

ABSTRACT

Title of Dissertation: WATER IN THE EARLY SOLAR SYSTEM:
INFRARED STUDIES OF AQUEOUSLY
ALTERED AND MINIMALLY PROCESSED
ASTEROIDS

Margaret M. McAdam, Doctor of Philosophy,
2017.

Dissertation directed by: Professor Jessica M. Sunshine, Department of
Astronomy

This thesis investigates connections between low albedo asteroids and carbonaceous chondrite meteorites using spectroscopy. Meteorites and asteroids preserve information about the early solar system including accretion processes and parent body processes active on asteroids at these early times. One process of interest is aqueous alteration. This is the chemical reaction between coaccreted water and silicates producing hydrated minerals. Some carbonaceous chondrites have experienced extensive interactions with water through this process. Since these meteorites and their parent bodies formed close to the beginning of the Solar System, these asteroids and meteorites may provide clues to the distribution, abundance and timing of water in the Solar nebula at these times. Chapter 2 of this thesis investigates the relationships between extensively aqueously altered meteorites and their visible, near and mid-infrared spectral features in a coordinated spectral-mineralogical study. Aqueous alteration is a parent body process where initially accreted anhydrous

minerals are converted into hydrated minerals in the presence of coaccreted water. Using samples of meteorites with known bulk properties, it is possible to directly connect changes in mineralogy caused by aqueous alteration with spectral features. Spectral features in the mid-infrared are found to change continuously with increasing amount of hydrated minerals or degree of alteration. Building on this result, the degrees of alteration of asteroids are estimated in a survey of new asteroid data obtained from SOFIA and IRTF as well as archived the Spitzer Space Telescope data. 75 observations of 73 asteroids are analyzed and presented in Chapter 4. Asteroids with hydrated minerals are found throughout the main belt indicating that significant ice must have been present in the disk at the time of carbonaceous asteroid accretion. Finally, some carbonaceous chondrite meteorites preserve amorphous iron-bearing materials that formed through disequilibrium condensation in the disk. These materials are readily destroyed in parent body processes so their presence indicates the meteorite/asteroid has undergone minimal parent body processes since the time of accretion. Presented in Chapter 3 is the spectral signature of meteorites that preserve significant amorphous iron-bearing materials and the identification of an asteroid, (93) Minerva, that also appears to preserve these materials.

WATER IN THE EARLY SOLAR SYSTEM: INFRARED STUDIES OF AQUEOUSLY
ALTERED AND MINIMALLY PROCESSED ASTEROIDS

by

Margaret M. McAdam

Dissertation submitted to the Faculty of the Graduate School of the
University of Maryland, College Park, in partial fulfillment
of the requirements for the degree of
Doctorate of Philosophy in
Astronomy
2017

Advisory Committee:

Professor Jessica M. Sunshine, Chair
Professor Kieren T. Howard
Dr. Michael S. P. Kelley
Professor Karen Prestegard
Professor Derek Richardson
Professor Richard Walker

© Copyright by
Margaret M. McAdam
2017

Dedication

In memory of Dr. Michael F. A'Hearn (1940-2017), a wonderful colleague and mentor.

Acknowledgements

I am grateful for the support and mentorship of my adviser, Jessica Sunshine as well as my committee members Derek Richardson and Michael Kelley. Thank you for your collaboration and the answers to my questions over the last six years.

To Tim McCoy, Kieren Howard and Conel Alexander, thank you for the great scientific discussions, edits on my papers and guidance.

I would also like to recognize the support and friendship of the Comet Group, especially Matthew Knight, Silvia Protopapa, Sam Crossley, and Carrie Holt. Thanks for all the chocolate!

To Ron Ballouz, thanks for being a great officemate!

I wish to also acknowledge all of the mentors, not yet mentioned, who have been instrumental to getting me where I am today. Starting with Dr. Bruce Gordon, my high school physics and astronomy teacher. You were the first person who taught me about planetary science and made me realize that I'm supposed to be a scientist. Thank you to Darby Dyar, Joanna Levine and Rachel Klima who were some of my incredible teachers at Mount Holyoke College. You taught me so much about astronomy in addition to being some of my most meaningful role models. To Karl Hibbitts, my very first boss, thank you for teaching me how to run a lab. Also thanks to Andy Rivkin. I really appreciate all the

beers and friendship. Finally, thank you Cari Corrigan for teaching me about meteorites and being a really inspiring scientist.

In addition to my mentors I wish to acknowledge the incredible network of scientists who I have the distinct privilege of calling friends. Thank you so much Erica Jawin, Rose Smith, Leah Cheek, Lauren Jozwiak, Hannah Susorney, and SONDY Springmann for the moral and scientific support.

To my family, Hugh, John and Ester, and especially my parents Bud and Terrie, you guys inspire me every day to be passionate and work hard. Thank you for all of the love and support.

To the Board Game Crew, all of my wonderful friends in DC and especially Aurora Coon, Rene Zelaya, Lauren Leffer, Rebecca Wener, Robert McCafferty, Chris Higgins, Jess Bell and Seth Puckett, thank you for all the laughs, deep conversations, dinner dates and little moments.

Last, but certainly not least, I'd like to recognize the incredible support and love of Mark Oscar Larson. Thank you for everything.

Table of Contents

Dedication	ii
Acknowledgements	iii
List of Tables	xi
List of Figures	xiii
List of Abbreviations	xviii
Chapter 1: Introduction	1
1.1 Asteroids, Meteorites and their Importance.....	1
1.2 Carbonaceous Chondrites: Properties, Parent Body Processing and Naming Conventions	4
1.2.1 Primary, Distinguishing Characteristics	4
1.2.2 Aqueous Alteration	6
1.2.3 Thermal Metamorphism.....	14
1.2.4 Meteorite Naming Conventions and Petrologic Types	15
1.3 Description of Carbonaceous Chondrite Chemical Groups.....	17
1.3.1 Ivuna-like Chondrites.....	18
1.3.2 Renazzo-like Chondrites	19
1.3.3 Mighei-like Chondrites	20
1.3.4 Ornans-like Chondrites	23
1.3.5 Vigarano-like Chondrites.....	24
1.3.6 Ungrouped Carbonaceous Chondrites	24
1.4 Asteroids: Classification and Evidence for Water	25
1.5 Spectroscopy: Remotely Determining Surface Properties.....	31
1.5.1 Visible and Near-infrared Spectroscopy	32
1.5.2 Mid-infrared spectroscopy	33

1.5.3 Spectroscopy of Carbonaceous chondrites and C-type asteroids	34
1.6 Summary Thesis Objectives	34
Preface to Chapter 2.....	39
Chapter 2: Aqueous Alteration on Asteroids: Linking the Mineralogy and Spectroscopy of CM and CI Chondrites	41
Abstract.....	41
2.1 Introduction.....	42
2.2 Background.....	44
2.2.1 Mineralogical Changes Associated with Aqueous Alteration	44
2.2.2 Mineralogy of the Meteorite Suite.....	47
2.2.3 Previous Spectroscopic Studies of CM/CI Chondrites	51
2.3 Data Collection	52
2.3.1 Samples	52
2.3.2 Spectral Measurements	53
2.3.3 Data	53
2.3.4 Visible and Near-Infrared Spectra	53
2.3.5 Mid-Infrared Spectra.....	54
2.4 Results.....	58
2.4.1 Visible/Near-infrared Spectral Relationships to Mineralogy	58
2.4.2 Trends in NIR Slope with Mineralogy.....	58
2.4.3 Lack of Correlation between Charge Transfer Band and Mineralogy.....	59
2.4.4 Mid-Infrared Spectral Relationships to Mineralogy	64
2.5 Connecting to Asteroids.....	74

2.5.1 Identifying Asteroid Mineralogy using MIR Results	74
2.5.2 Applications to Upcoming Missions.....	77
2.6 Conclusions.....	81
2.7 Acknowledgements.....	82
Preface to Chapter 3.....	83
Chapter 3: Spectral Evidence for Amorphous Silicates in Low-Metamorphic Grade CO Meteorites and Their Parent Bodies.....	85
Abstract.....	85
3.1 Introduction.....	86
3.2 Background.....	88
3.2.1 The least-altered CO meteorites.....	88
3.2.2 Disequilibrium Condensation of Amorphous Silicates.....	89
3.2.3 Spectroscopy of Amorphous Silicates and Glasses	90
3.2.4 Previous Spectral Studies of CO meteorites	93
3.3 Samples and Data Collection.....	94
3.3.1 Samples	94
3.3.2 Modal Mineralogy of Selected Samples	98
Type	100
3.3.3 Reflectance Spectra Data Collection	101
3.4 Results.....	101
3.4.1 Near-infrared Results	101
3.4.2 Mid-infrared Results	106
3.4.3 Comparison to metamorphosed COs	110

3.4.4 Comparison to other 3.0 Carbonaceous Chondrites	114
3.5 Evidence for Amorphous Material on Asteroids	118
3.6 Conclusions.....	125
Acknowledgements.....	127
Chapter 4: Mid-Infrared Observations of Main Belt Asteroids: Widespread Appearance of Hydrated Minerals and Variable Degrees of Alteration of Asteroids.....	129
Abstract.....	129
4.1 Introduction.....	131
4.2 Background.....	133
4.2.1 Spectral Signature of Aqueous Alteration in Carbonaceous Chondrites.....	133
4.2.2 Previous Detections of Hydrated Minerals using the Mid-infrared.....	139
4.3 Observations and Data Reduction.....	141
4.3.1 Archived Spitzer Observations	142
4.3.2 IRTF+BASS.....	147
4.3.3 SOFIA + FORCAST.....	152
4.3.4 Comparison of Observatories	153
4.3.5 Dataset Characteristics.....	155
4.4 Analysis	156
4.4.1 Thermal Modeling	156
4.4.2 Estimating Degree of Alteration	160
4.5 Results.....	178
4.5.1 Widespread and Variable Aqueous Alteration in the Main Asteroid Belt.....	178
4.5.2 Hydrated Asteroids Span the Range of Degrees of Alteration	184

4.5.3 Variability in the Themis Family	189
4.5.4 Notable Asteroids.....	193
4.6 Implications	199
4.6.1 Position of the Snow-line.....	199
4.6.2 Variability in the Themis Family	200
4.6.3 Asteroids with water-ice and hydrated minerals.....	202
4.7 Conclusions.....	203
Chapter 5: Summary of Conclusions and Future Work.....	209
5.1 Chapter 2 Conclusions	209
5.2 Chapter 3 Conclusions	210
5.3 Chapter 4 Conclusions	212
5.4 Limitations of this work.....	214
5.4.1 Survey Sample Limitations.....	214
5.4.2 Lack of Modal Mineralogy for Asteroids	214
5.4.3 Porosity and Grain Size Effects	215
5.5 Future Work:.....	216
5.5.1 Internal Thermal Evolution Models.....	216
5.5.2 Sample Return Missions	217
5.5.3 James Webb Space Telescope	219
5.5.4 Upcoming projects	219
5.6 Concluding Remarks.....	221
Appendices.....	223
Bibliography	355

List of Tables

Table 1.1: Average Petrologic Characteristics of Carbonaceous Chondrites (adapted from Weisberg et al., 2006)	18
Table 1.2: Bus-DeMeo Spectral Class Descriptions. Classes ordered by slope (largest to smallest) (Adapted from DeMeo et al., 2009).	31
Table 2.1: Summary of modal mineralogy, ferric iron content, and petrologic classification for the 16 CM/CI meteorite suite	50
Table 3.1: Meteorite Samples	97
Table 3.2: Modal mineralogy for selected samples.	100
Table 3.3: Spectral Modeling Components	109
Table 3.4: Minerva Observations.....	119
Table 3.5: Physical Properties of Minerva System.....	120
Table 4.1: Summary of Meteorite Mineralogy (adapted from Howard et al., 2009; 2010; 2011; 2015).	136
Table 4.2: Spitzer Observation Circumstances:.....	144
Table 4.3: Spitzer Target Physical Characteristics	146
Table 4.4: IRTF+BASS observations circumstances	148
Table 4.5: IRTF+BASS Asteroid Physical Characteristics	151
Table 4.6: SOFIA+FORCAST Observational Circumstances.....	153
Table 4.7: SOFIA+FORCAST Asteroid Physical Characteristics	153
Table 4.8: Thermal Modeling Best Fit Parameters.....	158

Table 4.9: Asteroid's Assigned Mineralogy	175
Table 4.10: Degree of alteration for asteroids with known water/hydration.	189
Table 4.11: Themis Family Asteroids.....	191

List of Figures

Figure 1.1: Average spectral types adapted from DeMeo et al (2009), courtesy of MIT.	30
Figure 2.1: Bidirectional reflectance spectra of CI/CM meteorites normalized to unity at 2.3- μm and offset for clarity.	55
Figure 2.2: MIR spectra of sixteen CM/CI meteorites normalized to unity at 8- μm and offset ~30% for clarity.	57
Figure 2.3: Reflectance ratio (2.4- μm /0.56- μm) plotted against the total abundance of phyllosilicates shows a general correlation between NIR slope and degree of aqueous alteration. However, despite consistent mineralogy across the suite, the NIR slope.....	62
Figure 2.4: Continuum removed spectra of meteorite suite in the 0.7- μm region plotted by increasing band depth.	63
Figure 2.5: 0.7- μm band depth vs. total abundance of phyllosilicates. Continuum removed band depth is uncorrelated with total amount of phyllosilicates and degree of alteration.	64
Figure 2.6: 0.7- μm band depth vs. relative abundance of ferric to total iron	65
Figure 2.7: Spectra of representative CM/CI meteorites, illustrating the characteristics of each subgroup.	70
Figure 2.8: Spectra in the 10-13- μm region vary continuously with degree of alteration.	71
Figure 2.9: Terrestrial analogs, olivine (Dyar et al., 2009) and antigorite (Bishop, et al., 2008b), compared to less and highly altered meteorites.	72
Figure 2.10: 10-13- μm peak position vs. total abundance of phyllosilicates.	73
Figure 2.11: The emissivity spectrum of asteroid (24) Themis (thermally corrected and normalized at 10- μm) compared to the spectra of representative meteorites: a less altered	

meteorite (QUE 97990), an intermediately altered meteorite (Mighei), and a highly altered	79
Figure 2.12: The emissivity minimum for asteroid (24) Themis superimposed on the meteorite reflectance peak positions vs. total volume of phyllosilicates.....	80
Figure 3.1: PSD-XRD Spectrum, model and residual for (a) ALH 77307 (CO 3.0), (b) DOM 08006 (CO 3.0), (c) Acfer 094 (CO 3.0) and (d) Felix (CO 3.3/3.4).	96
Figure 3.2: Near Infrared data. Near-infrared data (a), normalized and offset (+0.5) (b) and continuum removed and offset (c) ordered by weathering grade (top, minimally weathered to bottom, most weathered).....	103
Figure 3.3: Near-infrared slope vs. weathering grade.....	104
Figure 3.4: Band position vs. band depth. Terrestrially weathered samples have weaker (smaller band depths) that are centered $\sim 1.2\text{-}\mu\text{m}$	105
Figure 3.5: Mid-infrared spectra of low-metamorphic grade CO meteorites.	106
Figure 3.6: Four component spectra used for modeling: two olivines of differing iron content (Fo97 and Fo11), one enstatite, and a neutral darkening agent.	107
Figure 3.7: Example of mid-infrared spectral modeling.....	109
Figure 3.8: Residuals.	111
Figure 3.9: Near-infrared comparison to metamorphosed COs.....	112
Figure 3.10: PSD-XRD Spectrum, model and residual for (a) ALH 77307 (CO 3.0), (b) DOM 08006 (CO 3.0), (c) Acfer 094 (CO 3.0) and (d) Felix (CO 3.3/3.4).	113
Figure 3.11: Near-infrared comparison to 3.0 meteorites in other chemical groups.	116

Figure 3.12: Mid-infrared comparison of the spectra of 3.0 meteorites in other chemical groups.....	117
Figure 3.13: SPeX observation of 93 Minerva (offset +0.75) compared to low-metamorphic grade CO, DOM 08004 (CO 3.0/3.1).	121
Figure 3.14: SNR test.....	125
Figure 4.1: Meteorite endmembers.	137
Figure 4.2: Peak position vs. degree of alteration (amount of hydrated minerals) for anhydrous and aqueously altered meteorites. The peak position of the 10-13- μ m feature can be used to estimate the degree of alteration for asteroids.....	138
Figure 4.3: Histogram of taxonomic classifications for the dataset.....	154
Figure 4.4: Histograms of dataset's (a) albedo and (b) diameter.....	155
Figure 4.5: Relative emissivity difference compared to average error in the 10-13- μ m region.	161
Figure 4.6: (96) Aegle compared to a less altered meteorite.	164
Figure 4.7: Histogram of Goodness-of-fit values.	165
Figure 4.8: Excellent GoF example	166
Figure 4.10: Good GoF Example.....	166
Figure 4.9: Very good GoF example	166
Figure 4.11: Asteroids with mediocre fits to the laboratory data.	168
Figure 4.12: Asteroids with Poor goodness-of-fit values	169
Figure 4.13: Position of the 10-13- μ m feature is compared to the estimated degree using the best fit GoF value.....	171

Figure 4.14: Estimating the degree of alteration for BASS observations.....	172
Figure 4.15: (1284) Latvia and (267) Tirza compared to two Jupiter Trojan asteroids, (1172) Aneas and (624) Hektor (Emery et al, 2006) as well as Comet Tempel-2 (Kelley et al., 2017).	173
Figure 4.16: Degree of alteration by spectral type.....	174
Figure 4.17: C-complex variability of degrees of alteration.....	177
Figure 4.18: X-type asteroids variability observed by Spitzer.	178
Figure 4.19: Examples of Main Belt D-types.	179
Figure 4.20: Groups of degrees of alteration compared to their semi-major axis.	180
Figure 4.21: Groups of degrees of alteration compared to their diameters (on a logarithmic scale). There appears to be no relationship between asteroid size and degree of alteration.	181
Figure 4.22: Groups of degrees of alteration compared to their albedo. Highly altered asteroids may have a slight preference for lower-albedo asteroids.	182
Figure 4.23: Semi-major axis vs. Diameter of asteroid dataset.	183
Figure 4.24: Diameter vs Semi-major axis for asteroids with known hydration or water ice.	186
Figure 4.25: Asteroids with known hydration.	187
Figure 4.26: Asteroids with water-ice on their surfaces.	188
Figure 4.27: Emissivity spectra of the Themis Family members, ordered by number...	192

Figure 4.28: (1) Ceres emissivity spectrum and comparison to less altered meteorite. Ceres is interpreted to be similar to less altered meteorites with 60-75% hydrated minerals on its surface 194

Figure 4.29: Emissivity spectra of (10) Hygiea. Observed with SOFIA + FORCAST, Hygiea has features at 11.5 and 22- μm indicative of a highly altered surface (80-90% hydrated minerals) 195

Figure 4.30: (96) Aegle observed with Spitzer and IRTF+BASS. 196

Figure 4.31: (3200) Phaethon emissivity spectrum. Phaethon appears to be a highly altered asteroid with 80-90% hydrated minerals. This suggests that Phaethon has an inner solar system origin as opposed to a cometary origin. 198

List of Abbreviations

Chemical groups of carbonaceous chondrite meteorites:

CM – Mighei-like carbonaceous chondrite meteorites

CI – Ivuna-like carbonaceous chondrite meteorites

CR – Renazzo-like carbonaceous chondrite meteorites

CO – Ornans-like carbonaceous chondrites

CV – Vigarano-like carbonaceous chondrites

C-ung – Ungrouped carbonaceous chondrites

Spectroscopy abbreviations:

VNIR – visible/near-infrared spectroscopy (0.3-2.5- μm).

MIR – mid-infrared spectroscopy (referencing 8-25- μm spectral region).

Others:

PSD-XRD – Position Sensitive X-ray Diffraction is a method of determining the bulk mineralogy of samples using the diffraction of X-rays off of a powdered sample.

GoF - Goodness of fit value; a measure of how well an asteroid's spectrum matches laboratory meteorite data.

Chapter 1: Introduction

1.1 Asteroids, Meteorites and their Importance

The main asteroid belt, located between the orbits of Mars and Jupiter, contains more than 500,000 known objects (e.g., IAU Minor Planets Center). These asteroids range in size from ~1000 km in diameter (the dwarf planet Ceres) to small objects of a few hundred meters diameter that may be loosely held together by gravity (e.g., Scheeres et al., 2016). The asteroid belt represents the best record of the early inner Solar System, since these bodies are more primitive and less changed than larger planets. Asteroids, therefore, contain information about the composition of the starting materials of the Solar System, record parent body processes, and events in the disk. At early Solar System times, planets were being created through a process called accretion whereby smaller pieces of dust and rock aggregated into rocky planets. Some of those pieces of rock and dust were never accreted into a larger objects and therefore may retain more information about the Early Solar System.

One significant and outstanding question regarding this epoch is the distribution of water in the early Solar System. Water is a key component for life, however there is still debate about how the terrestrial planets, including Earth, obtained water. Canonically, the inner Solar System is denoted as the region interior to Jupiter's orbit. In this part of the Solar System, planets tend to be small and rocky unlike the gas and ice giants characteristic of the outer Solar System. Another important aspect of the inner Solar System is that it is interior to the 'snow-line' (e.g., Messenger et al., 2006). Outside of the snow-line,

temperatures are low enough so water can exist as solid ice. As the main asteroid belt is interior to the snow-line, the direct evidence for water in meteorites (pieces of asteroids transported to Earth) and telescopic evidence of water-ice on the surfaces of asteroids (e.g., Rivkin and Emery, 2010; Campins et al., 2010) indicates that this simple picture of a dry inner Solar System and icy outer Solar System does not adequately represent what is observed. There are a number of theories as to how water could be incorporated into asteroids and meteorites, including that the snow-line itself could have changed over time, migrating inwards into the region of the asteroid belt (e.g., Dodson-Robinson et al., 2009; Min et al., 2011) or, alternatively, that these objects formed past the snow-line and were later transported inwards (Walsh et al., 2011). The fundamental question becomes, how much water was in the main asteroid belt and where is it located? This answer may help constrain the position of the snow line, when water ice was available in the disk or potentially when giant planets migrated and transported material into the inner Solar System.

The purpose of this thesis is to identify the distribution of degrees of aqueous alteration in the asteroid belt in order to understand how the process of aqueous alteration affected the asteroid belt. The approach used here is to take well-characterized meteorites and measure them using a technique called spectroscopy. Spectroscopy, or the study of a material's interaction with light, is a tool that can be used from Earth to study asteroids remotely. This approach, coordinated spectral and mineralogical study, connects the bulk properties of the meteorites to their spectral features. If similar spectral features are observed on asteroids, this indicates that the asteroid may have similar bulk properties to

groups of meteorites. This work does not attempt to identify the parent bodies of meteorite groups but rather seeks to observe the process of aqueous alteration across many asteroids in the asteroid belt. Aqueous alteration is the chemical reaction between liquid water and silicate minerals producing hydrated minerals. The degree of alteration or amount of hydrated minerals produced can be used to trace the effects of water. This work uses the ground truth from the carbonaceous chondrite meteorites to understand the geologic context of aqueous alteration on asteroids.

With recent technological advances, refining of analytical techniques and increased numbers of asteroid and meteorite samples to study, there is more opportunity to investigate meteorites, their properties and relationships to spectroscopy. While many studies have been done on carbonaceous chondrites, one type of study that has not been accomplished is a coordinated spectral-mineralogical study. This type of study is presented in Chapter 2 of this thesis. Here, meteorite samples that were used for bulk mineralogical analyses were spectrally characterized. Knowing precisely the bulk mineralogy of these samples allowed us to determine the exact causes of a meteorite's spectral features. In this study, we found evidence of continuous spectral changes with degree of alteration for aqueously altered meteorites. This result provides a new tool for determining the bulk mineralogy of asteroids remotely (Chapter 4). Finally, recently some meteorites have been found to preserve amorphous iron-bearing silicate matrices. These amorphous materials condense out of the solar nebular and are easily destroyed by parent body processes once they have been accreted. For the first time, these have also been studied using spectroscopy. These results show (Chapter 3) that there are distinguishing spectral characteristics of these

rare meteorites. In the following sections of this chapter, I will describe the meteorites of interest to this work, what is currently known about asteroids and their water content, and how spectroscopy works.

1.2 Carbonaceous Chondrites: Properties, Parent Body Processing and Naming Conventions

1.2.1 Primary, Distinguishing Characteristics

Meteorites are generally grouped based on the characteristics of their mineralogy (composition and crystal structure of naturally occurring, inorganic chemical compounds), petrology (the abundances, textures, and structure of mineral assemblages), bulk chemical composition and oxygen isotopic compositions (Weisberg et al., 2006). Meteorite groups have distinct and unique bulk chemical compositions in addition to similarities in their mineralogy and petrology. Two or more groups of meteorites sharing broadly similar whole-rock chemical compositions, mineralogies and petrology, are called a class. The class of meteorites of interest to this thesis are the carbonaceous chondrites.

The carbonaceous chondrites are a subset of chondrites. Chondrites are characterized by the presence of chondrules or spherical droplets of igneous minerals (minerals that solidified from a melt or vapor). Chondrules are thought to be produced prior to the formation of the meteorite during a flash-heating event (e.g., Connolly and Jones 2017; Rubin, 2010; Jones et al, 2000). The exact nature of this heating event is under debate, however the event that created chondrules must have raised the local ambient

temperature of the disk in excess of ~2000K (Connolly and Jones 2017), vaporizing the dust. Some mechanisms that could plausibly produce chondrules are: interactions between the early active sun and the disk (Connolly and Jones, 2017), disk lightning (energy discharge caused by particle size sorting, perpendicular to the disk mid-plane; Jones et al, 2000), nebular shock wave of unknown origin, or impact jetting during planetesimal accretion (Connolly and Jones, 2017 and references therein). The presence of chondrules is characteristic of all chondrites, including carbonaceous chondrites.

Another important common characteristic of carbonaceous chondrites is the presence of organic matter (e.g., Cronin and Chang, 1993; Alexander et al., 2007). Organic matter may be partially responsible for the dark appearance of carbonaceous chondrite meteorites. It was erroneously thought to be pure carbon causing the color when this class was named. The organic matter includes many compounds such as amino acids. Due to the evidence of water in some carbonaceous chondrites and the presence of organic molecules, it has been suggested that these meteorites and asteroids related to them may be a significant building block of Earth (e.g., Alexander et al., 2012).

Organic matter is found in the matrices of carbonaceous chondrites. The matrix is defined as the material between the chondrules in meteorites. In the carbonaceous chondrites, matrix material tends to be relatively iron-rich silicates (minerals made primarily of Si, O, and Fe) compared to the chondrules, which generally are magnesium-rich silicates (minerals with Si, O and Mg primarily).

Groups of carbonaceous chondrites differ from each other in several ways including: average size of chondrules, amount of matrix relative to chondrules, mineralogy

of matrix, amount of metal and composition of olivine (if present), in addition to differences in oxygen isotopes and bulk chemistry. The mineralogy of carbonaceous chondrite matrices is generally hydrated minerals or olivine. Hydrated minerals or phyllosilicates are evidence that the meteorite has experienced interactions with water in a process called aqueous alteration. Matrix olivines (an anhydrous mineral) indicate that the meteorite has had minimal interaction with water but rather experienced thermal metamorphism. Both of these processes are discussed in the following subsections.

1.2.2 Aqueous Alteration

Aqueous alteration is the chemical reactions between liquid water and silicate minerals, producing hydrated minerals or phyllosilicates. Phyllosilicates found in carbonaceous chondrites have been suggested to form in the Solar nebula, prior to accretion (e.g., Grossman and Larimer, 1974). However, this idea has been largely ruled out though kinetic arguments of gas-grain reactions (e.g., Fegley, 2000) and phyllosilicates are generally thought to form on the parent body through aqueous alteration. Aqueous alteration occurs when water, coaccreted in the parent asteroid as water-ice, melts due to heating from short-lived radioactive nuclei. The process of aqueous alteration is very complex and still being studied. Aqueous alteration has been observed to some degree in a variety of meteorites from different chemical groups and classes (e.g., Tomeoka et al., 1989; Brearley, 2006; Alexander et al., 1989; Krot et al., 1995, 1997), including the ordinary chondrites (e.g., Alexander et al., 1989). Carbonaceous chondrites in the Ivuna-like, Renazzo-like and Mighei-like chemical groups are the most extensively aqueously altered meteorites (e.g., McSween, 1979; Brearley, 2006; Weisberg et al., 2006; Howard

et al., 2015). However, there is some evidence for water in Ornans-like and Vigarano-like carbonaceous chondrites (e.g., Brearley, 2006).

Aqueous alteration must have occurred relatively close to the beginning of the Solar System since the primary heat-source appears to be ^{26}Al , which has a half-life of $\sim 700,000$ years. The accretion of the carbonaceous chondrite parent asteroids occurred $\sim 3\text{-}4$ Ma after formation of calcium-aluminum-rich inclusions (CAIs; e.g., Fujiya et al., 2013; Brearley, 2006; Krot et al., 2006). CAIs were some of the first solids that formed in the protoplanetary disk and their formation marks the nominal ‘starting point’ of the Solar System. The onset of alteration likely occurred quickly after formation. Estimates of the period of aqueous alteration varies for the different groups of meteorites, however it seems that it was greater than ~ 7.5 Ma (e.g., Brearley, 2006). Furthermore, some evidence suggests that aqueous alteration may have been episodic in some carbonaceous chondrites (e.g., Brearley, 1999; Brearley and Hutcheon, 2000, 2002). Uncertainties in timing of accretion and water-to-rock ratios makes it difficult to determine the temperature of alteration. The estimates for the extensively altered carbonaceous chondrites (Ivuna-, Renazzo-, Mighei-like) range from very cool, $\sim 1^\circ\text{C}$ to 150°C (Brearley, 2006 and references therein).

Aqueous alteration replaces the original silicate minerals with phyllosilicates (e.g., Velbel et al, 2012). Phyllosilicates are layered minerals with alternating layers of tetrahedral- and octahedral-sheets. The tetrahedral sheets are composed of a cation, usually silicon or iron, surrounded by four oxygen atoms. The octahedral sheets have cations, usually magnesium or iron, in six-fold coordination with oxygens or hydroxyl groups. The alternating layers are held together by van der Waals forces, a weak intermolecular force.

Other accessory (minor) phases of minerals are created during aqueous alteration, including magnetite ($\text{Fe}^{2+}\text{Fe}^{3+}_2\text{O}_4$, an iron oxide), sulfides, tochillinite (a specific sulfide containing Fe, Ni and O), and calcite. The primary indication of the process of aqueous alteration is the presence and amount of phyllosilicates in a meteorite.

While aqueous alteration is a complex process of which, much remains poorly understood, the general stages and progression of alteration have been described in the literature (e.g., McSween, 1979; Bunch and Chang, 1980; Tomeoka and Buseck, 1985; McSween, 1987; McSween, 1989; Browning et al., 1996; Rubin, 2006; Howard et al., 2009, 2011, 2015). First, asteroids accrete their initial materials, chondrules (Mg-rich silicates with some metal and glass called mesostasis; e.g., Rubin et al., 2007), matrix materials (anhydrous silicates) and water ice. Heat is then released by short-lived radioactive nuclei. Aluminum-26 (^{26}Al) is thought to be the primary heat source producing aqueous alteration in the carbonaceous chondrites (e.g., Brearley, 2006; Young et al., 1999, 2003). The liquid water then reacts with the matrix materials converting them into phyllosilicates. These newly created phyllosilicates have the same elemental compositions to the precursor materials, with the addition of hydroxyl groups (OH) to the structure. In carbonaceous chondrites, these first matrix phyllosilicates are usually iron-rich. As the fluid is reacting with the matrix materials, it is simultaneously acting on the chondrules. Chondrules require more time to alter into phyllosilicates since they have defined boundaries and tend to have larger grains ('phenocrysts,' mm scale grains) of minerals. The first chondrule minerals to be altered are metal grains and amorphous chondrule glass (mesostasis), which are more susceptible to reacting with the fluid. The larger crystals of

olivines in chondrules take more time to react with the fluid. Chondrules and their components have a different composition than the matrix materials so the minerals produced as alteration progresses have different compositions. Chondrule glass and metal react with the fluid to form 'poorly characterized phases' or very fine-grained intergrowths of phyllosilicates from the matrix and tochillinite (Fe, S, Ni, and O). If there is still fluid present to react, the chondrule silicates, which are less susceptible than the chondrule glass and metal, are replaced by phyllosilicates as well. The process of aqueous alteration stops when there are no more fluids to react with silicates. This can occur because all of the initially accreted water-ice completely reacts to form phyllosilicates or, for some carbonaceous chondrites, the system is open and the water diffuses to the surface and is lost to space (e.g., Young et al., 1999, 2003).

The general process of aqueous alteration is to replace the initially accreted anhydrous minerals with hydrated phyllosilicates. There is also a dichotomy of composition of those phyllosilicates produced during aqueous alteration. The naming conventions of these phases has changed over the ~50 years that carbonaceous chondrites have been comprehensively studied (e.g., McSween, 1989, Browning et al, 1996; Rubin et al., 2006; Velbel et al., 2012; Howard et al., 2009, 2011). The nomenclature for carbonaceous chondrite phyllosilicates is further complicated because these minerals are rarely endmember compositions and therefore not easily named. We have adopted the nomenclature of Mg-rich phyllosilicates and Fe-rich phyllosilicates. These phyllosilicates tend to be in the serpentine group of minerals, indicating they have a layered structure with generally a divalent cation occupying the octahedral site. The phyllosilicates found in

carbonaceous chondrites are very different than those found on Earth. This difference is primarily caused by the setting of their formation; Earth-serpentines are formed in metamorphic settings while meteoritic-serpentines are low-temperature alteration products and can incorporate trivalent cations into their octahedral structures.

Aqueous alteration is a complex process that has affected chemical groups of carbonaceous chondrites differently. In certain carbonaceous chondrite chemical groups, aqueous alteration seems to have occurred in a closed system (e.g., Brearley, 2006). In a closed system, water cannot diffuse and escape, but rather all of the water reacts with anhydrous silicates and is incorporated into phyllosilicates. These close-system meteorites tend to be more highly altered (e.g., Brearley, 2006; Howard et al., 2009, 2011, 2015). It is not clear if all aqueously altered meteorites formed in closed-system settings. Some evidence indicates that Mighei-like chondrites, for example, may have altered in an open system which may be responsible for their highly variable degrees of alteration. Determining if a system was open or closed is not always possible. Similarly, determining the initial water-to-rock ratio is also difficult to determine. Estimates of the water-to-rock ratio for the carbonaceous chondrites varies from 0.3-1.2 (Brearley, 2006 and references therein). Furthermore, the timing of the onset of aqueous alteration is not always well constrained (e.g., Brearley, 2006).

To summarize, the general process of aqueous alteration (replacing initially accreted, anhydrous materials with phyllosilicates) is understood. The compositional and bulk mineralogical changes are fairly well constrained. However, the setting in which this alteration occurred as well as the temperature, timing of onset, and length of alteration are

not. Since the general process is understood, there have been many attempts to categorize individual meteorites by their degree of alteration. Categorizing meteorites in this way provides a method to investigate the process of alteration across chemical groups.

The first categorization of aqueously altered meteorites into degrees of alteration was by McSween (1979) who investigated the Mighei-like carbonaceous chondrites. As analytical techniques improved and more samples of aqueously altered meteorites became available through searches on the Antarctic ice-fields and deserts including the Sahara, the categorization and quantification of degrees of alteration similarly changed. Two of the most widely used schemes for the degree of alteration are the Mineralogical Alteration Index (MAI; Browning et al., 1996) and detailed petrologic properties (Rubin et al., 2007). These two methods use petrologic observations of meteorite thin sections. Thin sections are ~30 μm slices of meteorite mounted in epoxy on glass. These sections can be installed into an optical microscope or electron-microprobe analyzer (EPMA) and examined closely. In optical microscopy, minerals display unique properties (color, polarization etc.). It is possible to determine a variety of characteristics about meteorites from thin-section studies including composition and texture of the minerals. Texture is a crucial observation since it can be used to trace physical aspects of mineral formation including peak temperature, rapidity of cooling of a melt, temperature of aqueous alteration, etc. EPMA analyses investigate composition to a very high spatial precision. These analyses produce information about the elemental composition of a region of a thin section.

The Browning et al, (1996) and Rubin et al (2007) studies categorize Mighei-like meteorites into degrees of alteration based on several characteristics. The MAI of

Browning et al (1996) measures the change of Fe-rich phyllosilicates into Mg-rich phyllosilicates using three key parameters to determine degree of alteration: average matrix phyllosilicate composition, the volume of matrix silicates and finally the volume of chondrules in a meteorite. Unlike Browning et al (1996) who measure the substitution of Fe-rich phyllosilicates with Mg-rich phyllosilicates, Rubin et al, (2007) assign a petrologic type (2.0-2.6) based on the amount of alteration chondrule phenocrysts (large olivine grains) and volume of poorly characterized phases (fine-grained interwoven sulfides and phyllosilicates). They also identify other indicators such as the amount of iron-nickel metal grains, composition of accessory sulfides and carbonates. There are no CMs that appear to be unaltered; Rubin et al. (2007) choose the least-altered petrologic type arbitrarily to be 2.6.

Both of these alteration schemes have been criticized. The Browning et al. (1996) MAI work requires precision EPMA analyses and a complex algorithm to determine the degree of alteration. The schema by Rubin et al. (2007) appears to only apply to Mighei-like meteorites; it does not transcend chemical groupings in a functional way. This severely limits its efficacy in tracking the process of aqueous alteration across chemical groups or parent asteroids.

More recent classification schemes have attempted to quantify aqueous alteration using properties of meteorites that are unrelated to group characteristics (Howard et al., 2015). This schema, measuring the bulk mineralogy of meteorites, transcends chemical group and defines degree of alteration in a self-consistent way. The degree of alteration is defined as the total phyllosilicate fraction or the volume of phyllosilicates relative to the

volume of anhydrous silicates and phyllosilicates (or total silicate content). These volumes are measured using position-sensitive X-ray diffraction (PSD-XRD). As several chapters of this thesis utilize PSD-XRD results, I will briefly describe the technique.

During a PSD-XRD measurement, the powdered meteorite sample is bombarded with X-rays. These photons diffract off of the meteorite's crystal structure. Minerals in a meteorite have different elements and bonding environments that determine how X-rays interact with them. The diffracted X-rays are collected by a 120° detector arc, simultaneously. Since carbonaceous chondrites are complex mixtures of minerals, these diffraction patterns are correspondingly complex. Fitting techniques use standards of mineral measured under similar conditions to the meteorites (e.g., Bland et al., 2004; Howard et al., 2009, 2011, 2010). The deconvolution process involves accounting for intensities, counting times, flux of X-rays incident and the mass absorption coefficients for both the sample and the standard. Subsequently, the pattern-fits are converted into modal mineralogy (apparent volume of minerals in a sample) by accounting for the relative differences in X-ray absorption by the material (e.g., Bland et al., 2004; Howard et al., 2009, 2011, 2015). There are uncertainties associated with each step of this process, however, this technique has proven to be accurate within 1–3 vol.% of minerals in a sample (e.g., Howard et al., 2009, 2011, 2015).

The Howard et al. (2015) schema separates meteorites into degrees of alteration defined by increases in phyllosilicate fraction by 5 vol.% intervals. Type 3.0 is defined by <5% phyllosilicates relative the total silicate fraction, while 1.0 is defined as >95% phyllosilicates fraction relative to total silicate.

1.2.3 Thermal Metamorphism

Thermal metamorphism is the process of parent body heating. This process is driven, similarly to aqueous alteration, by heat release from ^{26}Al , however meteorites that are affected by thermal metamorphism likely do not appear to accrete with significant water (e.g., Brearley and Jones, 1998). Additionally, the distribution of ^{26}Al available during accretion of thermally metamorphosed carbonaceous chondrites may be variable in both space and time. After accretion of cold material, heat is released, which causes textural and mineralogical changes in the parent bodies (Brearley and Jones 1998, Weisberg et al., 2006; Huss et al., 2006). Texturally, the initial amorphous matrix materials are annealed into crystalline phases, creating a more compact (less porous) matrix (e.g., Huss et al., 2006). The peak temperatures reached for the thermally metamorphosed carbonaceous chondrites ranges from as low as $\sim 200^\circ\text{C}$ to $\sim 700^\circ\text{C}$ (e.g., Huss et al., 2006)

The timing of this parent-body process has been studied primarily in the ordinary chondrites where there are a large number of individual meteorites. The accretion of the ordinary chondrite parent body(s) occurred ~ 2 Ma after the formation of CAIs; the length of thermal metamorphism depends on the peak temperature reached. Low-metamorphic-grade meteorites (indicated by types 3.0–3.2) were heated until ~ 4 Ma post-CAI formation, while meteorites that experienced higher peak temperatures experienced heating for up to 7 Ma post-CAI formation (Huss et al., 2006). Ordinary chondrites appear to have accreted earlier and from a different reservoir of material than the carbonaceous chondrites. It is unclear if the timing and length of thermal metamorphism derived from the ordinary chondrites is applicable to carbonaceous chondrites. However, as the textural and

compositional markers are similar between the two classes of meteorites, it is possible that the thermally metamorphosed carbonaceous chondrites accreted and were heated in a similar manner to the ordinary chondrites.

1.2.4 Meteorite Naming Conventions and Petrologic Types

A shorthand indication for mineralogy, petrology, and degree of alteration or thermal metamorphism for carbonaceous chondrites is the petrologic type. This is a denotation that broadly defines the petrologic characteristics of a meteorite (e.g., the structure, texture and compositions of mineral assemblages). For carbonaceous chondrites there are three petrologic types: Type 3, which describes unequilibrated meteorites that have undergone some thermal metamorphism but are otherwise unchanged since accretion; Type 2, which refers to meteorites that have experienced aqueous alteration to some degree and Type 1, which indicates a high degree of aqueous alteration or that the meteorite is mostly comprised primarily of hydrated minerals. When modern meteorite classifications were first being developed, it was thought that since Ivuna-like meteorites are very old, they represented the first nebular materials. This implied that hydrated minerals were prevalent in the proto-planetary disk. These meteorites were assigned the petrologic type 1 to indicate that they are the most representative of the primordial Solar Nebula. It is known now that aqueous alteration is a parent body process and, in fact, type 3 meteorites are likely the least changed since accretion of the parent body. Nevertheless, this nomenclature persisted.

Carbonaceous chondrites are signified by their unique name, group identification and petrologic type. Some meteorites are observed falls. This means that the object was

seen to enter the atmosphere and subsequently collected. Falls are generally named after the city or region of where the meteorite fell (e.g., the Murray meteorite fell in the Murray, Kentucky). Meteorites in this thesis will be referred to by their name, group membership and petrologic type. For example, Orgueil (CI1) is in the carbonaceous chondrite class (shortened to 'C', CI1), in the Ivuna chemical group (abbreviated as 'I'; CI1) and has a petrologic type 1 (CI1) so it is primarily composed of hydrated minerals. Other meteorites are 'finds,' which indicates they were discovered without knowledge of when they arrived on Earth. Many meteorites are found in Antarctica or arid deserts such as the Sahara in Africa. The naming conventions differ for meteorite-finds depending on the institution collecting them and region of collection. Many of the meteorites studied in this thesis are collected by the US Antarctic Search for Meteorites program (ANSMET) in Antarctica. The naming convention for these meteorites is the geographic region where the meteorite was collected (e.g., Allan Hills, abbreviated as ALH), the last two digits of the year it was collected (the year of the summer season it was collected; '97' for a meteorite classified in 1997; '00' for a meteorite classified in 2000) followed by a random number. For example, ALH 77307 (CO3) is an Antarctic find from Allen Hills (a mountainous region on the Antarctic coast, near McMurdo Station), classified/collected in 1977; it is a carbonaceous chondrite (CO3) in the Ornans chemical group (CO3) that has experienced some thermal metamorphism (CO3). ANSMET has been conducting meteorite searches in Antarctica since 1976; therefore meteorites with year-designations from 76-99 are referring to meteorites collected/classified between 1976 and 1999 while meteorites with year-designations 00-17 are referring to meteorites collected in the 2000-2017 period.

These denotations will be used throughout this thesis as a shorthand to indicate different chemical groups and broad characteristics of those groups. Chemical groupings indicate that a meteorite originates from a specific, unique reservoir of material. Petrologic types provide a general framework for the type of minerals in a meteorite. Type 3 meteorites are anhydrous and sometimes heated; Type 2 meteorites are hydrated but highly variable in the degree of alteration; Type 1 meteorites are highly altered, hydrated meteorites.

Terrestrial weathering is a common feature of meteorite finds. Meteorites that sit for long periods of time exposed to air and precipitation may develop rust around metal grains and other products such as evaporite materials may form along fractures. Terrestrial weathering is a secondary process that occurs after the meteorite is on Earth; it is distinct from the parent body processes that affect meteorites on their parent bodies. For Antarctic finds, terrestrial weathering is measured on a scale (A – E) that describes the extent of rust and evaporites visible on the meteorite. These weathering products may affect the spectral signature of the meteorites. Some of these effects are described in Chapter 3.

1.3 Description of Carbonaceous Chondrite Chemical Groups

Several groups of carbonaceous chondrites will be discussed at length in this thesis. In the following subsections, I will describe the groups of carbonaceous chondrites that are studied in this thesis so that the reader has a general understanding of these meteorites. The major characteristics are listed in **Table 1.1**.

Table 1.1: Average Petrologic Characteristics of Carbonaceous Chondrites (adapted from Weisberg et al., 2006)

	<i>CI</i>	<i>CM</i>	<i>CR</i>	<i>CV</i>	<i>CO</i>
<i>Chondrule Abundance (vol.%)</i>	« 1	20*	50-60	45	48
<i>Matrix Abundance (vol.%)</i>	>99	70*	30-50	40	34
<i>CAI – AOA Abundance (vol.%)</i>	« 1	5	0.5	10	13
<i>Metal Abundance (vol.%)</i>	0	0.1	5-8	0-5	1-5
<i>Average Chondrule diameter (mm)</i>	N/A	0.3	0.7	1.0	0.15

*Highly variable; N/A – not applicable

1.3.1 Ivuna-like Chondrites

Ivuna-like carbonaceous chondrites (CIs) are a relatively small group with only 7 members (Ivuna, Orgueil, Alais, Tonk, Revelstoke, Yamato-86029, Yamato-86737, Yamato-980115, and Yamato-981034). The total mass of this group is approximately 35 kg. The small size of the CI group belies its importance to the study of meteorites and asteroids. CI chondrites most closely match the solar photosphere and corona, indicating that CI chondrites are elementally the most representative material of the early Solar nebula (Anders and Grevesse, 1989). Based on ^{53}Mn - ^{53}Cr age dating of CI meteorites (Fujiya et al., 2013), this group appears to have accreted ~3–4 million years (Ma) after the formation of CAIs. This means that the parent body (or bodies) of the CI meteorites accreted very close to the beginning of the Solar System.

The CI parent(s) experienced closed-system aqueous alteration, meaning the water chemically reacting with the minerals could not flow freely (e.g., Brearley, 2006). Furthermore, all the water reacted with the minerals (Brearley, 2006 and references therein). The size(s) of the CI parent(s) would have to have, at minimum, contained enough ^{26}Al to sustain liquid water for 9 Ma (Fujiya et al, 2013). In their internal thermal models,

Young et al (1999, 2003) suggest that asteroids of diameters ~80 km would satisfy constraints of closed-system aqueous alteration and oxygen isotopes observed in the CI group. This size is consistent with the results of Fujiya et al. (2013). More recent studies such as Bland et al., (2009) show that using estimates of permeability (e.g., a measure of a material's ability to allow fluid flow) from measurements of carbonaceous chondrites themselves (instead of estimates from terrestrial and lunar analogs, e.g., Grim and McSween, 1989) also satisfy oxygen-isotope and bulk chemistry constraints. These new models indicate that asteroids with high degrees of alteration did not necessarily have to originate from relatively small asteroids. Additionally, these new models resolve the paradox of pristine Solar-like bulk chemistry while experience pervasive aqueous alteration (Bland et al., 2009).

1.3.2 Renazzo-like Chondrites

Renazzo-like (CR) chondrites are a group of carbonaceous chondrites generally characterized by highly variable degrees of aqueous alteration. CR meteorites have generally experienced less extensive alteration than the Mighei-like (CM) and CI meteorites (e.g., Brearley, 2006 and references therein; Brearley and Jones, 1998). CRs tend to have a type 2 petrologic designation (indicating variable aqueous alteration), however there are two example of a type 1 CR, Grosvenor Mountains (GRO) 95577 and Al Rais. These meteorites appear to have been more extensively altered than other CRs while still being consistent with the group in oxygen isotopes and other bulk chemical signatures. In addition to this unusual member, two other CRs are notable.

Meteorite Hills (MET) 00426 and Queen Alexandra Range (QUE) 99177 are two CR meteorites which have abundant amorphous iron-bearing silicate matrices (e.g., Abreu and Brearley, 2010). These materials are thought to be produced through disequilibrium condensation (rapid cooling of vaporized phases, forming amorphous materials) in the disk. The exact nebular setting of this condensation is still under debate (e.g., Abreu and Brearley, 2010; Brearley, 1993). MET 00426 and QUE 99177 may represent CR meteorites that are the least-changed since the time of accretion, preserving critical information about the composition of the proto-planetary disk and the process of accretion. While these meteorites are the most pristine samples of the CR parent(s), this material is enriched in hydrogen and likely affected by aqueous alteration (Garenne et al., 2014). These materials may represent the ‘gel’ phase of alteration (e.g., Chizmadia and Nuth, 2006; Chizmadia, 2007), where water has just beginning to react with the initial anhydrous silicates but not progressed enough to produce phyllosilicates. MET 00426 and QUE 99177 may represent material from the outer unprocessed crust of the CR parent(s) that was altering on the interior (e.g., Young et al., 1999, 2003) or a parent body accreted from the same reservoir of CR-like silicate material with less-abundant water.

1.3.3 Mighei-like Chondrites

CM, Mighei-like carbonaceous chondrites, are a very large group of over 500 meteorites. CMs have experienced variable degrees of alteration (e.g., Howard et al., 2015). Some meteorites can be as highly altered as CI meteorites, but can have as little as ~60% hydrated minerals (i.e., 60% altered). Brecciation, or the process of impact shattering and

re-forming a meteorite comprised of angular pieces of the proto-lith (starting rock), is another common feature of CMs. Like alteration, CMs exhibit variable degrees of brecciation: some samples are unbrecciated and some are highly brecciated (e.g., Lauretta et al., 2000; Rubin et al. 2007). Brecciation destroys the original texture of the meteorite, therefore understanding the setting and nature of aqueous alteration in the CM parent(s) is difficult.

Aqueous alteration in CM meteorites is generally thought to have occurred on the CM parent(s) (e.g., Brearley, 2006). For example, the bulk chemical composition of CM meteorites is homogeneous (McSween, 1977; Bunch and Chang 1985). Additionally, as aqueous alteration increases in CMs, chondrules begin to alter into phyllosilicates, enriching these phyllosilicates in magnesium (McSween 1979; Lauretta et al., 2000; Velbel et al., 2012). The increase in magnesium is caused by the progressive conversion of chondrule silicates into phyllosilicates. Chondrules tend to be more magnesium rich than the surrounding matrix, thus as they are progressively altered, the phyllosilicates they form are more magnesium rich and the overall phyllosilicate content also increases in magnesium as they are altered. Additionally, during alteration, Fe-rich phyllosilicates recrystallize, incorporating Mg-ions while Fe-ions are mobilized in the fluid (e.g., Howard et al., 2015), enriching the bulk meteorite in Mg-rich phyllosilicates. This elemental exchange could only occur if the alteration was happening in a parent body. Furthermore, within one CM meteorite, the chondrules are generally altered to the same degree (e.g., Hanowski and Brearley, 2001). This again suggests that the process of aqueous alteration

was acting on the meteorite uniformly, which is predicted by an asteroidal-alteration scenario (e.g., Brearley, 2006; Lauretta et al., 2000; Hanowski et al., 2001).

There is some evidence that CM meteorites show pre-accretionary aqueous alteration (presumably in the nebula). This evidence is based generally on the presence of fine-grained rims on chondrules (Metzler et al., 1992; Bischoff et al., 1998; Zolensky et al., 1993). The mineral assemblages in the chondrule rims are hydrated or partially hydrated. If this hydration occurred on the parent body, parts of the chondrules should have reacted with the water as well. Since these chondrule phases (e.g., chondrule glass) have not been altered, the conclusion is that the fine-grained rims on these chondrules experienced hydration prior to being accreted onto the chondrule and subsequently accreted into the parent body (e.g., Brearley, 2006). While this evidence cannot be dismissed, some of the underlying assumptions do not account for complex geochemical micro-environments in which the reaction between water and the chondrule/chondrule rim material occurs. For example, metal grains in Yamato-791198 chondrule rims may have been preserved from destruction by the acidity of the fluid (Chizmadia and Brearley, 2003). Additionally, more recent studies of chondrule rims in CM meteorites indicate that these textures are consistent with formation on the parent body (e.g., Trigo-Rodriguez et al., 2006). In summary, there may be some nebular hydration of mineral assemblages, particularly in chondrule rims, in CM chondrites, however, most of the evidence indicates that the phyllosilicates in CMs were produced through parent-body aqueous alteration.

Some aqueously altered carbonaceous chondrites, including several in the CM group, show evidence of dehydration events (e.g., Nakaaura, 2005; Tonui et al., 2014).

There are ~25 such samples (Tonui et al, 2014; Nakamura, 2005) that exhibit a range in peak temperatures between $<250^{\circ}\text{C}$ to $>750^{\circ}\text{C}$ (Nakamura, 2005). Textural and trace-element evidence indicates that this dehydration occurred after or close to the end of aqueous alteration (e.g., phyllosilicates were produced and subsequently dehydrated). The source of heat to produce this dehydration event has been suggested to come from thermal metamorphism, similar to what is observed in type 3 carbonaceous chondrites, shock heating from impacts or radiation during a close passage to the Sun (e.g., Nakamura, 2005). These aqueously altered and heated samples are a further indication of the complexity of parent-body processes.

1.3.4 Ornans-like Chondrites

CO (Ornans-like) carbonaceous chondrites are thermally metamorphosed meteorites (e.g., McSween 1977; Kimura et al., 2008). These meteorites show evidence of peak temperatures ranging from ~ 200 to $>700^{\circ}\text{C}$. Certain CO samples that have low peak temperatures (e.g., ALH77307, Brearley, 1993; Alexander et al., in press) preserve pre-accretion composition and textures similar to the least-processed CRs described above. Unlike the CRs, the low-metamorphic-grade COs do not appear to have as much evidence of influence of water although there may have been some coaccreted water ice in the initial materials (e.g., Krot et al., 1995, 1997).

Some evidence suggests a ‘genetic’ relationship between the CO carbonaceous chondrites and the CM meteorites (e.g., Kallemeyn and Wasson, 1982). The anhydrous materials preserved in some CM meteorites share chemical characteristics (e.g., oxygen

isotopic signatures) with the CO meteorites. Furthermore in CMs where chondrules are still present (e.g., less aqueously altered), the average chondrule size is similar between the groups. The evidence against this genetic connection includes differences in matrix abundances (e.g., Weisberg et al., 2006) and composition of organics (e.g., Alexander et al., 2007).

1.3.5 Vigarano-like Chondrites

CV chondrites, Vigarano-like, may be the most well-studied and complex carbonaceous chondrites in this class (e.g., Weisberg et al., 2006; Huss et al., 2006; Howard et al., 2010). There is some evidence that they may have coaccreted with water (e.g., Brearley and Jones, 1998; Weisberg et al., 2006; Brearley, 2006) however, it was a much smaller proportion than what is seen in the CM/CI meteorites. CVs have experienced some heating, but are much less extensively heated than the COs with metamorphic grades of 3.3 or less (e.g., Brearley and Jones, 1998). The matrix materials of these meteorites have wide variability of mineral assemblages and olivine composition, however, the matrices tend to be dominated by iron-rich olivines.

1.3.6 Ungrouped Carbonaceous Chondrites

Several carbonaceous chondrites do not fit perfectly into an established chemical group (e.g., Essebi and Acfer 094). These meteorites may represent the first samples of a new chemical group (Weisberg et al., 2006). These meteorites are referred to as 'ungrouped', abbreviated to 'ung'. If they broadly fit into a petrologic type (e.g., hydrated

mineralogy), they are assigned this type similar to grouped meteorites. These will be identified and discussed in this thesis as required.

1.4 Asteroids: Classification and Evidence for Water

Water ice and hydrated minerals have been observed on the surfaces of some asteroids (e.g., Vilas and Gaffey, 1989; Rivkin and Emery, 2010; Campins et al., 2010; Takir and Emery, 2012). Hydrated minerals have been observed using primarily two spectral features: the 0.7- μm feature (e.g., Vilas and Gaffey, 1989) and the 3- μm feature (e.g., Lebofsky, 1980). The 3- μm feature has several different morphologies. The ‘checkmark’ shape indicates the presence of hydrated minerals (e.g., Lebofsky, 1980), while a ‘rounded’ shape indicates the presence of water ice (e.g., Rivkin and Emery, 2010; Campins et al., 2010). Two other 3- μm band morphologies were identified by Takir and Emery (2012): Ceres-like and Europa-like. Additionally, the presence of OH (thought to be the product of photo-dissociation of water; e.g., A’Hearn and Feldman, 1992) and water-vapor have been observed outgassing from the surface of Ceres (e.g., Küppers et al., 2014). More recently, a new class of objects, called activated asteroids (e.g., Hsieh and Jewett, 2006), have been observed to have comet-like activity by the presence of comae and tails. These features are thought to be the result of sublimating water ice but no ice or OH has been detected on these bodies due to the faintness of these objects (e.g., Hsieh and Jewett, 2006).

Water is clearly a significant component of the proto-planetary disk. The evidence for this is the extent of aqueous alteration in meteorites, the evidence of hydrated minerals and water ice on asteroids in addition to the ice-dominated bodies of the outer Solar System

such as comets and Oort-cloud objects. Researchers have been working to determine the distribution, abundance and epochs when water was present in the proto-planetary disk. The first indications of compositional stratification in the asteroid belt was noted by Gradie and Tedesco (1982). This work identified the distribution of compositional types with heliocentric distances. This was inferred to be related to compositional changes associated with increased hydrated minerals in the mid- and outer-Belt. Further studies found that hydrated asteroids, based on 3- μm observations, are preferentially found in the mid-Main Asteroid Belt (e.g., Jones et al., 1990; Vilas, 1994). The evidence of hydrated minerals disappears with increasing heliocentric distances. This was inferred to indicate that the mid-Belt experienced a mild heating event, inducing aqueous alteration, while the Outer Belt with more water and organics did not experience such an event (e.g., Grimm and McSween, 1989; 1993). Similarly, studies of the distribution of the 0.7- μm feature in the spectra of asteroids notice an increase in aqueously altered asteroids preferentially in the mid-Belt, however, hydrated asteroids were noted in a wider range of heliocentric distances than in the previous work of Jones et al (1980), Vilas (1994; Barucci et al., 1998; Fornaiser et al., 1999; Fornaiser et al., 2014).

A more recent survey of Outer Main Belt asteroids observed a more nuanced stratification. Takir and Emery (2012) find that hydrated asteroids ('checkmark' 3- μm features) are preferentially found in the mid-Belt, consistent with previous visible and 3- μm studies. However, Outer Main Belt asteroids preferentially have water-ice features (rounded 3- μm shapes). This result implied that the distribution of water increased with increasing heliocentric distance. In the Outer Belt, water represented a larger proportion of

the accreted materials. With longer accretion times, these asteroids experienced a lower heat flux from ^{26}Al in addition to a greater abundance of water, therefore Takir and Emery (2012) conclude that aqueous alteration did not occur on the Outer Main Belt objects. Water's high specific heat and a lower heat flux prevented the onset of aqueous alteration. In the mid-Belt, there was sufficient ^{26}Al and water ice for aqueous alteration to occur. While these studies find relationships between 0.7- μm , checkmark and rounded 3- μm features, these wavelength regions do not provide information about the degree of aqueous alteration.

One major difficulty in making connections between asteroids with low albedos and carbonaceous chondrite meteorites is the lack of spectral features in the visible and near-infrared. The 0.7- μm feature is indicative of the presence of hydrated minerals, however, it is not always observed in aqueously altered meteorites, nor is it related to the degree of alteration (e.g., McAdam et al., 2015a, b; see Chapter 2). Moreover, observations of asteroids in the 3- μm region have identified hydration on asteroids without the 0.7- μm feature (e.g., Rivkin et al., 2002). The absence of the 0.7- μm features does not indicate the absence of hydration on asteroids. The 3- μm feature is caused by the fundamental vibration of hydroxyl groups in the structure of hydrated minerals and water. As such, the position of this feature may be related to the degree of alteration of meteorites. Some studies (e.g., Takir et al., 2014) have started investigating the relationship between the 3- μm band position and petrologic type, however, more studies are needed in particular studies investigating the relationship with abundance of hydrated minerals. Furthermore, the atmosphere has a strong telluric absorption in the region where this feature occurs. The

atmosphere therefore may prevent the identification of compositional changes in this wavelength region from the ground. As a consequence, hydrated asteroids could be present in a number of groups, especially if these groups are defined in the absence of strong near-infrared features.

One significant goal of asteroid classification is to broadly group asteroids with similar compositions by parameterizing their spectra and identifying groupings (e.g., Tholen, 1984; Xu et al., 1995; Bus and Binzel, 2002; DeMeo et al., 2009; deMeo et al., 2016). For many asteroids classes, spectral similarity tracks well with asteroid mineralogy (e.g., V-types). However, for low-albedo asteroids, especially those with weak or no features, relationships with composition are not always as certain (see Chapter 2; McAdam et al., 2015a, b). The C-complex, or class of asteroids with broadly similar visible and near-infrared spectral characteristics, is subdivided into several types. These types of low-albedo asteroids have changed with the increasing number of asteroids observed with visible/near-infrared spectroscopy (e.g., Tholen, 1984; Bus and Binzel, 2002; deMeo et al., 2009). In the two most recent classification schemes made with spectroscopic measurements in the visible and near-infrared (Bus and Binzel, 2002; deMeo et al., 2009), there are six spectral types in the C-complex: B, C, Cb, Cg, Cgh, and Ch. These different classes correspond to spectral features, primarily the spectral slope or how the reflectance increases/decreases with increasing wavelength. Since asteroids classified with low albedos, weak features or variable slopes may be hydrated, a number of spectral types are investigated in this thesis. These spectral types that are studied are summarized in **Figure 1.1** (courtesy of Planetary Spectroscopy at MIT) and descriptions of the types are listed in **Table 1.2**.

C-type asteroids are found throughout the asteroid belt (e.g., DeMeo et al., 2016), however they dominate the mass and number of objects in the middle (2.5–2.82 astronomical units, AU, average distance from Earth to the Sun), and Outer Belt (2.82–3.3 AU; deMeo et al., 2016). The proportion of C-type asteroids is much greater than the proportion of carbonaceous chondrite falls. The number of meteorite falls is considered to represent the true flux of material from the Asteroid Belt. Since meteorites can be destroyed through erosional processes on Earth, meteorites made of very strong material (e.g., iron meteorites) preferentially survive to be collected as finds. Finds, therefore, do not represent the true flux of asteroidal material. Carbonaceous chondrites represent ~5% of the meteorite falls (Hughes, 1981), compared to >50% of asteroids in the middle to outer Asteroid Belt. This puzzling discrepancy may be related to the how asteroids are dynamically transported to the near-Earth space. Near-Earth Objects are taxonomically dominated by S-types while C-types make up a much smaller fraction of these objects (~6%; Binzel et al., 2004). Since this near-Earth space is likely the source region for the meteorites, the dynamical paths to this space must preferentially transport S-type/ordinary chondrite material.

Similarly, the large number of asteroids in the Main Belt of similar type means that the source of the carbonaceous chondrite groups is not a single parent asteroid. Planetesimal formation models (e.g., Levison et al., 2015) predict that multiple planetesimals can form out of the same local material, producing parent bodies of similar bulk properties including composition (Vernazza et al., 2014). It is therefore likely that carbonaceous meteorites

within a group could come from multiple parent asteroids of broadly similar bulk composition, including water content.

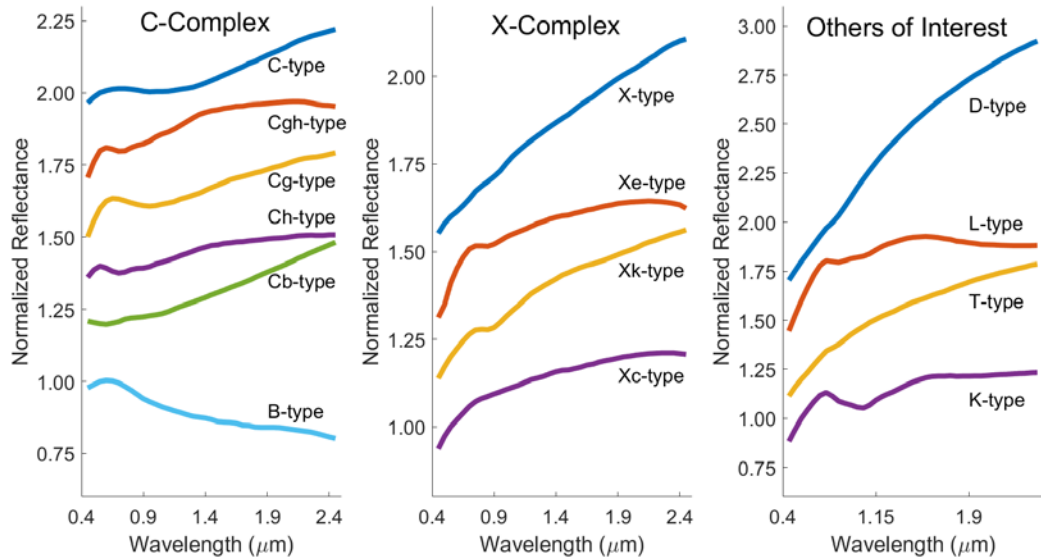


Figure 1.1: Average spectral types adapted from DeMeo et al (2009), courtesy of MIT

Left: The C-Complex asteroid taxonomies. C-complex asteroids tend to have low albedos some with features at 0.7- or 1.1- μm . (Center) X-complex asteroids tend to have higher albedos than the C-complex asteroids and may have some features. (Right) Other types of interest include D- and T-types which differ from C- and X-complexes by higher albedos. D-types tend to have more extreme red slopes. L- and K-types appear to have features caused by olivine and pyroxene that are weaker than what is observed in the S-complex. Their low albedos may indicate a relationship with the heated carbonaceous chondrites.

Table 1.2: *Bus-DeMeo Spectral Class Descriptions. Classes ordered by slope (largest to smallest) (Adapted from DeMeo et al., 2009).*

<i>Class</i>	<i>Description</i>
<i>D</i>	Linear spectrum, with steep slope
<i>L</i>	Steep slope in the visible, flat after 0.7- μm ; may have downward concave shape; may be a 2.0- μm feature
<i>T</i>	Linear spectrum with moderate – high slope; often concave-down shape
<i>X</i>	Linear spectrum with medium to high slope
<i>Xe</i>	Low to medium slope, concave-down shape; absorption at 0.55- μm
<i>Xk</i>	Low to medium slope concave-downward shape, weak feature between 0.8–1- μm
<i>K</i>	Wide absorption at \sim 1- μm
<i>Xc</i>	Low to medium slope slightly concave-down shape
<i>C</i>	Linear slope in the visible, often maximum at 0.6- μm , positive near-infrared slope; may have a feature longward of 1- μm
<i>Cgh</i>	Small positive slope beginning at \sim 1- μm , pronounced UV drop off; absorption band at 0.7- μm
<i>Cg</i>	Small positive slope beginning at \sim 1.1- μm , pronounced UV drop off
<i>Ch</i>	Small positive slope beginning at \sim 1.1- μm , slightly pronounced UV drop off, shallow absorption at 0.7- μm
<i>Cb</i>	Linear spectrum with small positive slope beginning at \sim 1.1- μm
<i>B</i>	Linear spectrum with negative slope; slight bump at 0.6- μm and/or slightly concave-up curvature between 1-2- μm

1.5 Spectroscopy: Remotely Determining Surface Properties.

Spectroscopy is one of the most fundamental tools at our disposal to determine the composition of the universe around us (e.g., Mustard, 2017). The region of the electromagnetic spectrum most relevant for the study of asteroids and meteorites is the visible–mid-infrared (0.3– \sim 30- μm). In this wavelength region, minerals have absorptions and vibrations that can be observed using spectrometers. Spectroscopy is a fast and non-destructive method for determining the bulk mineralogy of samples in the laboratory and, with telescopes, rocky materials in space. Since spectroscopy is the tool used in this thesis

to study meteorites and asteroids, I will briefly describe how minerals interact with light in the visible, near- and mid-infrared.

1.5.1 Visible and Near-infrared Spectroscopy

Spectral features in the visible and near-infrared are caused by several processes including: electronic processes (related to transition metals) and vibrational overtones. Vibrational overtones are produced by fundamental vibrations of minerals at longer wavelengths. These bands appear at integer multiples of the fundamental vibration's frequency. Fundamental vibrations will be addressed in Section 1.5.2.

Electronic processes include charge transfer and crystal field effects (e.g., Hunt, 1977). These spectral features are caused by transition metal ions in a mineral structure. Transition metals are elements that have unfilled d-orbitals (e.g., Clark, 1999; Clark et al, 1990; Burns, 1993; Hunt, 1977). For minerals studied in this thesis, the relevant transition metal is commonly iron. Crystal field effects involve distorting of the energy levels of the unfilled d-orbitals. In this situation, two energy states are created, a lower energy level and a higher energy level. The exact energy levels depend on the bonding environment (e.g., the number of bonds; 6 in octahedral coordination, 4 in tetrahedral coordination) and the symmetry of the bonding environment. In some crystal structures, a crystal-structural unit (e.g., tetrahedral or octahedral) may be distorted by adjacent units or by cations (a positively charged ion) in the sites (larger cations tend to warp the structure). When light interacts with transition metals in a crystal field, the photons that are absorbed are the ones that excite the transition metal's electron(s) from the low energy state to the high energy state. In a reflectance spectrum, this appears as a decrease in reflected light over a particular

wavelength region. Since the bonding environment and the symmetry of the site directly affect the energy splitting of the transition metal's energy levels, these bands are very useful for determining the mineralogy of materials remotely (e.g., Burns, 1993; Hunt, 1977). Charge transfer bands occur between two of the same cation with differing valence states (e.g., Fe^{2+} , Fe^{3+}). An electron is transferred between these two adjacent cations when photons of the appropriate energy are incident on the material. The energy of the photons depends on the bonding environment and the cations exchanging the electron.

1.5.2 Mid-infrared spectroscopy

Crystal structures also have vibrational modes (e.g., Clark, 1999; Estep-Barnes, 1977; Farmer and Palmieri, 1975). These modes depend on the bonds, the masses of the ions and their coordination in the crystal structure. The number of vibrational modes depends on the number of atoms in the molecule. In order for a molecule or mineral to be infrared active (i.e., to have fundamental vibrations in the infrared), the molecule must have a dipole (permanent or induced; Estep-Barnes, 1977; Clark, 1999). These lattice vibrations may be symmetric or asymmetric and bend or stretch the lattice structure. Depending on the mineral, lattice vibrations may be any combination of symmetric/asymmetric, bending or stretching. These terms define the appearance of the deformation of the lattice structure depending on its bonding environment and elements present. The crystal structure of a mineral depends on the composition and coordination of the atoms. The mid-infrared directly probes these properties and so can be used to identify mineralogy of samples.

1.5.3 Spectroscopy of Carbonaceous chondrites and C-type asteroids

Carbonaceous chondrites have been fairly extensively studied in the visible, near- and mid-infrared spectroscopy (e.g., Cloutis et al., 2011a, 2011b, 2012a, 2012b; Salisbury 1991; Takir et al., 2014). Carbonaceous chondrites tend to be very dark in the visible and near-infrared with few strong features (e.g., Cloutis et al., 2012a, b). Some aqueously altered meteorites, particularly in the CM chemical group, have a charge-transfer band (caused by an electron being exchanged between Fe^{2+} and Fe^{3+} ions in the structure of the hydrated minerals produced during aqueous alteration) at 0.7- μm (e.g., Cloutis et al., 2012). This feature has also been observed in the spectra of asteroids (e.g., Vilas and Gaffey, 1989). Mid-infrared studies of carbonaceous chondrites show evidence of their primary mineral phases, including phyllosilicates and olivine (e.g., Salisbury et al., 1991; Beck et al., 2013).

1.6 Summary Thesis Objectives

Presented in this thesis are three chapters that focus on understanding the relationships between meteorites' spectra and mineralogical changes associated with parent body processes and connecting meteorites to asteroids. Chapter 2 describes a coordinated spectral-mineralogical study of CM and CI meteorites that identifies a relationship between near- and mid-infrared spectra and bulk mineralogy. The exact same samples used for PSD-XRD measurements are observed using spectroscopy to determine mineralogy. We compared spectral changes directly to bulk mineralogy of each sample. Presented in this chapter are the continuous spectral changes associated with degree of

alteration (or amount of hydrated minerals) with mid-infrared spectral features. Aqueously altered meteorites can be categorized into three groups based on their mid-infrared spectral signature in 10-13- μm : highly, intermediately and less altered. These characteristics will be described in detail in this chapter. No relationships are found in the near-infrared with degree of alteration.

Chapter 3 investigates the laboratory spectroscopy of a suite of meteorites that have not experienced much change since the time of accretion. The characteristic bulk-mineralogical trait of these low metamorphic grade chondrites is large volumes (20-30%) of amorphous iron-bearing silicate matrices. These matrix materials are thought to form through disequilibrium condensation. They are highly susceptible to destruction through parent body processing (e.g., thermal metamorphism or aqueous alteration). Consequently, meteorites with these materials have experienced minimal parent body processing since the time of accretion. Several meteorites from different carbonaceous chondrites have similar petrology, however the CO meteorite group has a large number of these low-metamorphic grade samples. This chapter focuses on a suite of 8 CO meteorites. Furthermore, one asteroid is found to have similar spectral features in the near-infrared to the low metamorphic grade CO meteorites. This asteroid, (93) Minerva, appears to preserved materials from the earliest Solar System times on its surface.

Chapter 4 investigates the connection between meteorites and asteroids using mid-infrared spectroscopy. Since mid-infrared spectra of meteorites have diagnostic features that trace degree of alteration or lack thereof, this wavelength region can be used to constrain the extent of alteration of asteroids. This is the first time that the degree of

alteration, not simply the presence or absence of hydrated minerals, can be determined. Presented in this chapter are observations of 73 unique asteroids (75 observations total). These asteroids were observed using the Spitzer Space Telescope and the Infrared Spectrograph, NASA's Infrared Telescope Facility and the Broad band Array Spectrograph, and the Stratospheric Observatory for Infrared Astronomy FORCAST instrument. Asteroids' spectra are modeled with the Near Earth Asteroid Thermal Model (NEATM, e.g., Harris, 1998) to remove the thermal continuum from the data. The asteroids spectra and thermal models can be found in Appendix 1. After the thermal continuum is removed, the asteroids' emissivity spectra can be analyzed to determine degree of alteration. Asteroids are categorized into four groups: highly altered, intermediately altered, less altered and anhydrous based on their mid-infrared spectral features. The asteroids' emissivity spectra are in Appendix 2 and their meteorite comparisons are in Appendix 3. Hydrated asteroids appear to be widespread throughout the Main Asteroid Belt with varying degrees of alteration. The compositional stratification previously observed (e.g., Jones et al., 1990; Vilas, 1994; Barucci et al., 1998; Fornaiser et al., 1999, 2014; Takir and Emery, 2012) is not found in this dataset nor is there any relationship between asteroids' degree of alteration and heliocentric distance. Furthermore, asteroids with water-ice on their surfaces are found to also have hydrated minerals. In contrast to Takir and Emery (2012), aqueous alteration must have occurred on these asteroids despite the more prevalent water. The evidence of widespread hydrated minerals on low albedo main belt asteroids implies that temperatures in the proto-planetary disk must have been low enough to sustain water-ice at ~2 AU to 5 AU. Since carbonaceous chondrites have

accretion ages between 2.7-3.6 Ma post-CAI formation (Sugiura and Fujiya, 2014), the disk temperatures must have dropped around this period. This result is a departure from previous ideas of the Solar System's history which was thought to have water-ice in the mid-belt and beyond.

Finally, the last chapter of this thesis summarizes these results in more detail and the future opportunities for study.

Preface to Chapter 2

The following chapter is taken verbatim from McAdam, M. M., Sunshine, J. M., Howard, K. T., McCoy T. J. (2015) *Icarus*, 245, 320-332. This paper was submitted to *Icarus* on June 10, 2014, revised and resubmitted on September 15, 2014 and finally appeared in *Icarus* in January, 2015. The figure, table and section numbering have been updated to comply with the formatting requirements of the University of Maryland Graduate School and the references have been added to the Bibliography at the end of this document. Author McAdam analyzed the spectroscopy of the meteorites presented and primarily wrote this paper. Sunshine assisted with the analysis, sample procurement and editing. Author Howard prepared the samples, analyzed their bulk mineralogy, provided the samples for spectral analysis and assisted with interpretation of the results. Author McCoy assisted with the interpretation of the results and sample procurement.

Chapter 2: Aqueous Alteration on Asteroids: Linking the Mineralogy and Spectroscopy of CM and CI Chondrites

Abstract

CM/CI meteorites range in degree of aqueous alteration suggesting differences in initially accreted materials including water ice and possible spatial heterogeneities within their parent bodies. As alteration progresses, the total abundance and magnesium content of phyllosilicates increases. In this paper we present the results of a coordinated spectral-mineralogical study of a well-characterized suite of CM/CI meteorites that range from 60-90% alteration. By acquiring spectra of the same meteorite powders as Howard *et al* (2009, 2011) and Bland *et al* (2004), we are able for the first time to directly correlate mineralogy with features in reflectance spectra. At visible/near-infrared wavelength, the presence of a 0.7- μm charge transfer band is indicative of aqueous alteration. However, not all altered CM/CI meteorites exhibit this feature; thus the lack of a 0.7 μm absorption band in asteroids does not necessarily signify a lack of aqueous alteration. Furthermore, the position and depth of 0.7- μm charge transfer band shows no correlation with the mineralogical changes associated with aqueous alteration. Similarly, the near-infrared slope, which is not directly related to the mineralogic progression associated with increasing alteration, is not unambiguously related to degree of alteration in the CM/CI meteorites studied. However, the mid-infrared reflectance spectra of CM/CI meteorites contain a broad absorption feature in the 10-13- μm region, which is a convolution of

vibrational features due to Mg-rich phyllosilicates and unaltered olivine. The overall feature continuously changes with total phyllosilicate abundance from a shorter wavenumber/longer wavelength peak (815 cm^{-1} , $12.3\text{-}\mu\text{m}$) for less altered meteorites to a longer wavenumber/shorter wavelength (875 cm^{-1} , $11.4\text{-}\mu\text{m}$) peak in the highly altered meteorites, with roughly equal spectral contributions producing a doublet in intermediately altered meteorites. Using the results from the mid-infrared analyses of meteorite spectra, it is possible to estimate the degree of alteration on dark primitive asteroids. We find asteroid (24) Themis to have a $1000\text{-}700\text{ cm}^{-1}$ ($10\text{-}13\text{-}\mu\text{m}$) peak at longer wavelengths suggesting Themis has a complex surface mineralogy with approximately 70 vol. % phyllosilicates and 25 vol. % anhydrous silicates.

2.1 Introduction

CM and CI carbonaceous chondrites (CCs) experienced extensive interactions with water during the first 5 million years of the Solar System's evolution (de Leuw *et al.*, 2010). In addition to anhydrous silicates, these aqueously altered meteorites contain up to ≈ 13 wt. % water (Alexander *et al.*, 2013) bound as hydroxyl (OH) in the structure of phyllosilicates (e.g. serpentine), the dominant mineral phases in these meteorites. It is generally agreed that CM/CI carbonaceous chondrite meteorites experienced aqueous alteration while in their asteroid parent bodies (e.g. McSween, 1979; Bunch and Chang; 1980, Tomeoka and Buseck 1985; Tomeoka *et al.*, 1989). Additionally, the meteorites exhibit variations in degree of alteration (e.g. Browning *et al.*, 1996; Zolensky *et al.*, 1997; Lauretta *et al.*, 2000; Rubin *et al.*, 2007). CM and CI meteorites demonstrate a range of aqueous alteration from

less altered (~60 volume % phyllosilicates) to highly altered (~90 vol. % phyllosilicates) (Howard, *et al.*, 2009, 2011; Bland *et al.*, 2004; McSween, 1979; Bunch and Chang, 1980; Tomeoka and Buseck 1985; Tomeoka *et al.*, 1989; Browning *et al.*, 1996; Zolensky *et al.*, 1997; Lauretta *et al.*, 2000; Rubin *et al.*, 2007). These variations in alteration likely reflect differences in initially accreted materials, including relative abundances of iron and magnesium in silicates and amount of co-accreted water ice, which may vary laterally and vertically within the parent body.

This paper reports on the results of laboratory measurements of visible/near-infrared (VIS/NIR) and mid-infrared (MIR) reflectance spectra of a suite of 15 CM meteorites and one CI meteorite. Modal mineralogy was previously determined using 14 of the exact same CM meteorite powdered samples and the same CI meteorite powdered sample (Howard *et al.*, 2009, 2011; Bland *et al.*, 2004). CM/CI meteorites are complex, heterogeneous mixtures of chondrules and aqueously altered phases. Samples of the same meteorite can exhibit slightly different modal mineralogies because of this non-uniformity. Using the same sample powders that were used to determine modal mineralogy ensures the spectral interpretations are made with specific reference to the correct mineralogy of each sample rather than generalities of the meteorite's bulk mineralogy. Because of this unique aspect of this study, for the first time, a direct correlation between spectral features and mineralogy in CM/CI meteorites can therefore be established. The results from laboratory data are also directly applicable to the spectral analyses of dark asteroids acquired with ground-based and spacecraft-based observatories, facilitating the remote estimation of the degree of aqueous alteration. This approach is applied using the mid-infrared spectrum of

asteroid (24) Themis collected by the *Spitzer Space Telescope*. By extension, it is also possible to remotely map differences in aqueous alteration on dark asteroids throughout the asteroid belt and to quantify variations that may be observed on individual asteroids as they rotate, or are resolved by spacecraft such as the upcoming OSIRIS-REx (Lauretta, *et al.*, 2012) or Hayabusa-2 (Yoshikawa, *et al.*, 2008) missions to dark near-Earth asteroids.

2.2 Background

2.2.1 Mineralogical Changes Associated with Aqueous Alteration

Features in VIS/NIR to MIR regions are caused by charge transfer absorptions (Gaffey *et al.*, 1993), electronic transitions (Burns, 1993), and vibrational modes and overtones (Salisbury *et al.*, 1991; and are controlled by mineral structure and composition. Thus, in order to interpret and predict the features in the spectra of aqueously altered meteorites (and their asteroid parent bodies), it is necessary to understand the mineralogical progression of aqueous alteration. The most abundant mineral phases (>10 vol. %) are particularly important as they dominate VIS/NIR-MIR spectra.

The asteroids that formed CM/CI meteorites were initially composed of anhydrous components: chondrules and matrix silicates (*e.g.* Rubin *et al.*, 2007; Howard *et al.*, 2009, 2011). Chondrules are typically composed of relatively Mg-rich olivine (forsterite) with some glassy mesostasis and Fe-Ni metal (Rubin, *et al.*, 2007). The matrix silicates tend to contain more Fe-rich olivines (fayalite) (McSween, 1979). The iron in the matrices is typically more ferric (Fe^{3+}), while the iron in the chondrules is usually more ferrous (Fe^{2+}) (Howard *et al.*, 2009, 2011).

Aqueous alteration, the chemical reaction of water and anhydrous silicates, is triggered when radioactively decaying elements heat the asteroid melting the co-accreted water ice (McSween, 1979; Bunch and Chang, 1980; Tomeoka and Buseck 1985; Tomeoka *et al.*, 1989; Browning *et al.*, 1996; Zolensky *et al.*, 1997; Lauretta *et al.*, 2000; Rubin *et al.*, 2007). The phyllosilicates in CM/CI meteorites are dominated by serpentine group minerals (*e.g.*, $[\text{Mg,Fe}]_3\text{Si}_2\text{O}_5[\text{OH}]_4$). Serpentine group minerals are layered silicates with an alternating pattern of tetrahedral sheets and octahedral sheets. The tetrahedral sheets are comprised of silicon and oxygen tetrahedra, while the octahedral sheets have cations in octahedral coordination with oxygen ions or hydroxyl molecules. The sheets are connected by hydrogen bonds or van der Waals forces. For CM and CI chondrites, aqueous alteration reactions have converted most (on average 75 vol. %) of the anhydrous phases into hydrated phyllosilicates ranging in abundance from ~60-90 vol. % (Bland, *et al.*, 2004; Howard, *et al.*, 2009, 2011).

The composition of the phyllosilicates in CM/CI meteorites also varies depending on the degree of alteration (the amount of initial silicates converted to phyllosilicates) and the composition of the initially accreted anhydrous silicates. Fayalitic olivines, characteristically found in the matrices of the meteorites, are more susceptible to aqueous alteration (Velbel and Palmer, 2011). These phases are consequently the first to be converted into Fe-rich phyllosilicates. The Fe-rich phyllosilicates have dioctahedral structure containing ferric iron in two of the three octahedral *M*-sites (Howard *et al.*, 2009, 2011; Velbel and Palmer, 2011). These phases are typically referred to as cronstedtites (Tomeoka and Buseck, 1985; Calvin and King, 1997; Browning *et al.*, 1996; Lauretta *et*

al., 2000; Rubin *et al.*, 2007). Cronstedtite, in the strictest sense, is the iron endmember. However, Fe-rich phyllosilicates in CM/CI meteorites, always contain significant magnesium (*e.g.* $[\text{Mg}^{2+}, \text{Fe}^{2+}]_2\text{Fe}^{3+}[\text{Fe}^{3+}\text{Si}]\text{O}_5[\text{OH}]_4$) and are thus not cronstedtite endmembers. In addition, in CCs, cronstedtite can also be associated with intergrowths of the sulfide, tochilinite ($6\text{FeS}\cdot(\text{Mg}, \text{Fe}^{2+})(\text{OH})_2$). Since the structure of cronstedtite is not stable, it expels nucleons of ferrous iron, which contribute to the formation of magnetite in later stages of CM alteration (Howard *et al.*, 2014). Spectrally, the terrestrial cronstedtite endmember is very dark and has weak spectral features in the NIR and MIR (Calvin and King, 1997). The modal abundance of Fe-rich phyllosilicate plateaus when all of the initial Fe-rich olivine is converted. Thus, less altered meteorites have more of Fe-rich phyllosilicates relative to Mg-rich phyllosilicates and more abundant anhydrous materials than more altered meteorites.

The forsteritic chondrules produce Mg-rich serpentine family phyllosilicates. In this mineral, all three *M*-sites are filled with ferrous iron and magnesium (trioctahedral phyllosilicates). The altering chondrules enrich the surrounding material in magnesium, which drives a recrystallization of the Fe-rich phyllosilicates into structurally trioctahedral phyllosilicates relatively enriched in magnesium (Tomeoka *et al.*, 1989). Subsequently, as bulk hydration progresses, the relative proportion of Mg-rich phyllosilicates is expected to increase. Like cronstedtite, endmember Mg-serpentine compositions are also not found in meteorites.

Independent of differences in the processes involved in hydration reactions, the lack of phyllosilicate endmember compositions in CCs likely reflects the differences in the initial

anhydrous assemblages in CCs compared to terrestrial minerals. Specifically, terrestrial ultramafic rocks involved in serpentinization rarely contain fayalite and do not contain Fe-Ni metal. Asteroidal temperatures are also likely much lower than terrestrial settings of serpentinization and the supply of fluid more limiting (lower water/rock ratios). These differences imply that the spectra of terrestrial phyllosilicates are likely to be different than the spectra of CM/CI meteorites.

Observations of mineralogic changes with degree of alteration have been the basis of CM meteorites categorization schemes (*e.g.* McSween, 1979; Bunch and Chang, 1980; Tomeoka and Buseck, 1985; Burgess *et al.*, 1991; Zolensky *et al.*, 1993; Browning *et al.*, 1996; and Rubin *et al.*, 2007). For example, Rubin *et al.* (2007) scale the petrologic classification from 2.6 (least altered CM meteorites observed) to 2.0 (most altered CM meteorites) in intervals of 0.1. This classification is based specific criteria such as the presence of initial materials (*e.g.* mesostasis and Fe-Ni metal, unaltered chondrules/chondrule grains) and the presence intergrown phyllosilicates and sulfides. The Rubin petrologic classification for corresponding meteorites studied here are given in **Table 2.1**.

2.2.2 Mineralogy of the Meteorite Suite

In this study, the VIS/NIR and MIR spectra of 14 CM meteorites have been measured using the same powdered samples for which modal abundances have previously been determined by Howard *et al.* (2009; 2011). In most cases, Bland *et al.* (2012) have also obtained Mössbauer spectra of the same powders. We have also measured the reflectance spectrum of the CI Orgueil for which modal data was acquired by Bland *et al.*

(2004). Using the exact same samples as previous studies by Howard *et al.* (2009, 2011), Bland *et al.* (2004) and Bland *et al.*, (2012) allows spectral interpretations to be made using the specific mineralogy and ferric iron content for each individual sample as opposed to generalities of the meteorite. Two meteorites in this suite have undergone aqueous alteration prior to experiencing thermal metamorphism (Wisconsin Range 91600 and Pecora Escarpment 91008). In their recent paper, Tonui *et al.* (2014) describe the petrologic, chemical and spectroscopic evidence for thermal metamorphism for CM meteorites including PCA 91008 and WIS 91600. Modal mineralogy has not been derived for Pecora Escarpment 91008 (PCA 91008), but its spectrum and the spectrum of WIS 91600 are included because the effects of thermal metamorphism in the MIR have not previously been reported. All CM meteorites have pervasive alteration (Rubin *et al.*, 2007) and contain abundant phyllosilicates (both Fe- and Mg-rich), which comprise on average 75 vol. % of the mineral phases (Howard *et al.*, 2011). The CI meteorites also contain abundant phyllosilicates, but only minor anhydrous silicates and a greater of volume accessory phases than CMs including: carbonates, evaporites and iron oxides (Bland *et al.*, 2004; King *et al.*, 2014). The suite of meteorite samples used, a summary of their mineralogy (Howard *et al.*, 2009, 2011; Bland, *et al.*, 2004), their relative ferric iron content derived from Mössbauer spectra (Bland *et al.*, 2012), and their petrologic classification are listed in **Table 2.1**.

Trends in mineral abundances reflect the aqueous alteration process described in **Section 2.1** above. With increasing hydration, olivine and pyroxene abundances decrease and total phyllosilicate abundance increases. Furthermore as hydration progresses, Mg-rich

phyllosilicates are predominantly produced. The studies of Howard *et al* (2009, 2011) and the review by Velbel and Palmer (2011) indicate that the composition of the anhydrous phases is not necessarily uniform, contributing the differences in composition of the phyllosilicates produced. The Murray and Essebi meteorites are the only meteorites with homogeneous olivine composition (Fo₁₀₀ for both). Other meteorites studied here have at least two compositions of olivine ranging from Fo₁₀₀ to Fo₆₀. The accessory phases are uncorrelated with alteration and are typically near or less than 5 vol. % of the meteorites' mineral phases. Essebi and Orgueil have notably high accessory phases at ~10 vol. %. These two meteorites have similar abundances of calcite, gypsum and sulfides compared to the other meteorites in the suite but have much higher magnetite contents (~5 vol. %) compared to the ~1-2 vol. % of magnetite in the other meteorites.

Following aqueous alteration, thermal metamorphism can also occur in CM/CI meteorites (*e.g.* Tonui, *et al.*, 2014; Choe *et al.*, 2010; Rubin *et al.*, 2007). Both extensively altered and thermally metamorphosed (PCA 91008 and WIS 91600) meteorites show evidence of dehydroxylation that produces poorly crystalline, highly disordered, anhydrous phases (Tonui, *et al.*, 2014; Choe *et al.*, 2010; Rubin *et al.*, 2007).

Table 2.1: Summary of modal mineralogy, ferric iron content, and petrologic classification for the 16 CM/CI meteorite suite

Meteorite (Abbreviation)	Olivine (vol.%)	Orthopyroxene (vol. %)	Total anhydrous silicates (vol. %)	Accessory phases ¹ (vol. %)	Fe-rich phyllosilicates (vol. %)	Mg-rich phyllosilicates (vol. %)	Total phyllosilicates (vol. %)	% Ferric Iron [Fe ³⁺ /(Fe ²⁺ + Fe ³⁺)] (°)	Classification (Petrologic Subtype ³)
Queen Alexandra Range 97990 (QUE 97990)	22.5	7.5	30	2.6 ⁴	26.6	40.4	67	0.66	CM2(2.6)
Yamato 791198 (Y-791198)	17.1	9.8	26.9	2.5 ⁴	33.5	37.4	70.9	0.73	CM2(2.4)
Murchison	11.1	8.3	19.4	4.1	50.3	22.2	72.5	0.6	CM2(2.5)
Murray	17.3	5.6	22.9	3.2	49.1	25	74.1	0.67	CM2(2.5)
Wisconsin Range 91600 (WIS 91600)	14.8	1.4	16.2	10	0	73.5	73.5	–	CM2
Mighei	13.1	6.9	18.7	5.4	47.9	26.7	74.6	0.56	CM2
Essebi	14.5	2.1	16.6	9.1	0	74.5	74.5	0.47	C2-ung
Nogoya	14.6	3.9	18.5	5.6	43.4	32.8	75.85	0.55	CM2(2.2)
Cold Bokkeveld	11.5	4.9	16.4	6.8	23.3	54.1	77.3	0.67	CM2(2.2)
Allan Hills 81002 (ALHA 81002)	15.1	4.5	19.6	2.7	26.8	50.8	77.6	0.61	CM2
Queen Alexandra Range 93005 (QUE 93005)	11.1	1.4	12.5	5.4	20.8	61.3	82.1	0.48	CM2(2.1)
Scott Glacier 06043 (SCO 06043)	6.3	0	6.3	6	21.6	66	87.6	0.66	CM1
Meteorite Hills 01070 (MET 01070)	5.85	0.4	6.25	6.05	26.4	61.5	87.8	0.44	CM1(2.0)
Allan Hills 83100 (ALH 83100)	8.7	0.7	9.4	3.9	24.2	62.4	88.6	0.51	CM1/2
Orgueil	5.8 (°)	–	5.8 (°)	12.7 (°)	7.7 (°)	73.8 (°)	81.5 (°)	0.49	CI1
Pecora Escarpment 91008 (PCA 91008)	–	–	–	–	–	–	–	–	CM2

Data, unless otherwise indicated, is from Howard *et al.*, (2009, 2011)

¹ These phases include: Calcite, gypsum, magnetite, sulfides Fe, Ni metal ²Valence state of iron derived from Mössbauer analysis in Bland *et al.* (2012).

³Rubin *et al.* (2007)

⁴Meteorite has Fe, Ni metal at 0.2 vol. % level

⁵Data from Bland *et al.* (2004)

– Data unavailable

2.2.3 Previous Spectroscopic Studies of CM/CI Chondrites

Initial spectral studies of CM/CI meteorites cataloged the absorption features that occur at VIS to MIR wavelengths and related them to mineralogy (*e.g.* Cloutis *et al.*, 2011a, 2011b and references therein; Salisbury *et al.*, 1991). Calvin and King (1997) quantified these relationships in the VIS-MIR using linear mixtures of terrestrial phyllosilicates, including Fe-rich berthierines and nearly endmember Mg-serpentines. They were able to approximate the spectra of the CM meteorite Murchison and the CI meteorite Orgueil despite the expected structural/compositional differences between meteoritical and terrestrial phyllosilicates. More recent studies (*e.g.* Beck *et al.*, 2010, 2013 and Takir *et al.*, 2013) have focused on the 3- μm region, where the fundamental water and hydroxyl stretching vibrations is located. These studies show relationships between the 3- μm band position, shape and depth with mineralogy. In all cases, care was taken to measure the meteorite samples under conditions that minimize terrestrial adsorbed water.

In a study of reflectance spectra of a suite of 10 CM, CI and C-ungrouped meteorite powders under ultra-high vacuum conditions, Takir *et al.* (2013) found variation in the shape and position of 3- μm fundamental vibration of hydroxyl/water. The position and shape of the 3- μm feature is correlated with the type of phyllosilicate (Mg- or Fe-rich) as described by Howard *et al.* (2011) and with petrologic subgroupings (Rubin *et al.*, 2007; Browning *et al.*, 1996). While Takir *et al.* (2013) studied some sample from some of the same meteorites as Howard *et al.* (2009, 2011), the spectral analyses were produced using different meteorite powders than those for which Howard *et al.* (2011) derived modal mineralogy.

Using some corresponding meteorites to Howard *et al.* (2009) but different physical powders, Beck *et al.* (2010) also observed correlations in transmission spectra between 3- μm band parameters (including position and integrated band area) with degree of alteration as defined by Howard *et al.* (2009). In more recent work, Beck *et al.* (2013) examined MIR transmission spectra of a larger suite of 21 CM meteorites and 3 CI meteorites (some equivalent meteorites but different samples to Howard *et al.* 2009, 2011). In less altered meteorites, they observed features attributed to olivine that appeared as shoulders on a broad $\sim 10\text{-}\mu\text{m}$ feature they interpreted to be due to the phyllosilicate saponite. Nine of the CM and CI meteorites studied by Beck *et al.* (2013) with transmission spectra are also in the suite examined here with VIS/NIR-MIR reflectance spectra.

2.3 Data Collection

2.3.1 Samples

The 16 CM and CI meteorite samples used in this study were prepared by Howard *et al.* (2009, 2011) and Bland *et al.* (2004) for their position sensitive X-ray diffraction (PSD-XRD) analysis of bulk meteorite mineralogy. As described in these studies, 200 mg of each of the bulk meteorites samples were hand ground to approximately $35\text{-}\mu\text{m}$. A subset of the modal data acquired by Howard *et al.* (2009, 2011) and Bland *et al.* (2004) is included in **Table 2.1**. Fourteen of the same bulk meteorite samples were also characterized using Mössbauer spectroscopy (Bland *et al.*, 2012), which were used to derive the relative abundance of ferric iron as indicated in **Table 2.1**.

2.3.2 Spectral Measurements

Reflectance spectra of the suite of the well-characterized bulk meteorite samples were acquired at Brown University using the NASA/Keck Reflectance Laboratory (RELAB) facility. The bidirectional spectrometer was used to obtain data from 0.32 to 2.55- μm . These spectra were collected at incidence angle of 30° and emission angle of 0° with a spectral resolution of 5 nm. Pressed halon, with an approximate Lambertian surface, was used as a reflectance standard. MIR spectra were measured using the Thermo Nexus 870 FT-IR spectrometer. This off-axis bi-conical spectrometer uses a brushed gold standard. Data were obtained from 1 to 25 μm at a resolution of 4 cm^{-1} .

Unlike OH and H₂O vibrations in the 2.5- 3- μm region (*e.g.* Beck *et al.*, 2010, 2013; Takir *et al.*, 2013), fundamental Si-O stretching and bending vibrations in the MIR and their overtones in the NIR are unaffected by the adsorbed water. As such, all data for this study were taken under ambient temperature and pressure conditions.

2.3.3 Data

2.3.4 Visible and Near-Infrared Spectra

The VIS-NIR reflectance spectra are presented in **Figure 2.1**. These data have been normalized to unity at 2.3- μm . The thermally metamorphosed meteorites are plotted at the top in grays and the aqueously altered meteorites are ordered (top to bottom) by increasing total phyllosilicate abundance. Each meteorite exhibits the following features: a strong ultra-violet (UV) slope (0.32-0.6- μm), a variable NIR slope (0.5-2.5- μm) and often a ~0.7- μm charge transfer band. Slopes in the UV and NIR can be related to composition but can also be affected by physical properties of the material (*e.g.* grain size or compaction). The

~0.7- μm charge transfer band is caused by the exchange of an electron between a cation and an anion in the structure of phyllosilicates or oxides (Clark *et al.*, 1999). For the aqueously altered CM samples with limited or no heating, the NIR slopes of individual meteorites can vary greatly within subgroups (highly, intermediately, less altered) such that even in samples of similar degrees of hydration and with very similar bulk mineralogies, spectra can differ. CM meteorites typically have weak features between ~0.8- μm and 2.5- μm (Cloutis *et al.*, 2011). The position and depth of the 0.7- μm feature also varies, when present.

Three meteorites in the suite have unique spectra. CII Orgueil has a concave shape in the 0.5-2.5- μm spectral region. It also has a very small phyllosilicate and adsorbed water overtone feature at 1.9- μm , which are present in the spectra of only a few other meteorites. In addition, the spectra of CM meteorites, which have undergone thermal metamorphism, are also distinct from those that are only aqueously altered. PCA 91008 has a moderate NIR slope, lacks a 0.7- μm band but has a broad, weak 1.1- μm feature. In contrast, WIS 91600 has no absorption features and a reddened slope.

2.3.5 Mid-Infrared Spectra

The 1200-400 cm^{-1} (8-25- μm) spectra of the suite of meteorites are shown in **Figure 2.2**. These spectra are normalized to unity at 8- μm and offset for clarity. The aqueously altered meteorites are ordered (top to bottom) by total phyllosilicate abundance (Mg- and Fe-rich). All of the meteorite spectra have the following features: a Christensen feature (reflectance minimum, *e.g.* Salisbury *et al.*, 1992) near 8- μm , a broad restrahlen

absorption in the $1000\text{-}700\text{ cm}^{-1}$ ($10\text{-}13\text{-}\mu\text{m}$) region and phyllosilicate reststrahlen absorption features at short wavenumber/long wavelengths ($600\text{-}400\text{ cm}^{-1}$, $15\text{-}25\text{-}\mu\text{m}$).

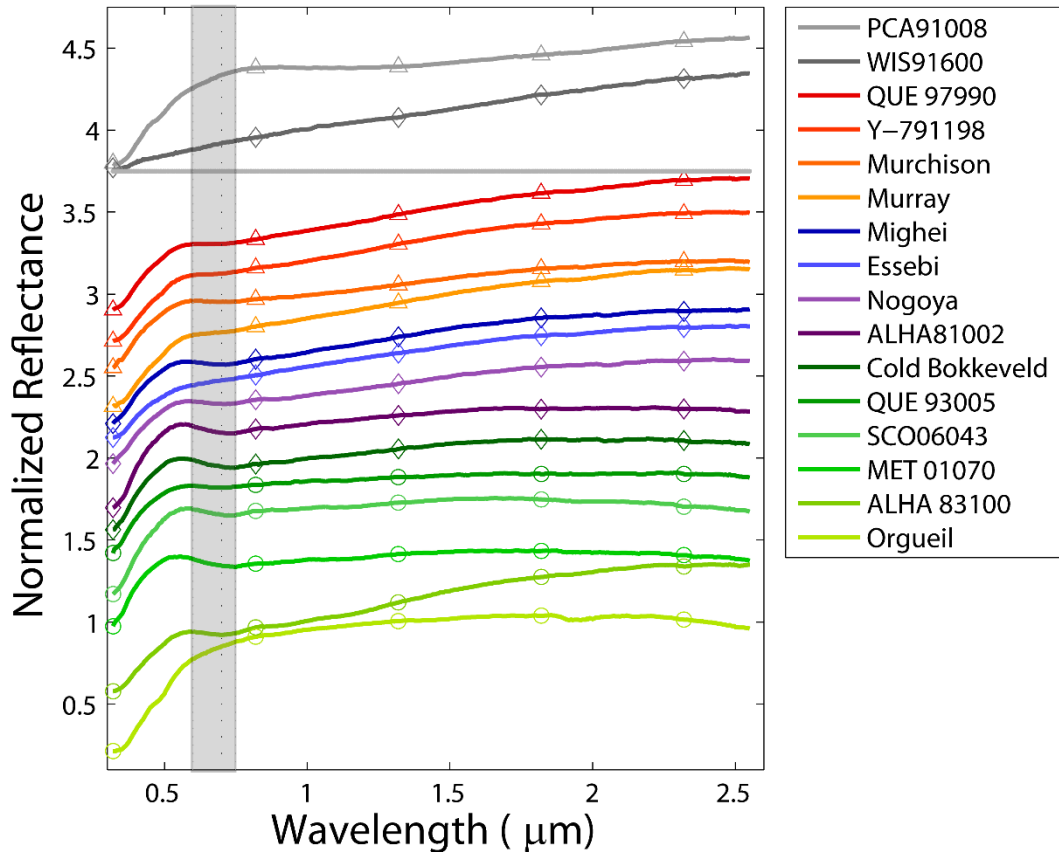


Figure 2.1: Bidirectional reflectance spectra of CI/CM meteorites normalized to unity at $2.3\text{-}\mu\text{m}$ and offset for clarity.

The thermally metamorphosed meteorites exhibit features that differ from the aqueously altered meteorites. PCA 91008 has a broad $1.1\text{-}\mu\text{m}$ feature while WIS 91600 has no features and a reddened slope. The fourteen other meteorites are ordered by increasing alteration. Less altered meteorites are in reds (offset 200-260%), intermediately altered meteorites in blues (offset 110-190%) and highly altered meteorites in greens (offset 0-90%). Some meteorites have a $0.7\text{-}\mu\text{m}$ charge transfer band; however the band is uncorrelated to degree of alteration (see **Section 2.4.1**)

Three groups of meteorites can be defined based on their spectral characteristics at $1000\text{-}700\text{ cm}^{-1}$ ($10\text{-}13\text{-}\mu\text{m}$) and $600\text{-}400\text{ cm}^{-1}$ ($15\text{-}25\text{-}\mu\text{m}$). The less altered meteorites

(reds) are characterized by a 1000-700 cm^{-1} (10-13- μm) feature peaking at shorter wavenumber/longer wavelengths, $\sim 815 \text{ cm}^{-1}$ ($\sim 12.3\text{-}\mu\text{m}$) and a single feature at $\sim 510 \text{ cm}^{-1}$ (19.5- μm). Highly altered meteorites have a longer wavenumber/shorter wavelength peak near 875 cm^{-1} (11.4- μm) in the 1000-700 cm^{-1} (10-13- μm) region and two features at $\sim 620 \text{ cm}^{-1}$ ($\sim 16\text{-}\mu\text{m}$) and $\sim 475 \text{ cm}^{-1}$ (21- μm). These last two features create a ‘W’ shape in the 600-400 cm^{-1} (15-25- μm) region. Intermediately altered meteorites have a doublet at the top of their 1000-700 cm^{-1} (10-13- μm) feature and intermediate spectral behavior between 600-400 cm^{-1} (15-25- μm). These spectral groupings are roughly consistent with corresponding meteorites defined in the 3- μm region by Takir *et al.* (2013).

The two thermally metamorphosed meteorites, PCA 91008 and WIS 91600, are spectrally consistent with the other meteorites in the suite. WIS 91600, with modal abundances of phyllosilicates similar to intermediately altered meteorites, has two peaks in the 1000-700 cm^{-1} (10-13- μm) region. Despite its thermal metamorphism, this meteorite is spectrally consistent with meteorites that have experienced similar degrees of aqueous alteration. PCA 91008 has experienced a higher grade of metamorphism (Tonui *et al.*, 2014) and has distinct spectral characteristics that are different to other CM meteorites. In the 1250-900 cm^{-1} (8-11- μm) region, PCA 91008 has several superimposed bands on the shoulder of the 1000-700 cm^{-1} (10-13- μm) feature. It also has the longest wavelength 1000-700 cm^{-1} (10-13- μm) feature of the suite of meteorites. These differences are likely related to the composition of the initial anhydrous materials and the phyllosilicates in this meteorite and the amorphous silicates produced as water/OH were removed from the structure of phyllosilicates during thermal metamorphism.

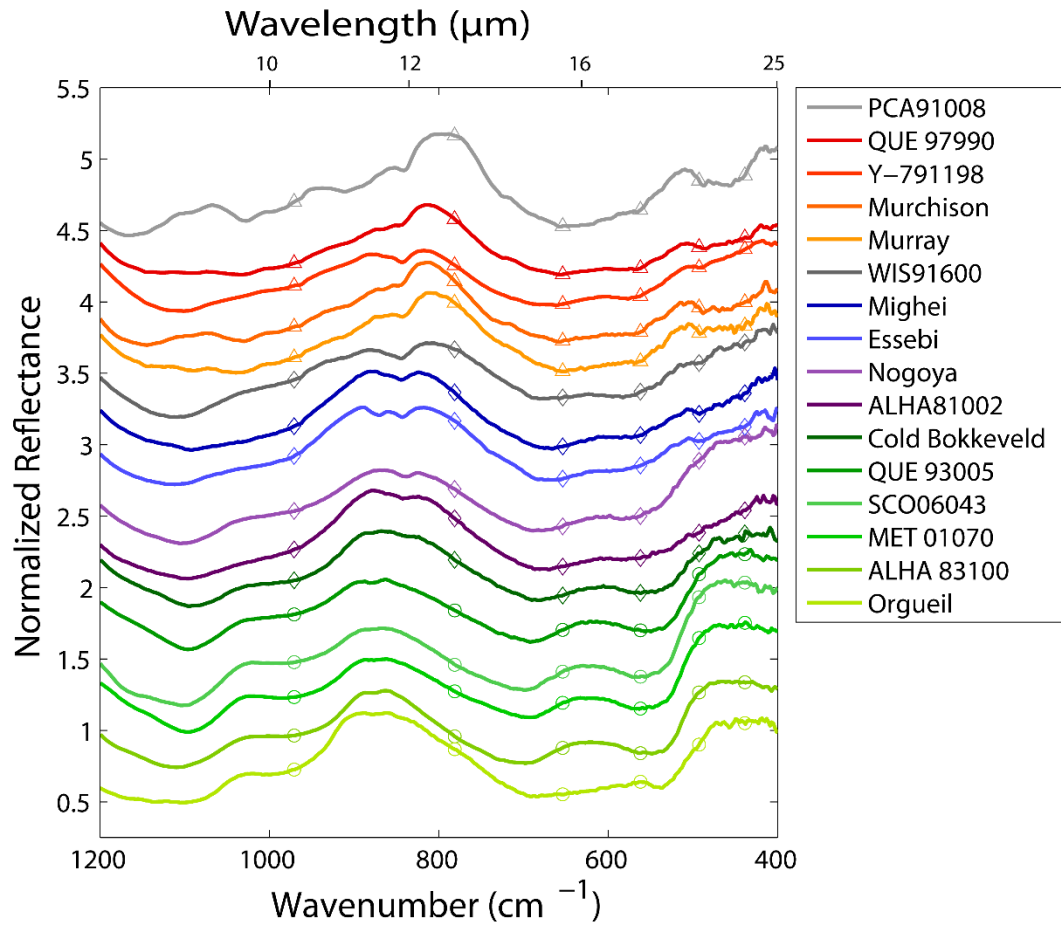


Figure 2.2: MIR spectra of sixteen CM/CI meteorites normalized to unity at 8- μm and offset $\sim 30\%$ for clarity

The fourteen aqueously altered meteorites are ordered by increasing alteration. Less altered meteorites are in reds, intermediately altered meteorites in blues and highly altered meteorites in greens. Two meteorites that have experienced both aqueous and thermal alteration are shown in gray.

2.4 Results

2.4.1 Visible/Near-infrared Spectral Relationships to Mineralogy

The VIS/NIR reflectance spectra of the CM/CI meteorites have few strong features except the overall NIR slope and a charge transfer band around 0.7- μm . In addition, weak and variable features attributed to crystal field transitions of iron in phyllosilicates at 0.9- and 1.1- μm have also been observed (Cloutis *et al.*, 2011). Dark asteroids are similarly feature-poor and are typically classified by the presence of the 0.7- μm band and the NIR slope (*e.g.* deMeo *et al.*, 2009; Vilas and Gaffey, 1989; Hiroi *et al.*, 1996; Clark *et al.*, 2010). Here, we evaluate the trends between mineralogy and the strongest features in the CM/CI meteorites: NIR slope and 0.7- μm charge transfer band.

2.4.2 Trends in NIR Slope with Mineralogy

The slope in the NIR is measured as the ratio of reflectance at 2.4- μm and 0.56- μm . **Figure 2.3** plots the reflectance ratios as a function of the total phyllosilicate abundance for each meteorite. The colors correspond to the total abundance of phyllosilicates (degree of alteration): reds are less altered meteorites, blues are intermediately altered and highly altered meteorites are greens. There appears to be relationship in between the slope and total abundance of phyllosilicates. Meteorites with less abundant phyllosilicates generally show strong red slopes (slope ratios of ~ 1.7). As the total abundance of phyllosilicates increases (increasing alteration) the slopes decrease approaching unity (flat spectrum). However there are two outliers to this trend, the highly altered meteorites CI1 Orgueil and CM1/2 ALH 83100, which are indistinguishable in NIR slope values from less to

intermediately altered meteorites. While they are outliers in NIR slope values, their modal abundances of phyllosilicates are well behaved (see **Table 2.1**).

Furthermore, the NIR slope can be affected by physical properties such as grain size, weathering and metal abundance. These physical affects and the ambiguous relationship between slope and mineralogy suggest that the NIR slope should not be used as a metric to determine the surface mineralogy of asteroids. Dark asteroids with similar slopes may be a manifestation of physical surface processes rather than alteration state.

2.4.3 Lack of Correlation between Charge Transfer Band and Mineralogy

The 0.7- μm charge transfer band is thought to be caused by the exchange of an electron between two adjacent atoms in a phyllosilicate or oxide (Gaffey, *et al.*, 1993). This spectral feature is seen on some dark asteroids and has been used to determine the presence of phyllosilicates and oxides that are rich in iron (*e.g.* Vilas and Gaffey, 1989). Asteroids with a 0.7- μm band have been shown to have 3- μm features indicating that the 0.7- μm feature is indicative of the presence of alteration on meteorites and asteroids (Rivkin *et al.*, 2013; Howell *et al.*, 2011; Rivkin *et al.*, 2002; Vilas *et al.*, 1994). However, in more recent work, Cloutis *et al.*, (2011b) do not find a relationship between charge transfer band depth and degree of alteration.

The VIS/NIR spectra of our suite of meteorites provide an opportunity to re-examine the mineralogical origins of the 0.7- μm feature. If this feature is caused by phyllosilicates and/or oxides, both of which are formed during alteration, the strength of the 0.7- μm band should be correlated with total abundance of phyllosilicates. Furthermore, if the charge transfer band is produced by iron with two valence states, it should be

correlated with relative ferric iron content. However, as discussed below, neither trend is seen, which suggests that the 0.7- μm charge transfer band may not be simplistically related to alteration.

The 0.7- μm region (0.6- to 0.75- μm) of the meteorite suite is presented in **Figure 2.4** ordered by band depth. These spectra are normalized to one at 0.6- μm and continuum removed. To find the band depth, a second order polynomial is fitted to the spectral segment and the minimum of the fitted polynomial is subtracted from the continuum. The minima of the fitted polynomials are denoted as asterisks in **Figure 2.4**. Most of the CM meteorites here studied have a 0.7- μm band, thus the presence of a 0.7- μm band is likely indicative of alteration. However, some highly altered meteorites (*e.g.* Orgueil) do not have this feature, which implies that the absence of a charge transfer band does not necessarily mean the absence of alteration. For most of the meteorites, the band is centered near 0.65- μm (not exactly 0.7- μm). As observed by Cloutis *et al.* (2011b), there is no apparent correlation between band center and degree of alteration. Additionally, the band depth of this feature is uncorrelated to total abundance of phyllosilicates (**Figure 2.5**). This was also observed by Cloutis *et al.* (2011b). The depth of this band is therefore insensitive to degree of alteration. Despite the mineralogical similarities, meteorites within the same subgroups (less, intermediately, highly altered) can have a wide variety of band depths. This is especially apparent in the highly altered meteorite group including CM1s and CM2s as well as the CI1 Orgueil. This group spans the range of band depths from the strongest band among all of the meteorites, ALH 83100 (2.6%) to moderately shallow band depth of SCO

06043 (1%) and finally, Orgueil, a highly altered meteorite with no charge transfer band at all.

The depth of the 0.7- μm band is also uncorrelated with the relative amount of ferric iron in the meteorite (**Figure 2.6**). The amount of ferric iron to total iron is derived from Mössbauer spectra of the same meteorite powders (Bland *et al.*, 2012). However, the iron content derived from these measurements is a bulk measurement and it is not possible to know whether the iron is in phyllosilicates or oxides specifically. If this feature is produced by homonuclear inter-valence charge transfer in a phyllosilicate or oxide, a sample with approximately equal abundances of ferric and ferrous iron would produce the charge transfer band. However, meteorites with relatively high ferric iron (~75%) seem to be as likely to have charge transfer bands as meteorites with relatively low ferric iron (~40%). This suggests that the strength and position of the charge transfer band may be a complex combination of the ferric to ferrous iron ratios in both Mg- and Fe-rich phyllosilicates. The Mössbauer results only provide bulk measurements of the ferric iron content.

While the presence of the 0.7- μm feature is indicative of alteration, it is otherwise insensitive to subtle differences in degrees of alteration. Furthermore, the absence of a charge transfer band does not necessarily indicate the absence of alteration. Our results confirm those of Cloutis *et al.*, (2011b), that depth and position of the 0.7- μm charge transfer band are not correlated to degree of alteration. Thus, multi-wavelength observations of asteroids are necessary to determine the alteration state.

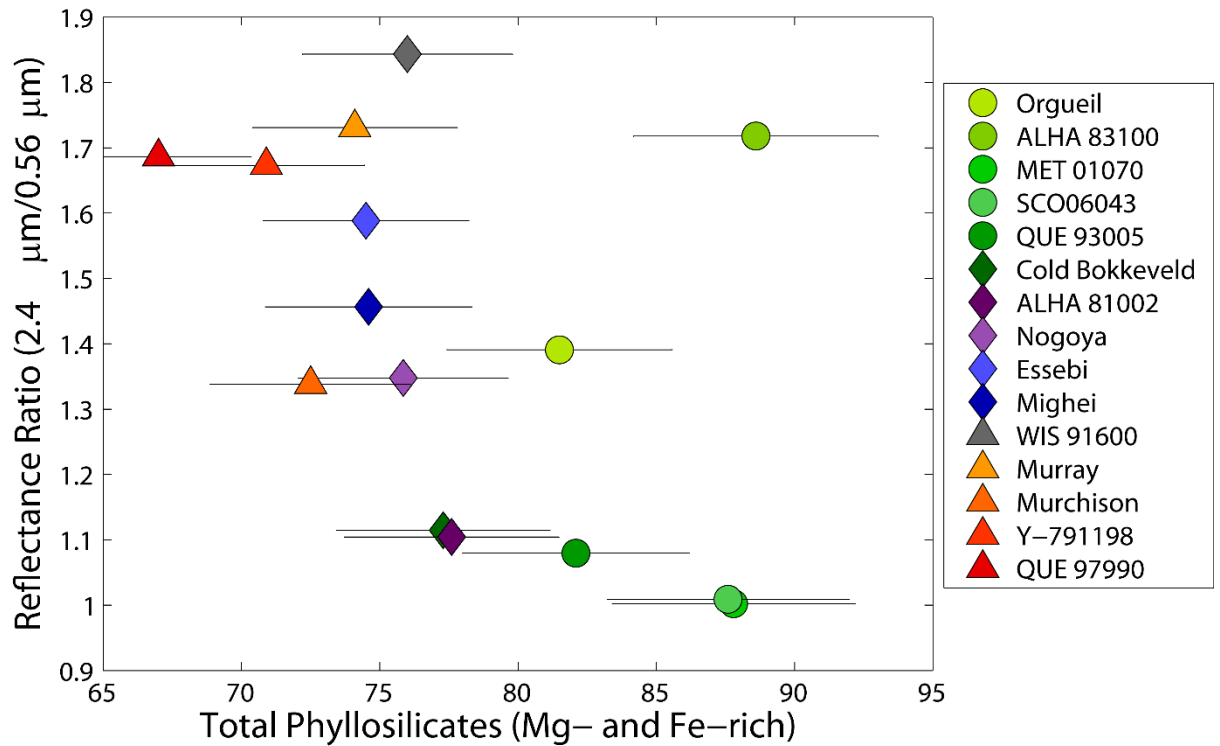


Figure 2.3: Reflectance ratio (2.4- μm / 0.56- μm) plotted against the total abundance of phyllosilicates shows a general correlation between NIR slope and degree of aqueous alteration. However, despite consistent mineralogy across the suite, the NIR slope

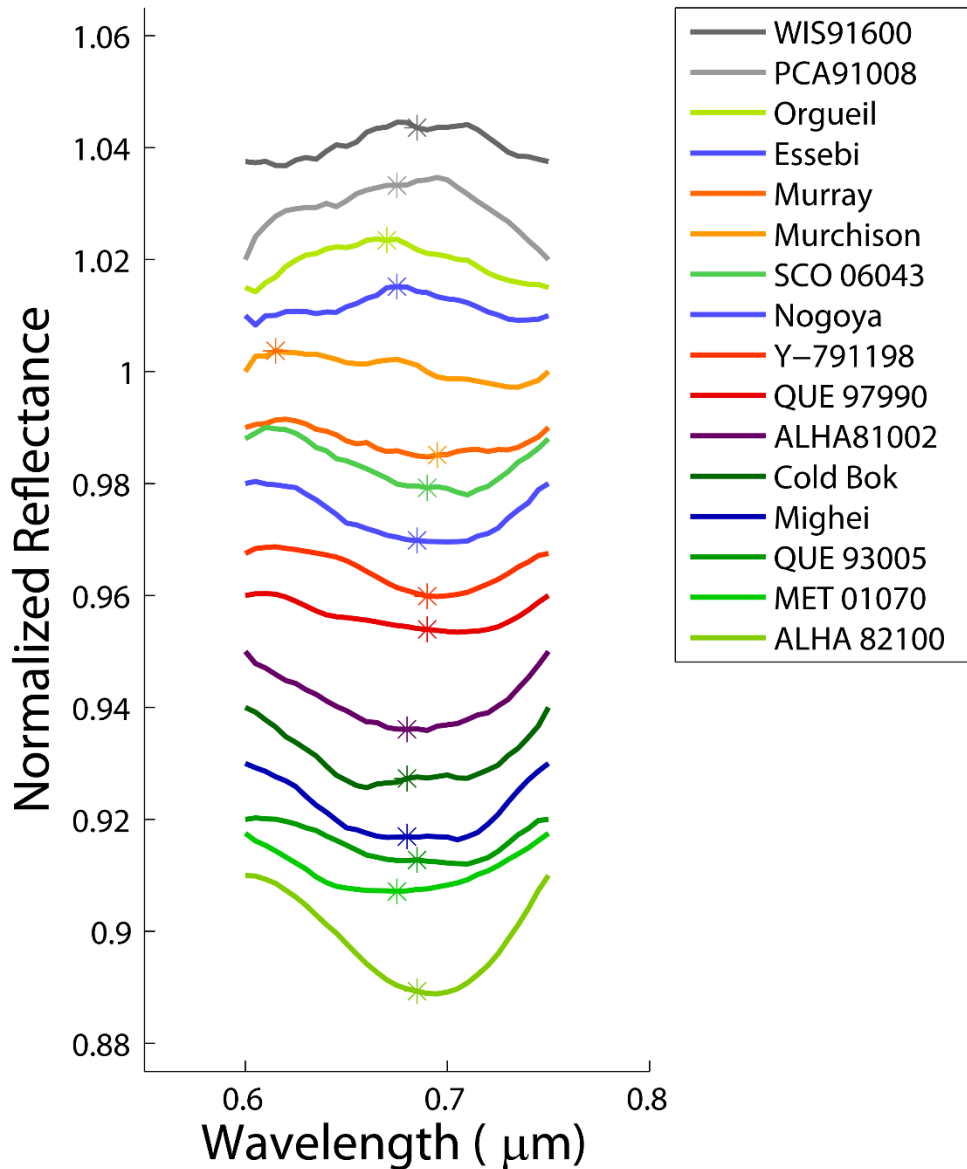


Figure 2.4: Continuum removed spectra of meteorite suite in the 0.7- μm region plotted by increasing band depth.

Asterisks represent the minima of the fitted second order polynomials. The normalized reflectance value of the spectra at this position is subtracted from the continuum to define the band depth. Some meteorites (Orgueil, PCA 91008, Essebi and WIS 91600) do not have a feature in this region. The twelve other meteorites have features that vary in position and depth and are not correlated with degree of aqueous alteration.

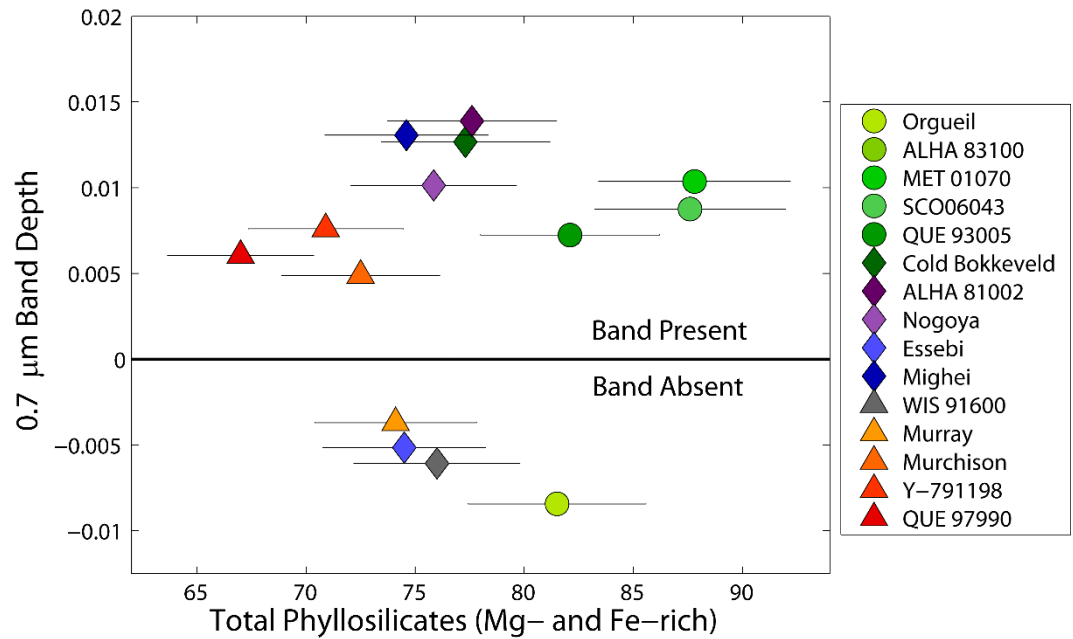


Figure 2.5: 0.7- μm band depth vs. total abundance of phyllosilicates. Continuum removed band depth is uncorrelated with total amount of phyllosilicates and degree of alteration.

2.4.4 Mid-Infrared Spectral Relationships to Mineralogy

The complex mineralogy of the meteorites is expressed in the MIR region where spectral changes are consistent with the mineralogical variations associated with the process of aqueous alteration found by Howard *et al.* (2011). However, one of the most challenging aspects of interpreting meteorite spectra in the MIR is the lack of good analog material. Since the phyllosilicates found in CM/CI meteorites are not endmember compositions of cronstedtite or serpentine, many terrestrial samples studied previously

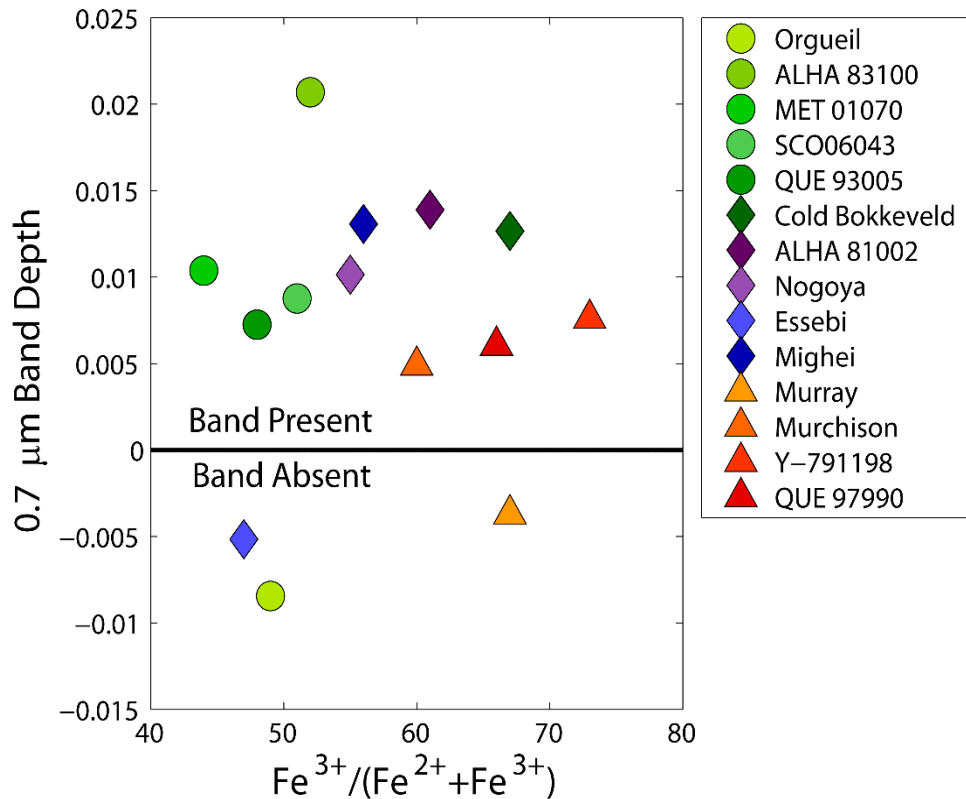


Figure 2.6: 0.7- μm band depth vs. relative abundance of ferric to total iron

Mössbauer spectra were collected for all meteorites (except PCA 91008 and WIS 91600) and are used to derive the valence state of iron. There is no correlation between 0.7- μm band depth and relative abundance of ferric iron.

(*e.g.* Calvin and King, 1997) do not include the same spectral features observed in the meteorites. These differences stem from different formation conditions (temperature and pressure) and different initial materials (*e.g.* fayalitic olivine and Fe-Ni metal are uncommon or nonexistent in rocks undergoing serpentinization on Earth). The differences in materials and conditions produce phyllosilicates that are not typically found in terrestrial settings. Terrestrial Fe-rich phyllosilicates (*e.g.* cronstedtite) have few spectral features in the MIR. While it is difficult to know for certain, Fe-rich phyllosilicates in meteorites are

therefore also not expected to contribute strongly in the 1000-700 cm^{-1} (10-13- μm) region. Mg-rich phyllosilicates in CM/CI meteorites have more iron than typical terrestrial serpentines, which may also affect the MIR spectral characteristics.

Although this lack of spectral analogs prohibits rigorous spectral modeling, MIR spectra of CM/CI meteorites show clear systematic evidence of both anhydrous silicates (olivine) and hydrated phyllosilicates. **Figure 2.7** shows representative spectra of the subgroups: highly, intermediately, and less altered meteorites. These spectra are normalized to unity at 8- μm and offset for clarity. The Christiansen features, near 1170 cm^{-1} (~8.5- μm), are marked by the arrows, the location of peak position in the 1000-700 cm^{-1} (10-13- μm) region at 875 cm^{-1} (11.4- μm) and 815 cm^{-1} (12.3- μm) are indicated by two vertical lines, and differences at long wavelengths from 600-400 cm^{-1} (15-25- μm) are denoted by highlighting.

The Christiansen feature is a reflectance minimum in MIR spectra of minerals caused when the real part of index of refraction of the medium the light is passing through becomes nearly equal to the index of refraction of the mineral (Salisbury *et al.*, 1992). This causes the scattering at this interface to be small and therefore almost none of the incident light is reflected. In many cases, the position of the Christiansen feature is diagnostic of a mineral (*e.g.* Nash and Salisbury, 1991). However, due to the mineralogic complexity of CM/CI the positions Christiansen features do not appear to have any correlation with total phyllosilicate abundance or phyllosilicate composition and cluster around a constant value. The small features in this region are not diagnostic of mineralogy. The overall shape in the region near Christiansen feature does, however, change with relation to the degree of

becoming more distinct and rounded with increasing alteration. Highly altered meteorites have a more pronounced Christiansen feature and the spectral region around it has a distinct rounded shape. Less altered meteorites can be flatter in this region but do not exhibit uniform spectral behavior.

The long wavelength spectral changes in the 600-400 cm^{-1} (15-25- μm) region are associated with structural changes in phyllosilicates. Fe-bearing dioctahedral phyllosilicates have 2 of the 3 octahedral M-sites filled with cations. In the iron rich endmember, cronstedtite, these sites would be filled with ferric iron atoms. In CM meteorites, the phyllosilicates have both ferric iron and magnesium cations filling these sites producing a single absorption feature in this region (Bishop et al., 2002). This feature is an overlapping vibration of the M-OH bending vibration in the octahedral layers and the Si-O bending vibration of the tetrahedral layers (Bishop et al., 2002; Michalski et al., 2005). In the less altered meteorites (reds) this absorption feature occurs at 510 cm^{-1} (19.5- μm ; Bishop et al., 2002; Michalski et al., 2005). Trioctahedral phyllosilicates with all three M-sites filled by cations have two distinct absorptions in the 15-25- μm region. The octahedral layers of the phyllosilicates in the highly altered meteorites (greens) are filled primarily with Mg- but have significant Fe-cations. A W-shape is created by the two absorptions: the OH-bending vibrations in Mg-rich trioctahedral phyllosilicates (620 cm^{-1} , ~16- μm) (Bishop et al., 2008) and the SiO_4 bending vibration at 475 cm^{-1} (21- μm) (Michalski et al., 2005 and references therein). Intermediately altered meteorites (blues) have intermediate spectral behavior.

The 1000-700 cm^{-1} (10-13- μm) feature (**Figure 2.8**) in CM/CI meteorite spectra is interpreted to be a convolution of the tetrahedral layer vibrations of phyllosilicates (Bishop *et al.*, 2008a) and the ν_1 fundamental stretching vibration in olivine at 775 cm^{-1} (12.9- μm) (Duke and Stephens, 1964; Tarte 1963; Dyar *et al.*, 2009). Less altered meteorites typically have more olivine present which causes a dominant peak at longer wavelengths (815 cm^{-1} , ~12.3- μm). Highly altered meteorites have more Mg-rich phyllosilicates and their 1000-700 cm^{-1} (10-13- μm) feature is therefore dominated by a shorter wavelength peak near 875 cm^{-1} (11.4- μm). The spectra of intermediately altered meteorites have roughly equal contributions of each phase creating a doublet.

Despite the dissimilarities with terrestrial analogs, comparisons with meteorite spectra are useful. Spectra of synthetic forsterite (Fo_{100}) (Dyar *et al.*, 2009) and an antigorite (Bishop *et al.*, 2008b) are shown in **Figure 2.9** in comparison to two meteorite endmembers. The strong ν_1 vibration in the olivine will contribute significantly to the spectra of the meteorites when olivine is at ~25 vol. % level. The Mg-rich phyllosilicates peak near 875 cm^{-1} (11.4- μm), but are typically poorly crystalline causing their features to be broad. The combination of the strong ν_1 olivine vibration at 875 cm^{-1} (~12.9- μm) and the broad tetrahedral layer vibration in Mg-rich phyllosilicates centered at 875 cm^{-1} (11.4- μm) combine to produce the 1000-700 cm^{-1} (10-13- μm) peak seen in meteorite spectra.

This continuous change in balance between the olivine and phyllosilicate peaks produces a strong spectral correlation with degree of alteration as shown in **Figure 2.10**, which shows the relationship between overall position of the 1000-700 cm^{-1} (10-13- μm) peak and the total abundance of phyllosilicates. The peak position of the band is determined

by the maximum of a second order polynomial fitted to the peak of the band. For the intermediately altered meteorites with characteristic doublets, the position of the overall peak (not those of the two individual peaks) is calculated. It should be noted that this relationship appears to also be valid for the WIS 96100, which has been both aqueously and thermally altered. Thermal metamorphism likely dehydrated some of the phyllosilicates and in so doing produced amorphous silicate phases (Tonui, *et al.*, 2014; Choe *et al.*, 2010; Rubin *et al.*, 2007). Since WIS 91600 has not experienced as extensive thermal metamorphism as PCA 91008, it still retains abundant Mg- and Fe-rich phyllosilicates. Modal mineralogy of this meteorite indicates that its abundances of phyllosilicates are in the intermediately altered meteorite range. As discussed in **Section 2.5.1** below, this correlation can be used to determine the alteration state of asteroids remotely.

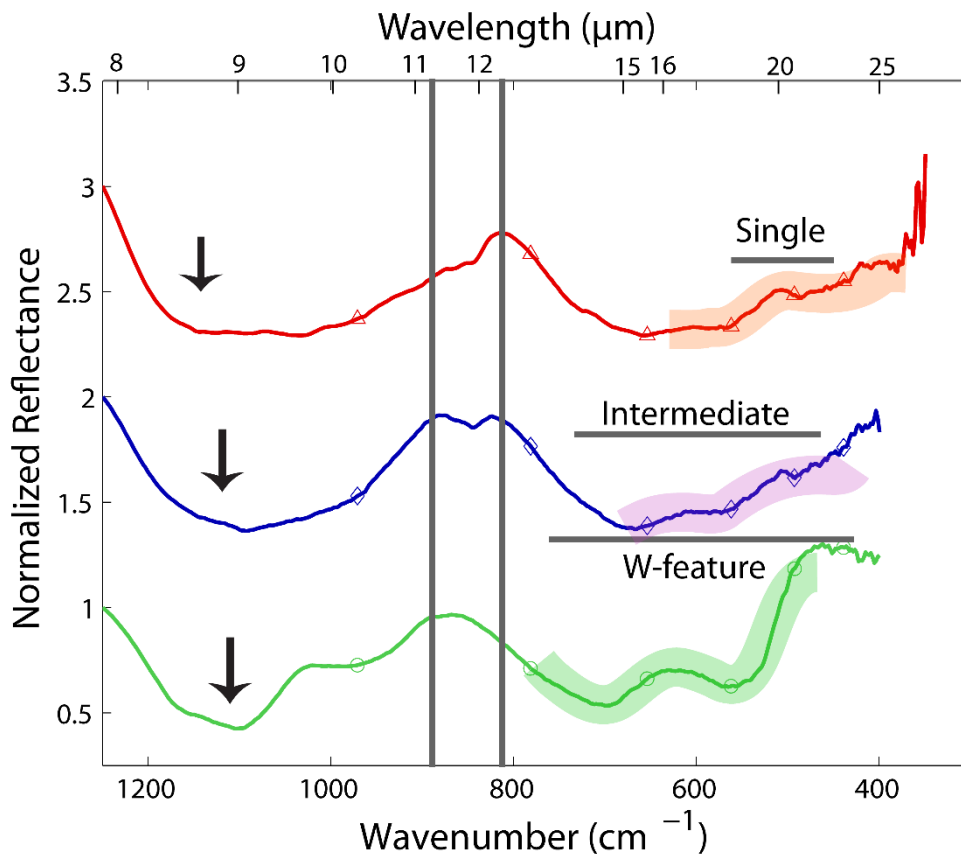


Figure 2.7: Spectra of representative CM/CI meteorites, illustrating the characteristics of each subgroup.

The Christensen features of the meteorites cluster around a single value of 1170 cm^{-1} however, there is some variation between meteorites. The black arrows indicate the approximate Christensen feature's position for each meteorite CM/CI spectra continuously change with increasing total alteration. Less altered meteorites have an 815 cm^{-1} ($12.3\text{-}\mu\text{m}$) and a single feature at 510 cm^{-1} ($19.5\text{-}\mu\text{m}$). As alteration increases, Mg-phyllsilicate abundance increases producing a doublet at in the $1000\text{-}700\text{ cm}^{-1}$ ($10\text{-}13\text{-}\mu\text{m}$) region and intermediate spectral behavior at longer wavelengths. Highly altered meteorites have very little olivine and their spectra are dominated by Mg-rich trioctahedral phyllsilicates in both the $1000\text{-}700\text{ cm}^{-1}$ ($10\text{-}13\text{-}\mu\text{m}$) with a peak at 875 cm^{-1} ($11.4\text{-}\mu\text{m}$) and at longer wavelengths with the W-feature (620 cm^{-1} , $\sim 16\text{-}\mu\text{m}$ and 475 cm^{-1} , $21\text{-}\mu\text{m}$).

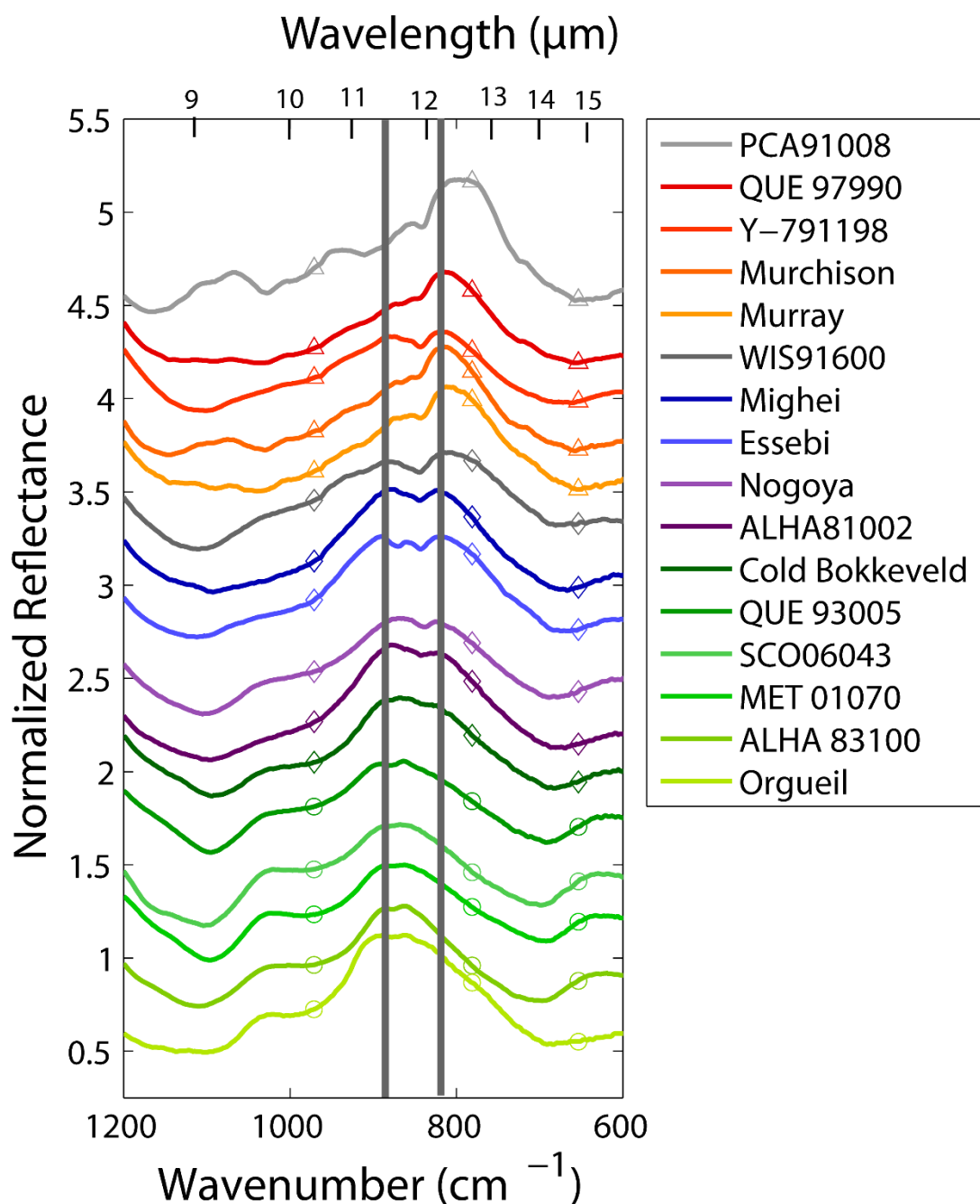


Figure 2.8: Spectra in the 10-13- μm region vary continuously with degree of alteration.

Less altered meteorites (reds) have a longer wavelength peak, intermediately altered meteorites have a doublet at the top of the absorption, and highly altered meteorites have a characteristically shorter wavelength peak.

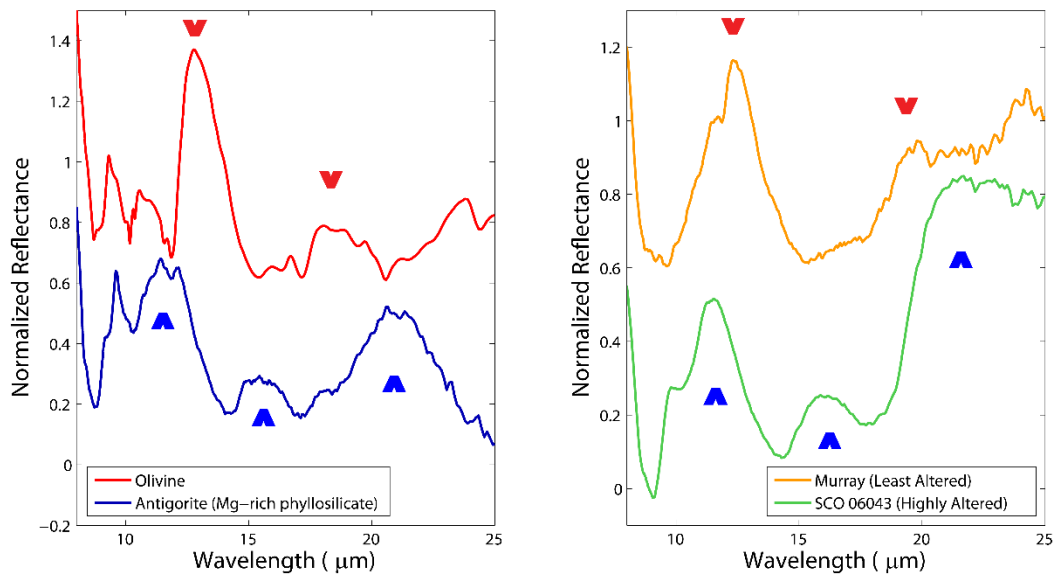


Figure 2.9: Terrestrial analogs, olivine (Dyar et al., 2009) and antigorite (Bishop, et al., 2008b), compared to less and highly altered meteorites.

The fundamental ν_1 vibration in olivine (775 cm^{-1} , $12.9\text{-}\mu\text{m}$), tetrahedral layer vibrations in antigorite (875 cm^{-1} , $11.4\text{-}\mu\text{m}$), OH-bending modes at 875 cm^{-1} ($16\text{-}\mu\text{m}$) and Si-O bending modes at 475 cm^{-1} ($21\text{-}\mu\text{m}$) also of antigorite are similar to the features in the CM meteorites. Differences in formation conditions and initial materials cause spectral differences making true quantitative analysis difficult.

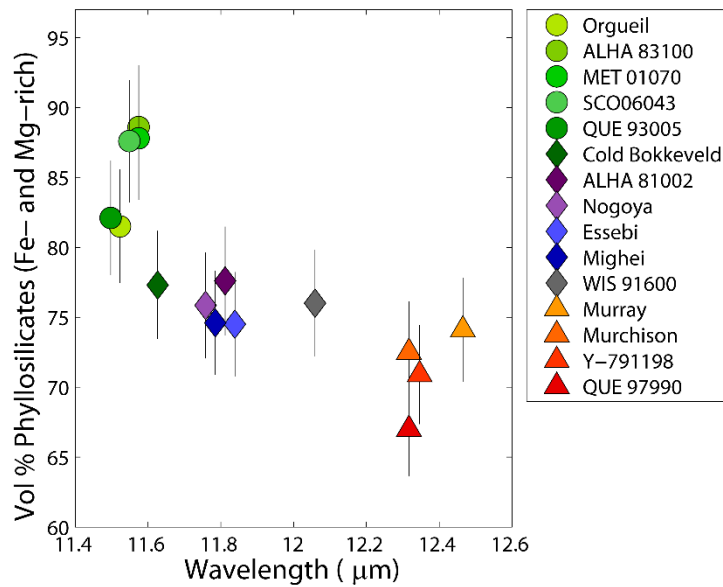


Figure 2.10: 10-13- μm peak position vs. total abundance of phyllosilicates.

The phyllosilicate abundances are from Howard *et al.* (2009, 2011) and have a 5% error bar on each value. The $1000\text{-}700\text{ cm}^{-1}$ (10-13- μm) peak is correlated with the degree of alteration, or the total abundance of phyllosilicates. Telescopic observations of this feature allows for the remote estimation of degree of alteration on asteroid surfaces.

2.5 Connecting to Asteroids

2.5.1 Identifying Asteroid Mineralogy using MIR Results

The trends in alteration established with laboratory spectra of our meteorite suite can be used to remotely identify alteration on asteroid surfaces. The 10-13- μm region, in particular, is useful because it falls into an atmospheric window observable using Earth-based and airborne platforms. Additionally, several space-based observatories have made observations of dark asteroids in this wavelength region. Studies in this wavelength region have included dark asteroids for example C- type (Lim *et al.*, 2005; Barucci *et al.*, 2002; Dotto *et al.*, 1999, 2002) and D-types (Emery, 2006). **Figure 2.11** shows a *Spitzer Space Telescope Infrared Spectrograph* (IRS) spectrum of the asteroid (24) Themis. Previous observations indicate that Themis is related to primitive, altered CM/CI meteorites (Clark *et al.*, 2011). It is a dark asteroid classified as C in the Bus-DeMeo and Tholen schemes (DeMeo *et al.*, 2009; Tholen, 1984) and B-type in the SMASS catalog (Bus and Binzel 2002a, 2002b). Themis has also been shown to have water ice on its surface (*e.g.* Rivkin and Emery, 2010; Campins *et al.*, 2010). Themis has a blue slope in the visible wavelength region and an overall concaved slope in the NIR (Clark *et al.*, 2010). This asteroid does not have a 0.7- μm charge transfer band but rather a broad 1.1- μm feature (Clark *et al.*, 2010).

The Themis spectrum emissivity data has been thermally corrected using the Near Earth Asteroids Thermal Model from Harris (1998). To reduce high-frequency

noise, the Themis data is further processed using a 5-channel boxcar smoothing algorithm. The resulting data have also been stretched between 0 and 1 to emphasize spectral features.

In order to compare the spectrum of Themis to the laboratory meteorite spectra, several factors that affect the absorption bands in the MIR must be considered. The first is pressure. Pressure, or more importantly interstitial gas, plays an important role in heat transport between grains on a surface (Logan *et al.*, 1973). Without interstitial gas, the top few microns of the surface, where MIR incident radiation is scattered, remains cold while the top few millimeters of the surface is heated by the absorption of visible light causing an increase in spectral contrast (Salisbury *et al.*, 1991; Logan *et al.*, 1973). This is referred to as the ‘cold skin’ model (Salisbury *et al.*, 1991; Logan *et al.*, 1973). The temperature difference between the outermost grains and interior grains increases spectral contrast. This effect, which can create large differences in contrast between spectra taken at ambient compared to the vacuum of space, is less pronounced for dark, opaque materials such as CM/CI meteorites and dark asteroids. Visible radiation cannot penetrate as deeply into the surface so a ‘cold skin’ never forms. Dark martials will, therefore, will have lower spectral contrast.

Additionally, grain size can affect the spectral contrast of the restrahlen bands in the MIR (*e.g.* Hunt and Vincent, 1968; Hunt and Logan, 1972; Salisbury and Eastes, 1985). For large grains (~100- μm or greater), spectral contrast is high because photons of MIR photons scatter quickly to the detector because they do not penetrate deeply into the grains (Hunt and Vincent 1968; Salisbury *et al.*, 1991; Salisbury *et al.*, 1992). Fine grains

(e.g. 0-45- μm) produce more volume scattering and therefore fewer photons reach the detector (Hunt and Vincent 1968; Salisbury *et al.*, 1991; Salisbury *et al.*, 1992).

Reststrahlen bands can also shift in position with variations of grain size, however, the magnitudes of these shifts are small (Hunt and Vincent, 1968). It is for these reasons that we stretch and smooth the spectrum of Themis and that our analyses focus on the relative spectral features, not their absolute magnitude.

Overlaid on the *Spitzer* data are meteorite spectra representative of three alteration groups (less, intermediately and highly altered), plotted to give spectral context. The meteorite spectra are approximated as emissivity using Kirchhoff's law and similarly stretched. While Kirchhoff's law is only strictly applicable for hemispherical spectroscopy, differences for bi-conical reflectance spectroscopy, used here, are minor and will only affect the magnitude of the features (Salisbury *et al.*, 1991, Clark, 1999).

Themis has a single feature in the 10-13- μm region at $\sim 12\text{-}\mu\text{m}$. The lack of a doublet and the position of this feature suggest that Themis is most similar to the less altered meteorites. This indicates that the surface of Themis likely contains both globally abundant phyllosilicates and anhydrous silicates. Using linear relationship between degree of alteration and phyllosilicate abundance, we estimate that Themis has ~ 70 vol. % phyllosilicates on its surface (**Figure 2.12**). Its similarity to the less altered meteorites (**Figure 2.11**) indicates that it has not undergone complete alteration on its surface. Since Fe-rich silicates alter more quickly than Mg-rich varieties, it is expected that Themis' surface mineralogy is enriched in Fe-rich phyllosilicates and unaltered Mg-rich olivine at levels of $\sim 10\text{-}20$ vol. % levels. Efforts are ongoing (McAdam *et al.*, 2013; McAdam *et*

al., 2014; see Chapter 4) to extend these efforts to the MIR spectra of other dark asteroids to compare their surfaces and to interpret their alteration state in the context of CM/CI meteorite mineralogy as we have done here for Themis.

2.5.2 Applications to Upcoming Missions

In the next decade, two sample return missions will be target dark, primitive near-Earth asteroids. Hayabusa-2 arrives at (162173) 1999JU3 (1999 JU3) in 2018 (Yoshikawa *et al.*, 2008) OSIRIS-REx will rendezvous with (101955) Bennu (Bennu) in 2020 (Lauretta *et al.*, 2012). Hayabusa-2 will have a NIR spectrometer (Yoshikawa *et al.*, 2008) and OSIRIS-REx will carry both a NIR spectrometer (OSIRIS-REx Visible and IR Spectrometer, OVIRS,) and the OSIRIS-REx Thermal Emissions Spectrometer (OTES) (Lauretta *et al.*, 2012). These spectrometers will acquire spatially resolved spectral data over the asteroid surfaces yielding insights into the mineralogical heterogeneity of the surfaces of these asteroids. Additionally spectral information of the subsurface of 1999 JU3 will be obtained when Hayabusa-2 launches a projectile into the surface of the asteroid (Yoshikawa *et al.*, 2008).

Earth-based NIR observations of 1999 JU3 (Vilas, 2008) have suggested that this asteroid has phyllosilicates on its surface by the presence of a $\sim 0.7\text{-}\mu\text{m}$ band. However, our analysis would suggest that little is known about the degree of alteration of this body. *Spitzer* IRS spectral observations (Campins, *et al.*, 2009) and photometric observations of 1999 JU3 made with the *Subaru* 8.2 m telescope (Hasegawa *et al.*, 2008) were used to determine physical properties such as thermal inertia for 1999 JU3. The photometric data

form *Subaru* observations indicate that the maximum flux in the 8-13- μm region occurs in the N-band filters centered on 11.7- μm with a width of $\sim 1\text{-}\mu\text{m}$. The 12.4- μm band filter has the next highest flux, significantly greater than photometric filters centered at shorter wavelengths (8.8-, 9.7-, and 10.5- μm). This may suggest that there is a feature in the region of 11.4-12.5- μm (where the large absorption caused by phyllosilicates and olivine is located in the spectra of CM/CI meteorites) but without higher resolution spectral data to show more clearly the position and shape, it is not possible to say anything about the mineralogy of 1999 JU3's surface.

NIR observations of Bennu suggest that it is a B-type asteroid with a blue slope and no charge transfer band at or around 0.7- μm (Clark *et al.*, 2011). However, slope is not unambiguously correlated to mineralogy (see **Section 2.4.1.1**) and the many physical processes that also affect NIR slopes (e.g. maturity, grain size and metal content). Similarly our results (see **Section 2.4.1**) indicate that a lack of a 0.7 μm does not imply lack of alteration. Emery *et al.* (2014) do not find conclusive mineralogical information within the noise levels of *Spitzer* MIR observations of Bennu and suggest that compaction may play a role in reducing spectral contrast in the MIR. While the nature of Bennu's surface mineralogy is not yet clear, on a global scale the combination of its physical state and degree of alteration does not seem to be similar to either the CM/CI meteorites or Themis.

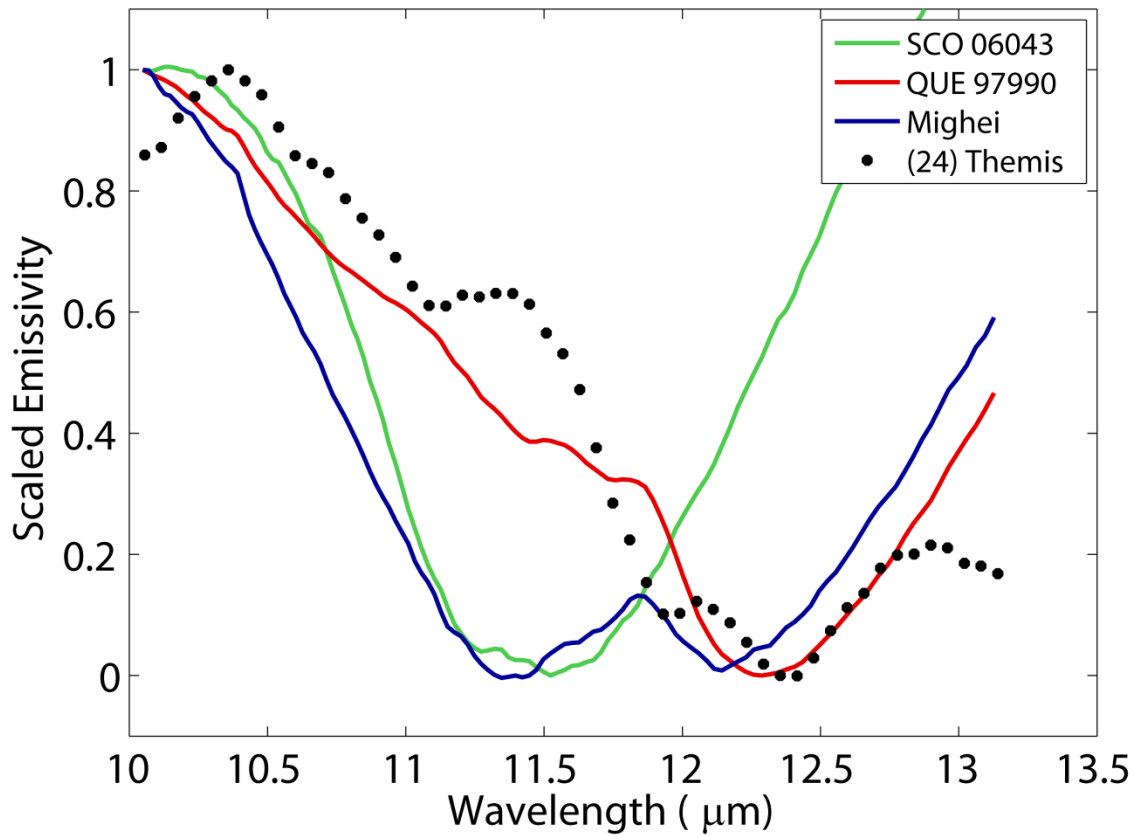


Figure 2.11: The emissivity spectrum of asteroid (24) Themis (thermally corrected and normalized at 10- μ m) compared to the spectra of representative meteorites: a less altered meteorite (QUE 97990), an intermediately altered meteorite (Mighei), and a highly altered

The meteorite spectra are approximated as emissivity using Kirckoff's law. Themis is spectrally similar to the less altered meteorites (single feature at ~12- μ m) and is therefore inferred to have both globally abundant phyllosilicates and anhydrous silicates.

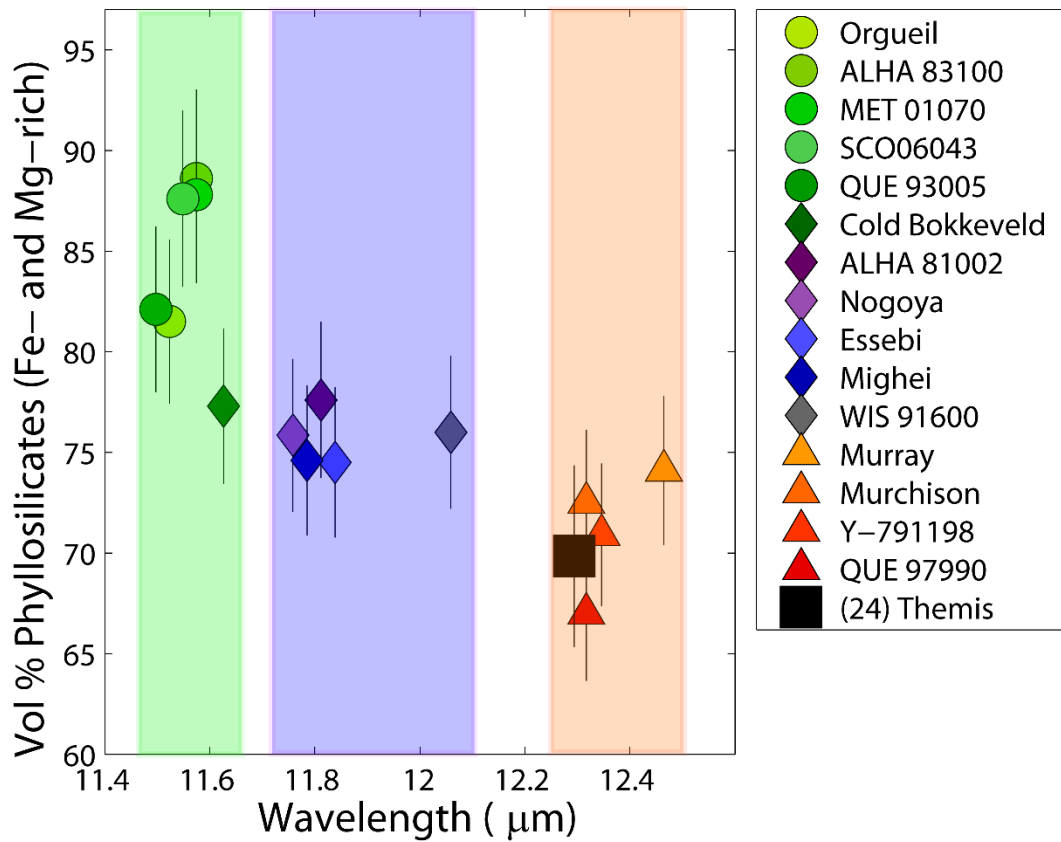


Figure 2.12: The emissivity minimum for asteroid (24) Themis superimposed on the meteorite reflectance peak positions vs. total volume of phyllosilicates.

Bars of color are overlaid to indicate the wavelength regions where degrees of alteration cluster: highly altered meteorites have peak positions around ~11.5-11.65-μm (green), intermediately altered meteorites peaks are between ~11.7-12.1-μm (blue) and less altered meteorites have peaks between ~12.3-12.5-μm. Themis is less altered an estimated to have ~70 vol. % phyllosilicates on its surface.

2.6 Conclusions

This coordinated spectral-mineralogical study of CM/CI meteorite powders provides a method to remotely determine the alteration state of asteroids using the VIS/NIR and MIR wavelength regions. While there is a trend in NIR slope and aqueous alteration, it is not directly related to mineralogy, and does not distinguish less or intermediately from highly altered meteorites. The presence of a 0.7- μm charge transfer band is an indicator of aqueous alteration, but is insensitive to the degree of alteration. Furthermore some CM/CI meteorites, which range in alteration from 60-90 vol. % phyllosilicates, do not have a charge transfer band implying that multi-wavelength observations of asteroids are crucial for determining both the state and degree of aqueous alteration.

In contrast, the MIR, and the 1000-700 cm^{-1} (10-13- μm) region in particular, is sensitive to total abundance of phyllosilicates and therefore the degree of alteration in meteorites. The spectra of CM/CI meteorites continuously change in this region, as the proportion of strong features in olivine and Mg-rich phyllosilicates systematically vary in relation to degree of alteration. The spectra of the less altered meteorites are dominated by the olivine peak at shorter wavenumber/longer wavelength (775 cm^{-1} , 12.9- μm), intermediately altered meteorites have roughly equal spectral contributions of olivine and Mg-rich phyllosilicates, producing a doublet in this region, while highly altered meteorites are dominated by Mg-rich phyllosilicates and have longer wavenumber/shorter wavelength peaks (875 cm^{-1} , 11.4- μm). The shape and position of this absorption feature can therefore be used to estimate the degree of alteration on asteroids. The asteroid (24) Themis is found

be dominated by a single feature centered near 12- μm , which suggests its surface is a complex mixture of 10-20 vol. % olivine and ~70 vol. % phyllosilicates. These results will be particularly useful for upcoming missions to dark, primitive near-Earth asteroids, Hayabusa-2 and OSIRIS-REx which will collect high spatial resolution spectra on the heterogeneity of alteration on these asteroids.

2.7 Acknowledgements

Spectra were acquired using the NASA Keck RELAB, a multiuser facility at Brown University. The efforts of Dr. T. Hiroi, who collected the RELAB spectra on our behalf, are greatly appreciated. Funding for this research by NASA's PGG Program (NNX10AJ57G) is gratefully acknowledged. We thank M. S. Kelley for his advice and assistance with processing the *Spitzer* data.

KTH was supported by NASA Cosmochemistry grant NNX14AG27G

We thank Andy Rivkin and an anonymous reviewer for their insightful comments and suggestions.

Preface to Chapter 3

Chapter 3 is taken verbatim from the recently submitted paper by McAdam, M. M., Sunshine, J. M., Howard, K. T., Alexander, C. M. O'D., McCoy, T. J., Bus, S. J. This work was submitted to the Journal Icarus on June 26, 2017 and is currently being reviewed. Figure, table, and section numbers have been updated to comply with the formatting requirements of the University of Maryland Graduate School. The reference list has been added to the Bibliography at the end of this thesis. Author McAdam analyzed the spectroscopy of the meteorites presented and primarily wrote the paper. Author Sunshine assisted with the spectroscopic analysis, interpretation and editing. Author Howard prepared the samples and provided some PSD-XRD measurements and derived modal mineralogy for this paper. Author Alexander assisted in sample procurement and assisted with the interpretation of the spectroscopic results and editing. Author McCoy assisted with interpreting the results. Finally, author Bus provided the spectrum of (93) Minerva fully calibrated for publication.

Chapter 3: Spectral Evidence for Amorphous Silicates in Low-Metamorphic Grade CO Meteorites and Their Parent Bodies

Abstract

Low-metamorphic grade carbonaceous chondrites are characterized by their predominately amorphous iron-rich silicate interchondrule matrices and chondrule rims. This material is highly susceptible to destruction by parent body processes of thermal metamorphism or aqueous alteration. The presence of amorphous material in a meteorite indicates that the parent body, or region of the parent body, has experienced minimal processing since the time of accretion. The CO chemical group of carbonaceous chondrites has a number of these low-metamorphic grade samples. We present visible/near-infrared and mid-infrared spectra of eight low-metamorphic grade CO meteorites (petrologic type 3.0-3.1). In the visible/near-infrared, these COs are characterized by a broad weak feature that was first observed by Cloutis et al (2012) to be at 1.3- μm and attributed to iron-rich amorphous silicate matrix materials. This feature is observed to be centered at 1.4- μm for the terrestrially unweathered, low-metamorphic grade CO meteorites. At mid-infrared wavelengths, a 21- μm feature, consistent with Si-O vibrations of amorphous materials and glasses, is also present. The spectral features of iron-rich amorphous silicate matrix are absent in both near- and mid-infrared spectra of high-metamorphic grade COs as these phases recrystallize into crystalline olivines. Furthermore, spectra of low-metamorphic grade meteorites in other chemical groups (CRs, MET 00426 and QUE 99177, and C2-

ungrouped Acfer 094), also exhibit a 21- μm feature. Thus we conclude that 1.4- and 21- μm features are characteristic of primitive, low-metamorphic grades in all chemical groups of carbonaceous chondrites. Finally, we present an IRTF+SPEX observation of asteroid (93) Minerva that has spectral similarities in the visible/near-infrared to the low-metamorphic grade carbonaceous chondrites. While Minerva is not the only CO-like asteroid (e.g., Burbine et al., 2001), Minerva is likely the asteroid that has experienced the least parent body processing observed to date.

3.1 Introduction

CO meteorites, named after their type member Ornans, are a chemical group of carbonaceous chondrites that are characterized by small chondrules that are set in a relatively FeO-rich fine-grained matrix (Rubin et al., 2010; McSween, 1977). Here matrix is used to include both interchondrule matrix and fine-grained rims on chondrules. Many CO meteorites contain abundant (a few percent) metal that is indicative of their formation under relatively reducing conditions. CO chondrites range in metamorphic grade from petrologic type 3.0 to 3.8 (Scott and Jones, 1990). Low-metamorphic grade CO meteorites (3.0-3.1) contain matrices with high abundances of amorphous material (e.g., Brearley, 1993), presolar grains (e.g., Nittler et al., 2013), and insoluble organic matter contents (Alexander et al., 2007, 2010, 2014). Until recently, only one CO 3.0 had been identified (ALH 77307, Brearley, 1993) and studied using infrared spectroscopy (Cloutis et al., 2012). As a result of annual searches conducted in Antarctica, many more low-metamorphic grade COs have now been identified, including at least one new unique CO

3.0 with several individual meteorite fragments (e.g., Alexander et al., 2014; Davidson et al., 2015). However, these new samples have not been extensively studied using spectroscopy.

A characteristic trait of low-metamorphic grade carbonaceous chondrites, including those in the CO chemical group, is the presence of amorphous material (iron-bearing silicates that lack long-range order) in their matrices (e.g., Alexander et al., in press). This amorphous material is thought to be the product of disequilibrium condensation from a gas (e.g., Brearley, 1993; Abreu and Brearley, 2010; Greshake, 1997; Leroux et al., 2015), and is very susceptible to modification by aqueous alteration and/or thermal metamorphism. Hence, the presence of this amorphous material in a meteorite indicates that it came from an asteroid or a region of an asteroid that experienced minimal processing after accretion. These samples are therefore likely to retain important chemical and geological information about events in the early Solar System.

Previous studies of Allan Hills (ALH) 77307, until recently the only known CO 3.0 (Grossman and Brearley, 2005), indicate that the amorphous component of its matrix is an iron-bearing silicate (Brearley, 1993; De Gregorio et al., 2016). Spectroscopically, the amorphous materials in low-metamorphic grade CO matrices behave like other amorphous phases, including impact and volcanic glasses, due to their structural similarity. They have been identified in the visible/near infrared by a broad band near 1.3- μm (Cloutis et al., 2012). Iron oxides (rust) can be present in low-metamorphic grade COs (e.g., Brearley and Jones, 1998; Grossman and Rubin, 2006), but generally their abundance is low and are

likely created by terrestrial weathering. Iron hydroxides and gypsum can also be present, but they are almost certainly the products of terrestrial alteration (Velbel et al., 1990).

Here we present visible/near-infrared and mid-infrared spectral data for eight low-metamorphic grade CO meteorites (3.0-3.1) to determine if the near-infrared spectral features identified by Cloutis et al., (2012) are representative of CO meteorites with minimal terrestrial weathering and to identify any characteristic spectral features in the mid-infrared. To investigate the spectral contribution of the amorphous iron-bearing silicate matrix in the mid-infrared, a first-order spectral model is used to remove the crystalline components. A potentially related asteroid for the low-metamorphic grade carbonaceous chondrites, (93) Minerva is identified. Minerva's near-infrared spectral features indicate it is potentially related to low-metamorphic grade carbonaceous chondrites. Minerva may represent the relatively less-processed parent body, or an asteroid that has experienced minimal heating and no aqueous alteration, while other asteroids related to COs (e.g., Burbine et al., 2001) are the thermally evolved parent asteroids. We explore the observational requirements for follow-up studies in the mid-infrared, which would confirm this potential detection and provide additional constraints on the origin of the low-metamorphic grade carbonaceous chondrites.

3.2 Background

3.2.1 The least-altered CO meteorites

The low-metamorphic grade CO meteorites are characterized by abundant chondrules (McSween, 1977; Rubin, 2010; Ebel et al, 2016), and fine-grained, largely

amorphous matrices (e.g., Brearley, 1993). These meteorites have experienced minimal heating, which is indicated by several factors including the structural grade of the insoluble organic matter (Bonal, et al., 2007, 2016; Alexander, et al., 2014), and the relatively high and homogenous chromium content in olivines (Grossman and Brearley, 2005; Davidson, et al., 2014). These COs can also have high presolar circumstellar silicate grain abundances (e.g., Nittler et al., 2013), which is another indication of minimal parent body processing.

The amorphous-rich matrices of these low-metamorphic grade COs have been extensively studied in certain CO samples (e.g., Brearley, 1993) and other primitive carbonaceous chondrites (e.g., Abreu and Brearley, 2010; Greshake, 1997; Le Guillou and Brearley, 2014). The matrices of low-metamorphic grade carbonaceous chondrites are dominated by truly amorphous material with little or no ordering, but do include some crystalline silicate grains (Brearley, 1993; De Gregorio et al., 2016). The matrix in ALH 77307 also contains highly localized ‘proto-phyllsilicates’ regions with some ordering, but these regions could be the result of terrestrial weathering (Brearley, 1993).

3.2.2 Disequilibrium Condensation of Amorphous Silicates

Amorphous silicates can form by several processes including disequilibrium condensation, quenching of silicate melts, particle irradiation of crystalline materials, impact shock, and early stages of aqueous alteration (e.g., Alexander et al., 1989; Abreu and Brearley, 2010; Chizmadia and Nuth, 2006; Chizmadia, 2007; Nuth et al., 2005). However, studies of low-metamorphic grade CO meteorites indicate that most of these processes can be ruled out as the formation mechanism for the amorphous materials (e.g., Brearley, 1993) and it is generally thought to be the product of disequilibrium condensation

from rapidly cooled gas. Meteorites that preserve amorphous materials formed through disequilibrium condensation include low-metamorphic grade carbonaceous chondrites in the CO, CR and ungrouped samples (e.g., Brearley, 1993; Abreu and Brearley, 2010; Greshake, 1997), CMs Paris and Yamato-791198 where these phases are preserved during heterogeneous aqueous alteration (Leroux et al, 2015; Chizmadia and Brearley, 2008). Furthermore, Glass Embedded with Metal and Sulfide (GEMS) grains found in interplanetary dust particles are also interpreted to form through disequilibrium condensation (Keller and Scott, 2011; Messenger et al, 2015).

Most of the amorphous materials found in the matrices of low-metamorphic grade carbonaceous chondrites likely formed in the solar nebula when temperatures in the disk were high and could vaporize dust (Wooden et al., 2007) or during transient heating events such as chondrule formation (e.g., Jones et al., 2000; Desch and Connolly, 2002; Connolly and Jones, 2017). These amorphous materials are highly susceptible to destruction through the parent body processes of thermal metamorphism and aqueous alteration. This paper confines itself to the study of low-metamorphic grade carbonaceous chondrites that have not experienced aqueous alteration, which can be considered both primitive and least-processed since they have high pre-solar grain abundances and are highly unequilibrated, unlike Paris and Y-791198 which have experienced significant interactions with water.

3.2.3 Spectroscopy of Amorphous Silicates and Glasses

Glasses are known to form in rapid cooling events such as impacts (e.g., Tompkins et al., 2010), volcanic eruptions (e.g., Crisp et al., 1990; Bell and Mao, 1976) and chondrule formation (e.g., Kurahashi et al., 2008). Additionally, observations of the interstellar

medium have spectral features at 10- and 20- μm that are attributed to amorphous silicates (e.g., Kemper et al, 2004, 2005)

The amorphous silicates found in the matrices of low-metamorphic grade COs are similar to other silicates lacking long-range order, including glasses formed by impact and volcanism. Structurally, glasses are comprised of units with short- to mid-range order ($\sim 15\text{-}20\text{-}\text{\AA}$; King et al., 2004). As discussed by King *et al.* (2004), when glass is formed, silicon and oxygen atoms form tetrahedra, locally. If there are other ions present, these enter the local structure as network formers or network modifiers. Network formers behave similarly to the silicon atoms, creating tetrahedra and increasing the ordering. These cations tend to be tri- or quadrivalent (e.g., Fe^{3+} , Ti^{4+} , or Al^{3+}). Mono- or divalent ions (e.g., Fe^{2+} , Mg^{2+} , Ca^{2+}) modify the local ordering by forming bonds with oxygens, thus limiting structural ordering by preventing bond formation between tetrahedra.

In the mid-infrared, the cation-oxygen bonds produce vibrations between 8-12.5- μm , and 16-25- μm . The exact positions of these mid-infrared features depends on several factors including the degree of polymerization (or the number of cation-oxygen bonds), cation substitutions in the tetrahedra, the number of network modifiers present and, for iron-rich glasses, the redox conditions (Mysen and Richet, 2005). The 8-12.5- μm features are caused by asymmetric stretching vibrations of the O-Si-O/Si-O-Si bonds. Glasses can have complex features in this region because ordering only exists locally and different units can create multiple features (King et al., 2004). Additionally, there are two asymmetric stretching modes that also produce multiple features between 8-10- μm and $\sim 12.5\text{-}\mu\text{m}$. Furthermore, the substitution of cations can change these frequencies. Increasing

polymerization of glasses, or the sharing of tetrahedrally coordinated oxygens, shifts spectral features to shorter wavelengths (from 9- μm to \sim 8- μm). Long-wavelength features (16-25- μm) are caused by the bending vibrations of the Si-O-Si bonds (King et al., 2004). Network formers other than silicon (e.g., aluminum) can change the frequencies of these vibrations, thus changing the wavelength of the 16-25- μm features (King et al., 2004).

In the visible/near-infrared, impact and volcanic glasses have well known crystal field features (e.g., Bell and Mao 1976; Moroz et al., 2009; Horgan et al., 2016; Morlok et al., 2016). Crystal field features are created through an electronic process where an ion with unfilled d-orbitals exists in a crystal structure. The bonding environment changes the energy levels of the d-orbitals generally splitting them into two energy states. Depending on the bonding environment (octahedral vs. tetrahedral), these states can be excited to produce absorption features in the visible/near-infrared. While the effects of ferric/ferrous iron on the near-infrared and mid-infrared spectra of glasses has not been extensively examined (e.g., Horgan et al., 2016), it has been suggested that ferric iron causes a broad absorption over the visible/near-infrared wavelengths that causes lower albedos and a moderately red-slope (Moroz et al., 2009). If ferrous iron cations are in local octahedral coordination, they produce the crystal field transitions seen at \sim 1- μm in spectra of natural and synthetic glasses (Moroz et al., 2009; Bell and Mao, 1976; Morris et al., 2000). Glasses with basaltic compositions have been extensively studied, but there is a paucity of studies that have investigated the simple iron/magnesium-silicon-oxygen system (e.g., King et al., 2004; Crisp et al., 1990).

3.2.4 Previous Spectral Studies of CO meteorites

Few studies (e.g., Cloutis et al., 2012) have documented the spectral characteristics of low-metamorphic grade CO meteorites. This is largely due to the lack of low-metamorphic grade COs in the meteorite collection. Previous spectral studies of COs mainly examined metamorphosed samples such as Ornans (3.4), Warrenton (3.7), and Lancé (3.5) (e.g., Johnson and Fanale, 1973; Gaffey, 1976; Salisbury et al., 1975). These higher metamorphic grade COs are characterized in the near-infrared and mid-infrared by absorptions caused by the olivine and pyroxene present in their chondrules and matrix. The first CO3.0 to be identified, ALH 77307, is spectrally characterized in the near-infrared by a flat slope and a broad, weak $\sim 1.3\text{-}\mu\text{m}$ feature that has been attributed to amorphous iron-bearing matrix silicates (Cloutis et al., 2012). In this wavelength region, ALH 77307 generally has a lower albedo than more metamorphosed COs (Cloutis et al., 2012).

Low-metamorphic grade CO chondrites are mineralogically and, therefore, spectrally distinct from other groups of carbonaceous chondrites (e.g., Alexander et al., in press). Carbonaceous chondrites such as CM1/2s, CI1s, and CR1/2s all have abundant hydrated minerals (e.g., Howard et al., 2009, 2011, 2015) produced by aqueous alteration. Hydrated minerals dominate the spectra of these carbonaceous chondrites in both the visible/near-infrared and mid-infrared. The aqueously altered CMs and CIs can have a charge transfer band at $0.7\text{-}\mu\text{m}$ in the near-infrared, as well as strong features at $11.5\text{-}12.5\text{-}\mu\text{m}$, $16\text{-}\mu\text{m}$ and $21\text{-}\mu\text{m}$ caused by the vibrational absorptions of the phyllosilicates. In the least altered CMs, which may contain $\sim 25\text{-}30\text{ vol.}\%$ olivine (Howard et al., 2009, 2011), a feature at $19.5\text{-}\mu\text{m}$ is also present in their spectra (Beck et al., 2014; McAdam et al., 2015a;

Chapter 2). Low-metamorphic grade COs are also spectrally distinct from more thermally metamorphosed carbonaceous chondrites, including COs and CVs. During thermal metamorphism minerals in chondrules and matrix equilibrate, strengthening vibrations in the mid-infrared (McAdam et al., 2015b). In the near-infrared, thermally metamorphosed meteorites exhibit olivine and pyroxene features at 1- μm and 2- μm . For meteorites with similar metamorphic grades as the COs studied here, there are both mineralogical and spectral similarities, which will be discussed further in *Section 3.4*.

3.3 Samples and Data Collection

3.3.1 Samples

The CO meteorites examined in this study are listed in **Table 3.1**, along with their metamorphic grades, weathering grades, and reference to studies that closely examined these meteorites. These meteorites were selected since they appear to be some of the least-processed COs (e.g., Alexander et al., in press) that contain amorphous iron bearing silicate matrices that comprise up to ~30 vol.% of the meteorite. Approximately 100 mg samples of each meteorite, sub-sampled from larger volumes prepared for Position-Sensitive X-ray analyses previously, were used for spectral characterization. Each aliquot was ground to ~35- μm grain size, which is estimated by optical microscopy. Multiple aliquots from four meteorites were analyzed for comparison purposes.

All of the samples show at least some evidence of terrestrial weathering. On a scale from A, least weathering to C, moderate weathering, most of the samples studied here have grades A, A/B or B, i.e., minor to moderate rust along fractures (including minor-moderate

rust halos on metal grains). Included in our suite are two meteorites that have more terrestrial weathering (Miller Range, MIL, 090073 and MIL 07687). These meteorites are reported to have moderate to severe rustiness, and in the case of MIL 07687 evaporite minerals are visible on its outer surface.

In previous analyses of these meteorites, organic solvents have been used successfully to remove terrestrial weathering for bulk isotope analyses (Greenwood *et al.*, 2016). A similar protocol was not used here, since the organic solvents could add spurious spectral features to the near- and mid-infrared spectral regions. Consequently, terrestrial weathering will affect the spectra presented here to some degree. These affects will be discussed in the following sections.

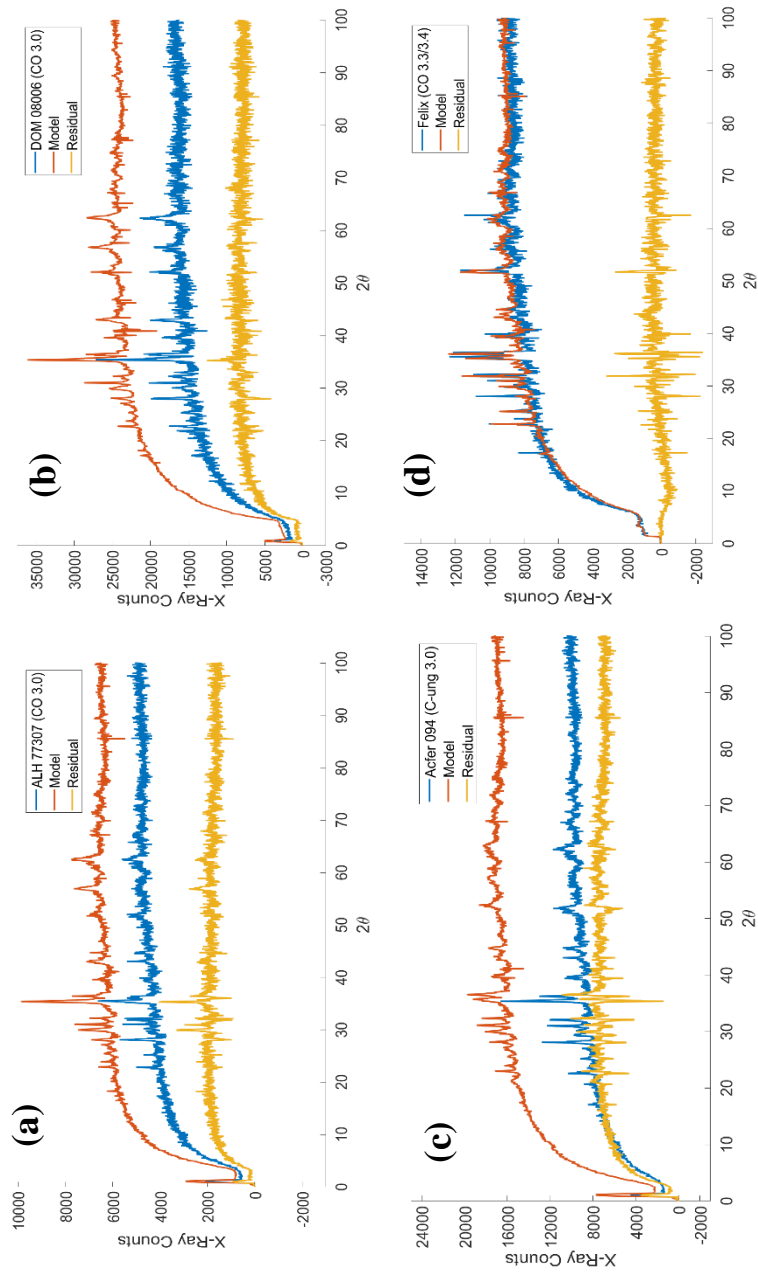


Figure 3.1: PSD-XRD Spectrum, model and residual for (a) ALH 77307 (CO 3.0), (b) DOM 08006 (CO 3.0), (c) Acfer 094 (CO 3.0) and (d) Felix (CO 3.3/3.4).

For ALH 77307, DOM 08006 and Acfer 094, crystallographic peaks in the X-ray patterns can be completely accounted for, however significant X-ray residuals remain. These X-ray counts are attributed to the poorly crystalline Fe-bearing matrix materials. Conversely, Felix has negligible amorphous materials; its spectrum can be completely modeled with crystalline standards without significant residuals. Felix has been heated to a higher peak temperature than DOM 08006, and ALH 77307 so the amorphous matrix materials have been recrystallized.

Table 3.1: Meteorite Samples

<i>Meteorite</i>	<i># of aliquots</i>	<i>Chemical Group</i>	<i>Metamorphic Grade</i>	<i>Weathering Grade</i>
<i>ALH 77307</i>	1	CO	3.0	Ae
<i>DOM 08004</i>	2	CO	3.1	B
<i>DOM 08006</i>	2	CO	3.0	A/B
<i>MIL 07687*</i>	1	CO	3.0	Ce
<i>MIL 090010</i>	1	CO	3.1	A/B
<i>MIL 07193</i>	2	CO	3.1	A
<i>MIL 07709</i>	2	CO	3.1	A
<i>MIL 090073</i>	1	CO	3.1	B/C
<i>MET 00426</i>	1	CR	3.0	B
<i>QUE 99177</i>	1	CR	3.0	Be
<i>Acfer 094</i>	1	Ungrouped	3.0	-
<i>Felix</i>	1	CO	3.3/3.4	-
<i>ALH 85003</i>	1	CO	3.5	A/B
<i>ALH 83108</i>	1	CO	3.5	A
<i>Allende</i>	1	CV	3.6	-

*This meteorite may not be a CO, but related to Acfer 094 (Brearley, 2012; Davidson et al., 2014).

3.3.2 Modal Mineralogy of Selected Samples

The powders used for the spectral analyses have previously been studied using position-sensitive X-ray diffraction (PSD-XRD) to constrain modal mineral abundances following the approach described previously and summarized below (Howard et al. 2015; Alexander et al., in press). Modal abundances for the suite of CO samples in this study have recently been reported in Alexander et al. (in press). Here we focus on three low-metamorphic grade COs (ALH 77307, DOM 08006; Acfer 094) and one thermally processed CO meteorite to illustrate the mineralogy of these samples and the changes associated with thermal metamorphism. The collected PSD-XRD patterns for these meteorites are shown in **Figure 3.1a-c**, along with phases identified using the ICDD database. To quantify proportions of mineral phases in meteorites, standards of pure minerals are measured under identical conditions. Then, peak intensities in the standard patterns are normalized for differences in collection times and scaled to match meteorite patterns. Sequentially standard patterns are subtracted from the meteorite pattern in identified proportions until a peak free residual is reached. Once the proportions of each standard are determined using the pattern fitting techniques, the pattern-proportions are converted into mineral proportions (wt. %) by correcting for relative difference in X-ray absorption using calculated mass absorption coefficients.

For ALH 77307, DOM 08006 and Acfer 094, the pattern fitting routines accurately account for all crystallographic peaks, however, significant X-ray residuals remain which,

represent the fluorescence signature of Fe bearing material without long-range crystallographic order. Both Fe-bearing silicates and Fe-oxides/hydroxides produced during terrestrial weathering are known to be X-ray amorphous in carbonaceous chondrites. The residual signature itself cannot discriminate the identity of the contributing phases; only the total contribution of residual X-ray counts to the bulk diffraction pattern can be quantified. However, the samples used in the PSD-XRD and spectral analyses were carefully chosen from the interior regions of the meteorites to reduce terrestrial weathering. Furthermore, observations of these meteorites using optical microscopy and Transmission Electron Microscopy (TEM; e.g., Brearley, 1993) excludes significant contributions to the X-ray residuals from Fe-oxides/hydroxides since the abundances of these phases could not create the residuals observed. Amorphous silicates in chondrules, (mesostases) tend to have low iron contents and will only contribute weakly to the X-ray residuals (Howard et al., 2015; Kurahashi et al, 2008). Sections of these low-metamorphic grade CO meteorites studied by TEM studies confirm the presence of abundant and amorphous Fe-rich silicate in the matrices of these samples (Brearley, 1993, Greshake, 1997, De Gregorio et al., 2016). Previous studies have used bulk compositions and petrography to demonstrate that most amorphous material identified by PSD-XRD in primitive CR 3.0 samples is also Fe-rich silicate in matrix (e.g., Howard et al., 2015a).

The resulting modal mineralogies are listed in **Table 3.2**. The CO meteorite Felix (**Figure 3.1d**) has experienced moderate metamorphism and is petrologically classified as 3.3/3.4. The petrologic grade of Felix is relatively low compared to other CO meteorites such as ALH 85003 (CO 3.5), which experienced higher peak temperatures. PSD-XRD

measurements indicate that unlike the low-metamorphic grade COs, Felix’s spectrum can be completely modeled using crystalline components. There is negligible X-ray residual for this meteorite and, therefore, negligible amorphous iron-bearing matrix. The lack of amorphous components in the PSD-XRD measurements of Felix is consistent with petrographic studies of this meteorite that show that even during mild to moderate heating, the amorphous silicate matrix materials are recrystallized into crystalline minerals.

Table 3.2: Modal mineralogy for selected samples.

<i>Meteorite</i>	<i>Typ e</i>	<i>Fo10 0</i>	<i>Fo9 0</i>	<i>Fo8 0</i>	<i>Fo7 0</i>	<i>Fo6 0</i>	<i>Fo4 0</i>	<i>Fo2 5</i>	<i>Tot. Olv.</i>
<i>ALH 77307</i>	3.00	0%	21%	0%	0%	0%	14%	0%	35%
<i>DOM 08006</i>	3.00	42%	0%	0%	0%	10%	0%	0%	42%
<i>Acfer 094</i>	3.00	0%	32%	0%	0%	0%	5%	0%	37%
<i>Felix</i>	3.3/ 3.4	0%	41%	0%	0%	0%	13%	7%	61%

<i>Meteorite</i>	<i>En.</i>	<i>ClinEn.</i>	<i>Tot. En.</i>	<i>Sulfide</i>	<i>Metal</i>	<i>Mag</i>	<i>Ph.</i>	<i>Am</i>	<i>Total</i>	
<i>ALH 77307</i>	27%		0%	27%	3%	2%	8%	4%	20%	100%
<i>DOM 08006</i>	22%		0%	22%	3%	1%	6%	2%	15%	100%
<i>Acfer 094</i>	24%		7%	31%	6%	2%	5%	0%	19%	100%
<i>Felix</i>	30%		0%	30%	3%	2%	4%	0%	0%	100%

Type – Petrologic Type; Olv – olivine; Fo – forsterite; En – enstatite; ClinEn – clino-enstatite; Mag – magnetite; Ph – phyllosilicate; Am – amorphous matrix.

3.3.3 Reflectance Spectra Data Collection

The reflectance data for all the carbonaceous chondrites measured in this study were acquired at the Brown University NASA/Keck Reflectance Laboratory. Visible/near-infrared measurement were obtained with the bi-directional spectrometer from 0.3- μm to 2.5- μm at a resolution of 10 nm with an incidence angle of 30° and emergence angle of 0° . Pressed halon, with an approximately Lambertian surface, was used as a reflectance standard. Mid-infrared spectra were measured using the Thermo Nexus 870 FT-IR spectrometer. This off-axis bi-conical spectrometer uses a brushed gold standard. Data were obtained from 1- μm to 25- μm at a resolution of 4 cm^{-1} .

3.4 Results

3.4.1 Near-infrared Results

The visible/near-infrared reflectance spectra of the suite of eight low-metamorphic grade CO samples are presented in **Figure 3.2**. A convex hull was used to remove the overall slope in the spectra, and enhance any features present. A broad weak feature centered near 1.4- μm is apparent for meteorites that have minimal terrestrial weathering. This feature has been previously attributed to amorphous iron-bearing silicates (Cloutis et al., 2012).

Weathering of the meteorites affects the near-infrared spectral slope, causing significant reddening (**Figure 3.3**). A 4th-order polynomial is fit the band and find the minimum for each spectrum is determined. For the minimally weathered samples the

position of the band is found to be at $\sim 1.4\text{-}\mu\text{m}$ (**Figure 3.4**). With increasing weathering grade, the position of the band shifts to shorter wavelengths, until it is not observable (e.g., MIL 07687). Weathering also reduces the depth of this feature (**Figure 3.4**). These changes are caused by hydrated iron oxides and gypsum produced during terrestrial weathering that mask the $1.4\text{-}\mu\text{m}$ feature. Small features at $0.9\text{-}\mu\text{m}$ and $1.9\text{-}\mu\text{m}$ also appear with significant terrestrial weathering. These are produced by evaporite minerals and terrestrial hydroxides (Velbel et al, 1990; Clark, 1999).

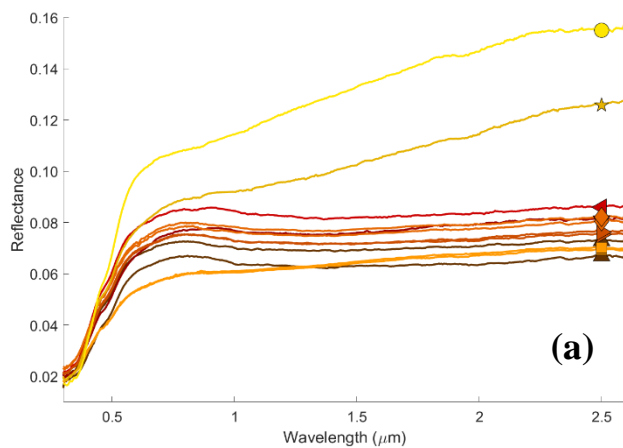
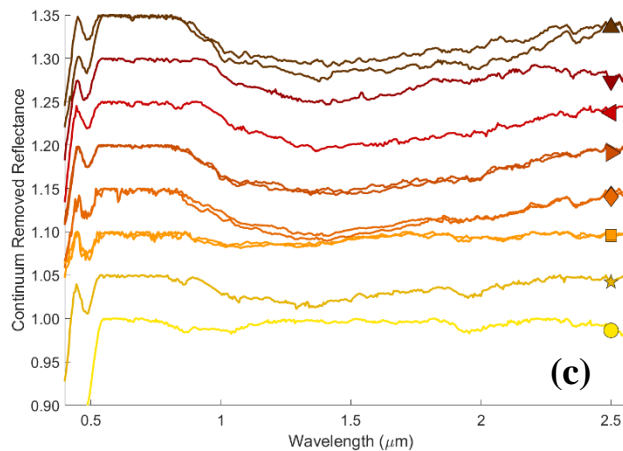
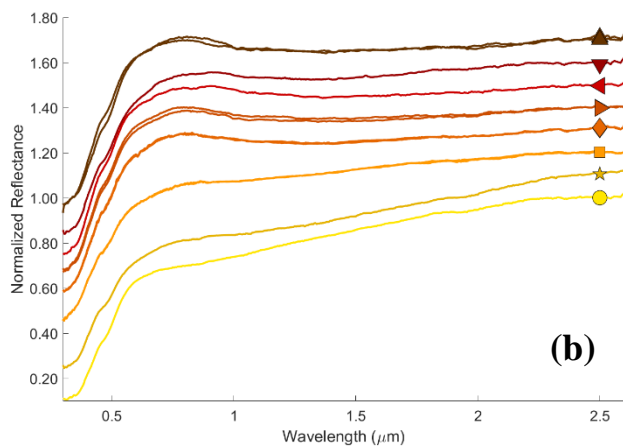


Figure 3.2: Near Infrared data. Near-infrared data (a), normalized and offset (+0.5) (b) and continuum removed and offset (c) ordered by weathering grade (top, minimally weathered to bottom, most weathered).

The color and symbol identify each sample. For minimally terrestrially weathered low-metamorphic grade COs, near-infrared spectra are fairly flat without strong features. Terrestrial weathering increases red slope and causes weak absorptions at 0.9- and 1.9- μm . Upon continuum removal, a broad weak feature ($\sim 2\text{-}5\%$) appears in the most pristine samples centered near 1.4- μm . This feature is masked by weathering products in weathered samples. A similar feature has previously been interpreted as the presence of iron-bearing silicate matrix (Cloutis, et al., 2012)



▲	MIL 07193	3.1,	A
▲	MIL 07193	3.1,	A
▼	ALH 77307	3.0,	Ae
▲	MIL 090010	3.1,	A/B
▲	MIL 07709	3.1,	A
▲	MIL 07709	3.1,	A
◆	DOM 08004	3.0/3.1,	B
◆	DOM 08004	3.0/3.1,	B
■	DOM 08006	3.0,	A/B
■	DOM 08006	3.0,	A/B
★	MIL 090073	3.0/3.1,	B/C
●	MIL 07687	3.0,	Ce

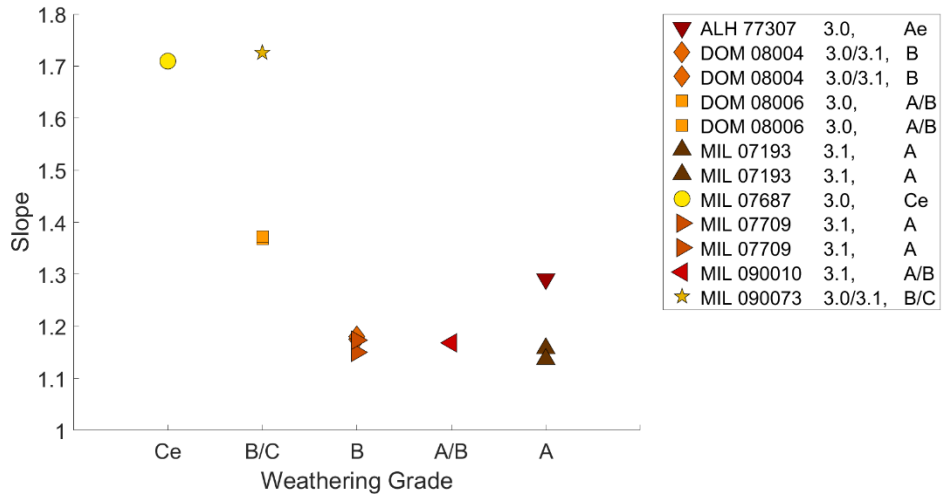


Figure 3.3: Near-infrared slope vs. weathering grade.

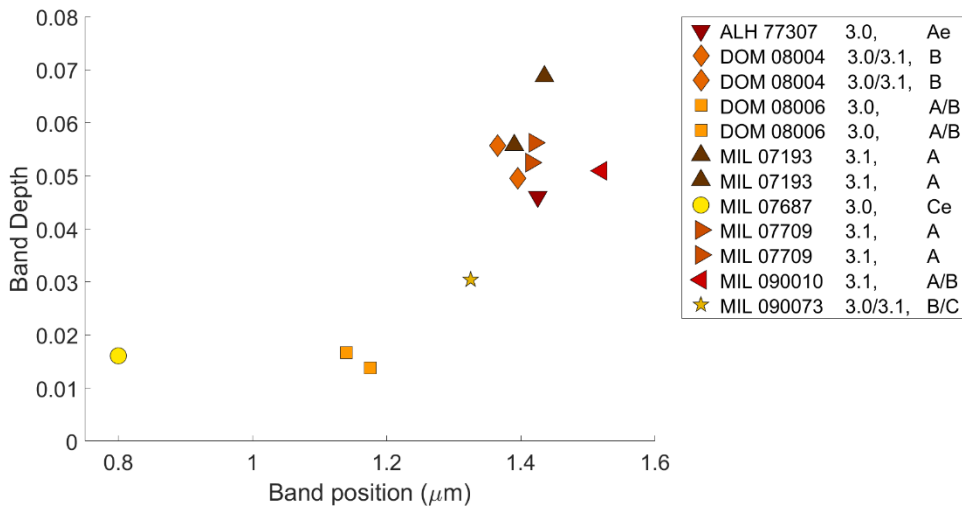
Minimally weathered low-metamorphic grade COs, with weathering grades A, A/B, or B, have a fairly flat slope (~1.1-1.2). Meteorites with more severe terrestrial weathering, grades B/C or Ce, have higher slope values indicating increased reddening.

The 1.4- μm feature in the low-metamorphic grade CO meteorites is qualitatively similar to features seen for certain natural and synthetic glasses (Cannon et al, 2017; Horgan, et al., 2014; Moroz et al., 2009). Generally, tektites, obsidians and other natural glasses exhibit a weak feature centered near 1.1-1.2- μm (Horgan et al., 2014). Fast-cooled synthetic glasses formed by rapid melting of JSC Mars-1 (an altered volcanic ash analogous to the Martian surface) show features that are similar in strength but at a shorter wavelength than the low-metamorphic grade CO meteorites (~1.2- μm for fast cooled synthetic glasses compared to 1.4- μm feature of the low-metamorphic grade COs). JSC Mars-1 has an iron content of 12-15 wt.%. Other studies (Cannon et al., 2017) have synthesized glasses with iron contents of ≤ 25 wt.% to simulate expected impact/volcanic glass compositions for Mars, the Moon and Mercury. The iron content of the synthetic glasses is lower than what is observed in the matrices of low-metamorphic grade CO meteorites which have

significantly higher iron contents (30-35 wt.% iron; Brearley, 1993). The near-infrared differences in wavelength between the low-metamorphic grade COs and natural/synthetic glasses may be attributable to the iron content of the CO meteorite samples. Since the amorphous matrix materials in these COs are olivine-normative, it is possible that the near-infrared spectral behavior will be similar to iron-rich olivines (Dyar et al., 1998). Fayalites have a $\sim 1\text{-}\mu\text{m}$ complex feature caused by three spin-allowed crystal field transitions of irons in the M1 and M2 sites (e.g., Burns and Huggins, 1972; Dyar et al., 2009). We suggest that since these amorphous silicates have olivine-normative compositions, the near-infrared spectral features for the pristine (minimally terrestrially weathered) low-metamorphic grade CO meteorites are caused by the amorphous iron-bearing silicate matrix materials, however more experiments are required to determine the exact cause of this feature.

Figure 3.4: Band position vs. band depth. Terrestrially weathered samples have weaker (smaller band depths) that are centered $\sim 1.2\text{-}\mu\text{m}$.

Minimally weathered low-metamorphic grade COs have bands around $1.4\text{-}\mu\text{m}$, with band depths of 5-7%. Color indicates the weathering grade, dark red symbols are less terrestrially weathered while lighter, yellow colors have more significant weathering.



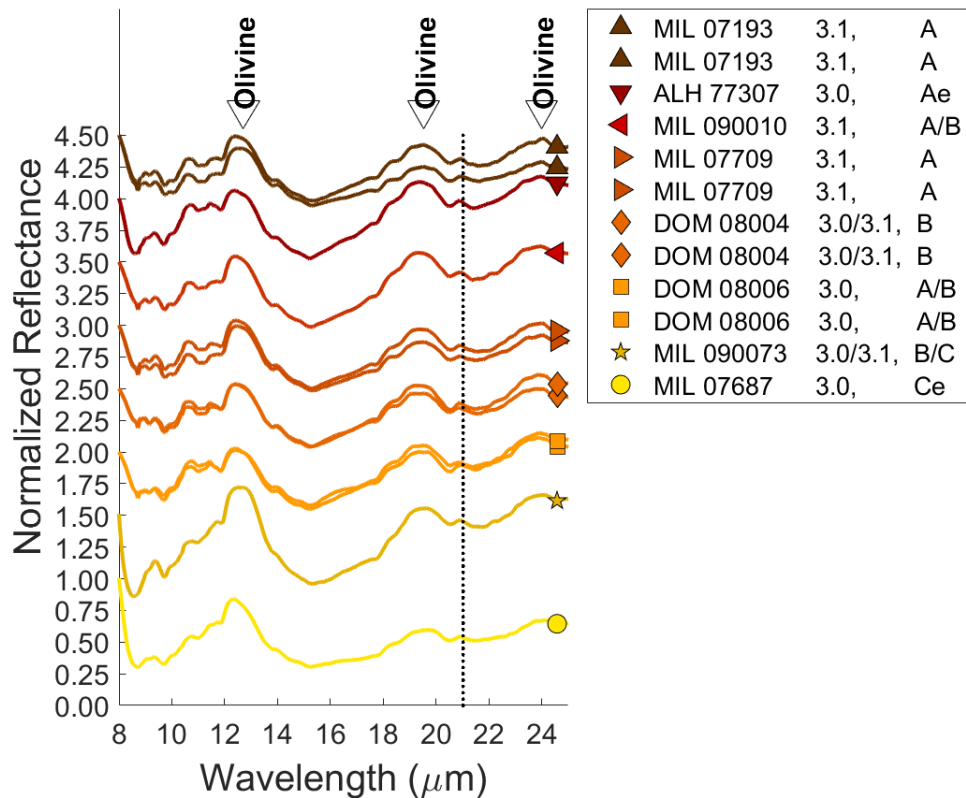


Figure 3.5: Mid-infrared spectra of low-metamorphic grade CO meteorites.

Normalized, offset data for eight CO meteorites ordered top to bottom by weathering grade (minimally terrestrially weathered samples at the top, more severely weathered samples at the bottom). Low-metamorphic grade CO meteorites exhibit strong features caused by olivine and pyroxenes in chondrules with features at ~ 12.7 , 19.5 - and 24 - μm . An additional feature at ~ 21 - μm is present in each spectrum. This is the Si-O vibration in the amorphous silicate matrix. Dashed lines indicate the positions of Si-O vibration in amorphous silicates and glasses.

3.4.2 Mid-infrared Results

In the mid-infrared (**Figure 3.5**), low-metamorphic grade CO meteorites exhibit features consistent with olivine and pyroxene in the chondrules, with strong absorption features centered at ~ 12.7 -, 24 - μm . Additional overlapping absorptions on the short-

wavelength side of the 12.7- μm feature are controlled by relative abundance of olivine and pyroxene. Some meteorites for which two samples are measured differ slightly primarily in slope (especially at long wavelengths). However, the positions of the features are the same. This is likely caused by differences in how the sample is placed in the sample dish (Salisbury and Eastes, 1985; Salisbury and Wald, 1992). Compared to the pristine low-metamorphic grade COs, terrestrially weathered samples have minor spectral differences in the mid-infrared wavelengths. MIL 090073 and MIL 07687 have a more extreme slope between 10- and 11.5- μm . However, the spectral features of olivine (12.7-, 19-, and 24- μm) and the 21- μm Si-O bending vibration are still apparent despite the weathering. In all of the spectra of the low-metamorphic grade COs, a feature can be seen at 21- μm that is attributable to Si-O bending vibrations in amorphous iron-bearing silicate matrix. This feature is ubiquitous and characteristic of low-metamorphic grade CO meteorites in this wavelength region.

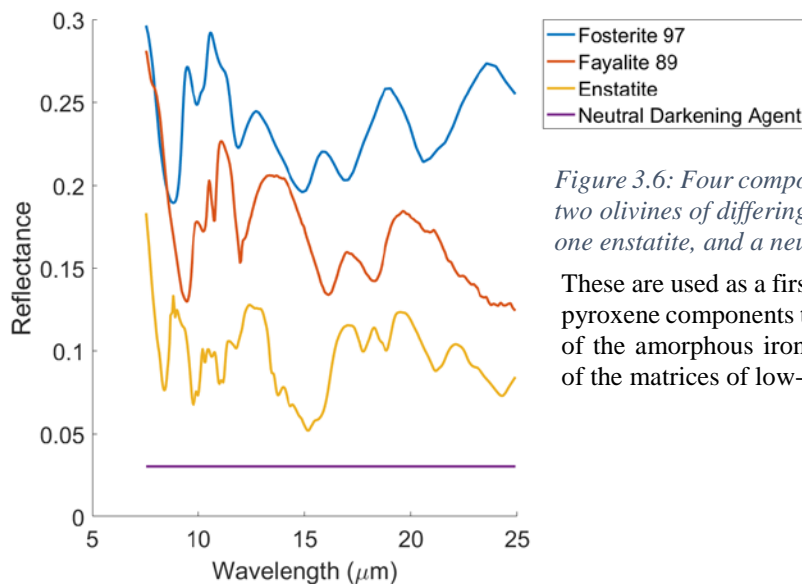


Figure 3.6: Four component spectra used for modeling: two olivines of differing iron content (Fo97 and Fo11), one enstatite, and a neutral darkening agent.

These are used as a first order model of the olivine and pyroxene components to enhance the spectral signature of the amorphous iron-bearing silicates characteristic of the matrices of low-metamorphic grade meteorites

To further examine the contribution of the amorphous matrix to the mid-infrared spectra, the crystalline component of each spectrum was approximated with a linear model (Thompson and Salisbury, 1993; Ramsey and Christensen, 1998) with four components (**Table 3.3**), including two olivines with different compositions (Fo97 and Fo11; Sunshine and Pieters, 1998), one enstatite (Bamble, Norway; MgSiO_3), and a neutral darkening agent. The standards used as model components have $<45\text{-}\mu\text{m}$ grain size and these data were also collected at RELAB. These components represent the approximate range of mafic minerals found in the low-metamorphic grade CO chondrules and lithic fragments (e.g., Davidson et al., 2013; Howard et al., 2014; 2015; **Table 3.2**). The neutral darkening agent is a constant that is used to lower the overall reflectance of a model. The component spectra are presented in **Figure 3.6**. Similar to previous spectral modeling efforts, these models rely on linear mixing of spectral component endmembers (e.g., Thompson and Salisbury, 1993; Ramsey and Christensen, 1998). Other mid-infrared spectral models used large databases of minerals to determine the relative abundances of minerals in a given spectrum. The spectral models presented here are a first order removal of the crystalline components of the meteorite spectra. The mid-infrared spectral models of the carbonaceous chondrites analyzed here are not intended to estimate modal mineralogies, but instead to broadly remove the crystalline components of the meteorites' spectra in order to emphasize the spectral features of the amorphous iron-bearing matrix. An example model fit to ALH 77307 is shown in **Figure 3.7**, along with the residual spectrum.

Table 3.3: Spectral Modeling Components

<i>Name</i>	<i>Mineral</i>	<i>Grainsize</i>	<i>Origin</i>	<i>References</i>
<i>Forsterite</i> 97	Mg-rich olivine	<45- μm	Cecchino, Rome, Italy	Sunshine and Pieters, 1998
<i>Fayalite</i> 89	Fe-rich olivine	<45- μm	Kiglipait intrusion.	Sunshine and Pieters, 1998; King and Ridley, 1987
<i>Enstatite</i>	Mg-rich pyroxene	<45- μm	Bamble, Norway	Sunshine and Pieters, 1998

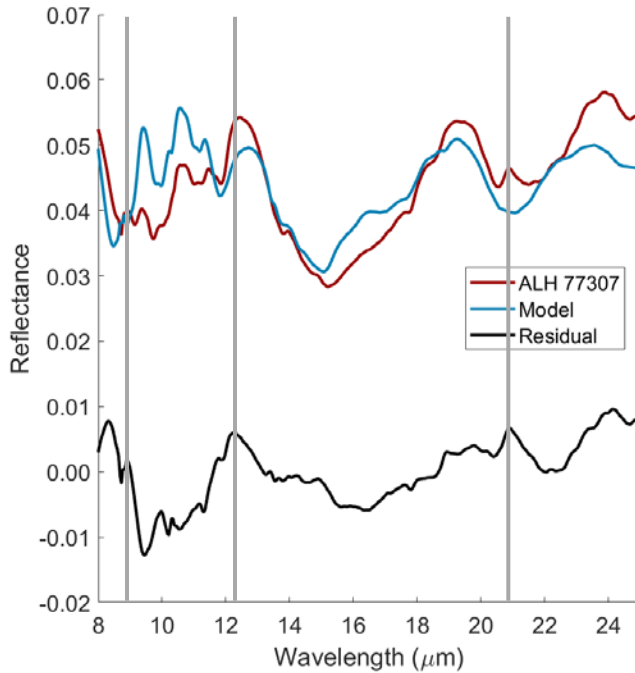


Figure 3.7: Example of mid-infrared spectral modeling.

The spectrum of ALH 77307 (red) is modeled using the non-negative linear least-squares approach with the four component spectra shown in Figure 6. The residual difference between the data (red) and the model (blue) is shown relative to zero error (bottom, black). Although the fit is poor in the region below 12 μm , the amorphous silicate features at 9.1-, 12.2-, and 21 μm are enhanced in the residual spectrum. The discrepancy between the model and data is due to the imperfect terrestrial analogs and non-linear mixing effects for the grain sizes of meteorite sample and modeling components.

The residual spectra for all low-metamorphic grade CO meteorites are presented in **Figure 3.8**. These residuals have two common characteristics: (1) all have negative residuals in the 8-11- μm region, and (2) all residuals exhibit positive features at ~9.1-, 12.2-

, and 21- μm . The negative residuals in the 8-11- μm region are caused by the model mineral spectra having significantly stronger features than the COs in this region. This may be caused by non-linear mixing in this spectral region, which can occur for samples with small grain sizes (e.g., <75- μm , Hunt and Vincent, 1968; Hunt and Logan, 1972; Salisbury et al., 1992; Salisbury and Eastes, 1985). The remaining features in the residuals (9.1-, 12.2-, and 21- μm) are caused by the absorptions of Si-O vibrations in the amorphous iron-bearing matrix. Qualitatively, these features are similar to the spectrum of condensed Fe/Mg-smokes (Hallenbeck et al, 2000; Hallenbeck et al., 1998; **Figure 3.8**). An example of the spectrum of a condensed Fe/Mg-smoke is shown in **Figure 3.8** (Hallenbeck et al, 1998). This material also has features at ~9.1- μm , a weak feature at 12.2- μm and a stronger 21- μm . The differences between the meteorite residuals and the Mg-smoke are the relative strengths of the vibrations and the slope at long-wavelengths. Since the matrix materials in the low-metamorphic grade COs do not have the same composition of the smokes, the vibration strengths and positions will be slightly different than the example presented. Additionally, the spectral model for the crystalline components is very simplistic and as a result the residual spectra almost certainly contain artifacts that contribute to the spectral discrepancies.

3.4.3 Comparison to metamorphosed COs

The secondary modification of the CO chondrites is dominated by the effects by thermal metamorphism on their parent body, however, the low-metamorphic grade COs have experienced only minimal heating, (~200-300°C). At the onset of metamorphism there was recrystallization of the amorphous matrix, followed by coarsening of the matrix,

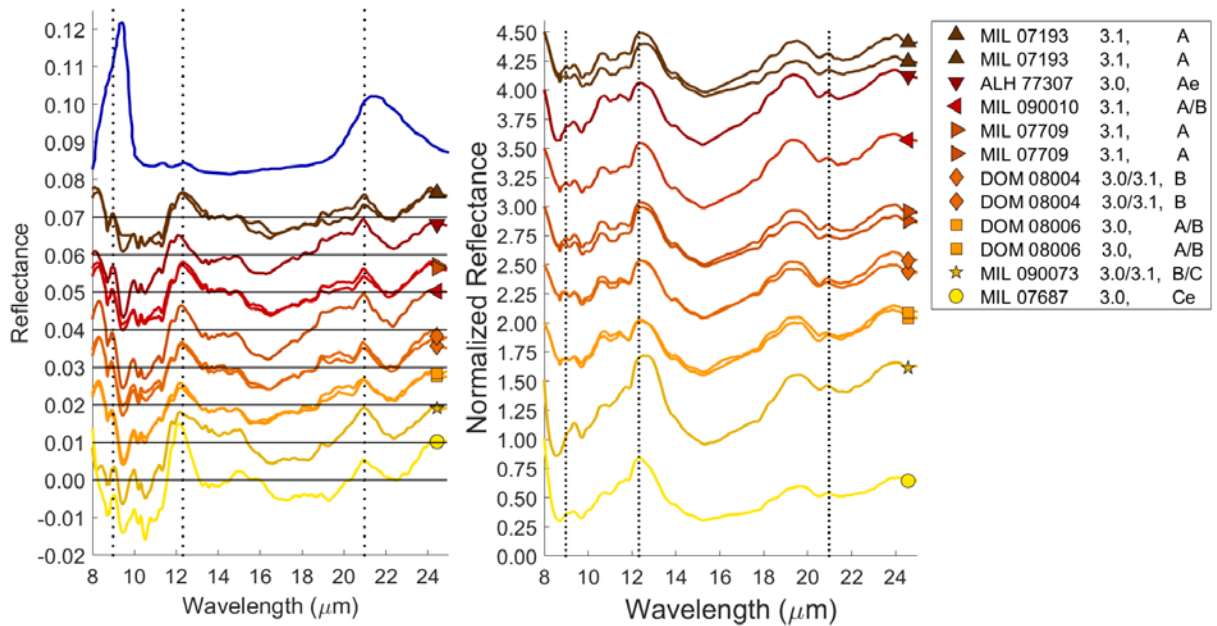


Figure 3.8: Residuals.

Residual spectra (after crystalline models are subtracted from data) for each of the low metamorphic grade CO meteorites. The positions of zero are indicated for each residual and are offset for clarity. They are ordered by weathering grade (pristine samples at the top). These first approximation models for the crystalline components poorly reproduce the 8-12 μm region where the residuals are consistently negative. However, these residual spectra show evidence for Si-O vibrations the 9.1-, 12.2-, and 21- μm as compared to the Fe-smoke (left, top blue curve), a laboratory condensate made of iron, silicon and oxygen (Hallenbeck et al, 1998). The low-metamorphic grade COs are qualitatively similar to the Fe-smokes. Differences in relative strengths of the Si-O vibrations is caused by the imperfect modeling techniques used and additionally, compositional differences exist between the Fe-smoke and the amorphous iron-bearing matrix silicates.

progressive equilibration between matrix and chondrule minerals, and recrystallization of the chondrule mesostasis. The maximum metamorphic temperatures experienced by any known members of the CO chemical group were $\sim 700^{\circ}\text{C}$ (McSween, 1977). These temperatures are high enough to recrystallize all amorphous material as well as equilibrate matrix and chondrule olivine compositions.

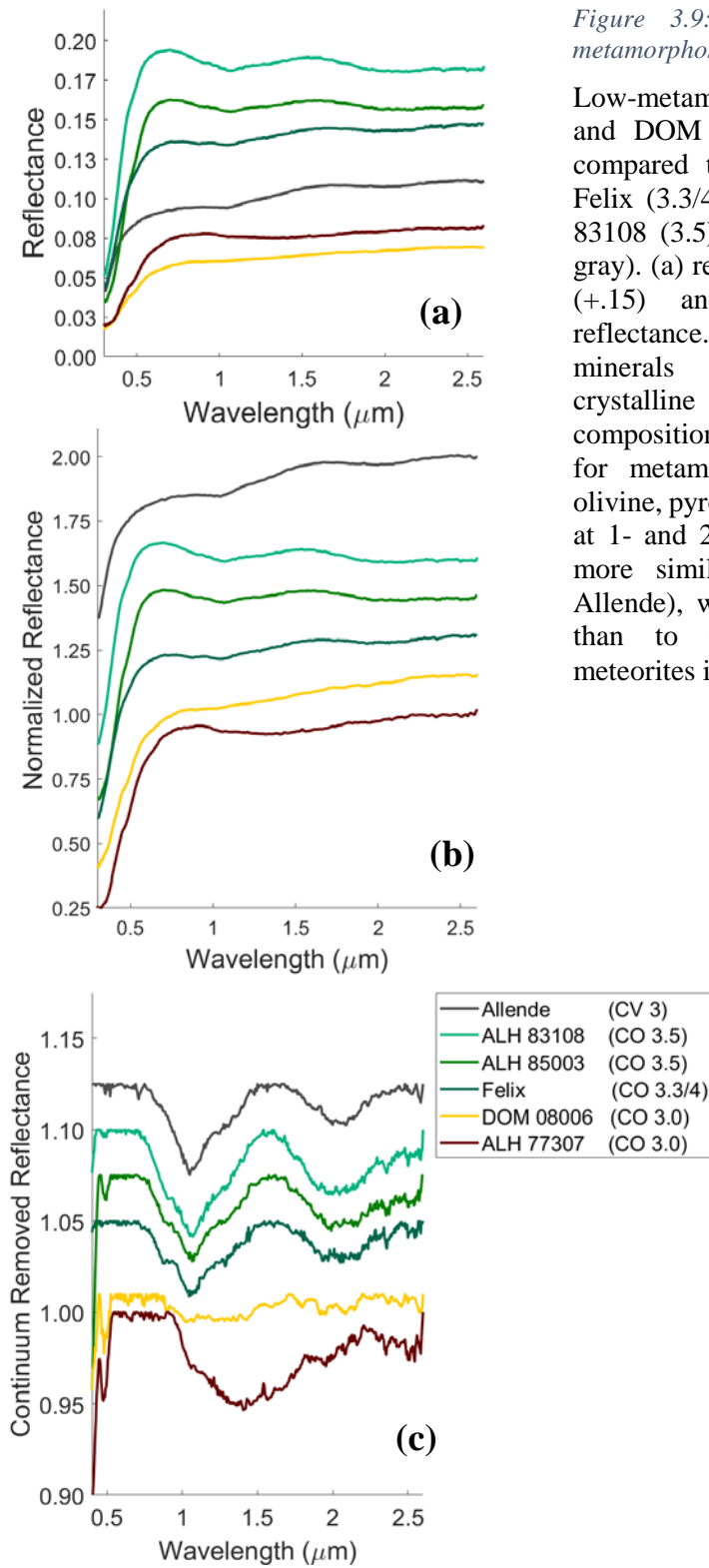


Figure 3.9: Near-infrared comparison to metamorphosed COs.

Low-metamorphic grade COs, ALH 77307 and DOM 08006 (red and yellow), are compared to three metamorphosed COs: Felix (3.3/4), ALH 85008 (3.5) and ALH 83108 (3.5), in green and Allende (CV3, gray). (a) reflectance, (b) normalized offset (+.15) and (c) continuum removed reflectance. During metamorphism, minerals equilibrate creating more crystalline olivine with homogenous composition. Features in the near-infrared for metamorphosed samples reflect the olivine, pyroxene composition with features at 1- and 2- μm . Metamorphosed COs are more similar to CV3 meteorites (e.g., Allende), which are also metamorphosed, than to the relatively less-processed meteorites in their own chemical group.

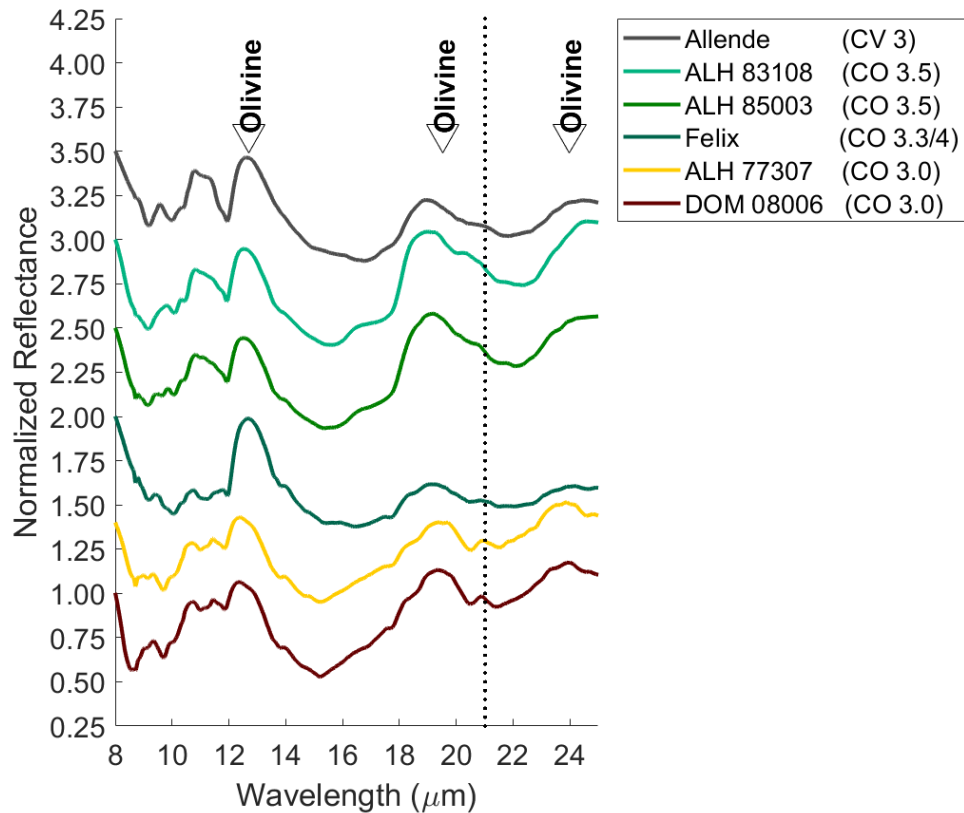


Figure 3.10: PSD-XRD Spectrum, model and residual for (a) ALH 77307 (CO 3.0), (b) DOM 08006 (CO 3.0), (c) Acfer 094 (CO 3.0) and (d) Felix (CO 3.3/3.4).

For ALH 77307, DOM 08006 and Acfer 094, crystallographic peaks in the X-ray patterns can be completely accounted for, however significant X-ray residuals remain. These X-ray counts are attributed to the poorly crystalline Fe-bearing matrix materials. Conversely, Felix has negligible amorphous materials; its spectrum can be completely modeled with crystalline standards without significant residuals. Felix has been heated to a higher peak temperature than DOM 08006, and ALH 77307 so the amorphous matrix materials have been recrystallized.

Felix is an example of a moderately metamorphosed CO. Its modal mineralogy, derived from PSD-XRD measurements, indicates that Felix has negligible amounts of amorphous material in its matrix and can be modeled using crystalline standards alone (see Section 3.2). Spectrally, this meteorite is significantly different from the low-metamorphic

grade COs, showing much stronger olivine features in the near- and mid-infrared spectral regions (**Figures 3.9 & 3.10**). Two higher metamorphic grade COs are also compared to low-metamorphic grade examples, ALH 85003 (CO 3.5), and ALH 83108 (CO 3.5). These samples were prepared similarly to the low-metamorphic grade COs and their spectra were also obtained at RELAB. ALH 85003 and ALH 83108 have been heated to higher peak temperatures than Felix and correspondingly exhibit stronger features caused by progressive increase in crystallinity and equilibration of crystalline phases, as well as further recrystallization of remaining chondrule mesostasis, during metamorphism. This has resulted in near-infrared features at 1- and 2- μm caused by equilibrated olivines. These features have replaced the 1.4- μm feature of the more primitive material. In the mid-infrared, mineralogical changes affect the spectra by increasing the strength of the ~12.7-19.5-, and 24- μm features. Additionally, this seems to significantly affect the 8-11- μm region where stronger olivine features appear. Carbonaceous chondrites in other heated groups, such as the CVs, contain similar minerals and have similar spectral features to the thermally metamorphosed CO meteorites. This is also shown in **Figures 3.9 & 3.10**, where the CV3 Allende is compared to the CO meteorites of various metamorphic grades.

3.4.4 Comparison to other 3.0 Carbonaceous Chondrites

Low-metamorphic grade meteorites are not limited to the CO chemical group. Several other meteorites have been reported to have amorphous matrices similar to what has been described in the low-metamorphic grade COs. Specifically, the CRs Meteorite Hills (MET) 00426 and Queen Alexandra Range (QUE) 99177 (Abreu and Brearley, 2010; Le Guillou and Brearley, 2014) and the ungrouped chondrite Acfer 094 (Greshake, 1997).

The CR chemical group of carbonaceous chondrites is characterized by aqueous alteration. The CR 3.0 meteorites may have experienced some interactions with water, however the amorphous phases are preserved in the CR 3.0 samples (e.g., Abreu and Brearley, 2010; Le Guillou and Brearley, 2014). These phases are preserved because conditions on the region of the parent body(s) prevented the formation of phyllosilicates since the interaction with water was minimal in these parent bodies/regions of parent bodies (Abreu and Brearley, 2010). Amorphous materials formed through disequilibrium condensation are also preserved in CM meteorites Paris and Y-791198 (Leroux et al., 2015; Chizmadia and Brearley, 2008). Unlike the CR 3.0, Paris and Y-791198 have evidence for extensive, but heterogeneous aqueous alteration (e.g. the presence of large abundances of phyllosilicates; e.g., Howard et al., 2011). This heterogeneity allowed some of the initially accreted amorphous materials to be preserved. In contrast to these CMs, the CR 3.0 meteorites, which do not show such extensive evidence for aqueous alteration, represent a parent body or region of a parent body that has undergone little change since the time of accretion. For this study, we confine ourselves to comparisons between the low metamorphic grade COs and these relatively less-processed 3.0 meteorites from the CR chemical group and Acfer 094. The CR 3.0s and Acfer 094 are similar to the low-metamorphic grade COs in terms of abundances of amorphous iron-bearing matrix silicates. The CM meteorites that an overall much smaller proportion of these phases.

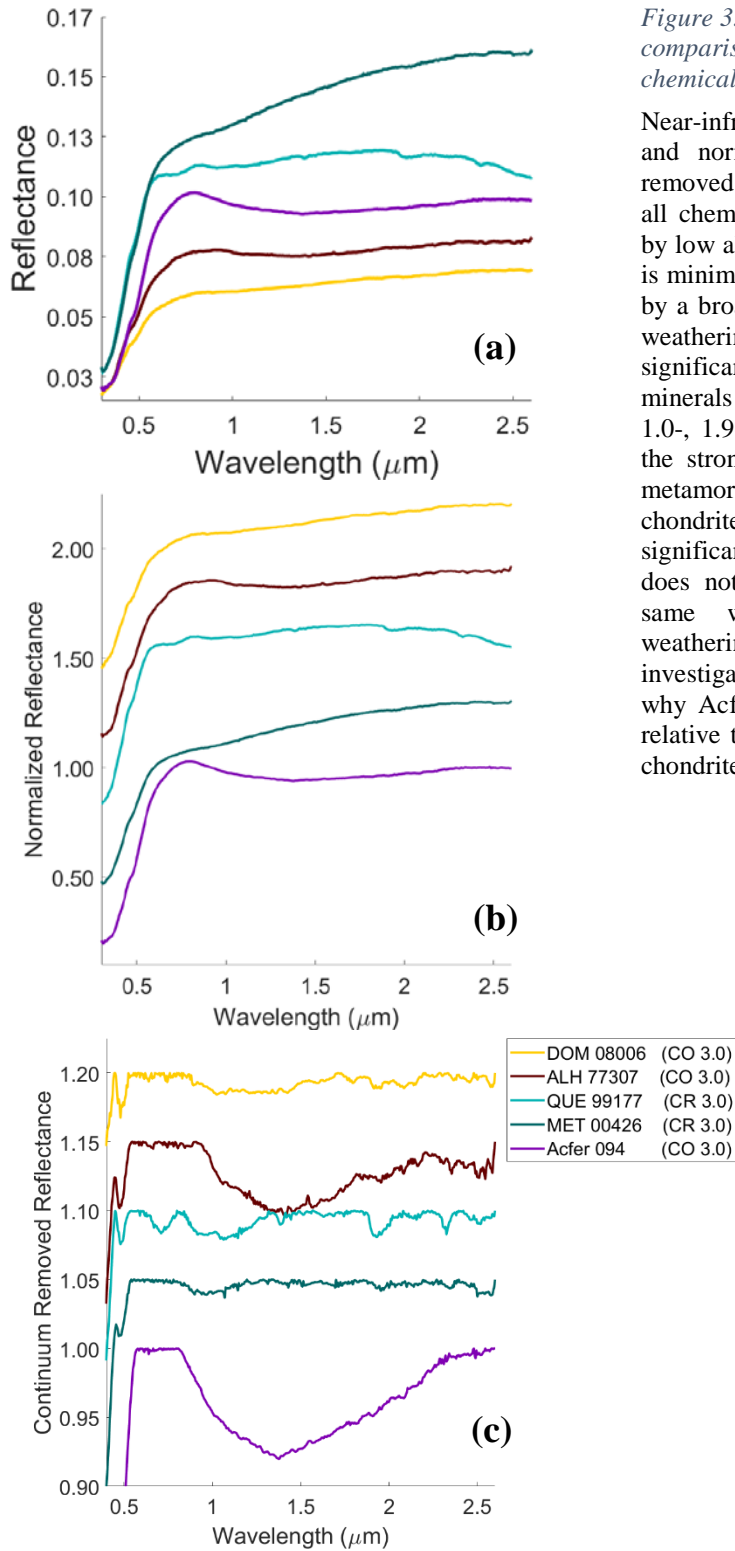


Figure 3.11: Near-infrared comparison to 3.0 meteorites in other chemical groups.

Near-infrared spectra (a), offset (+0.3) and normalized (b) and continuum removed (c) show that 3.0 meteorites of all chemical groups are characterized by low albedos, and where weathering is minimal, they are also characterized by a broad 1.4- μm feature. Terrestrial weathering affects the CRs significantly, with clay and evaporite minerals producing features at 0.7-, 1.0-, 1.9- and 2.4- μm . Acfer 094 has the strongest 1.4- μm of all the low-metamorphic grade carbonaceous chondrites studied. This sample has significant terrestrial weathering which does not affect the spectrum in the same way Antarctic terrestrially weathering affects the CR3.0s. Further investigation is required to determine why Acfer 094's feature is so strong relative to the other 3.0 carbonaceous chondrites.

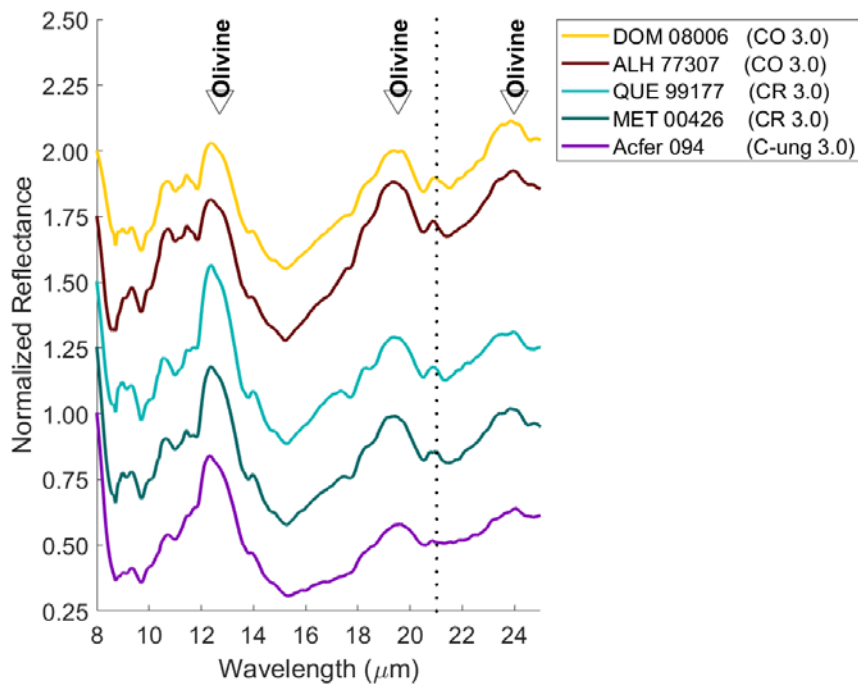


Figure 3.12: Mid-infrared comparison of the spectra of 3.0 meteorites in other chemical groups.

In the mid-infrared, the spectra of all low-metamorphic grade carbonaceous chondrites exhibit 12.7-, 19.5- and 24- μm features caused by the olivine and pyroxenes in their chondrules. Additionally, they all have the 21- μm produced by the Si-O bonds from their amorphous iron-bearing silicate matrices.

The CR samples have some terrestrial weathering and thus their near-infrared spectra are comparable to the weathered COs. Acfer 094 has a feature at $\sim 1.4\text{-}\mu\text{m}$ that is even deeper than what is observed in the low-metamorphic grade COs (**Figure 3.11**). However, this meteorite was found in the Sahara and is likely to be more weathered than the Antarctic COs and CRs presented here. Further investigation is required to understand why Acfer 094 does not have terrestrial alteration features similar to the CRs and the more weathered Antarctic CO meteorites presented here. Since Acfer 094 was found in the Sahara, the terrestrial weathering may be different (perhaps drier) than terrestrial

weathering of the Antarctic. In the mid-infrared, the CRs and Acfer 094 exhibit features caused by the Si-O vibrations produced by the amorphous iron-bearing silicates characteristic in these low-metamorphic grade samples (**Figure 3.12**). This comparison indicates that the 21- μm feature is indicative of the presence of amorphous iron-bearing phases. The presence of these materials indicates the asteroid/meteorite underwent minimal processing (potentially some interactions with water or heating to 200-300°C) and therefore record information about the composition and nebular processes at early Solar System times.

3.5 Evidence for Amorphous Material on Asteroids

There is evidence for the presence of amorphous materials on at least one asteroid: (93) Minerva. The spectrum of Minerva collected with SpeX at the NASA's Infrared Telescope Facility (IRTF) is shown in **Figure 3.13**. The near infrared data from SpeX is scaled to the visible data from the Small Main-Belt Asteroid Spectroscopic Survey (Xu et al., 1995; Bus and Binzel, 2002; normalized at 0.55- μm) to produce the final spectrum. SpeX is a medium resolution cryogenic instrument (Rayner et al., 2003), which has been used to observe a large number of asteroids in the near-infrared (e.g., DeMeo et al., 2009; Clark et al., 2010). Observational circumstances and the standard stars used during those observations are listed in **Table 3.4**. The spectrum of Minerva shown in **Figure 3.13** is normalized to unity at 2.4- μm and compared to DOM 08004 (CO 3.0/3.1; normalized to unity at 2.4- μm ; Minerva data is offset by +0.75). Spectrally classified as a C-type (Xu et al., 1995; Bus and Binzel, 2002), Minerva's overall low albedo (0.062 +/- 0.015; Marchis

et al., 2013) and broad $\sim 1.4\text{-}\mu\text{m}$ feature are very similar to low-metamorphic grade COs. Although some asteroids, which are thought to be related to angrite meteorites (clinopyroxene dominated achondritic meteorites; Burbine et al., 2006), have some similarities to Minerva and the low-metamorphic grade COs, they have much stronger features ($\sim 15\%$) and much higher albedos. Based on the presence and similarity of the $1.4\text{-}\mu\text{m}$ feature and its low albedo, Minerva is interpreted to be compositionally similar to the low-metamorphic grade meteorites.

Table 3.4: Minerva Observations

<i>Asteroid</i>	<i>Date (UT)</i>	<i>Start Time (UT)</i>	<i>End Time (UT)</i>	<i>Int. (Min)</i>	<i>Airmass</i>	<i>Standard</i>
(93) Minerva	2003-04- 27	08:31:05	08:59:29	18.0	1.132- 1.137	Landolt (SA) 107-684, Landolt (SA) 107-998

Minerva is a triple system, with two satellites that likely formed as a result of a recent collision (Marchis et al., 2013; Yang et al., 2016). Detailed observations of this system constrain the physical properties of Minerva (e.g., Marchis et al., 2013; Yang et al., 2012). These are presented in **Table 3.5**. The satellites appear spectrally similar to the primary in the visible and near-infrared (Yang et al, 2016), however these measurements are difficult to make and heavily affected by the image processing to remove the signal of the primary. Furthermore, these observations have significant atmospheric absorption between $1.3\text{-}1.5\text{-}\mu\text{m}$ so that the $1.4\text{-}\mu\text{m}$ feature cannot be detected.

Table 3.5: Physical Properties of Minerva System

<i>Asteroid</i>	<i>Albedo</i>	<i>Diameter</i>	<i>Mass</i>	<i>Bulk Density</i>
(93) Minerva ¹	0.062 +/- 0.013	154 +/- 6 km	3.35 +/- 0.54 x 10 ¹⁸ kg	1.75 g/cm ³
(I) Aegis ²	0.062 +/- 0.013*	4.3 +/- 1.5 km	-	-
(II) Gorgoneion ²	0.062 +/- 0.013*	3.6 +/- 1.0 km	-	-

*assumed from Marchis et al., 2013.

¹Marchis et al., 2013

²Yang et al., 2016.

The impact that created the satellites likely occurred relatively recently, ~1 billion years ago, based on estimates on the rigidity of the primary and the specific tidal dissipation (Marchis et al., 2013; Yang et al., 2016). However, this system may be older if it experienced non-tidal effects such as gravitational interactions with other asteroids or late-inward migration of Jupiter (Marchis et al., 2013). The satellite-creating impact likely caused Minerva to have significant macro-porosity (Marchis et al., 2013) that lowers the bulk-density of the asteroid. Furthermore, this impact was probably large enough to resurface part or all of the asteroid, removing any effects of surface processing (e.g., Thomas and Robinson, 2005). C-type asteroids are not strongly affected by optical and near-infrared spectral changes due to space weathering (e.g., Clark et al., 2002; Lantz et al., 2015). Furthermore, our observations of Minerva are hemispherically averaged. The presence of a 1.4- μ m band therefore implies that Minerva's surface contains a significant amount of amorphous material over a large fraction of the asteroid. Marchis et al., (2013) also report IRTF+SpeX observations of Minerva. These data are similar to our observations

in albedo, but the Marchis spectrum does not appear to have a 1.4- μm feature. This may indicate some heterogeneity for Minerva, perhaps related to its impact history.

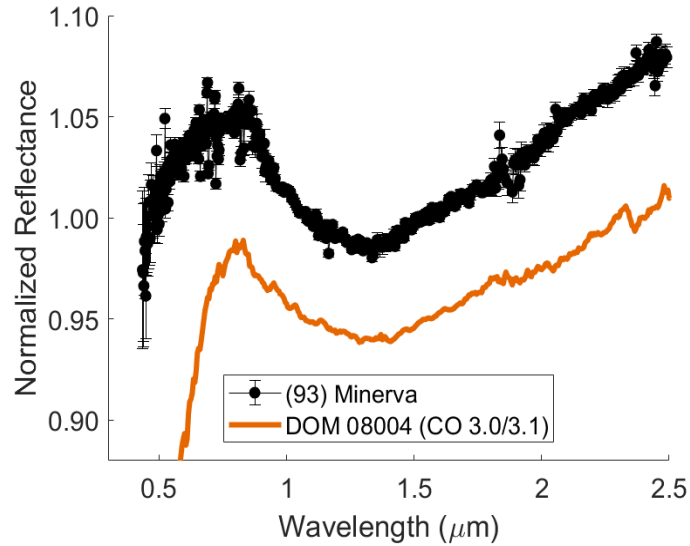


Figure 3.13: *SPeX* observation of 93 Minerva (offset +0.75) compared to low-metamorphic grade CO, DOM 08004 (CO 3.0/3.1).

The similarity between the shape and position of the 1.4- μm and similar low albedo indicates that amorphous materials may be abundant on the surface of Minerva. Minerva is the best candidate for follow up observations in the mid-infrared to confirm the presence of amorphous iron bearing silicates.

In order to preserve a significant amount of amorphous iron-bearing phases on Minerva it must not have experienced significant heating, which is possible if the asteroid accreted late or the amorphous materials are part of an outer, unprocessed shell unaffected by interior heating. In the late accretion scenario, Minerva likely accreted ~ 4 Ma after CAI formation (Sugiura and Fujiya. 2014), missing the peak heat flux from ^{26}Al . Without significant heating, the asteroid would have escaped all but the mildest thermal metamorphism, and it is likely that the interior mineralogy is similar to the surficial

mineralogy. In the alternative case, this CO-like parent body may have undergone interior heating, with increasing thermal metamorphism with increasing depth (e.g., onion-shell model; Taylor et al., 1987; Huss et al., 2006). In this case, the outer layers of the parent body experienced minimal heating (200-250°C; e.g., Bonal et al., 2016). The major impact that created the satellites may have resurfaced the asteroid and created macro-porosity, but left these outer layers largely intact. It may be possible to distinguish between these scenarios using rotationally resolved spectroscopy of Minerva. Large, recent impacts may excavate materials from depth on to the surface of the asteroid (e.g., Binzel et al, 1997). If these interior materials have spectral signatures of thermal metamorphism, the onion-shell model would be confirmed. If there are no rotational heterogeneities, the late-accretion model best matches Minerva's history.

While Minerva appears to be related to the low-metamorphic grade CO meteorites, other asteroids have been suggested to be related to the more extensively thermally metamorphosed CO meteorites. In particular, two K-type asteroids (221) Eos and (653) Berenike have been reported to have near-infrared spectral features similar to those of the thermally metamorphosed CO, Warrenton (CO 3.7; Burbine et al, 2001). However, while Eos and Berenike are dynamically related near 3.0 AU, Minerva's semi-major axis at ~2.7 AU indicates that it is a distinct body. Thus while there may be some compositional evidence suggesting CO meteorites could originate from a single, distributed parent body (e.g., Weisberg et al., 2006), it's clear from observations of the asteroid belt that at least some low- and high-metamorphic distinct CO-like asteroids exist. If the CO meteorites are

from multiple parent bodies, Minerva may represent a parent body for less-processed samples while Eos and Berenike represent thermally evolved parent bodies.

It is also possible that Minerva is related to other carbonaceous chondrites that preserve amorphous iron-bearing silicates. The early stages of aqueous alteration may preserve some amorphous silicates and pre-alteration textures, which has been observed for the CM meteorites Paris and Yamato-791198, and CR 3.0 meteorites (Leroux et al, 2015; Chizmadia and Brearley, 2008; Abreu and Brearley, 2010). A few ordinary chondrites (e.g., Semarkona and Bishunpur) also have amorphous phases, in their matrices (Alexander et al., 1989; Dobirca and Brearley, 2011), but since matrix makes up much smaller volume fractions in the ordinary chondrites than in CM, CO and CR chondrites the amorphous material is unlikely to produce strong features in their spectra. Paris, Yamato-791198 Paris, Yamato-799198 and more aqueously altered CRs (e.g., Howard et al., 2015b), are characterized by the presence of large volumes of phyllosilicates produced during aqueous alteration that have strong mid-infrared spectral features (McAdam et al., 2015a, b; Chapter 2). Furthermore, thermally metamorphosed carbonaceous chondrites (e.g., thermally metamorphosed COs and CVs) lose the characteristic 21- μm feature, while strengthening olivine features in the mid-infrared (McAdam et al, 2015b; Chapter 2). Therefore using rotationally resolved, mid-infrared observations of asteroids, including Minerva, it will be possible to distinguish between a CM/CR, aqueously altered mineralogy, a CO, thermally metamorphosed mineralogy or a rotationally homogenous body that accreted late.

The target asteroids of the on-going sample return missions OSIRIS-REx and Hayabusa-2, (101955) Bennu and (162173) Ryugu, will soon become the standards of comparison for low-albedo asteroids. Based on the presence of the 0.7- μm feature (Vilas, 2008) Ryugu appears to be an aqueously altered asteroid and so it is unlikely to have significant amorphous materials on its surface. The spectrum of Bennu does not have either the 1.4- μm feature or 21- μm and therefore Bennu does not appear to have amorphous-iron bearing silicates on its surface. Mid-infrared observations of Bennu did not have sufficient signal-to-noise to detect the 21- μm , Si-O feature (Emery et al., 2014). However, the vastly improved spatial resolution of the upcoming orbital observations of Bennu will help determine if Bennu contains amorphous silicates.

In addition to the sample return missions to asteroids, the upcoming James Webb Space Telescope (JWST) will have both near- and mid-infrared instruments capable of observing asteroids. The Mid-Infrared Instrument (MIRI) has spectral coverage from 5-28- μm with medium-high resolution. The resolving power ($\lambda/\Delta\lambda$) of this spectral mode is ~1550-3250 (Swinyard et al, 2004; Wells et al, 2015). This resolving power is somewhat high to determine the surface mineralogy of Minerva or other asteroids. As a consequence, longer integration times will be required to obtain sufficient signal-to-noise to determine mineralogy. However, binning the data to resolution of ~500 or less should allow the identification of mineralogy including the presence of the 21- μm feature indicative of amorphous iron-bearing silicates. The signal-to-noise ratio (SNR) requirements for observing the diagnostic feature of amorphous materials at 21- μm are estimated by resampling the laboratory spectra of CO meteorites to spectral resolution ~500, then adding

noise to that spectrum and determining empirically the minimum signal-to-noise where the 21- μm feature is detectable. We find that a SNR of ~ 50 could allow a marginal detection (e.g., **Figure 3.14**). A detection can be reliably made, however, with a SNR of ~ 100 .

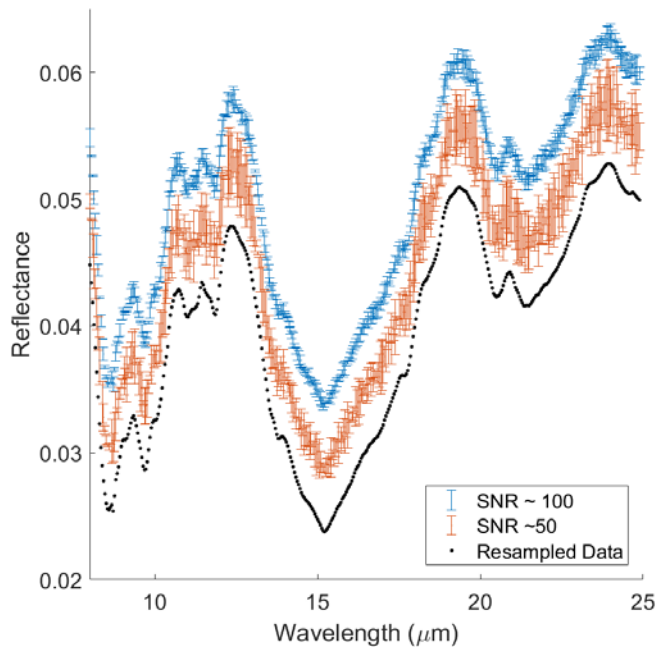


Figure 3.14: SNR test.

To estimate the minimum required SNR to detect the 21- μm feature, Gaussian distributed noise is added to laboratory data that has been resampled $R \sim 200$. We find that a SNR of ~ 50 could produce a marginal detection, if binning is employed, however, a SNR ~ 100 or greater would ensure a detection. We suggest a minimum SNR of ~ 100 to detect this material on the surface of an asteroid.

3.6 Conclusions

Carbonaceous chondrites that have experienced little thermal processing are characterized by amorphous iron bearing silicates in their interchondrule matrices and chondrule rims. The low-metamorphic grade meteorites occur in several chemical groups, particularly among CO meteorites. We have presented visible/near-infrared and mid-infrared spectroscopy of a suite of 8 such low-metamorphic grade COs. Previous near-infrared spectral studies of ALH 77307 reported the presence of a $\sim 1.3\text{-}\mu\text{m}$ feature that was

attributed to the iron-bearing amorphous silicates (Cloutis et al., 2012). We find that this spectral feature, centered at 1.4- μm in our analysis, is characteristic of all low-metamorphic grade CO meteorites that have had relatively minor terrestrial weathering. Additionally, we present for the first time mid-infrared spectroscopy for low-metamorphic grade CO meteorites. In the mid-infrared, low-metamorphic grade COs are characterized by chondrule olivines and pyroxenes. However, an additional feature at 21- μm is present in the spectra of all low-metamorphic grade COs. This 21- μm feature is caused by the Si-O vibrations of the amorphous iron bearing silicate matrix in these samples. This is the first mid-infrared spectral evidence of amorphous material reported for any low-metamorphic grade carbonaceous chondrite. Upon modeling the crystalline spectral component of these data, additional spectral features at 9.1 and 12.2- μm are revealed. All of these mid-infrared spectral features, 9.1, 12.2 and 21- μm , are caused by the amorphous iron-bearing silicate materials in the matrix and are qualitatively similar to those seen in synthetic glasses.

We also present the near- and mid-infrared spectra of two CR 3.0s, MET 00426 and QUE 99177 and Acfer 094 an ungrouped carbonaceous chondrite. We find that all low-metamorphic grade carbonaceous chondrites, regardless of chemical group, exhibit similar spectral features in the near- and mid-infrared; specifically they all exhibit at 1.4- and a characteristic 21- μm features.

Finally, we present visible and near-infrared spectrum of asteroid (93) Minerva. The primary asteroid of this triple system is low in albedo and spectrally similar in the 1.4- μm region to the low-metamorphic grade COs. We interpret Minerva to have a fresh surface dominated by amorphous iron-bearing silicates exposed after a relatively recent (~

1 Ga) impact event. Amorphous iron-rich materials on Minerva's surface could be preserved in one of two ways, either Minerva is an asteroid that accreted late, escaping extensive heating from short-lived radioactive nuclei and therefore the surface mineralogy is representative of the entire asteroid, or Minerva has an onion-shell layers that have increasing thermal metamorphism with increasing depth. In this latter case, the outer layers of the asteroid experienced less heating than interior layers and the amorphous materials are preserved. Using rotationally resolved spectroscopy, especially in the mid-infrared, it may be possible to distinguish between these scenarios. JWST and the MIRI instrument will be able to help constrain the history of Minerva and similar asteroids related to the low metamorphic grade CO meteorites. A reliable detection of the 21- μm feature can be made with an SNR of ~ 100 if binning of the 5-28- μm region is employed.

The preservation of amorphous materials on the surface of Minerva and potentially other asteroids provide strong evidence that they have experienced minimal heating and aqueous alteration. Thus, asteroids rich in amorphous materials provide a unique window into the earliest epochs of the Solar System, prior to the onset of parent body processing, and offer an opportunity to explore the compositions and physical processes that occurred in nebula and early accretionary phases of asteroid formation.

Acknowledgements:

Spectra were acquired using the NASA Keck RELAB, a multiuser facility at Brown University. The efforts of Dr. T. Hiroi, who collected the RELAB spectra on our behalf, are greatly appreciated. This research is funded by the NASA Earth and Space Sciences Fellowship and by NASA Cosmochemistry grant NNX11AG27G.

Chapter 4: Mid-Infrared Observations of Main Belt Asteroids: Widespread Appearance of Hydrated Minerals and Variable Degrees of Alteration of Asteroids

Abstract

While hydrated minerals have been observed on asteroids using visible/near-infrared spectroscopy, it has not been possible to constrain the amount of hydrated minerals using these wavelength regions. We present mid-infrared spectra of 73 asteroids, determining their degree of alteration using the mid-infrared emissivity features as a trace of degree of alteration. The mid-infrared spectral region, particularly in the 10-13- μm region, is diagnostic of degree of alteration. We find that aqueous alteration is widespread in the main asteroid belt. No relationship is found between degree of alteration and heliocentric distance, which contrasts with stratification of taxonomic types and the apparent relationship between 3- μm morphology and heliocentric distance previously noted using visible and near-infrared studies (e.g., Takir and Emery, 2012; Fornaiser et al., 2014). Furthermore, asteroids may be hydrated to any degree regardless of their spectral type, albedo or diameter. Asteroids with known hydration either from the 0.7- μm or 3- μm feature are shown to have have variable degrees of alteration. Asteroids that have water-ice on their surfaces also have evidence for hydrated minerals on their surfaces as well. Previously, hydrated minerals and water ice have not been observed on the same objects. Since the 3- μm region and the mid-infrared observations probe different depths into the surface, it appears that the water-ice is confined to the upper few microns of the asteroids

while hydrated minerals are found at ~10- μm depths. The Themis family appears to contain variable degrees of alteration, which may be related to secondary aqueous alteration caused by the impact that disrupted the parent body or heterogeneous alteration on the parent b Ceres and Hygiea, two of the largest asteroid in the main asteroid belt, are shown to have different degrees of alteration (less and highly altered respectively). The difference between Ceres and Hygiea in estimated degree of alteration and the presence of large abundances of hydrated minerals on both asteroids suggest that newer models of aqueous alteration on asteroids such as the mud ball model (Bland et al., 2017), may more accurately reflect the process of aqueous alteration on asteroids.

The implication of these results is that the disk temperatures at the time of aqueously altered asteroid accretion must have been low enough for a substantial abundance of water ice to be present between 2 and 5 AU. Since the accretion ages for carbonaceous chondrites are well known (Fujiya et al., 2013; Sugiura and Fujiya, 2014), the change in disk temperatures can be timed. Anhydrous carbonaceous chondrite meteorites (or meteorites that accreted with only small amounts of water) accreted slightly before aqueously altered carbonaceous chondrites (~2.7 Ma post CAI formation compared to 3-4 Ma post-CAIs). This indicates that the disk temperatures were dropping at ~2.7 Ma post-CAIs and were cool enough for water ice to be present by at least 3-4 Ma post-CAIs while the parent bodies of aqueously altered asteroids were accreting. Furthermore, the disk must have been locally heterogeneous in water ice since asteroids of all sizes may be variously altered. These local heterogeneities could give rise to the variability observed.

4.1 Introduction

The meteorite record indicates that water was a significant component of the protoplanetary disk especially when carbonaceous chondrite meteorites (which may have very extensive aqueous alteration) were accreting. Even the ordinary chondrite Semarkona, the most pristine sample of the early solar nebula, has evidence of coaccreted water (e.g., Alexander et al., 1989). The timing of the availability of water-ice for accretion, the distribution of water ice in the solar nebula and the abundance of coaccreted water into parent asteroids are still significant open questions for our understanding of the history of the early Solar System. Studies of meteorites have provided significant insights and constraints onto setting and timing of alteration on asteroids, however to more fully understand the geologic context of alteration and distribution of water, observations of asteroids are required.

The degree to which an asteroid/meteorite is altered (measured by the amount of hydrated minerals present) is controlled by the abundance of initially accreted water ice, the internal distribution of that water within the parent body and the internal thermal evolution of the parent body. Parent bodies that accreted in a region of the nebula with more water ice may have a higher degree of alteration since they have more water to react with the initially accreted silicates. Additionally, the degree of alteration may also be controlled by the reservoir of material that the asteroids/meteorites accretion. For example, recent geochemical studies of meteorites indicate that carbonaceous chondrites as a class have unique isotope signatures (e.g., Warren, 2011) suggesting these bodies accreted from

a chemically unique reservoir of material. The location of this reservoir in the disk may be related to distance from the Sun (e.g., Warren, 2011). The degree is likely controlled by the internal distribution of water and the internal thermal evolution of the parent asteroid. A parent body with a heterogeneous internal distribution of water, for example, could experience variable degrees of alteration in different regions of the body (e.g., Benedix et al., 2003). Additionally, the degree of alteration of asteroids is related to the setting of the alteration. Parent asteroids that aqueously alter in a closed setting (e.g., the CI meteorites; Brearley, 2006) likely react all of the initially accreted water with silicates. If aqueous alteration occurs in an open system (e.g., Young et al., 1999, 2003), some of the initially accreted water may escape the system, stopping reaction from continuing. Open-system aqueous alteration has been suggested as a mechanism that could create the wide variability of degrees of alteration for the CM meteorites (e.g., McSween, 1979). To disentangle this complexity (heterogeneous parent body alteration; initially accreted water abundance; open vs. closed system setting), missions to aqueously altered main belt asteroids are likely needed. However, Earth and space-based observations of asteroids may provide some insights into these complexities.

The goal of this chapter is to investigate the large scale distribution of aqueously altered asteroids. These results may provide some insights into the amount of water available for accretion at early Solar System times, the setting of alteration by investigating the size distribution of hydrated asteroids and the internal heterogeneity of water by observing asteroid families. The tool used to identify hydrated minerals on the surfaces of asteroids is mid-infrared spectroscopy. In a coordinated spectral-mineralogical study

(McAdam et al., 2015a, b; Chapter 2), mid-infrared spectral features are shown to change continuously with degree of alteration or amount of hydrated minerals present. The mid-infrared is a tool for identifying the degree of alteration not simply the presence of hydrated minerals.

4.2 Background

4.2.1 Spectral Signature of Aqueous Alteration in Carbonaceous Chondrites

CM, CI and CR carbonaceous chondrites have experienced extensive aqueous alteration (e.g., McSween, 1979; Bunch and Change, 1980; Howard et al., 2009, 2010, 2015). Aqueous alteration converts silicate minerals into phyllosilicates, referred to here as hydrated minerals. The setting of alteration, distribution of water in a parent body and initially accreted water abundance control the degree to which an asteroid/meteorite is altered. While different groups of aqueously altered meteorites may have different settings of aqueous alteration (closed vs. open settings), aqueous alteration appears to be acting on their parent asteroids concurrently (Fujiya et al., 2013). Similarly, carbonaceous chondrite parent asteroids have similar accretion ages (e.g. Sugiura and Fujiya, 2014). Internal thermal evolution models of aqueously altered asteroids suggest that highly altered, closed-system alteration affect asteroids of ~80 km diameter or smaller (Young et al., 1999, 2003). Larger asteroids may have convective flow of liquid water due to gravitational instabilities (Young et al., 1999, 2003). This may result in the release of the water if reaches the surface (e.g., Young et al., 1999, 2003).

The systematic mineralogical changes associated with aqueous alteration can be measured using Position Sensitive X-ray diffraction (PSD-XRD) techniques. These studies use bulk meteorite powders and measure the volume of minerals in a given sample (e.g., Howard et al., 2009, 2010, 2015). Petrologic type 1 meteorites are the most extensively aqueously altered meteorites. The CI, CM and CR chemical groups have examples of type-1 meteorites. The mineralogy of these samples is dominated by hydrated minerals (>80 vol.%). The CM chemical group has highly variable degrees of aqueous alteration, with as little as 60 vol.% hydrated minerals. Aqueous alteration appears to be highly variable for CM meteorites. Two samples, Paris and Yamato-791198, have been extensively aqueously altered but also preserve amorphous materials similar to what has been found in low-metamorphic grade CRs and COs that have experienced minimal parent body processing (e.g., Chizmadia and Brearley, 2008; Leroux et al., 2015). This suggests heterogeneity of alteration within the parent asteroids. Even for samples such as Yamato-791198, the bulk mineralogy of CMs tends to be ~60 vol.% hydrated minerals or greater (e.g., Howard et al., 2011). The CR meteorites also exhibit highly heterogeneous alteration. CRs Meteorite Hills (MET) 00426 and Queen Alexandra Range (QUE) 99177 have experienced only minimal interactions with water, preserving amorphous nebular materials (e.g., Abreu and Brearley, 2010) while Grosvener Mountains (GRO) 95577 exhibits extensive aqueous alteration with a hydrated mineral fraction (abundance of hydrated minerals over total silicates) of 0.89, similar to the CIs and CM1s (Howard et al., 2015). Other carbonaceous chondrites have experienced only minimal interactions with water. These meteorites include the Vigarano-like (CV) and Ornans-like (CO) chemical groups. There is some

evidence to suggest that the CVs may have coaccreted with some water ice (e.g., Weisberg et al., 2006), however the CVs and COs are generally characterized by thermal metamorphism.

Studying a suite of aqueously altered meteorites using spectroscopy (McAdam et al., 2015a, b; Chapter 2) that were previously analyzed using PSD-XRD methods, we have found continuous mid-infrared spectral changes that vary with degree of alteration. These meteorites can be generally spectrally classified into three groups (**Figure 4.1**): highly altered, intermediately altered and less altered. The highly altered meteorites are characterized by 80-90 vol.% hydrated minerals and have spectral features controlled by those hydrated minerals at 11.5, 16 and 21- μm . Intermediately altered meteorites have 75-80% hydrated minerals. These have a doublet with absorptions at 11.5 and 12.3- μm with a weak 19.5- μm feature that may or may not be present. Less altered meteorites have 60-75% hydrated minerals and ~25-30% anhydrous minerals (primarily olivine). These meteorites have a feature at 12.3- μm and 19.5- μm . These features are controlled by the olivine which is relatively abundant in these meteorites. Meteorites that do not have extensive alteration, such as the CVs, are spectrally distinct from the aqueously altered meteorites. The mineralogy of CVs is dominated by olivine (up to ~85 vol.%). While the less altered meteorites may have significant olivine their mid-infrared spectral features are considerably modified by the hydrated minerals present. The CVs show stronger olivine features at ~12.7 and 19.5- μm . The spectral characteristics are summarized in **Figure 4.1** and their mineralogy in **Table 4.1**. Identifying these spectral features on the surfaces of asteroids would allow us to estimate the asteroid's degree of alteration at its surface.

Table 4.1: Summary of Meteorite Mineralogy (adapted from Howard et al., 2009; 2010; 2011; 2015).

<i>Spectral Groups</i>	<i>Total olivine range (vol. %)</i>	<i>Total Anhydrous range (vol. %)</i>	<i>Total accessory range (vol. %)</i>	<i>Total phyllosilicate range (vol. %)</i>
<i>Highly Altered Meteorites</i>	22.5 – 14.8	5.8 – 12.5	3.4 – 12.7	82.1 – 88.6
<i>Intermediately Altered Meteorites</i>	15.1 – 11.5	16.6 – 19.6	5.4 – 2.7	74.6 – 77.6
<i>Less Altered Meteorites</i>	8.7 – 5.8	16.2 – 30	2.6 – 10	67 – 73.5
<i>Anhydrous meteorites (CV3s)</i>	76.6 – 85	81.4 – 93.1	5.8 – 11.8	0 – 4.2

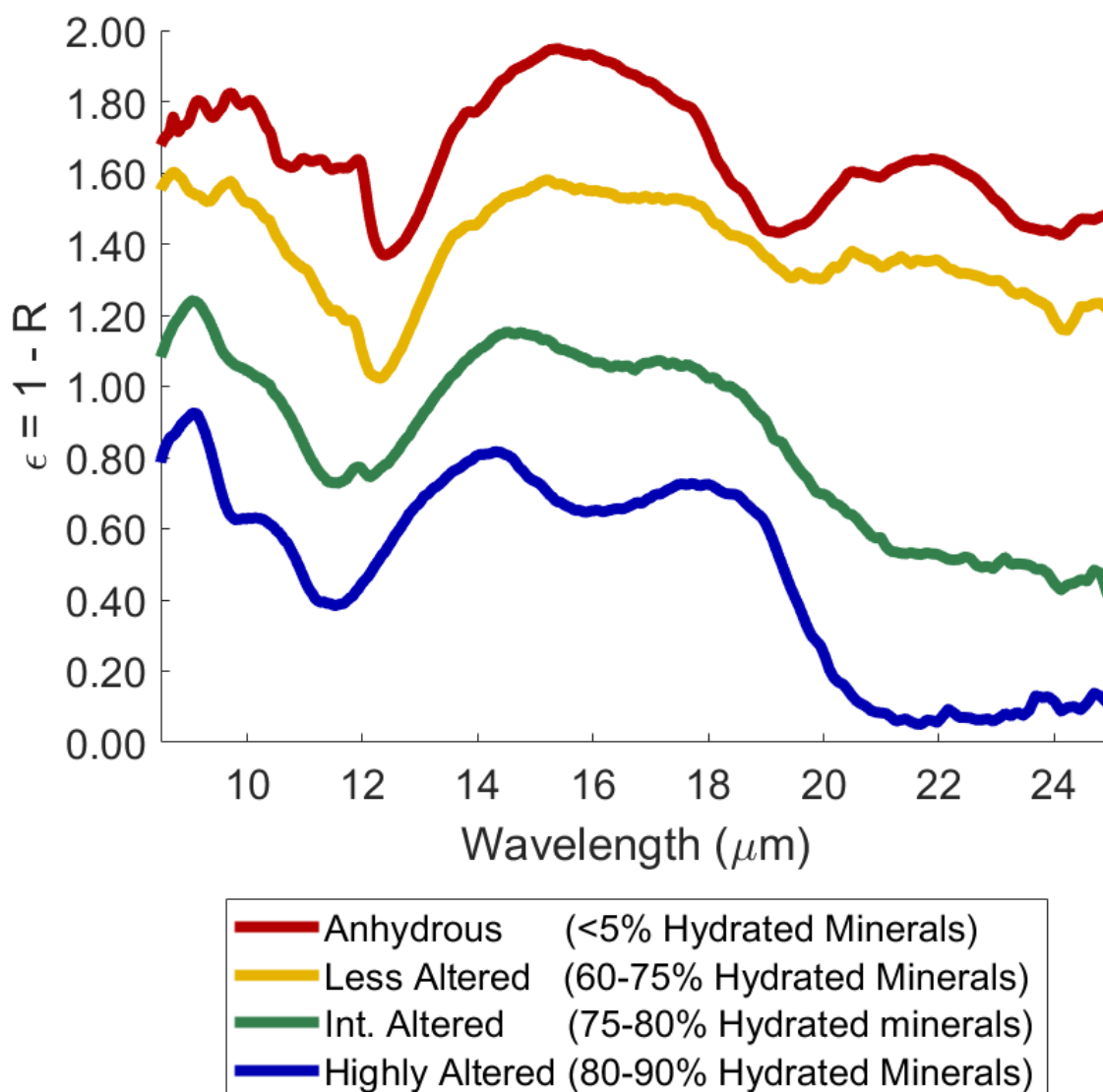


Figure 4.1: Meteorite endmembers.

Here, the meteorite endmembers from the coordinated spectral-mineralogical study are presented. They have been approximated as emissivity using Kirckoff's law. Spectral features change continuously with degree of alteration. Anhydrous meteorites (Vigarano, CV3) has strong olivine features at 12.7-, 19.5- μm ; Less altered meteorites (Murchison, CM2) have significant hydrated minerals (60-75%) which modify the mid-infrared spectral features. Less altered meteorites have features at 12.3- and a weaker 19.5- μm . Intermediately altered meteorites have a doublet in the 10-13- μm region and variable behavior in the 16-25- μm region. Finally, highly altered meteorites have 11.5-, 16 and 22- μm controlled by the abundant hydrated minerals (80-90%).

In this chapter, asteroid spectra are compared to four example meteorite endmembers. These are Orgueil (CI1, highly altered meteorite), Mighei (CM2, intermediately altered), Murchison (CM2, less altered meteorite) and Vigarano (CV3, olivine dominated). These meteorites are representative of the behavior of each subgroup of degree of alteration.

The 10-13- μm region is particularly useful for determining the mineralogy of asteroids. The meteorites have strong spectral features that change continuously with degree of alteration (e.g., **Figure 4.2**). This wavelength region is in an atmospheric window making it possible to observe asteroids using ground based and airborne telescopes.

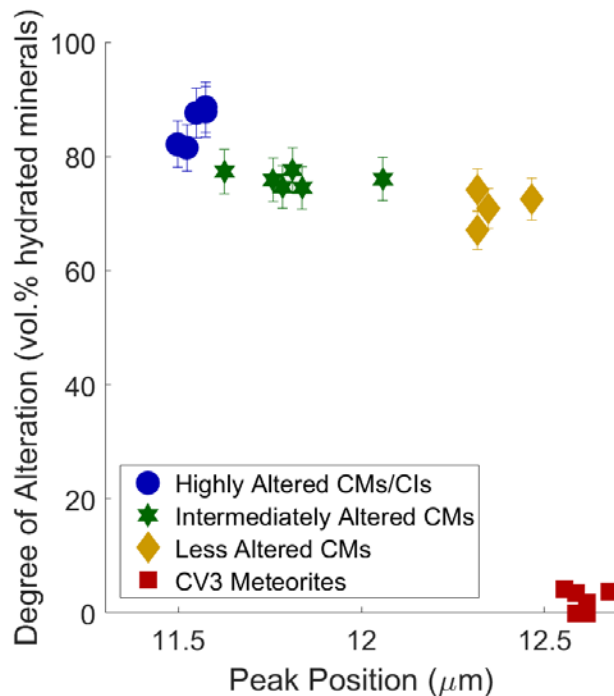


Figure 4.2: Peak position vs. degree of alteration (amount of hydrated minerals) for anhydrous and aqueously altered meteorites. The peak position of the 10-13- μm feature can be used to estimate the degree of alteration for asteroids.

Additionally, the Spitzer Space Telescope observed a large number of asteroids in this wavelength region providing a large archived dataset useful for the purposes of this work.

4.2.2 Previous Detections of Hydrated Minerals using the Mid-infrared

Hydrated minerals have been observed on the surfaces of asteroids using mid-infrared spectroscopy. Kuiper Airborne Observatory identified silicate features in the spectrum of (1) Ceres (e.g., Cohen et al., 1998; Rivkin et al., 2009; Milliken and Rivkin, 2009). The Thermal Emission Spectrometer on the Mars Global Surveyor has been used to identify hydrated minerals on the surface of Phobos and Deimos (e.g., Giuranna et al., 2011). The Infrared Space Observatory (ISO) identified hydrated minerals on several asteroids including (308) Polyxo and (10) Hygiea (Dotto et al., 1999, 2002). These observations relied on comparisons to spectral databases including Arizona State University's TES Spectral Library and the NASA/Keck Reflectance Laboratory (RELAB) database (Pieters et al., 2004). More recently, emission features in spectra of Themis family asteroids have been interpreted using results from our coordinated spectral-mineralogical study. Landsman et al., (2016) find that the Themis family asteroids tend to be similar to the less altered meteorites.

Connections have also been made between asteroids and meteorites using mid-infrared observations. (10) Hygiea has been linked to the Ornans-like chemical group of carbonaceous chondrites (e.g., Barucci et al., 2002). Barucci et al., (2002) find that their fits between asteroids and laboratory spectra were not in complete agreement, however the COs represent the best comparison. CH chondrites have spectral similarities to (21) Lutetia

(Moyano-Cambero et al., 2016) in the visible/near- and mid-infrared spectral regions. Previous Visible/Near-infrared studies of asteroids

Surveys of asteroids have investigated the relationship between spectral types and heliocentric distance (e.g., Gradie and Tedesco, 1980; DeMeo et al., 2016), 0.7- μm features and heliocentric distance (e.g., Fornaiser et al., 2014) and 3- μm band morphology and heliocentric distance (e.g., Takir and Emery, 2012). These studies find compositional stratification of the asteroid belt. The inner belt is dominated by S-type asteroids while outer belt asteroids are much darker with few spectral features (Gradie and Tedesco, 1980; DeMeo et al., 2016). Recently, Fornaiser et al (2014) and Takir and Emery (2012) noticed that asteroids with hydrated minerals (either 0.7- μm feature or ‘checkmark’ 3- μm band morphologies) are predominately in the mid-main belt which is consistent with previous studies (e.g., Lebofsky, 1980; Jones et al., 1990; Vilas, 1994; Barucci et al., 1998; Fornaiser et al., 1999). This has been suggested to mean that aqueous alteration only affected the mid-belt either because this is a ‘Goldilocks’ zone where there is enough water ice and heat from ^{26}Al to produce hydrated minerals (e.g., Grimm and McSween, 1989; 1993) or that water ice was preferentially available in this particular region of the disk (e.g., Vilas, 1994; Barucci et al., 1998; Fornaiser et al., 2014). The Grimm and McSween models rely on assumptions of accretion times that vary with heliocentric distance. Accretion in the outer belt occur at slightly later times than in the inner belt which, controls the amount of heat available in these asteroids. These models also rely on permeability (ability of water to flow) that are based on terrestrial and lunar analog material. Both of these assumptions

have been addressed in new models of planet formation and internal thermal evolution of asteroids.

Turbulence and streaming instabilities may significantly affect the accretion times of asteroids (e.g., Johansen et al., 2007; Johansen et al., 2014; Turner et al., 2014). Additionally grain collisions and growth processes also may affect growth of asteroids and the timescales of this process (e.g., Dominik et al., 2007). Recent models of aqueous alteration on asteroids have had more success producing a significant abundance hydrated minerals on asteroids of large sizes, unlike the Young et al., 1999, 2003 models. In the Young et al., (1999; 2003) models, the parent asteroid was assumed to be lithified prior to aqueous alteration. In this case, the flow of water would significantly change the chemical signatures such as the oxygen isotopes and the elemental similarity between CIs and the Sun. If, however, asteroids were not lithified, the parent asteroid would be a loose conglomerations of silicates and water in a ‘mud ball’ (Bland et al., 2017). Under these assumptions, aqueous alteration can occur to high degrees on asteroids of sizes up to 400 km (Bland et al., 2017) while also preserving the elemental and isotopic signatures observed in meteorites.

4.3 Observations and Data Reduction

The asteroids analyzed in this work were observed using three different platforms and instruments: the Spitzer Space Telescope (*Spitzer*) with the Infrared Spectrograph (IRS), the Stratospheric Observatory for Infrared Astronomy (SOFIA) with the Faint Object Infrared Camera for the SOFIA Telescope (FORCAST) and NASA’s Infrared

Telescope Facility (IRTF) with the Broadband Array Spectrograph System (BASS), a visiting instrument. The following subsections describe the observations and data reduction steps for each platform and instrument. Physical characteristics for the asteroids including diameter (Tedesco et al., 2004), albedo (Tedesco et al., 2004) and semi-major axis are the JPL Small-Body Database Browser¹.

4.3.1 Archived Spitzer Observations

During the cryogenic portion of its mission, *Spitzer* (Werner et al., 2004) observed a large number of low albedo asteroids using the IRS instrument (Houck et al., 2004). The majority of the Spitzer observations used here were made using the short-low (SL) module which covers the wavelength range of 5.2-14.5- μm with resolutions of ~ 100 . This mode contains two orders, SL1 covering 7.4-14.5- μm and SL2, 5.2-7.7- μm . Several asteroids were observed using both the short-low and the long-low modules. The long-low (LL) module covers the wavelength region of 14.0-38.0- μm with a similar resolution to the SL module. The low-resolution modes, SL and LL use a slit design to observe asteroids. The slits are divided into two, in-line subslits that allow for the instrument to observe two orders in the same mode. The source is centered in each of the subslits, the light is then passed through a bandpass filter and dispersed onto the detector. While the source is being observed in one subslit for one mode (e.g., SL1 or LL1), the other subslit is exposed to the sky background. Each asteroid is background corrected by co-adding the images with the asteroid in the opposite slit, then the co-added image is subtracted from the observation.

¹ ssd.jpl.nasa.gov/sbdb.cgi

After background corrections, the spectrum is extracted using the Spitzer IRS Custom Extraction (SPICE) program. This Java-based program generates a spatial flux profile and extracts the spectrum along the maximum of the flux profile. After SPICE extraction, the spectra that are best centered in the slit are averaged together to improve the over-all signal-to-noise ratio.

In total, 47 asteroids from the *Spitzer* archive are analyzed here. The dates and observations specifics for each asteroid are listed in **Table 4.2**. In addition to the circumstances of the observation, the program that observed them is also listed. The observation campaigns that observed these asteroids had a variety of goals many of which included physical characterization of these bodies. These asteroids range in size (Tedesco et al., 2004), albedo (Tedesco et al., 2004), semi-major axis and spectral type (Tholen, 1984; DeMeo et al., 2009). These properties are listed in **Table 4.3**. Occasionally, asteroid observations will have spurious features around 9.5- μm that may be caused by bad pixels that were poorly masked or by emission features from the interstellar medium. These spurious data points are removed prior to thermal modeling and estimating the degree of alteration.

Several of these observations have been previously published. Lincandro et al., (2012) and Landsman et al., (2016) investigated Themis family asteroids. Lincandro et al., (2012) constrained the thermos-physical properties of these asteroids, finding that they are characterized by fine-grained regolith with similar fairy-castle structure observed on Trojan asteroids (e.g., Emery et al., 2006). Landsman et al., (2016) found that the Themis family asteroids had denser regolith structures and/or larger grain sizes than the Trojans.

Additionally, Landsman et al., (2016) estimated the degree of alteration for the Themis family asteroids to be consistent with the less altered meteorites. Another Themis family asteroid (90) Antiope was presented in Hargrove et al., (2015). Hargrove et al., find that Antiope does not have a fairy-castle structure similar to Themis. Asteroids from the Cybele dynamical group were investigated in Lincandro et al., (2011) and Hargrove et al., (2012). Hargrove and collaborators identify a diversity of composition between the three objects they observed in both the 3- μ m and 10- μ m regions. Lincandro et al., (2011) suggest that (65) Cybele is has an anhydrous mineralogy and a fine-grained surface structure in addition to water-ice on its surface. Marchis et al., (2012) investigated a large number of asteroids in this study, focusing on binary objects. In this paper, Marchis et al. (2012) constrain the thermophysical properties of these bodies and physical properties of these systems (e.g., density).

Table 4.2: Spitzer Observation Circumstances:

<i>Name</i>	<i>Program</i>	<i>Date</i>	<i>Int. Time</i>	<i>H</i>	<i>Delta</i>	<i>Rh</i>	<i>phase</i>
			s	mag	AU	AU	Deg.
<i>(24) Themis</i>	2	6/8/2005	6.9	7.08	3.2	3.5	16.3
<i>(65) Cybele</i>	2	2/8/2005	14.7	6.62	3.5	4.0	14.8
<i>(90) Antiope</i>	1	7/12/2004	29.4	8.27	3.1	3.1	16.2
<i>(92) Undina</i>	5	1/14/2006	12.6	6.61	2.7	3.0	18.7
<i>(96) Aegle</i>	1	7/13/2004	14.7	7.67	3.1	3.5	16.9
<i>(107) Camilla</i>	3	2/29/2008	12.6	7.08	2.7	3.4	13.2
<i>(114) Cassandra</i>	1	10/20/2004	14.7	8.26	2.3	2.5	23.6
<i>(121) Hermione</i>	3	1/0/1900	0	7.31	2.9	3.4	16.1
<i>(130) Elektra</i>	1	4/22/2005	14.7	7.12	3.1	3.5	16.0
<i>(135) Hertha</i>	5	12/13/2005	121.9	8.23	2.2	2.9	16.6
<i>(161) Athor</i>	5	11/19/2005	12.6	9.15	2.1	2.1	27.4
<i>(201) Penelope</i>	5	6/24/2006	29.4	8.43	1.4	2.3	15.9
<i>(216) Kleopatra</i>	5	2/2/2006	121.9	7.3	2.9	3.3	15.9

(222) <i>Lucia</i>	4	12/9/2008	182.8	9.13	2.7	3.5	10.7
(223) <i>Rosa</i>	4	9/10/2008	44	9.68	3.4	2.9	15.9
(253) <i>Mathilde</i>	1	6/26/2004	61	7.08	3.1	3.1	18.8
(261) <i>Prymno</i>	1	9/30/2004	14.7	6.61	2.1	2.3	25.6
(267) <i>Tirza</i>	2	11/17/2005	61	10.1	2.7	3.0	19.0
(269) <i>Justitia</i>	2	4/15/2005	6.3	9.7	1.5	2.1	25.1
(283) <i>Emma</i>	3	5/27/2008	12.6	8.72	2.1	2.9	13.5
(284) <i>Amalia</i>	8	3/21/2005	25.2	10.05	1.5	2.1	25.5
(316) <i>Goberta</i>	4	9/11/2008	182.8	10.1	3.8	3.6	15.2
(325) <i>Heidelberg</i>	5	12/11/2005	121.9	8.65	2.6	3.0	18.1
(334) <i>Chicago</i>	2	7/6/2005	61	7.6	3.4	3.8	14.6
(336) <i>Lacadiera</i>	2	10/3/2004	6.3	9.76	1.9	2.4	22.6
(368) <i>Haidea</i>	1	3/25/2004	121.9	9.93	3.2	3.7	14.6
(379) <i>Huenna</i>	2	10/24/2004	60.95	8.87	2.9	3.2	18.2
(383) <i>Janina</i>	4	11/28/2008	44	9.91	3.0	2.9	18.9
(468) <i>Lina</i>	4	7/10/2008	58.7	9.82	3.6	3.6	16.1
(492) <i>Gismonda</i>	4	12/15/2008	182.8	10	2.9	3.5	13.3
(497) <i>Iva</i>	5	2/3/2006	725.5	10.02	3.3	3.7	14.5
(515) <i>Athalia</i>	4	1/8/2009	18.9	11.23	2.7	2.7	21.2
(526) <i>Jena</i>	4	3/4/2009	44	10.17	2.1	2.9	15.7
(554) <i>Perga</i>	1	9/14/2005	6.3	9.2	2.6	2.7	22.1
(762) <i>Pulcova</i>	2	9/28/2004	29.4	8.28	2.8	3.0	19.6
(785) <i>Zwetana</i>	5	6/25/2006	12.6	9.45	2.4	2.8	20.7
(1086) <i>Nata</i>	4	1/24/2009	37.8	9.5	2.3	3.0	14.9
(1268) <i>Libya</i>	7	11/29/2003	29.4	9.12	4.0	4.2	13.6
(1284) <i>Latvia</i>	2	3/20/2005	121.9	10.24	2.5	3.1	16.7
(1373) <i>Cincinnati</i>	2	7/17/2004	14.7	11.5	2.1	2.5	23.1
(1580) <i>Betulia</i>	1	3/11/2005	241.8	14.5	1.9	1.9	30.2
(1702) <i>Kalahari</i>	2	7/3/2005	241.9	11.03	2.8	3.1	19.2
(1922) <i>Zulu</i>	6	4/27/2007	426.6	12.3	3.0	3.1	18.7
(2428) <i>Kamenyar</i>	4	4/2/2009	243.8	11.5	2.5	3.4	8.8
(2934) <i>Aristophanes</i>	4	3/9/2009	182.8	11.7	2.4	3.1	14.1
(3090) <i>Tjossem</i>	4	1/17/2009	304.7	13	3.0	3.0	18.8
(3200) <i>Phaethon</i>	2	1/14/2005	58.7	14.6	0.7	1.1	60.2

Delta – distance between the asteroid and Earth; Rh – heliocentric distance.

1 – Extinct comets and low albedo asteroids (PI: Cruikshank)

2 – Extinct comets and low albedo asteroids -2 (PI: Cruikshank)

3 – A survey of Binary Asteroids with Spitzer/IRS (PI: Marchis)

4 – A comparative study of the Themis and Veritas Asteroid Families (PI: Campins)

5 – IRS spectroscopy of M-class asteroids and 375 Ursula.

6 – Surface mineralogy of Trojan asteroids and extinct comets as a proxy

7 – IRS Campaign R

8 – SIRTf IRS Calibration Program.

Table 4.3: Spitzer Target Physical Characteristics

<i>Name</i>	<i>Tholen</i>	<i>Bus-DeMeo</i>	<i>Family</i>	<i>Diameter</i>	<i>Albedo</i>	<i>semi-major axis</i>
				km		AU
(24) <i>Themis</i>	C	C	Themis	198.0	0.07	3.1
(65) <i>Cybele</i>	P	Xk	Cybele (dyn)	237.3	0.07	3.4
(90) <i>Antiope</i>	C	C	Themis/Beagle	116.0	0.06	3.2
(92) <i>Undina</i>	X	Xc	-	126.4	0.25	3.2
(96) <i>Aegle</i>	T	T	Aegle	177.8	0.05	3.1
(107) <i>Camilla</i>	C	X	Sylvia	210.4	0.06	3.5
(114) <i>Kassandra</i>	T	K	-	94.2	0.09	2.7
(121) <i>Hermione</i>	C	Ch	Cybele (dyn)	209.0	0.05	3.4
(130) <i>Elektra</i>	G	Ch	-	180.7	0.09	3.1
(135) <i>Hertha</i>	M	Xk	Nysa-Polana	79.2	0.14	2.4
(161) <i>Athor</i>	M	Xc	-	41.0	0.23	2.4
(201) <i>Penelope</i>	M	Xk	-	85.9	0.04	2.7
(216) <i>Kleopatra</i>	M	Xe	-	124.0	0.12	2.8
(222) <i>Lucia</i>	B	-	Themis	55.4	0.13	3.1
(223) <i>Rosa</i>	X	-	Themis	79.8	0.02	3.1
(253) <i>Mathilde</i>	-	Cb	-	52.8	0.04	2.7
(261) <i>Prymno</i>	B	X	-	50.0	0.14	2.3
(267) <i>Tirza</i>	D	D	-	56.0	0.05	2.8
(269) <i>Justitia</i>	-	D	-	50.7	0.06	2.6
(283) <i>Emma</i>	X	-	Emma	132.4	0.02	3.1
(284) <i>Amalia</i>	C	Ch	-	53.0	0.06	2.4
(316) <i>Goberta</i>	-	-	Themis	56.1	0.06	3.2
(325) <i>Heidelberg</i>	M	-	-	75.7	0.11	3.2
(334) <i>Chicago</i>	C	-	-	198.8	0.04	3.9
(336) <i>Lacadiera</i>	D	Xc	Vesta	67.5	0.04	2.3
(368) <i>Haidea</i>	D	-	-	69.3	0.04	3.1
(379) <i>Huenna</i>	B	C	Themis	84.8	0.05	3.1
(383) <i>Janina</i>	B	B	Themis	43.5	0.10	3.1
(468) <i>Lina</i>	C/P/F	Xc	Themis	60.2	0.06	3.1
(492) <i>Gismonda</i>	-	-	Themis	53.4	0.07	3.1
(497) <i>Iva</i>	M	-	-	40.9	0.12	2.9
(515) <i>Athalia</i>	I	Cb	Themis	41.9	0.04	3.1
(526) <i>Jena</i>	B	-	Themis	44.8	0.08	3.1
(554) <i>Perga</i>	F/C	Ch	Flora	95.9	0.05	2.4
(762) <i>Pulcova</i>	F	-	-	147.3	0.04	3.2
(785) <i>Zwetana</i>	M	Cb	-	49.5	0.12	2.6

<i>(1086) Nata</i>	-	Ch	Veritas	66.3	0.08	3.2
<i>(1268) Libya</i>	P	-	-	96.7	0.04	4.0
<i>(1284) Latvia</i>	T	L	-	41.1	0.07	2.6
<i>(1373) Cincinnati</i>	-	Xk	-	19.4	0.16	3.4
<i>(1580) Betulia</i>	C	-	-	5.8	0.08	2.2
<i>(1702) Kalahari</i>	D	L	-	34.6	0.07	2.9
<i>(1922) Zulu</i>	-	-	-	20.6	0.06	3.2
<i>(2428) Kamenyar</i>	-	Ch	Veritas	23.7	0.12	3.2
<i>(2934) Aristophanes</i>	-	Ch	Veritas	21.9	0.11	3.2
<i>(3090) Tjossem</i>	-	Cg	Veritas	14.3	0.12	3.2
<i>(3200) Phaethon</i>	F	B	-	5.1	0.11	1.3

4.3.2 IRTF+BASS

The IRTF is a 3-m class telescope located at the summit of Mauna Kea, Hawaii. BASS is a visiting instrument that has been used to observe asteroids and comets from IRTF previously (e.g., Lynch et al., 2007). BASS is a liquid-helium cooled, 3-14- μm low-resolution spectrometer that uses two sodium prisms and two photoconductor arrays to make observations (Hackwell et al., 1990).

Twenty-two asteroids were observed between January 27 and January 31, 2017. Sixteen of these asteroids have a spectral classification of Ch or Cgh. These asteroids therefore are known to be aqueously altered. The goal of these observations was to constrain the amount of hydrated minerals on their surfaces. The remaining 6 asteroids are main belt asteroids with T- or D-types. The goal of this proposal was to determine if main belt T- and D-types have similar spectral behavior to Jupiter Trojan asteroids with T/D classifications (e.g., Emery et al., 2006). Some of these T/D-types asteroids have been studied in the near-infrared (e.g., Takir and Emery, 2012) and are known to have water ice on their surfaces (361 Bononia) or hydrated minerals (308 Polyxo).

Table 4.4: IRTF+BASS observations circumstances

<i>Name</i>	<i>Date</i>	<i>Standard</i>	<i>Airmass</i>	<i>Int. Time</i> (s)	<i>H</i>	<i>Delta</i> (AU)	<i>Rh</i> (AU)	<i>phase</i> (deg.)
(1) <i>Ceres</i>	1/30/201 7	Alpha Tau	1.099-1.128	960.0	3.34	2.82 3	2.80 9	20.50
(13) <i>Egeria</i>	1/29/201 7	Alpha Tau	1.252-1.152	2340. 0	6.74	1.49 5	2.36 3	14.50
(96) <i>Aegle</i>	1/28/201 7	Beta Gem	1.041-1.038	960.0	7.67	1.89 9	2.80 0	9.90
(98) <i>Ianthe</i>	1/28/201 7	Beta Gem	1.172-1.253	1500. 0	8.84	2.09 2	2.49 5	22.70
(105) <i>Artemis</i>	1/30/201 7	Beta Gem	1.210-1.275	3840. 0	8.57	1.63 5	2.18 2	12.55
(106) <i>Dione</i>	1/29/201 7	Alpha Boo	1.001-1.100	1020. 0	7.41	2.22 5	3.20 1	2.80
(109) <i>Felicitas</i>	1/28/201 7	Beta Gem	1.257-1.228; 1.091-1.072	2040. 0	8.75	1.97 0	2.67 0	17.40
(144) <i>Vibilia</i>	1/28/201 7	Beta Gem	1.229-1.171; 1.120-1.118	3600. 0	7.91	2.98 0	3.28 1	17.20
(156) <i>Xanthippe</i>	1/27/201 7	Beta Gem	1.101-1.167	2640. 0	8.64	1.57 4	2.51 4	8.50
(162) <i>Laurentia</i>	1/30/201 7	Beta Gem	1.050-1.102	2520. 0	8.83	1.63 1	2.55 4	9.70
(187) <i>Lamberta</i>	1/29/201 7	Alpha Tau	1.048-1.078	2340. 0	8.16	2.33 1	3.00 8	15.50
(200) <i>Dynamene</i>	1/29/201 7	Alpha Tau	1.036-1.061	1320. 0	8.26	1.61 9	2.53 6	10.10
(233) <i>Asterope</i>	1/27/201 7	Alpha Boo	1.148-1.189; 1.239-1.341; 1.219-1.323	2520. 0	8.21	2.26 4	2.92 7	8.21
(257) <i>Silesia</i>	1/29/201 7	Alpha Boo	1.010-1.000; 1.000-1.012	3900. 0	9.47	2.02 7	2.99 6	4.20
(266) <i>Aline</i>	1/28/201 7	Beta Gem	1.250-1.264; 1.351-1.460	2580. 0	8.80	1.94 3	2.88 2	7.20
(308) <i>Polyxo</i>	1/29/201 7	Alpha Tau	1.138-1.225	2040. 0	8.17	2.76 2	2.79 1	20.40
(342) <i>Endymion</i>	1/28/201 7	Beta Gem	1.029-1.019	2220. 0	10.22	1.30 2	2.26 5	7.00
(361) <i>Bononia</i>	1/30/201 7	Alpha Tau	1.024-1.064	3240. 0	8.22	2.71 4	3.12 6	17.70
(415) <i>Palatia</i>	1/30/201 7	Beta Gem	1.080-1.106; 1.160-1.231	2700. 0	9.21	1.23 4	2.20 8	5.10
(442) <i>Eichfeldia</i>	1/29/201 7	Alpha Tau	1.083-1.091; 1.148-1.172; 1.237-1.271	2280. 0	10.03	1.80 3	2.44 6	20.50
(490) <i>Veritas</i>	1/30/201 7	Alpha Tau	1.021-1.111	4440. 0	8.32	2.46 7	3.06 0	16.50

(773) <i>Irmintraud</i>	1/29/201 7	Alpha Boo	1.347-1.302	3840. 0	9.10	2.42 1	2.92 6	18.60
----------------------------	---------------	--------------	-------------	------------	------	-----------	-----------	-------

During the BASS observations, asteroids were observed contemporaneously with standard stars that are well characterized in the mid-infrared. Standards were observed throughout each night, at multiple airmasses. The asteroids observed by IRTF+BASS are listed in **Table 4.4** with their heliocentric distance, distance from Earth, phase, integration time, standard star and airmass of the observation. The physical characteristics (spectral types, diameters, albedo and semi-major axis) are listed in **Table 4.5**.

To reduce the BASS observed targets, the sky background is removed and the data is flux calibrated. The asteroid's observed spectrum is divided by the standard star's spectrum. This unitless quantity is multiplied by an exponential term that accounts for the differences between the standard's star airmass (X_{standard}) and the asteroid observation's airmass (X_{asteroid}). The opacity term (κ) in the exponent accounts for the strength of the telluric absorption. The flux model is absolute flux of the standard star at each wavelength. The resulting spectrum is converted from SI units into Janskys for further analysis. This calibration process is summarized in Equation (1):

$$\left[\left(\frac{\text{Asteroid Observation}}{\text{Standard Observation}} \right) e^{-\kappa(X_{\text{standard}} - X_{\text{asteroid}})} \right] * \text{Flux Model} \quad (1)$$

Each asteroid is observed by chopping and nodding to reduce the sky background. The integration times for each asteroid can vary depending on the brightness of the target from 4-64 minutes. If additional time was required, the asteroid was recentered and the chop-nodding is resumed. These chop and nod pairs are averaged before being reduced. Standards are observed periodically over each night at airmasses similar to the asteroids. These observations are ~9 minutes of integration at different airmasses. The division of the

standard star removes atmospheric absorptions especially at $\sim 9.2\text{-}10.2\text{-}\mu\text{m}$, where ozone strongly absorbs. To account for changing conditions over a given night of observing and any difference between the asteroid's airmass and the standard's, the exponential term uses the wavelength dependent opacity (κ) and the difference in airmass to further remove any atmospheric contamination. The opacity of the atmosphere is calculated by determining the slope of the line between the natural logarithm of the standard's flux at a given wavelength and the airmass of that observation.

Table 4.5: IRTF+BASS Asteroid Physical Characteristics

<i>Name</i>	<i>Tholen</i>	<i>Bus-DeMeo</i>	<i>Family</i>	<i>Diameter (km)</i>	<i>Albedo</i>	<i>Semi-Major Axis (AU)</i>
<i>(1) Ceres</i>	G	C		939.4	0.09	2.8
<i>(13) Egeria</i>	G	Ch		222.8	0.07	2.6
<i>(96) Aegle</i>	T	T	Aegle	177.8	0.05	3.1
<i>(98) Ianthe</i>	C,G	Ch		132.8	0.03	2.7
<i>(105) Artemis</i>	C	Ch		112.3	0.02	2.4
<i>(106) Dione</i>	G	Cgh		207.9	0.04	3.2
<i>(109) Felicitas</i>	C,G	Ch		82.6	0.06	2.7
<i>(144) Vibia</i>	C	Ch		142.4	0.06	2.7
<i>(156) Xanthippe</i>	C	Ch		143.3	0.03	2.7
<i>(162) Laurentia</i>		Ch		97.0	0.05	3.0
<i>(187) Lamberta</i>	C	Ch		147.3	0.04	2.7
<i>(200) Dynamene</i>	C	Ch		128.3	0.05	2.7
<i>(233) Asterope</i>	T	Xk		99.7	0.09	2.7
<i>(257) Silesia</i>		Ch		72.7	0.05	3.1
<i>(266) Aline</i>	C	Ch		109.5	0.06	2.8
<i>(308) Polyxo</i>	T	T		128.6	0.05	2.7
<i>(342) Endymion</i>	C	Ch	Konig	60.9	0.04	2.6
<i>(361) Bononia</i>	D,P	-		154.3	0.04	4.0
<i>(415) Palatia</i>	D,P	-		83.6	0.06	2.8
<i>(442) Eichfeldia</i>	C	Ch		62.2	0.04	2.3

<i>(490) Veritas (773) Irmintraud</i>	C	Ch	Veritas	118.8	0.06	3.2
	D	T		91.7	0.05	2.9

4.3.3 SOFIA + FORCAST

The SOFIA observations are reduced using the FORCAST Redux pipeline version v1.2.0. This pipeline was recently updated and the data reprocessed. The SOFIA results here use this updated pipeline. A full description of the data pipeline and reduction steps can be found in the SOFIA Guest Observer Handbook for FORCAST Data products (v5.0.0). The raw data images undergo a number of steps including cleaning for bad pixels (caused by extreme dark current), droop correction (reduced signal on the pixel array caused by the signal itself), and non-linearity correction (empirically derived correction for non-linear response of the detector to signal greater than 60% saturation). At this point, the data are background corrected by stacking chopped image pairs then subtracting nodded image pairs. For bright point sources or bad pixels, large differences in signal across adjacent pixels can cause cross talking between pixels which appears as streaking on the stacked images. A ‘jailbar’ correction is used to remove this effect. The spectra are then extracted from the corrected, stacked data products using an optimal extraction protocol described by Cushing et al., (2004). Both the positive and negative chop/nod images are extracted with the negative image multiplied by -1. Next, the spectra are corrected for telluric absorptions, instrument response and flux calibrated. Finally each spectrum is merged into a single output file which is then thermally corrected and analyzed for degree of alteration.

The observation circumstances, including the altitude of observation, are listed in **Table 4.6** for the SOFIA observed targets. Their physical properties can be found in **Table 4.7**.

Table 4.6: SOFIA+FORCAST Observational Circumstances

<i>Name</i>	<i>Cycle</i>	<i>Date</i>	<i>Altitude (ft.)</i>	<i>Int. time (s)</i>	<i>H</i>	<i>Delta (AU)</i>	<i>Rh (AU)</i>	<i>Phase (deg)</i>
<i>(10) Hygiea</i>	4	2/18/2016	42005 _{.4} ⁺²	39.5	5.43	2.1	2.9	10.2
<i>(165) Loreley</i>	3	11/4/2015	41123 _{.10} ⁺¹⁹	48.2	7.65	2.3	3.1	13.6
<i>(194) Prokne</i>	3	6/3/2015	42999 _{.6} ⁺⁵	43.4	7.68	1.5	2.9	14.7
<i>(36) Atlante</i>	3	11/13/2015	43093 _{.7} ⁺²⁹	47.0	8.46	1.7	2.1	27.3
<i>(52) Europa</i>	4	2/17/2016	43002 _{.4} ⁺¹³	46.0	6.31	1.8	2.8	2.0
<i>(266) Aline</i>	3	6/4/2015	45006 _{.0} ⁺¹	22.1	8.80	2.611	2.476	22.80

Table 4.7: SOFIA+FORCAST Asteroid Physical Characteristics

<i>Name</i>	<i>Tholen</i>	<i>Bus-DeMeo</i>	<i>Family</i>	<i>Listed D (km)</i>	<i>Listed Albedo</i>	<i>Semi-Major Axis (AU)</i>
<i>(10) Hygiea</i>	C	C	Hygiea	407.1	0.07	3.1
<i>(165) Loreley</i>	C	Cb		180.1	0.05	3.1
<i>(194) Prokne</i>	C	-		161.7	0.06	2.6
<i>(36) Atlante</i>	C	-		115.2	0.04	2.8
<i>(52) Europa</i>	C	C		303.9	0.06	3.1
<i>(266) Aline</i>	C	Ch		109.5	0.06	2.8

4.3.4 Comparison of Observatories

The three observatories and instruments used to study asteroids are all low-medium resolution spectrometers. SOFIA+FORCAST has the highest resolution of ~250, while *Spitzer*+IRS and IRTF+BASS have lower resolutions of ~100 and ~50 respectively. SOFIA and IRTF+BASS have the disadvantage of telluric absorptions, such as ozone

between 9.2-10.2- μm , methane and carbon dioxide. The IRTF+BASS data reduction steps using a standard star observation generally removes the ozone absorption well, however some contamination may remain. The ozone absorption region is masked before thermal modeling and meteorite comparison. The SOFIA+FORCAST observations tend to have significant telluric absorptions and the 9.2-10.2- μm region is similarly masked. Additionally, SOFIA data is binned prior to thermal modeling and meteorite comparison to improve the signal-to-noise ratio. *Spitzer* and SOFIA can also be used to observe asteroids in the Q-band (17.7-27.7- μm or longer) where additional spectral features related to the degree of alteration appear. IRTF+BASS is designed to make spectroscopic observations between 3-14- μm and so cannot make observations in the 17.7-27.7- μm region.

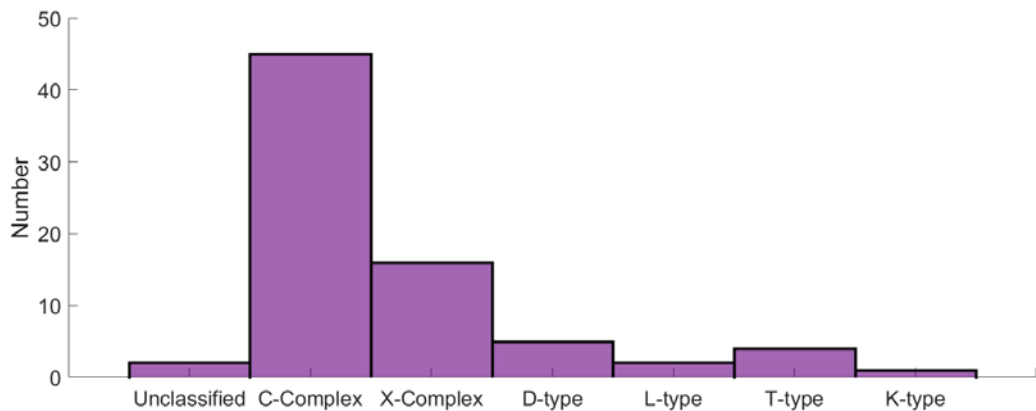


Figure 4.3: Histogram of taxonomic classifications for the dataset.

60% of the sample have a C-complex taxonomy. ~20% have an X-complex classification. The remaining sample have D-, T-, L-, K-types and two are unclassified.

4.3.5 Dataset Characteristics

Figure 4.3 shows a histogram of the taxonomic classification of the asteroids analyzed in this study. Most (60%) of the asteroids studied are in the C-complex. This includes asteroids with classifications of B, C, Cb, Cg, Cgh, and Ch, which all have low albedos. The remaining 40% have either X-complex classifications (X, Xc, Xk, Xe), D-, T-, L- or K-types. Two asteroids (492 Gismonda and 1922 Zulu) are currently unclassified but were included because of their low albedo (Zulu) or albedo and family membership (Gismonda). The asteroids in this dataset range in visible light albedos (**Figure 4.4a**) but are in general less than 15%. With the exception of two asteroids, (1) Ceres and (10) Hygiea that have diameters of ~950 km and 407 km respectively, the asteroids studied here are less than 350 km in diameter (**Figure 4.4b**), most having sizes of 80-150 km.

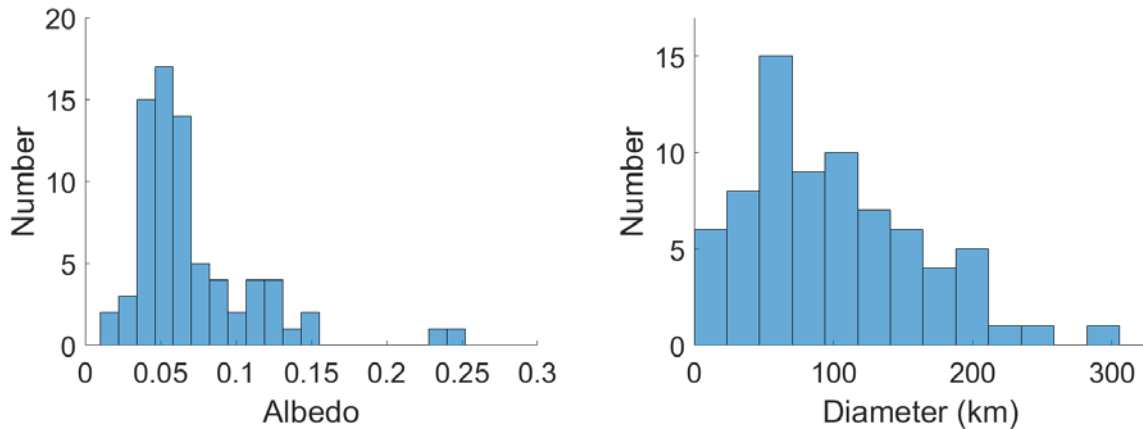


Figure 4.4: Histograms of dataset's (a) albedo and (b) diameter.

The asteroids studied here tend to have low albedos (<16%). Two asteroids, (92) Undina and (161) Athor, have high (20-25%) albedos. These asteroids with Xc spectral classification were included for comparison purposes. With the exception of (1) Ceres and (10) Hygiea (not shown), the dataset ranges in diameter from ~5 - ~200 km. Ceres and Hygiea are considerably larger (~950 km and ~410 km, respectively).

4.4 Analysis

Each asteroid observation after being reduced is analyzed in two subsequent ways: thermal modeling and assessment of degree of alteration. This section will describe these data analysis techniques.

4.4.1 Thermal Modeling

Each asteroid is modeled using the Near-Earth Asteroid Thermal Model (NEATM, e.g., Harris, 1998). This model describes the thermal emission from a non-spherical asteroid with a rough surface. The NEATM solves the equation (2):

$$F_{\lambda} = \frac{\varepsilon D^2 h c^2}{\Delta^2 \lambda^5} \int_0^{2\pi} \int_{-\pi/2}^{\pi/2} \frac{1}{\exp(hc/\lambda\kappa T(\theta, \varphi)) - 1} \times \cos^2(\varphi) \cos(\theta - \varphi) d\theta d\varphi \quad (2)$$

Where,

$$T(\theta, \varphi) = T(0) \cos(\varphi)^{1/4} \cos(\theta)^{1/4} \quad (3)$$

and,

$$T(0) = \left[\frac{(1-A)S}{\varepsilon\sigma\bar{\eta}} \right] \quad (4)$$

Here, ε is the emissivity value (set to 0.9 for this analysis), D is the diameter of the asteroid, h is Plank's constant, c is the speed of light, diameter (D), distance from the Earth (Δ) and temperature of the surface, λ is the wavelength of light, T is the temperature, α is the phase of the asteroid during the observation, θ describes the latitude of the asteroid and φ longitude. The surface temperature of the asteroid can vary over its surface depending on how it is illuminated.

F_λ (Equation 2) determines the grey body emission from the visible surface of an asteroid, illuminated by the sun. This emission from a surface depends on the asteroid's diameter (D), distance from the Earth (Δ) and temperature of the surface. The asteroid's hottest spot is the subsolar point ($T(0)$). The temperature of the asteroid's surface, including $T(0)$, varies depending on the heliocentric distance of the asteroid, phase, albedo and incident flux on the asteroid's surface (S). Furthermore, it is dependent on the emissivity (ϵ) and beaming parameter (η). Emissivity for these thermal models is fixed to 0.9. This value describes the efficiency that a surface absorbs and reemits the solar radiation. The beaming parameter is a free parameter in this model that describes the surface roughness. This integral is numerically solved at each wavelength to determine the grey body contribution to the asteroid's spectrum. There are two free parameters in this model: diameter and beaming parameter. The best fitting thermal model is found using a grid search technique. An array of diameters and beaming parameters are passed to the empirical solver. The goodness of fit is determined by minimizing X^2 between the data and the NEATMs. The model with the lowest X^2 is chosen as the best model and its parameters are used to describe the thermal contribution to the spectrum. For a given diameter (in kilometers), the geometric albedo can be calculated using (Fowler and Chillemi, 1992):

$$albedo = \left[\frac{1329 \times 10^{-H/5}}{D} \right]^2 \quad (5)$$

The best fitting diameter, beaming parameter, emissivity and calculated albedo are listed in **Table 4.8**. All observations with their best fit thermal models can be found in *Appendix I*.

Table 4.8: Thermal Modeling Best Fit Parameters

<i>Best Fit Parameters:</i>	<i>Name</i>	<i>Best fit D</i>	<i>albedo</i>	<i>η</i>
<i>Spitzer+IRS Observation</i>		km		
	(24) Themis	185	0.08	0.975
	(65) Cybele	291	0.05	0.8
	(90) Antiope	107	0.08	0.775
	(92) Undina	150	0.18	1.125
	(96) Aegle	164	0.06	0.925
	(107) Camilla	189	0.07	1.025
	(114) Kassandra	95	0.10	0.975
	(121) Hermione	154.5	0.09	0.964
	(130) Elektra	189	0.07	1
	(135) Hertha	79	0.14	1.1
	(161) Athor	54	0.13	0.9
	(201) Penelope	65	0.18	1
	(216) Kleopatra	123	0.14	1.15
	(222) Lucia	41	0.23	0.75
	(223) Rosa	67	0.07	0.8
	(253) Mathilde	47	0.06	0.675
	(261) Prymno	49	0.12	1.15
	(267) Tirza	46	0.08	0.8
	(269) Justitia	44	0.12	0.8
	(283) Emma	116	0.04	0.85
	(284) Amalia	51	0.06	1.05
	(316) Goberta	48	0.07	0.8
	(325) Heidelberga	86	0.08	1.125
	(334) Chicago	195	0.04	0.875
	(336) Lacadiera	64	0.05	0.925
	(368) Haidea	72	0.04	0.9
	(379) Huenna	83	0.07	1.025
	(383) Janina	56	0.06	0.975
	(468) Lina	63	0.05	0.8
	(492) Gismonda	36	0.15	0.75
	(497) Iva	27	0.24	0.775
	(515) Athalia	55	0.02	0.975
(526) Jena	34	0.13	0.85	
(554) Perga	110	0.03	0.9	
(762) Pulcova	124	0.06	0.95	
(785) Zwetana	40	0.18	0.8	

IRTF+BASS Observations

(1086) Nata	54	0.10	0.9
(1268) Libya	106	0.04	0.9
(1284) Latvia	41	0.08	1.15
(1373) Cincinnati	18	0.14	1.125
(1580) Betulia	7	0.06	1.5
(1702) Kalahari	42	0.04	1
(1922) Zulu	15	0.09	0.6
(2428) Kamenyar	22	0.09	0.65
(2934) Aristophanes	21	0.08	0.675
(3090) Tjossem	14	0.06	0.7
(3200) Phaethon	7	0.23	1.625

(1) Ceres	945	0.09	0.9
(13) Egeria	236	0.06	1
(96) Aegle	197	0.04	1.15
(98) Ianthé	96	0.06	0.875
(105) Artemis	121	0.05	0.95
(106) Dione	186	0.06	0.95
(109) Felicitas	230	0.01	2
(144) Vibia	256	0.02	1.4
(156) Xanthippe	156	0.03	1.275
(162) Laurentia	96	0.06	0.85
(187) Lamberta	159	0.04	0.875
(200) Dynamene	153	0.04	0.85
(233) Asterope	130	0.05	0.95
(257) Silesia	84	0.04	0.95
(266) Aline	185	0.02	1.15
(308) Polyxo	169.5	0.03	1.075
(342) Endymion	82	0.02	1.25
(361) Bononia	143.5	0.04	0.75
(415) Palatia	132	0.02	0.975
(442) Eichfeldia	45	0.08	0.7
(490) Veritas	132	0.05	0.95
(773) Irmintraud	134.5	0.02	1

***SOFIA+FORCAST
Observations***

(10) Hygiea	390	0.08	0.775
(36) Atlante	102	0.07	0.85
(52) Europa	302	0.06	1
(165) Loreley	200	0.04	1.1
(194) Prokne	152	0.06	0.525

4.4.2 Estimating Degree of Alteration

Using the best fit thermal model, the thermal contribution of the asteroid's spectrum can be removed by dividing the data by the model. This residual contains information about the asteroid's surface mineralogy. Figures showing the emissivity spectra of the asteroids in this study are located in *Appendix 2*.

In order to estimate an asteroid's degree of alteration, it is first necessary to determine if the asteroid has an emissivity feature in the 10-13- μm region. From the laboratory studies of meteorites, asteroids are expected to have emissivity minima between 11.5-13- μm , depending on the degree of alteration. To make this determination, value of the emissivity at the minimum in the 11.5-13- μm region is subtracted from the value of the spectrum at 10- μm . This is defined as the relative emissivity difference. The relative emissivity difference is compared to the average error of the spectrum in the 10-13- μm range in **Figure 4.5**. The average error in the 10-13- μm region is an indication of the signal-to-noise ratio of a spectrum. Several of the asteroids have large average error values compared to their relative emissivity depths (data points below the 1:1 correlation between relative depth and average error). This indicates that the observation has large point-to-point scatter. These observations have poor signal-to-noise-ratio and so are rejected from the dataset. Additionally, asteroids with relative emissivity depths of less than 2% or less are rejected since these asteroids, upon visual inspection, do not appear to have features. Asteroids with large relative emissivity differences compared to the average error have

strong features in the 10-13- μm range. $\sim 75\%$ of the data set (56 of 75) asteroid spectra have features in the 10-13- μm range.

In order to compare the asteroid's emissivity spectra, the laboratory reflectance data (R) must be approximated as emissivity (ϵ) using Kirchhoff's law: $\epsilon = 1 - R$. This is valid as a first order approximation except for very small grain sizes or for surfaces that do not have a strong thermal gradient (e.g., Salisbury et al., 1994; Henderson et al., 1996). These deviations can be up to 6% of the emissivity. Carbonaceous asteroids do not have large thermal gradients due to their low albedos. Asteroid's emissivity spectra can further be

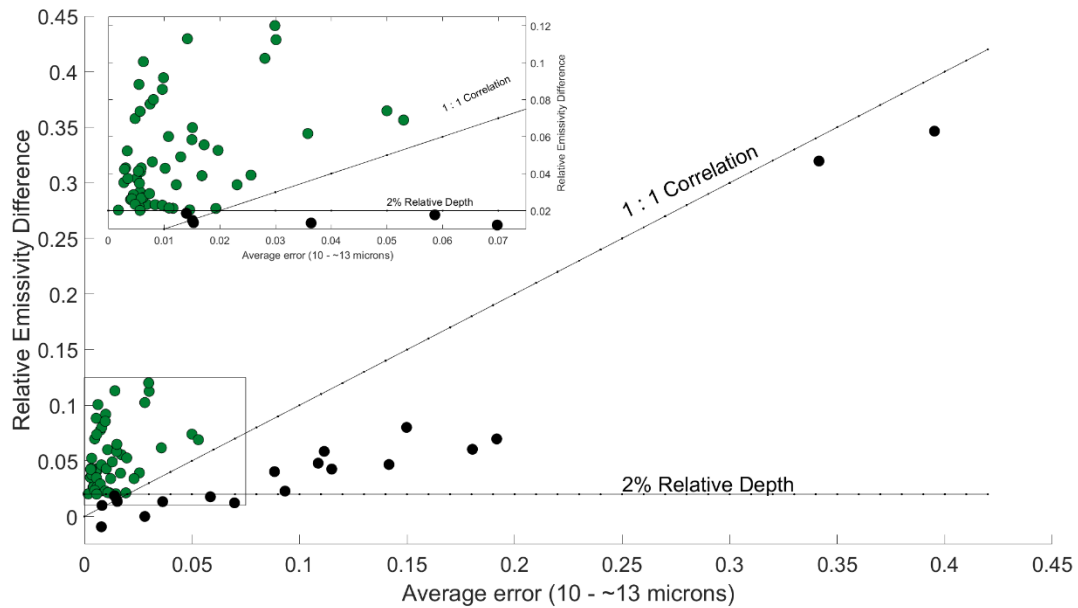


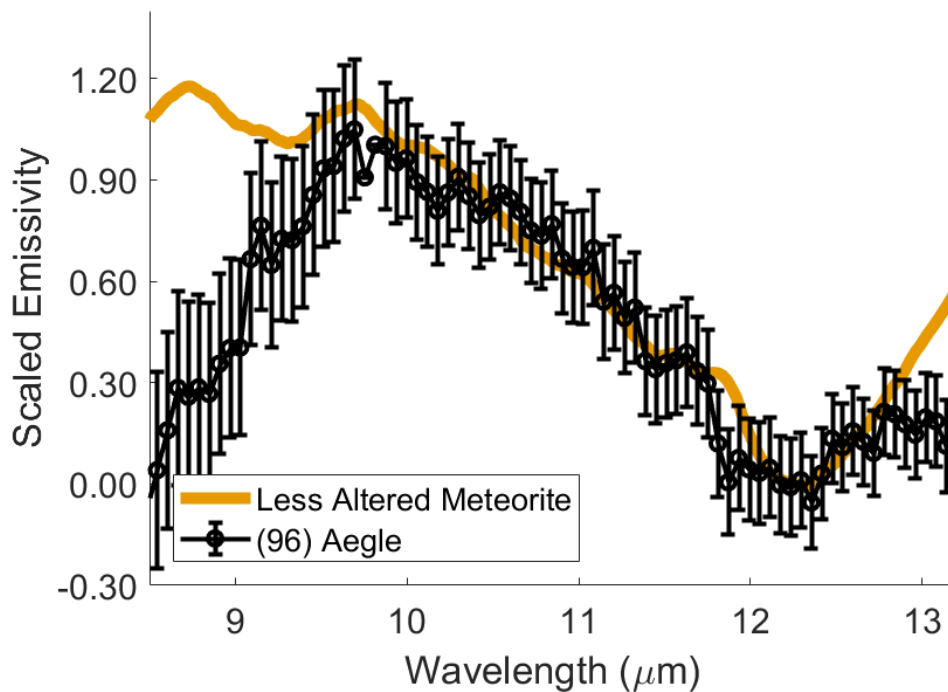
Figure 4.5: Relative emissivity difference compared to average error in the 10-13- μm region.

The 75 observations of 73 asteroids are assessed to determine if a feature is present. The emissivity difference is defined as the difference in emissivity values at 10- μm and the minimum of the spectrum in the 11-13.2- μm range. This difference indicates the strength of the feature. The average error in the 10-13- μm region is a proxy measure of the signal-to-noise ratio of the spectrum. Asteroids are said to have a feature if the relative emissivity depth is large compared to the relative error. Asteroids that have average errors below the 1:1 correlation indicates an observation with large point-to-point scatter and therefore poor signal to noise. Asteroids with relative emissivity depths of 0.02 (2%) or less do not appear to have a feature upon visual inspection and are rejected.

affected by grain size and porosity. Grain size effects have been fairly well studied in the laboratory (e.g., Hunt and Vincent, 1968; Hunt and Logan, 1972; Logan et al., 1973; Salisbury and Eastes, 1985; Mustard and Hays, 1997; Ramsey and Christensen, 1998; Cooper et al., 2002). These studies show that for silicate minerals, decreasing grain size decreases overall spectral contrast (or the depth of emissivity features). As grain sizes decrease, emission features decrease in relative depth and become more difficult to detect. Porosity similarly effects the spectral contrast (e.g., Salisbury and Eastes, 1985; Logan et al., 1973). Surfaces that have a fairy castle structure (e.g., particles in a very low density configuration held up by van der Waals forces) show changes in overall spectral contrast compared to packed particles or solid surfaces (e.g., Logan et al., 1973). Changes in peak positions have been noted for certain materials in fairy castle structures (e.g., Logan et al., 1973). These studies of grain size effects, thermal gradients and porosity investigated minerals that are not analogous to those in the carbonaceous chondrites since these minerals (e.g., quartz) are not found in large abundances in carbonaceous chondrites. More studies are needed in order to fully understand the changes in position of vibrational features for carbonaceous chondrites. The laboratory studies (McAdam et al., 2015a,b; Chapter 2) used to compare to the spectra of asteroids have $\sim 30\text{-}\mu\text{m}$ grain size (McAdam et al., 2015a, b; Chapter 2), which is a grain size regime where the Kirchhoff's law as a first order approximation is valid.

In order to account for differences in spectral contrast associated with both grain size and porosity differences between the laboratory measurements and the asteroids' spectra, the laboratory data is stretched between 0 and 1. The zero-point is taken to be the

position of the vibrational feature in the meteorite's spectrum between 8-13- μm which is dependent on the mineralogy and degree of alteration. The normalization point is taken to be at $\sim 10\text{-}\mu\text{m}$ where the spectra of the meteorites are relatively featureless. Asteroids' spectra are treated similarly. A parabola is fitted to the 11-13- μm feature, if present. The minimum of the parabola is defined as the zero-point and the spectrum is then normalized at 10- μm . Since the asteroids' spectra can be noisy the zero and normalization points are the average of the adjacent 3-5 emissivity values.



Over the 8-13- μm region, the asteroid data and the laboratory tend not to match in the 8-9.5- μm . The Christensen feature (the emissivity maximum usually found in the 8-9.5- μm region) can vary in position depending on the medium the light is traveling through (e.g., vacuum or atmosphere), grain size and physical properties of the surface (e.g., compaction etc.). These changes do not affect the position of the features in the 10-13- μm region. The meteorite comparison therefore is made between 10-13- μm .

When the asteroid data are directly compared (for example, **Figure 4.6**), the laboratory data often deviates from the asteroid spectrum in the 8-9.5- μm region. This discrepancy is likely related to the differences in Christiansen features between the laboratory data and the asteroid data. The Christensen feature is an emissivity maximum caused when the real part of index of refraction of the medium the light is passing through becomes equal to the index of refraction of the material. When this occurs, the scattering of photons at the interface between the material and the medium is low, so almost all of the light is transmitted (creating the emissivity maximum). The position of this feature is affected by both the medium (e.g., vacuum of space, atmosphere in the laboratory) and may also be affected by surface properties such as grain size, porosity and thermal gradients (e.g., Hunt and Vincent, 1968; Hunt and Logan, 1972). These affects are still being studied for carbonaceous chondrites (e.g., Donaldson-Hanna et al., 2017). As a consequence, it is not possible to modify the laboratory spectra to account for the expected difference between the laboratory data's Christiansen feature and the asteroid's Christensen features in vacuum. However, the positions of the emissivity features are consistent in laboratory

Figure 4.6: (96) Aegle compared to a less altered meteorite. measurements even when the Christiansen features shift. However, the positions of the Reststrahlen features are consistent in laboratory measurements even when the Christiansen features shift, since the Christensen features are strongly affected by scattering while the Reststrahlen bands are not. Therefore, directly comparing the asteroid data to the laboratory data longwards of the Christiansen feature is valid. The estimated degrees will therefore be assessed by a direct comparison between the asteroid spectrum and laboratory data in the 9.5-13- μm region.

In order to estimate the degree of alteration, the goodness of fit (*GoF*) between the asteroid and the laboratory data is assessed using the Equation (6):

$$GoF = \sum(A(\lambda) - L(\lambda))^2 \quad (6)$$

Where $A(\lambda)$ is the asteroid's spectrum at a given wavelength and $L(\lambda)$ is the laboratory spectrum at a given wavelength. The laboratory data are resampled to the same resolution of the asteroid's data. The asteroid's spectrum is compared to each of the four endmembers presented in Figure 4.1: highly altered, intermediately altered, less altered and anhydrous. The lowest goodness-of-fit value is then used as the degree of alteration with this value indicating the certainty of this estimation. Since this quantity is squared, differences between the laboratory data and the asteroid are accentuated by large goodness-of-fit values, while excellent fits have small values. **Figure 4.7** shows a histogram of the

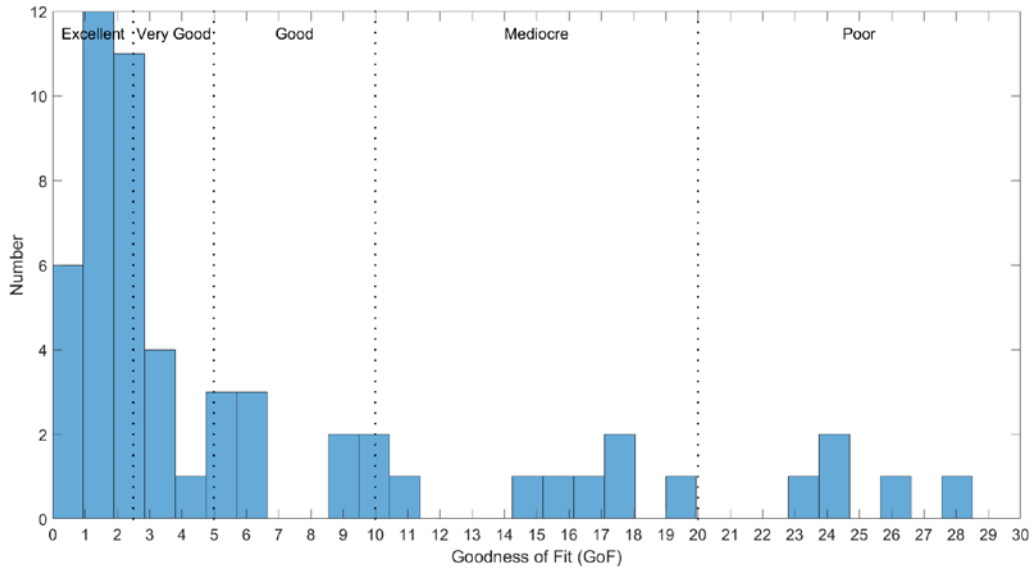


Figure 4.7: Histogram of Goodness-of-fit values.

Most of the asteroids with clear mineralogical features have goodness-of-fit values in the excellent, very good and good range. Several asteroids have mediocre and poor fits. These are investigated further as discussed below.

goodness-of-fit values for the asteroids with emissivity features. These goodness-of-fit values are then categorized, based on visual inspection, into the following groups: excellent fits ($0.2 \leq \text{GoF} \leq 2.5$), very good fits ($2.5 \leq \text{GoF} \leq 5$), good fits ($5 \leq \text{GoF} \leq 10$), mediocre fits ($10 \leq \text{GoF} \leq 20$) and poor fits ($20 \leq \text{GoF} \leq 30$). Most of the dataset (43 of 56) have goodness-of-fit values in the excellent (e.g., **Figure 4.8**), very good (**Figure 4.9**), or good

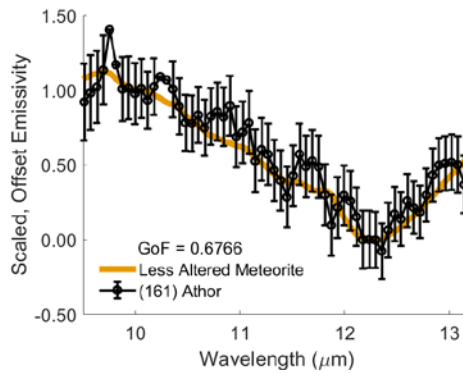


Figure 4.8: Excellent GoF example

161 Athor compared to a less altered meteorite. Athor is an example of an excellent fit. Its goodness-of-fit value is less than 1.

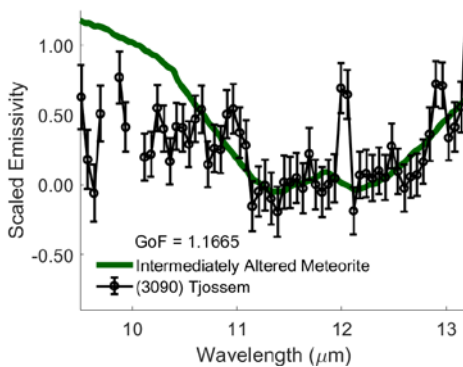


Figure 4.10: Very good GoF example

3090 Tjossem compared to an intermediately altered meteorite. This is an example of a very good fit between the asteroid and the meteorite data. The GoF value is between 2.5 and 5.

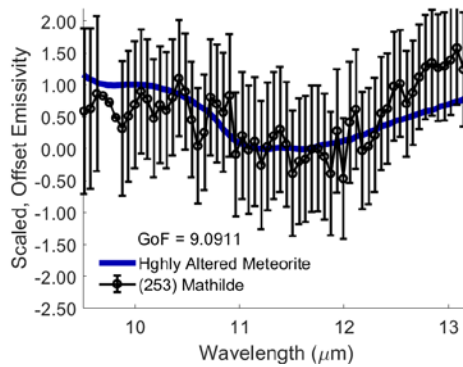


Figure 4.9: Good GoF

253 Mathilde compared to a highly altered meteorite. Mathilde is an example of a good fit with a GoF value between 5 and 10.

(**Figure 4.10**) range, indicating that the asteroids and the meteorite endmember match very well. The estimated degrees of alteration for the dataset is listed in **Table 4.9**, including the goodness-of-fits for the assigned degree.

Asteroids with goodness-of-fits in the mediocre or poor fits undergo additional visual inspection before their degree is estimated. Asteroids with mediocre fits are presented in **Figure 4.11** with the meteorite endmembers that have the best goodness-of-fit values. (90) Antiope appears to be a hydrated asteroid, with the best goodness-of-fit value between the data and the highly altered meteorite endmember ($GoF = 9.9$). Antiope's spectrum in the 12-13- μm range is much steeper than other asteroids in this dataset. This slope increase is mirrored in the highly altered meteorite endmember although the shape near 11.5- μm of Antiope's spectrum is not as comparable. Antiope is therefore assigned a highly altered degree. (223) Rosa, like Antiope, has an extreme slope in the 12-13- μm region. This again caused a discrepancy between the meteorite endmembers. However, the best fit is found between the CV3 meteorite and the Rosa data. Based on the visual inspection of the position of the minimum of the feature, this asteroid is assigned a less altered degree. (316) Goberta is a somewhat noisy spectrum leading to large goodness-of-fit value. This asteroid, upon visual inspection, appears to be a highly altered asteroids which is consistent with the best goodness-of-fit value found between the data and the highly altered meteorite endmember. (325) Heidelberga appears to be very consistent with the less altered meteorite endmember in the 9.5-.12.2- μm region. However, the asteroid's spectrum is unusually flat in the 12.5-13.2- μm range. This unusual shape causes the best goodness-of-fit value to occur between the anhydrous CV3 meteorite and the data. This

asteroid is estimated to be a less-altered degree since the data is far more consistent with this meteorite endmember than the CV3 meteorite, despite the lower goodness-of-fit value.

(492) Gismonda has a large goodness-of-fit values with the lowest occurring for the intermediately altered endmember and the data. This observation appears to be somewhat noisy, causing the large goodness-of-fit value. However, the visual comparison indicates that the intermediately altered meteorite endmember best matches this asteroid's spectrum.

(2428) Kamenyar similarly is somewhat noisy leading to large goodness-of-fit values. The

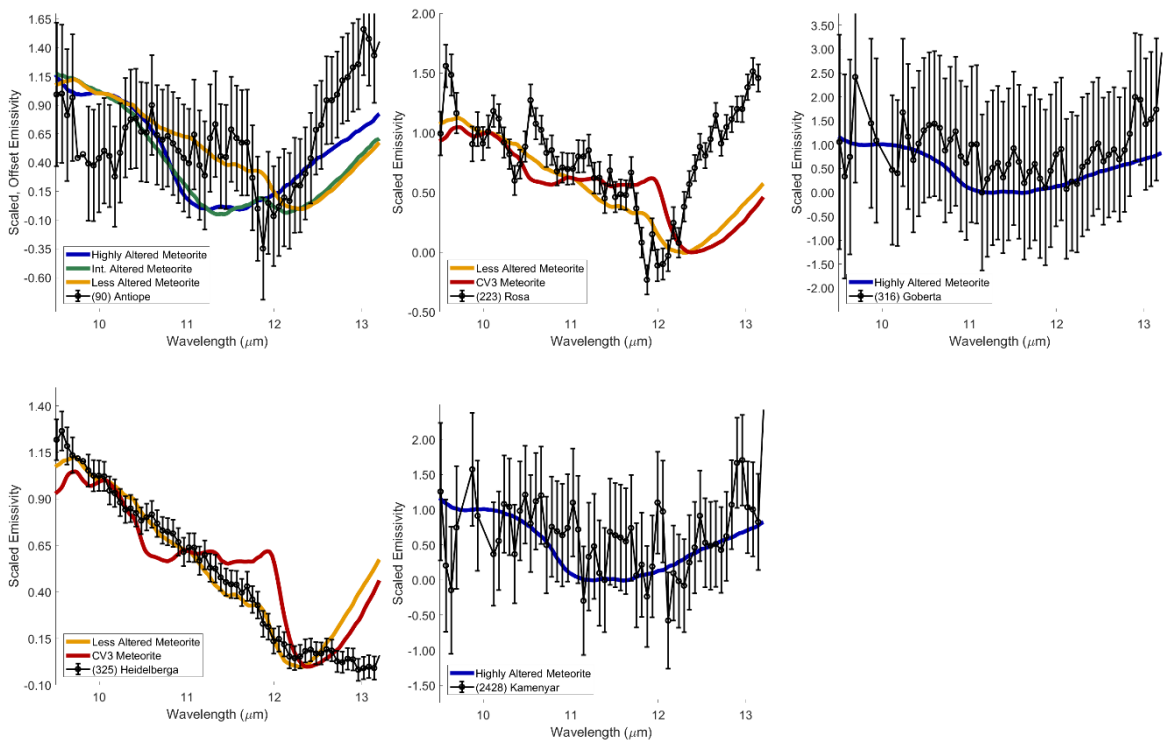


Figure 4.11: Asteroids with mediocre fits to the laboratory data.

These asteroids are visually assessed before degree of alteration is estimated. (90) Antiope is assigned a highly altered degree; (223) Rosa is assigned a less altered degree; (316) Goberta is assigned a highly altered degree; (325) Heidelberg is assigned a less altered degree; (415) Palatia is assigned a highly altered degree and finally (2428) Kamenyar is a highly altered degree.

best goodness-of-fit occurs between the asteroid and the highly altered meteorite endmember. This is consistent with the visual inspection of this observation.

Asteroids with poor goodness-of-fit values are also visually inspected. These asteroids are presented in **Figure 4.12**. These fits tend to be poor due to high signal-to-noise ratios or in the case of (1580) Betulia, high frequency sinusoidal fringing on the spectrum. In order to estimate the degrees of these asteroids, best-fit model based on the minimum goodness-of-fit value is compared to the minimum of the feature (**Figure 4.13**). The minimum of the feature is found by fitting a parabola to the data between 10-13- μm . The position of the 10-13- μm can be used as a first order approximation of the degree of alteration. The comparison between the best goodness-of-fit estimate and the position of the feature provides a method to check if the goodness-of-fit test is providing an accurate degree. In general, the position of the feature is consistent with the degree estimated using the goodness-of-fit technique. However, since these fits are poor, these asteroids are considered to be hydrated, with an unknown degree. Two asteroids with poor-fits cannot

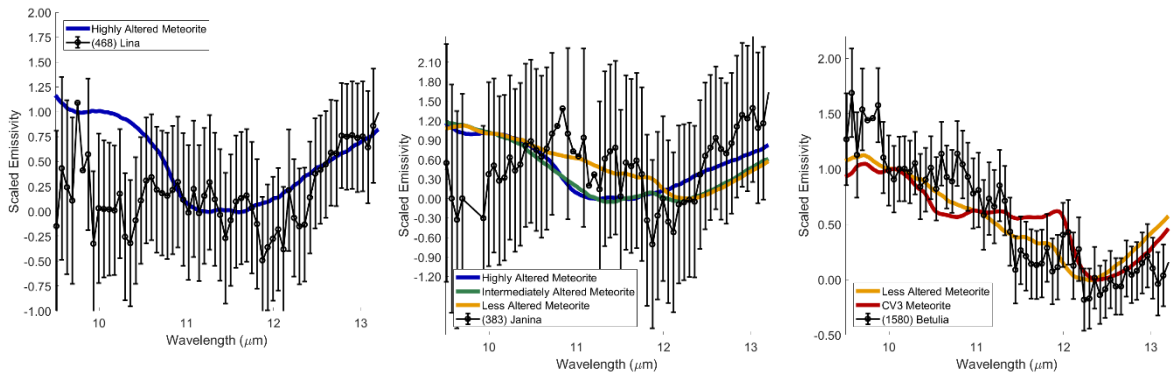


Figure 4.12: Asteroids with Poor goodness-of-fit values

These asteroids, with the exception of (1580) Betulia, are found to be hydrated but since these fits are so poor, a degree cannot be estimated. Betulia, since it could be either a less altered or anhydrous, is not assigned a degree.

be assigned a degree. (1580) Betulia's feature could be consistent with a less-altered degree however the goodness-of-fit test indicates that this asteroid is anhydrous. Since we do not independently know if this asteroid has hydrated minerals based on visible/near-infrared spectral measurements, it is not possible to assign a degree for this target

The BASS data has a much lower spectral resolution than the Spitzer and SOFIA observations. This can produce spurious fits between the laboratory data and the asteroid spectra using the goodness-of-fit technique. For example, (1) Ceres best GoF value is the highly altered meteorite, however, this seems to be a product of poor fits on either side of $\sim 12\text{-}\mu\text{m}$ balancing canceling each other out. These data are treated with a visual inspection in addition to the GoF test. (1) Ceres is estimated to be a less altered asteroid. (415) Palatia has fairly large point-to-point scatter, indicating a high signal-to-noise ratio for this observation. The lowest goodness-of-fit value for this asteroid is found between the data and the less-altered meteorite endmember. However, visual inspection of this asteroid indicates that it has a highly altered degree. (342) Endymion also has a large point-to-point scatter, creating disparities between the laboratory data. Similar to the poor GoF asteroids, the position of the feature for Endymion (e.g., **Figure 4.13**) suggests that this asteroid is hydrated but a degree of alteration cannot be assigned. (96) Aegle, similar to Endymion, is interpreted to be hydrated but no degree is assigned. (156) Xanthippe does not appear similar to the meteorite data. This observation may have a calibration issue leading to the unusual features. This asteroid is also not assigned a degree.

Asteroids (267) Tirza and (1284) Latvia are dissimilar to the other asteroids in this study. Tirza and Latvia (**Figure 4.15**) have much more extreme spectral contrast at 10- μ m region. This spectral shape has been noted in some Jupiter Trojan asteroids (Emery et al., 2006) and the nuclei of comets (Kelley et al., 2017). These asteroids are compared to two Trojan asteroids and comet Tempel 2 in **Figure 4.15**. This spectral contrast or trapezoidal

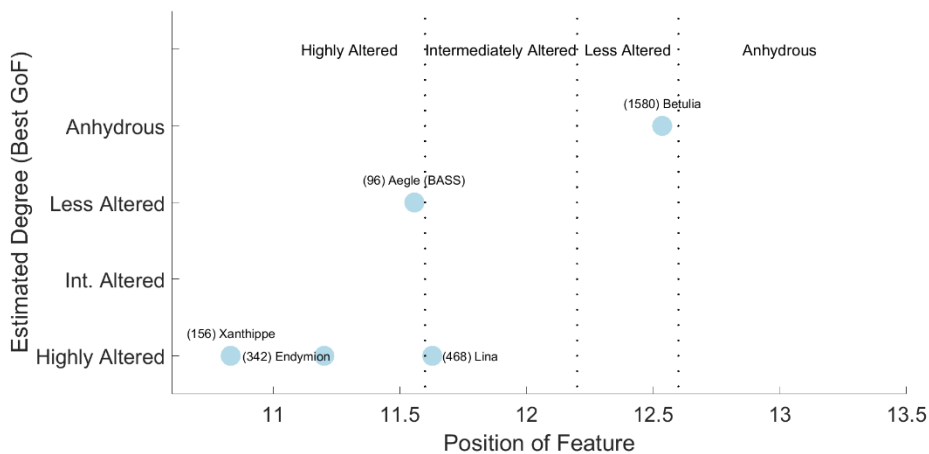


Figure 4.13: Position of the 10-13- μ m feature is compared to the estimated degree using the best fit GoF value.

With the exception of Xanthippe and Betulia, the estimated degree and the position of the feature indicate a hydrated mineralogy. However, because these fits are so poor, these asteroids are considered hydrated with an unknown degree. Xanthippe does not appear to be meteorite like. Betulia could be less altered or anhydrous. Therefore, a degree cannot be estimated for this object.

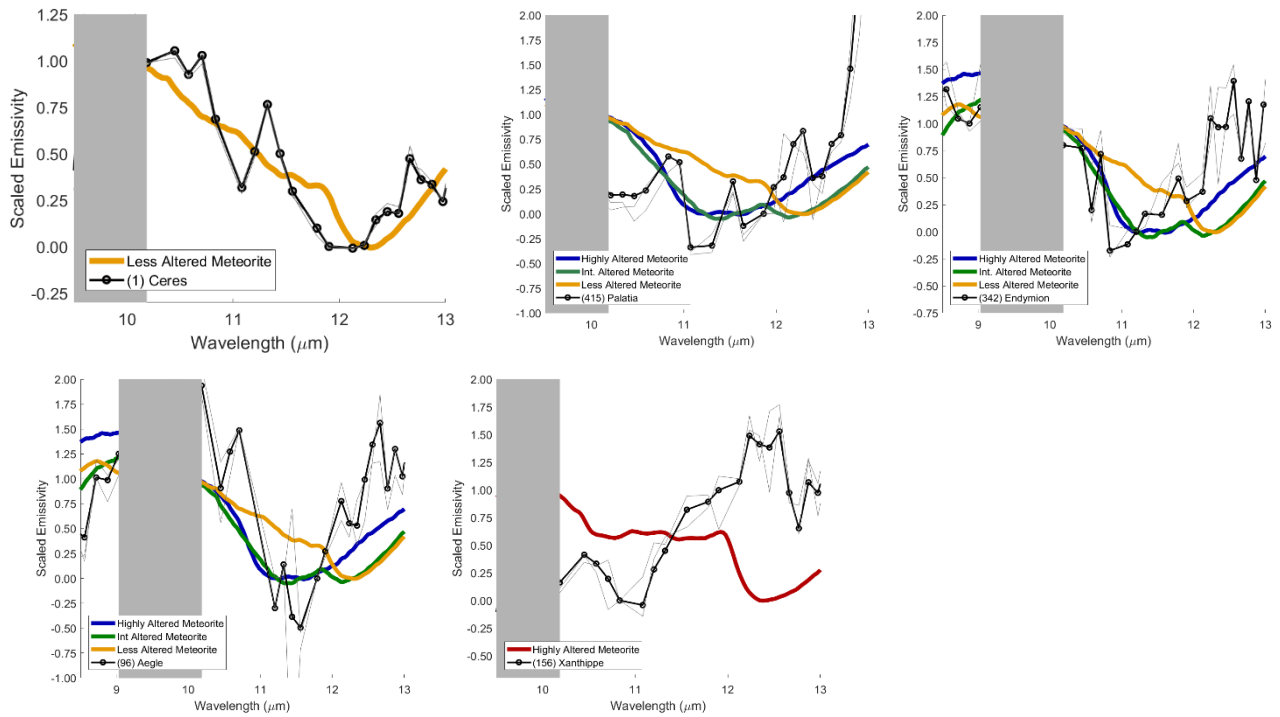


Figure 4.14: Estimating the degree of alteration for BASS observations.

Since BASS has a much lower resolution than Spitzer and SOFIA, the GoF test tends to give spurious results or mediocre to poor fits. These asteroids are all visually inspected when a degree is estimated. Ceres is interpreted to be a less altered asteroid. (415) Palatia is a highly altered body. (342) Endymion and (96) Aegle are hydrated but not assigned a degree due to the dissimilarity between the laboratory data and the asteroid spectra. Finally, (156) Xanthippe is not meteorite like and therefore a degree cannot be assigned.

shape in the 10- μm region has been interpreted to be caused by very low porosity surfaces (e.g., Emery et al, 2006; Kelley et al., 2017) and possibly related to the origin of these objects. Although comets are dominated by water ice (referred to as dirty snow balls, Whipple, 1957), they have not experienced aqueous alteration (e.g., Davidsson et al., 2016). Comets never reached an internal temperature high enough to melt water ice and induce the onset of aqueous alteration (e.g., Davidsson et al., 2016). Tirza and Latvia are interpreted to be similar to comet nuclei and Trojan D-types potentially having a different

origin than other asteroids in the Main Belt and/or very low surface porosities. They have not experienced aqueous alteration but we cannot infer further information about the surface composition.

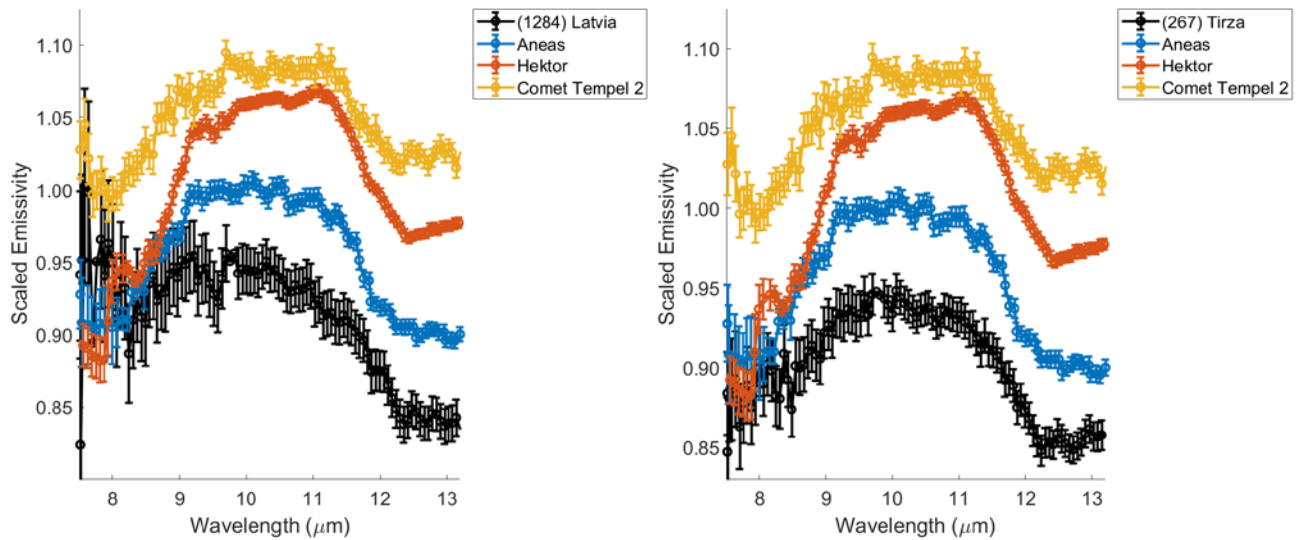
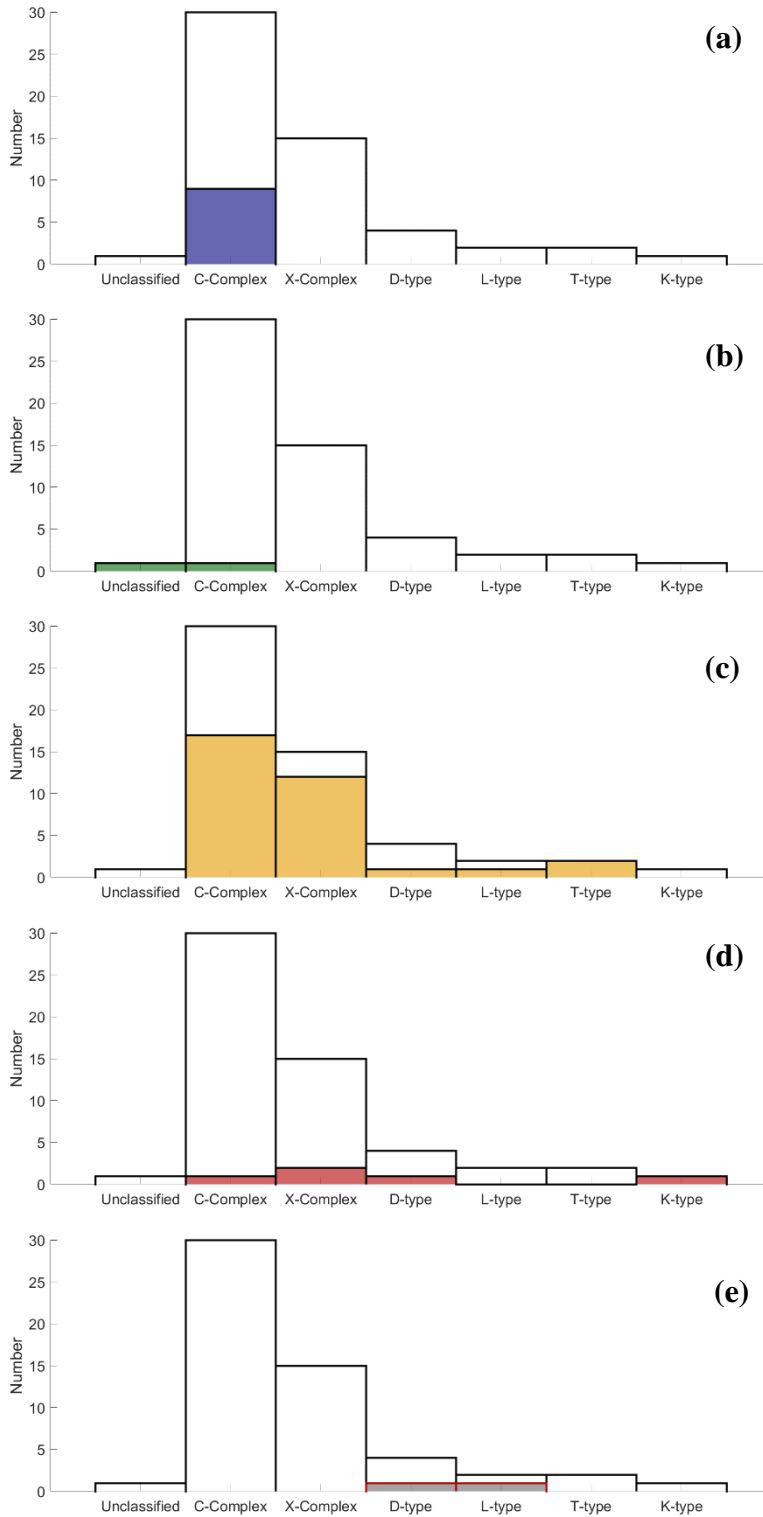


Figure 4.15: (1284) Latvia and (267) Tirza compared to two Jupiter Trojan asteroids, (1172) Aneas and (624) Hektor (Emery et al, 2006) as well as Comet Tempel-2 (Kelley et al., 2017).

Hektor, Aneas, and Tempel-2 have a trapezoidal shape in the 10- μm region. Tirza and Latvia appear to be more similar to Jupiter Trojan and Comet Tempel-2. Latvia and Tirza may have different origins than the other main belt asteroids observed or have more porous surfaces. They likely have not experienced aqueous alteration, however we cannot infer anything else about their surfaces with this observation alone.

Figure 4.16: Degree of alteration by spectral type.



(a)

(b)

(c)

(d)

(e)

(a) Highly altered asteroids are found in C-complex asteroids (b) Two asteroids are found to be intermediately altered asteroids one C-complex asteroid and one unclassified. (c) Less altered asteroids, which are the most numerous in the dataset are found in the C- and X-complex with at least one T-type example. (d) Asteroids that appear to be anhydrous are found in the C- and X-complexes and L-types and K-types. (e) Asteroids with trapezoidal features are found in the D-types and L-types.

Table 4.9: Asteroid's Assigned Mineralogy

<i>Spitzer+IRS Observations</i>	<i>Name</i>	<i>Parabola min. Positon</i>	<i>Estimated Degree</i>	<i>Goodness-of-fit</i>
	(24) Themis	12.2	Less Altered	5.91
	(65) Cybele	12.2	Less Altered	3.30
	(90) Antiope	11.3	Highly Altered	10.08
	(92) Undina	12.6	Anhydrous	1.17
	(96) Aegle	12.5	Less Altered	0.73
	(107) Camilla	12.4	Less Altered	2.28
	(114) Cassandra	12.7	Anhydrous	2.10
	(121) Hermione	12.1	Less Altered	4.16
	(130) Elektra	12.3	Less Altered	1.43
	(135) Hertha	12.4	Less Altered	1.02
	(161) Athor	12.2	Less Altered	0.68
	(201) Penelope	12.9	Less Altered	1.75
	(216) Kleopatra	12.3	Less Altered	5.48
	(223) Rosa	11.5	Less Altered	15.32
	(253) Mathilde	11.4	Highly Altered	9.09
	(261) Pymno	13.0	Less Altered	2.68
	(267) Tirza	13.1	Trapezoidal	0.00
	(269) Justitia	13.0	Anhydrous	1.60
	(283) Emma	12.4	Less Altered	1.19
	(284) Amalia	13.0	Less Altered	1.81
	(316) Goberta	11.6	Highly Altered	19.67
	(325) Heidelberga	13.0	Less Altered	10.11
	(334) Chicago	12.5	Less Altered	1.95
	(336) Lacadiera	12.5	Less Altered	2.33
	(368) Haidea	13.0	Less Altered	2.13
	(379) Huenna	12.4	Less Altered	2.58
	(383) Janina	11.8	Hydrated*	10.75
	(468) Lina	11.6	Hydrated*	24.09
	(492) Gismonda	11.8	Intermediately Altered	17.13
	(497) Iva	12.3	Anhydrous	0.24
	(515) Athalia	12.4	Less Altered	1.54
	(526) Jena	11.9	Highly Altered	17.49
	(554) Perga	12.4	Less Altered	2.56

<i>IRTF+BASS Observations</i>	(762) Pulcova	12.1	Less Altered	3.73
	(785) Zwetana	13.0	Anhydrous	5.95
	(1086) Nata	12.2	Less Altered	3.64
	(1268) Libya	12.8	Less Altered	1.64
	(1284) Latvia	13.2	Trapezoidal	0.00
	(1373) Cincinnati	12.4	Less Altered	3.72
	(1580) Betulia	12.5	Uncertain	28.46
	(1702) Kalahari	13.2	Less Altered	1.06
	(2428) Kamenyar	11.6	Highly Altered	14.95
	(2934) Aristophanes	12.2	Less Altered	2.63
	(3090)Tjossem	11.9	Intermediately Altered	2.53
	(3200) Phaethon	11.6	Highly Altered	5.19
	<i>SOFIA+FORCAST Observations</i>	(1) Ceres	12.1	Highly Altered
(96) Aegle		11.6	Hydrated*	26.03
(156) Xanthippe		10.8	Uncertain	22.89
(342) Endymion		11.2	Hydrated*	23.90
(415) Palatia		11.3	Highly Altered	16.63
(10) Hygiea		11.4	Highly Altered	5.25
(36) Atlante		11.7	Highly Altered	9.32
(52) Europa		12.9	Less Altered	1.02
(165) Loreley		12.3	Less Altered	2.49
(194) Prokne		11.0	Highly Altered	6.04
(266) Aline	22.4	Highly Altered	0.32	

Hydrated* - unknown degree

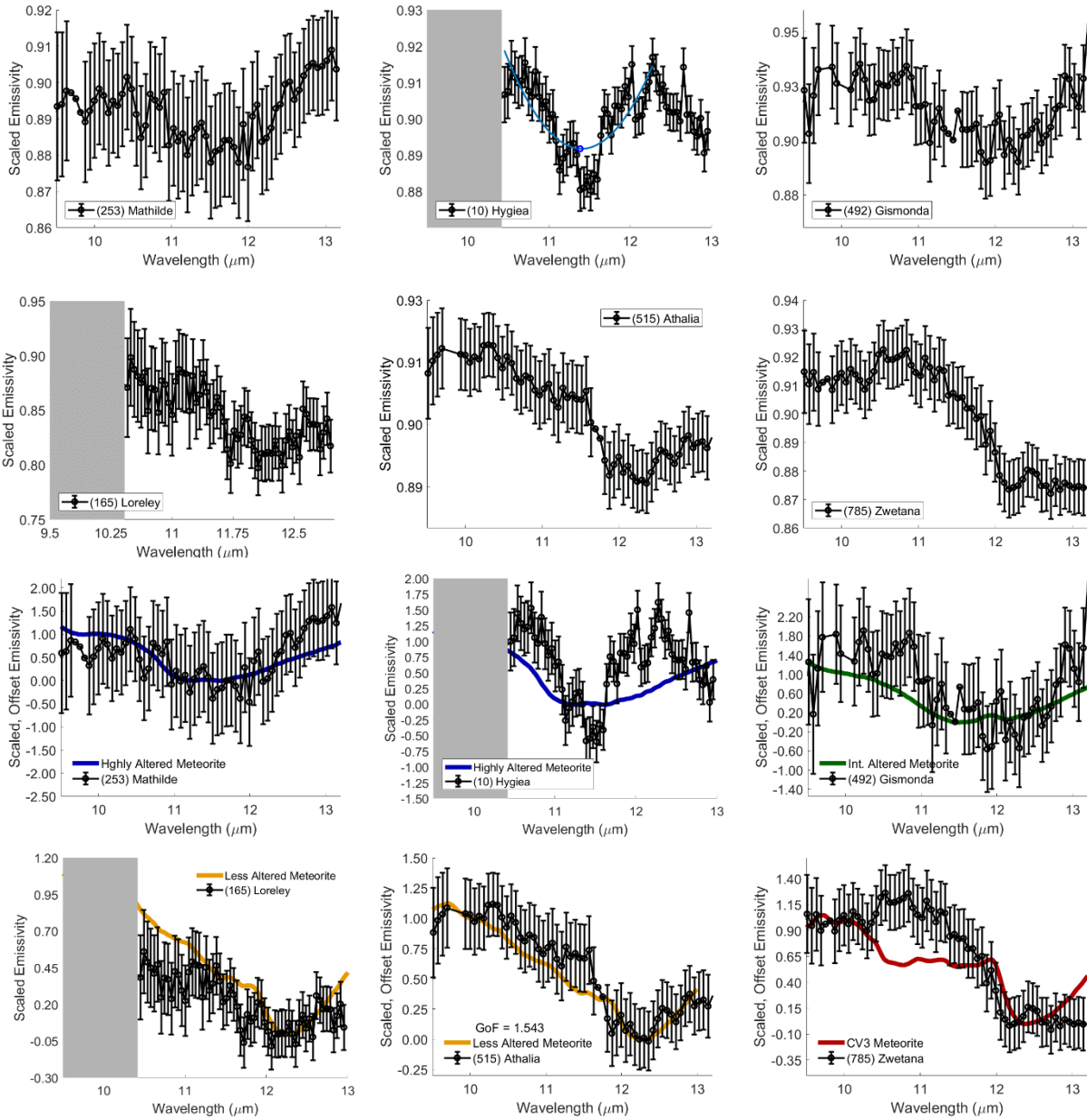


Figure 4.17: C-complex variability of degrees of alteration.

Top row: highly altered asteroids (253) Mathilde observed with Spitzer, Cb-type and (10) Hygiea observed with SOFIA+FORCAST, C-type and intermediately altered asteroid (492) Gismonda (unclassified, Themis family). Second line: Less altered asteroids (165) Loreley observed with SOFIA, (515) Athalia observed by Spitzer and the anhydrous asteroid (785) Zwetana (Cb-type). Data collected in this wavelength region may have residual ozone which is masked in order to observe the mineralogy. The 3rd and 4th lines show the comparison of the asteroid data to the meteorites.

4.5 Results

4.5.1 Widespread and Variable Aqueous Alteration in the Main Asteroid Belt

Figure 4.16 shows the histograms of the degree of alteration by spectral type. Highly altered asteroids (10 asteroids) are found in the C-complex. Intermediately altered asteroids and likely intermediately altered asteroids (2 objects) are (3090) Tjossem and (492) Gismonda. Tjossem is a C-complex asteroid. Gismonda is currently unclassified but it is a member of the Themis family indicating it is likely a C-complex body. Less altered asteroids are the most numerous in the dataset (30 objects). These objects maybe in the C-complex, X-complex, and T-types. Anhydrous asteroids (5) do not have hydrated minerals but rather appear most similar to CV3 meteorites. These asteroids are interpreted to be

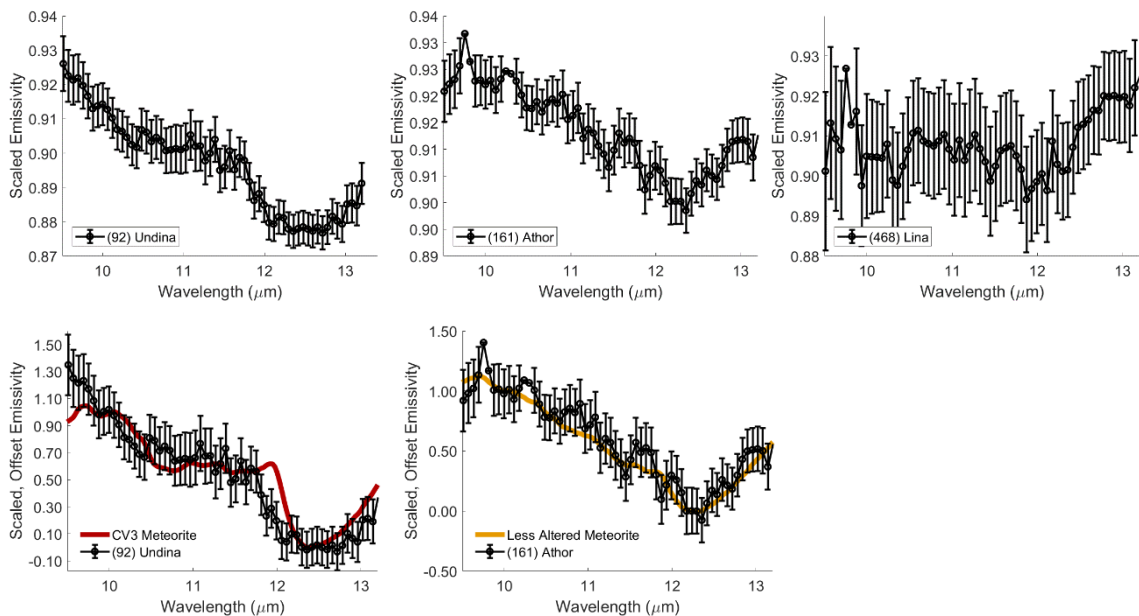


Figure 4.18: X-type asteroids variability observed by Spitzer.

(92) Undina appears to be anhydrous likely olivine dominated, (161) Athor appears to be less altered and (468) Lina that appears to be hydrated but its goodness of fit value is poor so the degree is unknown.

olivine-dominated and have not experienced extensive interactions with water. Anhydrous asteroids do not have a preferred spectral type but appear in C- and X-complexes as well as D-types.

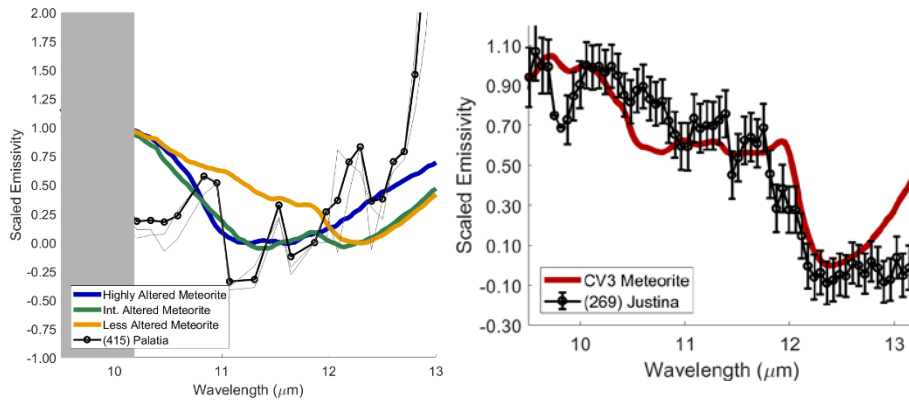


Figure 4.19: Examples of Main Belt D-types.

(415) Palatia (observed with IRTF+BASS) appears to be a highly altered asteroid while (269) Justina (observed with *Spitzer*) appears anhydrous. Two other Main Belt D-types appear meteorite-like and anhydrous (361 Prymno and 368 Haidea). (267) Tirza however appears comet-like (see Figure 4.6).

C-complex (**Figures 4.17**) asteroids have examples of degrees of alteration ranging from anhydrous to highly altered. X-complex (**Figure 4.18**) asteroids seem to have lower degrees of alteration than the C-complex asteroids, however many have hydrated minerals on their surfaces. Main Belt D-types have a variety of surface compositions (**Figure 4.19**). Three of the five observed appear to be anhydrous, one is highly altered. The remaining asteroid (267) Tirza appears similar to comet nuclei and Jupiter Trojan asteroids (see **Figure 4.15**) Three Main Belt T-types are observed. Two are featureless. (96) Aegle was observed using both IRTF+BASS and *Spitzer*. This asteroid appears a less altered degree in the *Spitzer* data while the BASS data cannot be assigned a degree since the signal-to-

noise ratio is higher for this observation. Asteroids exhibiting hydrated minerals appear throughout the asteroid belt (**Figure 4.20**). Hydration occurs on asteroids of all sizes (**Figure 4.21**). There does not appear to be a systematic relationship between visible albedo and degree of alteration (**Figure 4.22**).

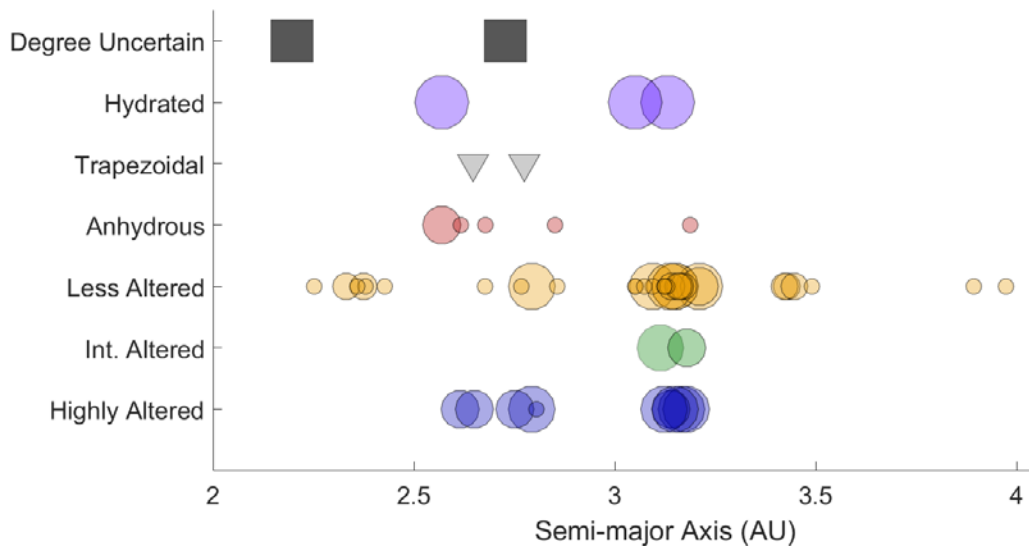


Figure 4.20: Groups of degrees of alteration compared to their semi-major axis.

Here, the size of the symbol indicates the GoF value (small symbols for small values). The transparency for each symbol is set to 0.33 so darker colors indicate more observations.

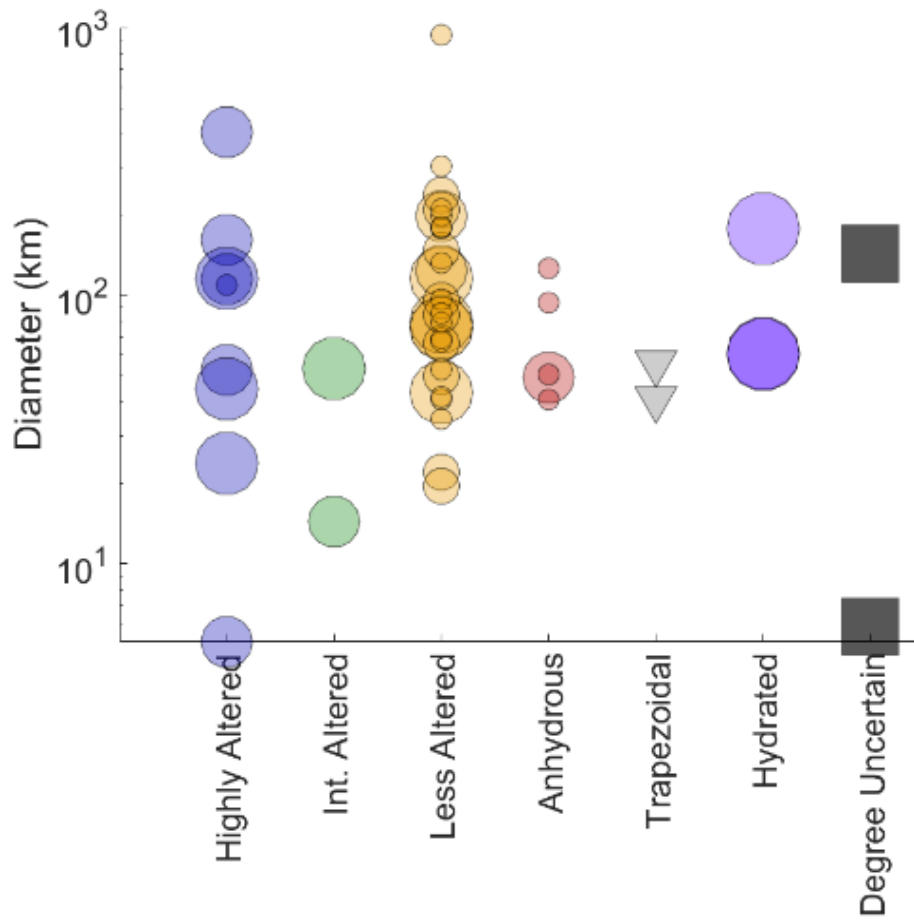


Figure 4.21: Groups of degrees of alteration compared to their diameters (on a logarithmic scale). There appears to be no relationship between asteroid size and degree of alteration.

Here, the size of the symbol indicates the GoF value (small symbols for small values). The transparency for each symbol is set to 0.33 so darker colors indicate more observations.

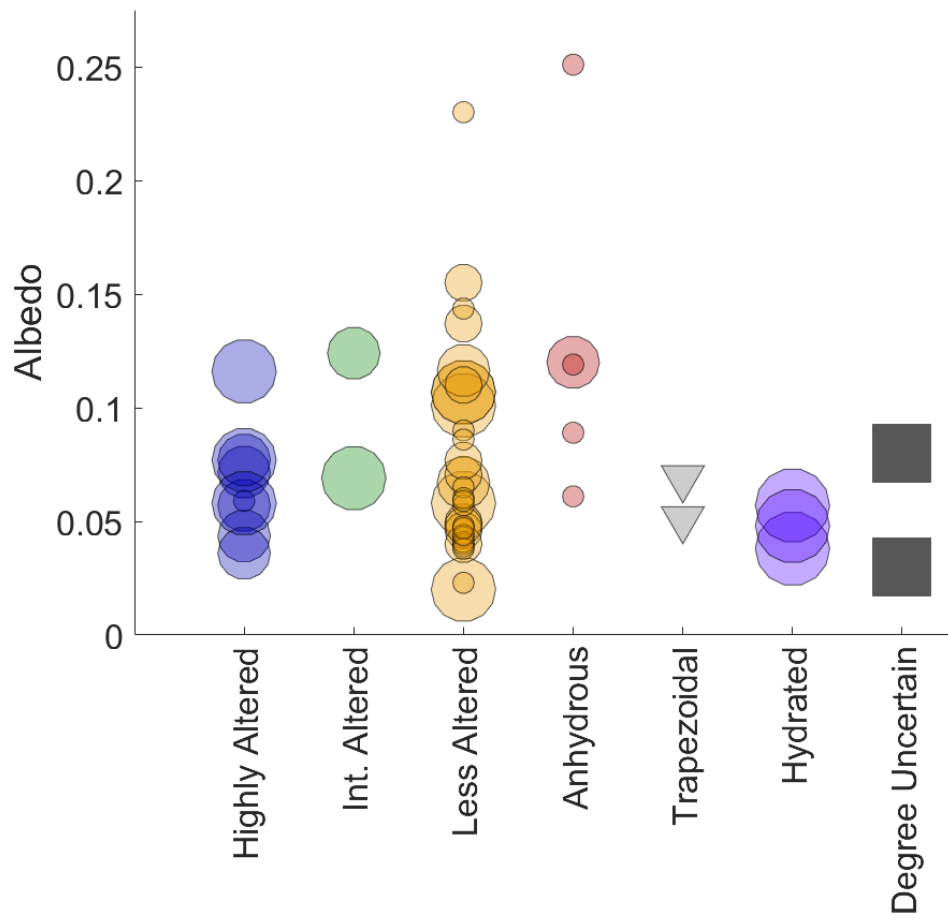


Figure 4.22: Groups of degrees of alteration compared to their albedo. Highly altered asteroids may have a slight preference for lower-albedo asteroids.

Less altered asteroids have a wider range of albedos that can be similar to the highly altered asteroids. There does not appear to be a systematic relationship between degree of alteration and albedo.

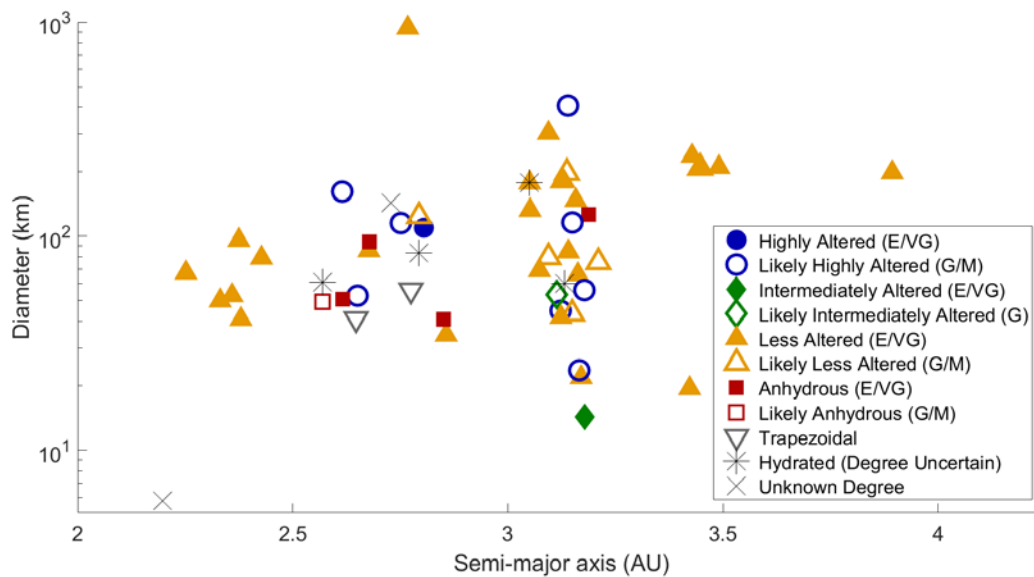


Figure 4.23: Semi-major axis vs. Diameter of asteroid dataset.

The diameter and semi-major axis of each asteroid is plotted. The symbol represents the degree of aqueous alteration for the targets: blue, filled circles are highly altered with GoF values of 0.2-5, open blue circles are highly altered asteroids with GoF values of 5-10, open green diamonds are likely intermediately altered asteroids with GoF values of 5-10, filled green diamonds are intermediately altered (GoF values 0.2-5), open yellow triangles are likely less altered (GoF 5-10), filled yellow triangles are less altered with GoF of 0.2-5, filled red squares are not hydrated (likely olivine dominated) and open gray triangles have trapezoidal features and are likely not hydrated. Additionally, asteroids with poor GoF values are black asterisks indicating they are hydrated but with an unknown degree. Finally, asteroids that cannot be assigned a degree are represented by black 'x' symbols. There does not appear to be a relationship between degree of alteration and heliocentric distance or size. Asteroids of all size ranges and semi-major axes may be aqueously altered or anhydrous.

The widespread appearance and variability of aqueous alteration is shown in **Figure 4.23** where the orbital semi-major axes of the asteroids are plotted against their diameters with the symbol indicating their degree of aqueous alteration. This dataset has few asteroids with $25 \text{ km} \leq D \leq 200 \text{ km}$ between 3.5 and 4 AU. As a consequence, it is not possible to

say with certainty how the alteration state of outer main belt asteroids differs from the mid- and inner-belt as a population. However, with the few asteroids that are currently available, it appears that aqueous alteration has affected the entire asteroid belt. There does not appear to be any relationships between heliocentric distances and degree of alteration similar to previous studies (e.g., Gradie and Tedesco, 1982; Takir and Emery, 2012; Fornaiser et al., 2014). In addition to aqueous alteration affecting asteroids throughout the main belt, there are also examples of anhydrous asteroids throughout the main belt. The implications of these observations are discussed in Section 4.6.

Using the methods of Howard et al., (2015), the minimum amount of water-ice accreted to produce the observed degree of alteration can be estimated. For less altered meteorites/asteroids, the parent body required 15.6 wt.% water-ice when accretion. The highly altered parent bodies required slightly more, 17.3 wt.% water. The main asteroid belt, between 2 and 5 AU, therefore must have had at least 15 wt.% water ice at the time of carbonaceous chondrite parent body accretion to produce the amount of hydration observed in this dataset.

4.5.2 Hydrated Asteroids Span the Range of Degrees of Alteration

Hydrated minerals have been identified on the surfaces of asteroids using visible and near-infrared studies. The ‘checkmark’ feature near 3- μm is indicative of hydrated minerals (Lebofsky, 1980; Vilas, 1994). The Ch-type are defined by the presence of the 0.7- μm feature (e.g., Bus and Binzel, 2002; DeMeo et al., 2009) which is also indicative of hydrated minerals. Rivkin et al (2015) showed that Ch-type asteroids typically have a ‘checkmark’ 3- μm morphology. There are 23 Ch-type asteroids in the dataset presented

here, that may be less or highly altered (e.g., **Figure 4.24; Table 4.10**): Five are highly altered, twelve with less altered mineralogy, one hydrated asteroid that could not be assigned a degree and one asteroid that had an uncertain degree since its spectrum did not match the laboratory data. Asteroids with a 3- μm observations but without the Ch-classification (Takir and Emery, 2012) also have a range in degrees of aqueous alteration. These asteroids can have checkmark features, Ceres-like (e.g., (10) Hygiea) or Europa-like 3- μm morphologies (Takir and Emery, 2012). These asteroids do not have a preferred alteration state but rather have surfaces that are less or highly altered. Example emissivity spectra of asteroids previously known to be hydrated are shown in **Figure 4.25** with meteorite comparisons.

Water-ice on asteroids has been noted by a rounded 3- μm shape (e.g., Rivkin and Emery, 2010; Campins et al., 2010; Lincandro et al., 2011; Hargrove et al., 2012; Hargrove et al., 2015) and through the 10- μm emission plateau (e.g., Lincandro et al., 2011). Four of the five asteroids in this dataset that have a rounded 3- μm features also have sufficient signal-to-noise to identify degree of alteration. These asteroids, (24) Themis, (65) Cybele, (90) Antiope, and (107) Camilla, are interpreted to have hydrated minerals, similar to the less altered meteorites (**Figure 4.26**). The water ice present on these asteroids appears to be masking hydrated minerals in the 3- μm region. This result suggests that simple stratification models of the asteroid belt such as Grimm and McSween (1989; 1993) do not completely reproduce what is observed here, since hydrated minerals are observed on asteroids with water-ice.

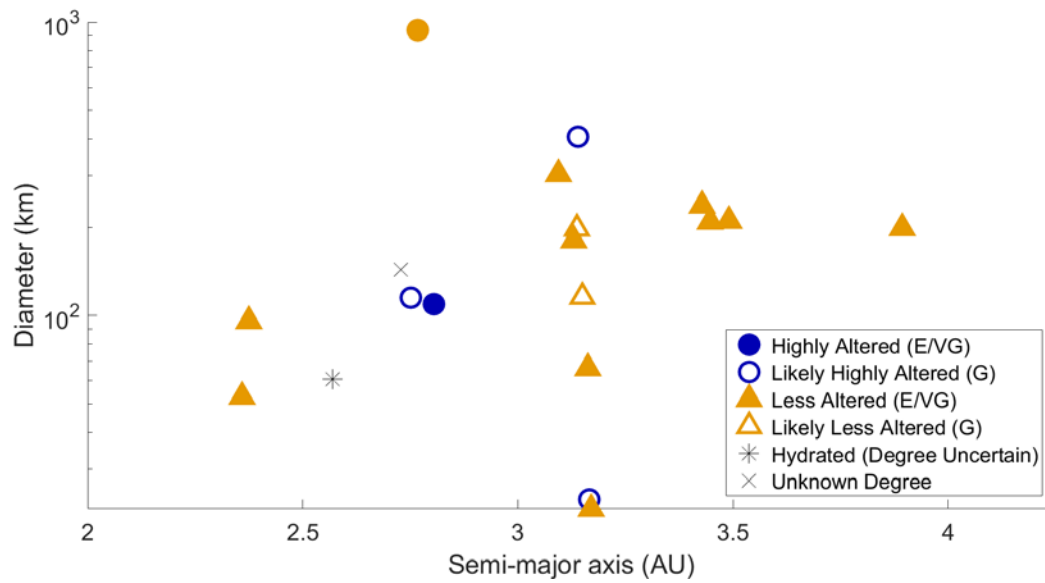


Figure 4.24: Diameter vs Semi-major axis for asteroids with known hydration or water ice.

All asteroids with known hydration appear to have hydrated minerals on their surfaces in the mid-infrared (with the exception of 156 Xanthippe which cannot be assigned a degree). Hydrated asteroids may be any degree of alteration even those with 'checkmark' 3- μm or 0.7- μm features. There does not appear to be a preferred alteration state.

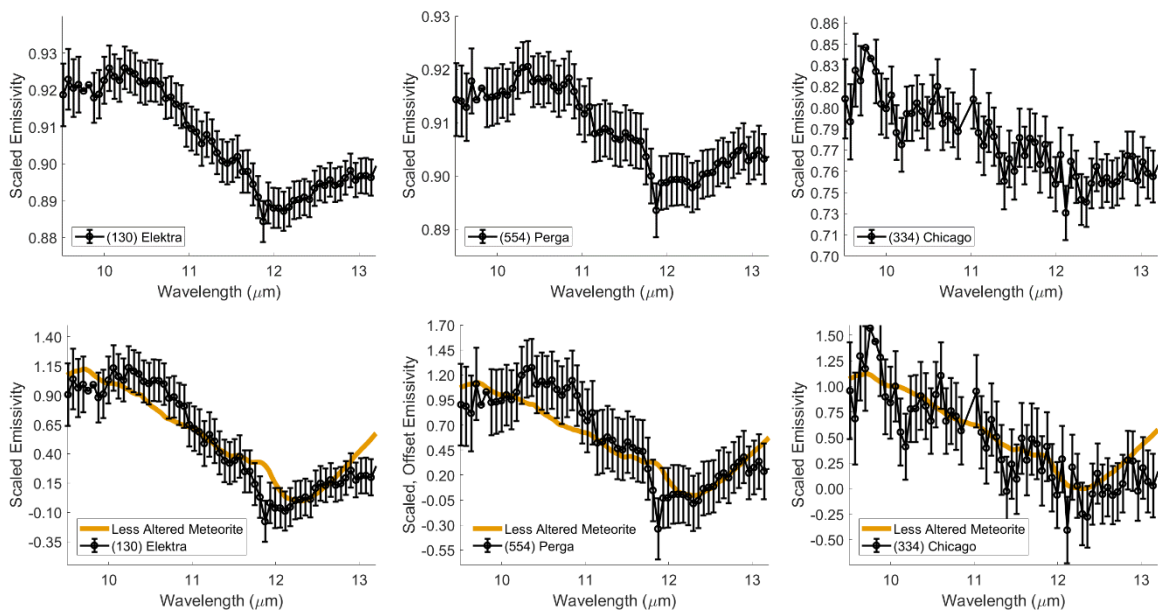


Figure 4.25: Asteroids with known hydration.

Asteroids (130) Elektra, and (554) Perga have both checkmark 3- μm absorptions and 0.7- μm features. These asteroids appear to be similar to the less altered meteorites. (334) Chicago does not have a 0.7- μm feature but does have a checkmark 3- μm shape. It too appears to be aqueously altered similar to the less altered meteorites.

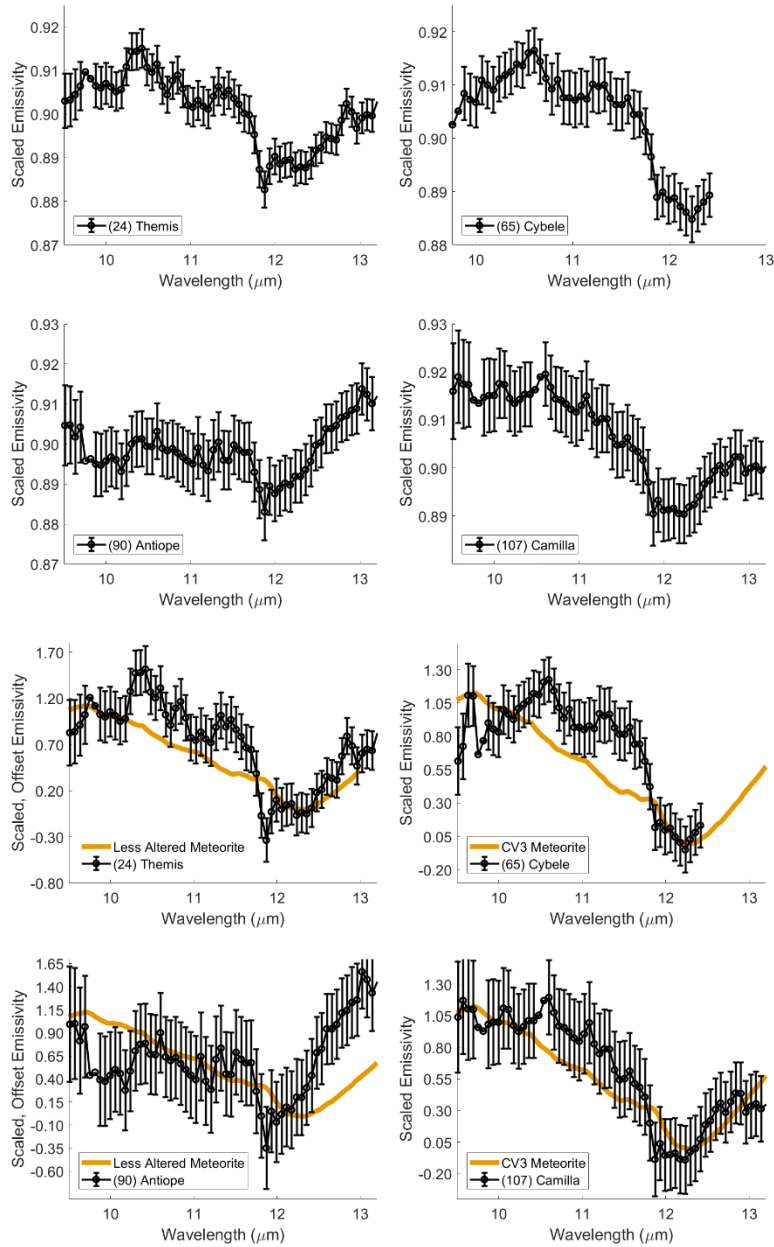


Figure 4.26: Asteroids with water-ice on their surfaces.

Asteroids with rounded 3- μm features appear to be aqueously altered. The asteroids with sufficient signal-to-noise appear to be less altered or likely less altered. Cybele (2nd and 4th rows, right) appears somewhat different than the other water-ice rich asteroids. Water ice appears to be masking aqueous alteration on these asteroids. This indicates that while water ice might be a more abundant component of accreted materials in the Outer Belt, there was sufficient heat to induce aqueous alteration.

Table 4.10: Degree of alteration for asteroids with known water/hydration.

<i>Name</i>	<i>Tholen</i>	<i>Bus-DeMeo</i>	<i>3-μm morph.</i>	Estimated Degree	<i>Goodness-of-fit</i>
<i>(1) Ceres</i>	G	C	Ceres-like	Highly Altered	1.35
<i>(10) Hygiea</i>	C	C	Ceres-like	Highly Altered	5.25
<i>(24) Themis</i>	C	C	Rounded	Less Altered	5.91
<i>(36) Atlante</i>	C	-	Sharp	Highly Altered	9.32
<i>(52) Europa</i>	C	C	Europa-like	Less Altered	1.02
<i>(65) Cybele</i>	P	Xk	Rounded	Less Altered	3.30
<i>(90) Antiope</i>	C	C	Rounded	Less Altered	10.08
<i>(107) Camilla</i>	C	X	Rounded	Less Altered	2.28
<i>(121) Hermione</i>	C	Ch	Sharp	Less Altered	4.16
<i>(130) Elektra</i>	G	Ch	Sharp	Less Altered	1.43
<i>(266) Aline</i>	C	Ch	-	Highly Altered	0.32
<i>(284) Amalia</i>	C	Ch	-	Less Altered	1.81
<i>(308) Polyxo</i>	T	T	Sharp	Less Altered	1.95
<i>(334) Chicago</i>	C	-	Sharp	Less Altered	2.33
<i>(342) Endymion</i>	C	Ch	-	Hydrated*	23.90
<i>(554) Perga</i>	F/C	Ch	Sharp	Less Altered	2.56
<i>(1086) Nata</i>	-	Ch	-	Less Altered	3.64
<i>(2428) Kamenyar</i>	-	Ch	-	Highly Altered	14.95
<i>(2934) Aristophanes</i>	-	Ch	-	Less Altered	2.63

4.5.3 Variability in the Themis Family

The Themis collisional family is a low-albedo family located in the in the mid-belt. This is a dynamically old family (e.g., Nesvorný et al, 2003) that formed 2.5+/- 1 Ga ago. The progenitor asteroid, (24) Themis, is taxonomically classified as a C- (Tholen, 1984) or B-type (DeMeo et al., 2009). This indicates that Themis has an overall low albedo with a flat to blue slope. Family members observed by *Spitzer* have a variety of spectral types that are generally in the C-complex but a few have X-complex types (**Table 4.11**). Evidence of aqueous alteration has been noted for some Themis family members in the visible

wavelength region (e.g., Florczak et al., 1999). In the near-infrared, the Themis family tends to have red slopes (e.g., Ziffer et al., 2011) indicating older surfaces. The results of previous spectral modeling studies of the Themis family indicate a significant spectral component is chondritic porous interplanetary dust particles and ultra-fine (<2- μm grain size) Fe-bearing olivine glasses (Marsset et al., 2016). Themis family members have been interpreted to have larger grain size and/or a denser regolith structure than Jovian Trojan Asteroids (Licandro et al., 2012; Landsman et al., 2016). Furthermore, Landsman et al (2016) suggest that the Themis family asteroids are similar to less altered meteorites which is consistent with the analysis of Themis presented previously (Chapter 2; McAdam et al., 2015). The technique used to arrive at this conclusion in Landsman et al., (2016) was to fit a polynomial to the emission spectra and determine the position of the minima.

Themis has been shown to have water ice and organics on its surface (e.g., Rivkin and Emery, 2010; Campins et al., 2010). This water is thought to be coaccreted with the other asteroidal materials and preserved in the subsurface until the present day. Furthermore, several small Themis family members appear to have comet-like activity (e.g., Hsieh and Jewett, 2006). These observations have been used to suggest that Themis may have had enough water ice to prevent the onset of aqueous alteration (e.g., Takir and Emery, 2012; Grimm and McSween, 1989, 1993). We suggest that Themis family asteroids may range in degrees of aqueous alteration from less to intermediately altered (**Figures 4.27**). Of the Themis family asteroids that have known slopes from Ziffer et al., (2011), there does not appear to be any relationship between slope and degree of alteration (**Table 4.11**). The water ice preserved on Themis may have coaccreted and been preserved on

these bodies, however aqueous alteration did occur on this asteroid. These observations may indicate that the process of aqueous alteration is a highly heterogeneous within a parent asteroid. It is possible that the impact responsible for the collisional breakup of the proto-Themis asteroid could have heated the asteroid enough to induce secondary aqueous alteration. Experiments of impact induced heating indicate that large impacts may raise the global temperature of an asteroid by a few degrees (Kiel et al., 1997). This may be enough heating to induce water-ice melting and the onset of aqueous alteration, however more theoretical studies are required to determine if this is the case.

Table 4.11: Themis Family Asteroids

<i>Name</i>	<i>Tholen</i>	<i>Bus-DeMeo</i>	<i>Slope Value¹</i>	<i>Meteorite best fit</i>	<i>GoF</i>
<i>(24) Themis</i>	C	C	0.17	Less Altered	5.91
<i>(90) Antiope</i>	C	C	-	Less Altered	10.08
<i>(222) Lucia</i>	B	-	0.08	No feature	n/a
<i>(223) Rosa</i>	X	-	-	Less Altered	15.32
<i>(316) Goberta</i>	-	C	0.06	Highly Altered	19.67
<i>(379) Huenna</i>	B	C	0.21	Less Altered	2.58
<i>(383) Janina</i>	B	B	0.03	Less Altered	10.75
<i>(468) Lina</i>	C/P/F	Xc	-	Hydrated*	24.09
<i>(492) Gismonda</i>	-	-	-	Intermediately Altered	17.13
<i>(515) Athalia</i>	I	Cb	-	Less Altered	1.54
<i>(526) Jena</i>	B	-	-	Highly Altered	17.49

¹Ziffer et al., 2011.

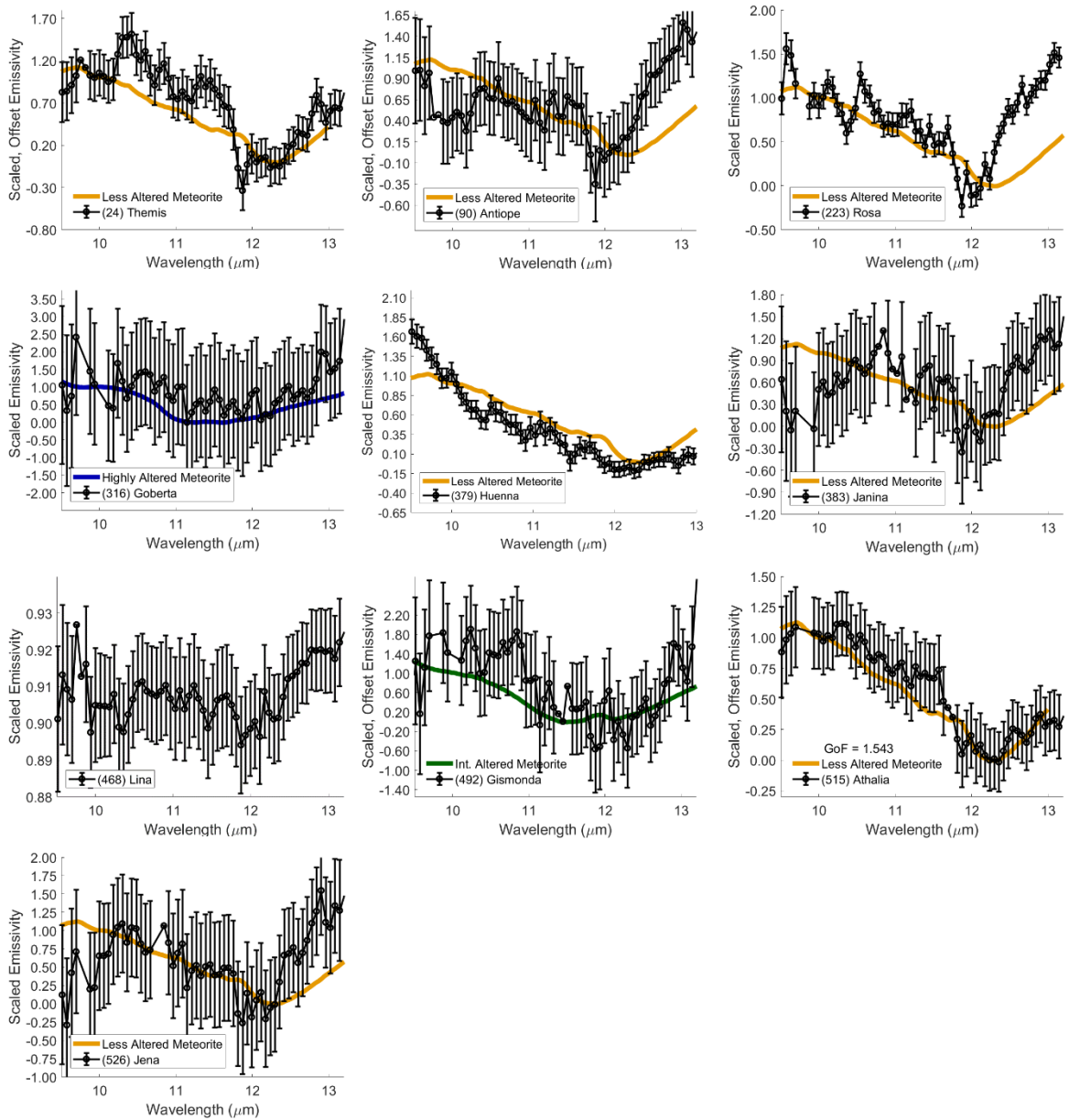


Figure 4.27: Emissivity spectra of the Themis Family members, ordered by number.

The Themis family asteroids appear to be hydrated to any degree, less, intermediately and highly altered. Asteroid (222) Lucia is featureless and not included in this plot since it is featureless. This variability indicates that either that the process of aqueous alteration is highly heterogeneous within a parent body or that the impact that caused collisional break-up may have induced secondary aqueous alteration.

4.5.4 Notable Asteroids

(1) Ceres

Ceres has the distinction of being the largest object in the asteroid belt and one of the targets of the Dawn Mission. It has a mostly spherical shape due to its size. The Dawn mission has constrained Ceres' global geometric albedo to 0.094 ± 0.007 (Ciarniello et al., 2017). Ceres has bright spots that have significantly higher albedos than the surrounding surface (e.g., Ciarniello et al., 2017). Prior to the arrival of Dawn, Ceres had been shown to have iron-rich clays on its surface (e.g., Rivkin et al. 2006; Milliken and Rivkin, 2009). Results from the Dawn mission suggest that Ceres has ammoniated phyllosilicates on its surface (e.g., De Sanctis et al., 2016) that are uniformly distributed (e.g., Ammannito et al., 2016). In addition to the detection of ammonia, recent spectral models also rule out brucite (Mg-rich hydroxide), as previously suggested by Millikin and Rivkin (2009), as a significant component of Ceres' surface (e.g., De Angelis et al., 2016). Additionally, OH was observed outgassing from its surface (e.g., A'Hearn and Feldman, 1993; Küppers et al., 2014). Water-ice has been observed on its surface by Dawn (e.g., Combe et al., 2016; Platz et al., 2016). Mid-infrared observations of Ceres identify the presence of hydrated minerals on its surface based on a 10 and 22- μm feature (Vernazza et al., 2017). Vernazza et al. (2017) further compare SOFIA observations and ISO observations of Ceres to mineral samples diluted in potassium-bromide pellets to simulate the low porosity of regolith surfaces. These comparisons, they conclude, indicate the presence of enstatite (Mg-rich pyroxene) at the level of 20 vol.% in addition to a hydrated mineral component (Vernazza et al., 2017). Ceres has also been observed in the MIDAS survey (Lim et al., 2005) where

it was one of a few asteroids that had an emission feature. Lim et al., (2005) do not comment on the mineralogy of Ceres. Our results of Ceres studied with the IRTF+BASS indicate that it is a hydrated asteroid, in agreement with both the Dawn Mission results (De Sanctis et al., 2016) and previous ground/airborne studies (e.g., Cohen et al., 1998, Rivkin et al., 2009; Millikin; Vernazza et al., 2017). We suggest that Ceres is similar to the less altered meteorites (**Figure 4.28**) with a surface that is 60-75% hydrated minerals. The Dawn mission observed hydrated minerals across the whole surface of Ceres (e.g., Ammannito et al., 2016) and it has been suggested that Ceres could have formed with a higher water to rock ratio than the CM meteorites (e.g., McSween et al., 2016). This result is inconsistent with a high water-to-rock ratio, suggested by McSween et al., (2016). Ceres appears to have experienced extensive aqueous alteration and has a significant amount of hydrated minerals at its surface, however, the high degree of alteration observed by the Dawn mission and through modeling is not reproduced here.

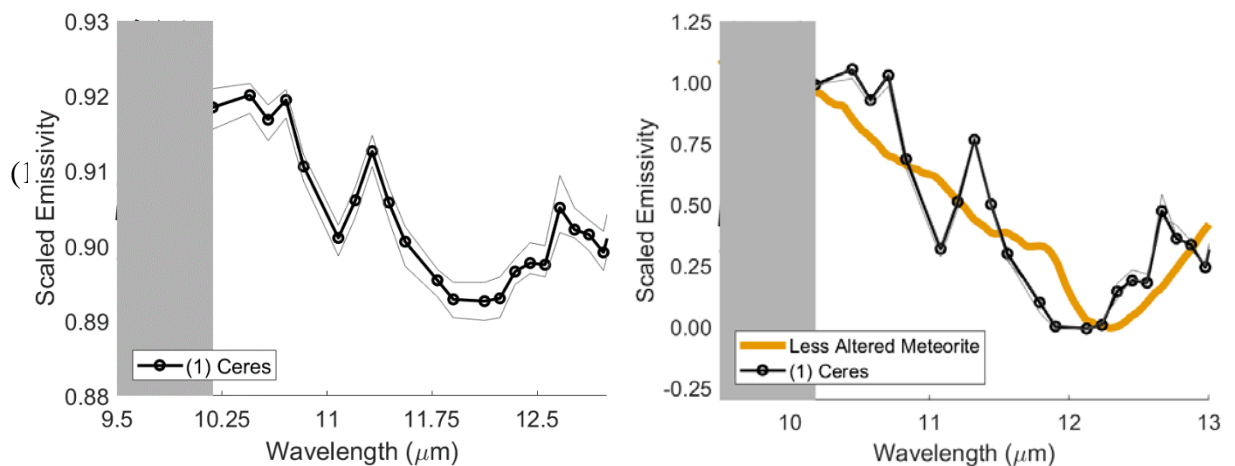


Figure 4.28: (1) Ceres emissivity spectrum and comparison to less altered meteorite. Ceres is interpreted to be similar to less altered meteorites with 60-75% hydrated minerals on its surface

Hygiea (**Figure 4.29**) has spectral similarity in the 3- μm region to Ceres (e.g., Takir and Emery, 2012). Hygiea has been observed in the mid-infrared by ISO (Barucci et al., 2002) and was found to be similar to the anhydrous CO meteorites. Barucci et al., (2002) note that this spectral comparison is not satisfactory, but this comparison is the best they identified. Ceres and Hygiea are thought to have undergone similar parent body processes due to their large size. We find that Hygiea is spectrally distinct from Ceres in the mid-infrared. Presented in **Figure 4.29** is the SOFIA observation of Hygiea. SOFIA observed this asteroid in two wavelength ranges, 8-13- μm and 17.7-27- μm . Both channels indicate that Hygiea is similar to the highly altered meteorites with an 11.5- μm and 22- μm features. These features are somewhat different than the laboratory data, which may suggest some compositional differences between Hygiea and the meteorite endmember used. Hygiea appears to be a highly altered body indicative of large abundances (80-90%) of hydrated

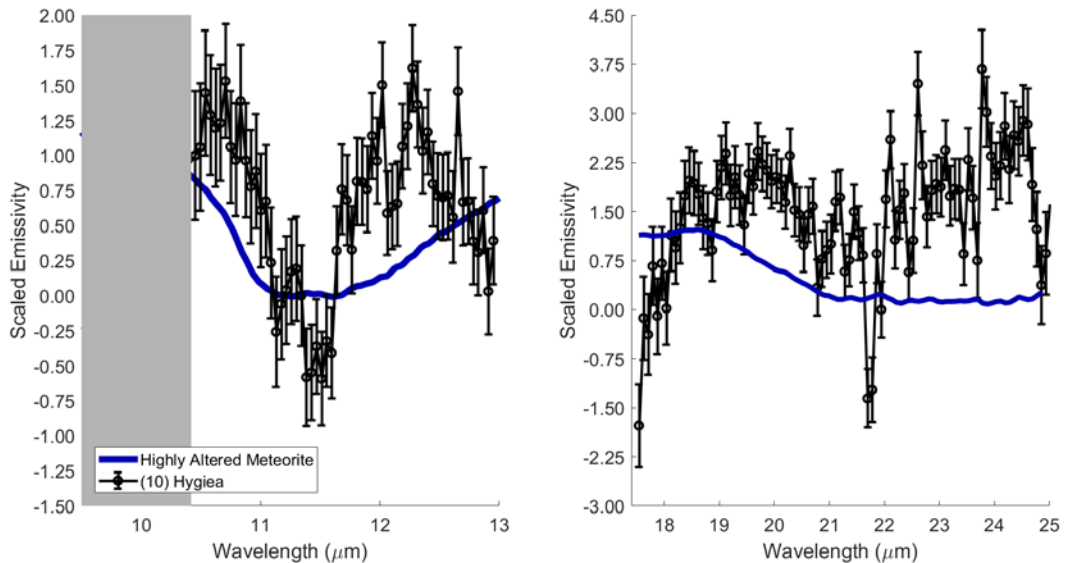


Figure 4.29: Emissivity spectra of (10) Hygiea. Observed with SOFIA + FORCAST, Hygiea has features at 11.5 and 22- μm indicative of a highly altered surface (80-90% hydrated minerals)

minerals. Young et al (1999, 2003) suggest that highly altered meteorites formed on asteroids that have diameters of less than 80 km. Asteroids larger than this would have pore water convection resulting in the loss of water from the system. This observation that

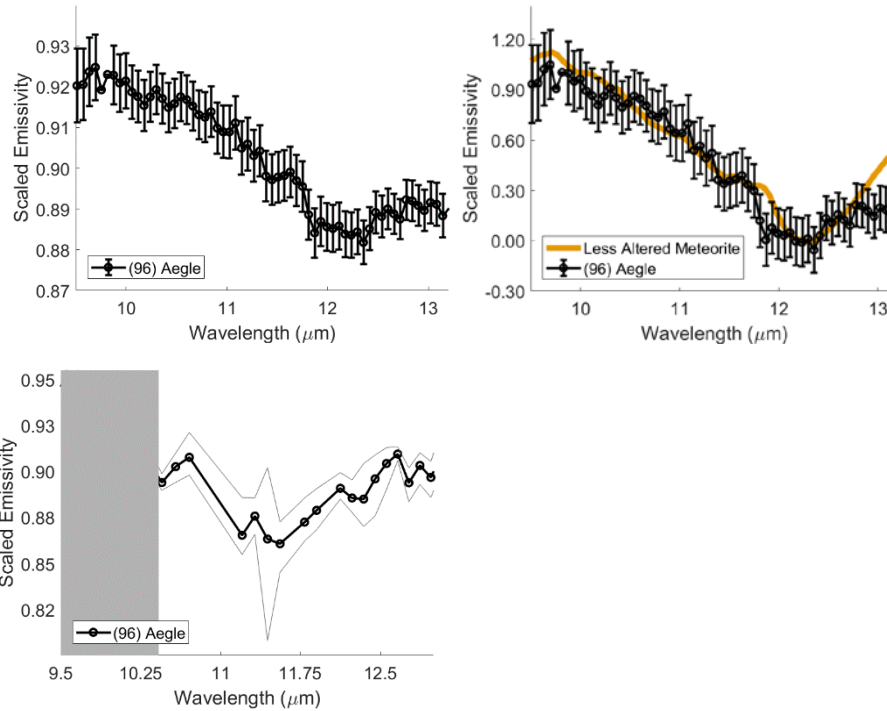


Figure 4.30: (96) Aegle observed with *Spitzer* and *IRTF+BASS*.

These observations indicate that Aegle is hydrated. However, the *Spitzer* data indicates a less altered degree while the *BASS* data suggests a highly altered degree. This difference may be related to a calibration issue or rotational heterogeneity.

Hygiea is highly altered somewhat contradicts the conclusions of Young et al (1999, 2003).

The observation that very large bodies, such as *Hygiea*, have an estimated high degree of alteration may be consistent with new ‘mud ball’ models of asteroid formation and alteration (e.g., Bland et al., 2017). These models suggest that asteroids of larger sizes could experience more extensive alteration, in contrast to the Young et al., (1999; 2003) models.

(96) Aegle

Aegle was observed using *Spitzer* and the *IRTF+BASS* (**Figure 4.30**). These results show that Aegle, a T-type located in the mid-asteroid belt, has hydrated minerals on its

surface. IRTF+BASS observations have a poor goodness-of-fit value and therefore a degree of alteration could not be assigned. Both observations indicate that Aegle is a hydrated body. Aegle may be exhibiting heterogeneity between the Spitzer and IRTF+BASS observations. This could suggest something about the process of aqueous alteration on this asteroid. However, the Spitzer data has a significantly higher signal-to-noise ratio and therefore is much more reliable. More observations of this asteroid are needed to determine if heterogeneity is present.

(3200) Phaethon

(3200) Phaethon is a near-earth object (NEO) that has limited comet-like surface activity (e.g., Jewitt and Li, 2009). This is the progenitor body for the Geminids meteor shower (Fox et al., 1984). It is spectrally a B-type with a negative slope and no features in the near infrared (e.g., DeMeo et al., 2009). This NEO has been suggested to be a comet (due to observed activity) or an asteroid (e.g., Lincandro et al., 2007), because of its spectral type (comets do not have this near-infrared spectral characteristics). Phaethon may possibly from the Pallas Family (e.g., de Leon et al., 2010). Pallas is also a B-type (e.g., Clark et al., 2010) and has a ‘checkmark’ 3- μm feature (e.g., Larson, 1983; Feierberg et al., 1981). The Spitzer observation of 3200 Phaethon (**Figure 4.31**) indicates a surface dominated by hydrated minerals particularly in the 10-13- μm region. In the longer wavelengths (15-25- μm), Phaethon does not appear to be similar to the laboratory data. There does not appear to be a 16 or 22- μm feature despite the distinct similarity to the highly altered meteorites in the 10-13- μm region. Phaethon lacks a distinct trapezoidal shape characteristic of comet nuclei (e.g., Kelley et al., 2017). This result supports an inner Solar System origin for this

asteroid. Comets do not have hydrated minerals since they never experienced enough heating to melt the water-ice (Davidsson et al., 2016).

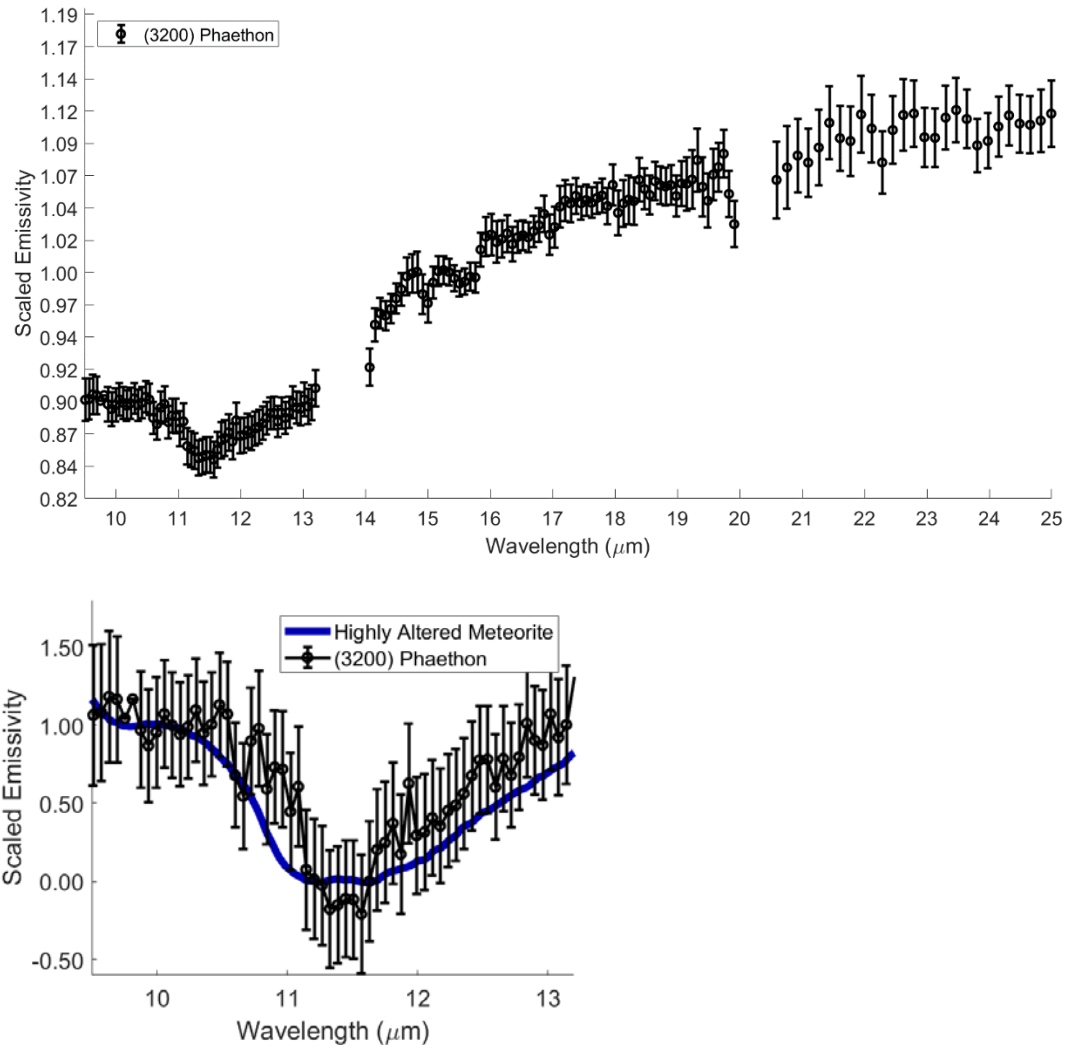


Figure 4.31: (3200) Phaethon emissivity spectrum. Phaethon appears to be a highly altered asteroid with 80-90% hydrated minerals. This suggests that Phaethon has an inner solar system origin as opposed to a cometary origin.

4.6 Implications

4.6.1 Position of the Snow-line

The snow-line is the approximate distance from the sun in the proto-planetary disk beyond which the temperature is cool enough for water to exist as ice (e.g., Hayashi, 1981; Lunine, 2006). The position of the snow-line was first suggested to be at 2.7 AU (Hayashi, 1981) during planet accretion. Since the conditions of the disk vary with time, the position of the snow line likely has changed over the course of the Solar System's early history (e.g., Dodson-Robinson et al., 2009). In some proto-planetary disk models, the snow-line could have migrated in toward the Sun as close as 1 AU depending on the accretion rate onto the central star (Sasselov and Lecar, 1999). Other disk modeling suggests that water in the form of vapor or small ice or dirty ice particles may survive in the inner Solar System, where the disk temperatures are nominally too hot to sustain water ice (e.g., Cyr et al., 1998; Podolak and Zucker, 2004; Chick and Cassen, 1997). These grains could then be incorporated into asteroids during accretion. The dataset presented here suggests that water ice had to be a significant component of the disk in the 2-5 AU region. Less altered asteroids appear throughout the main asteroid belt from 2-4 AU in this dataset. These asteroids require a minimum of 15 wt.% water at accretion to produce the amount of hydrated minerals observed. Furthermore, since accretion ages of carbonaceous chondrites indicate that these meteorite chemical groups were accreting between 2.7-4 Ma post CAI-formation (Fujiya et al., 2013; Sugiura and Fujiya, 2014), water-ice must have been a significant component in this epoch. Additionally, since asteroids have variable degrees of

alteration throughout the main belt, the water ice was likely locally heterogeneous. Asteroids could then accrete variable abundances of water-ice possibly contributing to the variability in degrees observed throughout the main belt.

It has been suggested that the carbonaceous chondrite materials, including C-type asteroids (e.g., Warren, 2011; Walsh et al., 2011) may have formed beyond the orbit of Jupiter where volatiles including water are abundant, then subsequently transported into the asteroid belt during dynamical mixing. The results presented here suggest that, counter to the Grand Tack Theory, water appears to have been a significant component of the disk materials in throughout the main asteroid belt. If the Grand Tack Theory were correct, outer Solar System materials were delivered much further into the main belt than previously thought.

4.6.2 Variability in the Themis Family

The variability in the Themis family may be indicating something fundamental about collisional processing or aqueous alteration on asteroids. Impact induced heating may raise the global temperature of an asteroid a few degrees (Kiel et al., 1997). Aqueous alteration occurs at fairly low temperatures (e.g., Brearley, 2006) so this global increase of a few degrees may be sufficient to induce secondary alteration. The timescale of this global heating would have to be sustained for a significant period of time. Studies of meteorites show that aqueous alteration occurred over a few Ma timescale. Future studies are needed to determine if induced secondary alteration is possible.

Alternatively, the variability in the Themis family may be intrinsic to the proto-Themis asteroid. Recent internal thermal models of Themis (Castillo-Rogez et al., 2010)

indicate that the peak temperature of the parent body may vary depending on initially accreted materials. This thermal heterogeneity may be responsible for the varying degrees of alteration seen in the Themis family members observed by *Spitzer*.

Internal thermal evolution models of asteroids suggest that high degrees of alteration should occur only on small asteroids with diameters of less than 80 km (Young et al., 1999; 2003). Convection of liquid water due to gravitational instability would transport water of hydration to the surface of asteroids larger than this size, and release it to space. More recent internal thermal evolution models of Ceres (e.g., Neveu et al., 2015) suggest a similar convection to produce the amount of hydrated minerals on Ceres' surface. These models are consistent with what is observed on Ceres and Hygiea. Both objects have high degrees of alteration. Additionally, more recent models of asteroid formation and evolution may more accurately reproduce the variable degrees of alteration observed on asteroids in a large size range. The new 'mud ball' models (Bland et al., 2017) reject the underlying assumption in the Young et al., (1999, 2003) models that the asteroid had to be lithified before alteration occurred. If asteroids were not lithified, but rather a loose conglomeration of materials, the Solar-like elemental composition, geochemical signatures (e.g., oxygen isotopes) and variable degrees of alteration can be reproduced on asteroids of a variety of size ranges. Since there is no relationship between degree of alteration and diameter of the asteroid, these results are more consistent with a mud-ball style of internal evolution. More work, however, is required to determine if the mud-ball models can reproduce what is observed in the asteroid belt.

4.6.3 Asteroids with water-ice and hydrated minerals

Four asteroids with rounded 3- μm features appear to be similar to less altered meteorites. This is the first time hydrated minerals and water-ice have been observed on the surfaces of small bodies. Previously, water-ice has been observed in the presence of anhydrous silicates (e.g., comets or hydrated minerals have been observed in the absence of water ice). The observation of water-ice has been made using the 3- μm region while the detection of hydrated minerals is made using a longer wavelength region. It appears that the water-ice frost, which has been suggest to be a very thin layer (45 nm for Themis; Rivkin and Emery, 2010; Campins et al., 2010) is sitting on the hydrated minerals. These two detections are not inconsistent but rather are made by probing different depths into the surface of these asteroids.

Based on the results of internal thermal evolution models of Grimm and McSween (1989, 1993), Takir and Emery suggest that asteroids with water-ice on their surfaces did not experience aqueous alteration. The identification of hydrated minerals on asteroids with surficial water ice suggests that while water-ice may be a more significant component of these asteroids' accretionary materials, its presence did not prevent aqueous alteration. This result may indicate that the internal thermal history of these asteroids is more complex than previously thought. One possibility is that while the heat flux from ^{26}Al may have been lower (because these bodies accreted slightly later; Grimm and McSween, 1989, 1993), there was sufficient heating to melt some water ice and induce aqueous alteration. There may have been an initial period when water melted, inducing the onset of aqueous alteration, covering 60-75% of the silicates into hydrated minerals, then the water refroze

and is preserved until the present. Alternatively, these asteroids may have highly heterogeneous internal distributions of water allowing for alteration to have occurred in some regions while preserving ice in others. The lack of an observed checkmark feature may be indicating that the composition of these hydrated minerals on these asteroids may be different than what is observed on asteroids with checkmark shapes. The fundamental vibration may be in the telluric absorption and therefore unseen in the 3- μm data. Future studies of these asteroids and internal thermal evolution modeling is required to determine how hydrated minerals and water-ice could coexist on asteroids and investigate any differences in composition of the hydrated minerals produced.

In recent years, several active asteroids have been identified in the main asteroid belt (e.g., Hsieh and Jewett, 2006). Several of these asteroids, including 133P/Elst-Pizarro are in the Themis family. The activity observed on 133P has been suggested to be the result of sublimating water ice, however, since this object is so faint and small, it has not been possible to determine this for certain. The dust in 133P's coma should be compositionally different from cometary comae since 133P is related to Themis and Themis is an aqueously altered body. If 133P were to be observed in the mid-infrared, the dust in its coma is expected to be at least 60% hydrated minerals based on the observations of both the Themis family and asteroids with water-ice on their surfaces. The dust in its coma or on its surface may have some olivine since the less altered meteorites still have some unaltered chondrules but the primary mineralogy should be hydrated.

4.7 Conclusions

The presence of hydrated minerals has been previously observed on the surfaces of asteroids using visible, near and mid-infrared spectroscopy (e.g., Fornaiser et al., 2014; Takir and Emery, 2012; Dotto et al., 2002). Using the results from a coordinated spectral-mineralogical study of carbonaceous chondrite meteorites, the amount of hydrated minerals on the surfaces of asteroids can be constrained for the first time, using mid-infrared spectroscopy. We present mid-infrared spectra of 73 unique asteroids observed using *Spitzer*+IRS, IRTF+BASS and SOFIA+FORCAST. These asteroids range in size, albedo, heliocentric distance and spectral type. We find that the hydration is widespread and variable in the main asteroid belt. Asteroids of all sizes, albedos and many spectral types may be hydrated. Spectral type in particular does not seem related to degree of alteration. C-complex asteroids are observed to have any degree of alteration including anhydrous. Similarly, the X-complex asteroids tend to have lower degrees than the C-complex asteroids but may still have hydrated minerals on their surfaces. Additionally, we find that the near-Earth object, (3200) Phaethon, which has been suggested to be either a comet (due to its activity) or an asteroid (based on dynamical arguments and spectral similarities to Pallas), is most similar to the highly altered meteorites and is interpreted to have a main belt origin. Ch-type asteroids and asteroids with ‘checkmark’ 3- μm morphology are all hydrated but exhibit varying degrees of aqueous alteration.

Hydrated minerals are widespread in the main belt. There does not appear to be a relationship between degree of alteration and heliocentric distance. Additionally, asteroids in the main belt have variable degrees of alteration unrelated to size, or distance from the Sun. This may be caused by local heterogeneities in the disk that could allow for more

water-ice to be accreted into asteroids producing more aqueous alteration. Previously observed relationships between 0.7 and 3- μm features and heliocentric distance are not reproduced in this dataset. Furthermore, asteroids with water-ice on their surfaces are observed to be aqueously altered. These represent a new category of object: bodies with both evidence for water and hydrated minerals. Previously, either hydrated minerals have been observed on asteroids or water-ice is present with anhydrous minerals. This indicates that while water-ice may be a more significant accretionary component for outer main belt asteroids, it did not prevent the onset of aqueous alteration on these asteroids. The duration of aqueous alteration may have been shorter for these asteroids or these bodies may have highly heterogeneous internal distributions of water.

The widespread appearance and variability of aqueous alteration, even on asteroids with water-ice, is in contrast to studies using visible (e.g., Fornaiser et al., 2014) and near-infrared measurements (e.g., Takir and Emery, 2012) that conclude there is a nexus in the mid-main belt where aqueous alteration occurred at early times. This result implies that the disk temperatures must have been low enough for water ice to be stable between 2-5 AU from ~2.7-4 Ma after CAI formation. This is the range in accretion times for the carbonaceous chondrites. Anhydrous carbonaceous chondrites (e.g., CVs and COs; accreted with only small amounts of water) formed slightly earlier than aqueously altered carbonaceous chondrites. We observe anhydrous, olivine dominated asteroids similar to CVs to appear throughout the main asteroid belt as well. This implies that the disk temperatures were dropping in the main belt around the time of the olivine-dominated, CV-

like asteroids' accretion, then were cool enough for water ice to be stable as the aqueously altered asteroids accreted.

For the first time, it is possible to identify the degree of alteration of asteroids not simply the presence or absence of hydrated minerals. Furthermore, with the large number of observations, it is possible to examine the distribution of degrees of alteration in the asteroid belt. The widespread appearance of hydrated minerals was not previously observed. This provides important insights about the proto-planetary disk's temperature, particularly during carbonaceous chondrite parent body accretion. While these results are a significant step forward in our understanding of the early Solar System and the distribution of water, there are still significant open questions yet to be answered. The intriguing variability of degrees of alteration in the Themis family, different degrees of alteration for Ceres and Hygiea, and a lack of relationship between degree of alteration and asteroid diameter suggest internal thermal evolution models are not accurately describing the process of alteration. Recent mud ball models of aqueous alteration on asteroids (e.g., Bland et al., 2017) may more accurately reflect what is observed. Furthermore, the Themis family variability may indicate internal heterogeneity of alteration within parent asteroids.

The OSIRIS-REx and Hayabusa-2 missions to small, low albedo NEOs may provide insights into how aqueous alteration occurred on asteroids. Both of these missions are sample return so in addition to their orbital characterization of their target asteroids, Bennu and Ryugu, materials from these objects will be studied in the laboratory. Ryugu is an aqueously altered asteroid (Vilas, 2008) but the alteration state of Bennu is currently unknown. The results of these missions may provide a geologic context for aqueous

alteration, timing of accretion and potentially other insights that will be significant for a fuller understanding of aqueous alteration of asteroids in the main belt.

Chapter 5: Summary of Conclusions and Future Work

The primary goal of this thesis is to connect asteroids and carbonaceous chondrite meteorites using spectroscopy. The second and fourth chapters investigate connections between meteorites and asteroids that have evidence for extensive interactions with water through the process of aqueous alteration. Aqueous alteration is a complex process that depends on the amount of coaccreted water ice, the internal heterogeneity of water within the parent body and the setting of alteration (e.g., open vs. closed system setting). To truly unravel all of these complexities, missions to main belt aqueously altered asteroids are likely needed. However, this investigation of a large number of asteroids that connects their spectral features to well-studied meteorites has provided insights into the Solar System's early history. The third chapter investigates meteorites and asteroids that preserve significant amounts of iron-rich amorphous materials. This material is formed through disequilibrium condensation and is highly susceptible to destruction through parent body processing including aqueous alteration and thermal metamorphism. Its presence indicates that the asteroid/meteorite has not undergone parent body processing and so preserves primitive Solar System material and has experienced minimal processing since accretion.

5.1 Chapter 2 Conclusions

In Chapter 2, spectral changes as a function of degree of alteration are investigated for a suite of CM and CI meteorites that had known bulk mineralogies from previous PSD-XRD studies (Howard et al., 2009, 2011). The visible and near-infrared spectral region

does not contain strong relationships between spectral features and degree of alteration. The near-infrared slope and 0.7- μm band depth are not correlated with abundance of hydrated minerals. The presence of the 0.7- μm band indicates the presence of hydrated minerals, but the lack of such a feature does not indicate the lack of hydration. The mid-infrared region, in contrast, does have strong features that change continuously with degree of alteration. The 10-13- μm feature is particularly useful for determining the degree of alteration of asteroids since this is in a telluric window and so can be used from Earth to study asteroids. In the 10-13- μm region, meteorites can be grouped into three categories based on spectral behavior: highly altered meteorites have an 11.5- μm feature, intermediately altered meteorites have a doublet with peaks at ~ 11.5 and ~ 12.3 - μm and less altered meteorites have features at ~ 12.3 - μm . Additionally, features in the 16-25- μm region also change with degree of alteration. As an example, (24) Themis is estimated to 60-75% hydrated minerals on its surface based on similarities between the emissivity spectrum and the less altered meteorites.

5.2 Chapter 3 Conclusions

Chapter 3 investigates a different group of carbonaceous chondrites that rather than being characterized by aqueous alteration appear to be some of the least processed carbonaceous chondrites. This chapter examines the visible, near and mid-infrared spectroscopy of eight low-metamorphic grade CO meteorites. These low-metamorphic grade CO meteorites have abundant amorphous iron-bearing silicate matrices. The presence of this amorphous material indicates that these chondrites have not experienced

extensive aqueous alteration. Further, they have only undergone mild heating of up to ~200°C. These meteorites record information about accretion and the early solar nebula available nowhere else.

Near-infrared and mid-infrared spectra are reported for these meteorites. Features at 1.4- and 21- μm are attributed to the iron-bearing amorphous silicates. Furthermore, low metamorphic grade meteorites from other chemical groups, CRs MET 00426 and QUE 99177 as well as the ungrouped meteorite Acfer 094, are characterized by similar materials and have the same diagnostic spectral features observed in the low-metamorphic grade COs. CO meteorites of higher metamorphic grades lack these features since the thermal metamorphism that affects them recrystallized their amorphous silicates into olivines. These results provide a tool for identifying the least-processed asteroids if similar near and mid-infrared features are observed. To that end, one asteroid's near-infrared spectrum is presented. (93) Minerva, observed using IRTF+SpeX, has a 1.4- μm features similar to the low-metamorphic grade CO meteorites. This indicates that Minerva has hemispherically abundant iron-bearing amorphous silicates on its surface and likely represents one of the least-processed bodies in the asteroid belt. Future studies of Minerva must first confirm the near-infrared detection with mid-infrared spectroscopy to investigate rotational heterogeneity which will help constrain formation mechanisms for the low metamorphic grade meteorites.

5.3 Chapter 4 Conclusions

Chapter 4 further investigates the distribution of hydrated asteroids in the main belt. Observations of 73 asteroids from three different observatories are analyzed to estimate the degree of alteration of these bodies. Asteroids are assigned a degree of alteration based on their mid-infrared spectral similarity to the laboratory spectra of meteorites (Chapter 2; McAdam et al., 2015a, b). These degrees are: anhydrous (<5% hydrated minerals), less altered (60-75% hydrated minerals), intermediately altered (75-80% hydrated minerals) and highly altered (80-90% hydrated minerals). Asteroids of all degrees of alteration are found throughout the Main Belt. There does not appear to be any relationship between presence or amount of hydrated minerals with heliocentric distance like what has been previously reported (e.g., Takir and Emery, 2012). This result indicates that the disk temperatures in the 2-5 AU region must have been cool enough to sustain water-ice between ~2.7-4 Ma post-CAI formation, when carbonaceous chondrite parent bodies were accreting (Fujiya et al., 2013; Sugiura and Fujiya, 2014). Furthermore, local heterogeneities of water-ice must have been present to produce the variability of degrees observed. This result is a significant departure from previous work (e.g., Takir and Emery, 2012) where water-ice is thought to be a larger proportion of the outer main belt accretionary materials. Aqueous alteration is prevented when water represents a larger proportion of the accretionary materials since there are fewer silicates that contain the heat source, ^{26}Al . Additionally, the accretion times may be later in the outer main belt compared to the inner belt. Combined with water's high specific heat, the accreted ^{26}Al is not

sufficient to melt the water, thus preventing the onset of aqueous alteration. In addition to the widespread, variable abundances of hydrated minerals in the asteroid belt, asteroids that have previously been observed to have water-ice on their surfaces by a rounded 3- μm feature are found to be aqueously altered. In particular, (24) Themis, (65) Cybele, (90) Antiope and (107) Camilla appear to be similar to the less altered meteorites. This indicates that, while water ice may be a more significant component of the accretionary materials, there was sufficient heat to induce aqueous alteration, for at least a period, in some regions of these asteroids. The evidence of water ice in addition to hydrated minerals indicates that these asteroids are a new category of small body. Hydrated minerals have never before been identified in the presence of water ice previously.

In addition to the hydration observed on asteroids with water-ice, there are other indications that asteroid internal thermal evolution is not fully understood. For example, Ceres and Hygiea, thought to have experienced similar internal thermal histories, appear to have different degrees of alteration (Ceres being less altered, Hygiea highly altered). Furthermore, the diameter of asteroids is not related to their degree of alteration as has been predicted by internal thermal evolution models (e.g., Young et al., 1999, 2003). Additionally, Themis family asteroids appear to have varying degrees of alteration. These asteroids may be less or intermediately altered. This variability in degrees of alteration for family members may be related to secondary aqueous alteration induced by the collision that formed the family or it could be heterogeneous alteration on this parent body.

5.4 Limitations of this work

Results of a coordinated-spectral mineralogical study of meteorites in the laboratory provide new tools for determining the degree of alteration of asteroids remotely in addition to identifying some of the most pristine nebular condensates in the asteroid belt. This work also provides new insights about the process of aqueous alteration on asteroids. The identification of a new category of asteroid (those with evidence for water ice and aqueous alteration) and variability in the Themis family indicate potentially heterogeneity of aqueous alteration in the parent body show that the geologic setting of aqueous alteration is perhaps more complex than previously thought. Furthermore, this work challenges ideas about the history of the solar nebula. While it has been hypothesized that the position of the snow line may have changed over the Solar System's history, here it is shown that the snow line must have been at ~ 2 AU during the time of carbonaceous chondrite accretion. However, this work has certain limitations.

5.4.1 Survey Sample Limitations

A significant limitation of the study of asteroids is a lack of targets with diameters between 50 and 125 km in the Outer Belt (3.5-4 AU). These asteroids are understandably difficult to detect but observing them to determine their degree of alteration may further help constrain how aqueous alteration has affected the asteroid belt.

5.4.2 Lack of Modal Mineralogy for Asteroids

While this work estimates the degree of alteration of asteroids, it is unable to estimate the modal fractions of minerals on their surfaces. The main reason for this is a

spectral library of endmember minerals does not exist for carbonaceous chondrite meteorites. As has been mentioned in the chapters above, carbonaceous chondrite minerals, especially the hydrated minerals, do not have good terrestrial analogs. The setting of meteorite mineral formation is significantly different from terrestrial settings, including temperature and pressure regimes. Consequently, terrestrial phyllosilicates in particular do not have the same spectral features and therefore cannot be used for spectral modeling. Future studies must establish appropriate endmember spectra to do this modeling.

One way to obtain endmember carbonaceous chondrite relevant mineral spectra is to use FTIR microscopy to obtain spectra on thin sections of meteorites. This technique would allow the researcher to obtain the spectra of individual grains or regions of meteorite matrix. Using FTIR microscopy and electron microprobe analyses it will be possible to identify the composition of the minerals being investigated as well as their spectra. Carbonaceous chondrites are tremendously variable on all scales. Consequently, this study must obtain FTIR microscopic spectra of many thin sections within groups. Studying a large number of meteorite thin sections would provide the researcher with a comprehensive library of meteorite mineral phases. Once these are collected, linear mixing models can be used to determine the modal fractions of minerals in an asteroid's spectrum.

5.4.3 Porosity and Grain Size Effects

Further study is also needed to understand how carbonaceous material behaves with porosity and grain size. These effects have been well studied in the laboratory (e.g., Logan et al., 1973; Henderson et al., 1996) but with minerals that are not relevant to the carbonaceous chondrites. Two asteroids were observed to have significantly different mid-

infrared spectra than meteorites. (267) Tirza and (1284) Latvia appear to have larger spectral contrast in the 9 to 11- μm region compared to other asteroids in the dataset. Spectral features similar to this have been observed for comet nuclei and Jovian Trojan D-type asteroids. These features have been previously interpreted to be related to the asteroids' grain size and surface configuration of the grains (e.g., fairy castle structures). The Trojan D-types have been interpreted to have a different origin than the main belt asteroids, which explains their spectral distinctiveness. Asteroids Tirza and Latvia are interpreted to either have small grains in a fairy castle structure or to have a different origin than the other main belt objects studied. More work is required to understand these objects to better understand their mineralogy.

5.5 Future Work:

5.5.1 Internal Thermal Evolution Models

Several results from Chapter 4 indicate that the current understanding of the internal thermal evolution of asteroids does not reflect what is observed: the lack of relationship with degree of alteration and asteroid diameter, the different alteration states of Ceres and Hygiea as well as the Themis family variability. The success of the Young et al. (1999, 2003) models were that they reproduced the oxygen-isotope distribution observed in the CI and CM meteorites. Recent modeling efforts show that asteroids in a much larger size range compared to Young et al., (1999, 2003) may experience extensive aqueous alteration (Bland et al., 2017). These models reject the underlying assumption that the asteroid had to be lithified prior to alteration. Instead, asteroids are treated as 'mud balls', loose

conglomerations of liquid water and silicates. This treatment simultaneously preserves geochemical markers observed in meteorites (e.g., oxygen isotope signatures and Solar-like elemental composition) and predicts aqueous alteration may occur to any degree on asteroids of sizes below ~400 km. The models of Bland et al., (2017) are promising for understanding of alteration on asteroids, it is necessary to compare the predicted distributions of hydrated minerals at the surfaces of asteroids (depending on size and initial water to rock ratios) to observations of asteroids. Additionally, internal thermal models of asteroids must additionally investigate if heterogeneity is possible and how this might be expressed (e.g., layering, depth dependency, onion skin layers etc.).

Internal thermal modeling is also relevant for the study of asteroids linked to low metamorphic grade CO meteorites. (93) Minerva may have some compositional heterogeneity on its surface. If Minerva is homogeneous, this implies that this object and the low metamorphic grade CO meteorites, formed after the peak heat flux from ^{26}Al . Without significant heating these meteorites/asteroids escaped parent body processing. If however rotational heterogeneity is observed this may imply a more complex internal thermal evolution. Thermal models may need to investigate how to preserve amorphous materials on a heated or aqueously altered body.

5.5.2 Sample Return Missions

Ongoing sample return missions will provide key insights into the process of aqueous alteration on asteroids. NASA's OSIRIS-REx and JAXA's Hayabusa-2 missions are sample return missions visiting low albedo near Earth objects Bennu and Ryugu. These two asteroids are near-Earth objects and so likely have their origin in the main belt. Bennu

is rubble pile object (Chesley et al., 2014) indicating it has an extensive collisional history. The mass and bulk density of Ryugu is currently unknown. While these asteroids are significantly different from many of the main belt asteroids studied in Chapter 4, Ryugu and Bennu are likely related to main belt objects. These missions will, therefore, provide observations of the geological settings of aqueous alteration on asteroids. In addition to their orbital characterization of these bodies, samples from Ryugu and Bennu will be returned for study in the laboratory. As a consequence of both the orbital characterization and sample returns, these asteroids will be the standard of comparison for aqueous alteration in the asteroid belt. The results of these missions will provide key insights that will significantly improve our understanding of alteration on asteroids.

Ryugu appears to be an aqueously altered body (e.g., Vilas, 2008), however, there is some evidence for spectral variability. Lazzaro et al. (2013) do not observe a 0.7- μm feature that had previously been identified. In the absence of mid-infrared observations with sufficient signal-to-noise to identify surface mineralogy, it is not currently possible to determine the degree of alteration of this asteroid. However, Ryugu is likely related to the aqueously altered meteorites. It may be any degree of alteration from less to highly altered. Hayabusa-2 is not carrying a mid-infrared spectrometer, however its near-infrared spectrometer can globally map the presence of the 0.7- μm but the degree of alteration for this asteroid will not be known until the sample is returned to the laboratory.

Bennu has a B-type classification indicating a blue near-infrared slope. Mid-infrared studies of Bennu (Emery et al., 2014) do not have sufficient signal-to-noise to determine the degree of alteration for this object. Two asteroids in the dataset presented in

Chapter 4 have B-type classifications: (3200) Phaethon and (383) Janina. Phaethon and Janina are aqueously altered bodies but with different degrees (highly and less altered respectively). Bennu could be any degree of alteration, including anhydrous since it is not possible to constrain the degree of alteration using near-infrared features and slopes. OSIRIS-REx is carrying a mid-infrared instrument that will be able to globally map the degree of alteration of Bennu prior to sample collection. Using the results from this thesis, the OSIRIS-REx team may be able to contextualize the differences in degrees of alteration between the region where the sample is collected and the rest of the asteroid.

5.5.3 James Webb Space Telescope

The James Webb Space Telescope (JWST) is carrying the Mid-Infrared Instrument (MIRI) that will be able to observe asteroids in the 5--38- μm range. JWST will be capable of observing small, faint objects that are difficult if not impossible to observe from Earth. This observatory will be able to identify the degrees of alteration for asteroids and potentially surface mineralogy of asteroids. For example, JWST and MIRI may be able to identify the 21- μm feature in the spectrum of Minerva (if present) to confirm the presence of amorphous iron-bearing silicates.

5.5.4 Upcoming projects

Preserving amorphous material on (93) Minerva. As discussed in Chapter 3, near-infrared observations of Minerva indicate it has significant amorphous material on its surface. This material may be preserved there in several ways including as the outer unprocessed shell on an asteroid whose interior has experienced processing (aqueous alteration or thermal metamorphism) or the asteroid accreted late and the whole body is

characterized by the presence of this material. In order to determine which preservation hypothesis is correct, mid-infrared rotationally resolved spectroscopy of this asteroid is required. Either Minerva will be rotationally homogeneous, supporting the late-accretion theory of formation or it will be rotationally heterogeneous. Rotational heterogeneity can occur when a large impact excavates subsurface material. Using the mid-infrared spectral region, it will be possible to determine if this subsurface material is hydrated or anhydrous. Hydrated subsurface material indicates that Minerva is likely related to the CR meteorites that may preserve amorphous iron-bearing materials but are also characterized by aqueous alteration. Alternatively, these subsurface materials may be anhydrous. This would indicate that Minerva is related to the CO meteorites, characterized by thermal metamorphism. Finally, it is unlikely that Minerva is the only asteroid that preserves these materials. The near-infrared spectral signature of the amorphous iron-bearing materials provides a useful tool for identifying asteroids similar to Minerva and the low-metamorphic grade carbonaceous chondrites. To find other asteroids with abundant amorphous materials, a survey of archived and new data will be undertaken in order to understand these objects as a population.

Timing of Phaethon's orbit change. (3200) Phaethon appears to be similar to the highly altered meteorites, indicating its surface is 80-90% hydrated minerals. Phaethon's orbit has a passes very close to the sun with a perihelion distance of 0.14 AU. This close approach coupled with the observed activity (e.g., Jewett and Li, 2010) make the observation of significant hydrated minerals somewhat surprising. The fact that there are still significant hydrated minerals that have not been destroyed through dehydration

processes (e.g., Tonui et al., 2014) may provide a method to time when Phaethon experienced its orbital change. To time this change, laboratory dehydration experiments on highly altered meteorites are required. Simulating the thermal flux that Phaethon has experienced and observing when the 11.5- μm feature changes or disappears may provide this constraint. Additionally, asteroids such as (10) Hygiea have been shown to be similar to heated CM meteorites (e.g., Hiroi et al., 1992) in the near-infrared. It is possible that Phaethon, like Hygiea potentially or naturally dehydrated CM meteorites (e.g., Tonui et al., 2014) may have experienced heating/dehydration prior to its orbital change. These laboratory studies must investigate dehydration on meteorites with varying degrees of alteration. Additionally, surveys of aqueously altered with subsequent heating are required to constrain the amount of heating Phaethon could have experienced before its orbital change.

5.6 Concluding Remarks

This work represents the first step towards a more in depth understanding of aqueous alteration in the asteroid belt. Previously, it was only possible to identify the presence of hydrated minerals or water ice. The new techniques presented here provide a tool for remotely estimating the degree of alteration of asteroids which has implications for the timing and abundance of water-ice in the early Solar System. These results provide new constraints on planet formation by estimating the abundance of water in the asteroid belt during carbonaceous chondrite accretion or alternatively, the extent of dynamical mixing that occurred. More studies are needed to continue to understand aqueous alteration in the

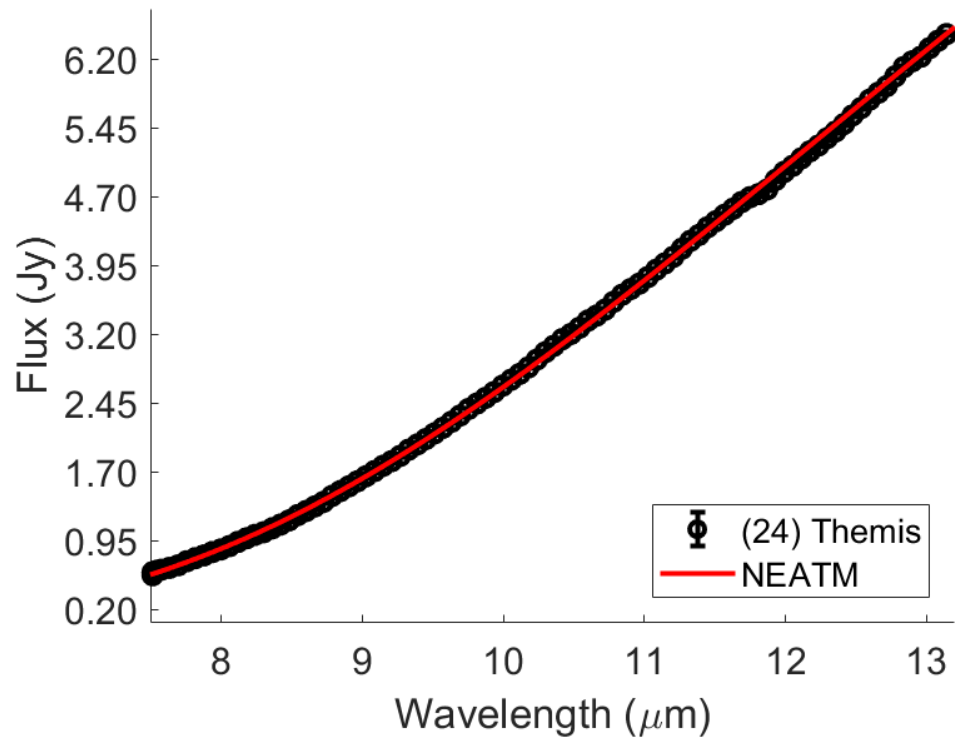
asteroid belt. Upcoming missions to small, low albedo asteroid that may be hydrated will provide new insights into the formation, processing and timing of aqueous alteration on asteroids. One unique aspect of this work is the focus on connecting laboratory studies of meteorites to asteroids. This synergy between laboratory studies and remote sensing techniques will continue to provide more insights into parent body processing, formation and timing of solar system and parent body events. The continuing connection between these two disciplines is essential for future progress in our understanding of aqueous alteration and the distribution of volatiles in the early Solar System.

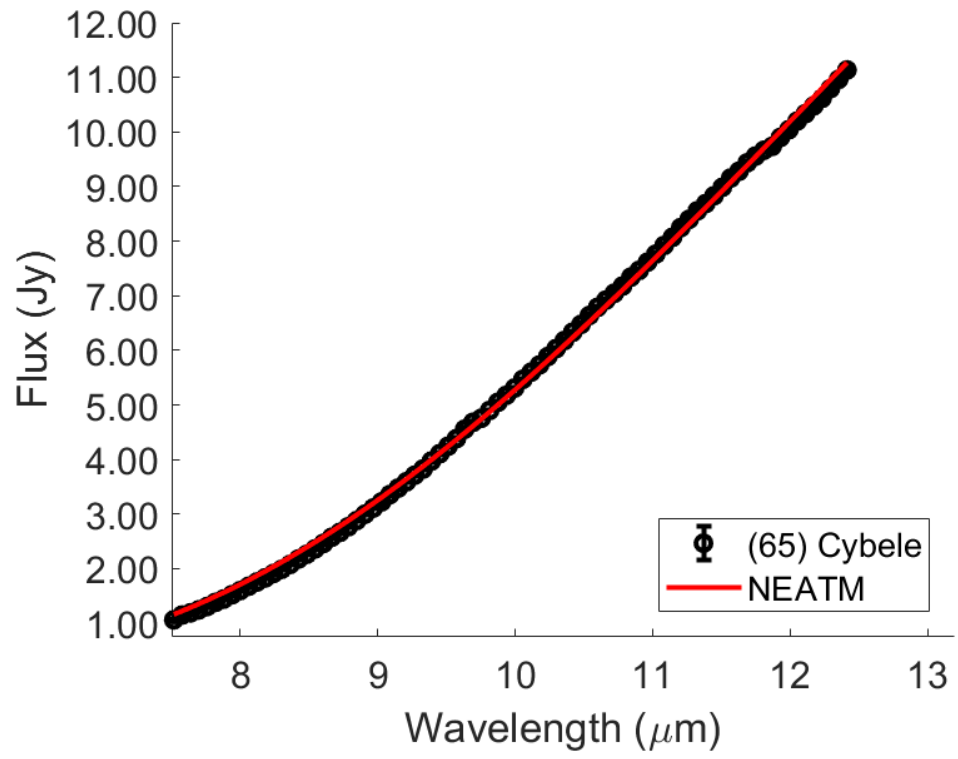
Appendices

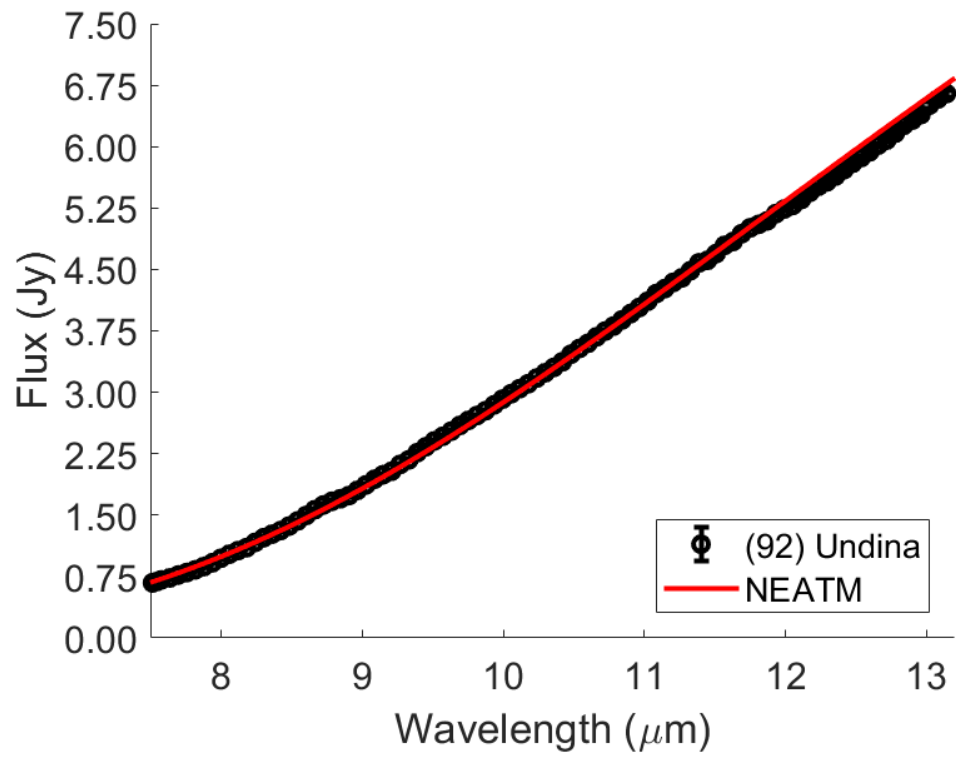
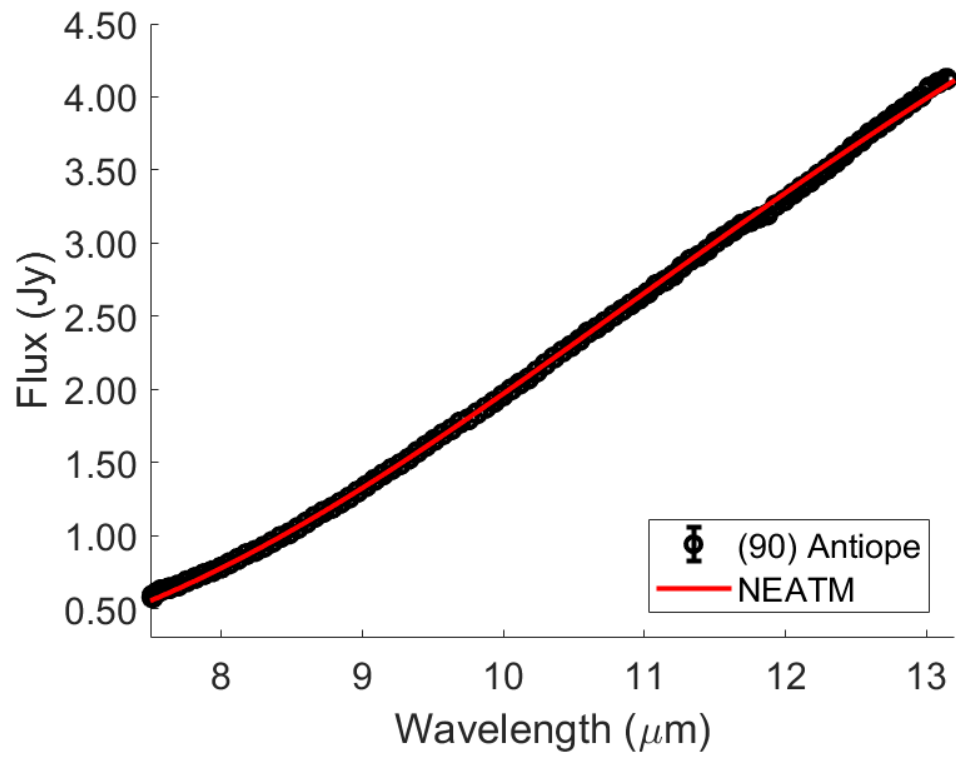
Appendix 1: Asteroid Data and Thermal Models

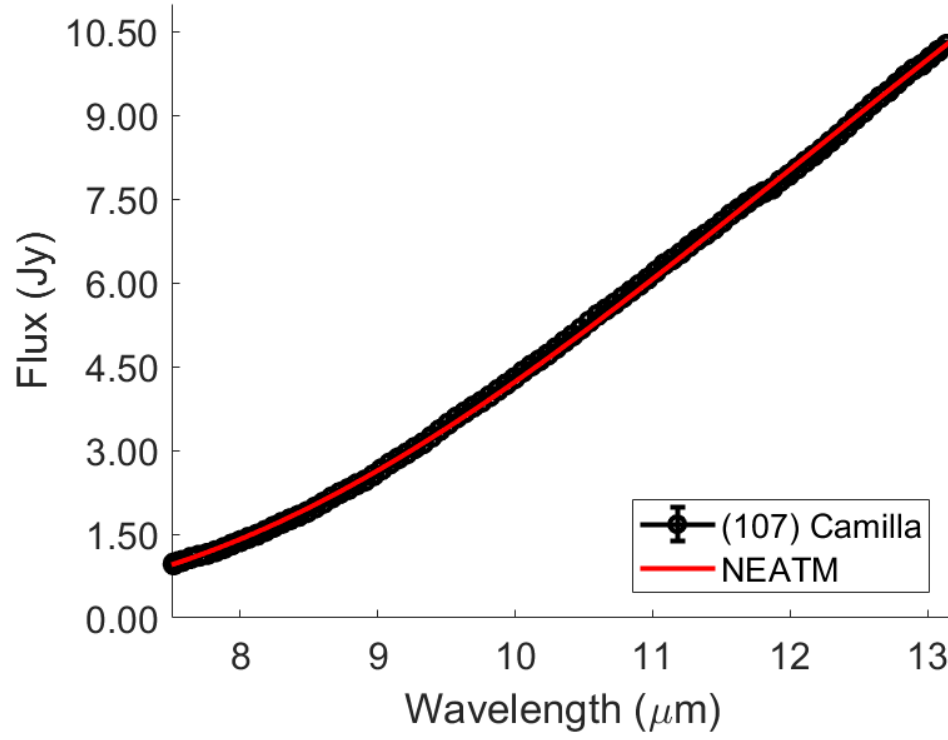
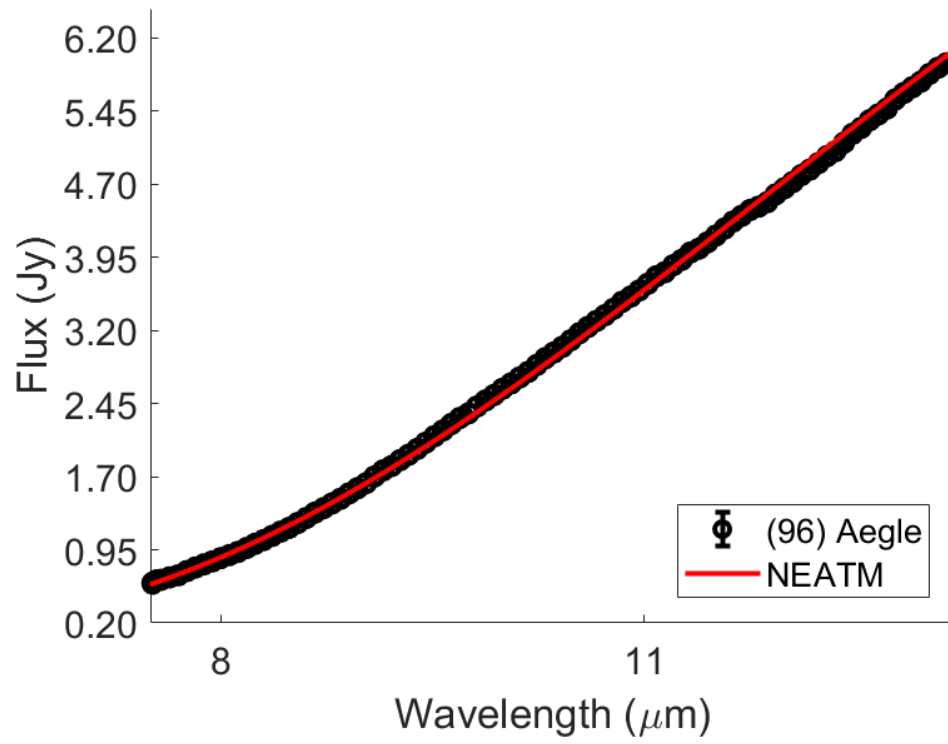
Presented here are asteroid data with their best fit Near Earth Asteroid Thermal Models (NEATM; e.g., Delbo and Harris, 2002). Best fit parameters for each model can be found in **Table 4.9**

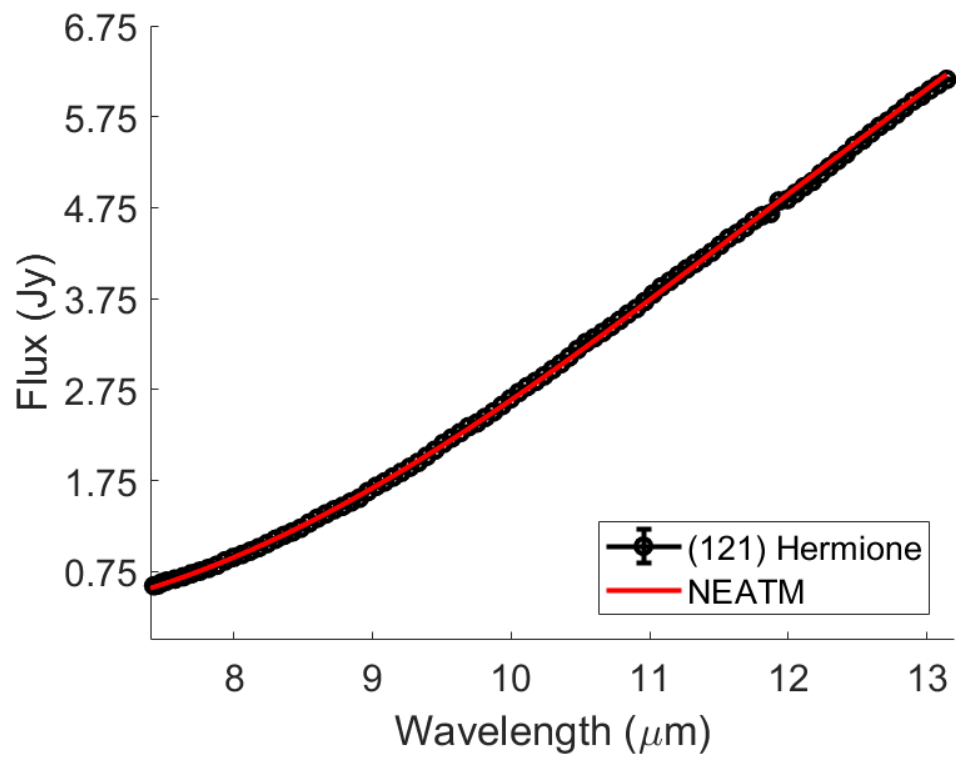
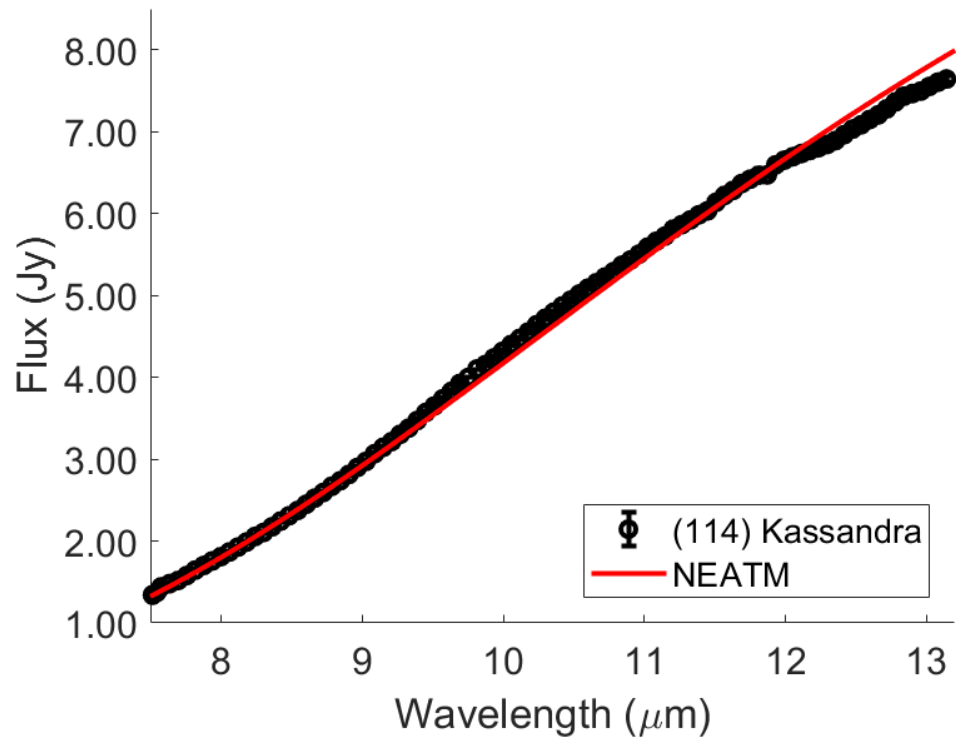
Spitzer+IRS Observations:

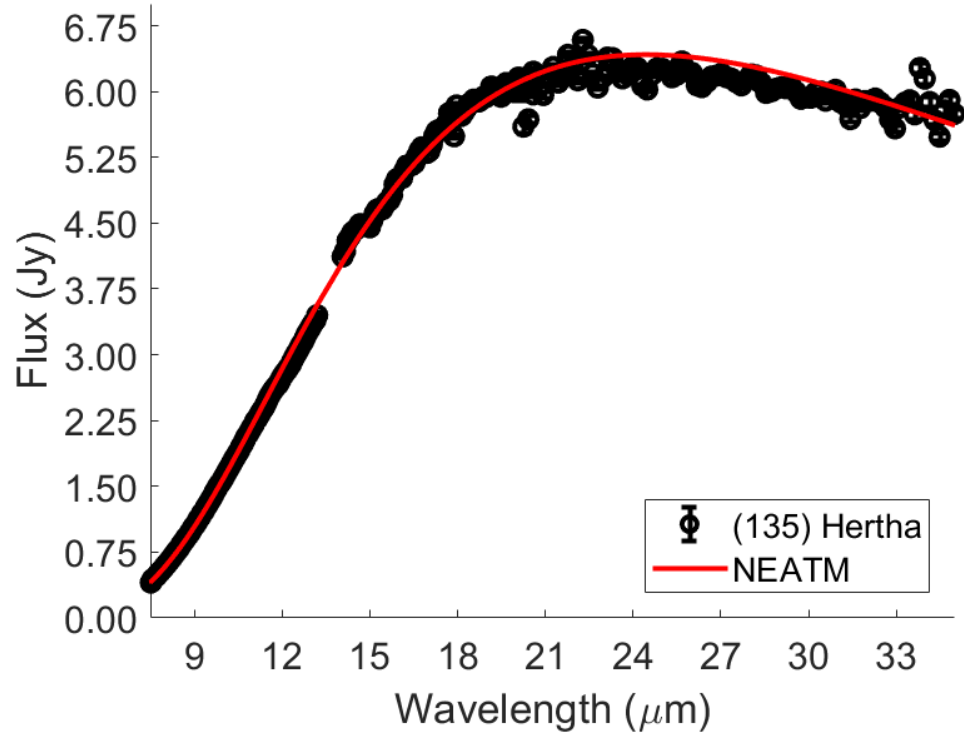
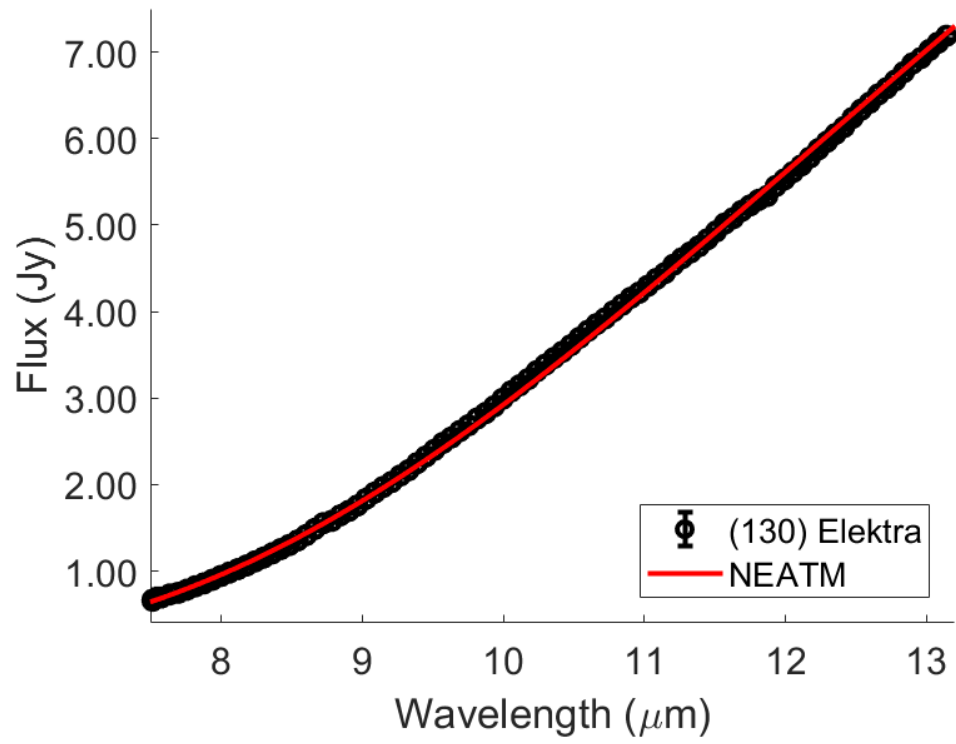


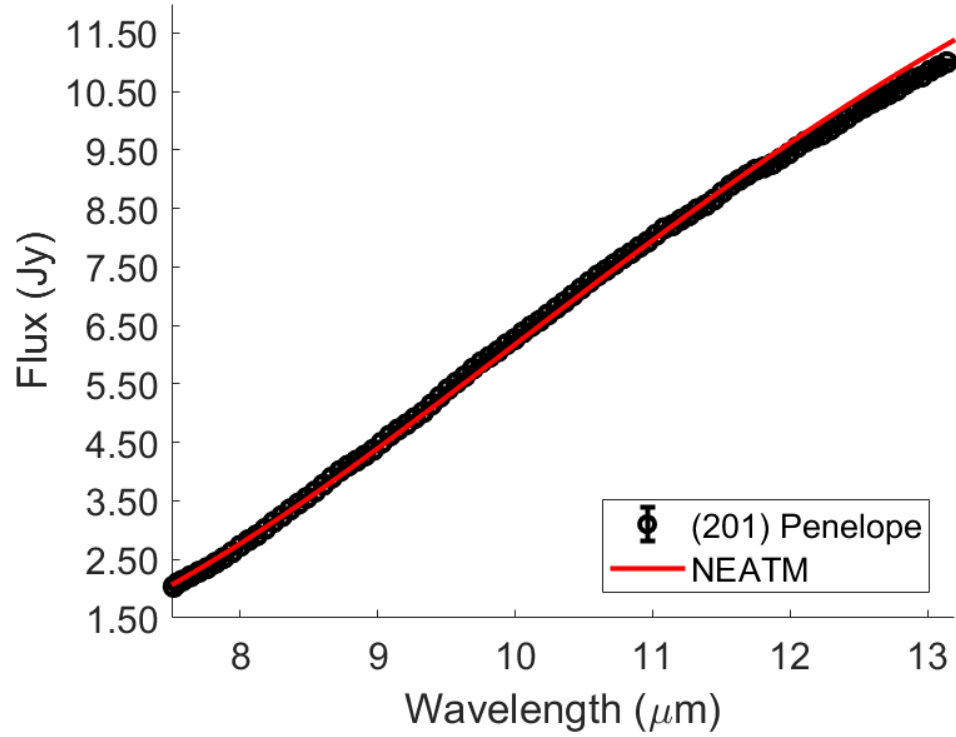
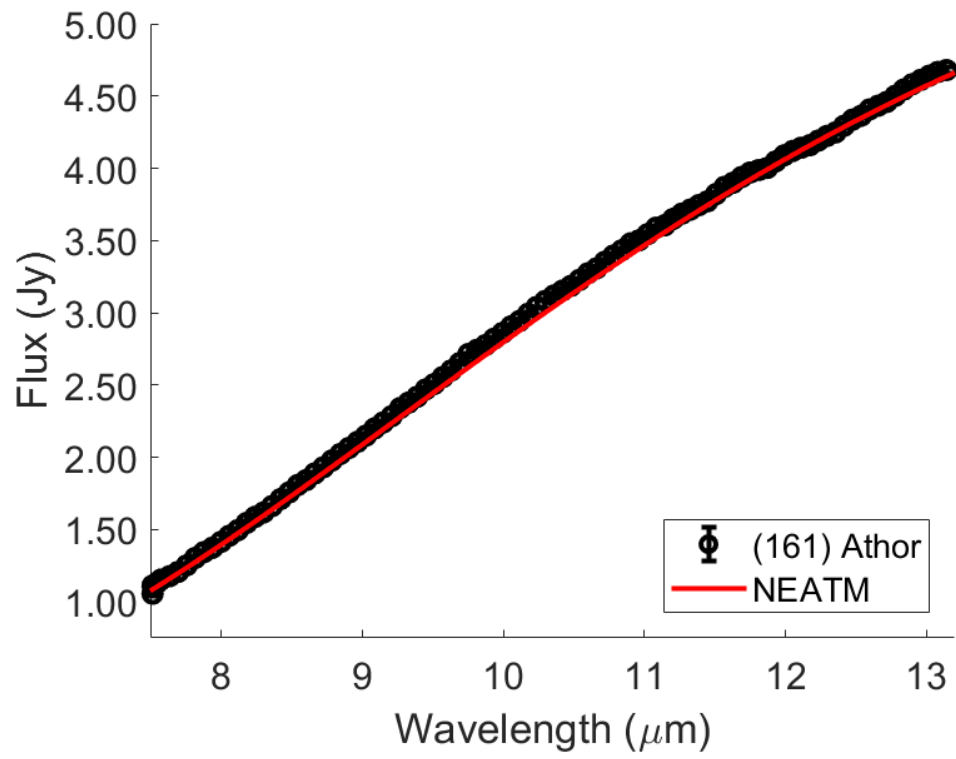


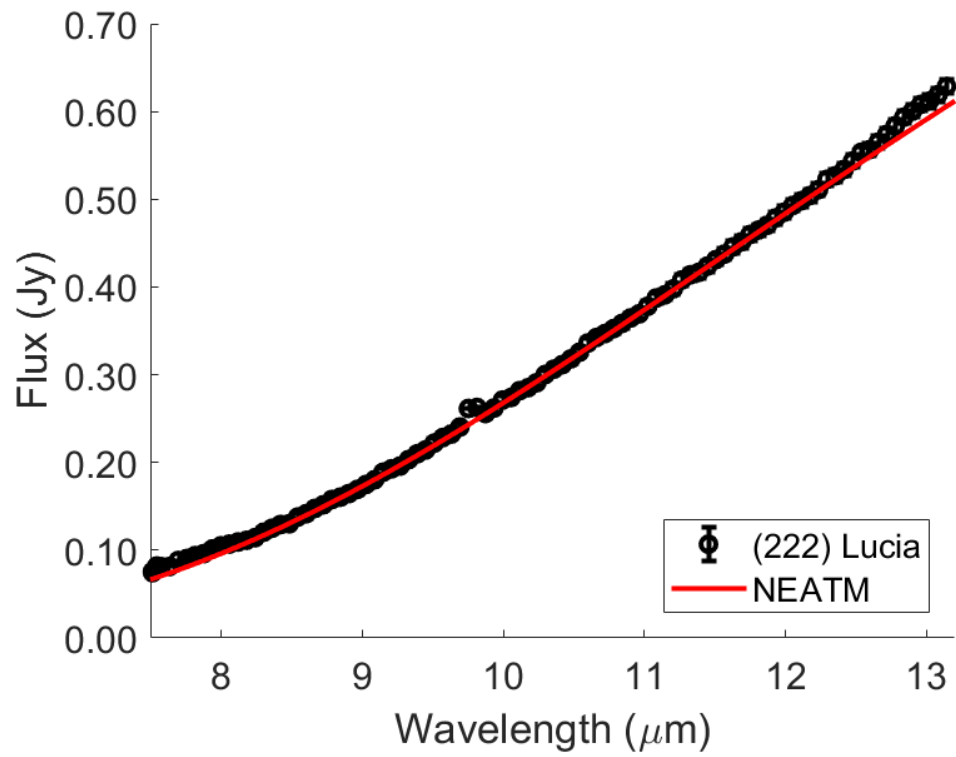
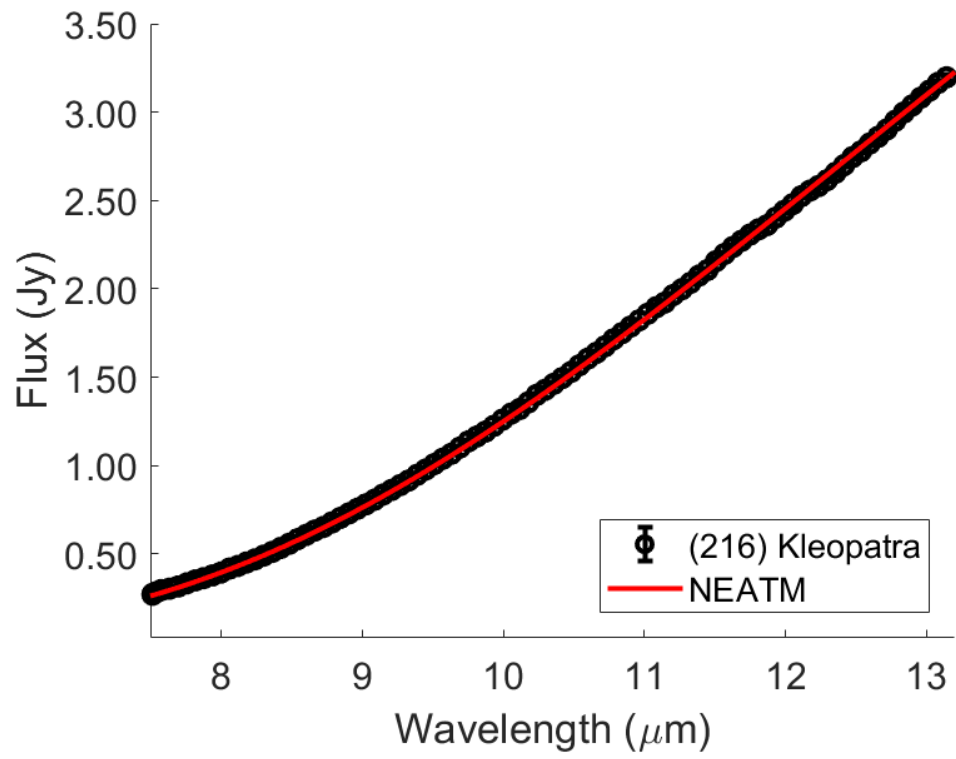


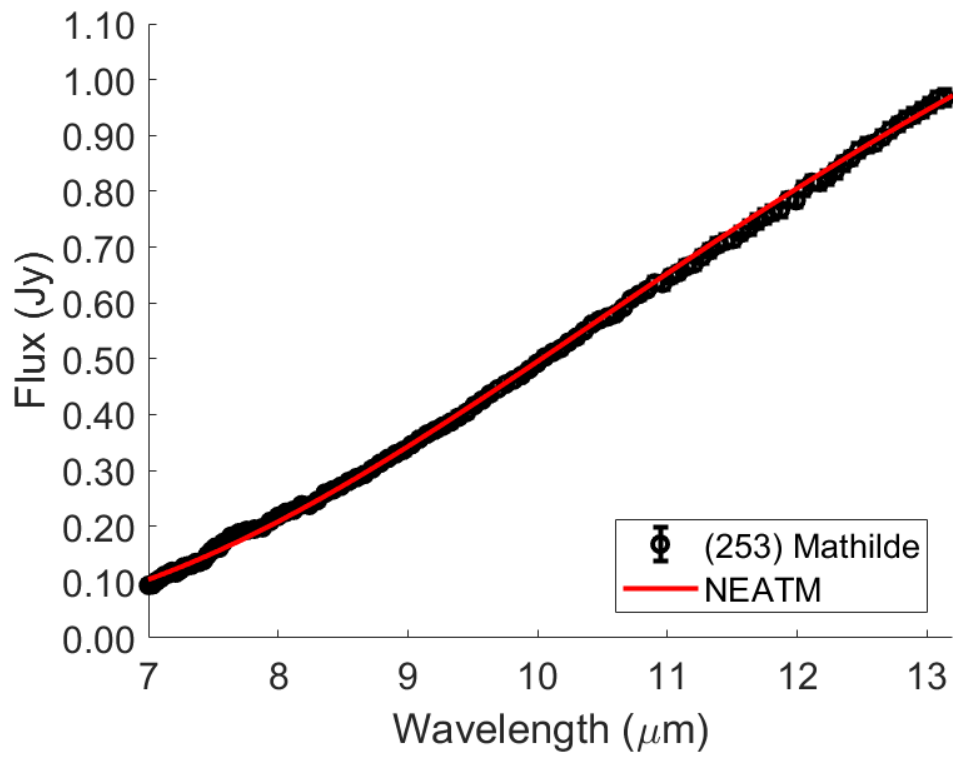
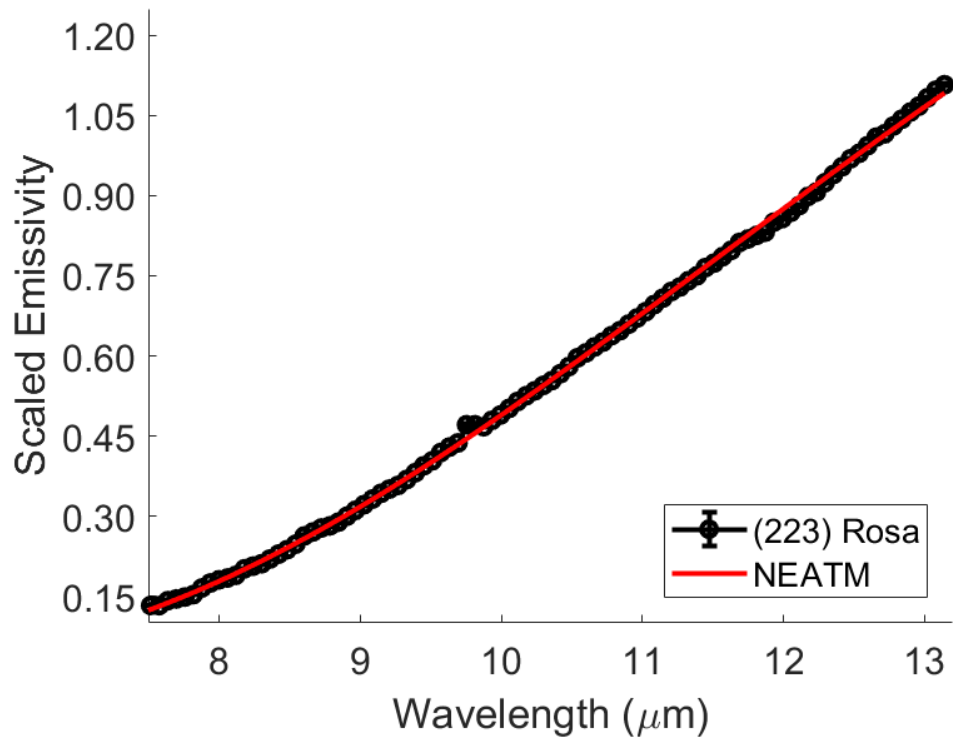


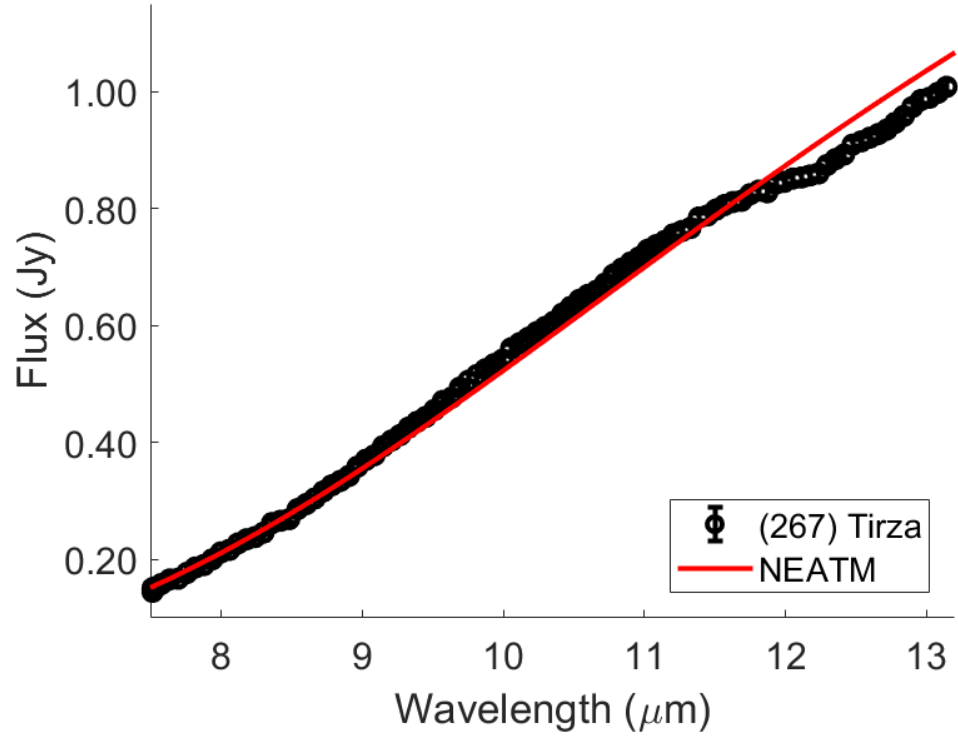
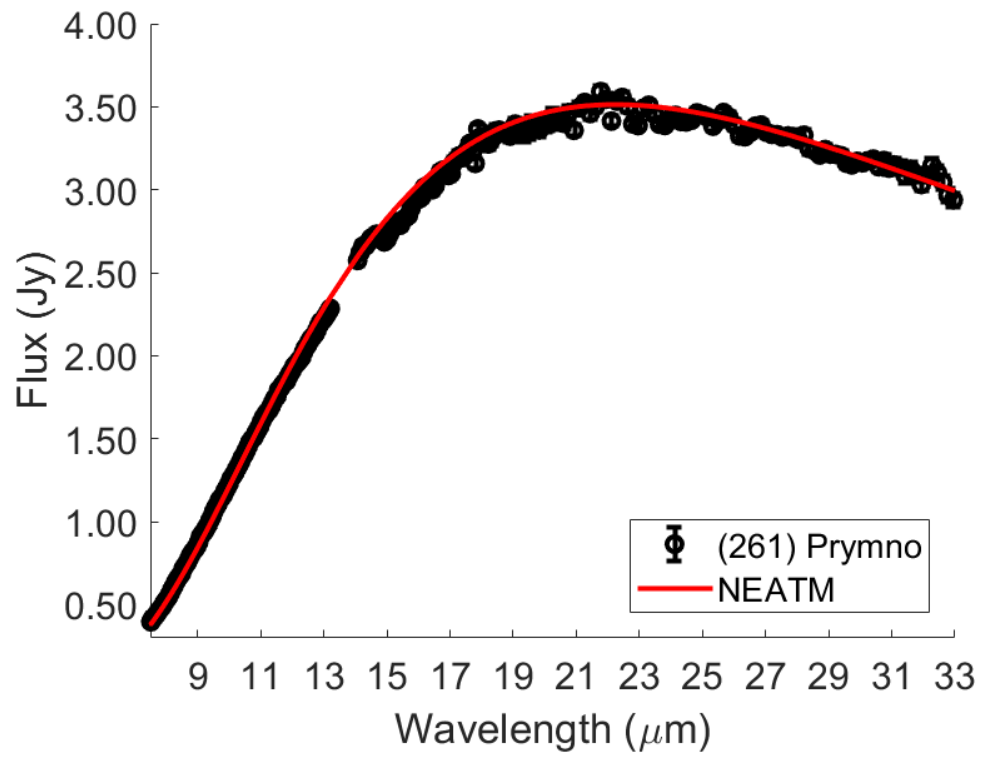


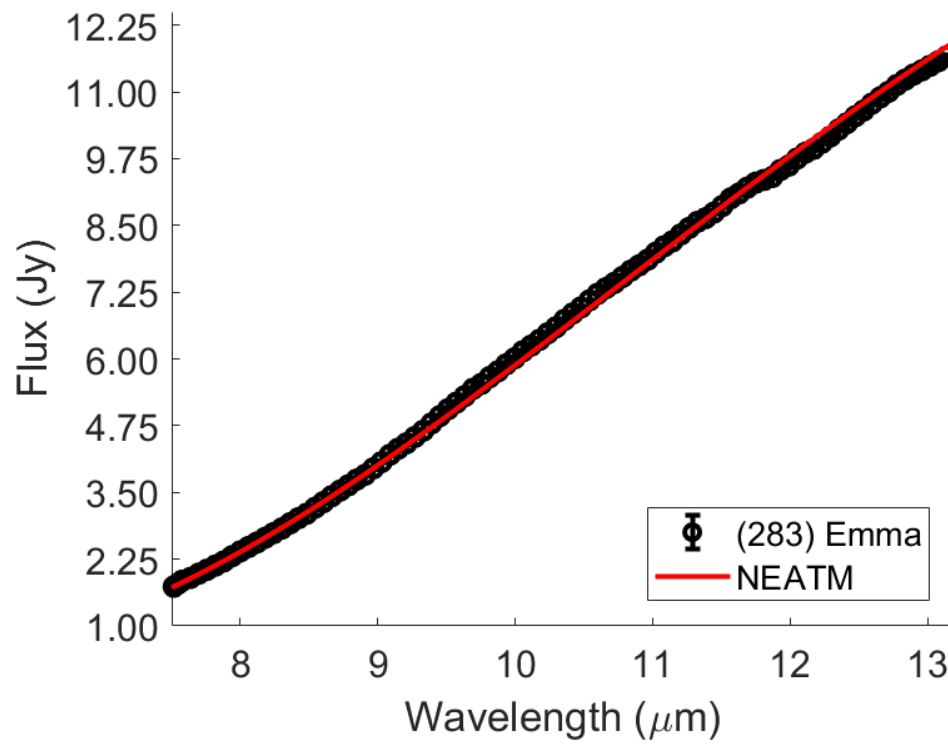
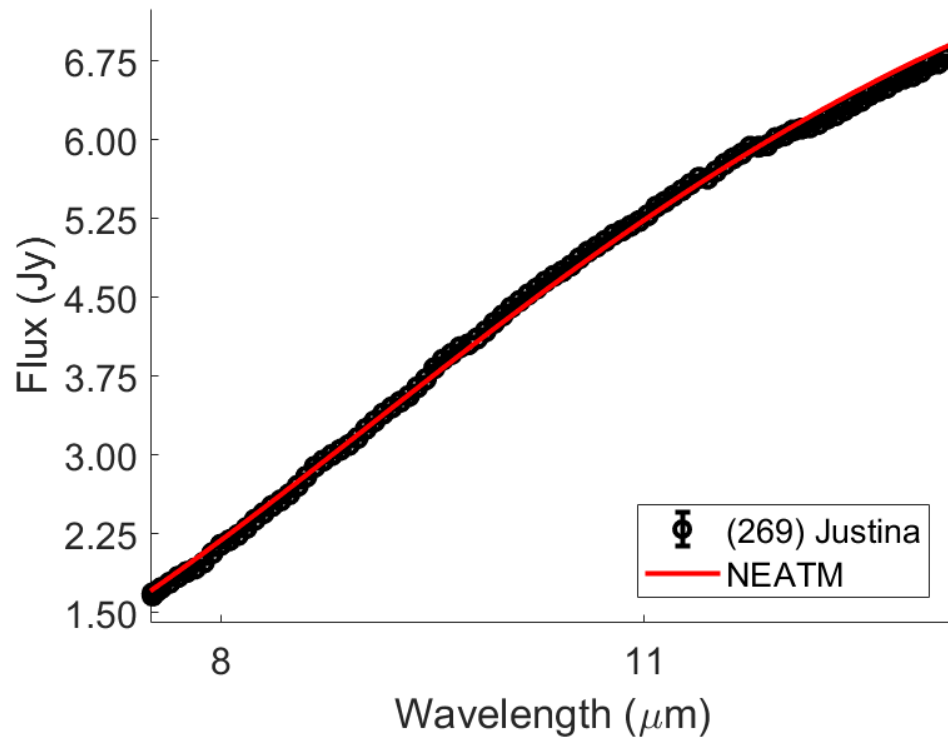


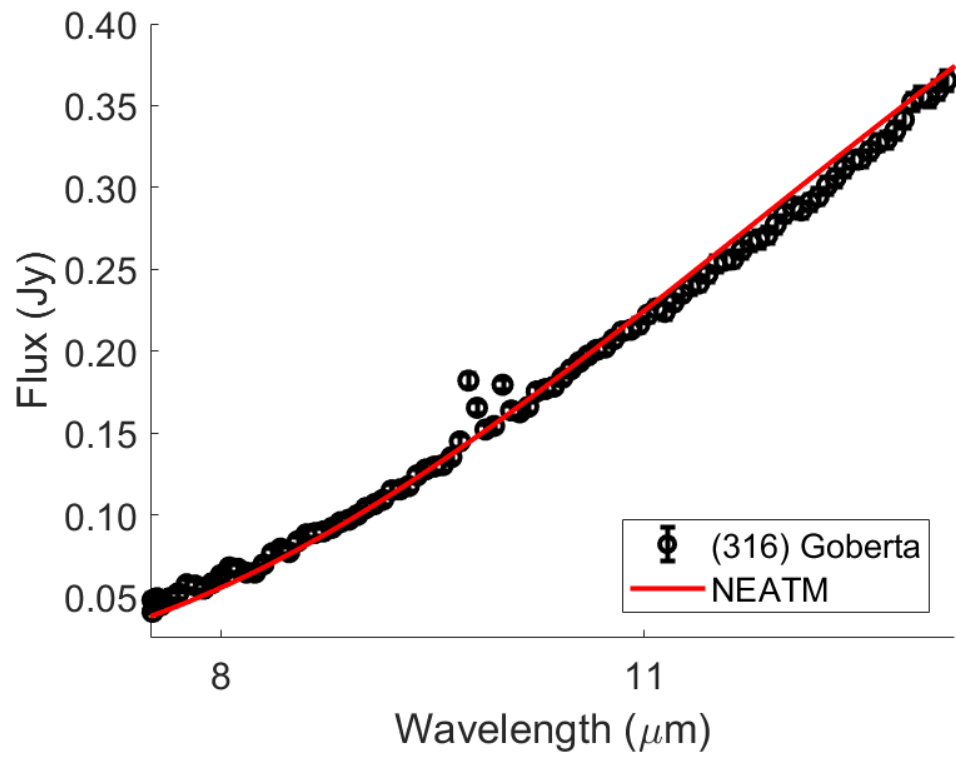
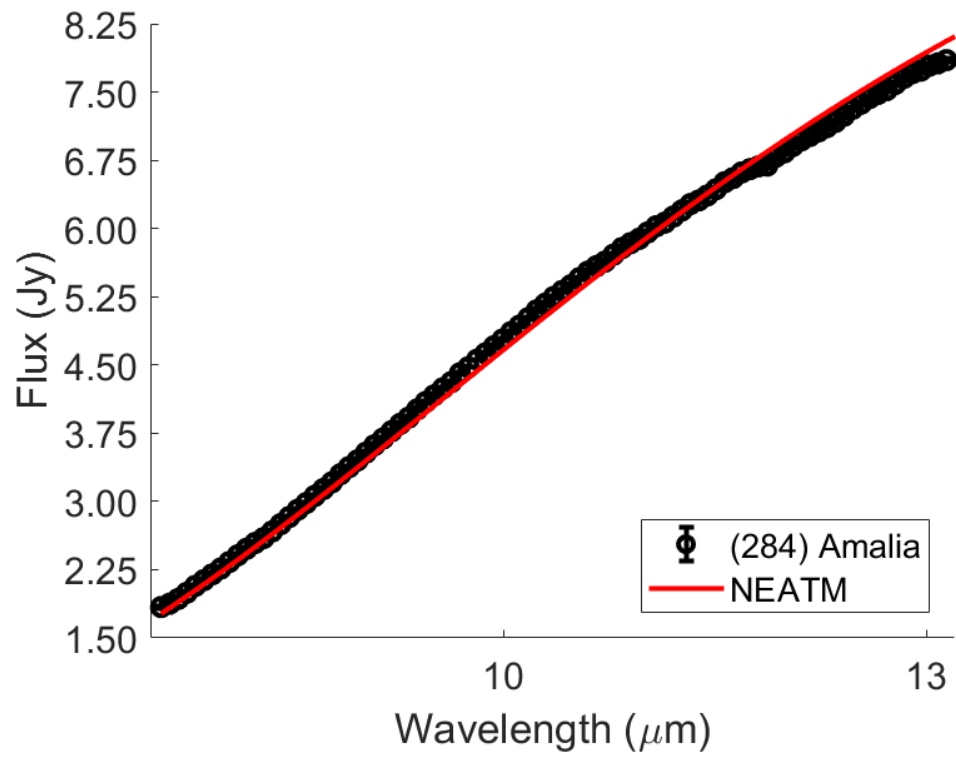


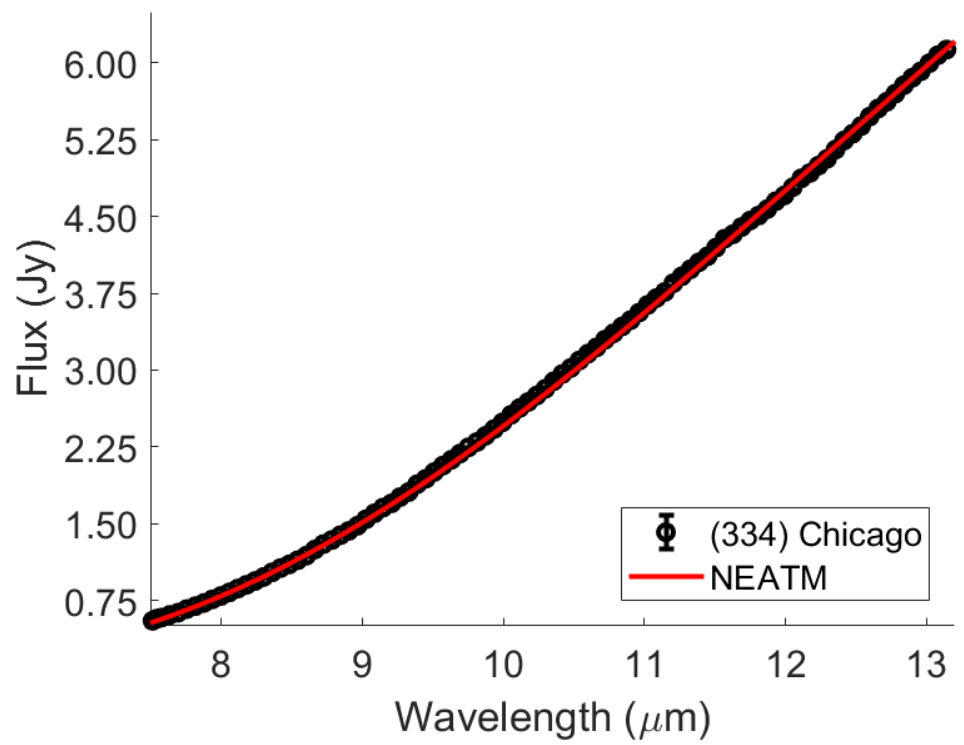
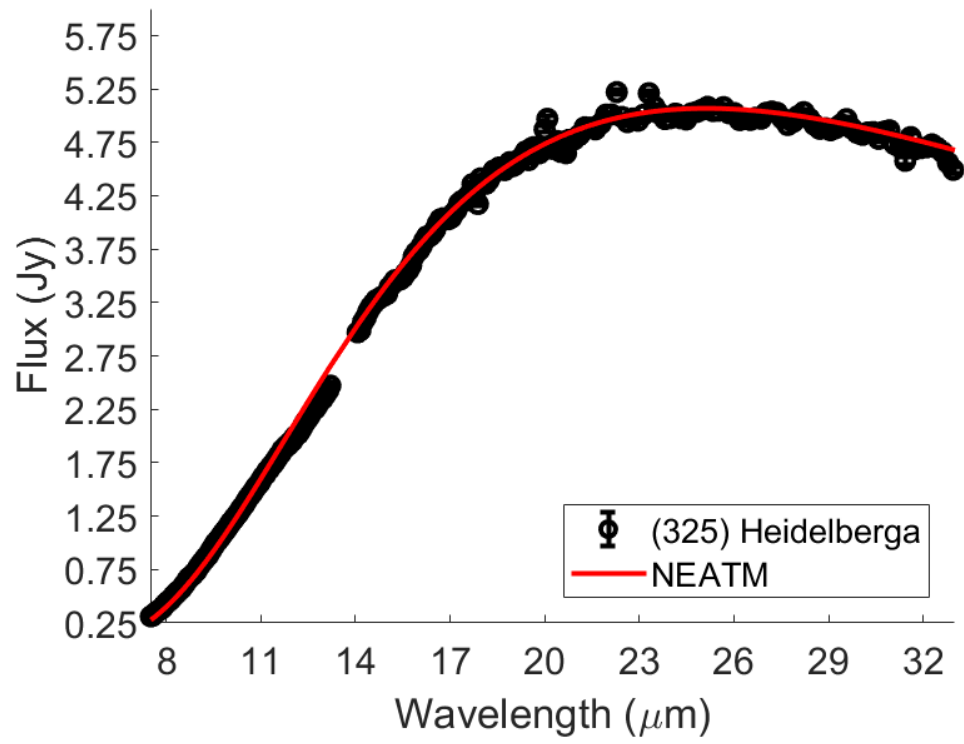


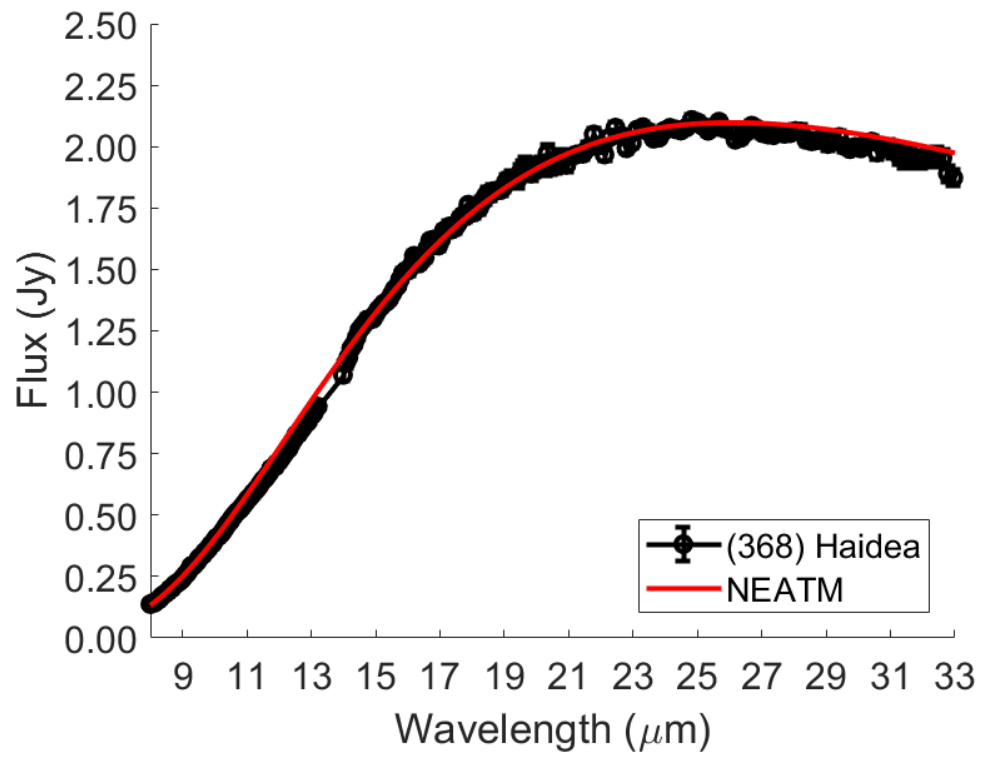
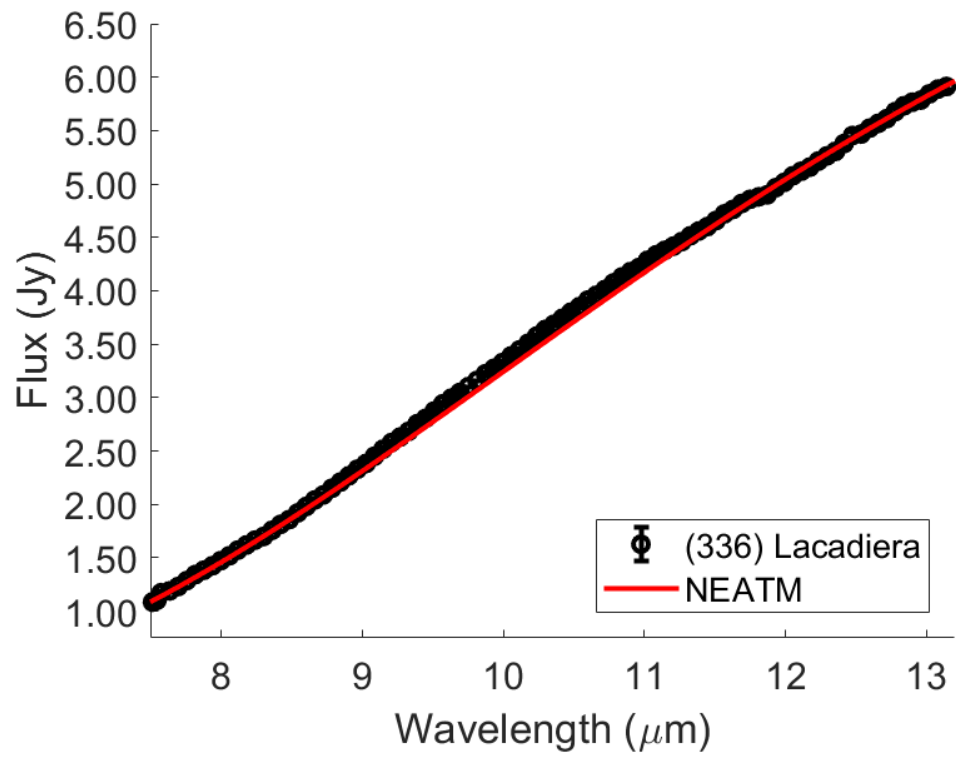


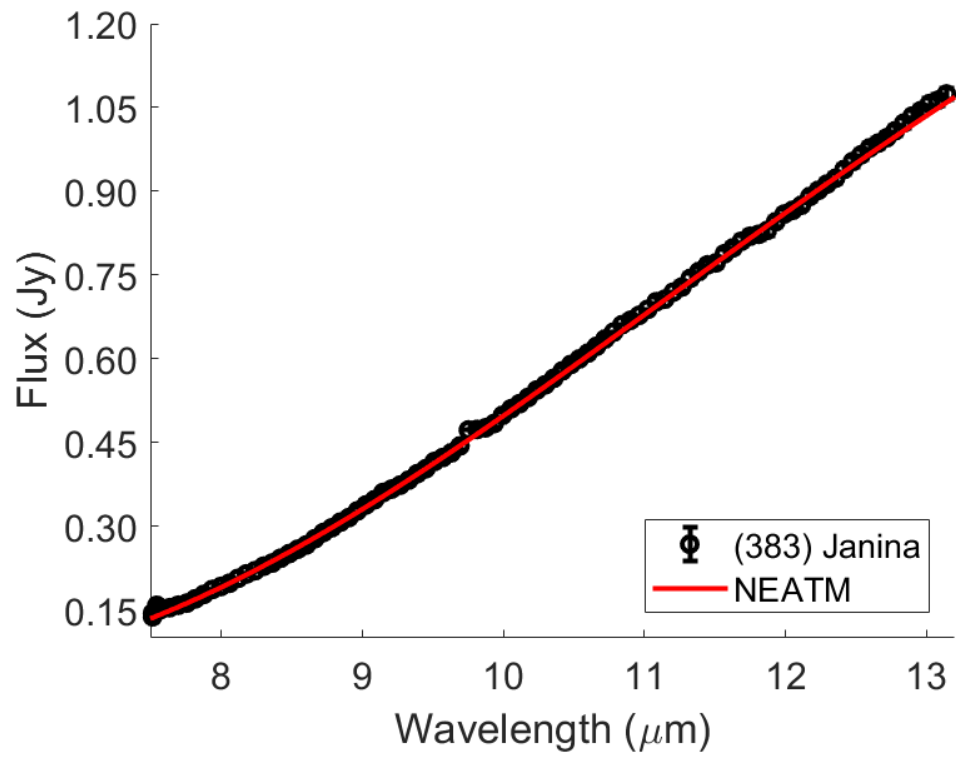
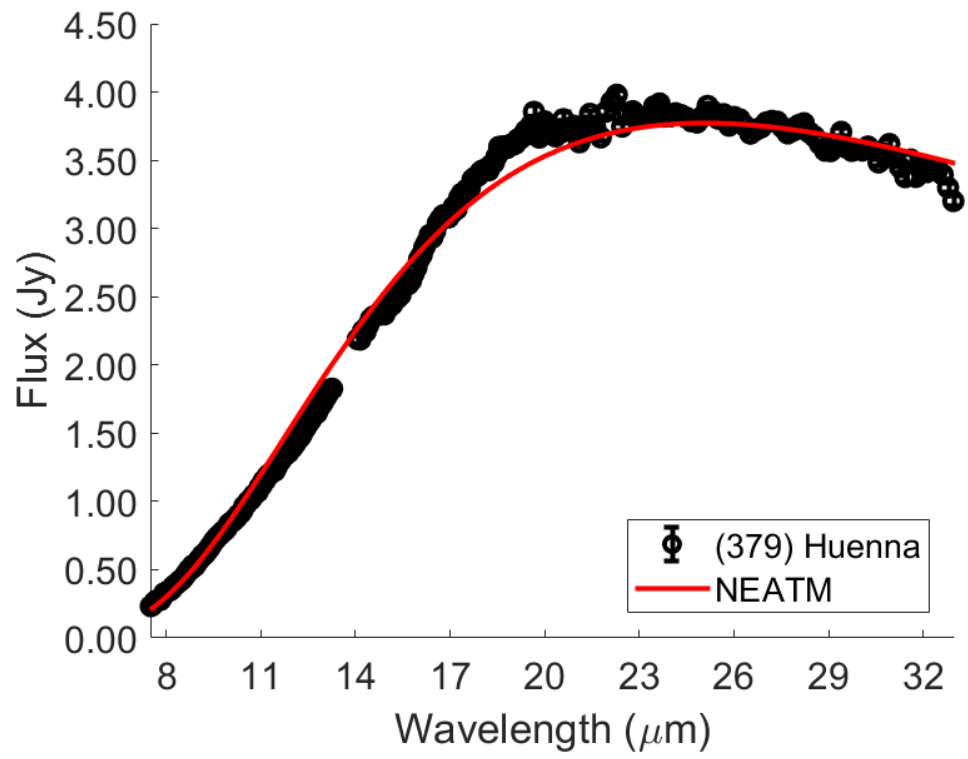


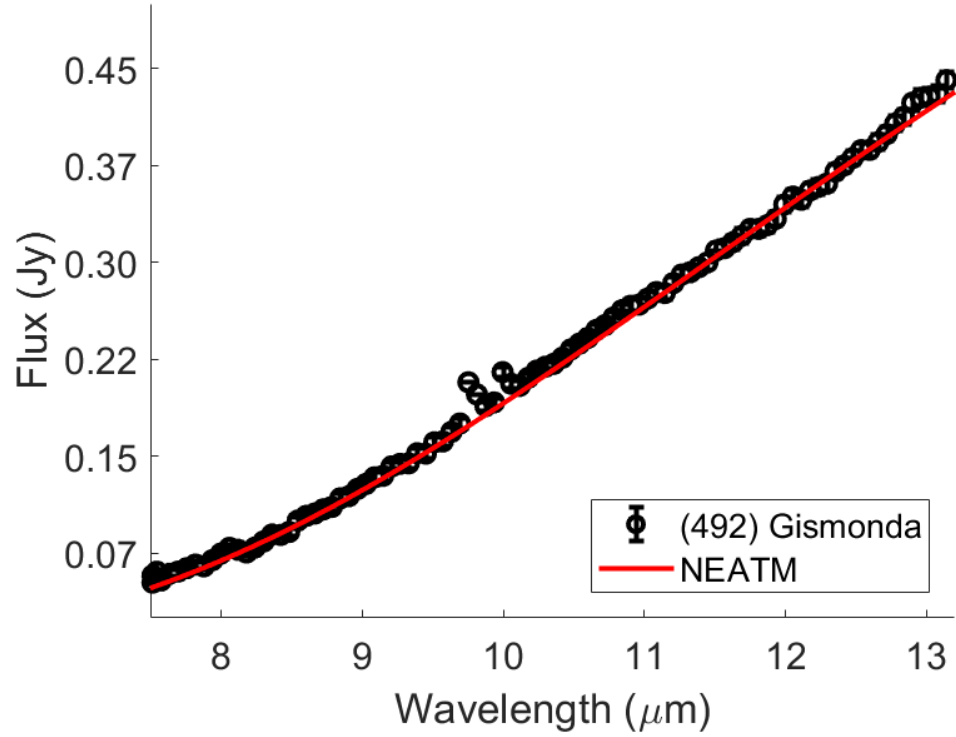
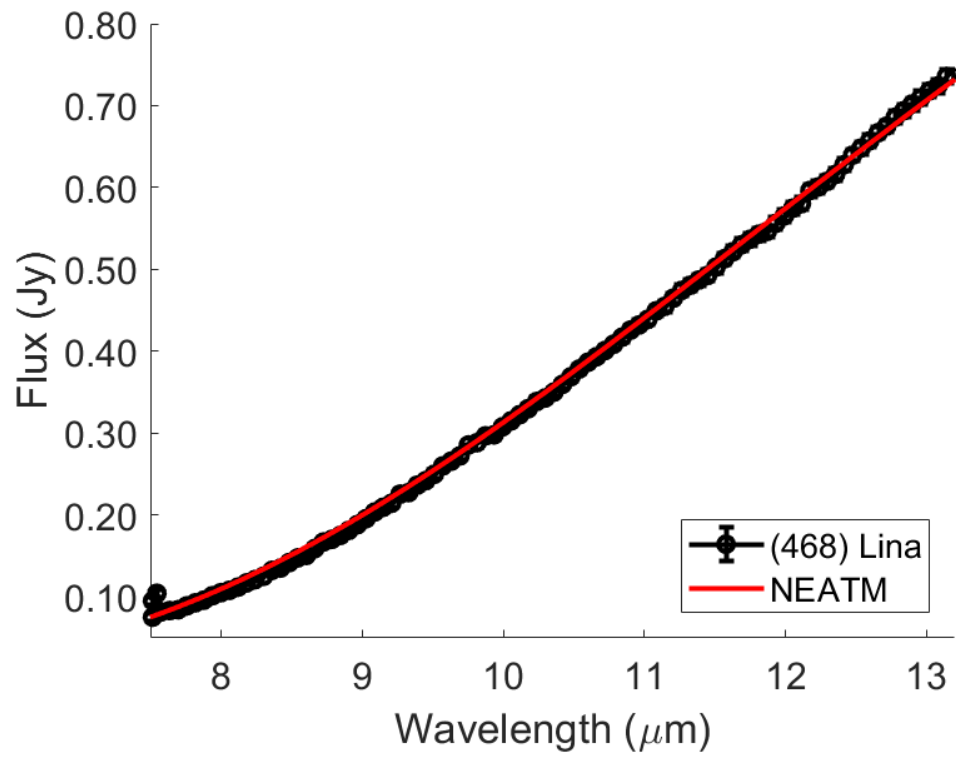


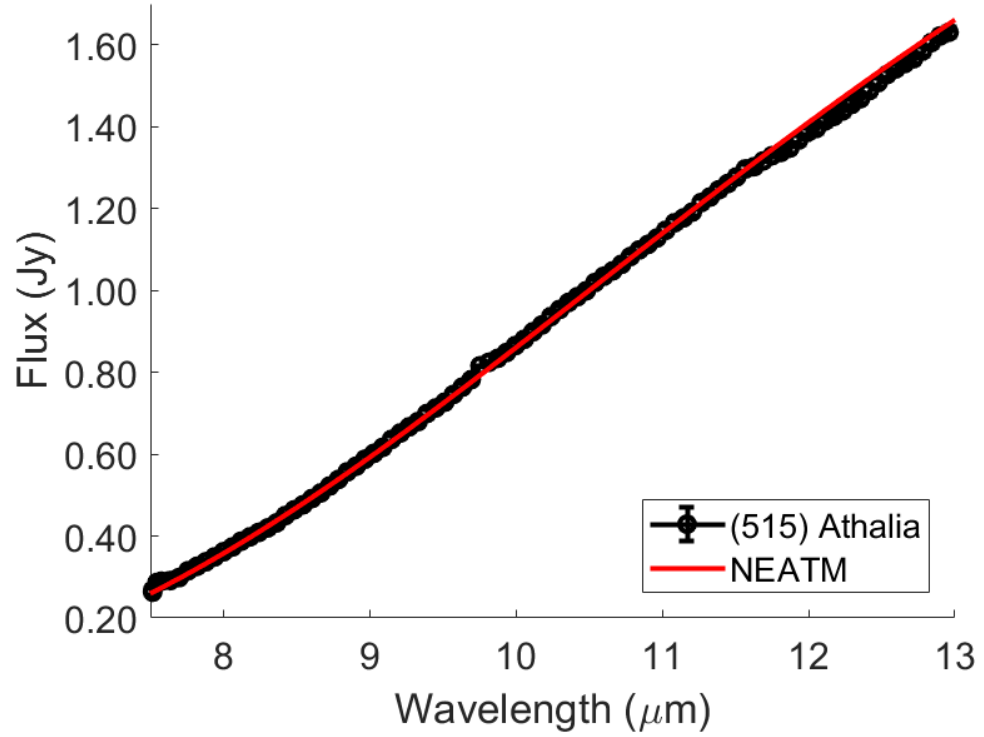
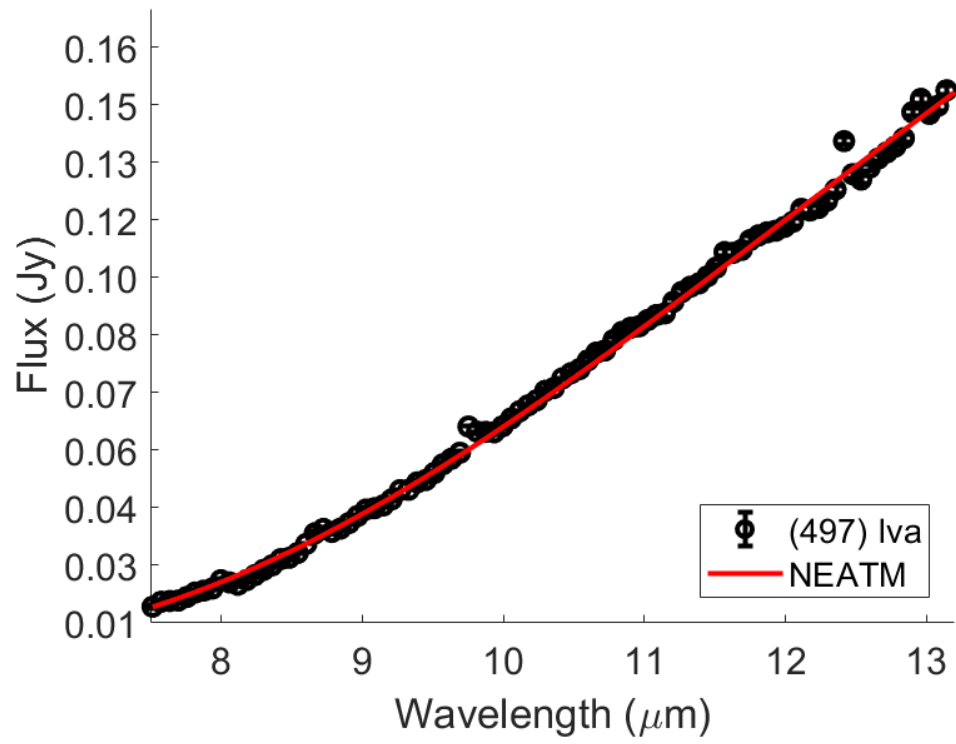


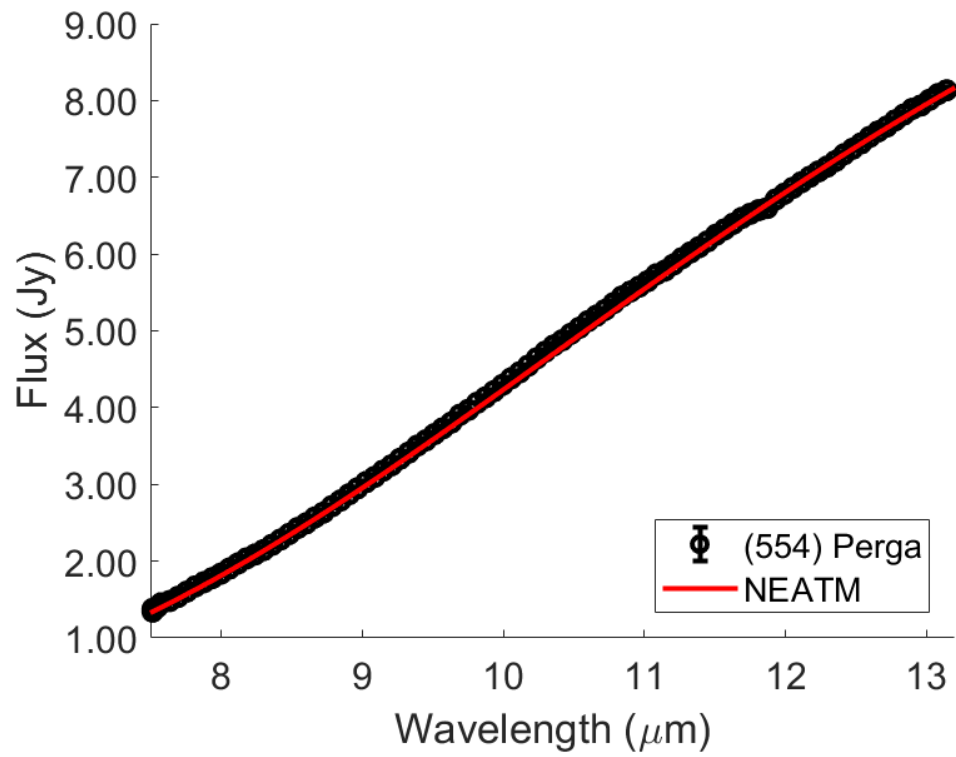
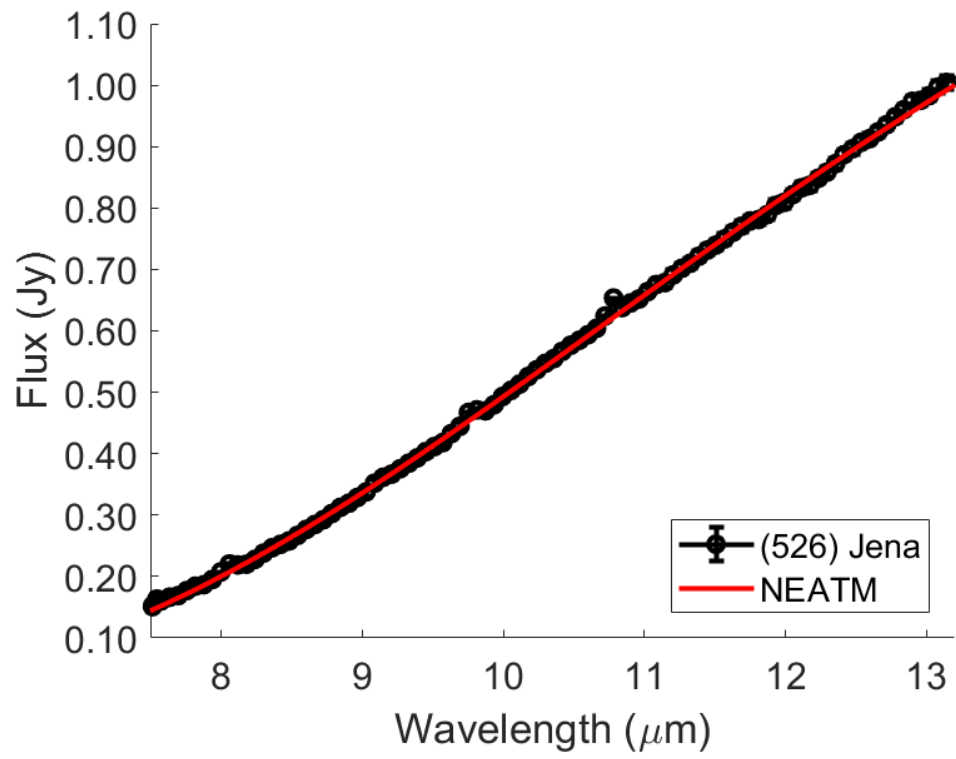


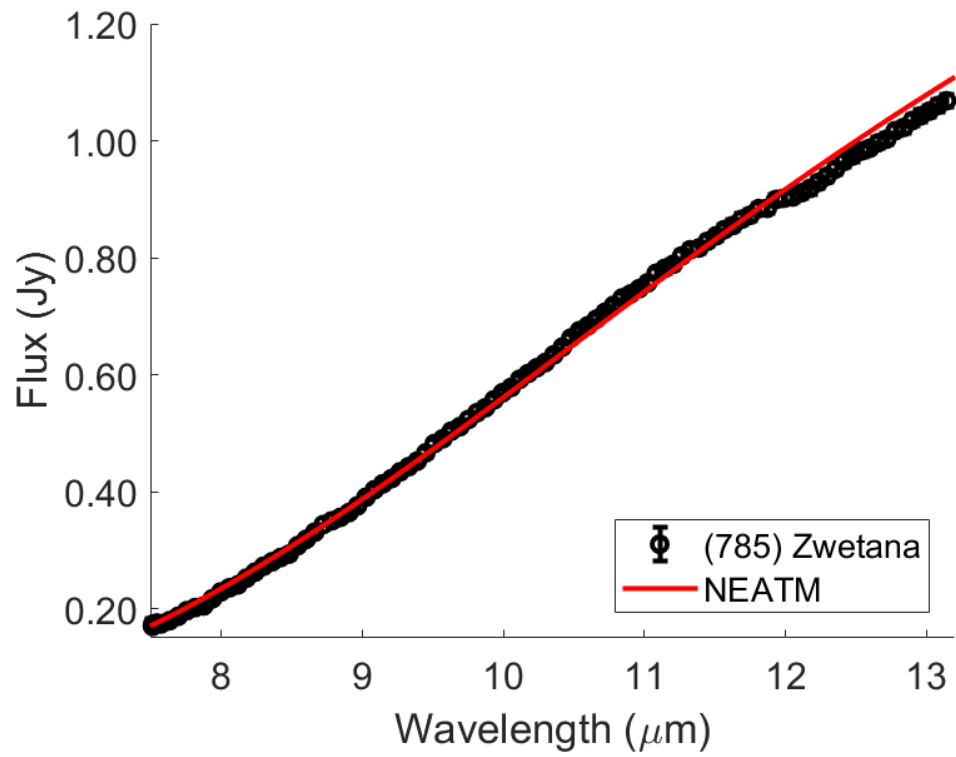
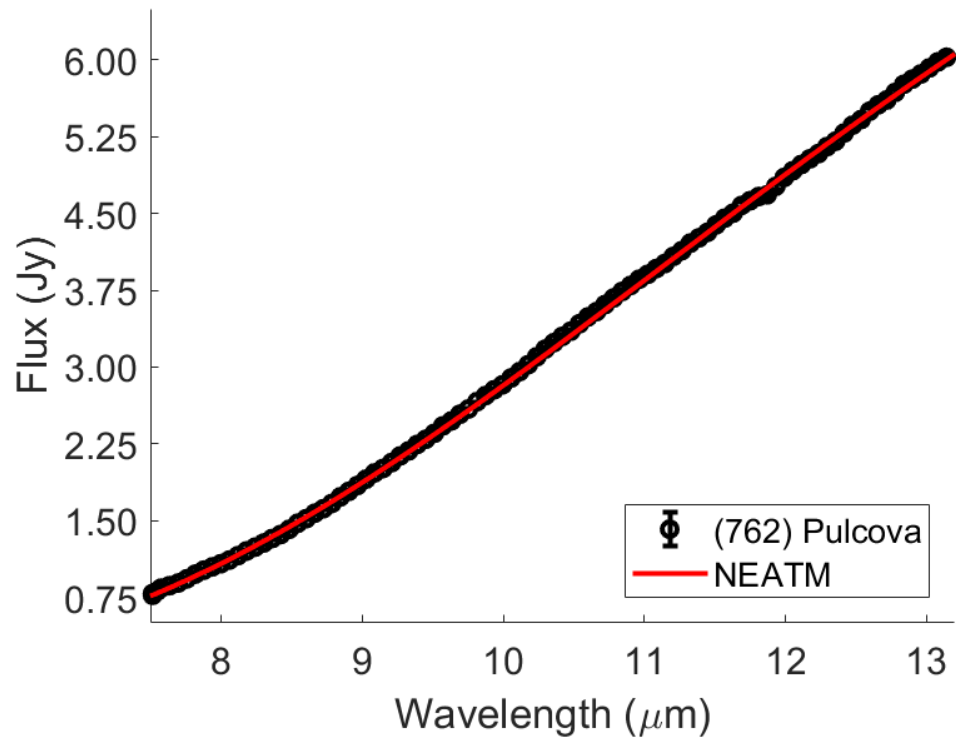


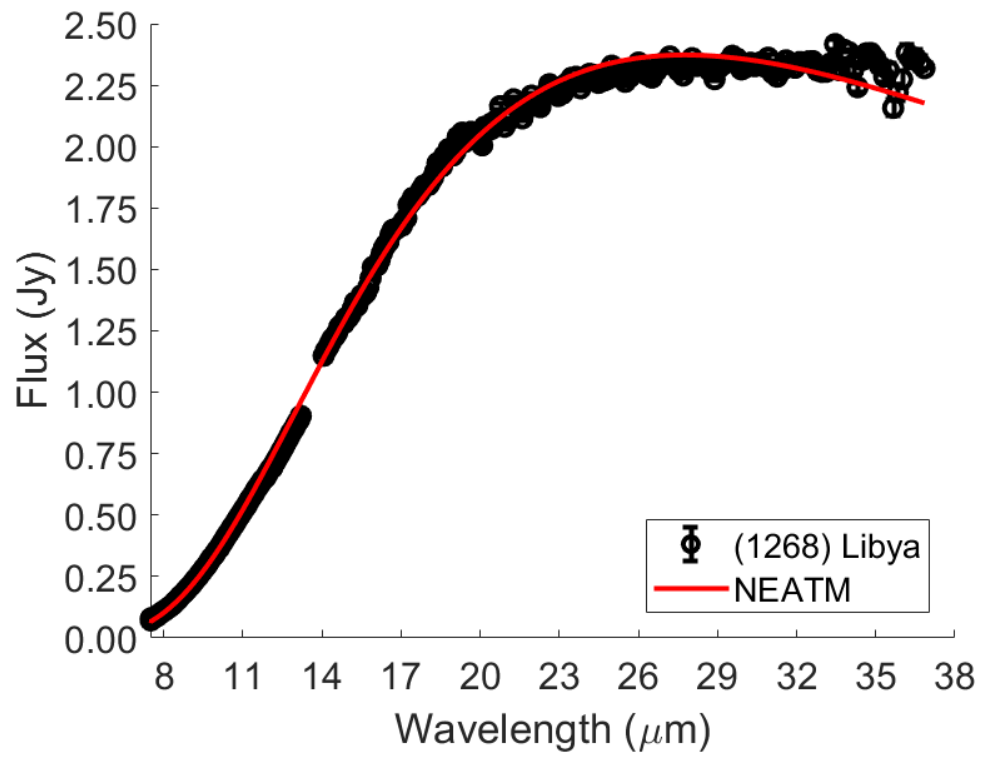
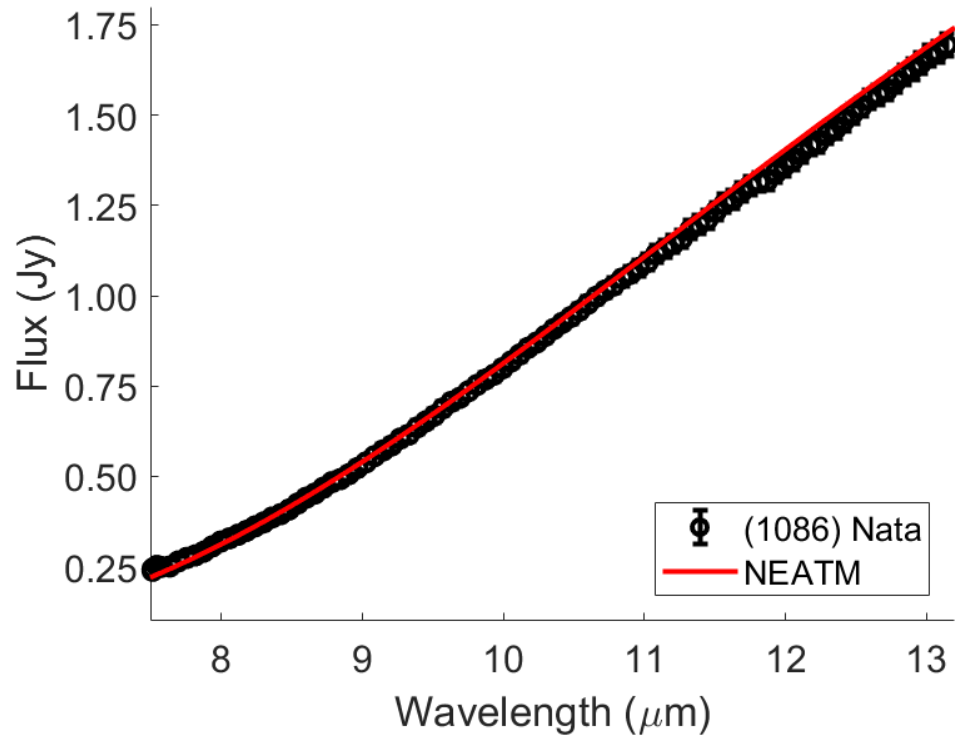


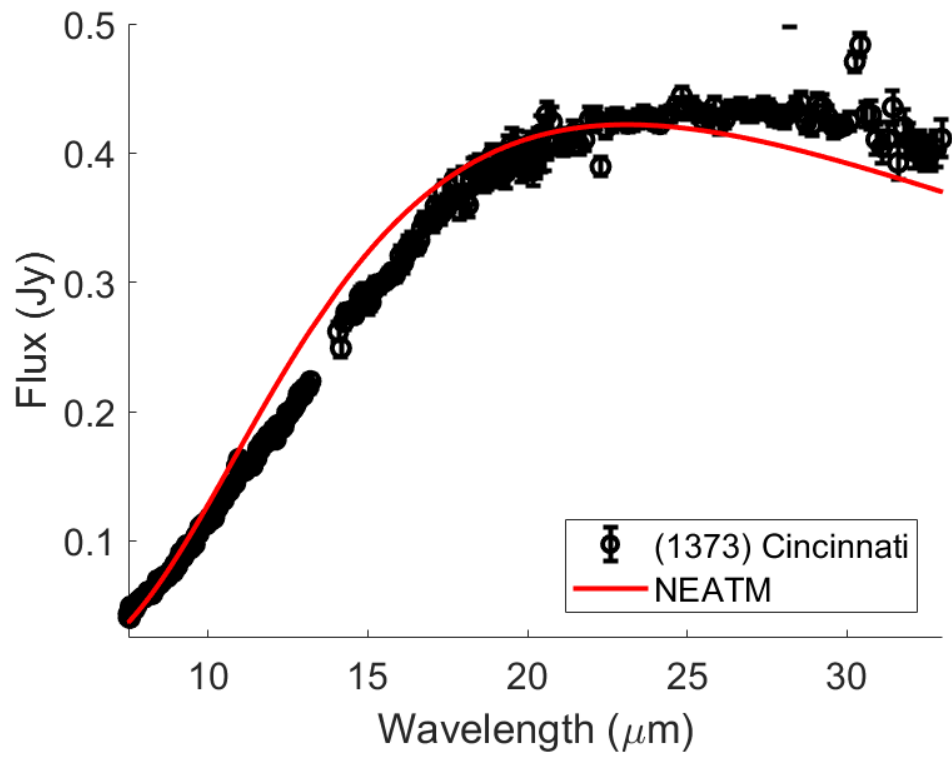
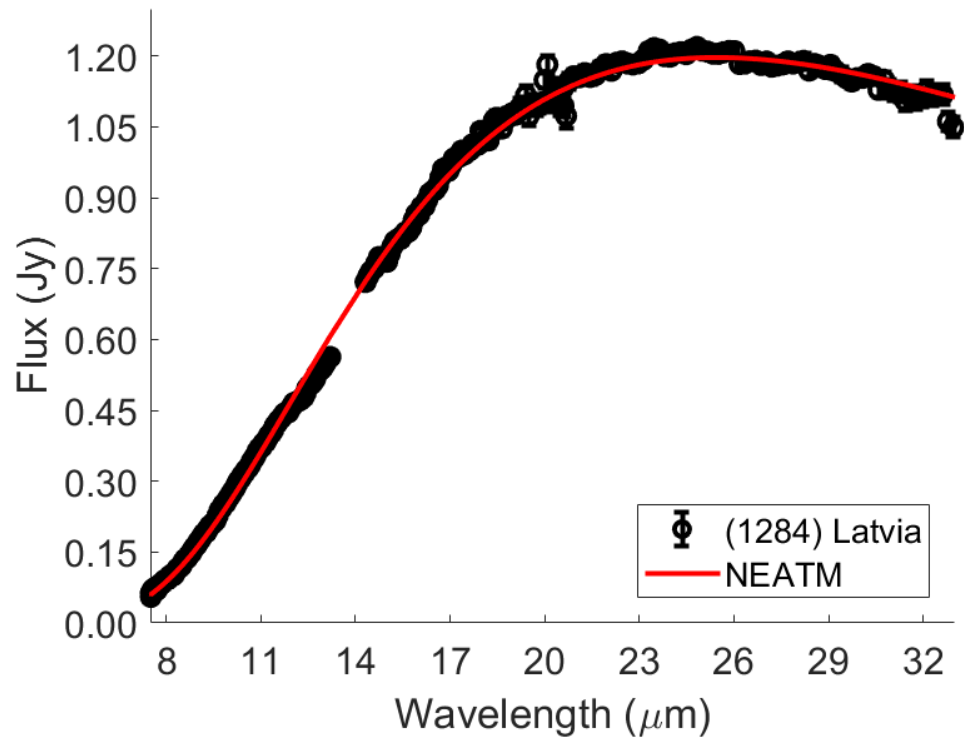


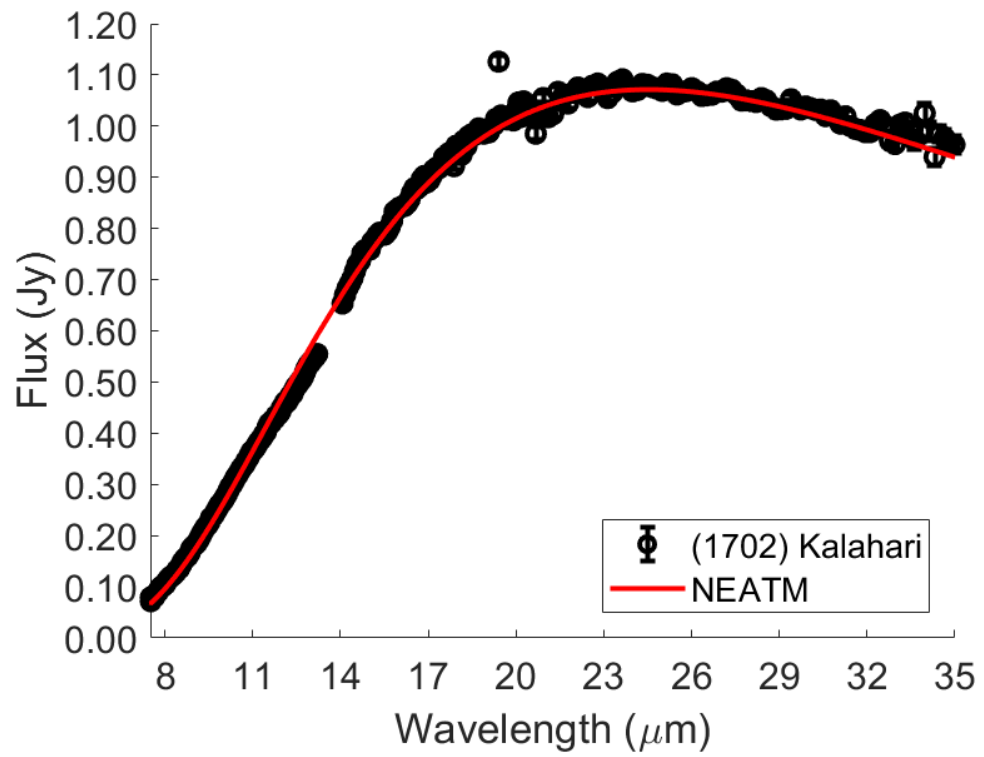
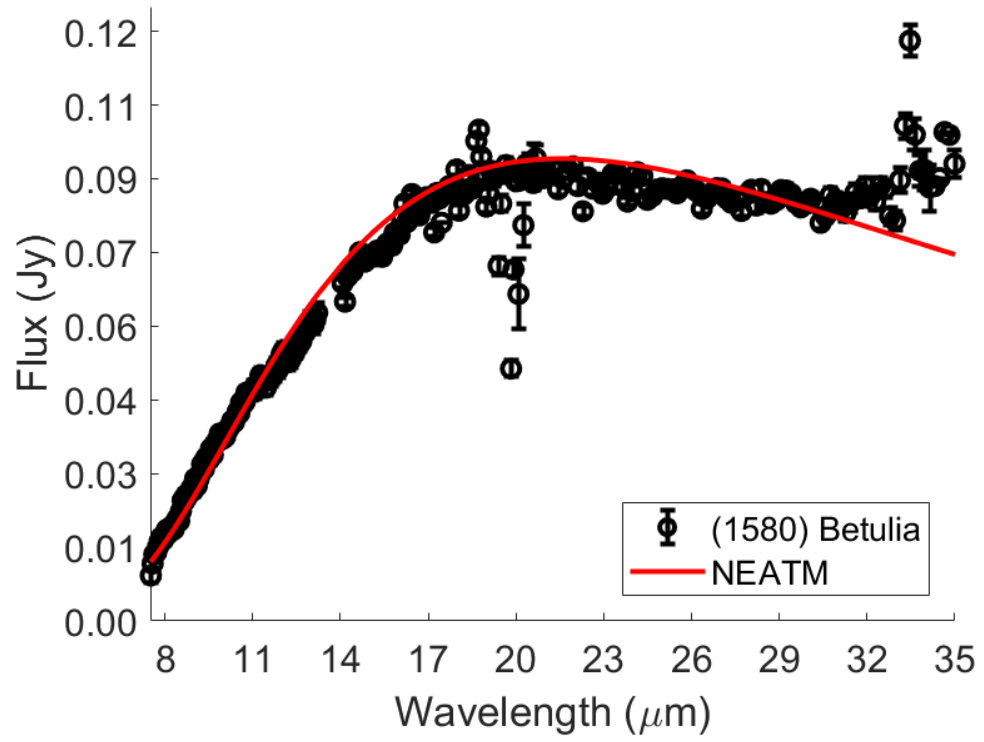


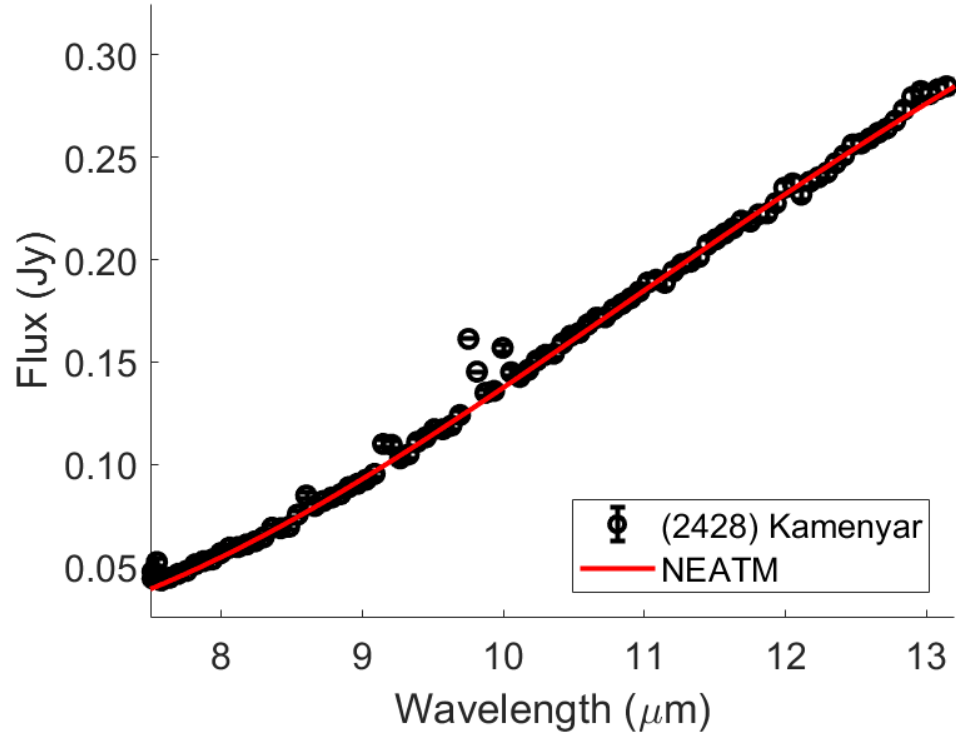
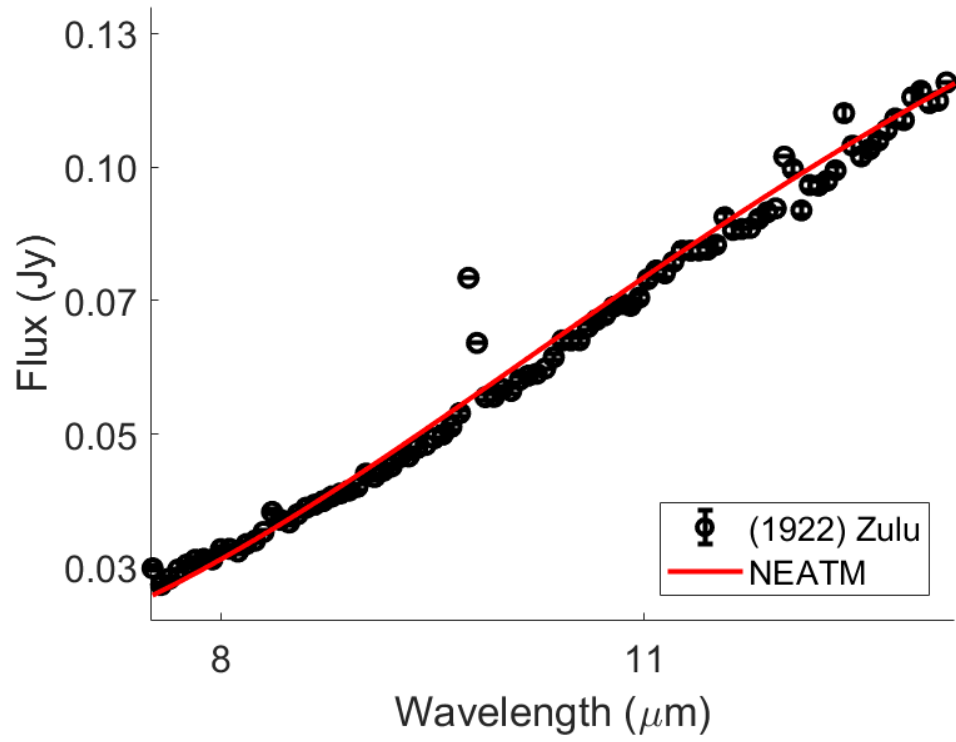


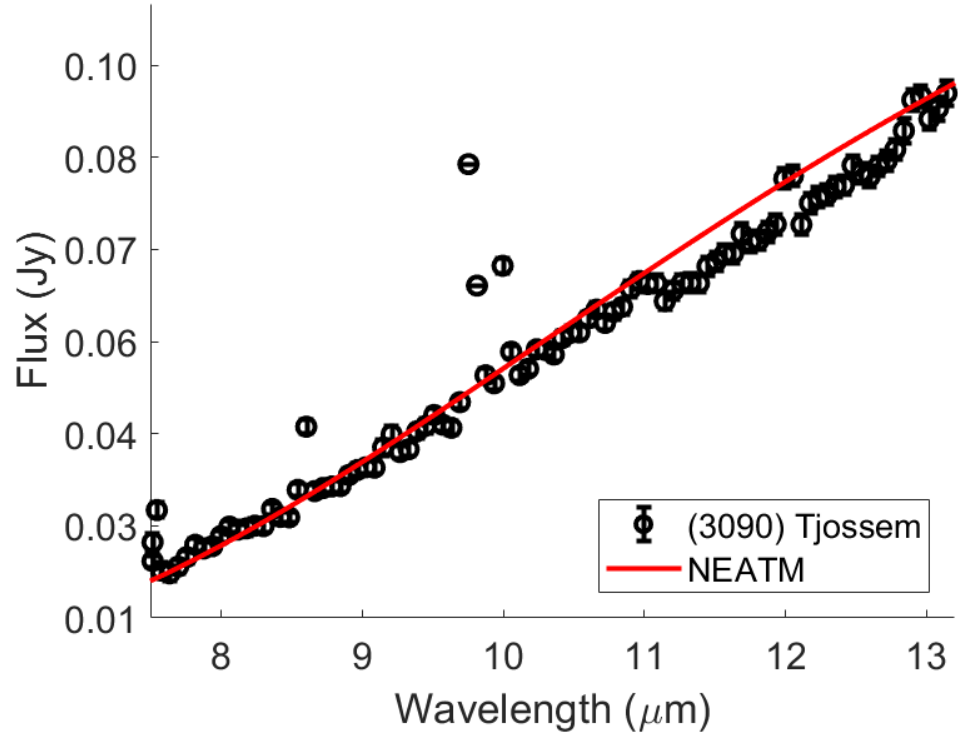
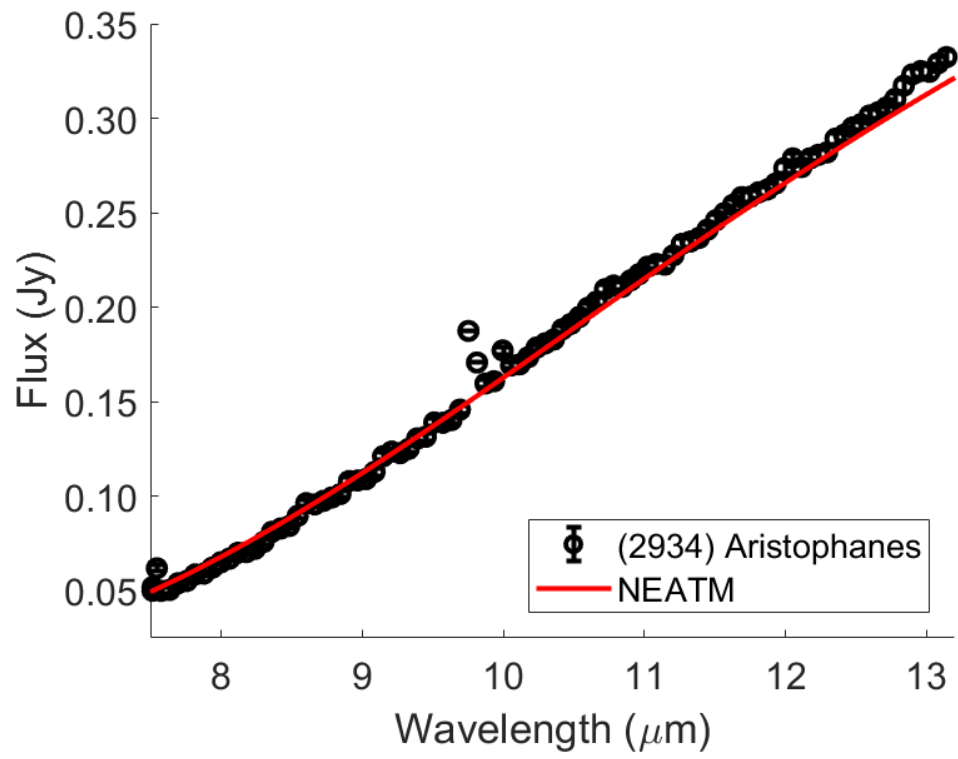


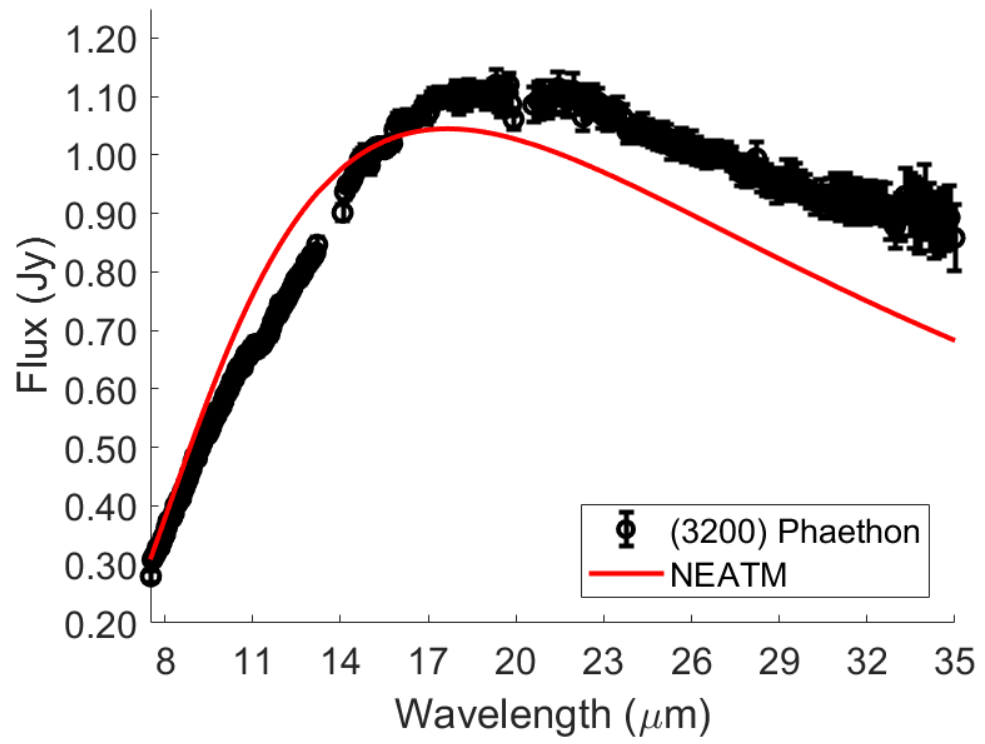




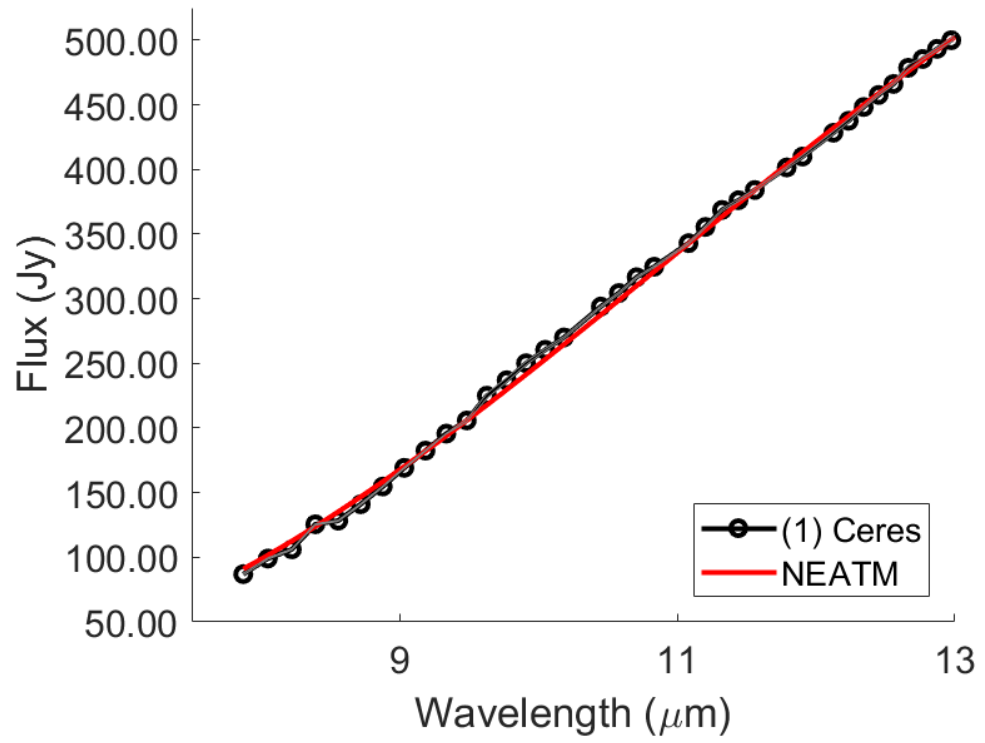


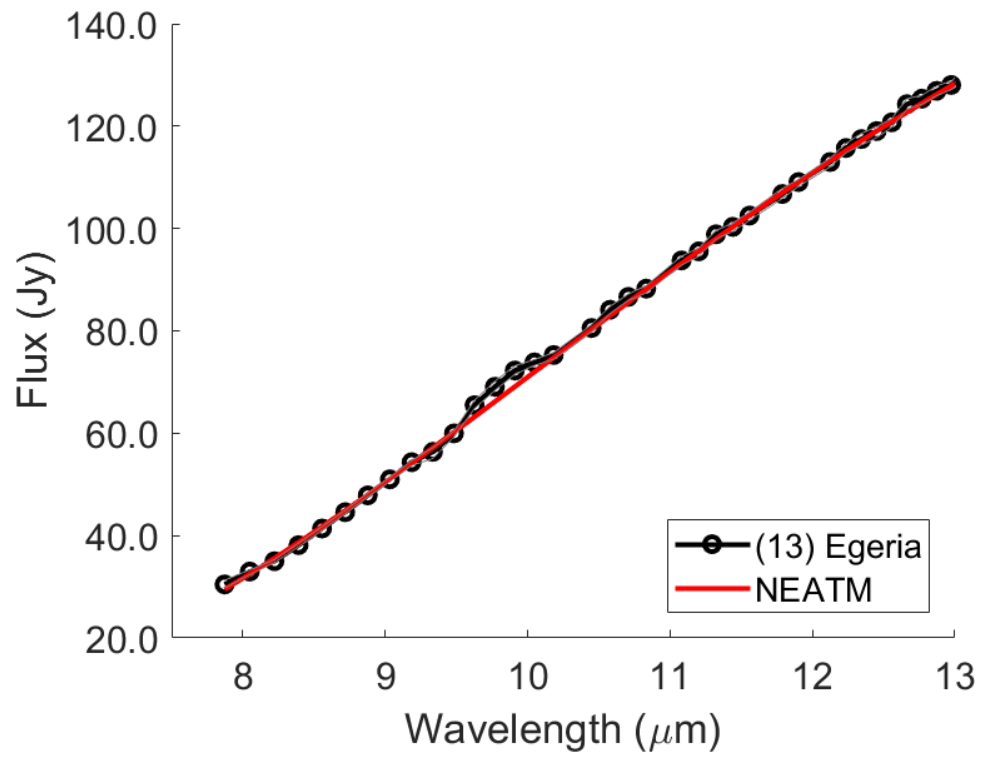


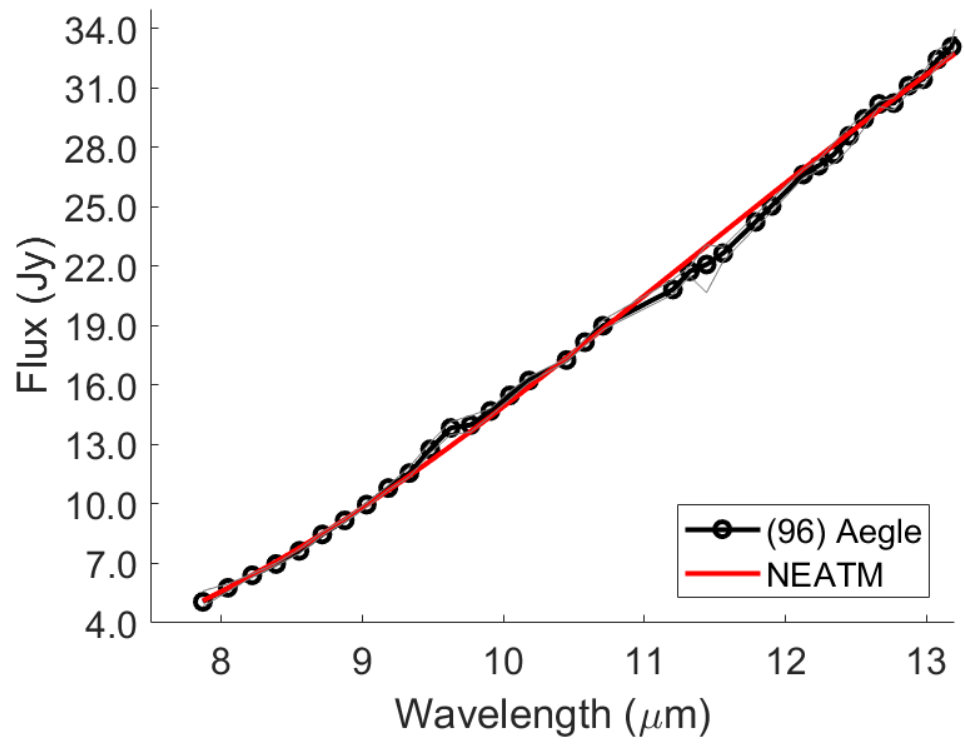


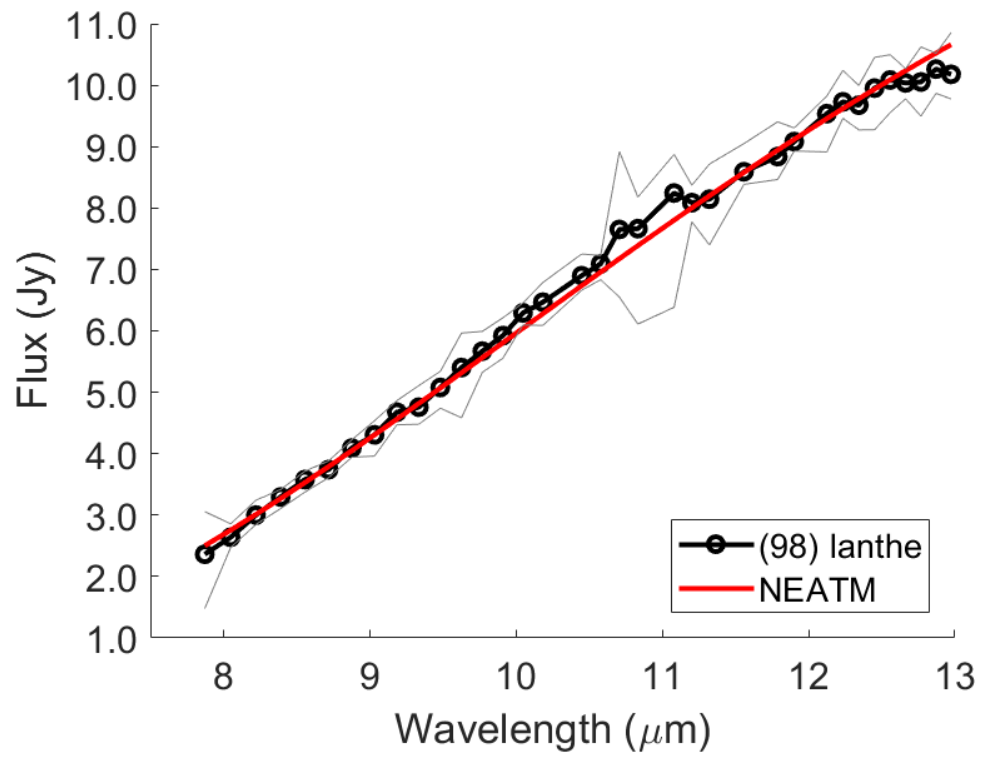


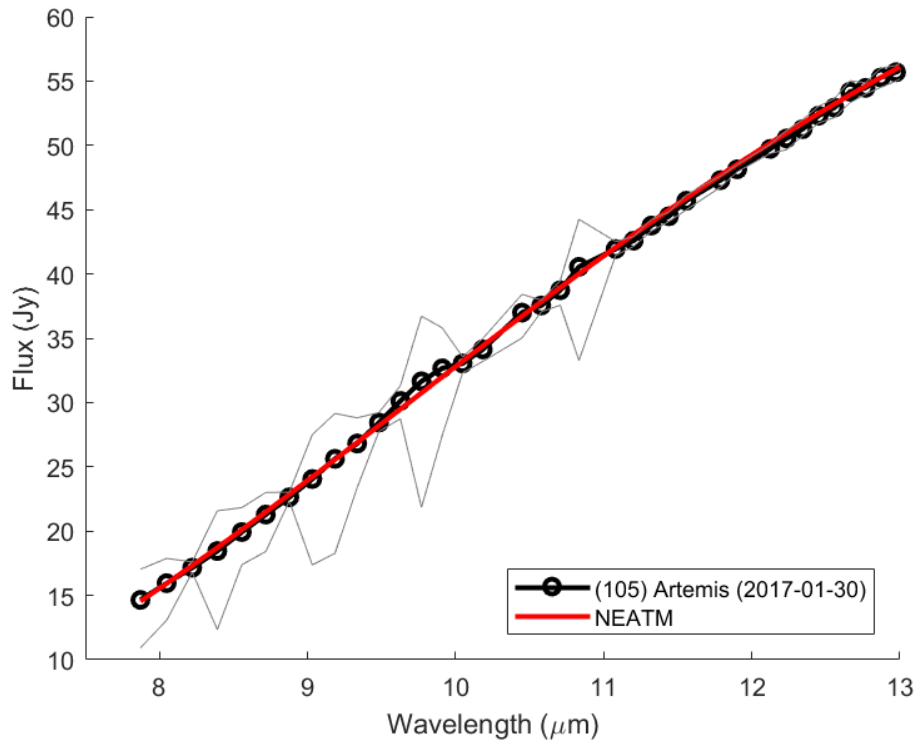
IRTF+BASS Observations:

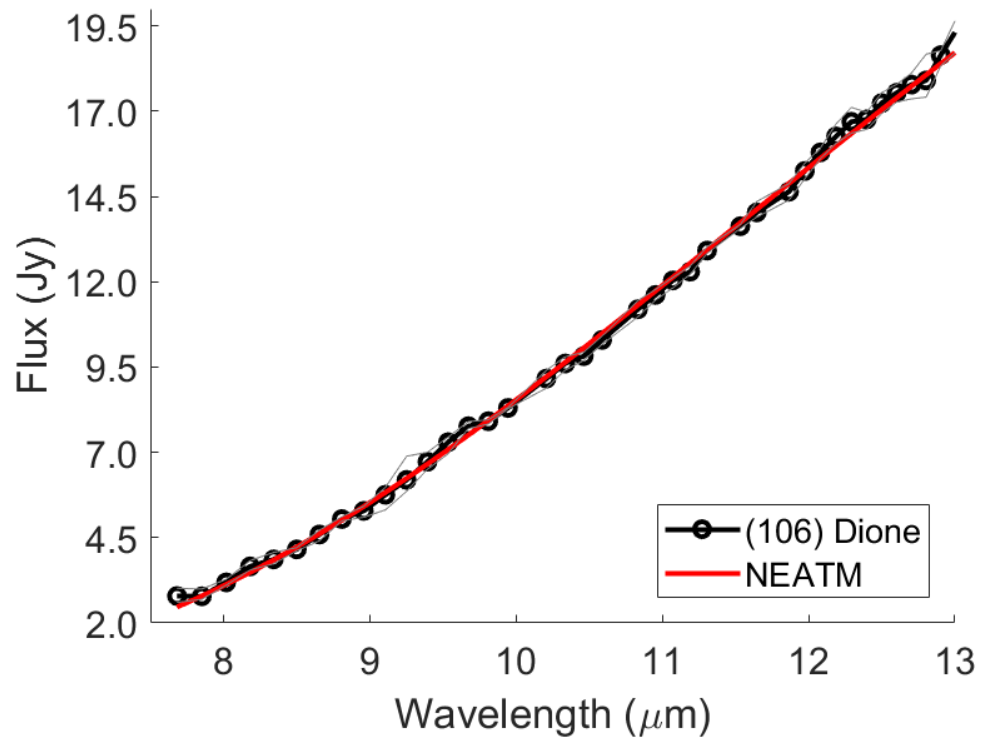


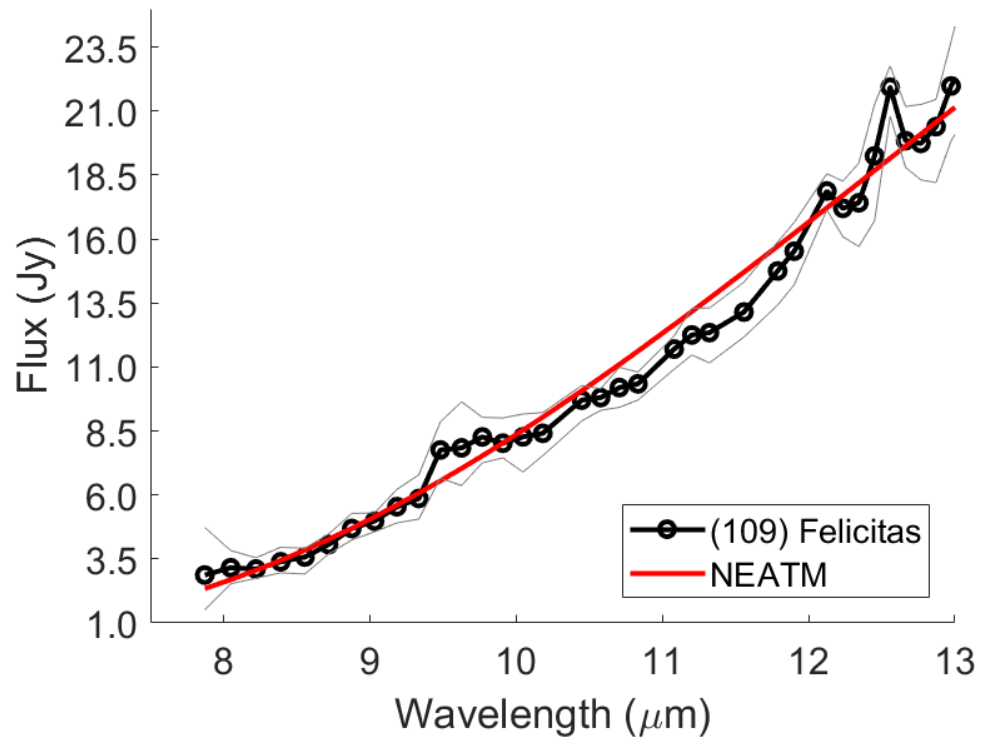


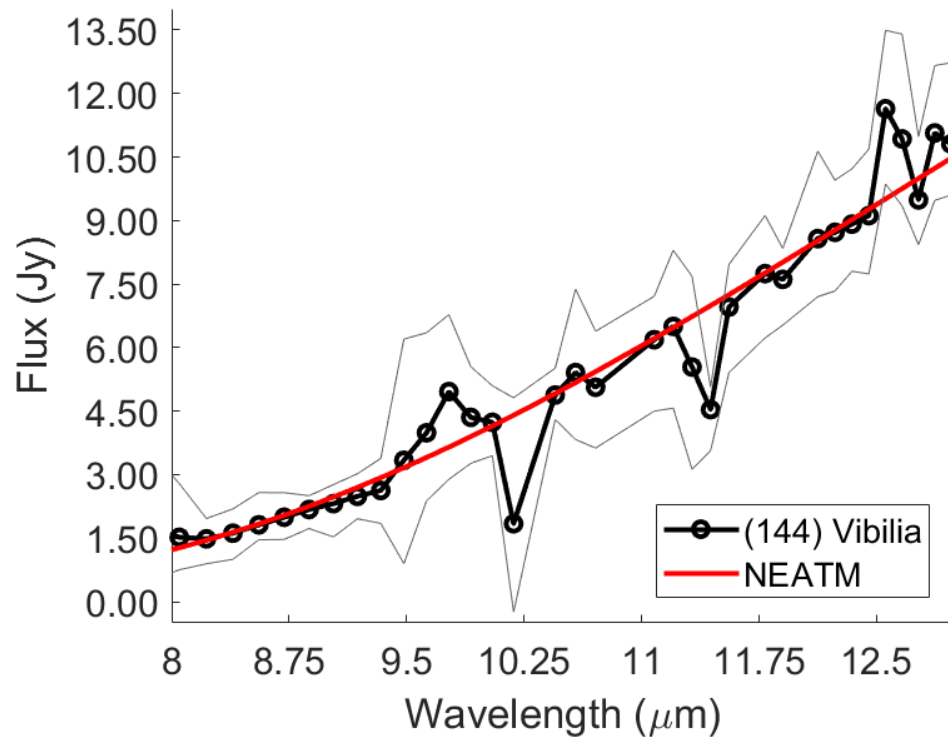


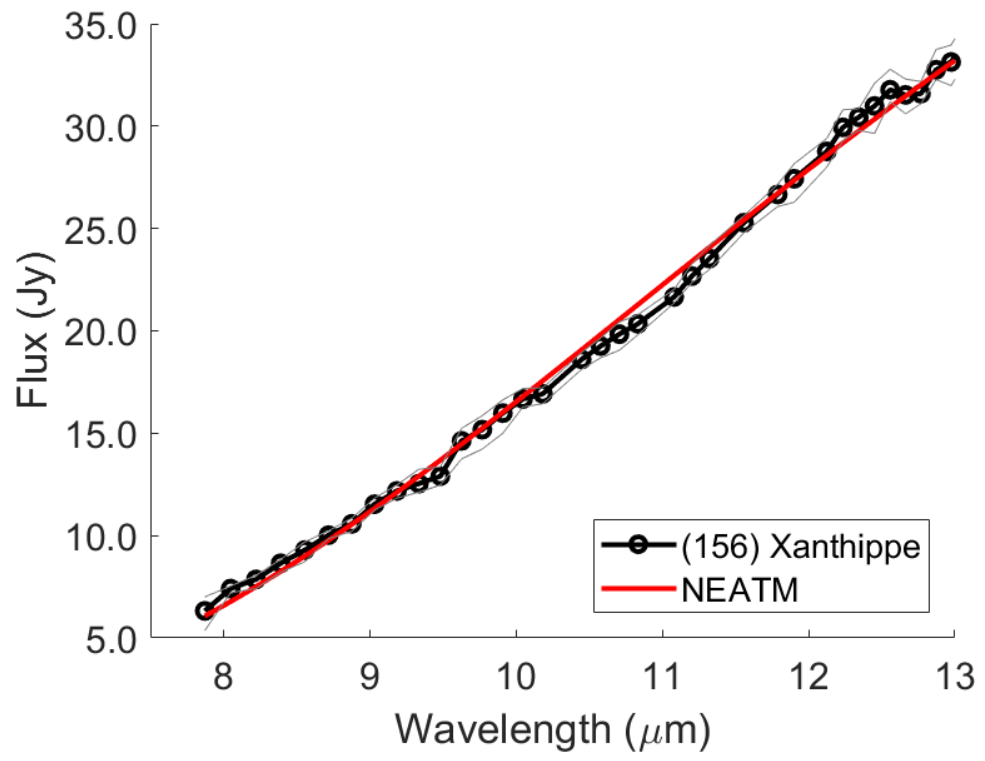


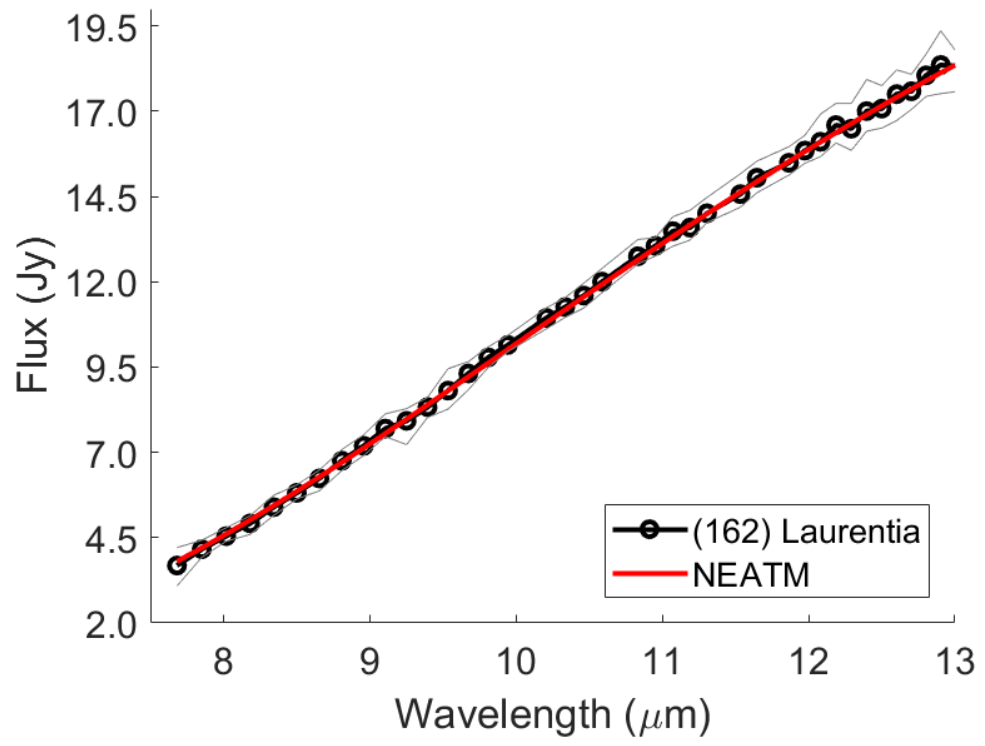


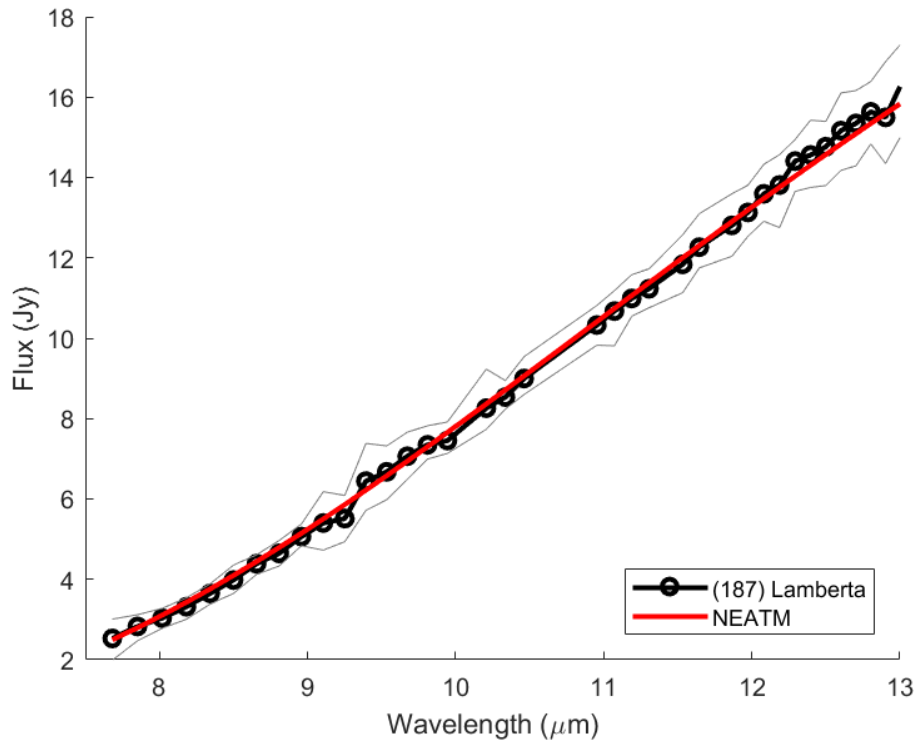


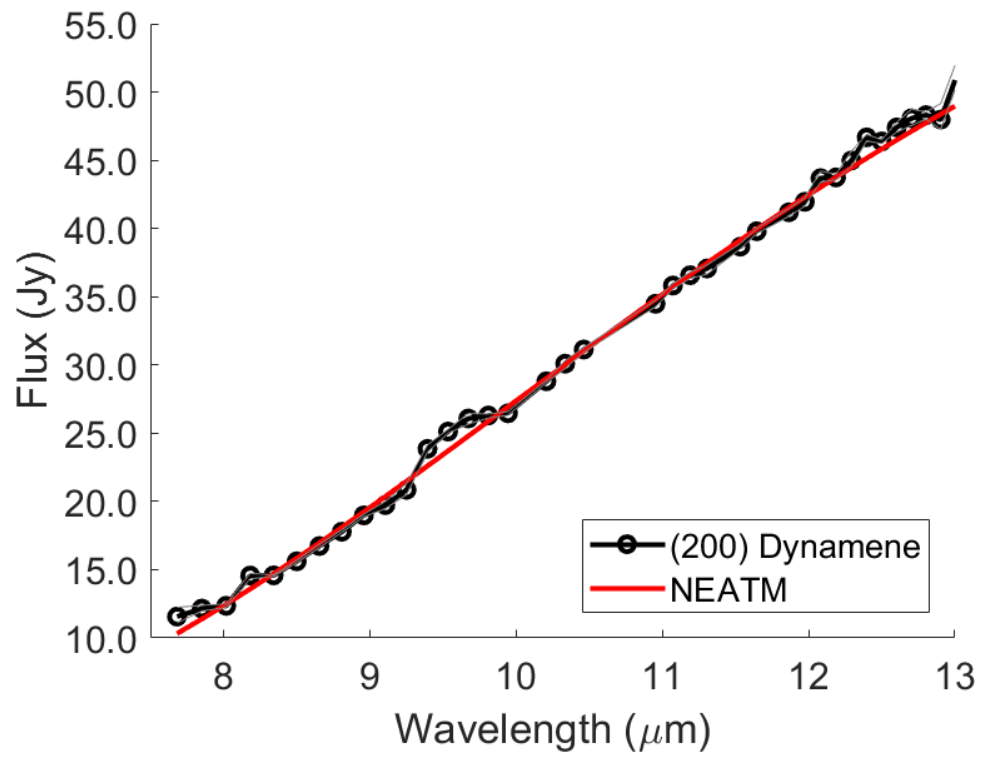


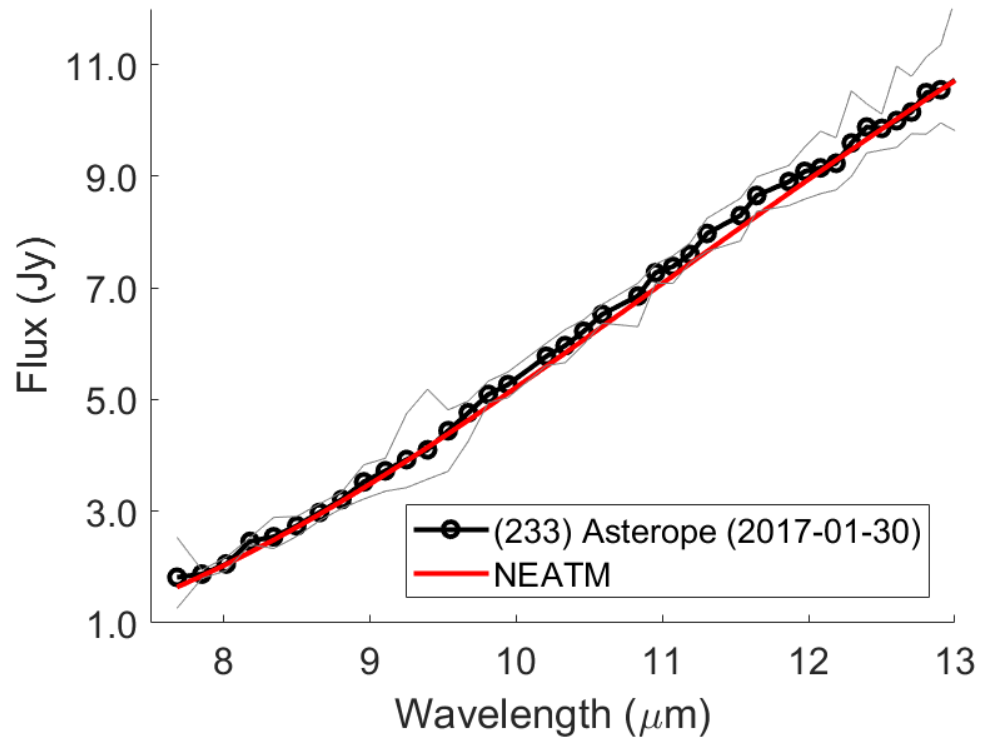


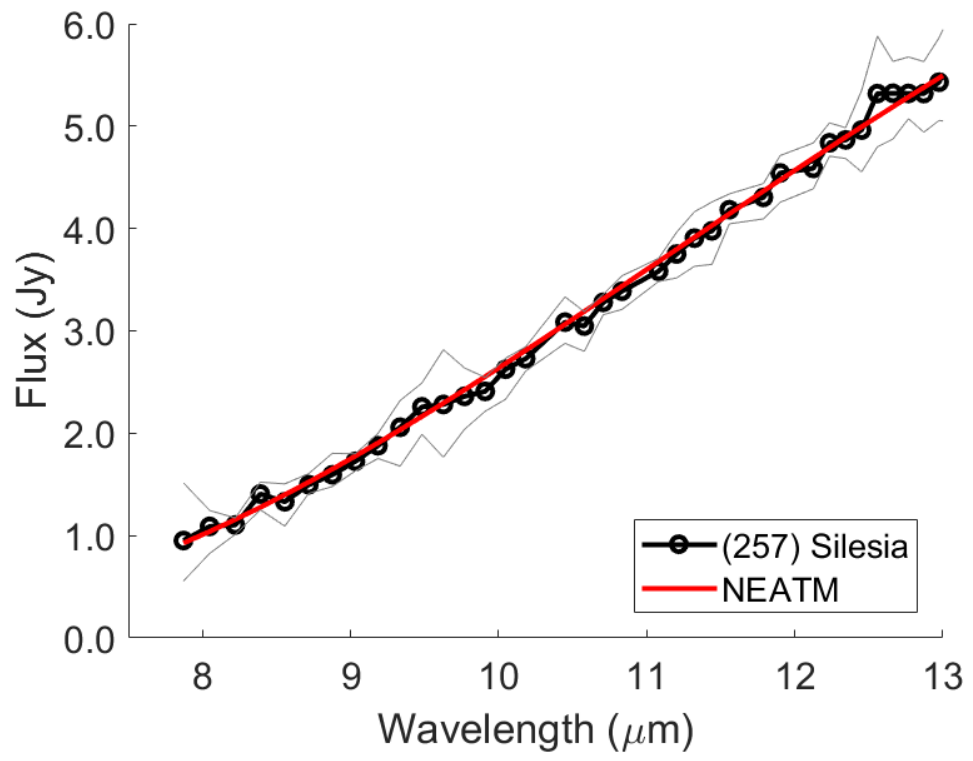


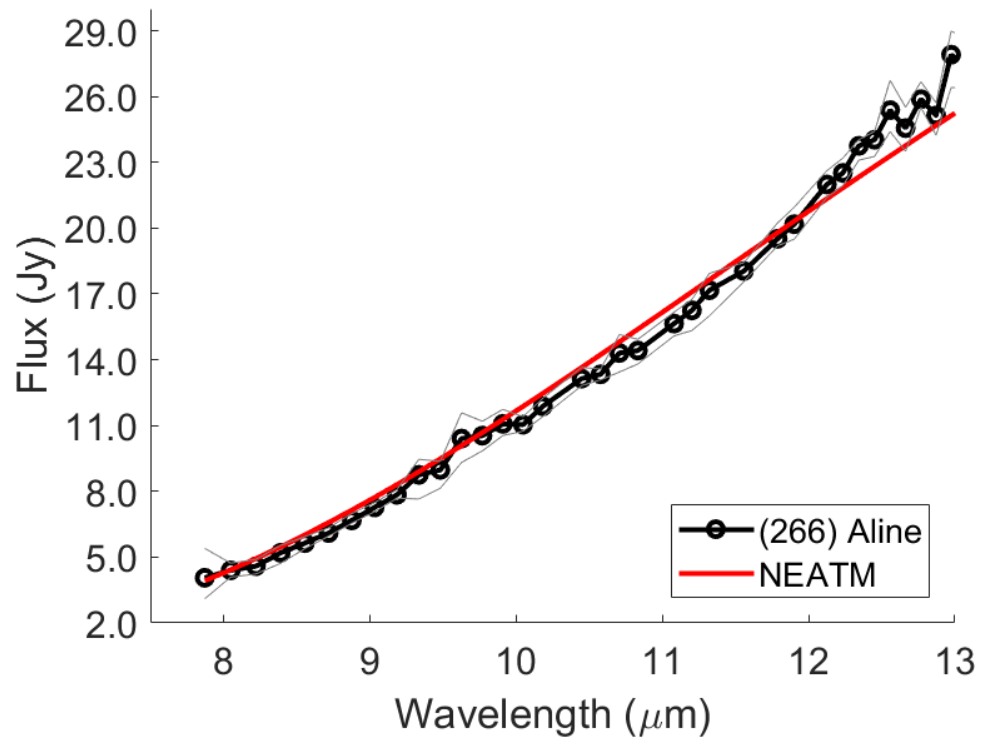


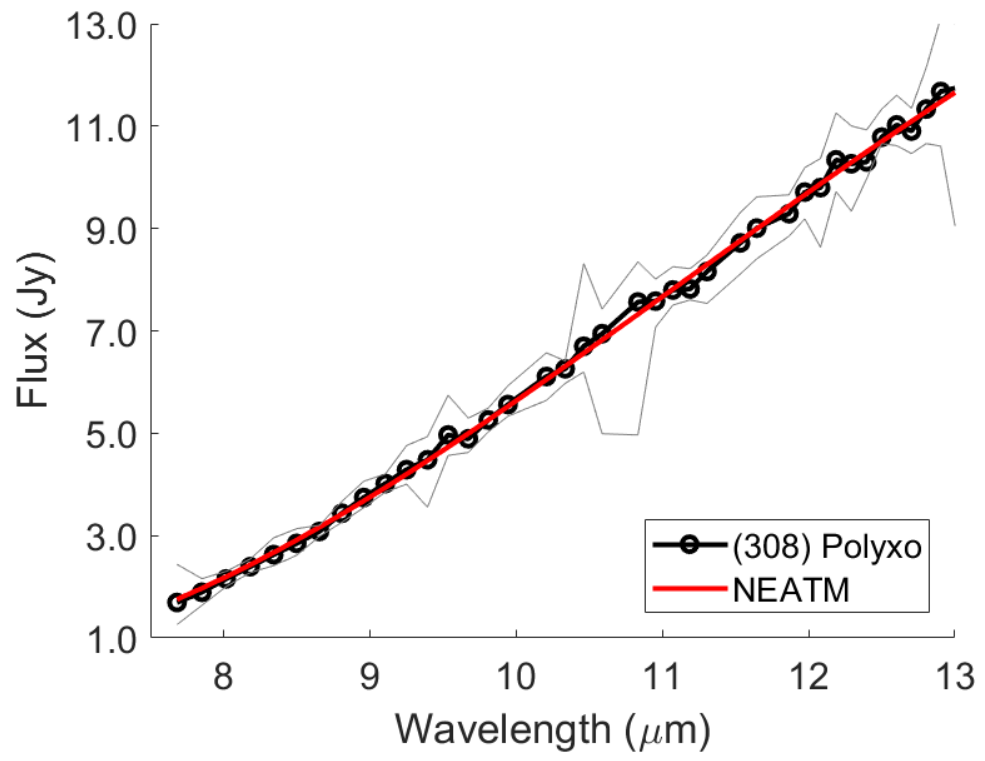


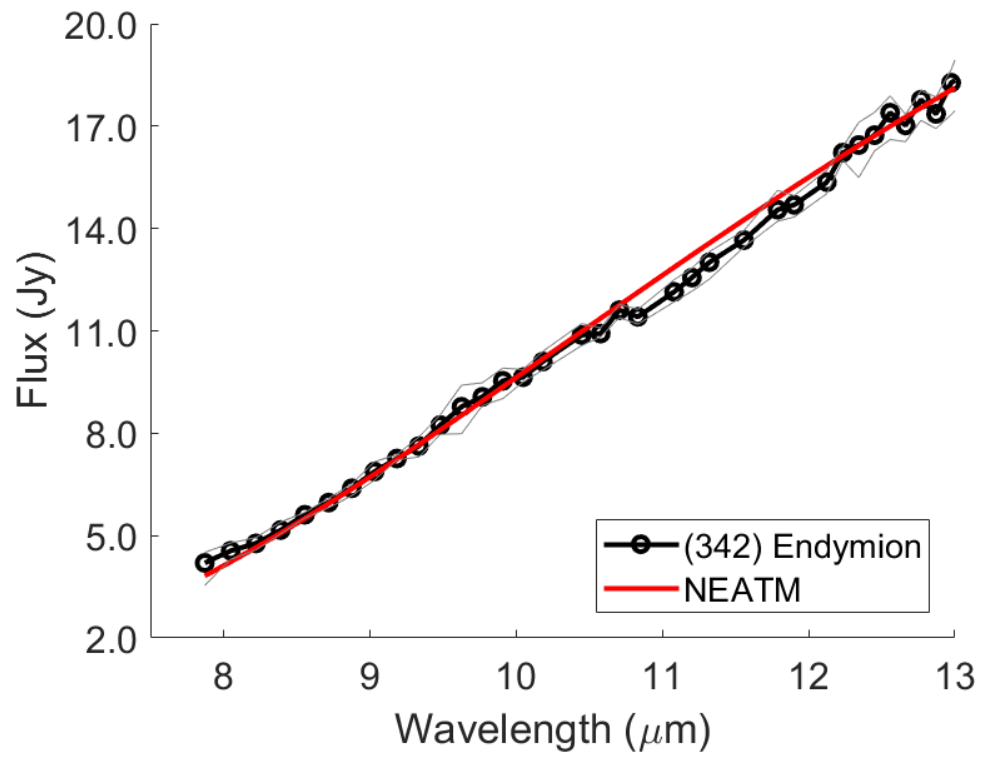


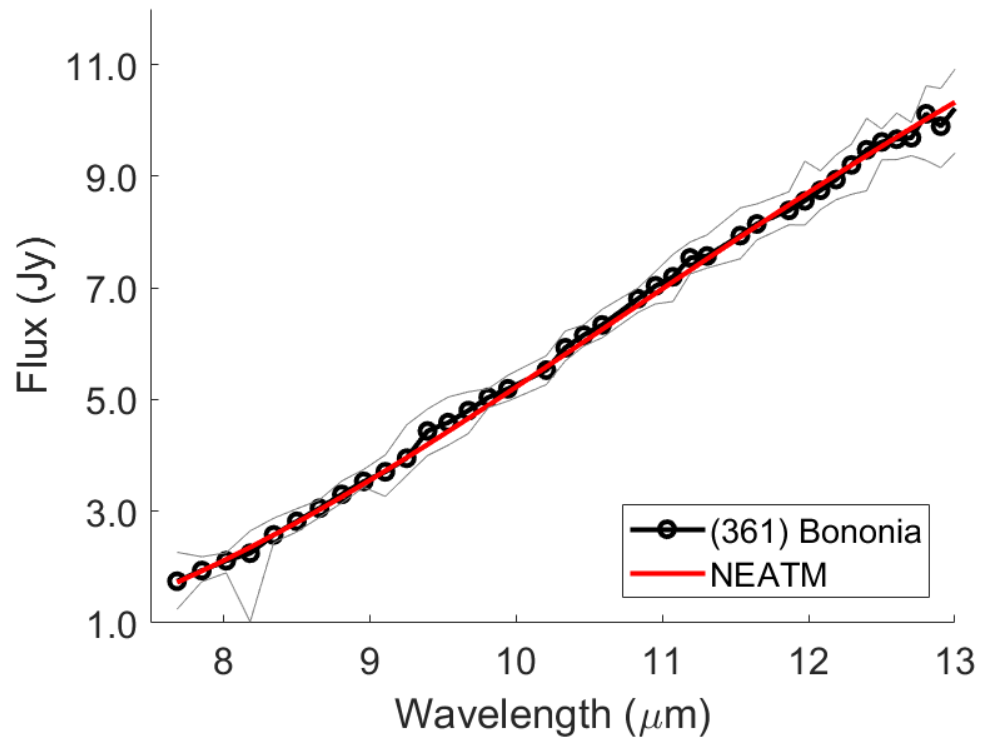


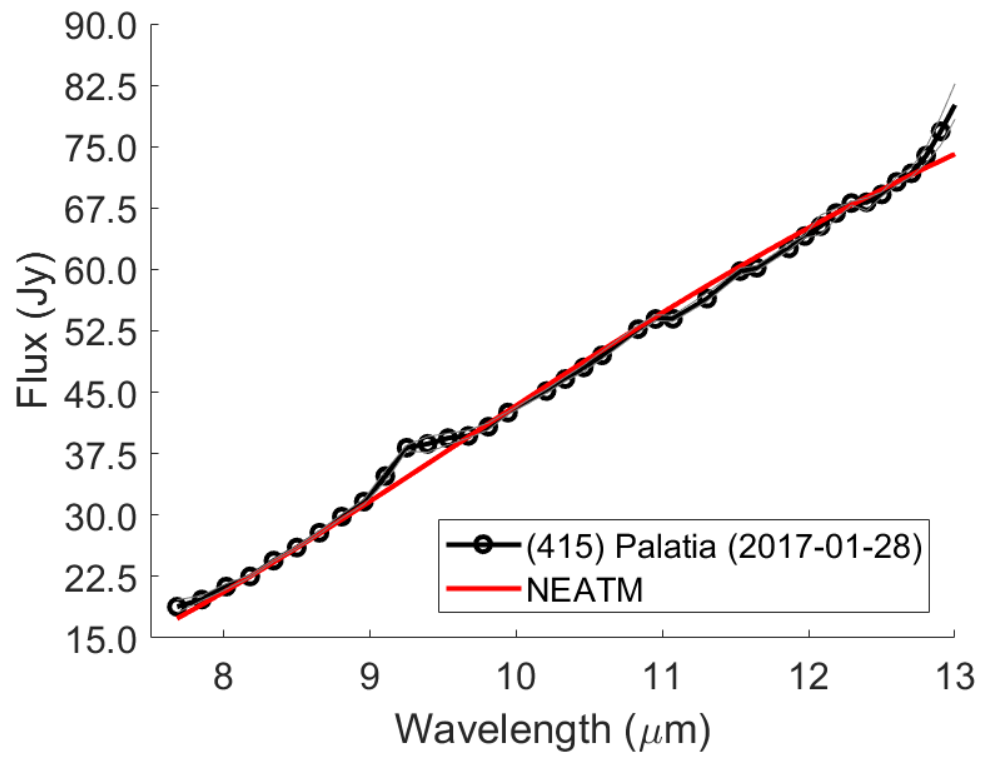


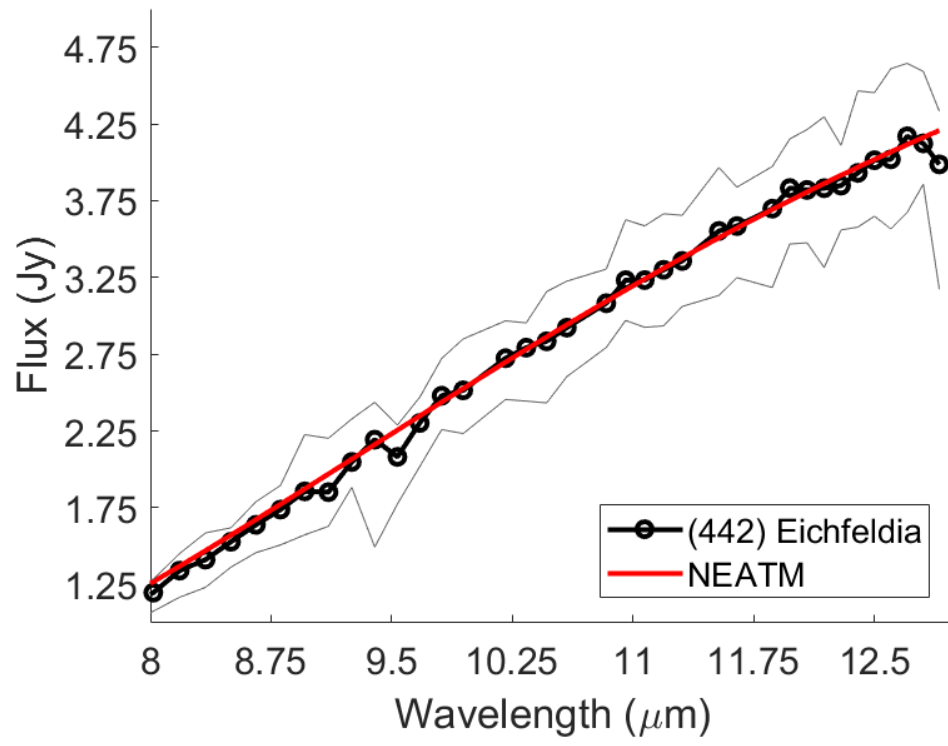


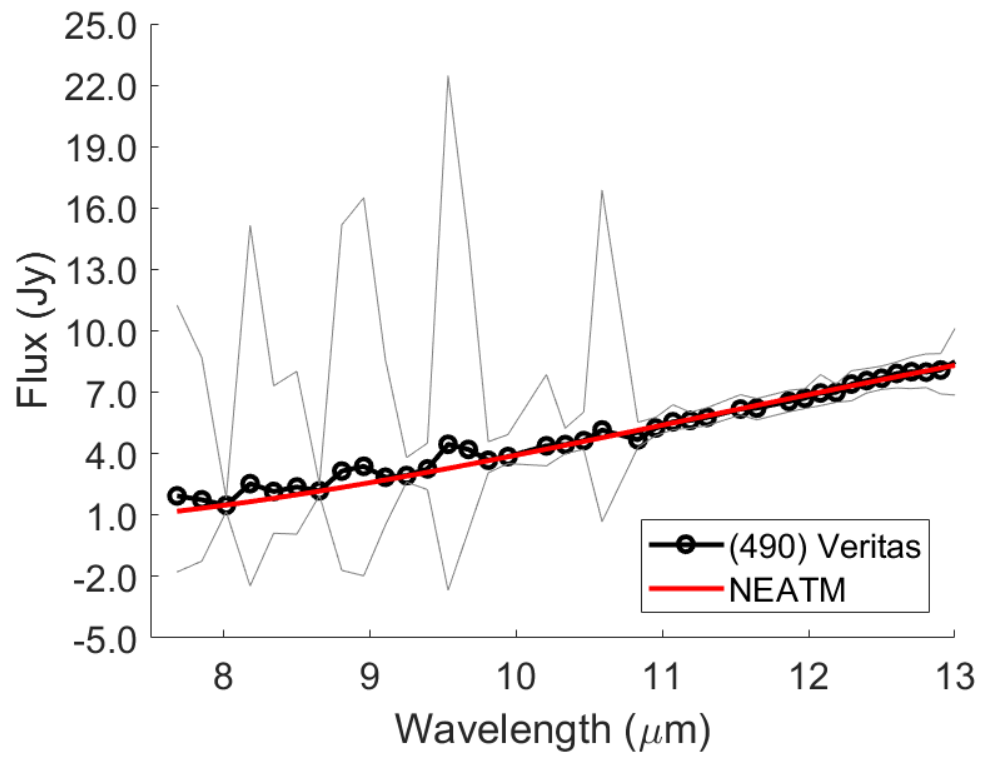


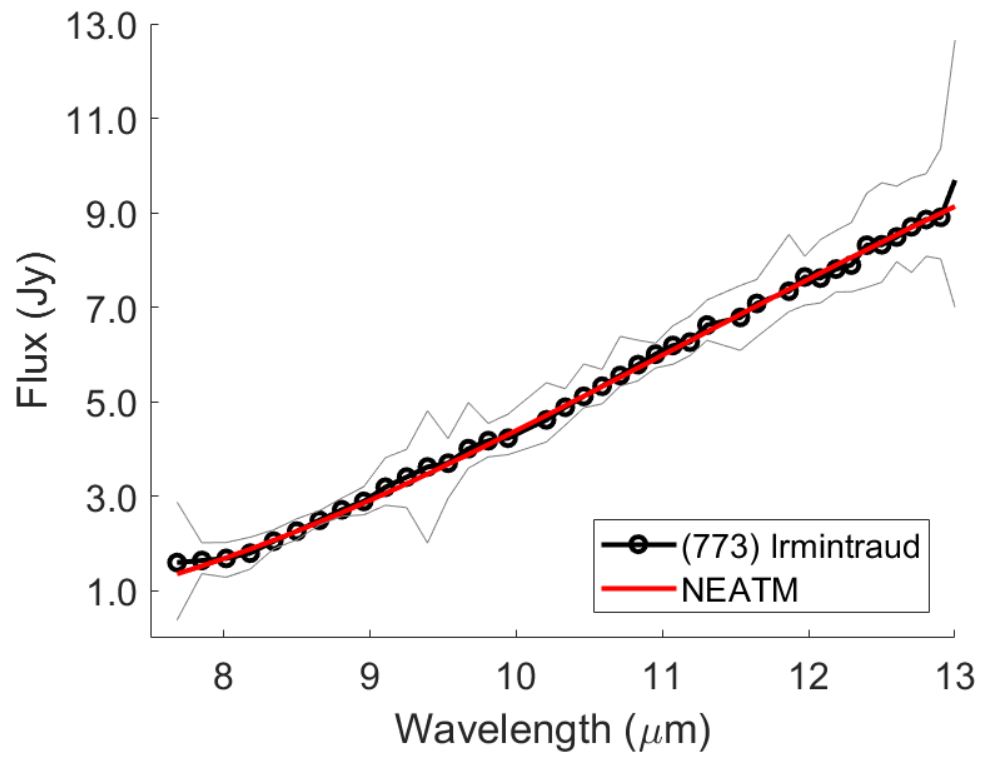




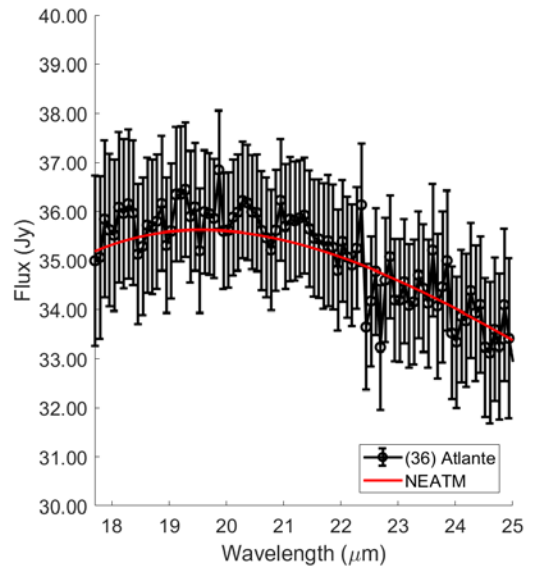
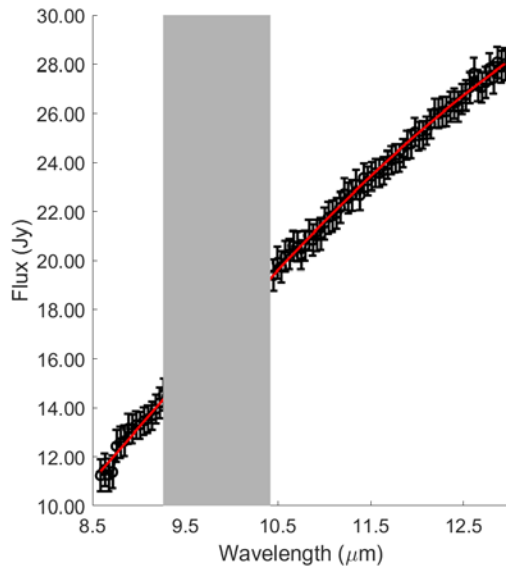
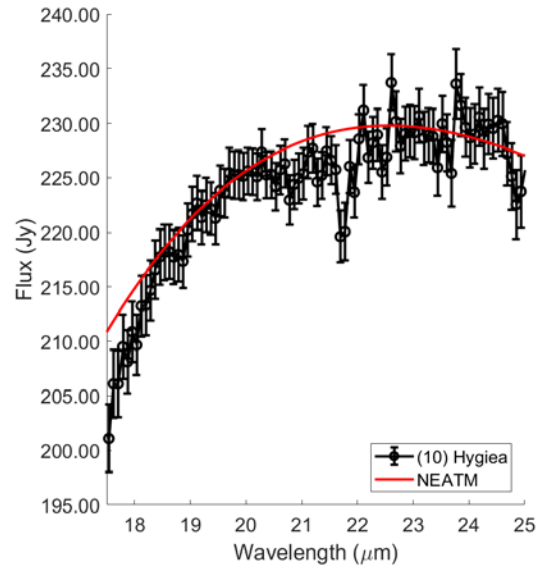
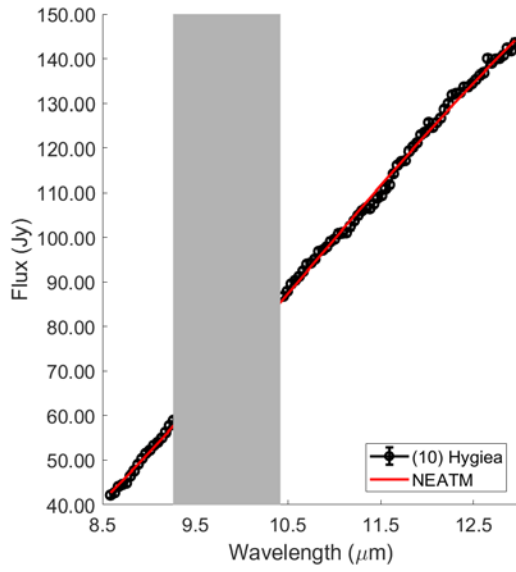


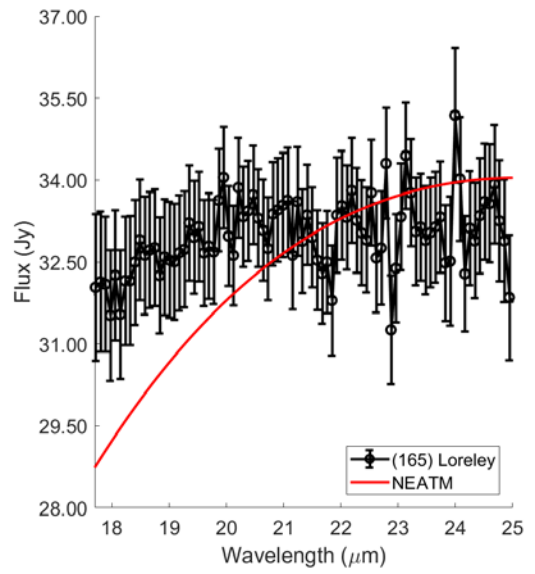
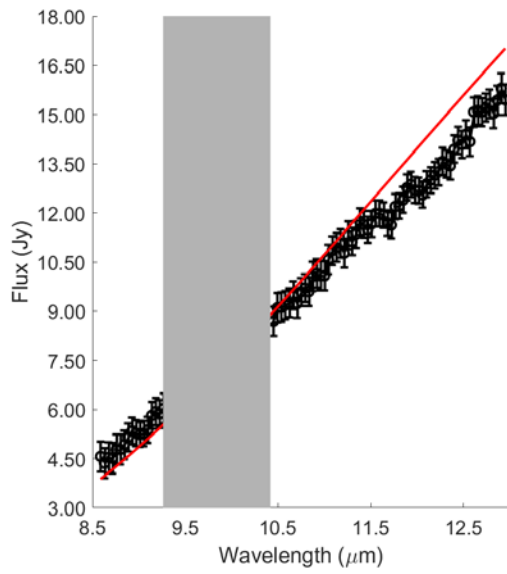
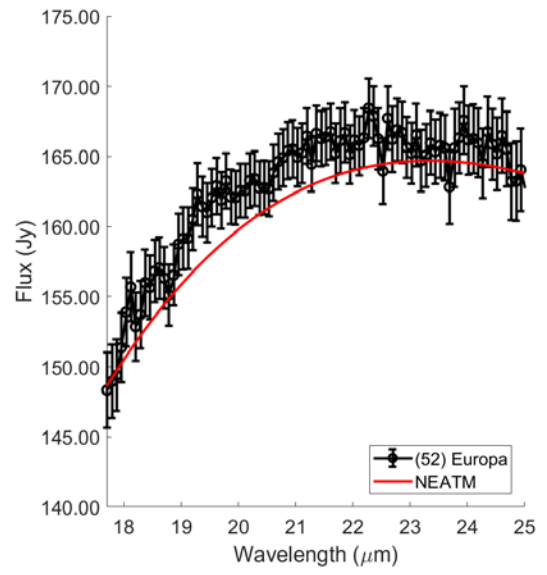
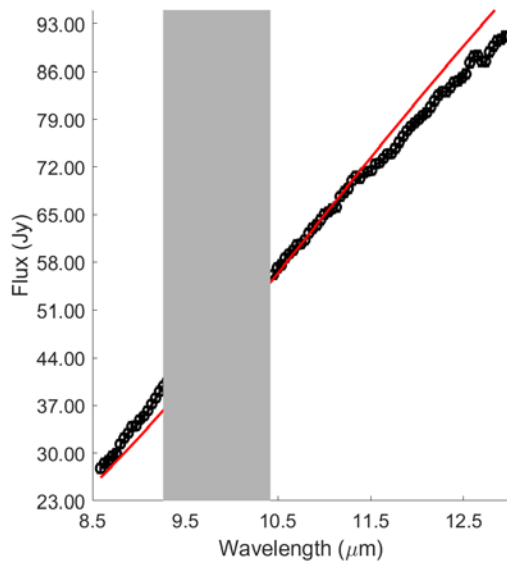


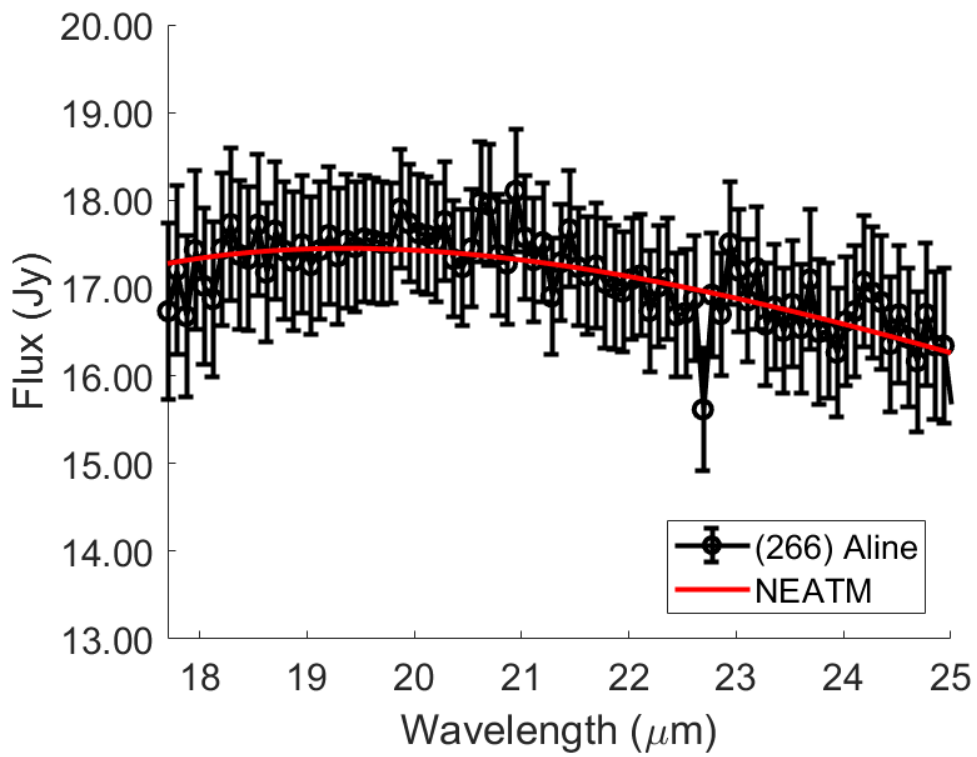
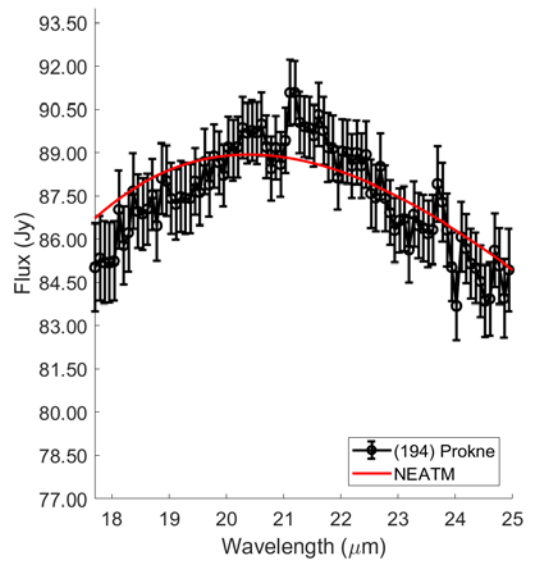
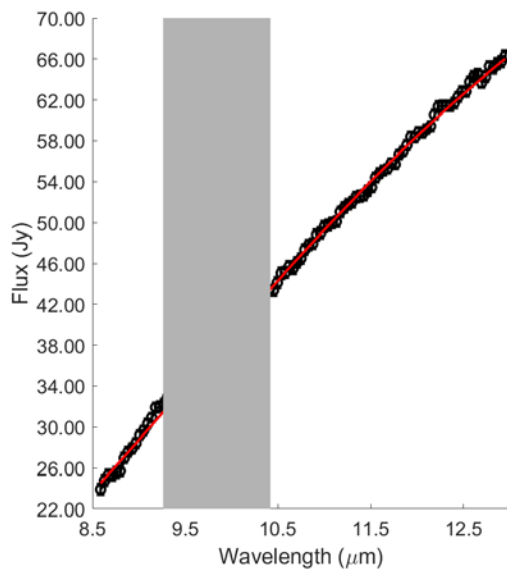




SOFIA+FORCAST Observations:



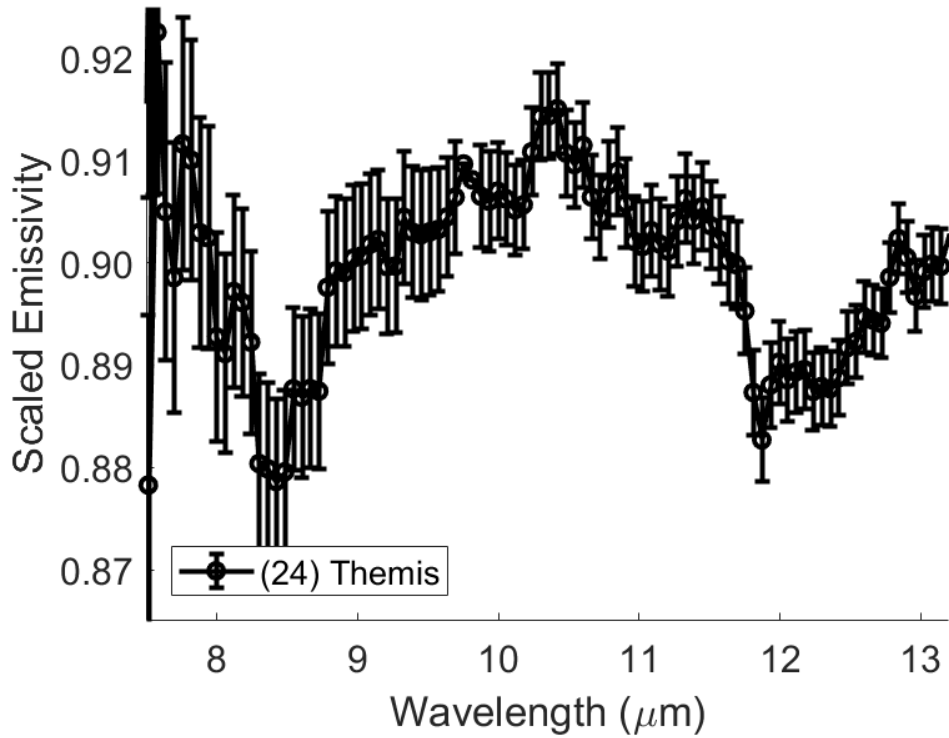


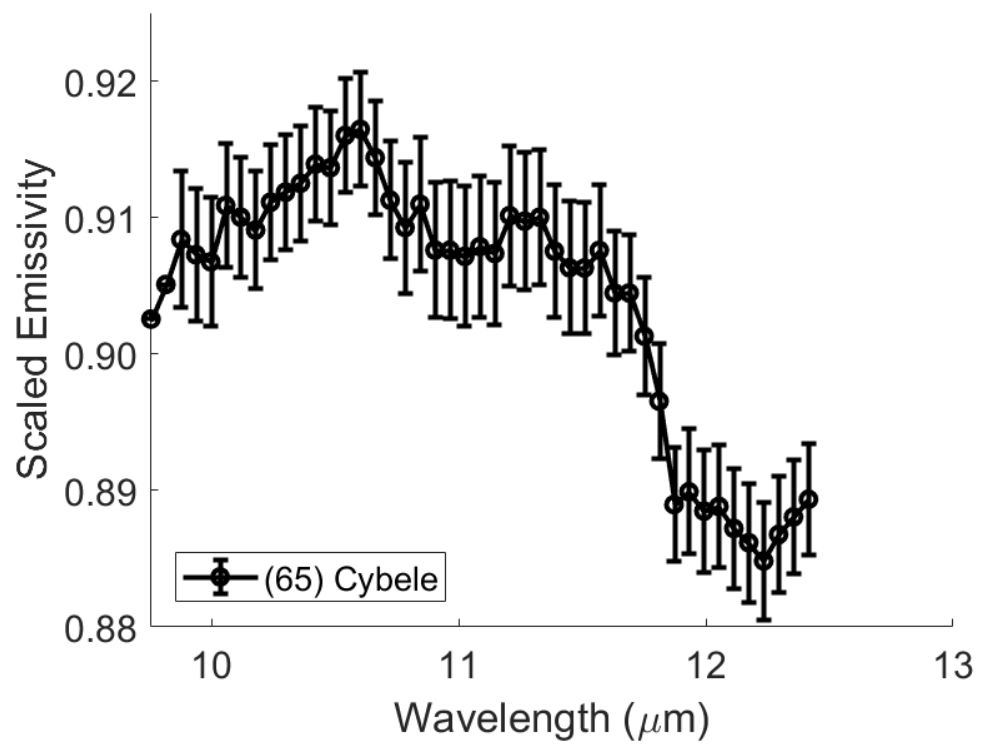


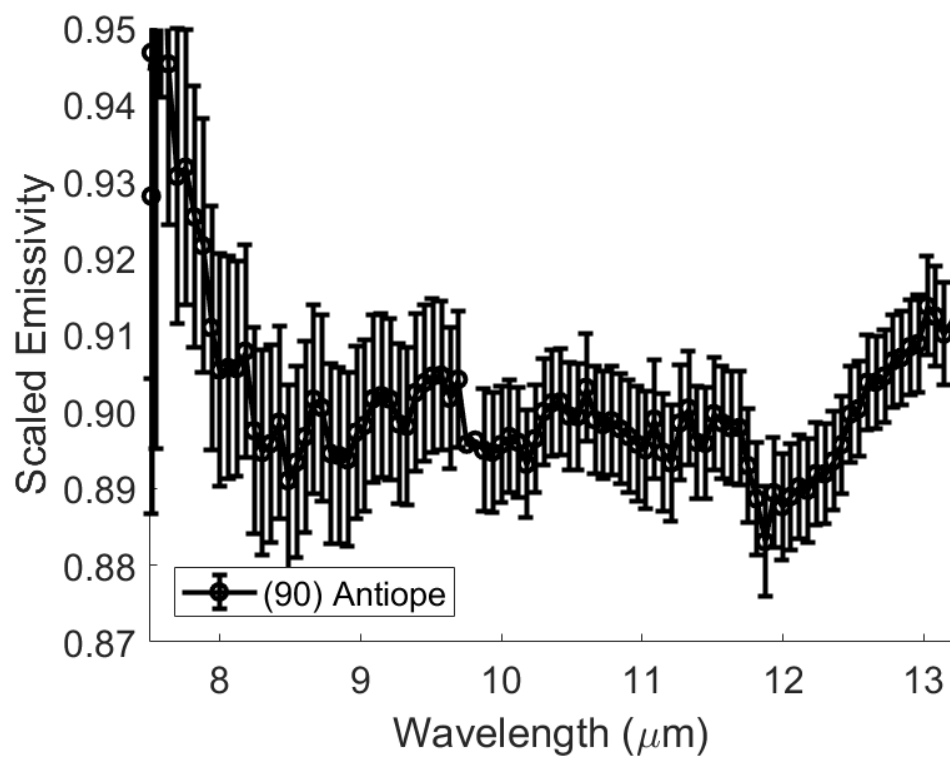
Appendix 2: Asteroid Emissivity Spectra

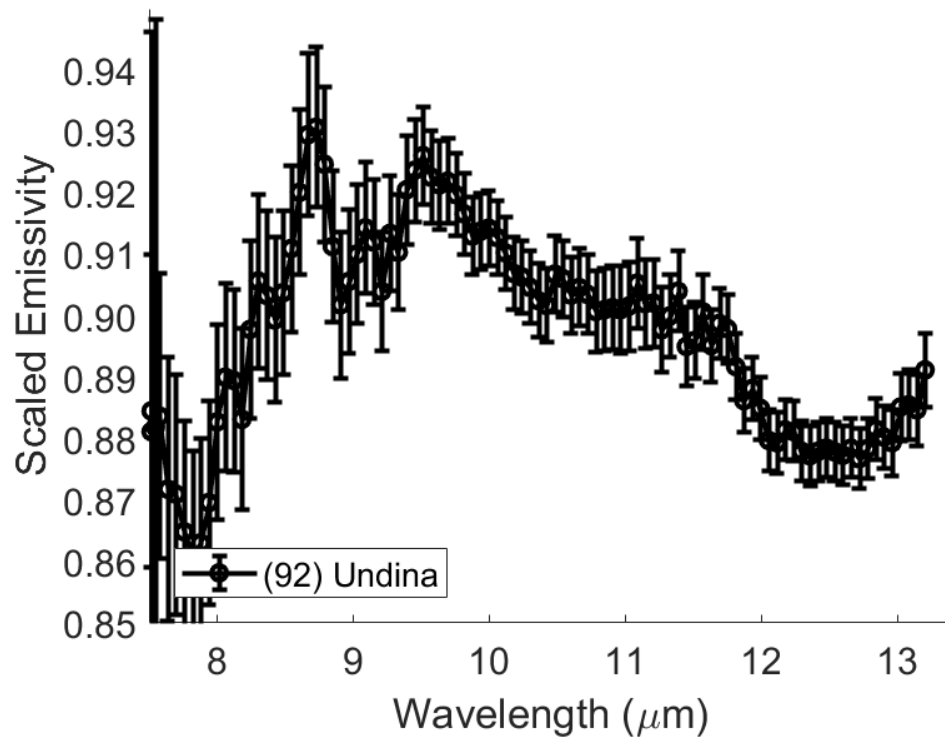
Emissivity spectra of asteroids are produced by dividing the asteroid data by the best fit thermal model. They are presented here.

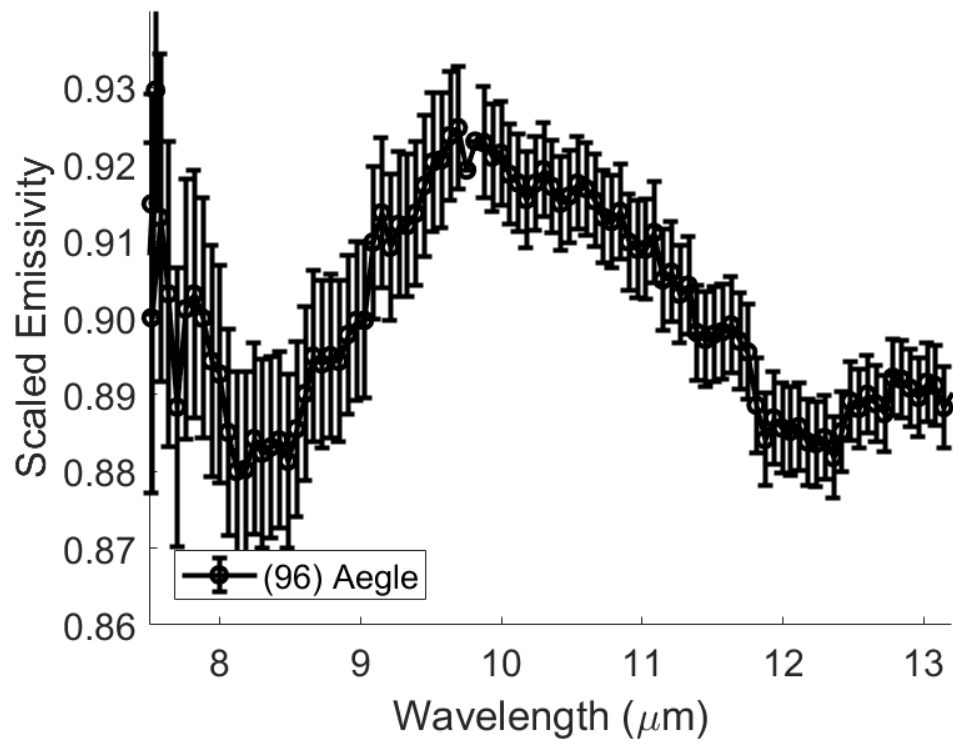
Spitzer+IRS Observations:

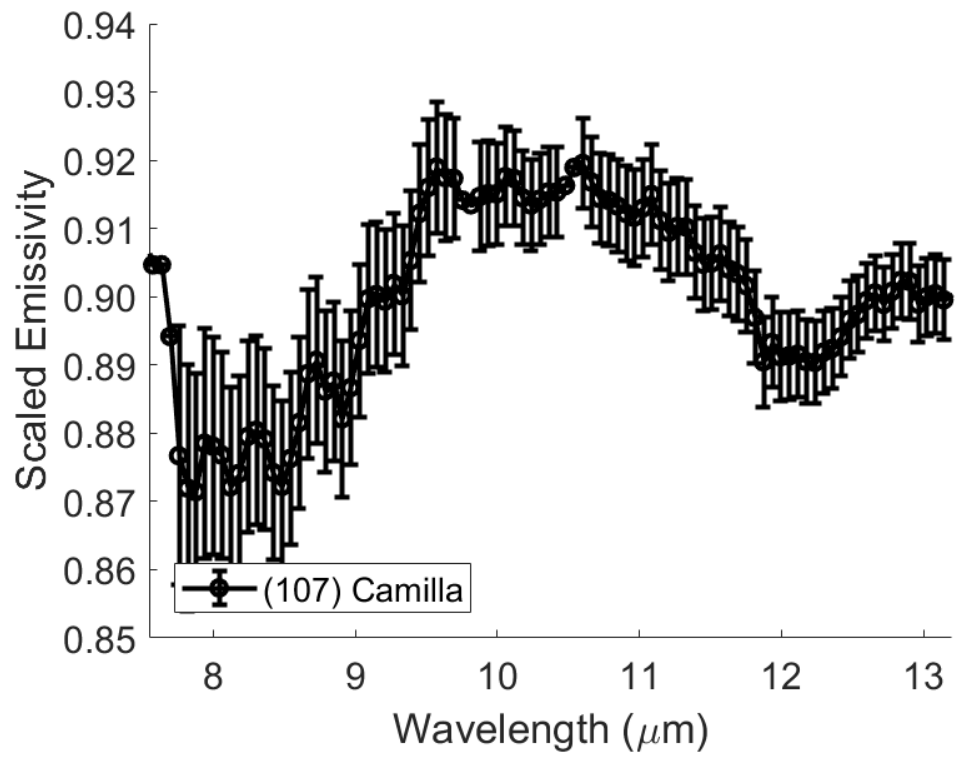


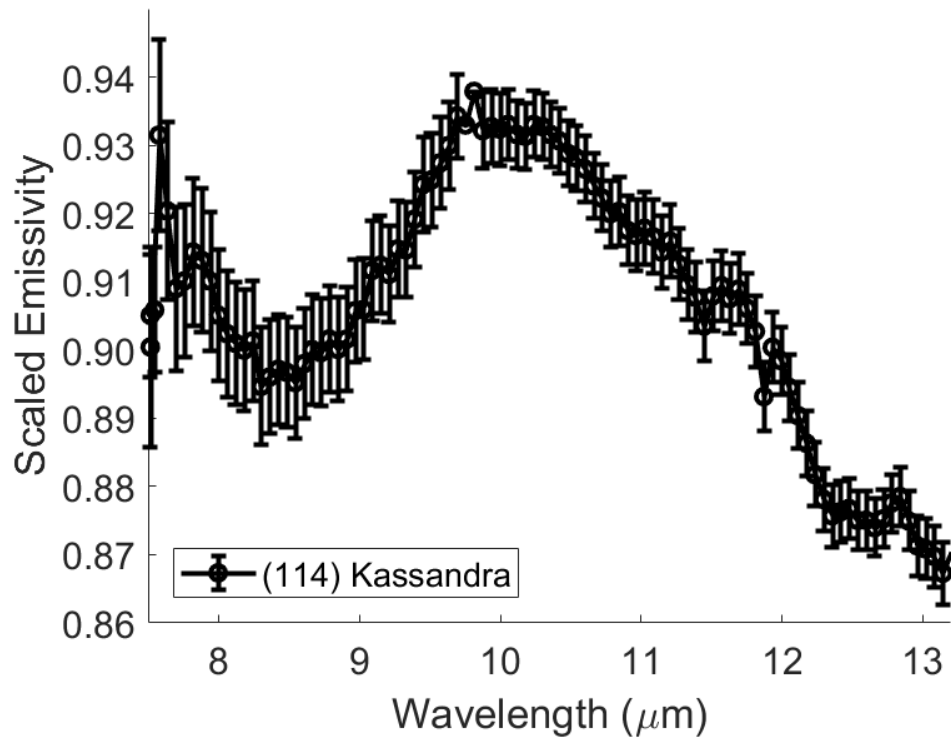


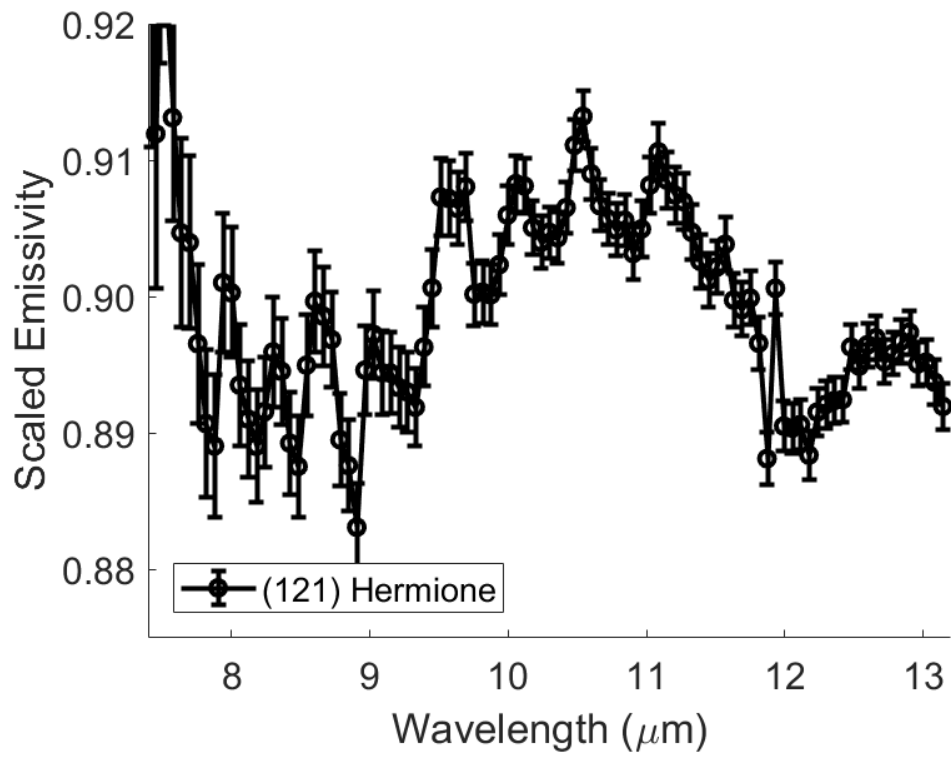


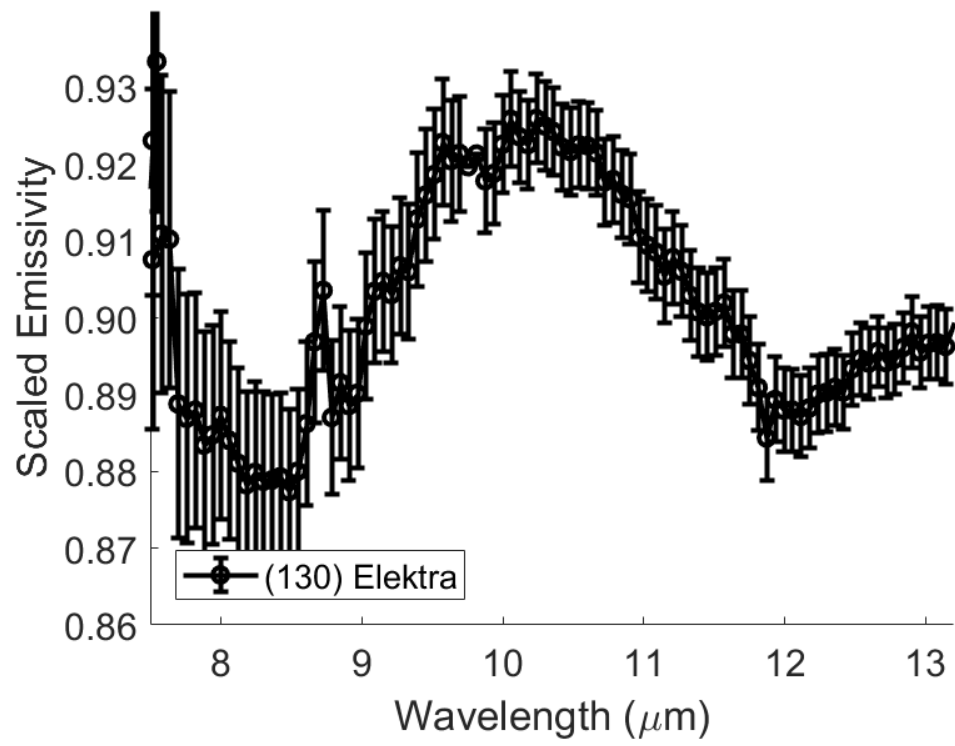


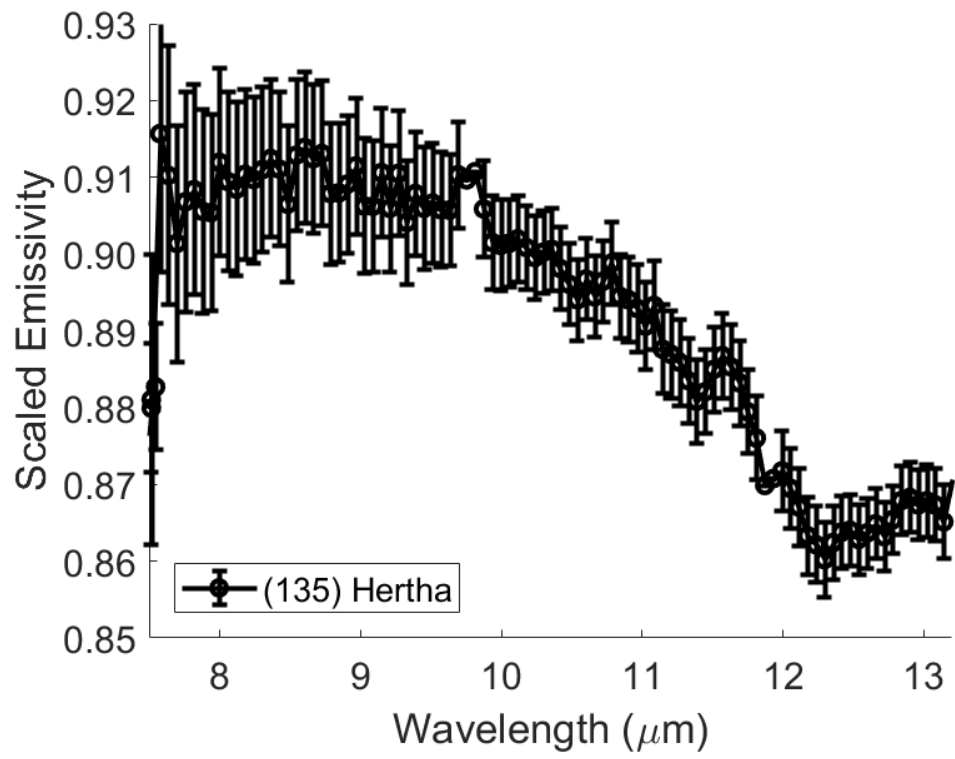


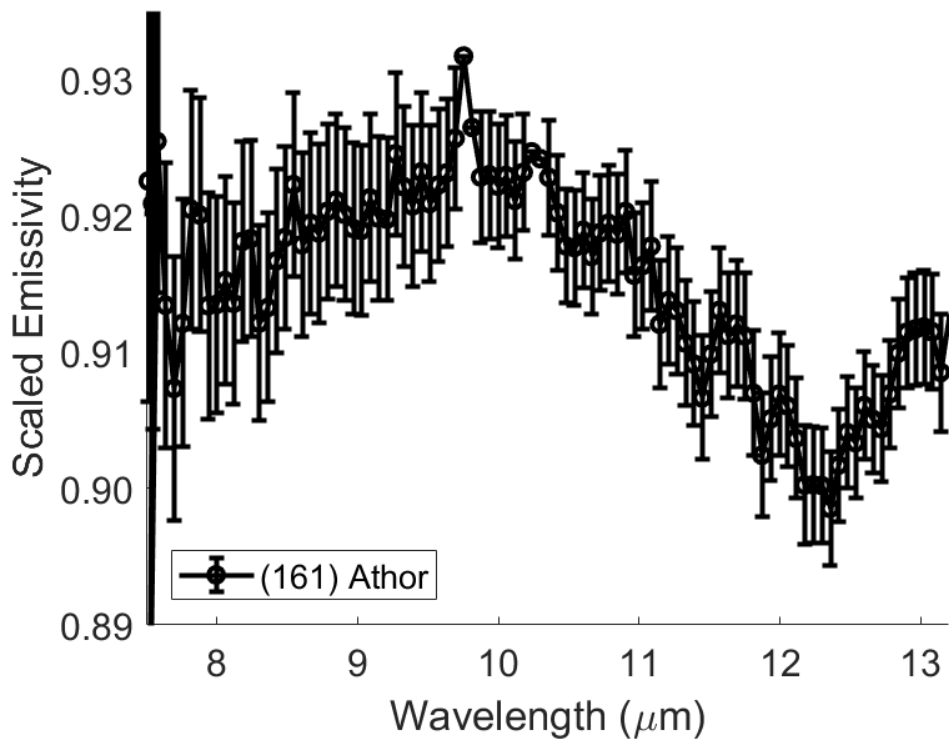


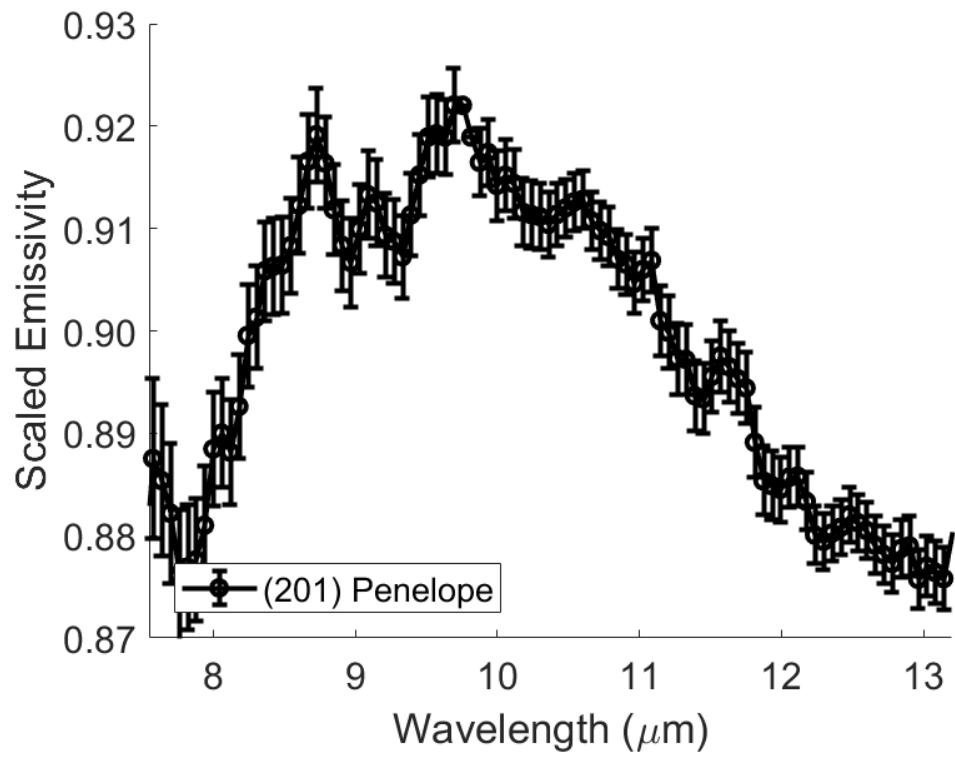


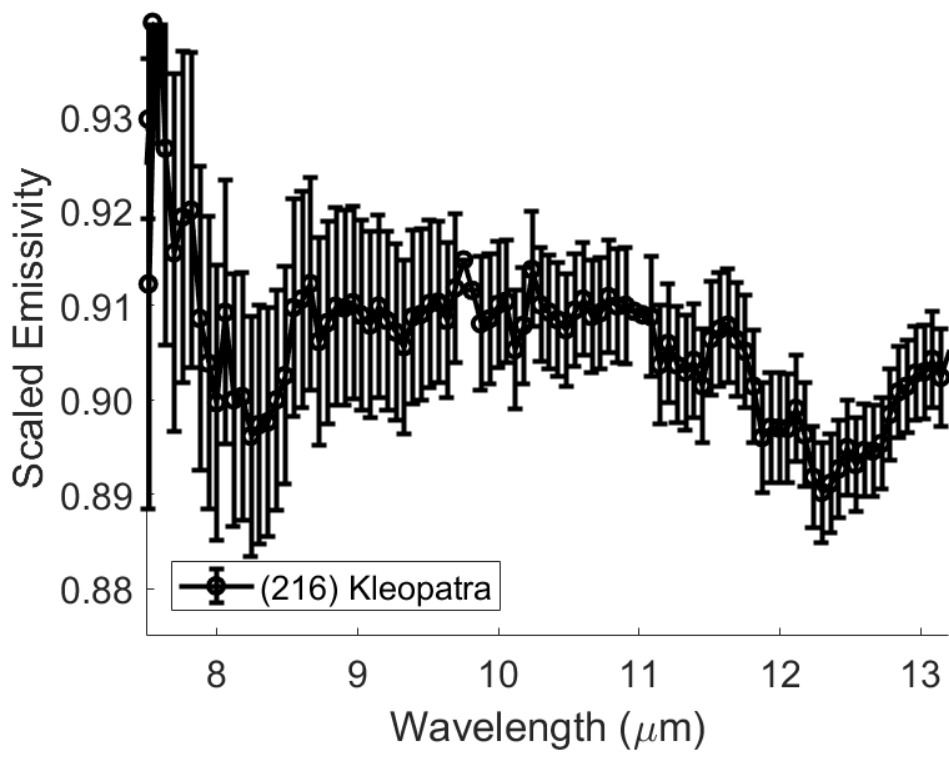


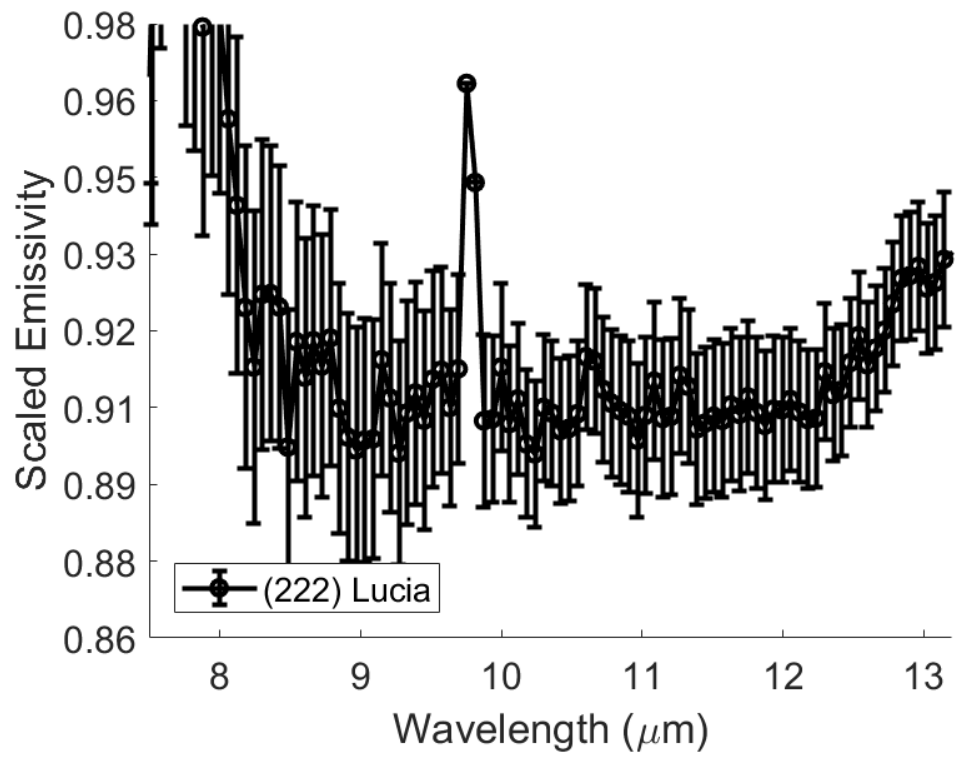


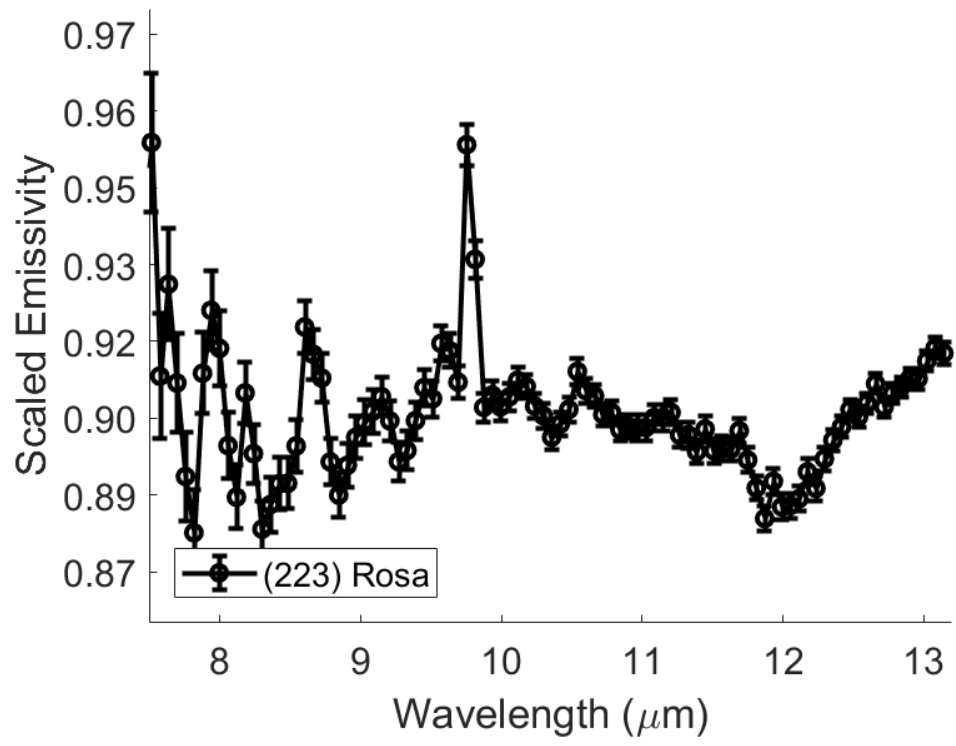


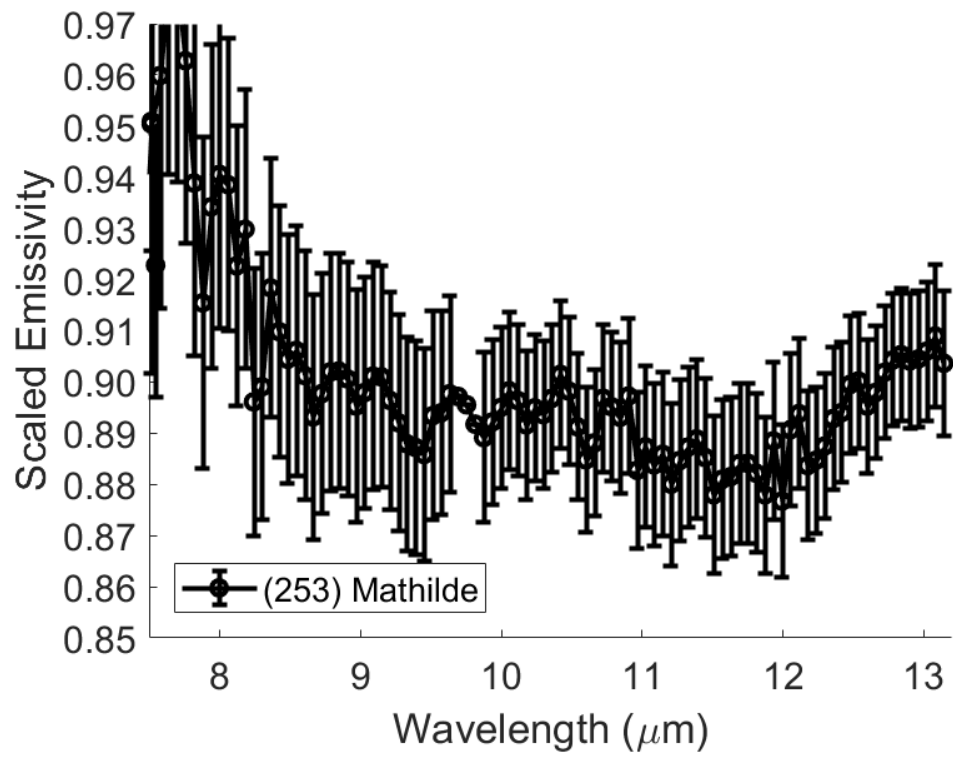


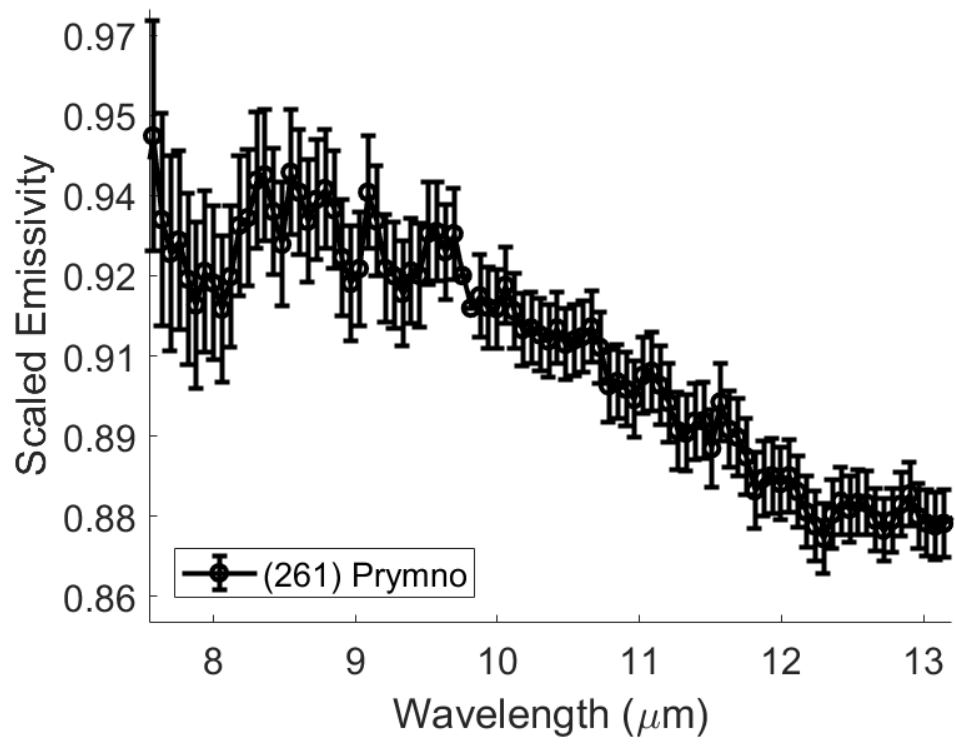


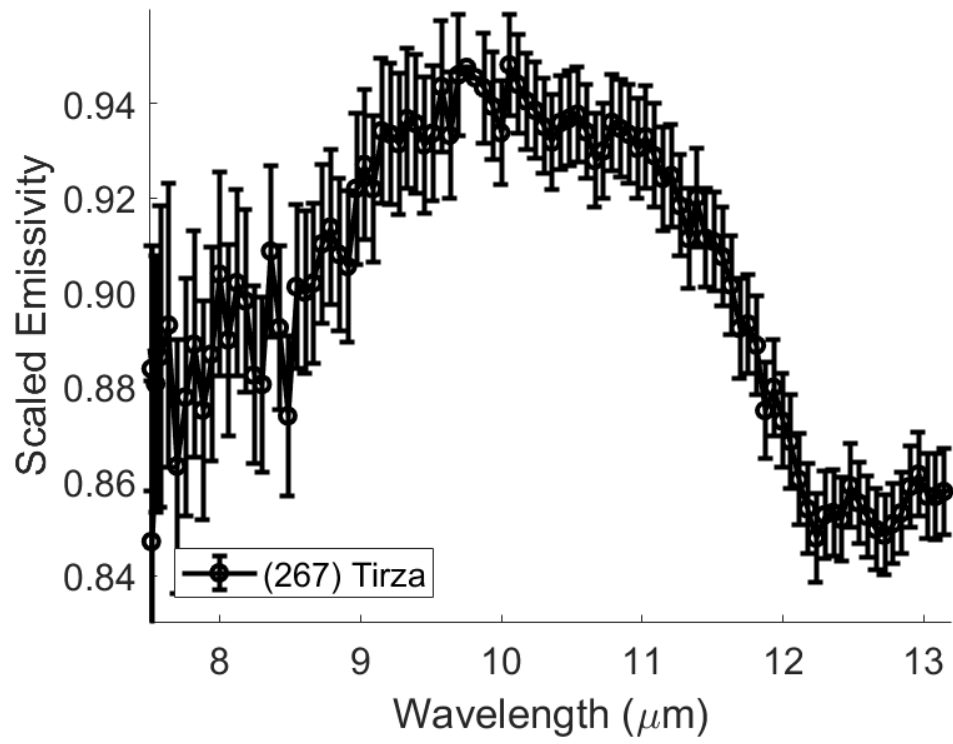


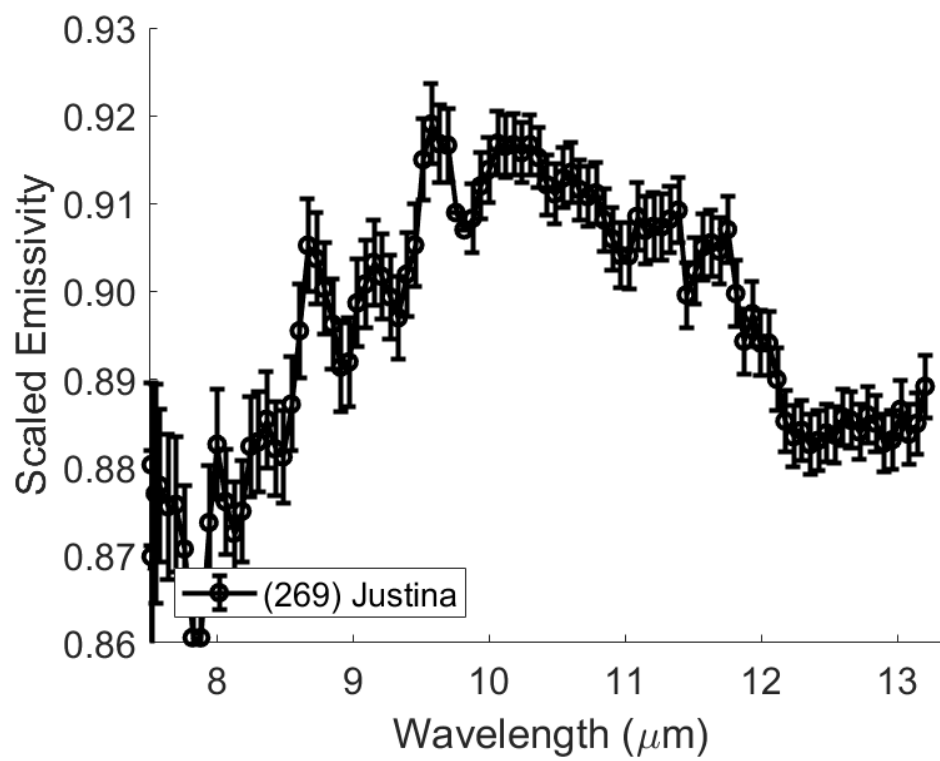


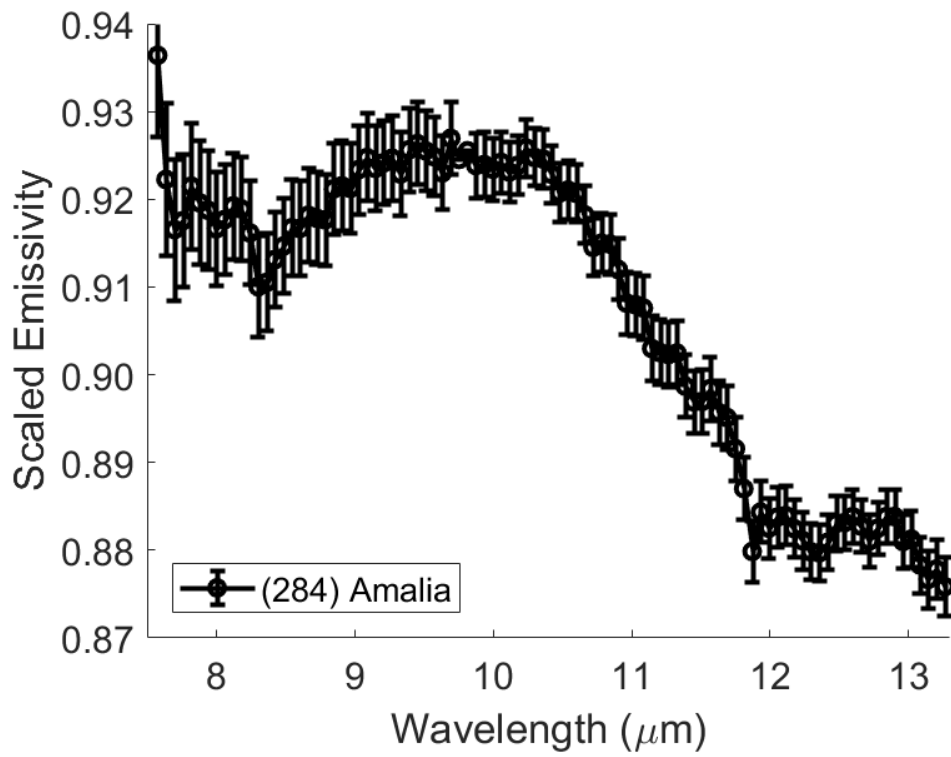
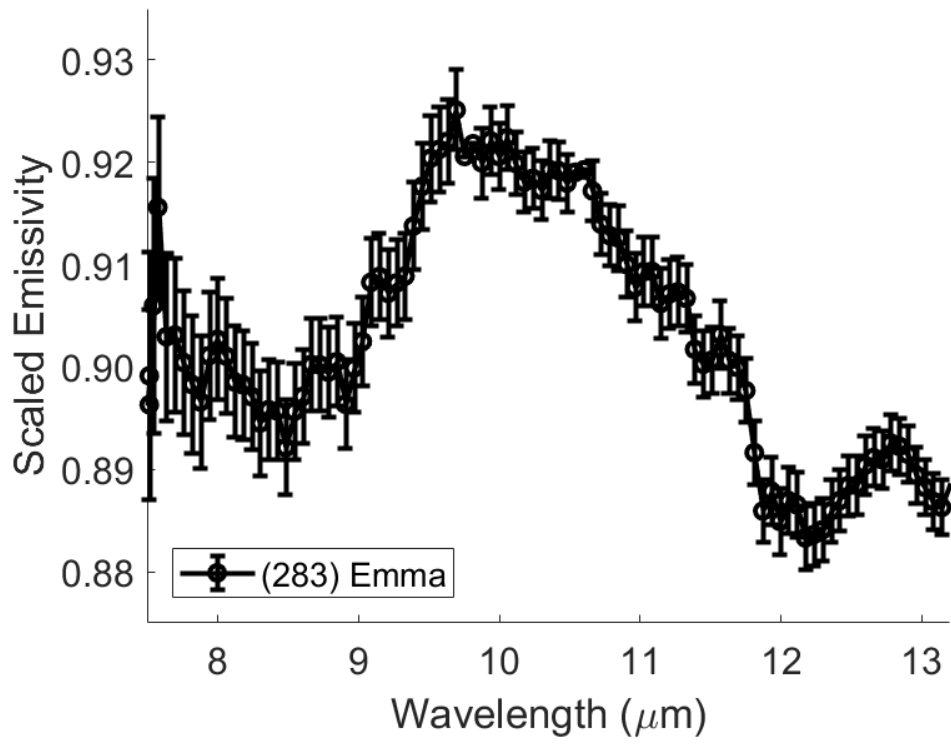


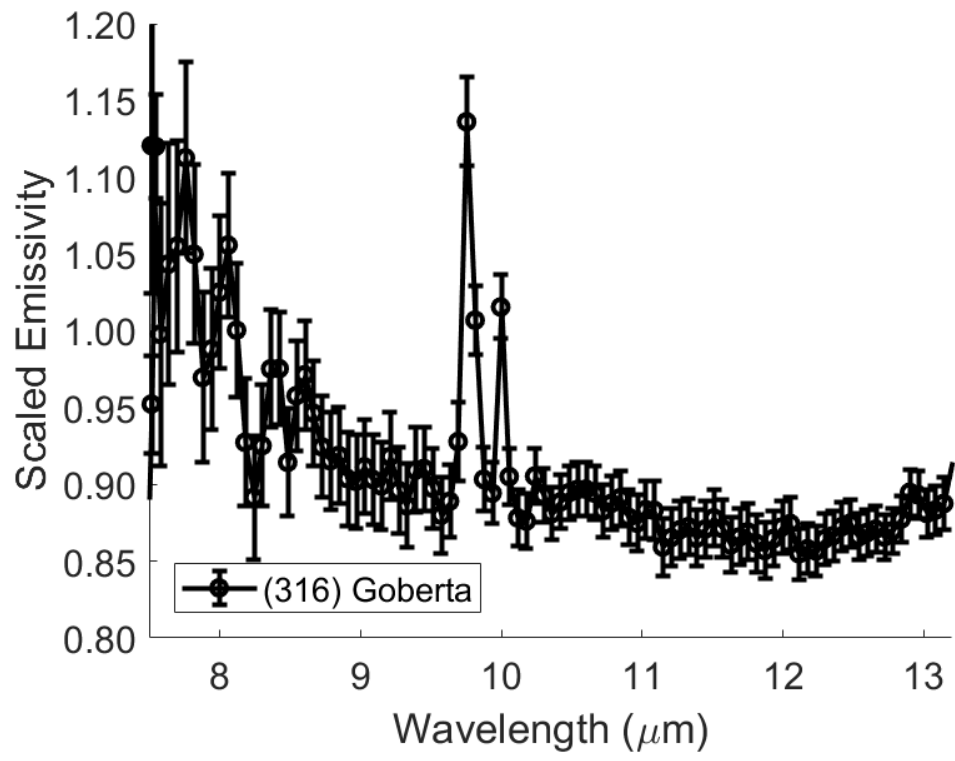


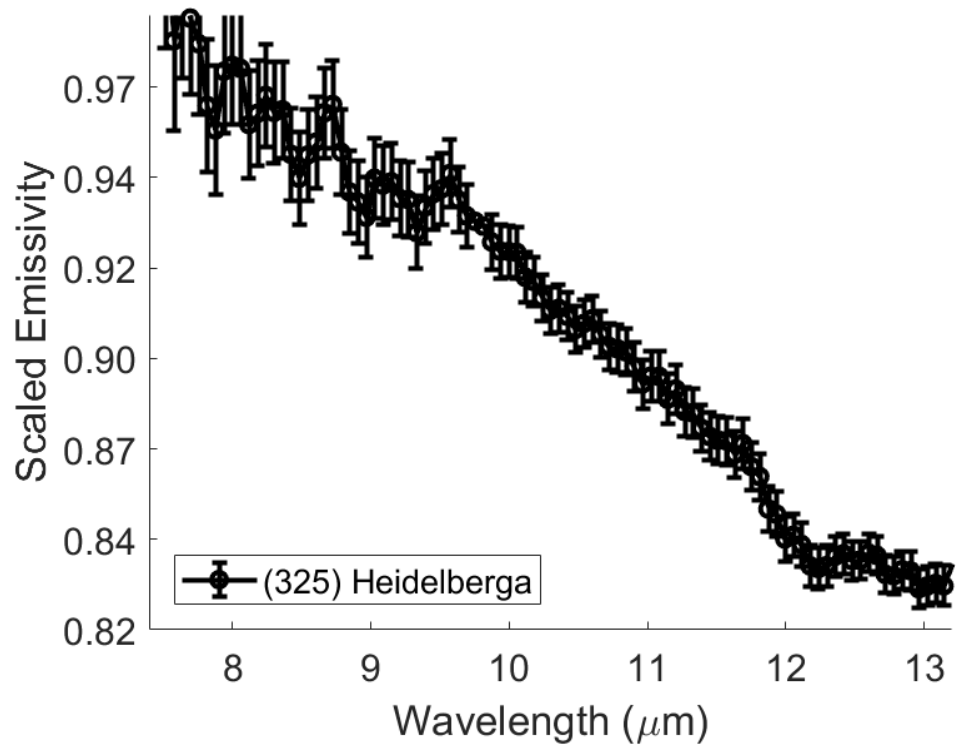


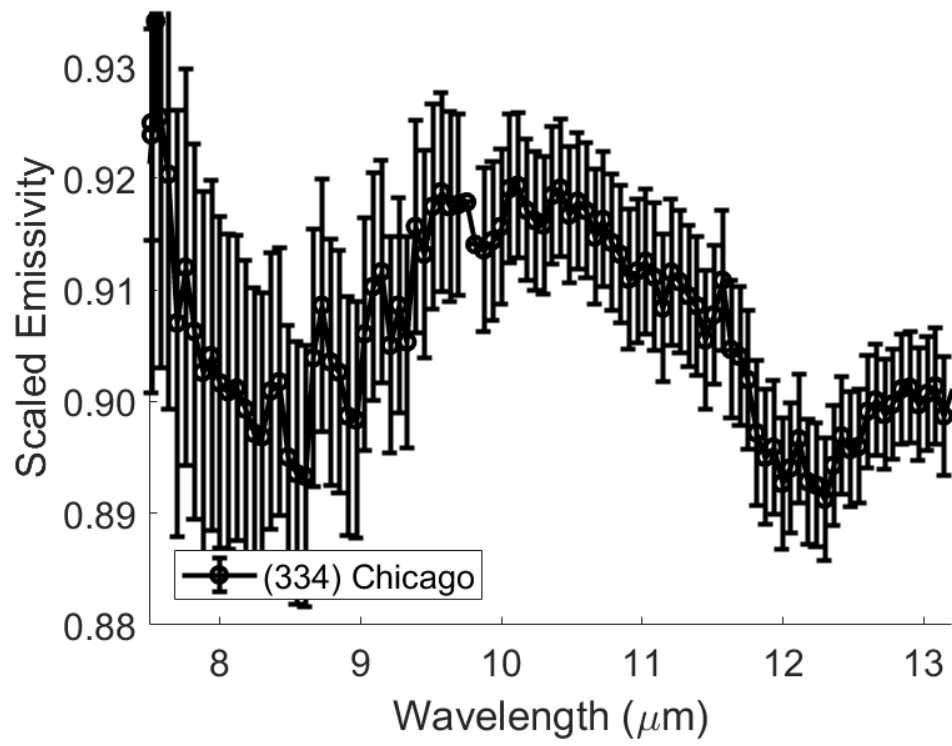


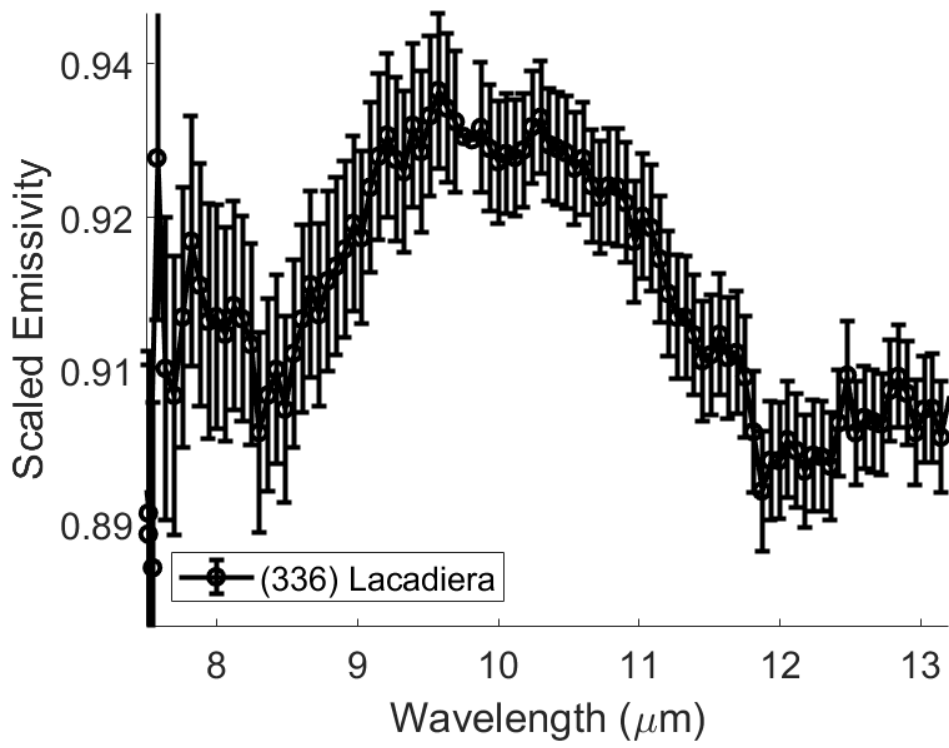


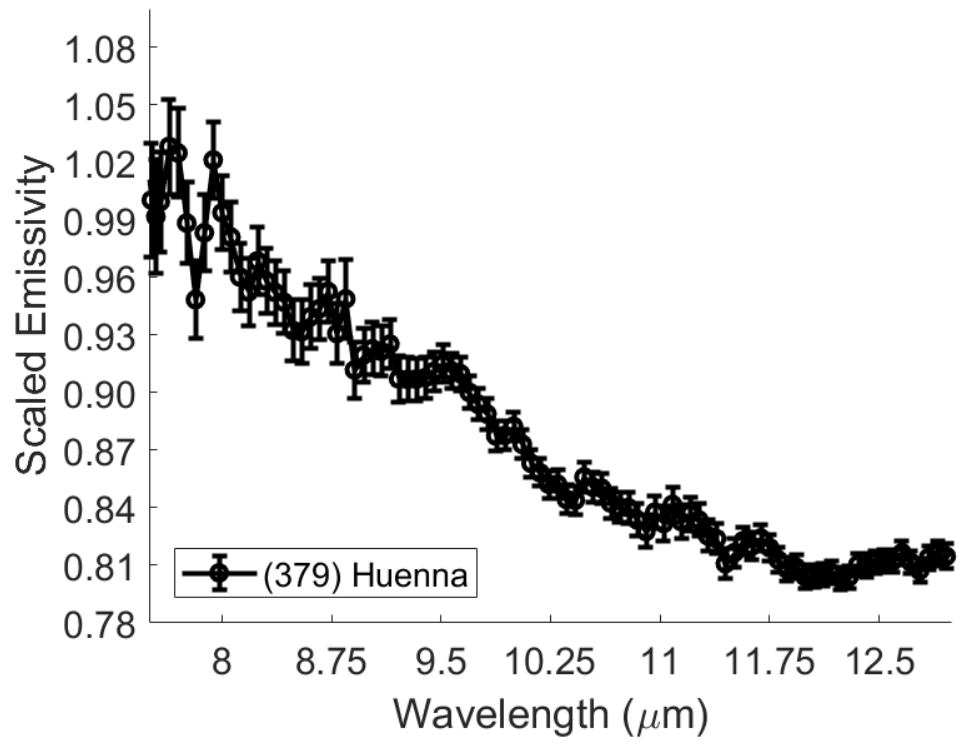


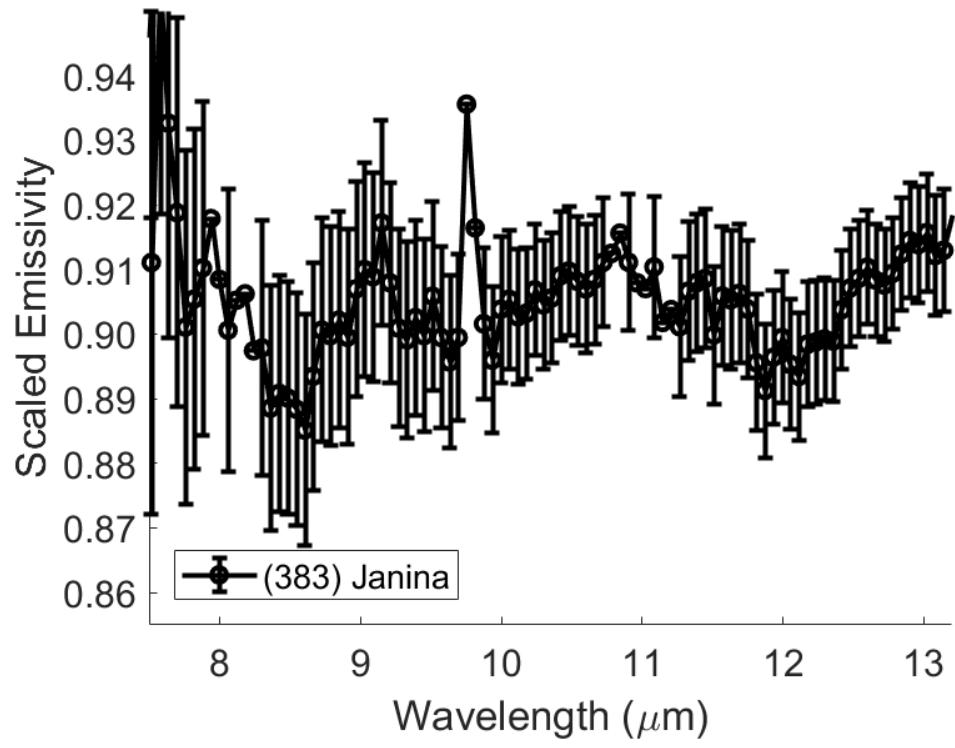


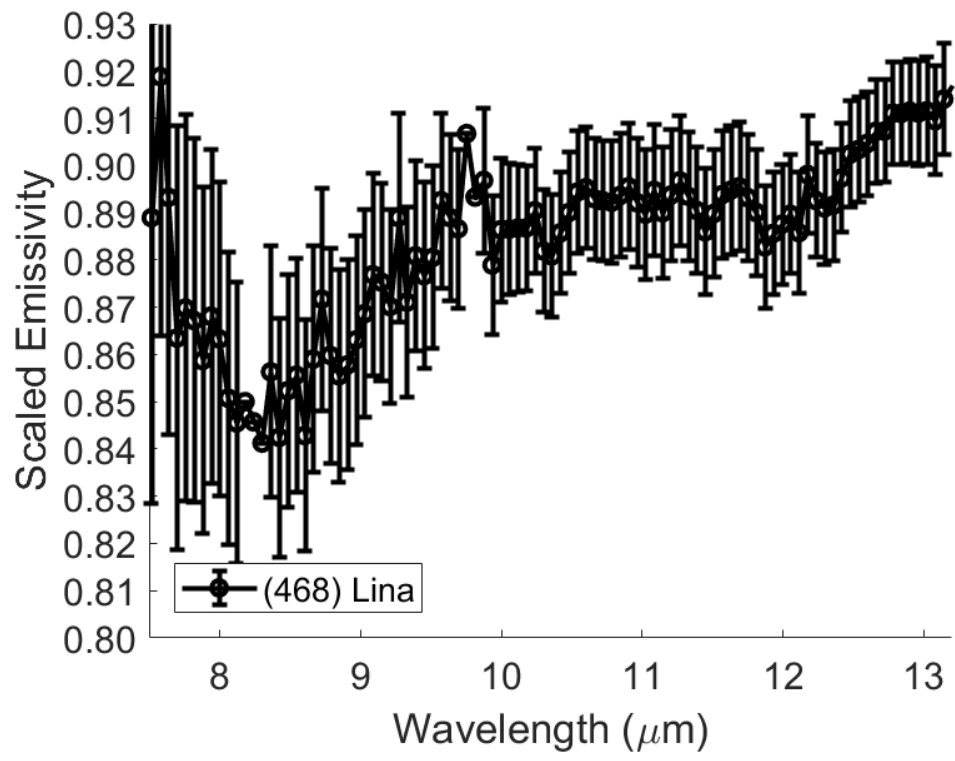


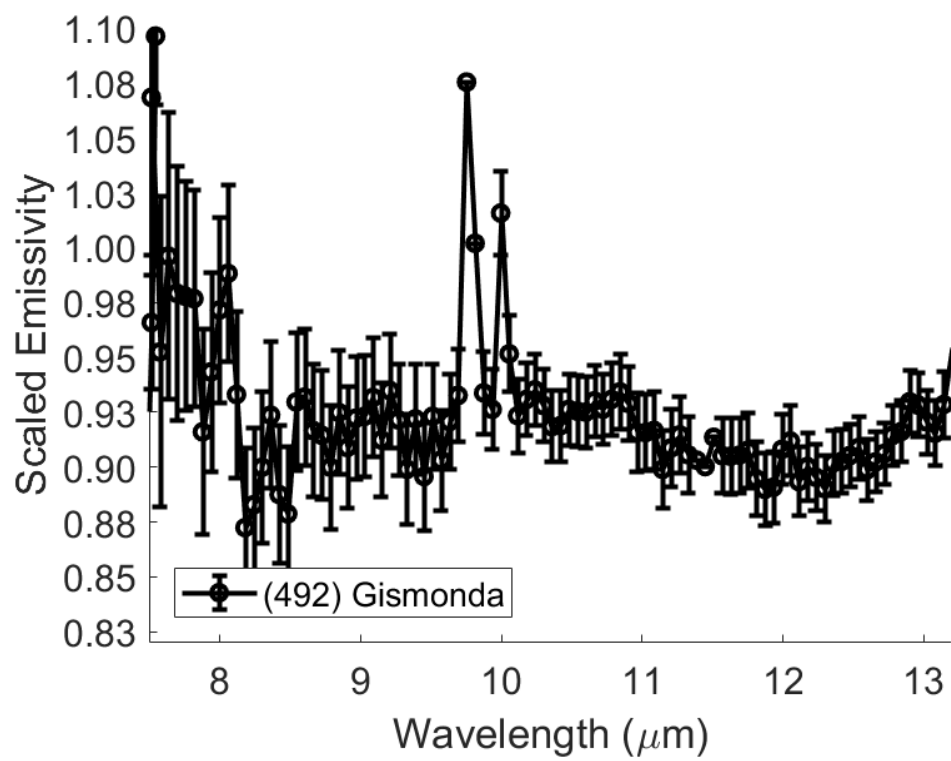


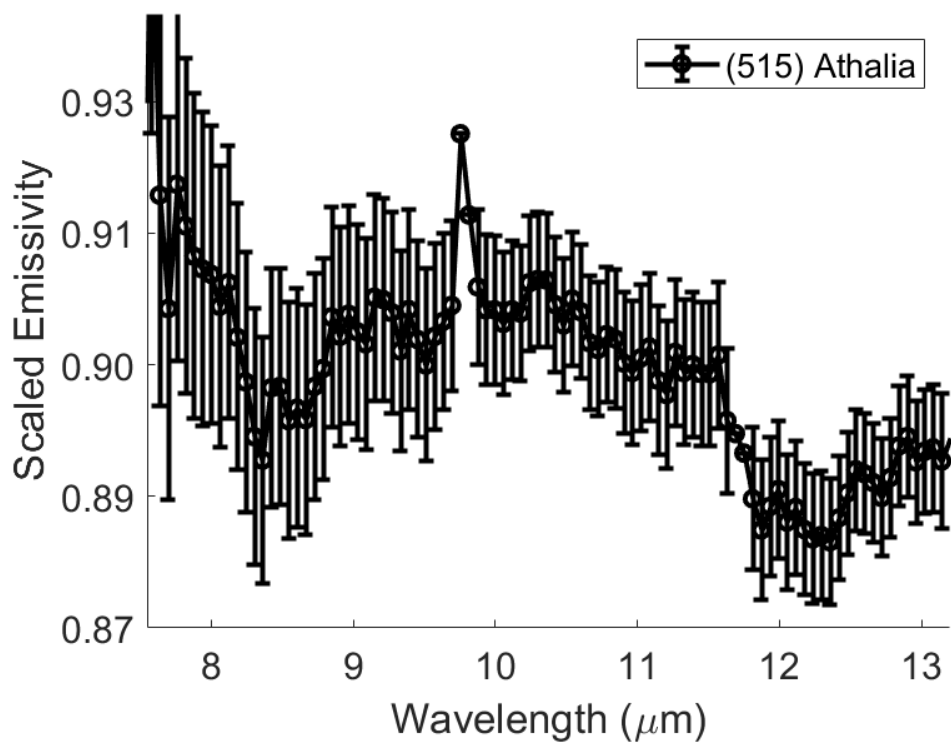
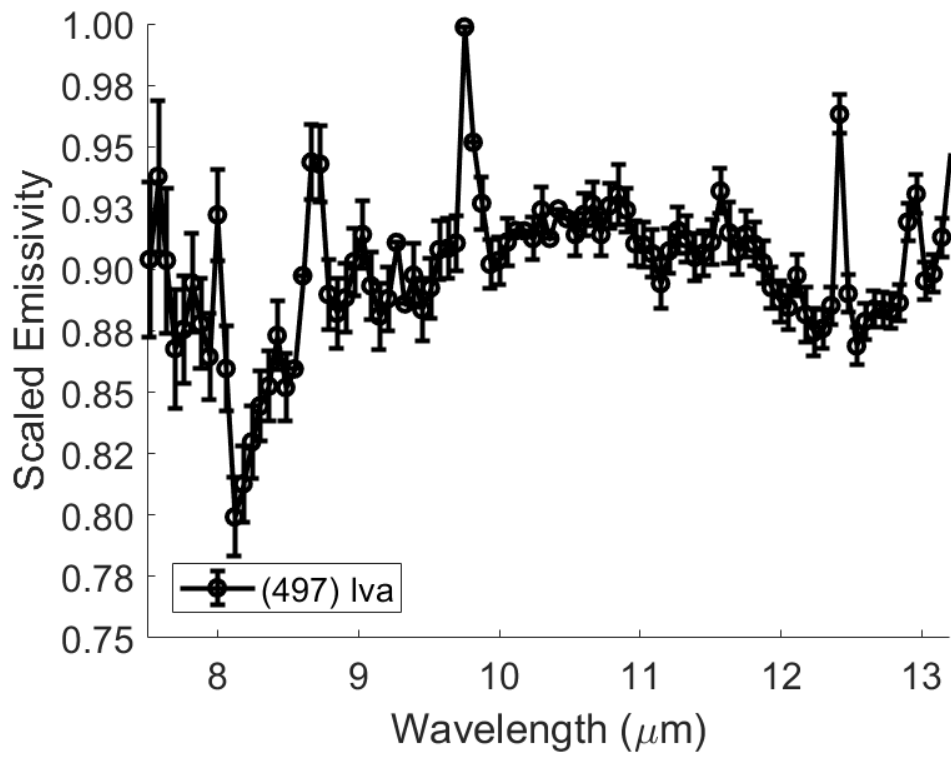


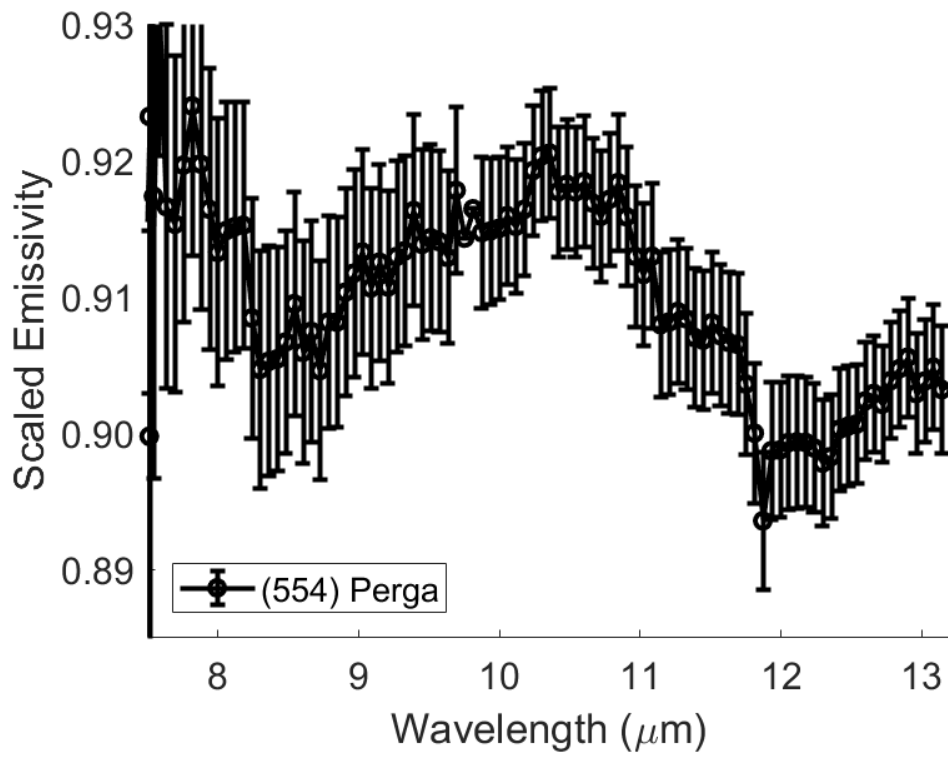
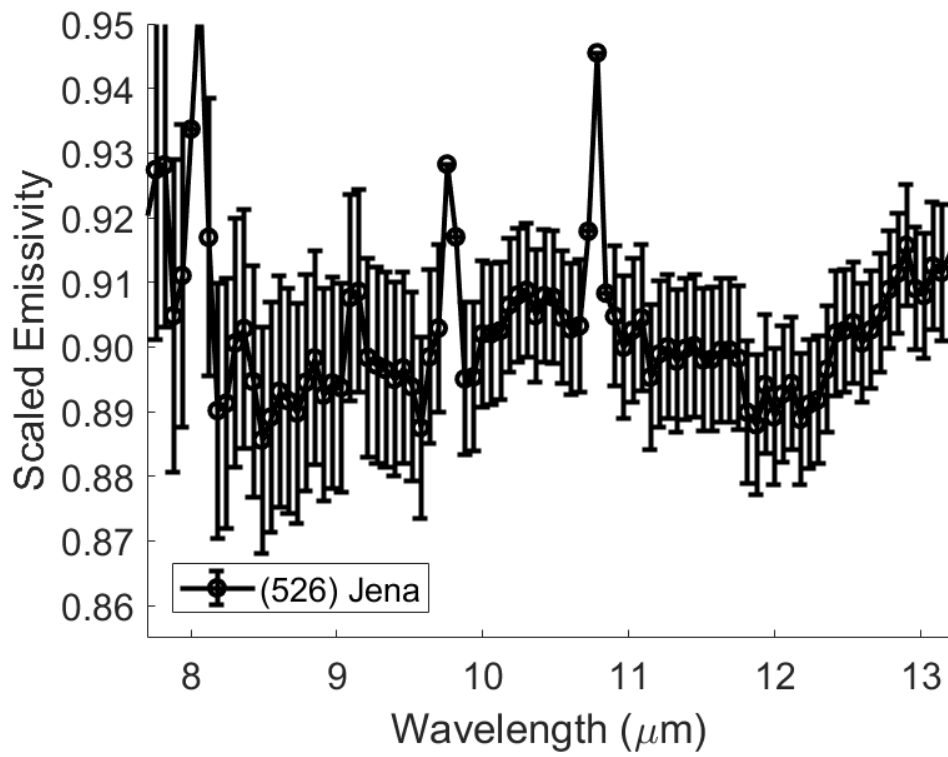


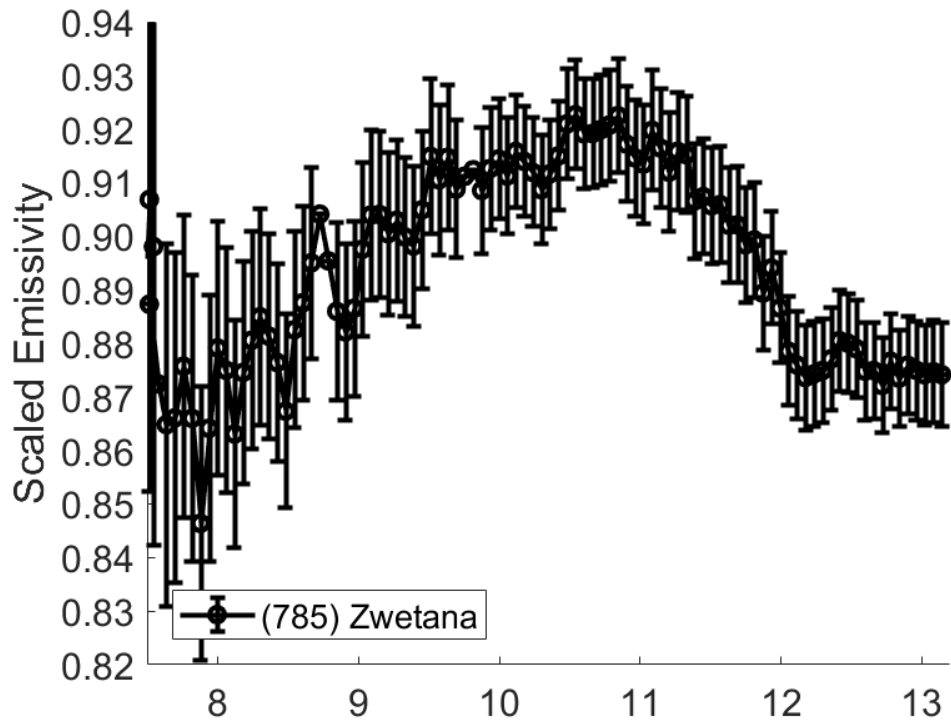
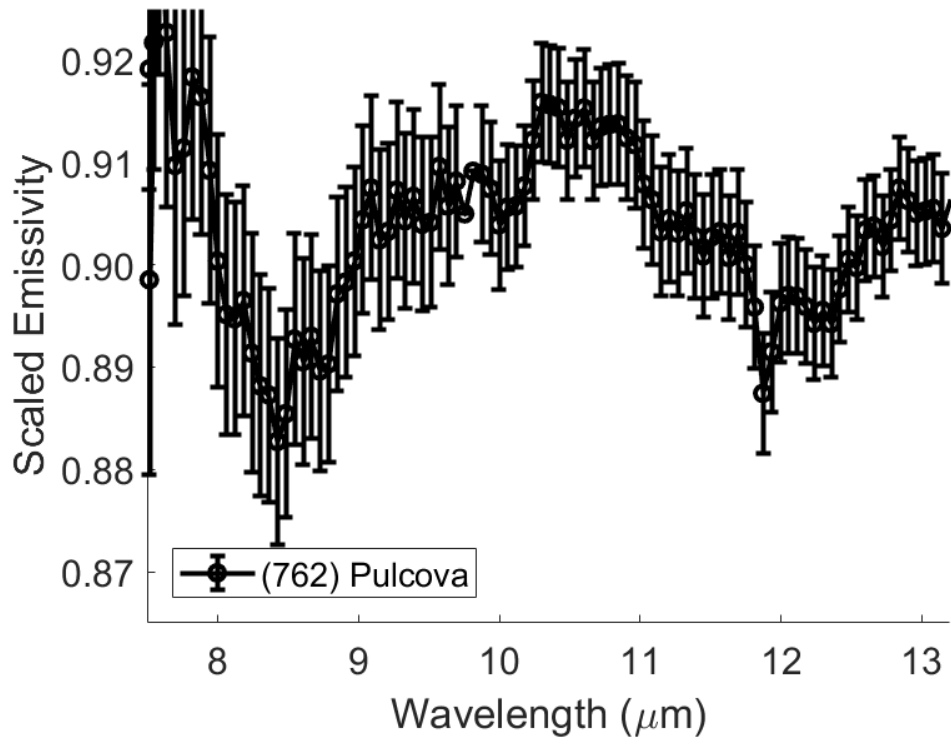


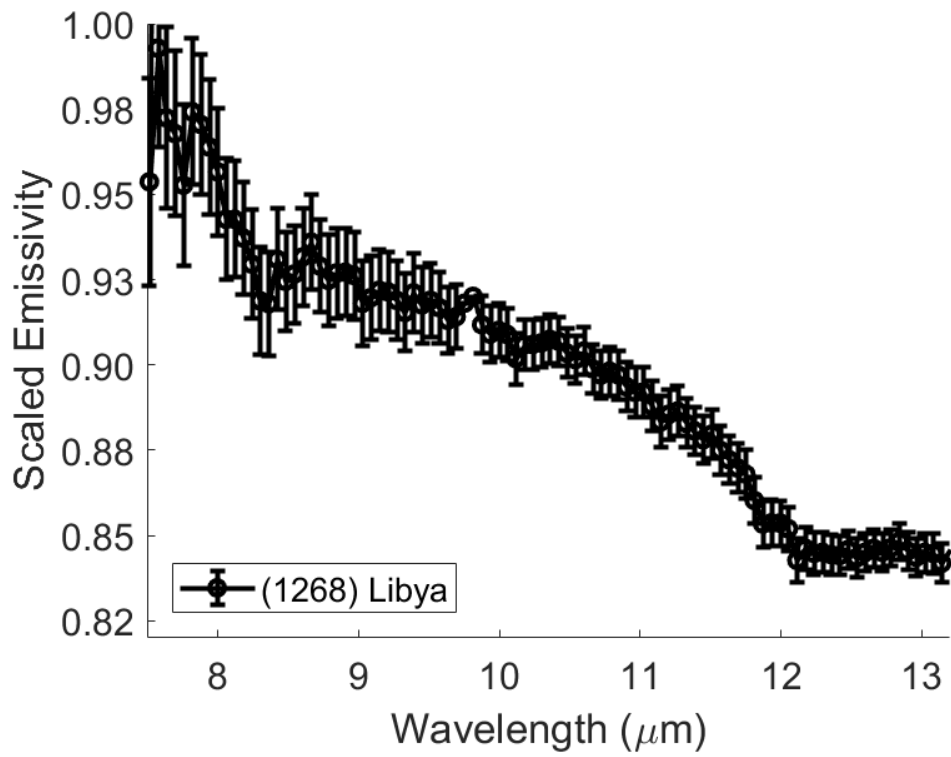
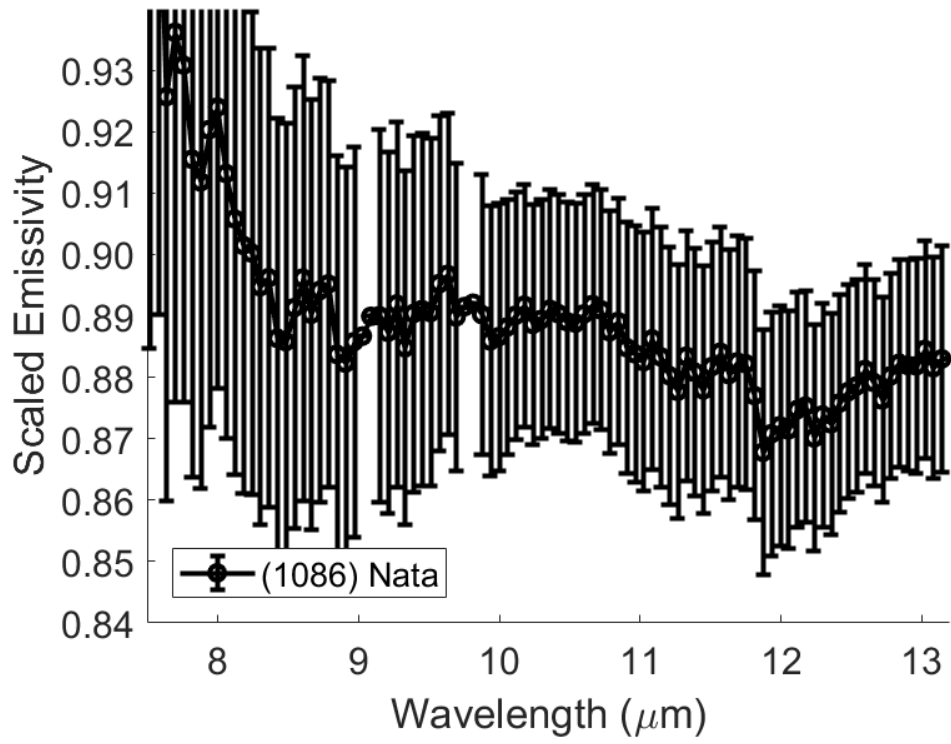


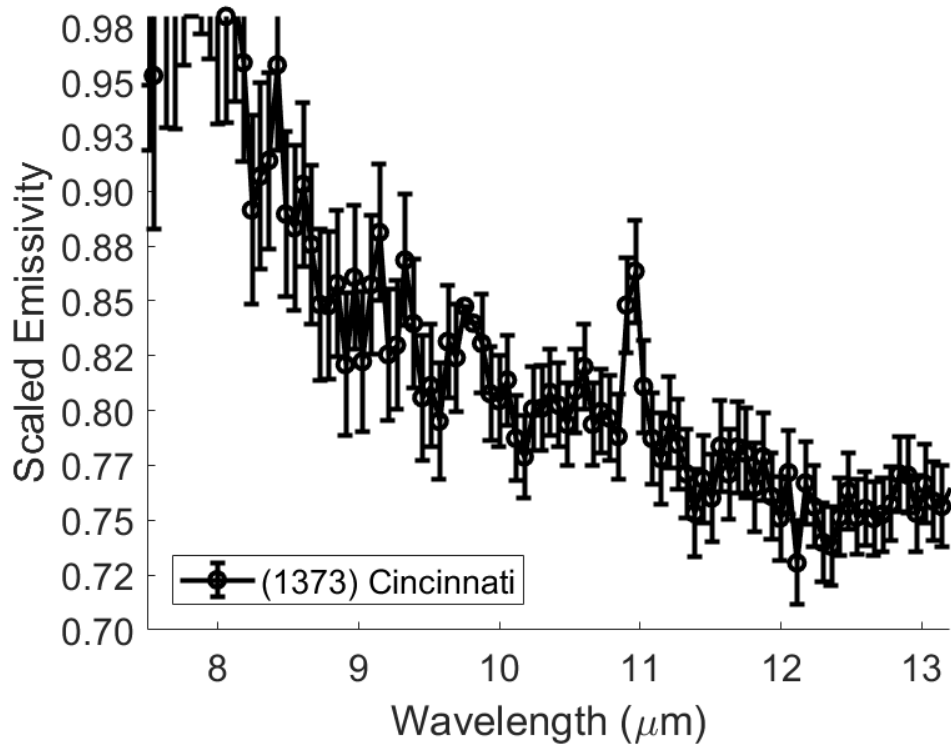
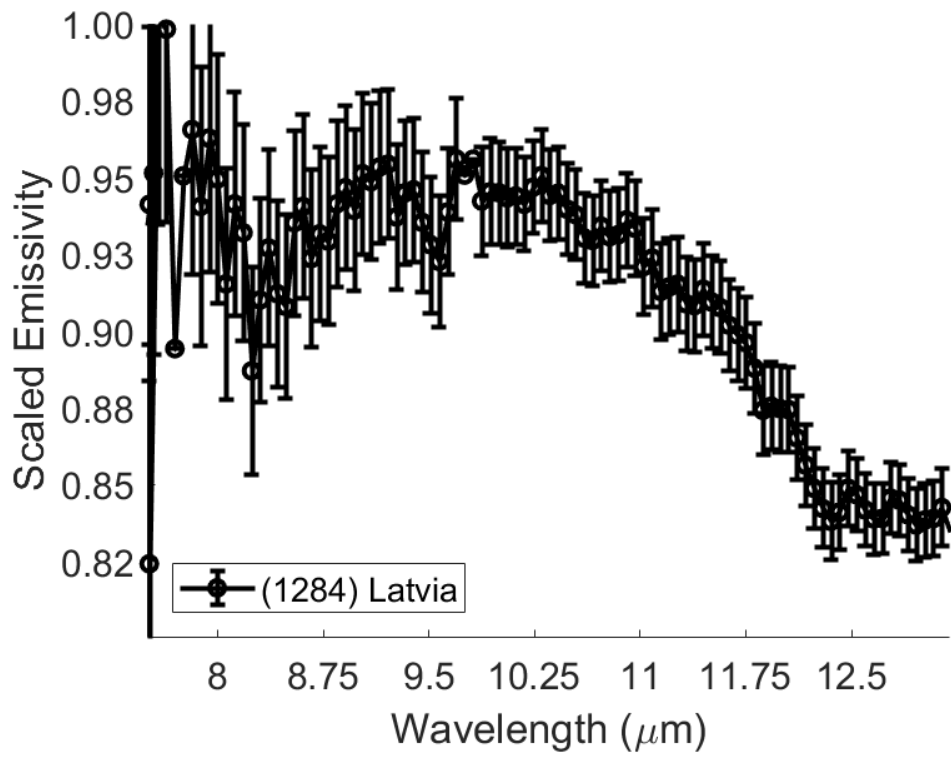


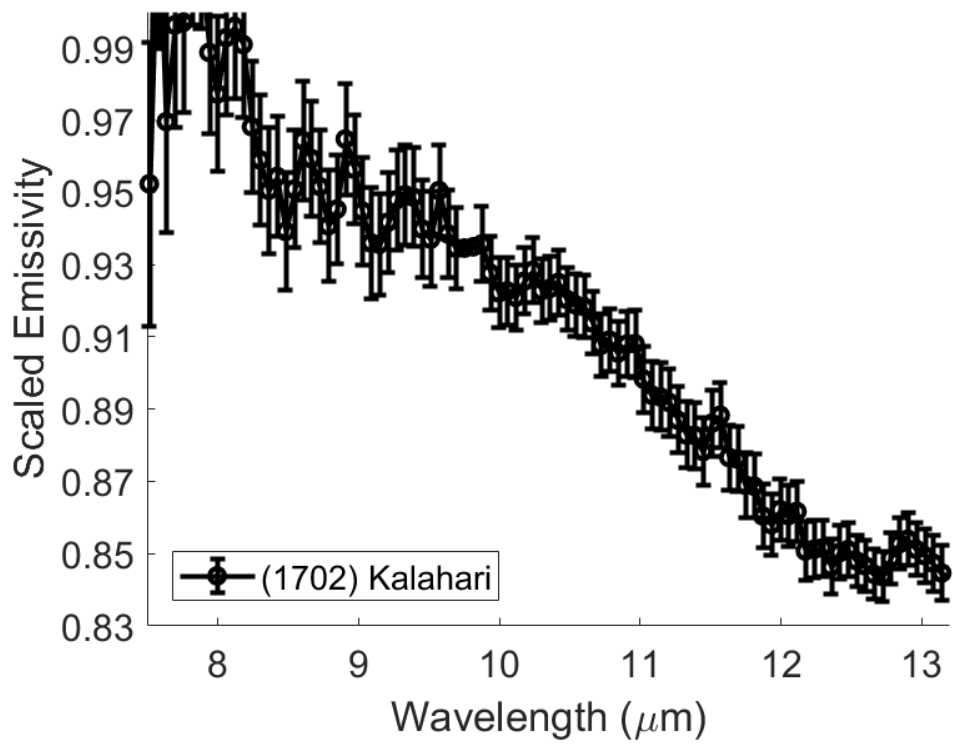
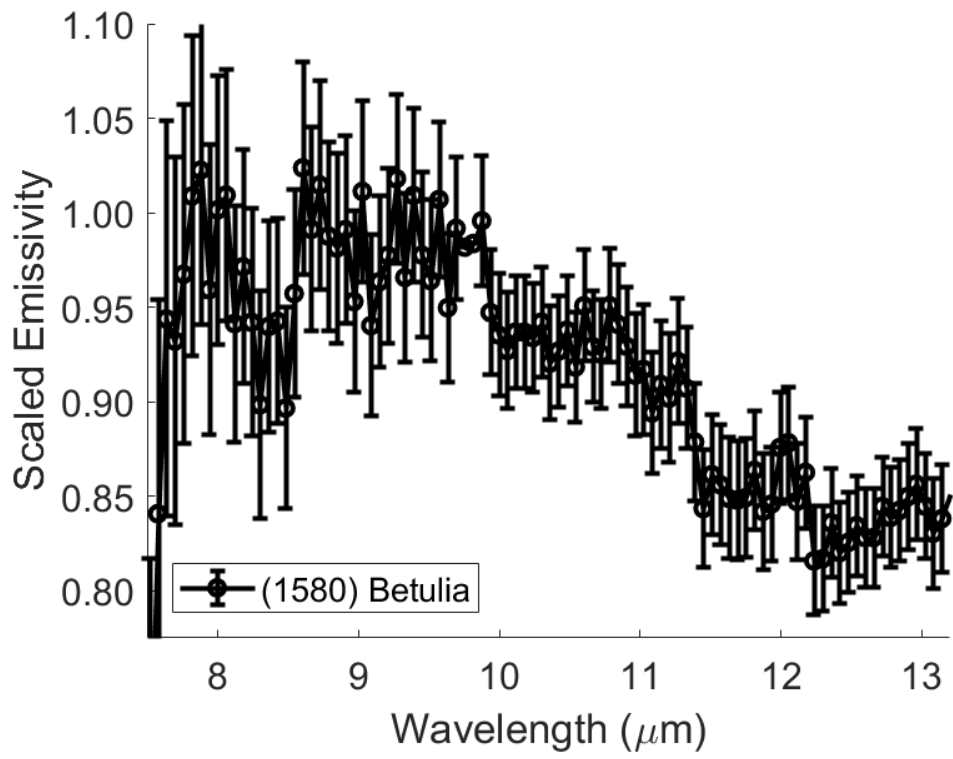


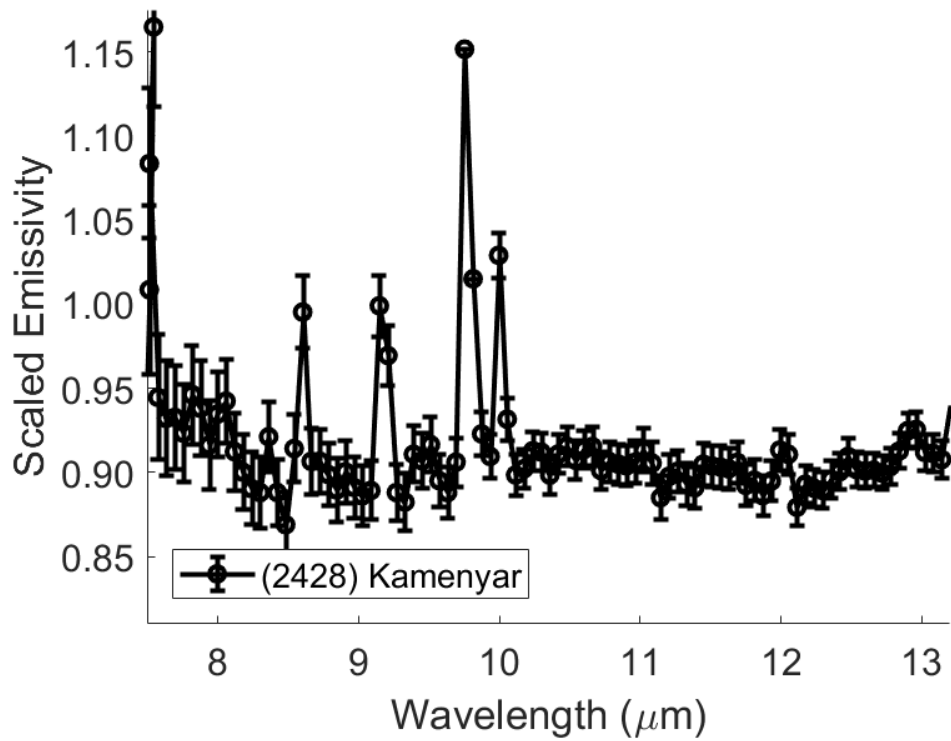
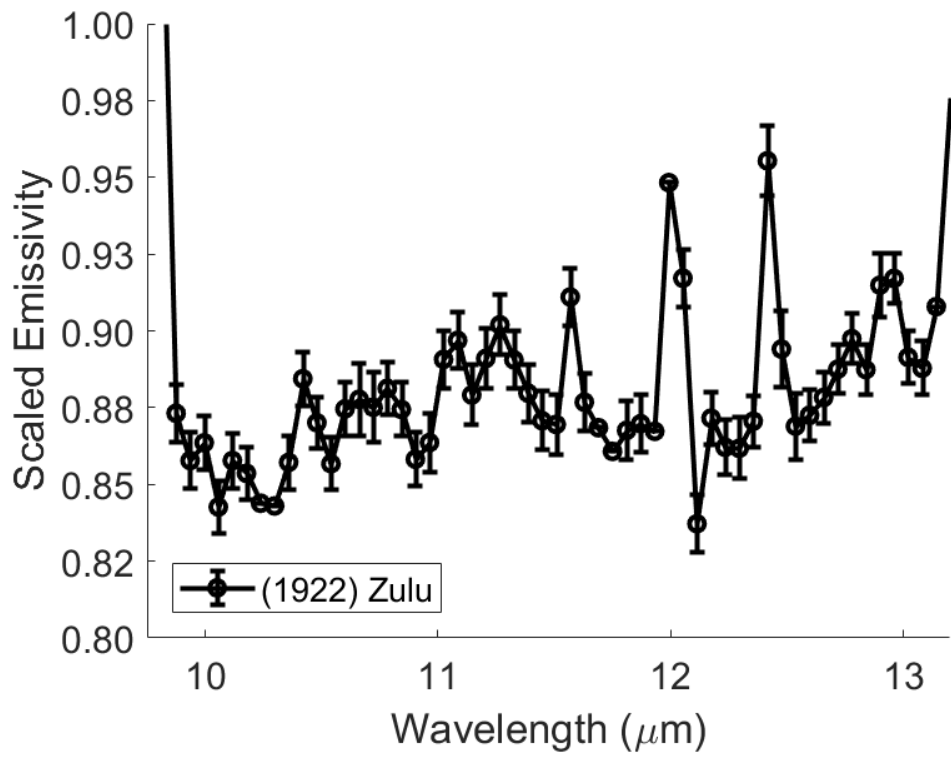


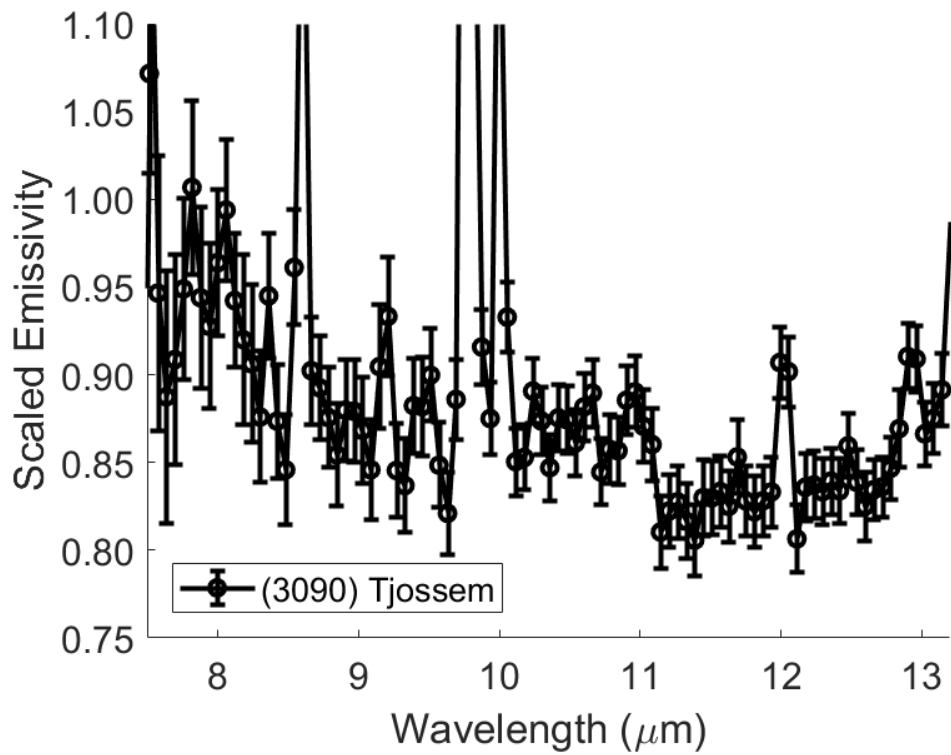
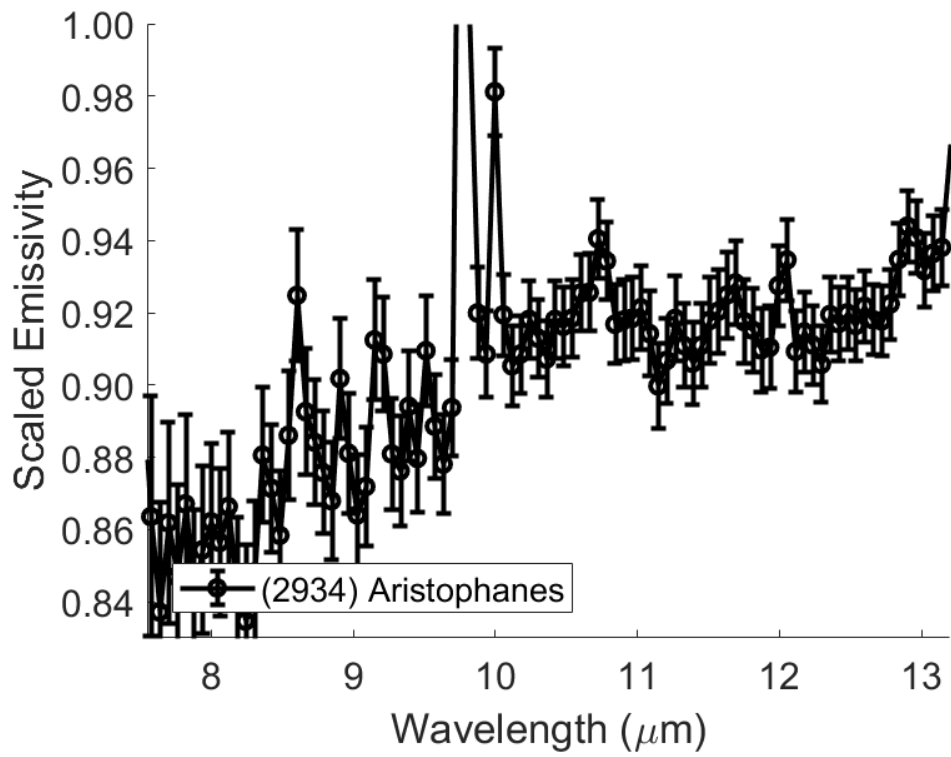


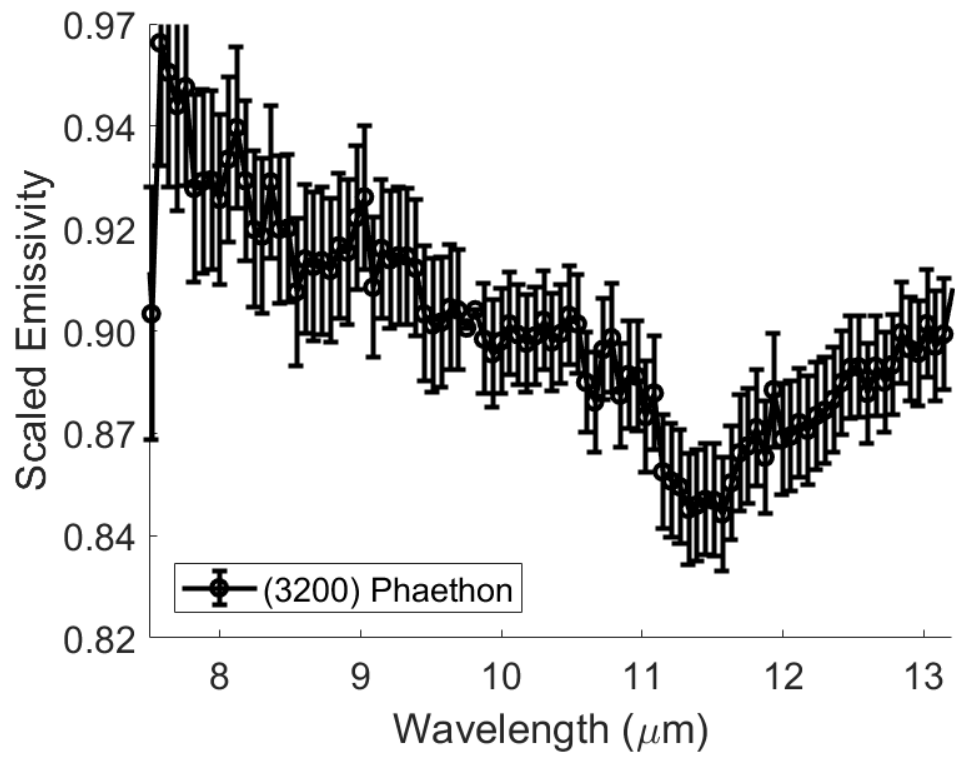




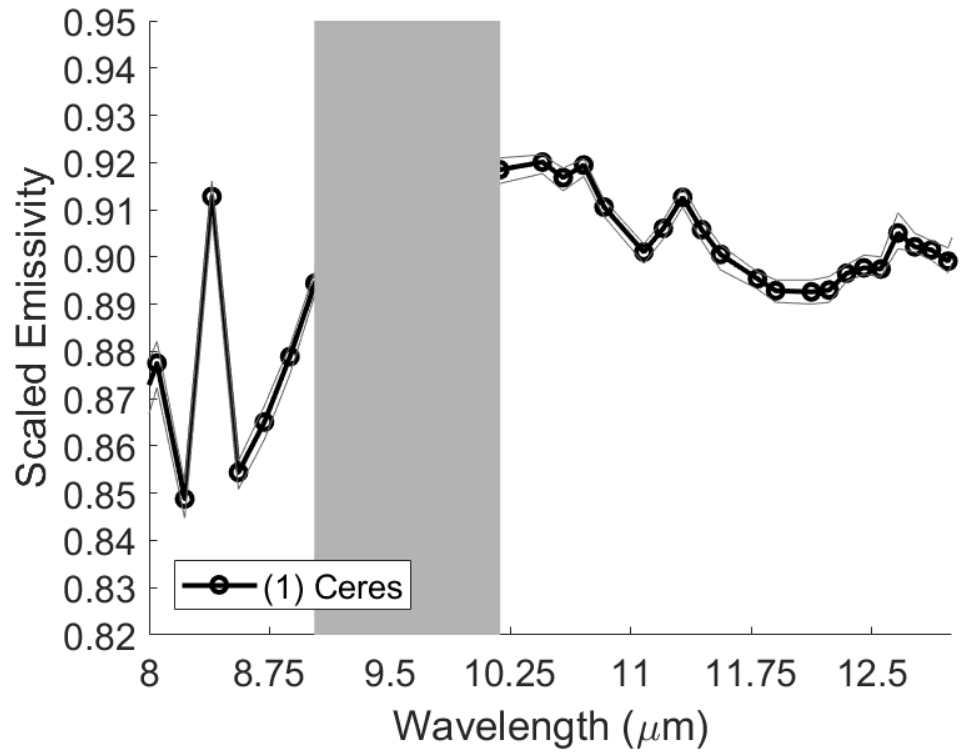


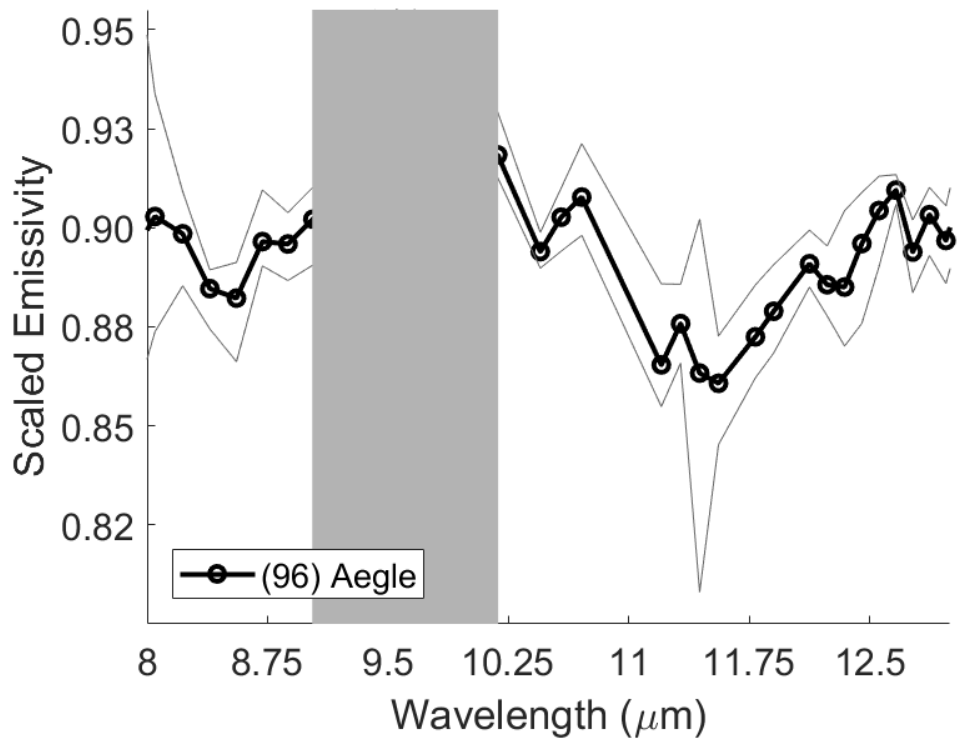
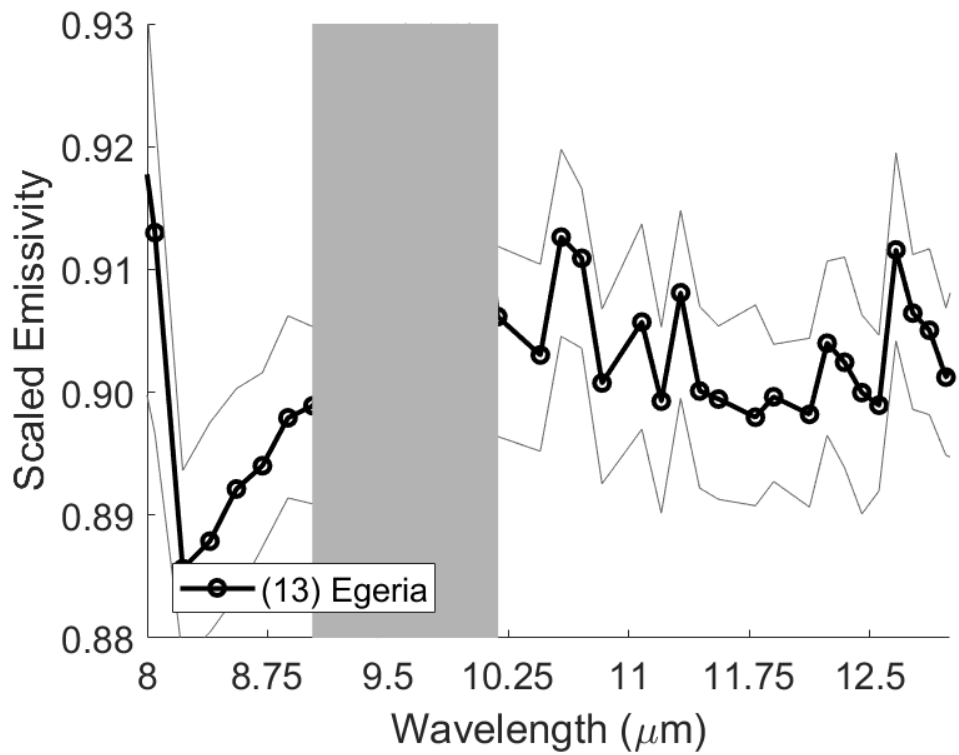


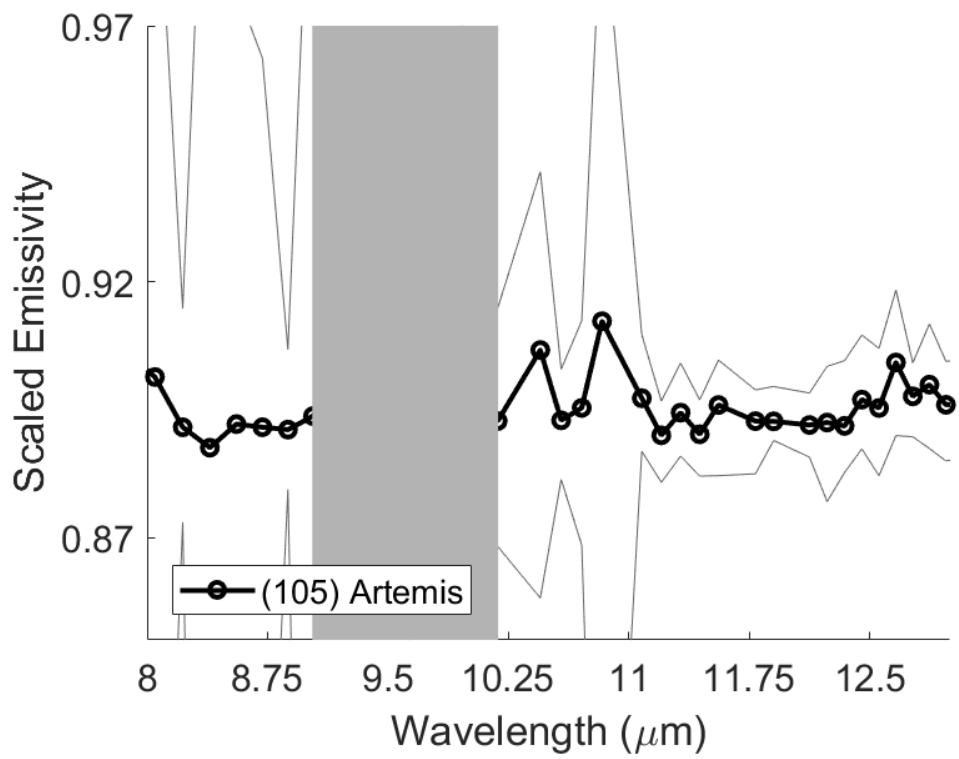
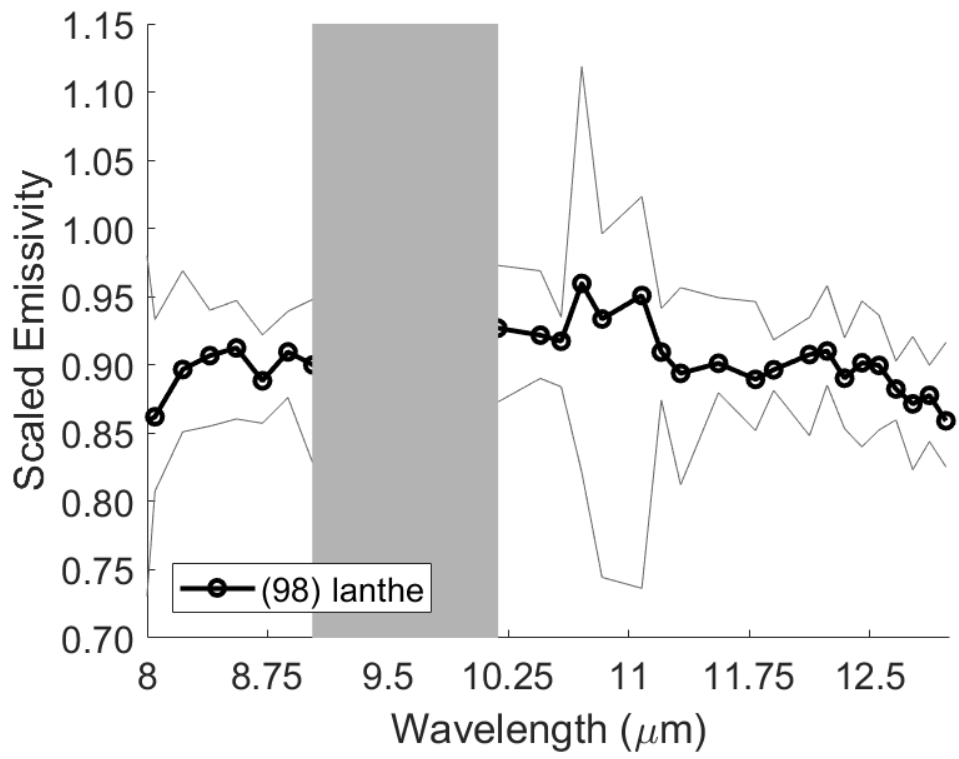


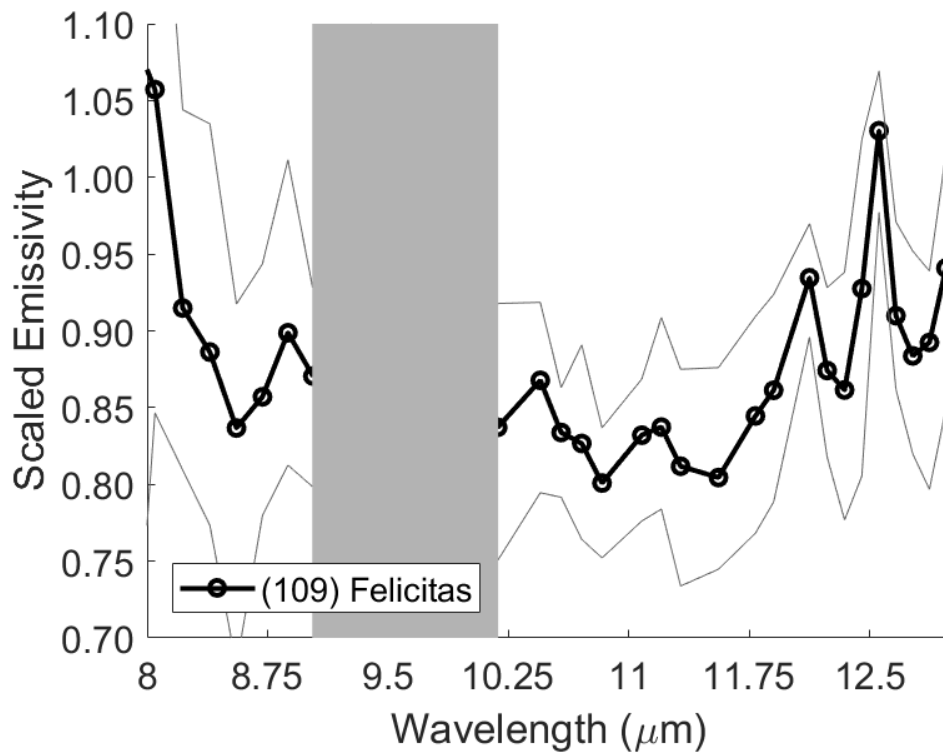
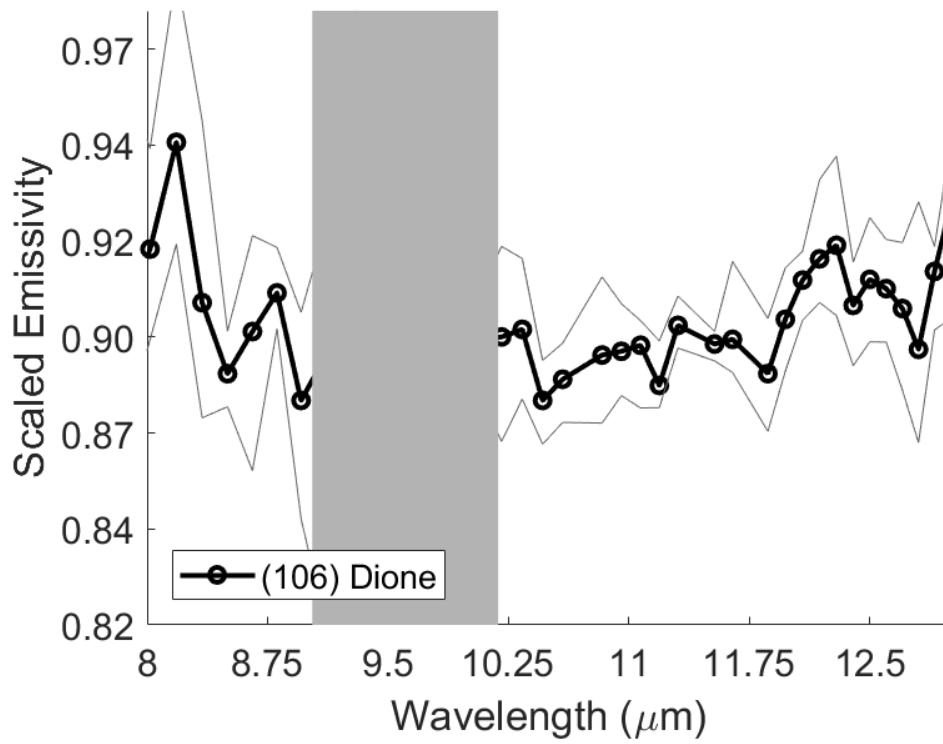


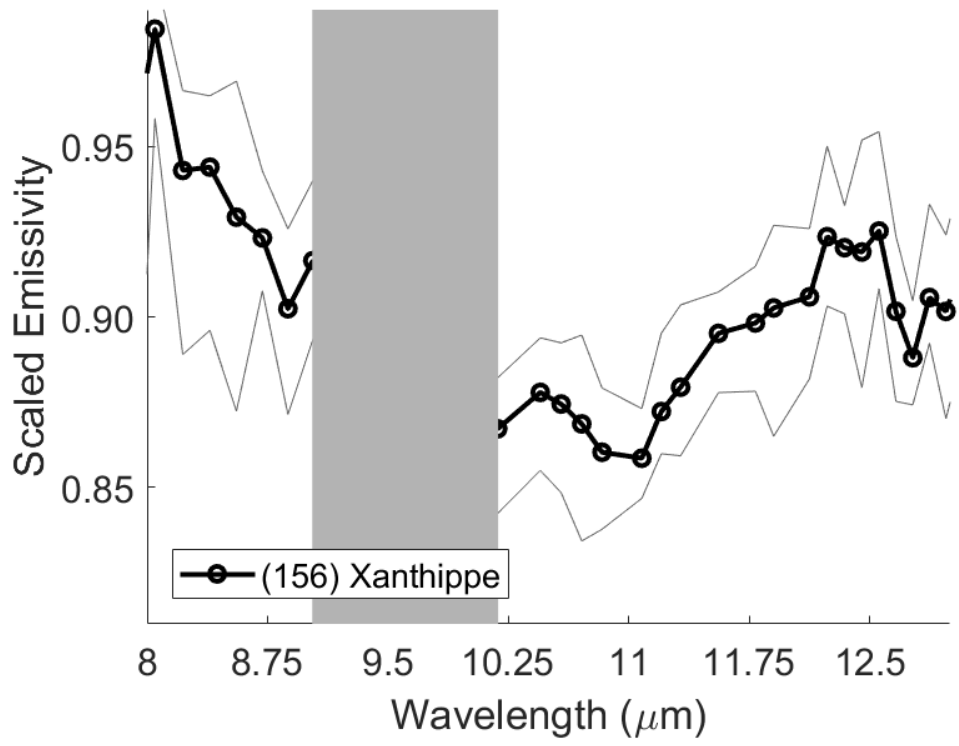
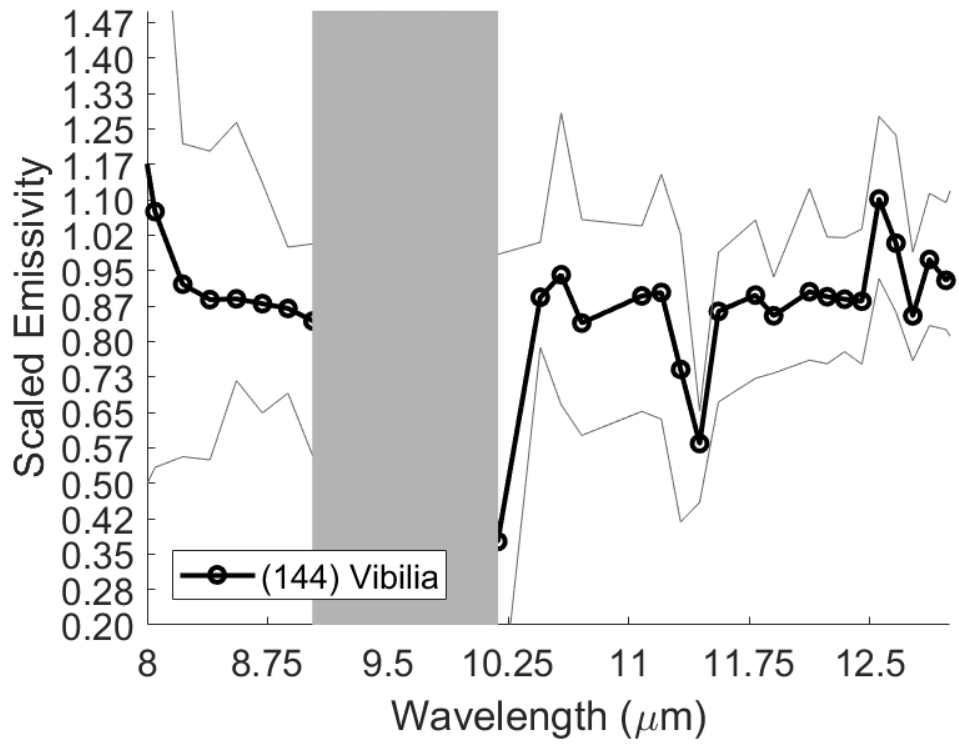
IRTF+BASS Observations:

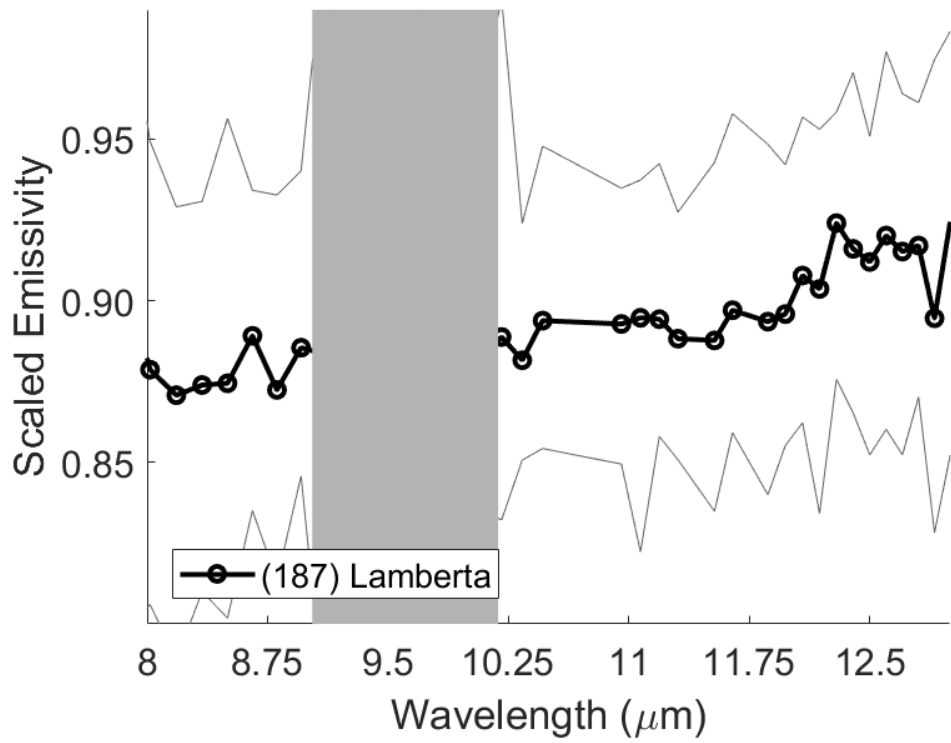
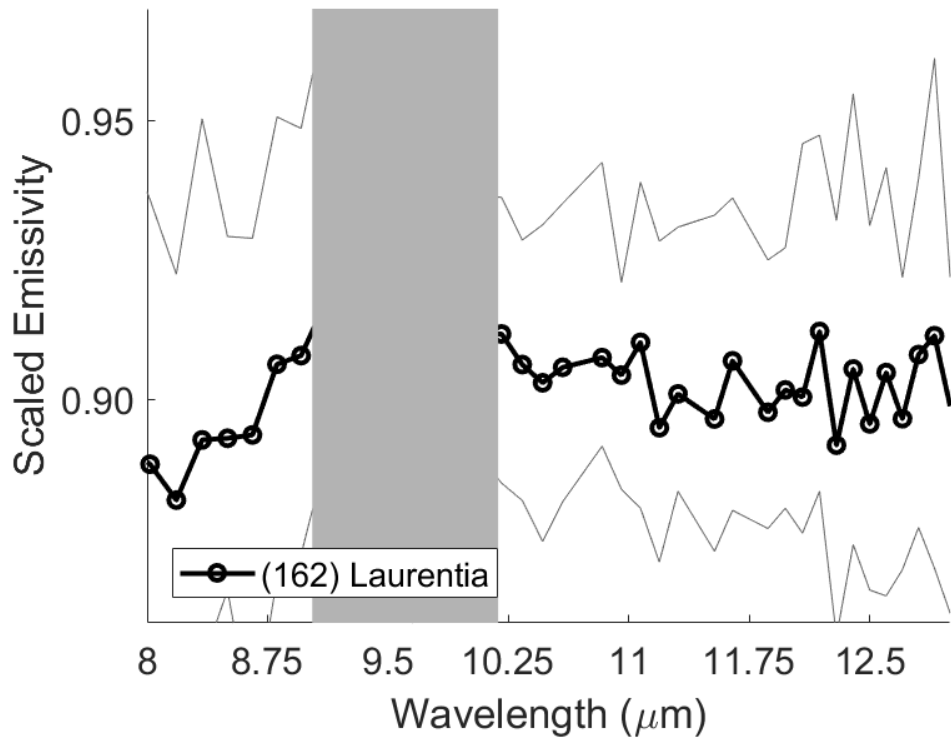


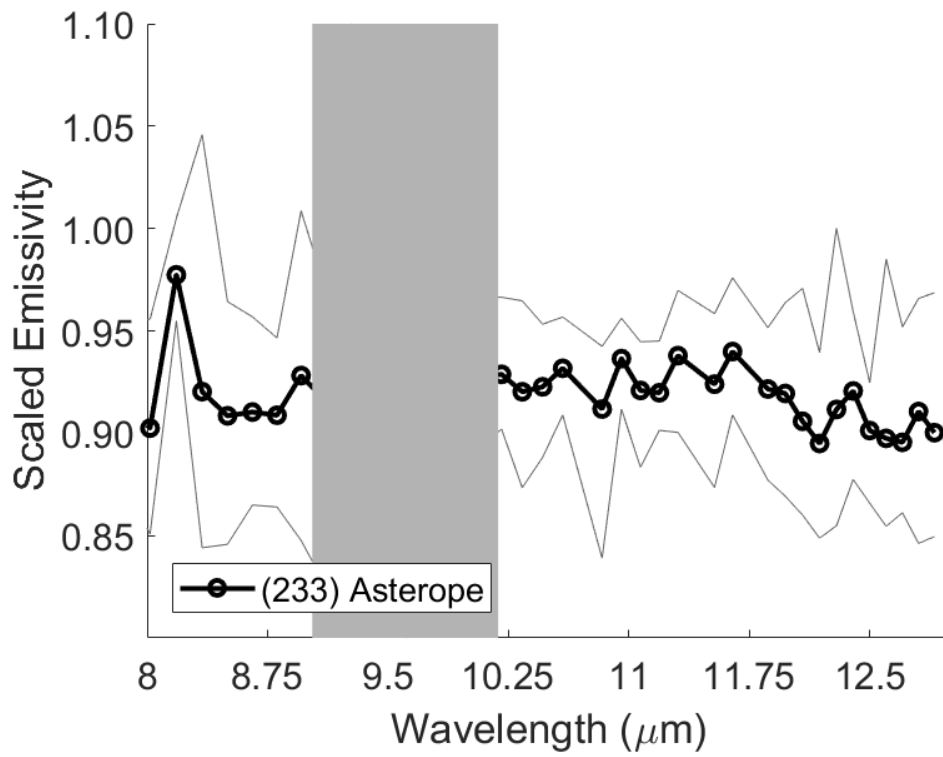
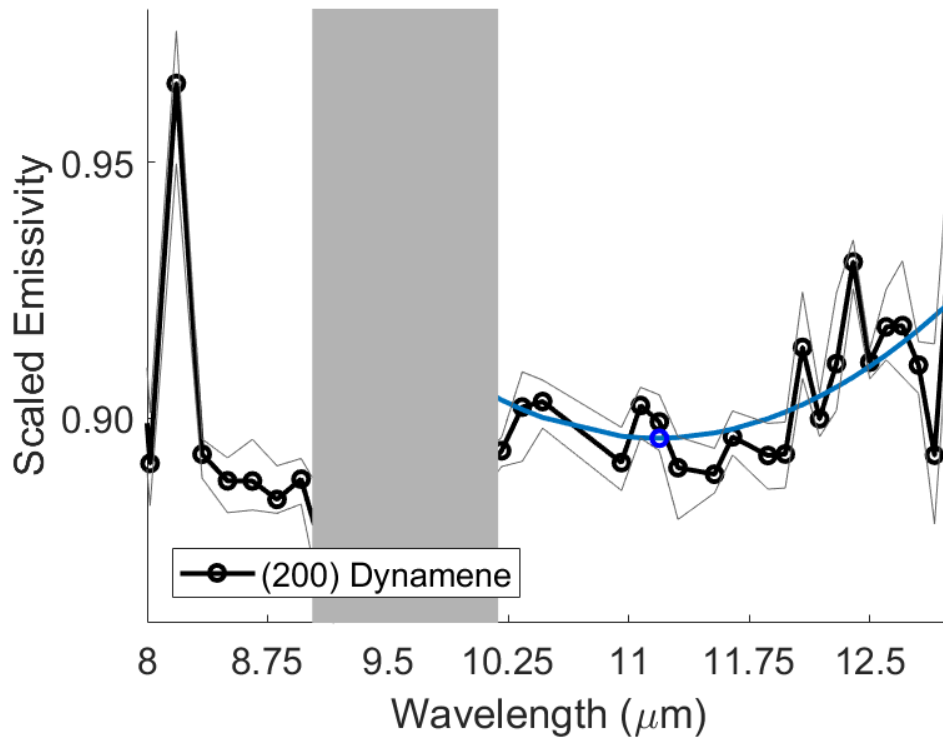


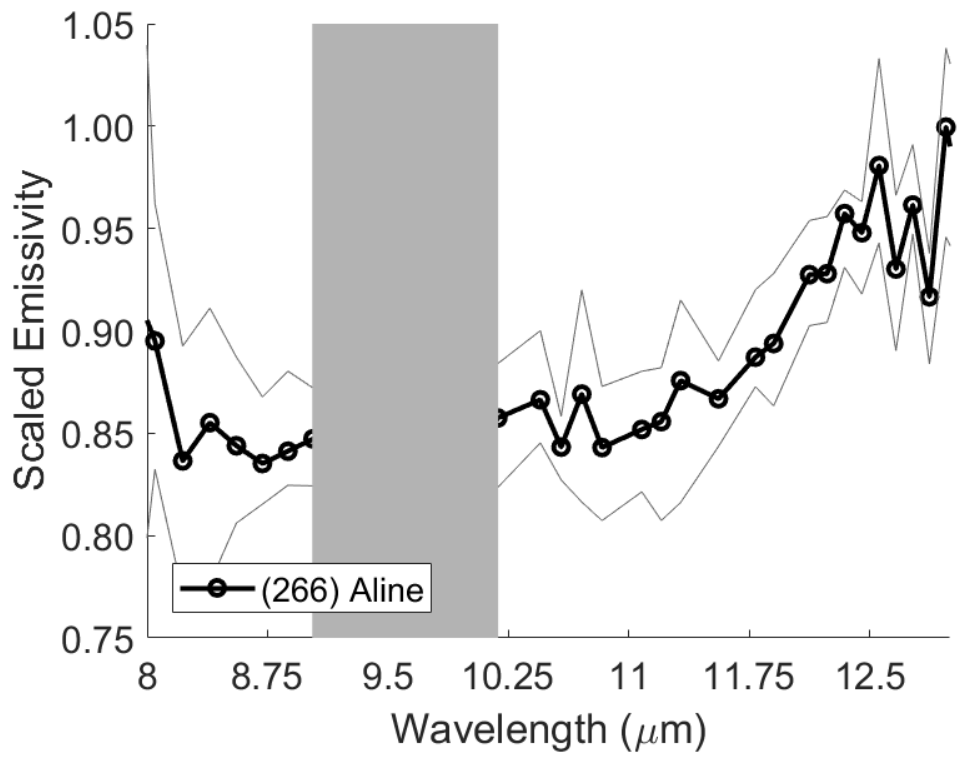
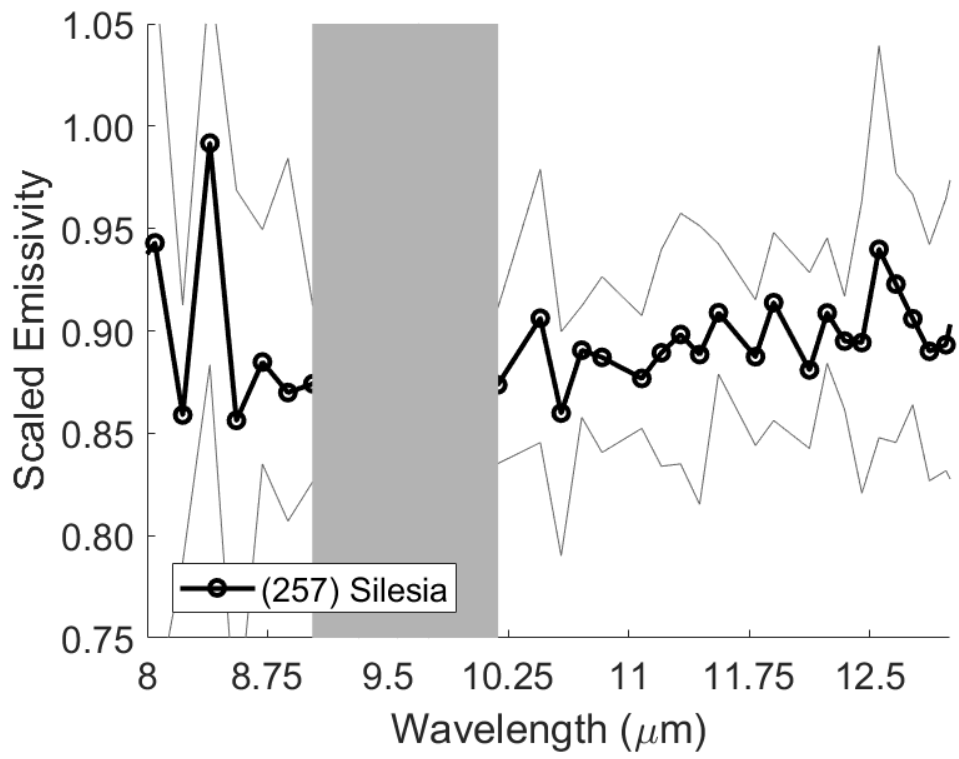


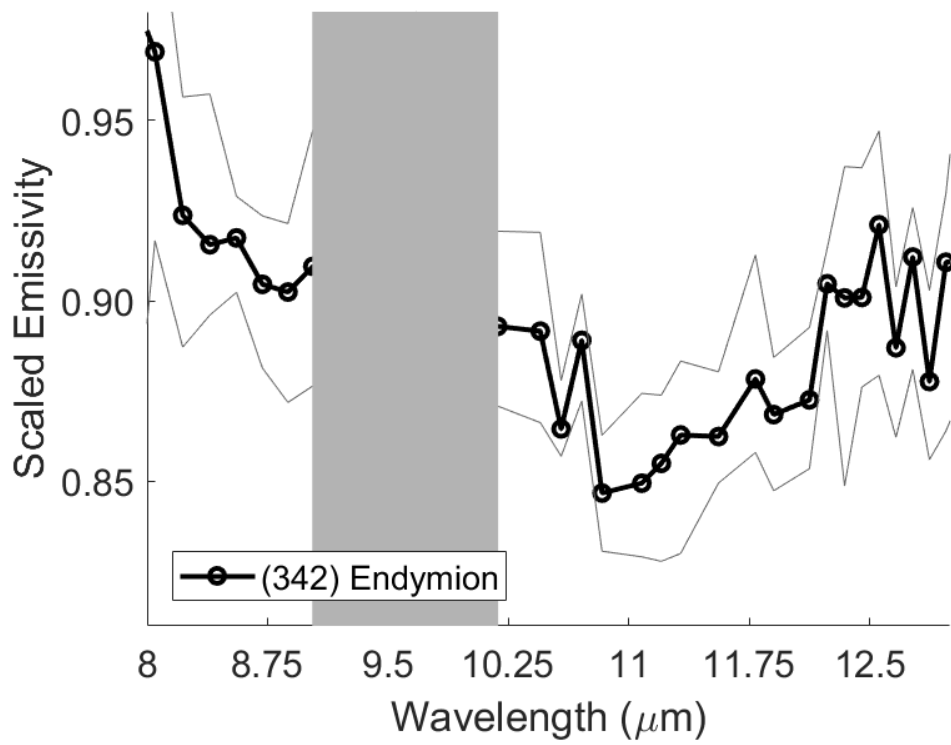
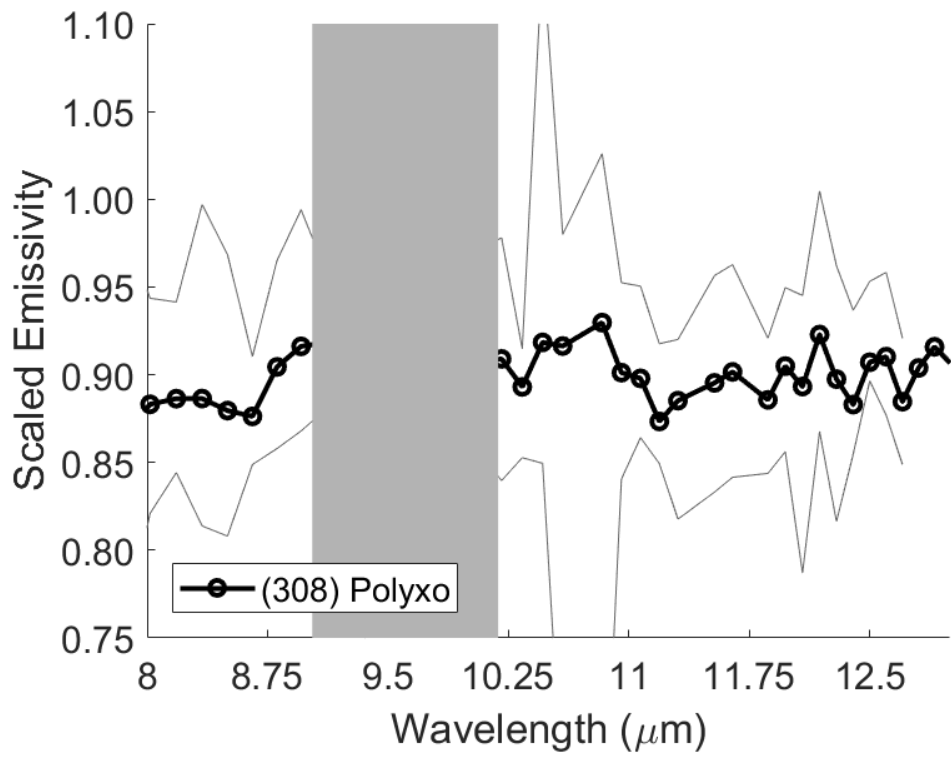


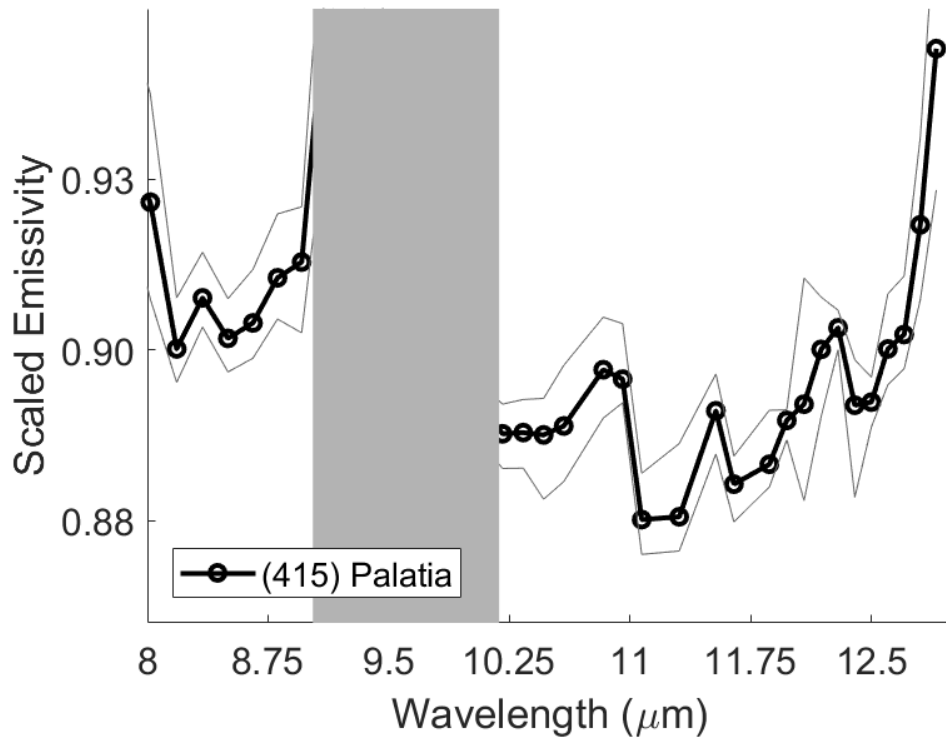
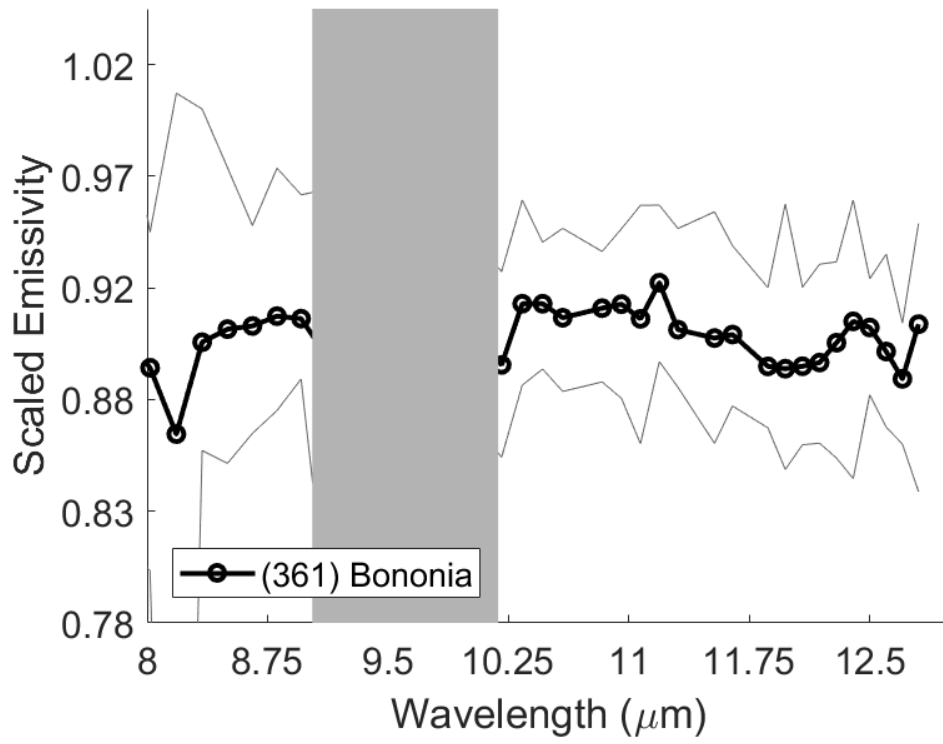


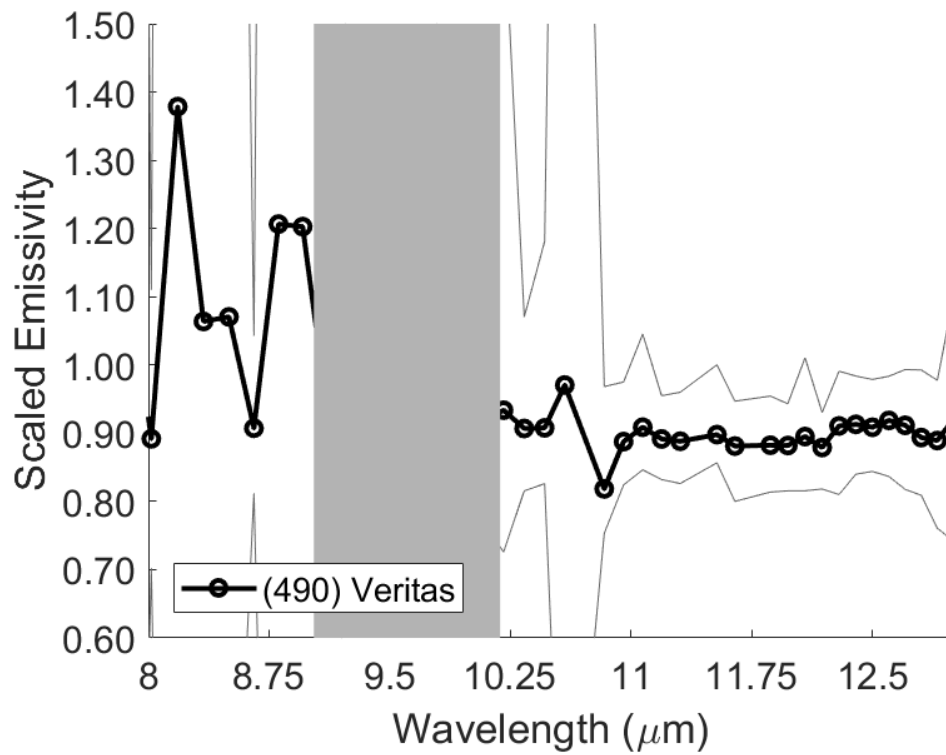
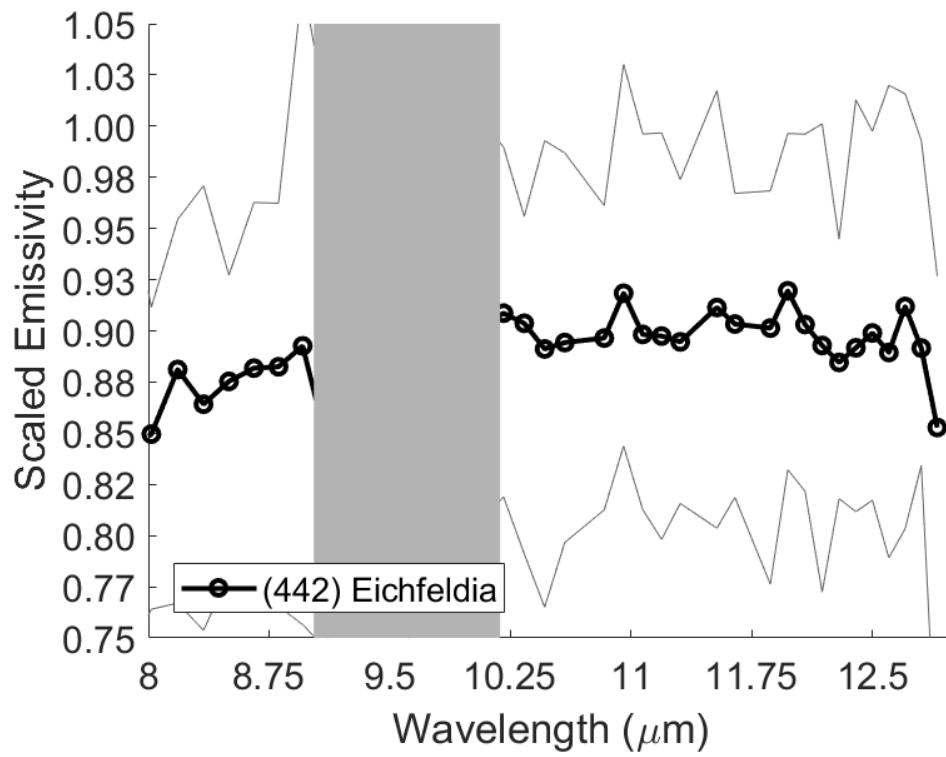


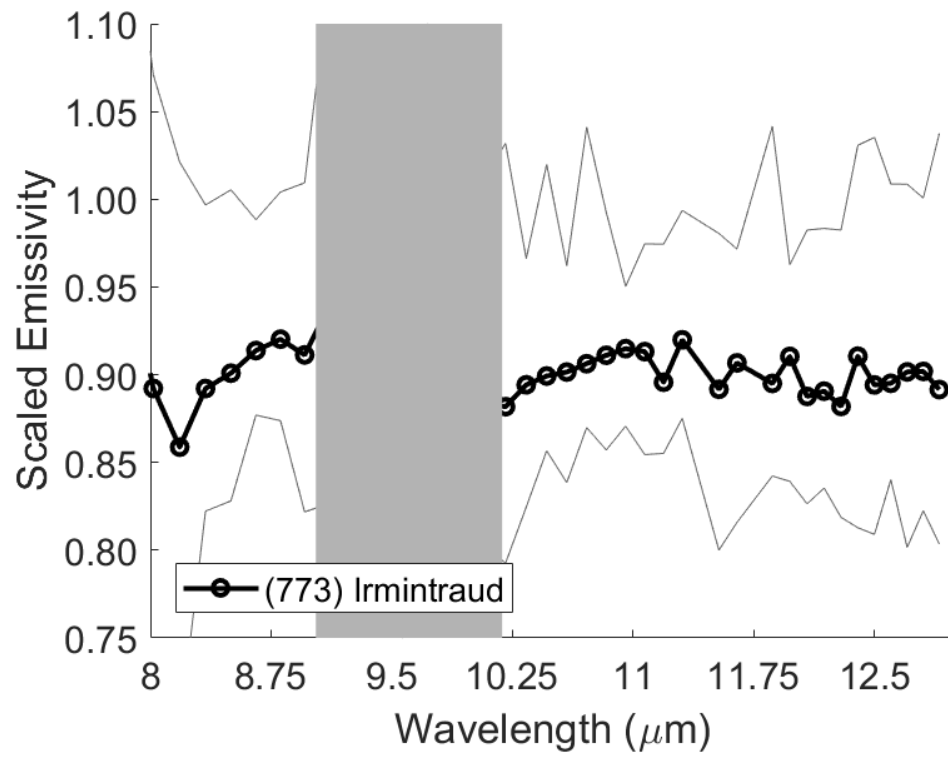




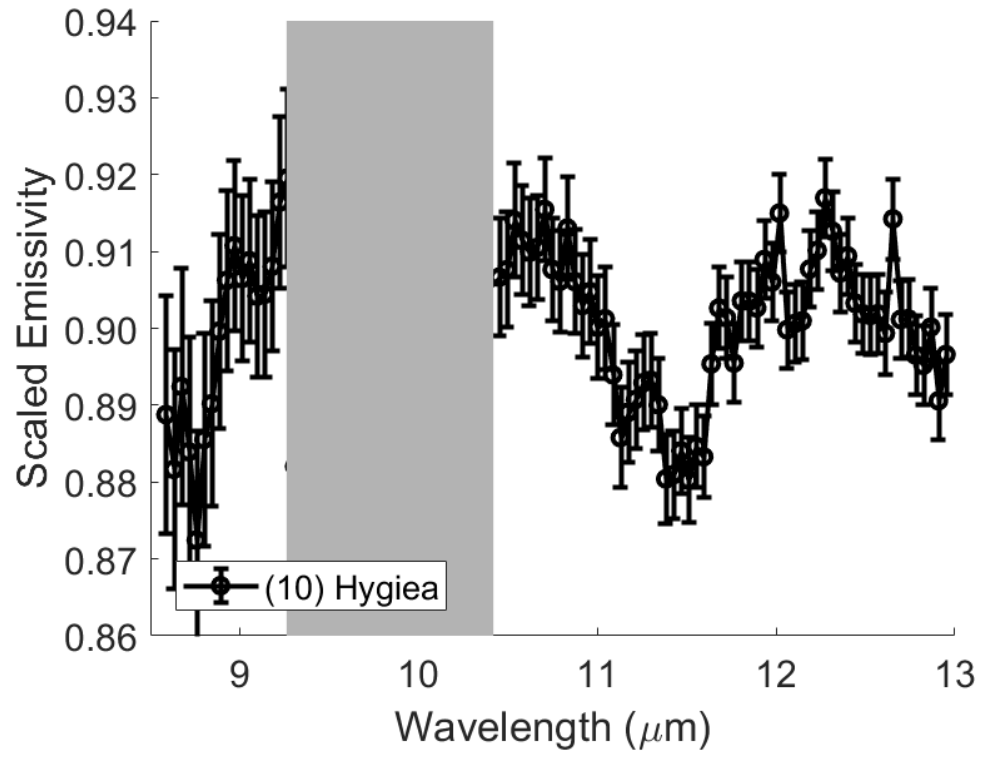


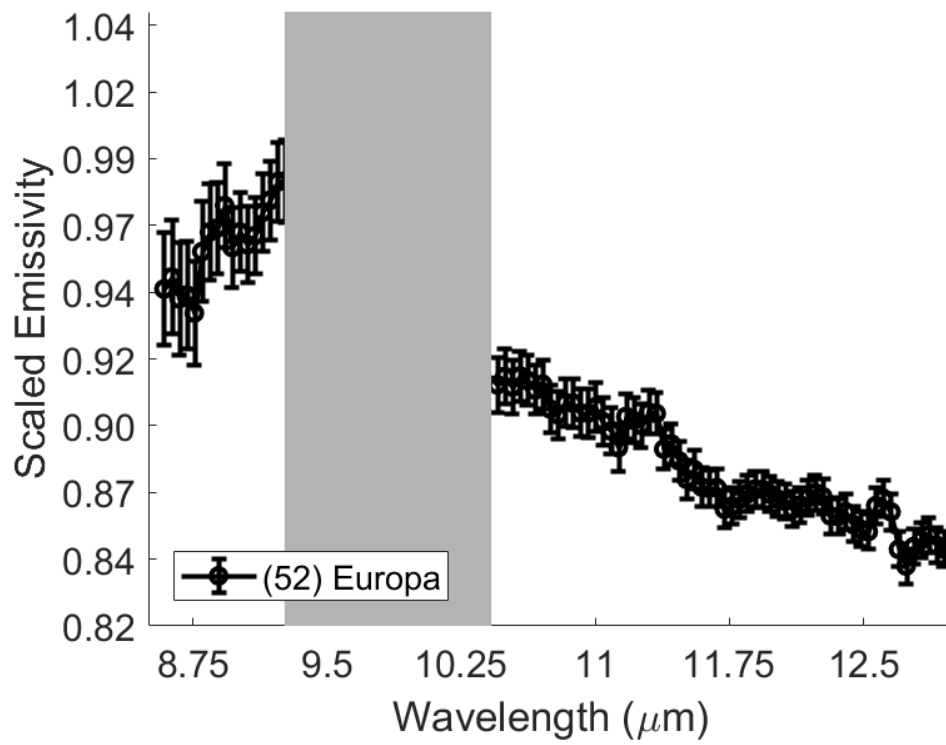
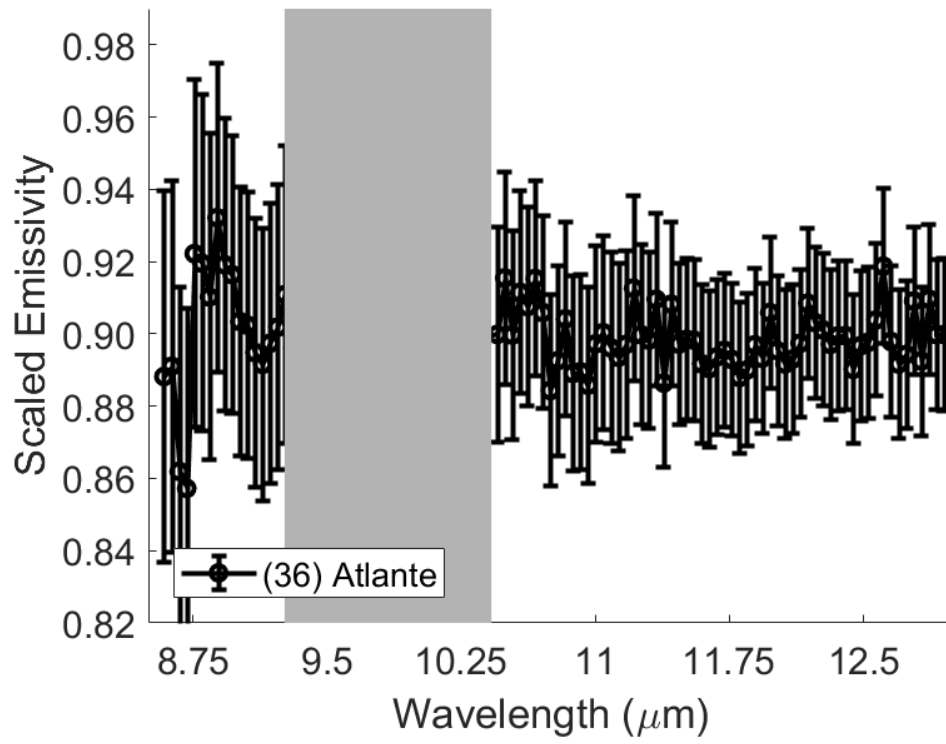


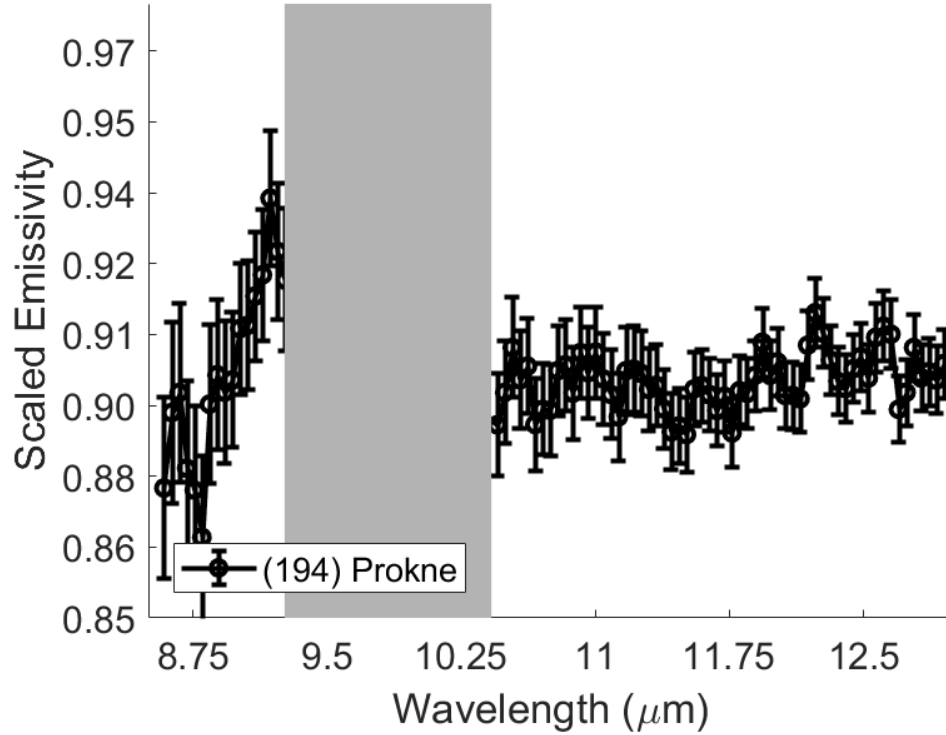
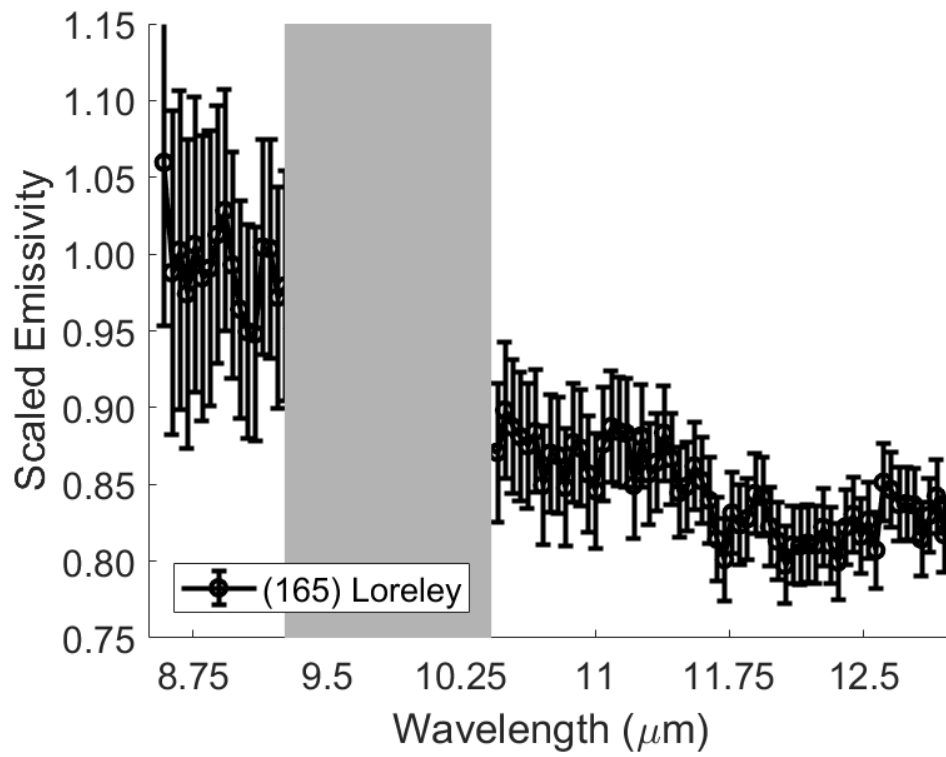


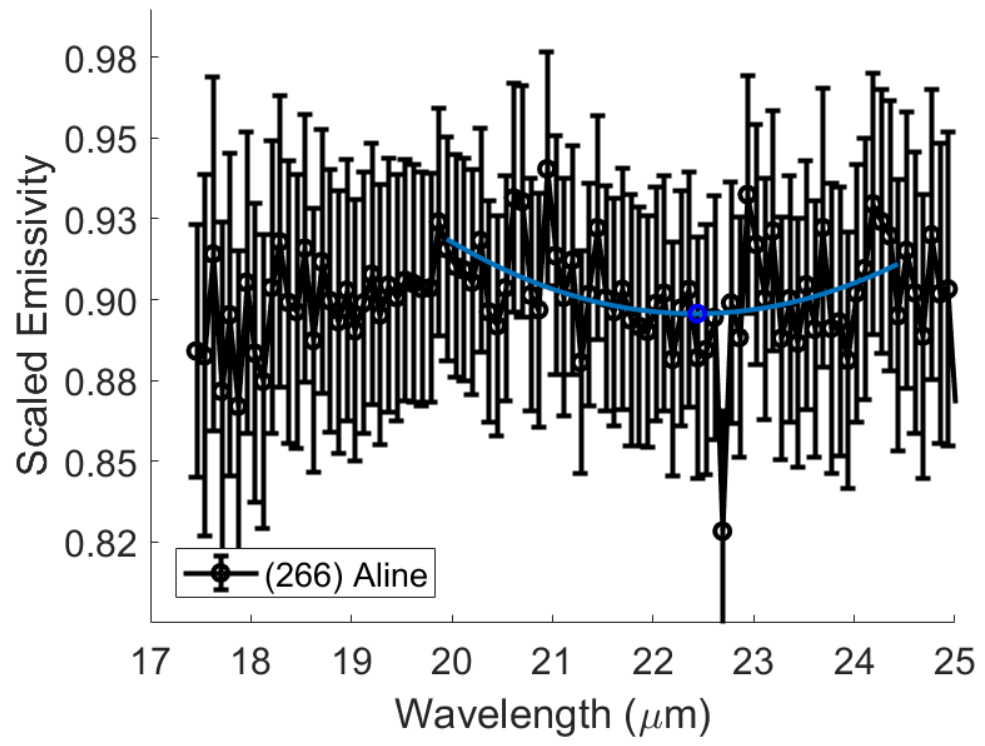


SOFIA+FORCAST Observations:





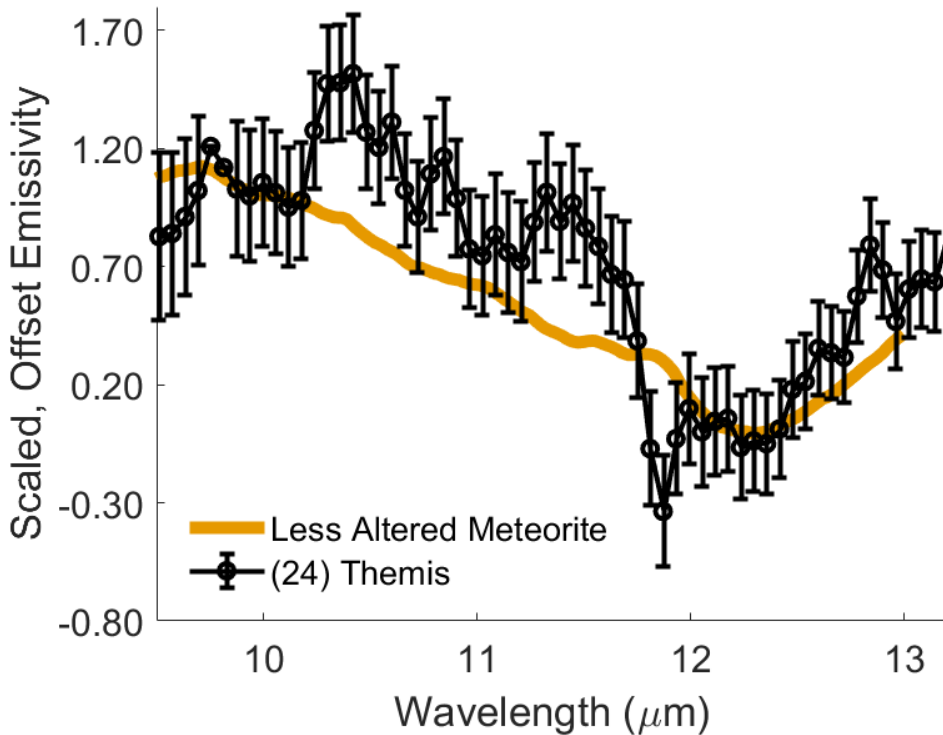


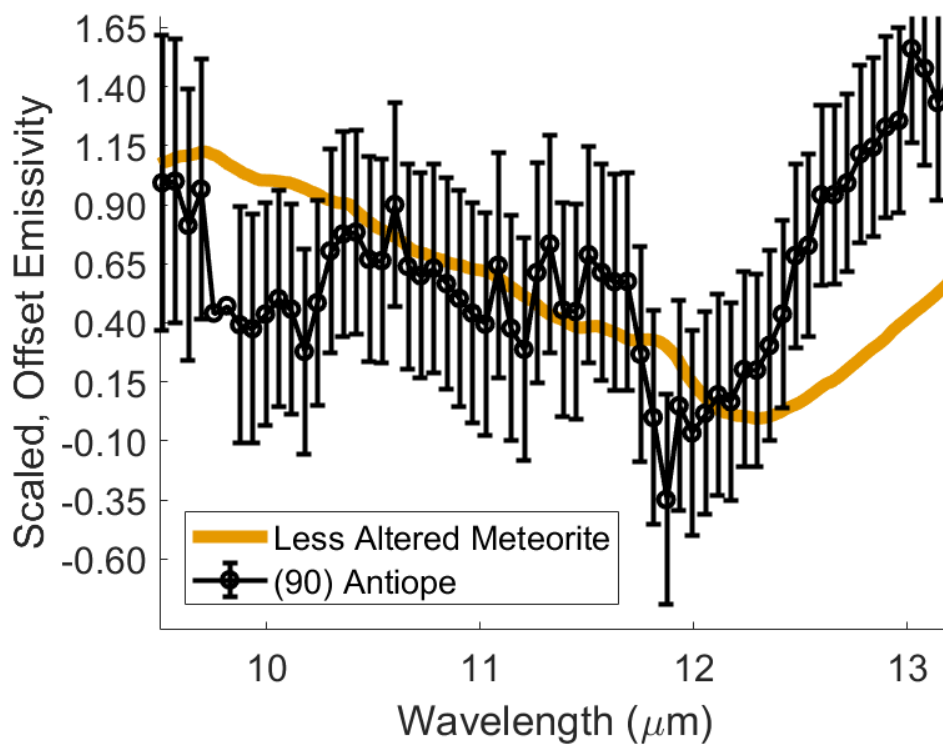
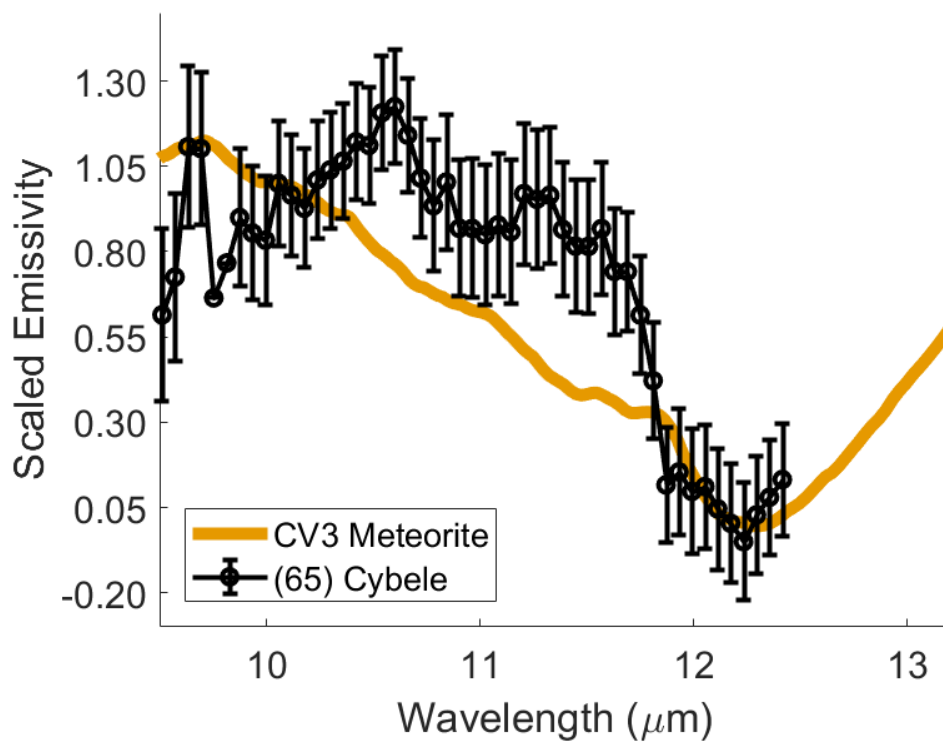


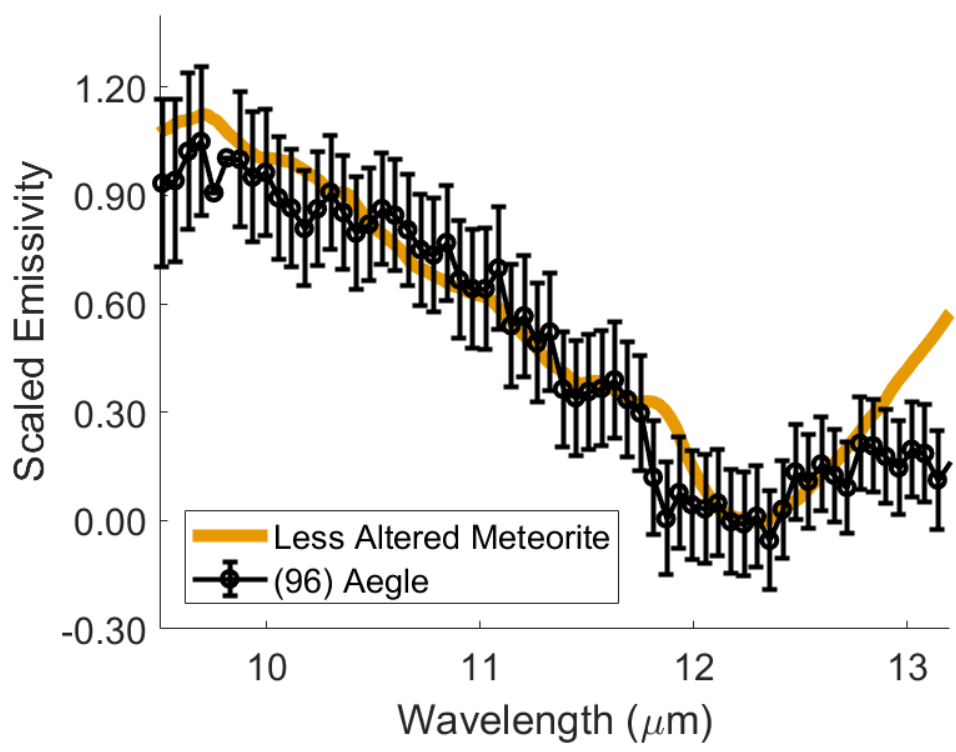
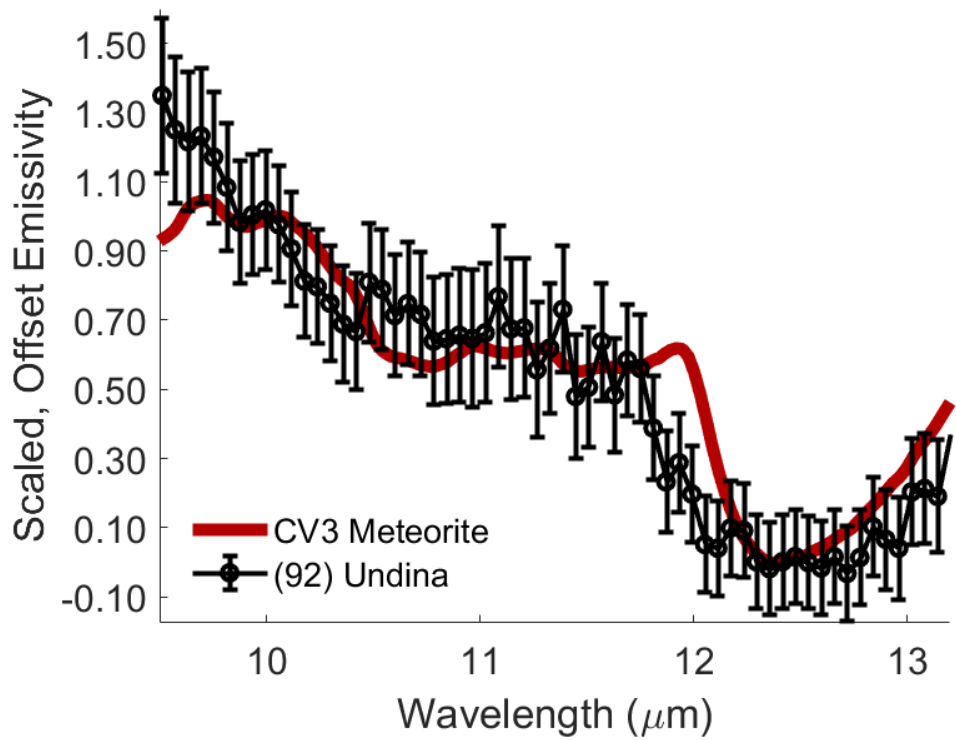
Appendix 3: Degree of Alteration Assignment for Asteroids

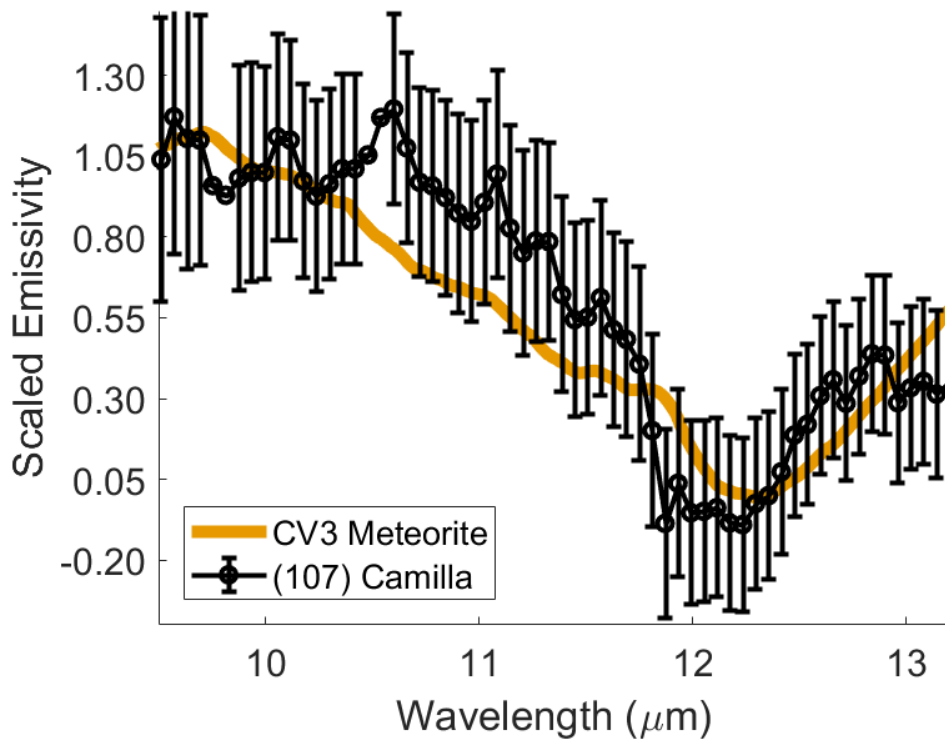
Emissivity spectra of asteroids are compared to meteorites. Laboratory meteorite data are first approximated as emissivity using Kirchhoff's law, $E = 1 - R$, then stretched between 0 and 1 to remove any effects of grain size or porosity. Asteroid emissivity spectra are similarly stretched to remove any grain size, porosity or thermal gradients that may affect their overall spectral contrast. The asteroid is assigned mineralogy based on comparison of the stretched emissivity spectra to the meteorite data. Featureless asteroids are not included in this appendix.

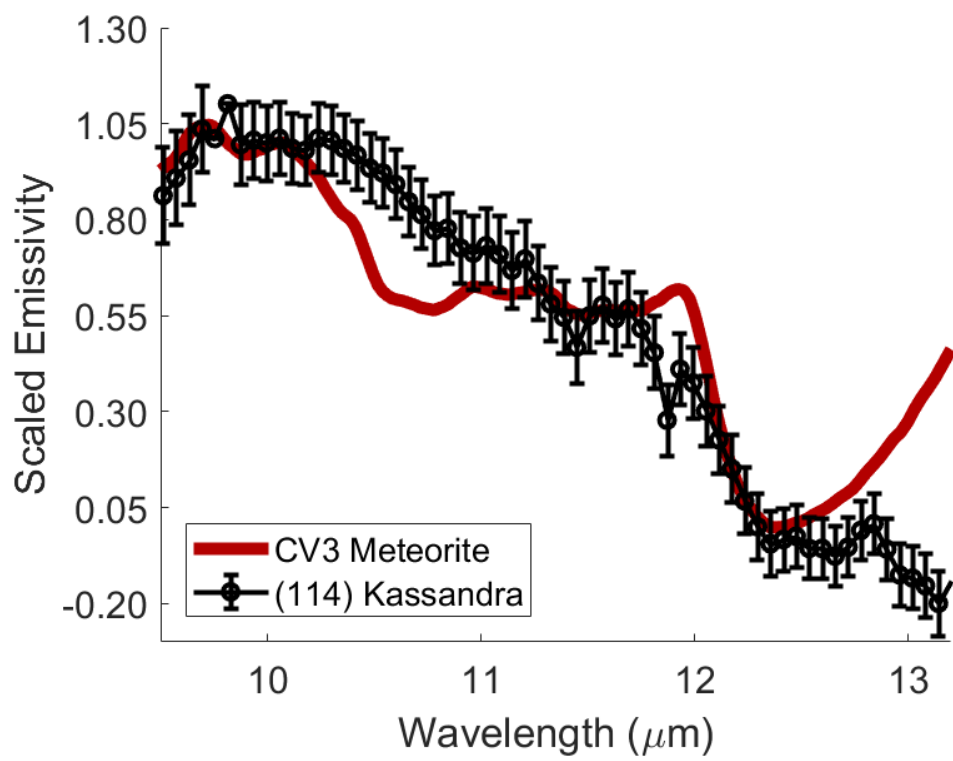
Spitzer+IRS Observations

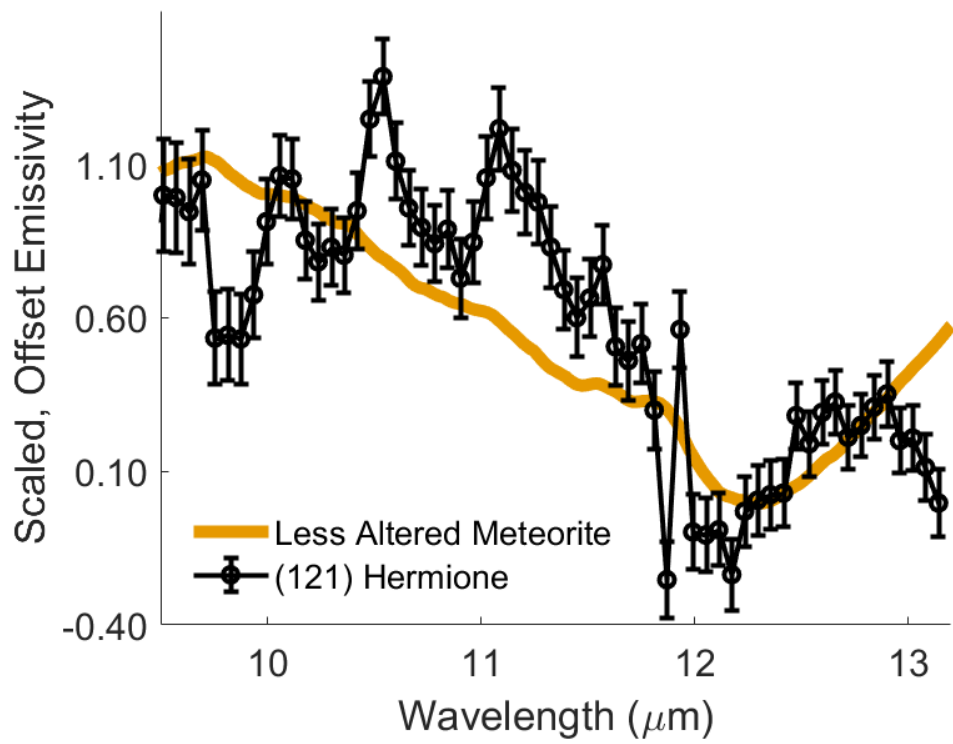


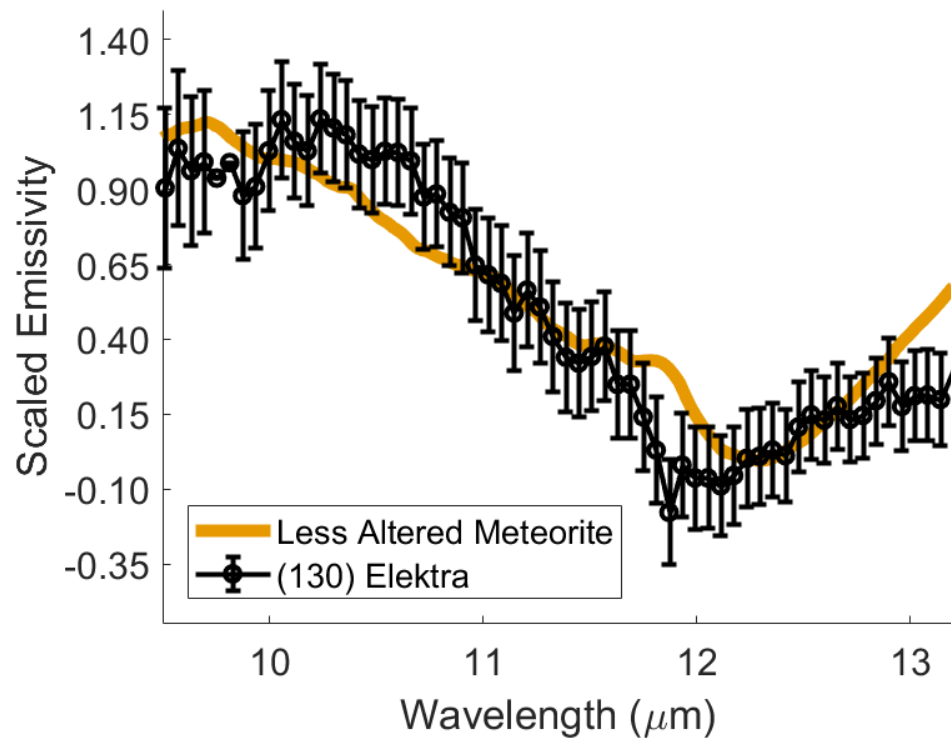


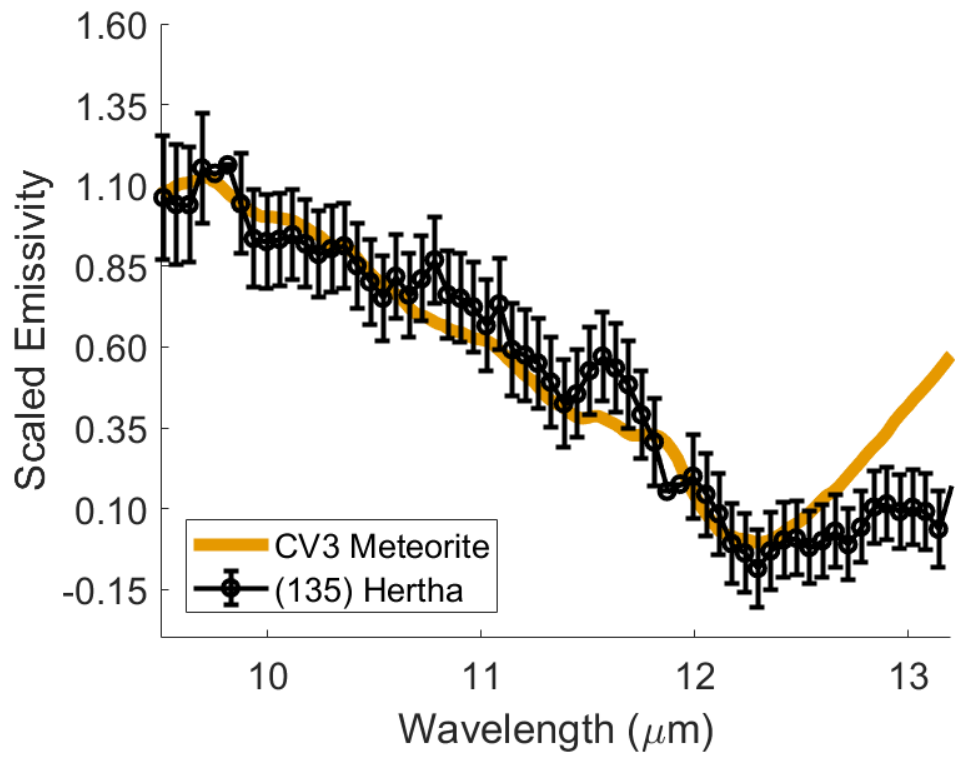


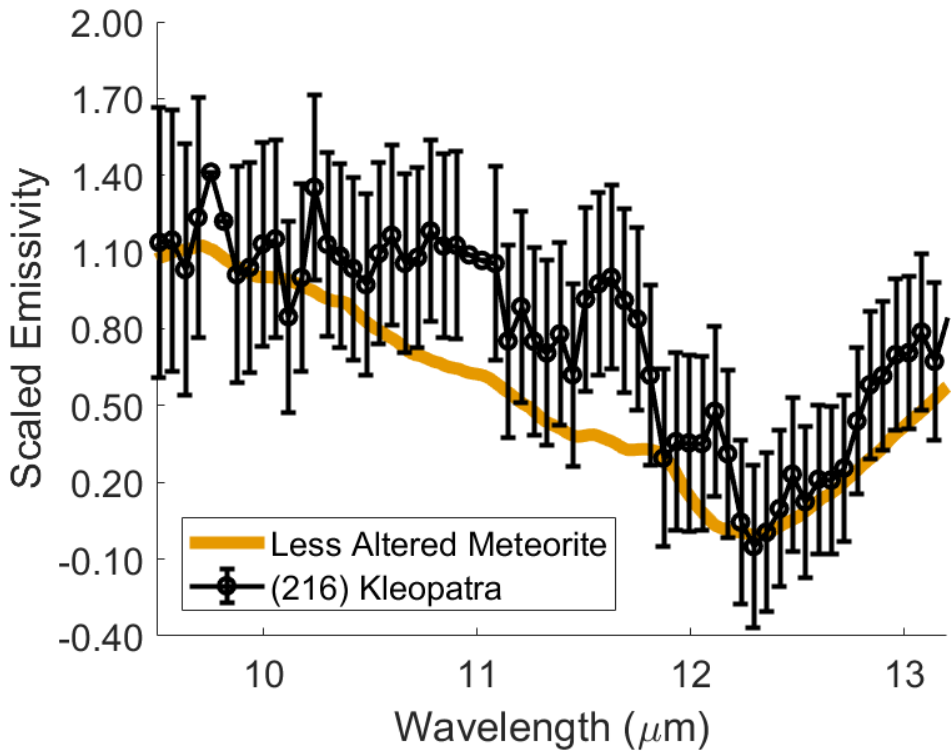
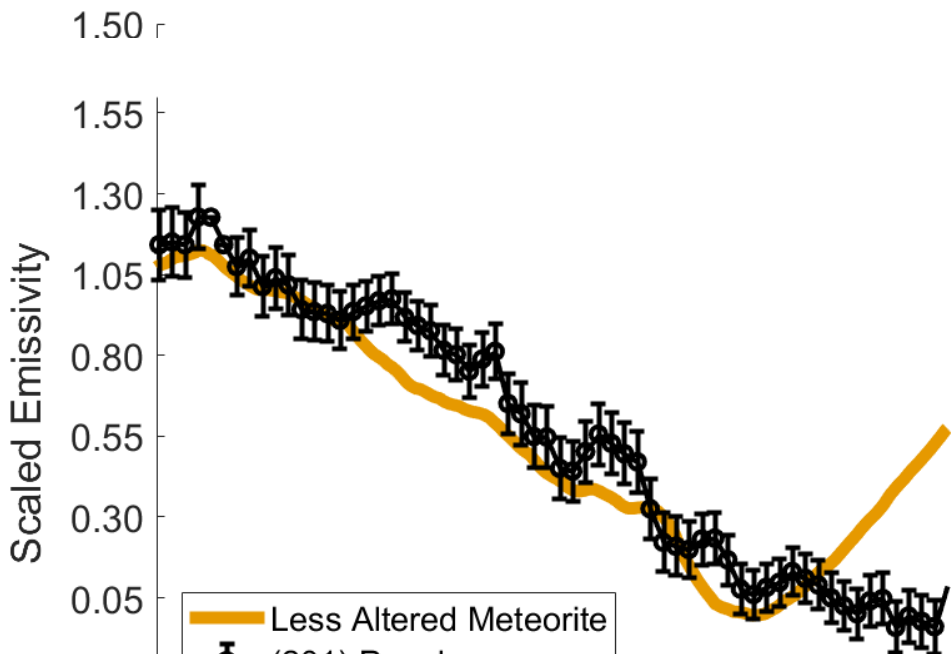


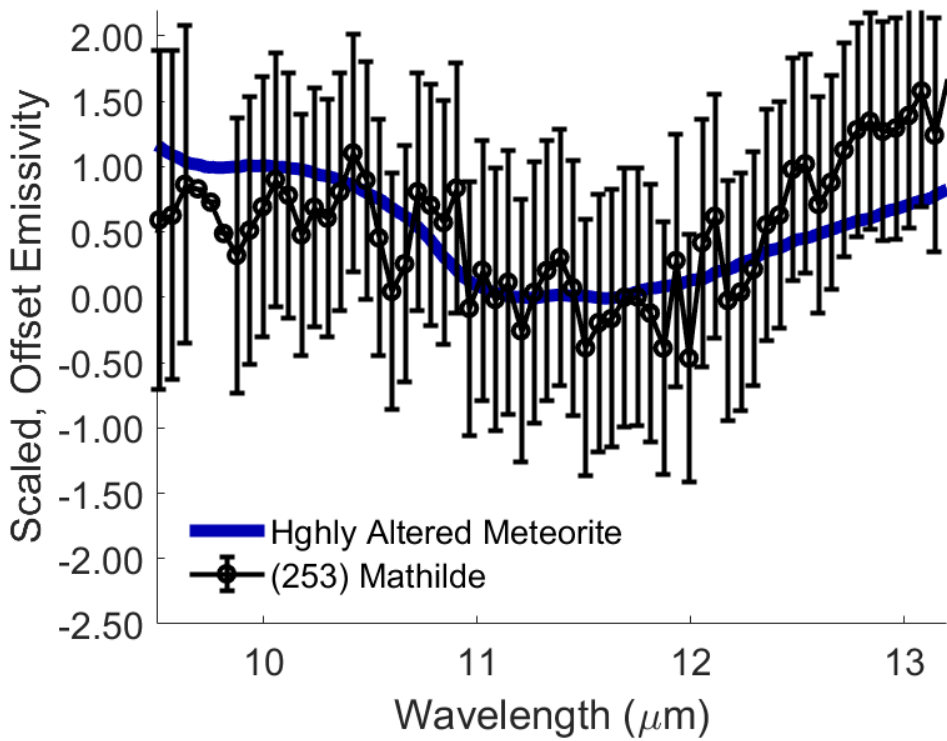
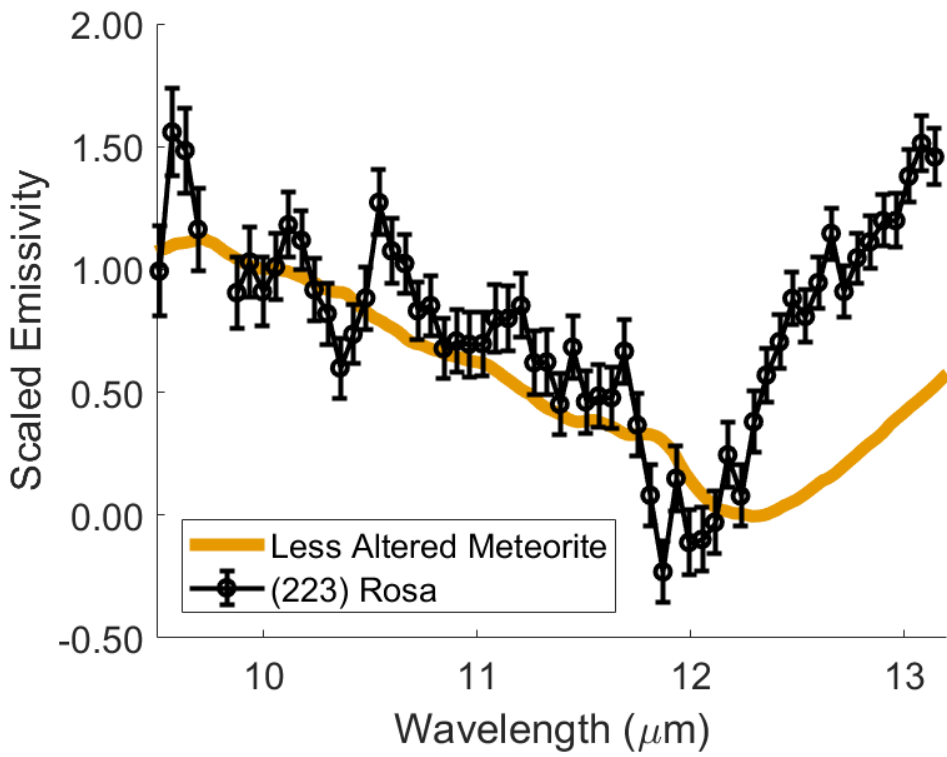


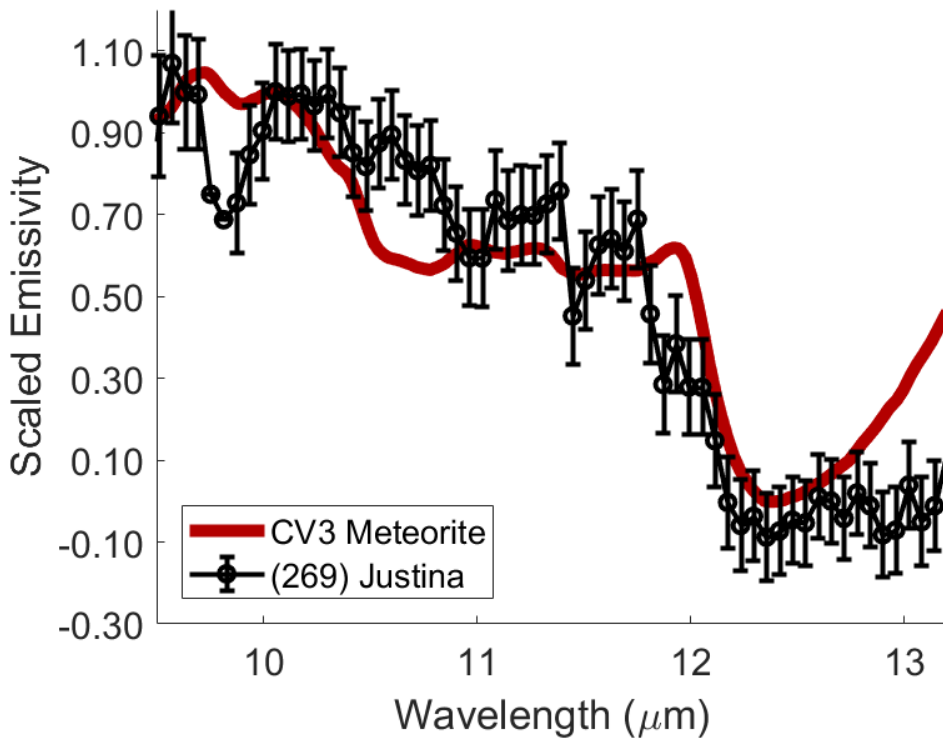
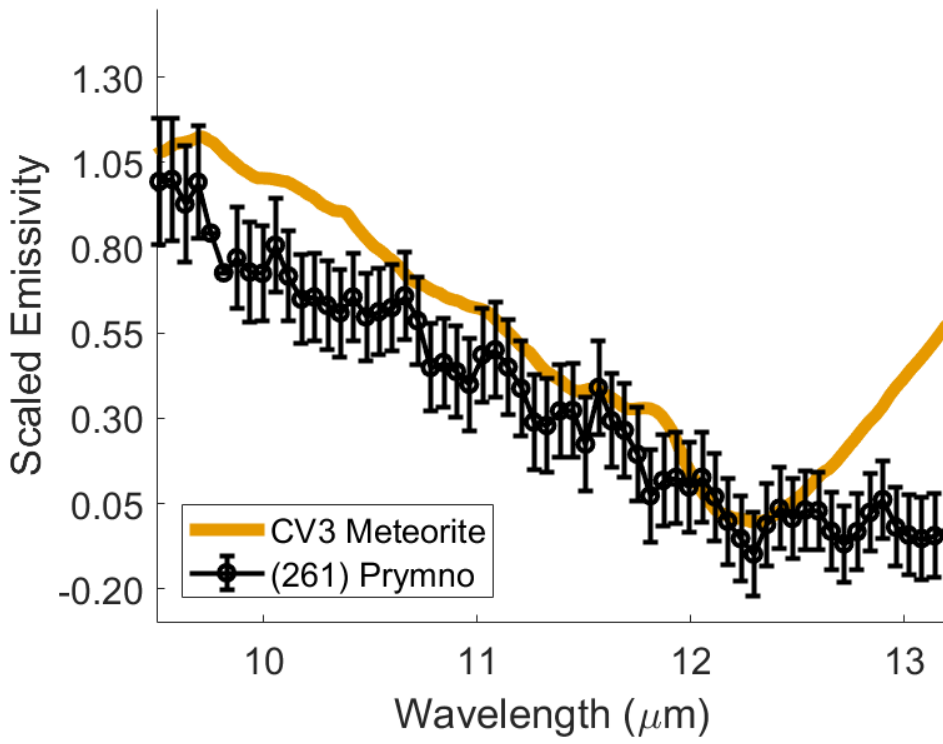


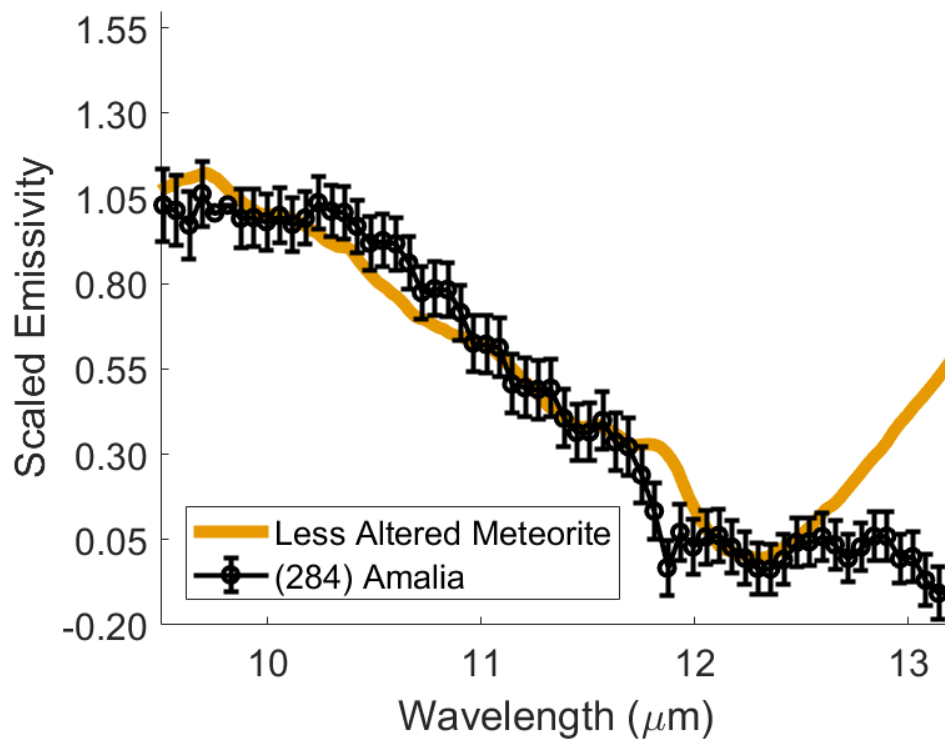
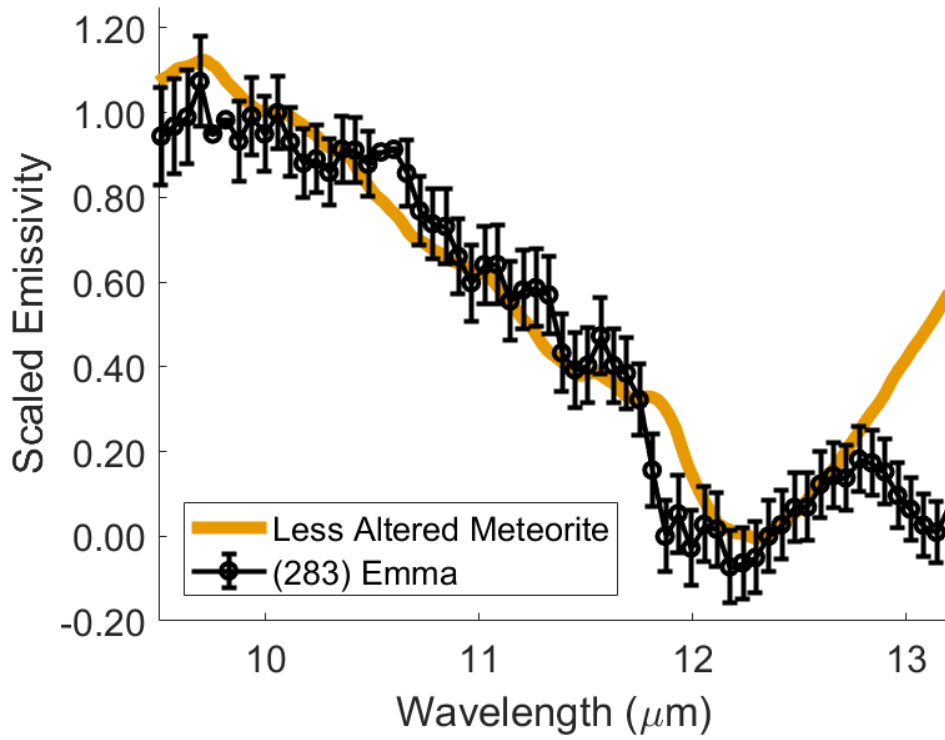


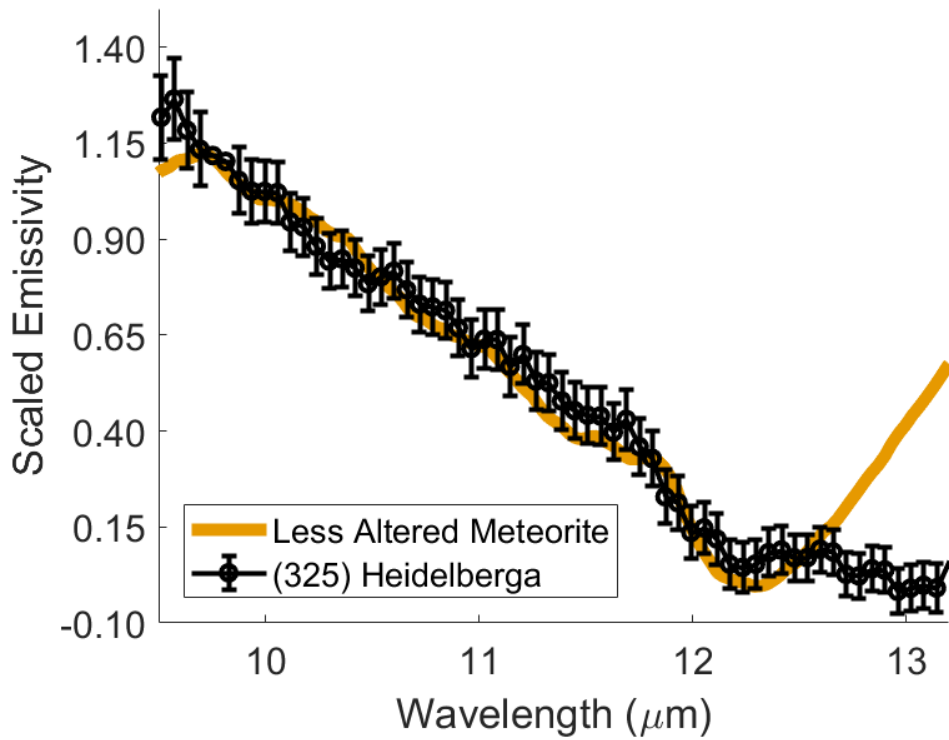
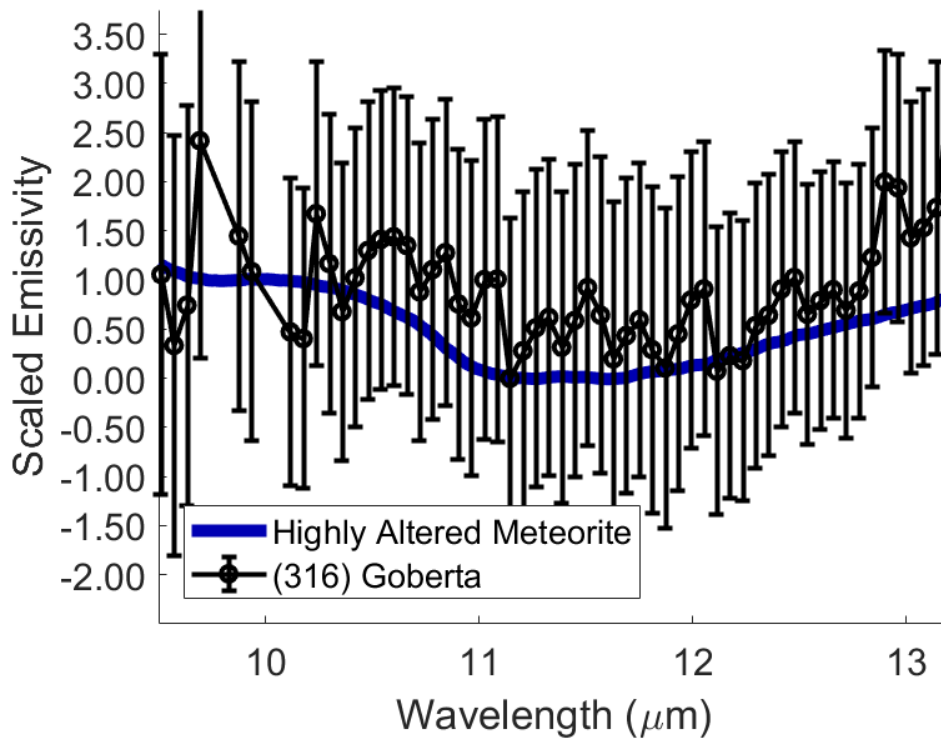


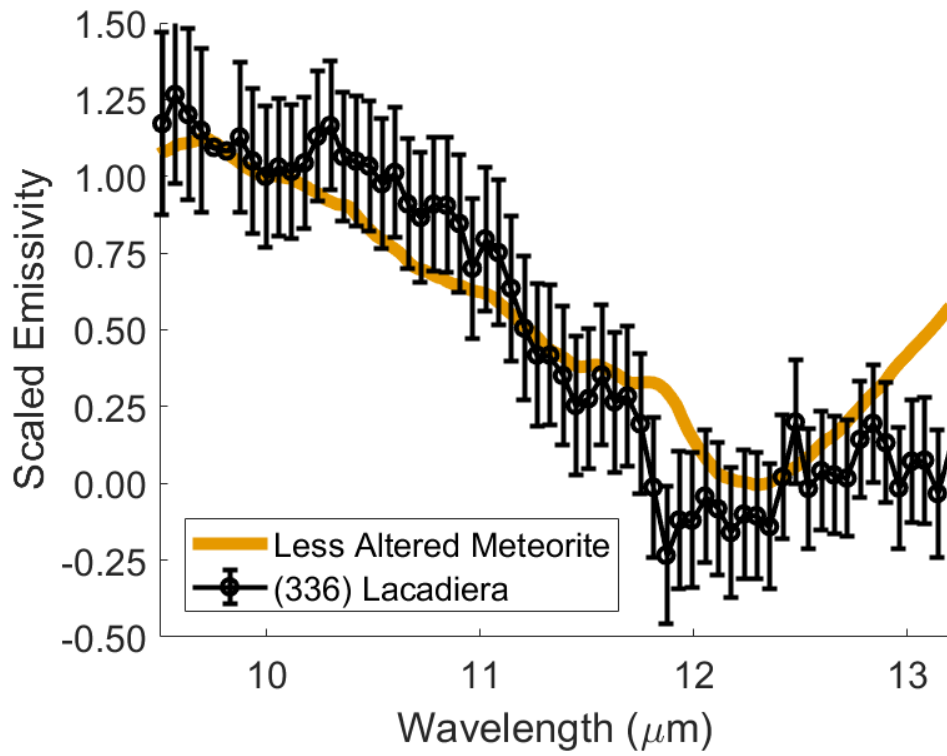
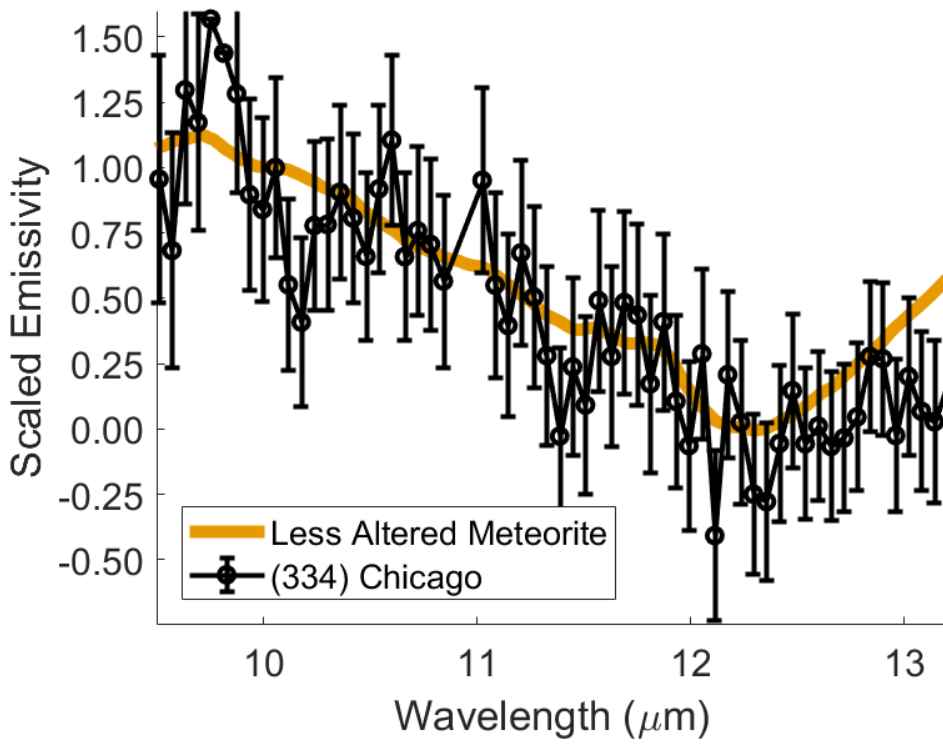


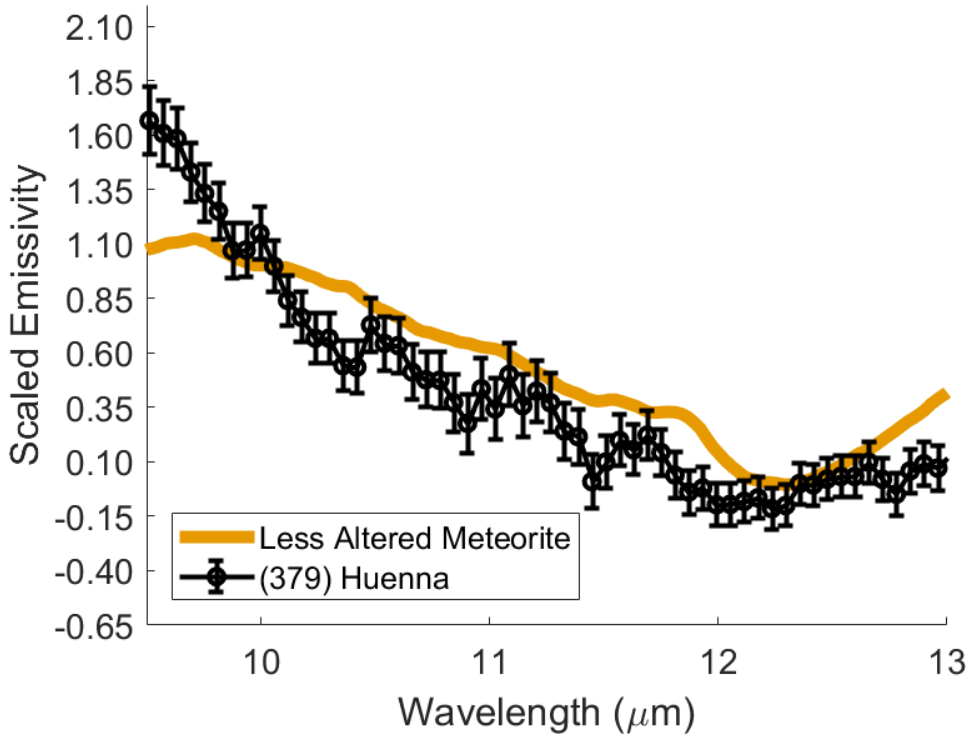
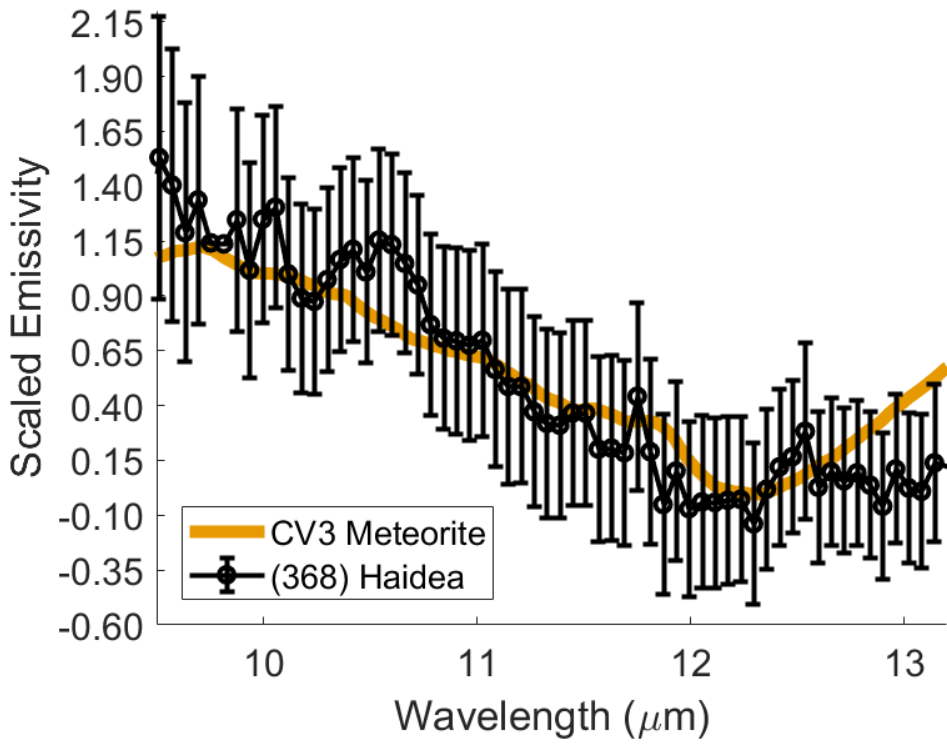


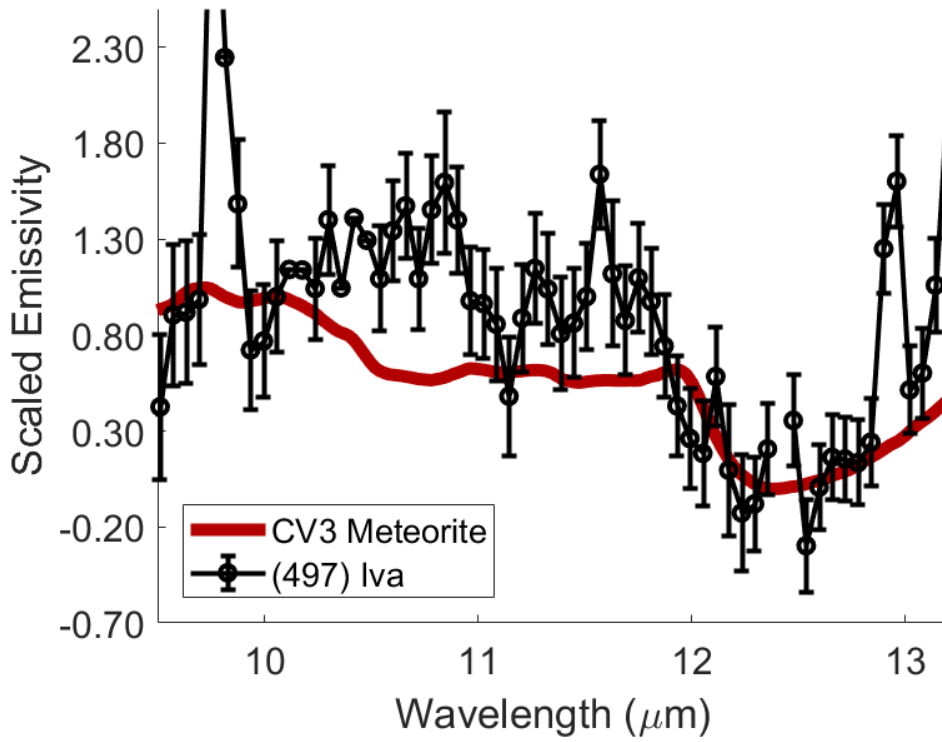
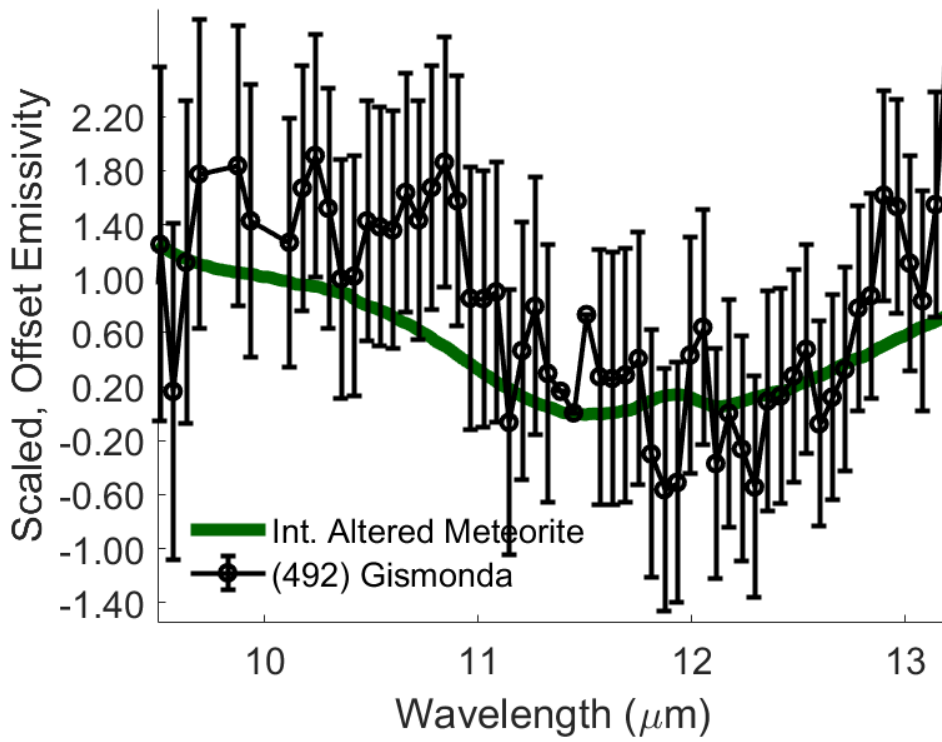


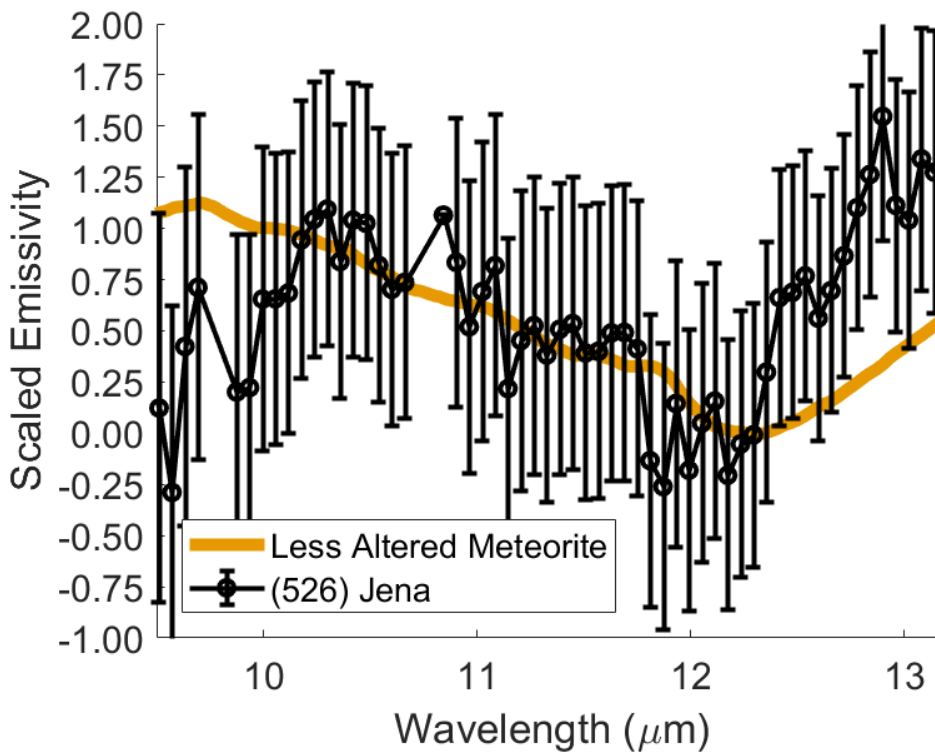
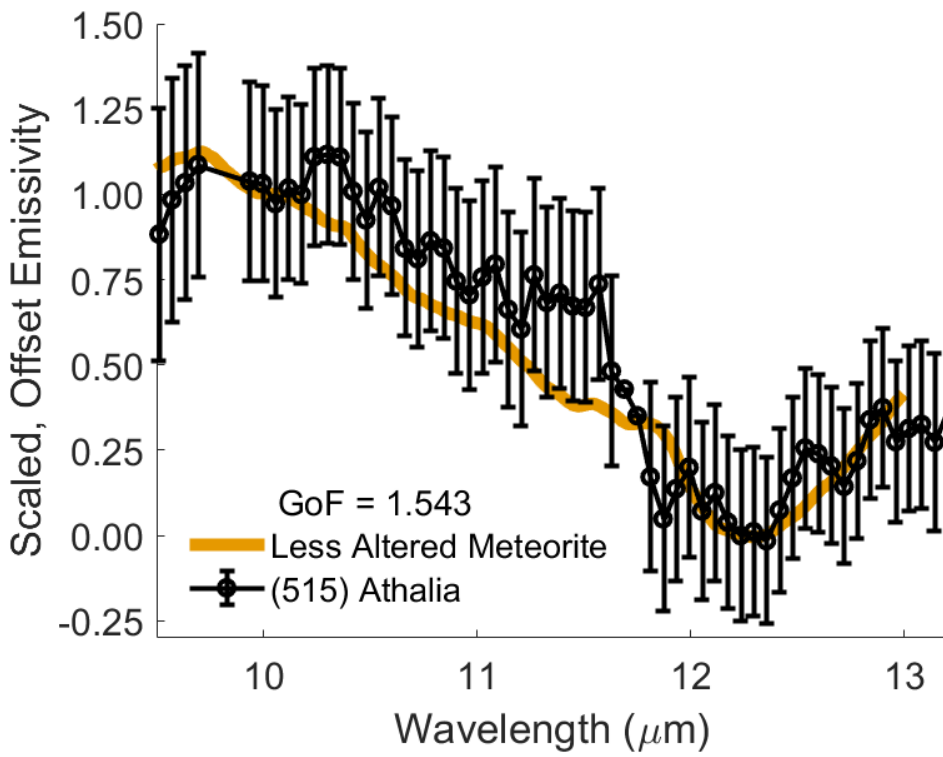


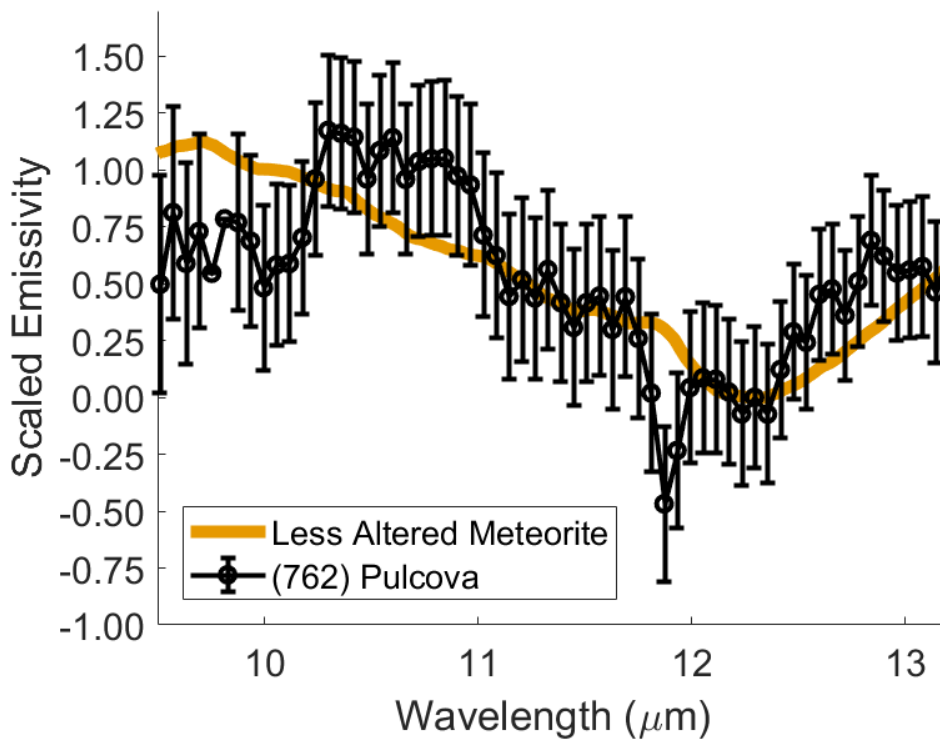
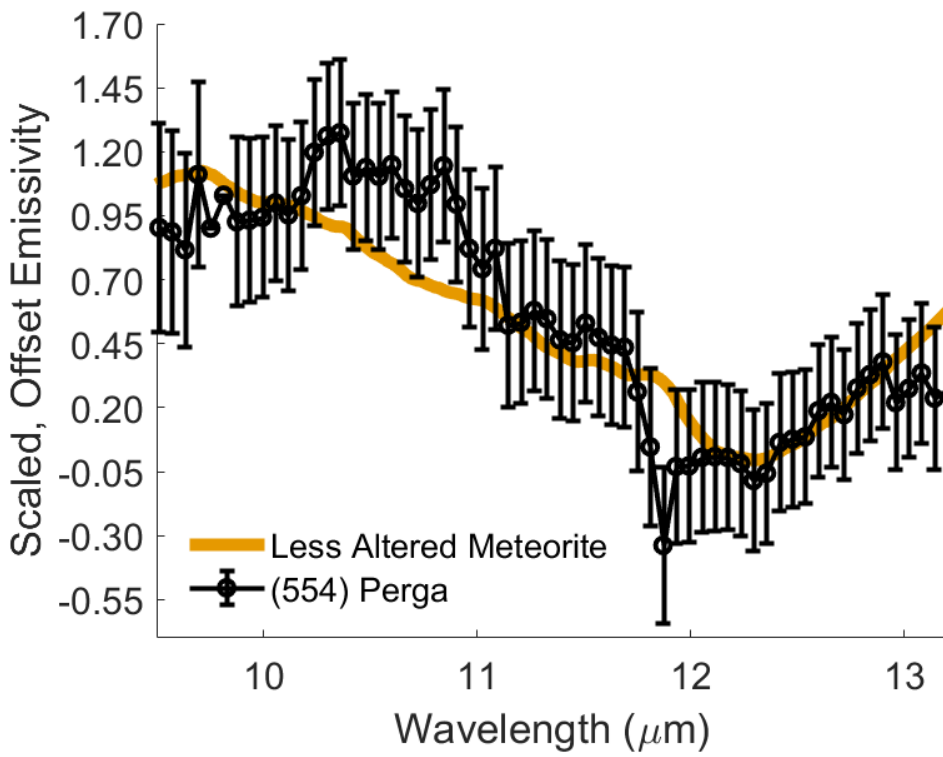


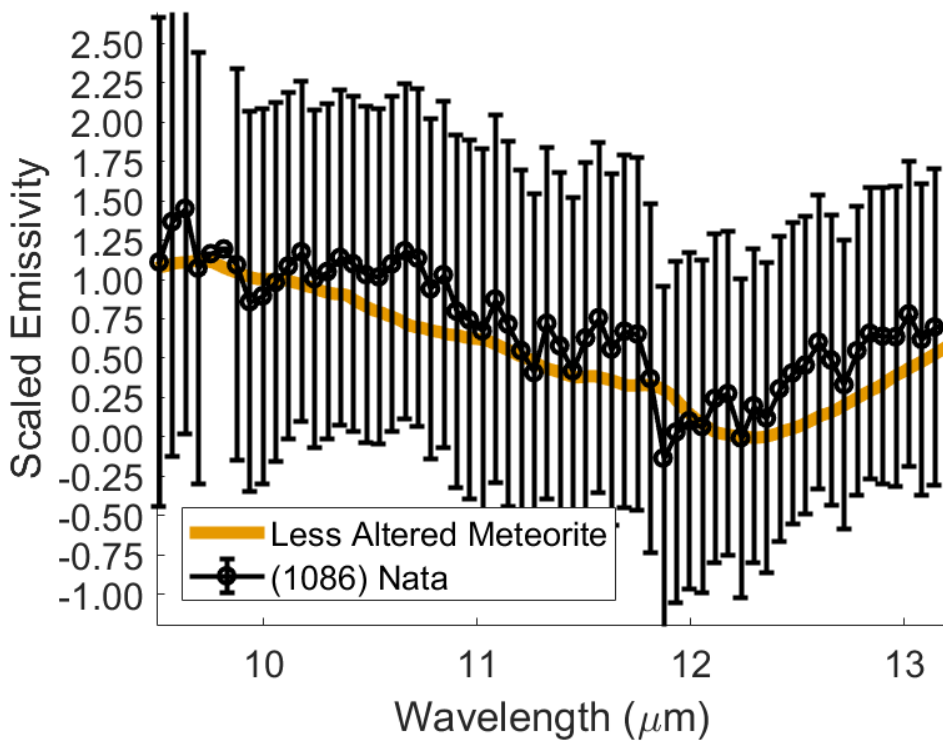
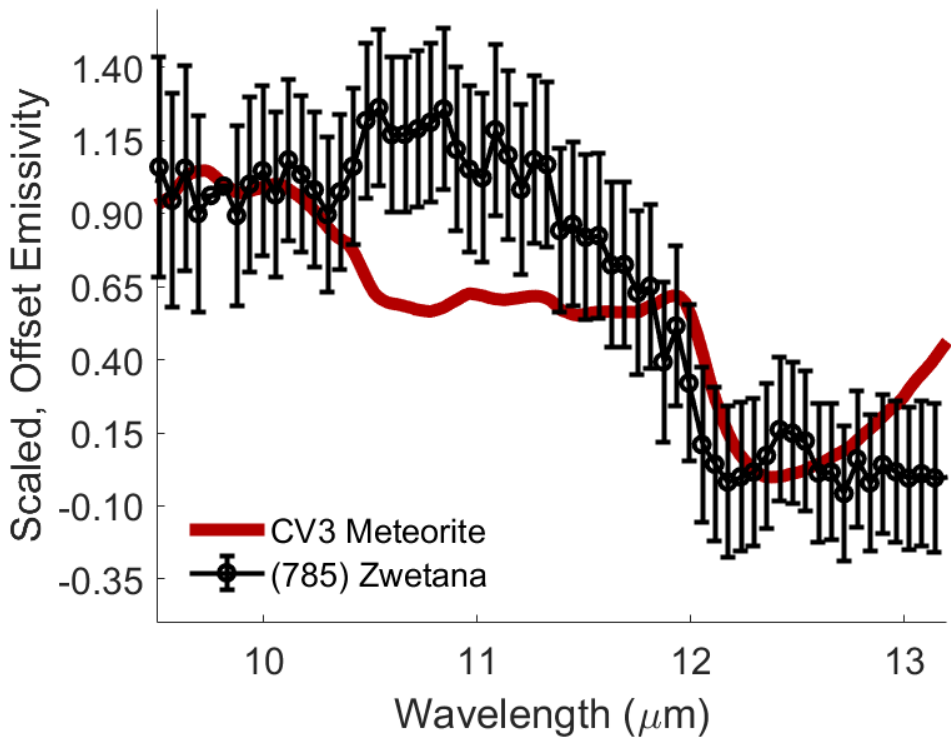


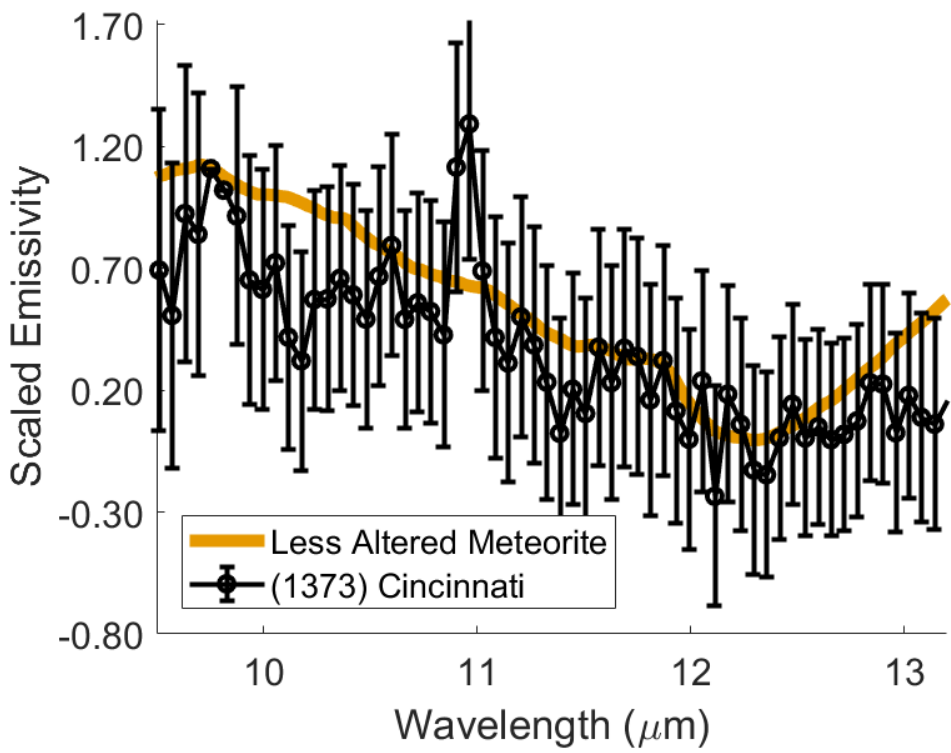
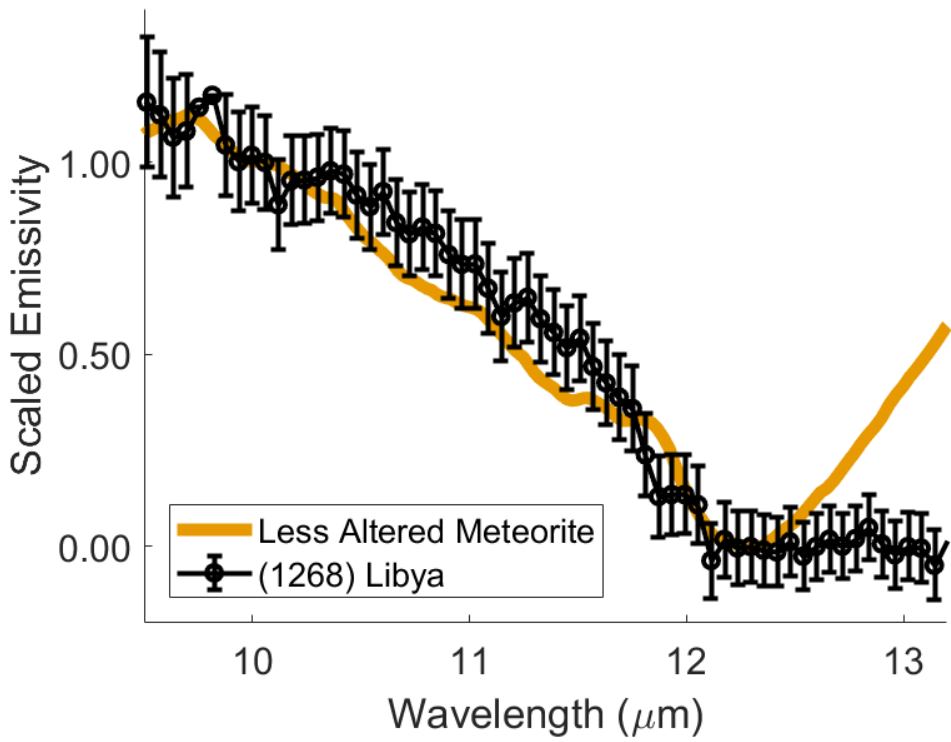


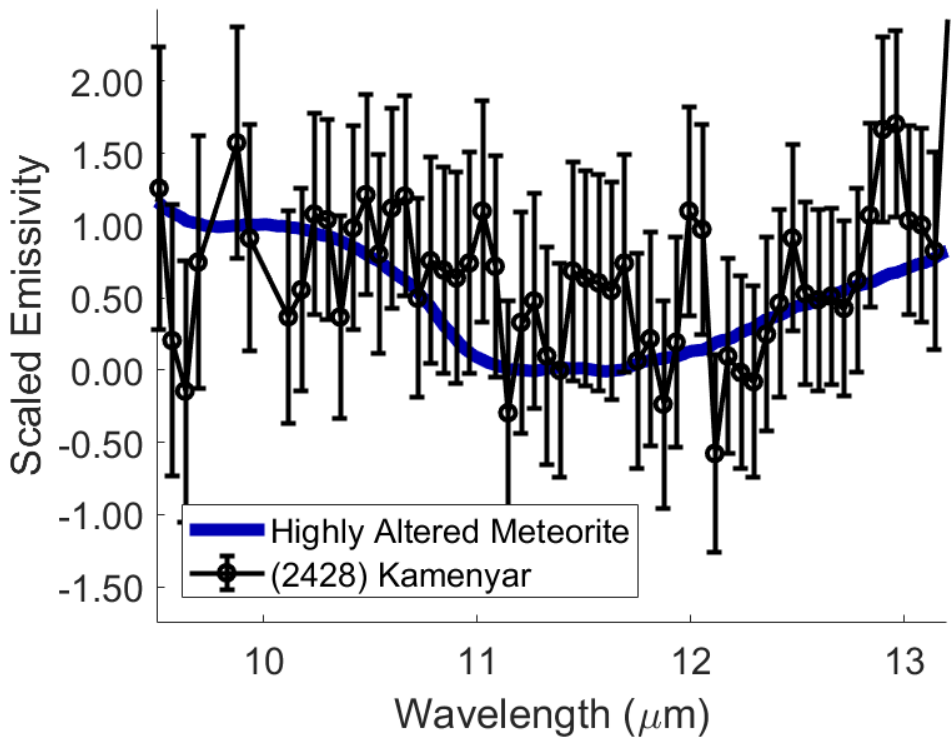
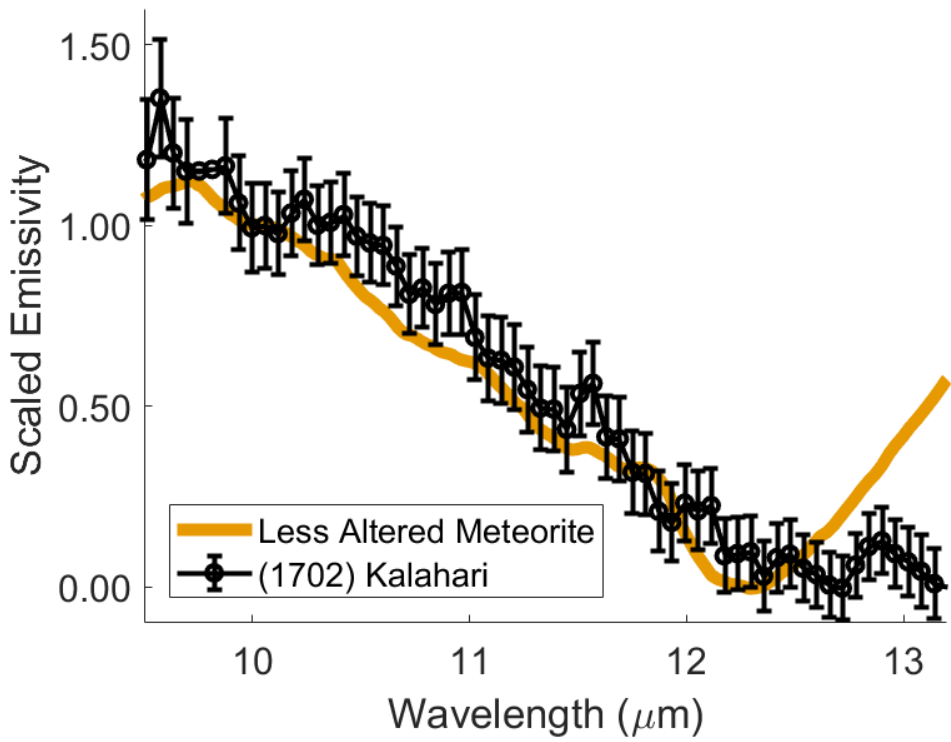


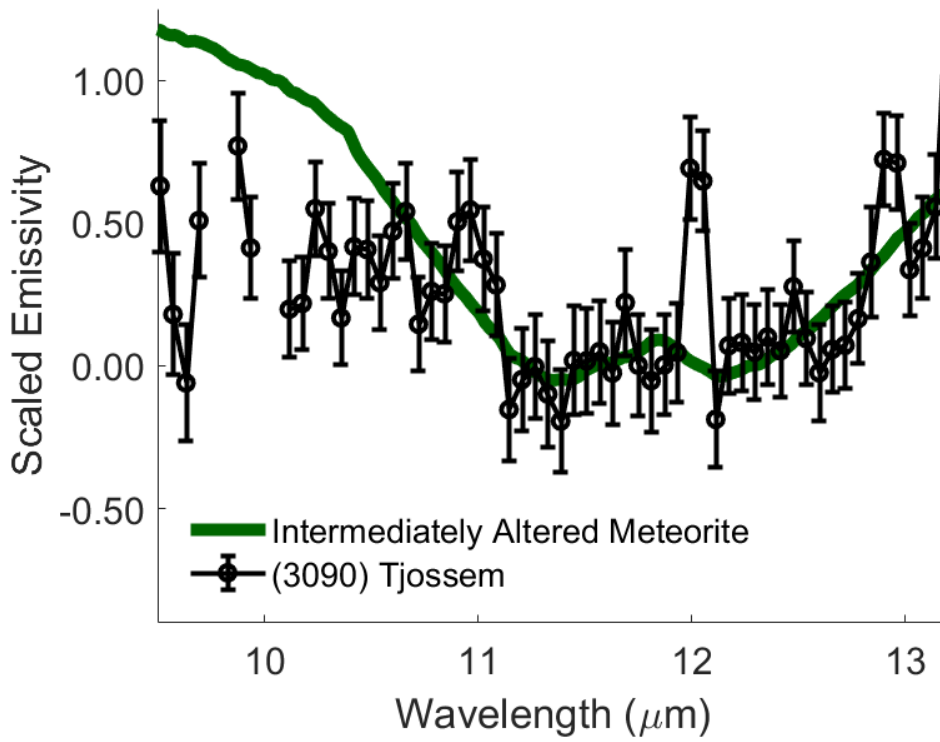
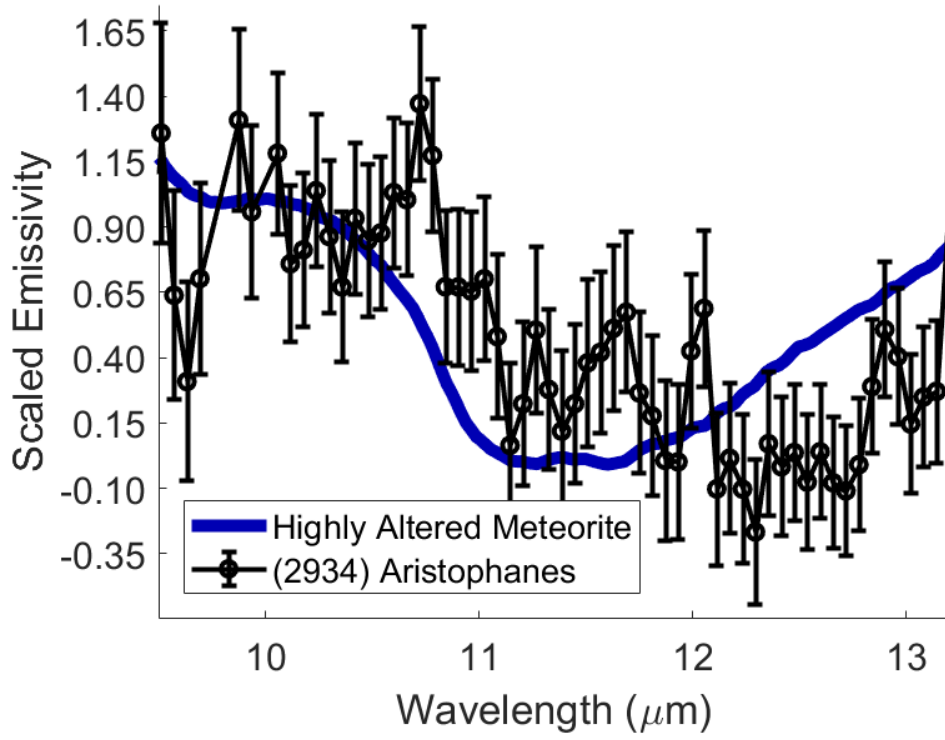


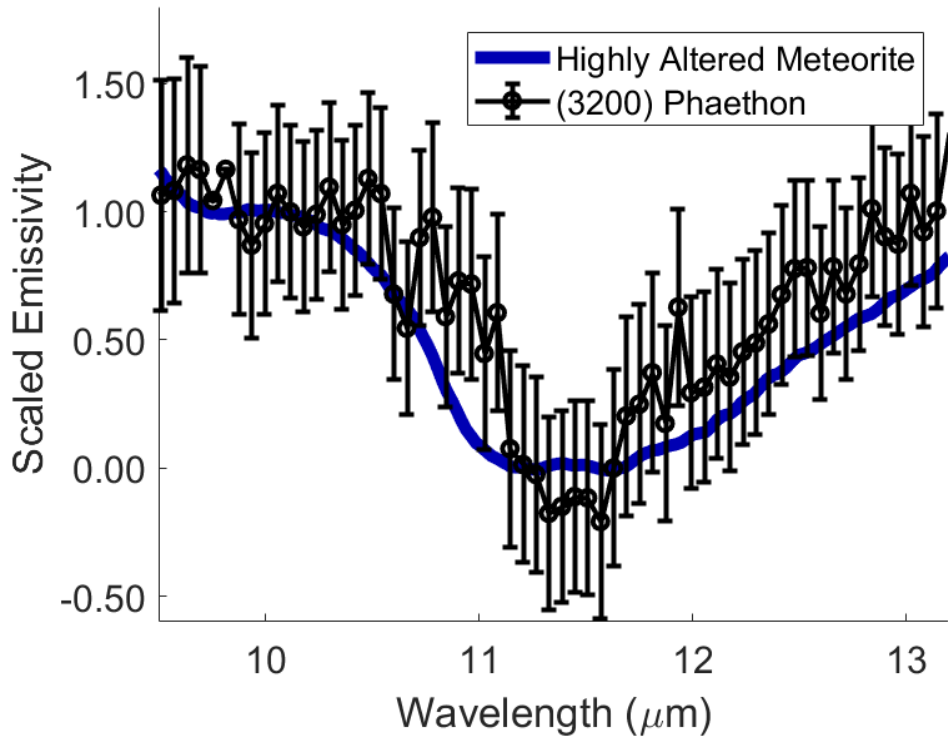




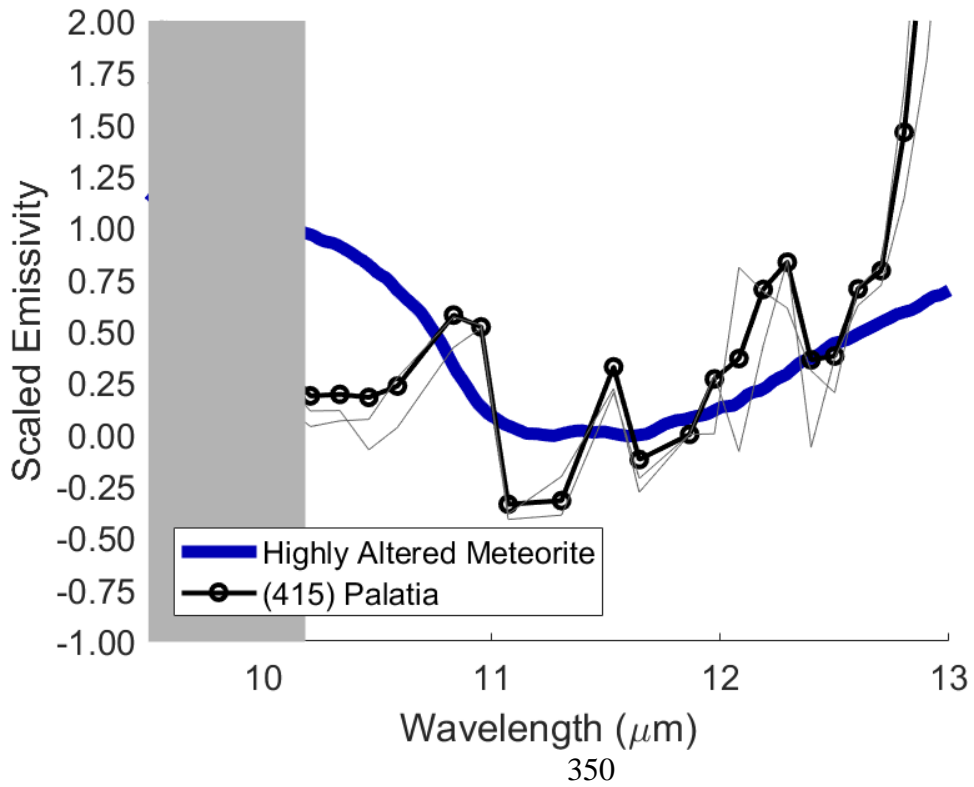
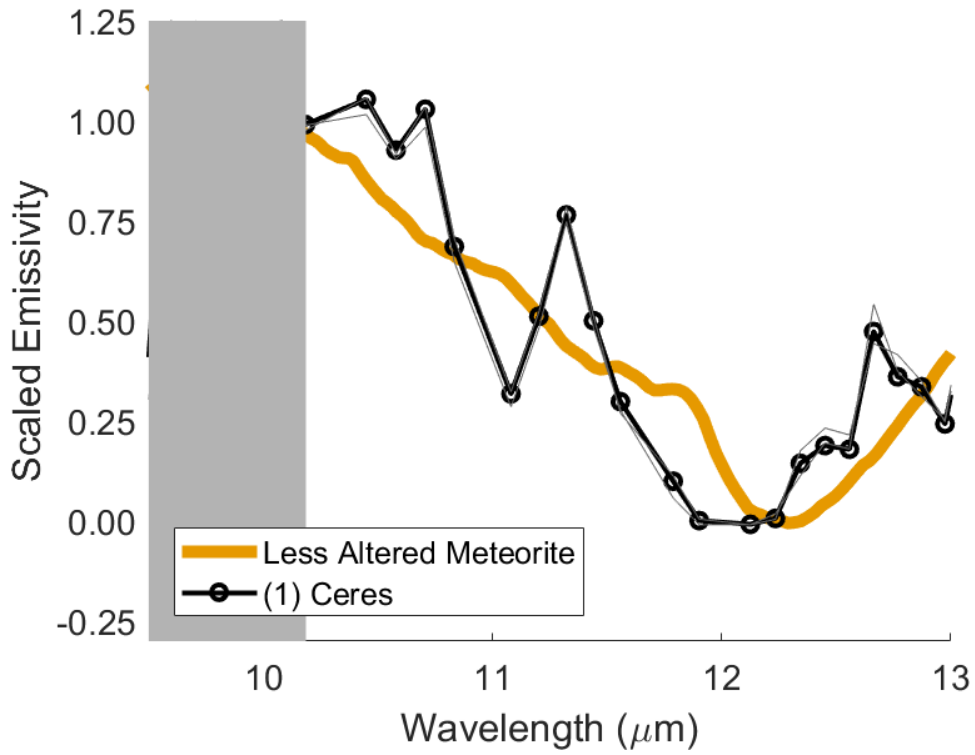


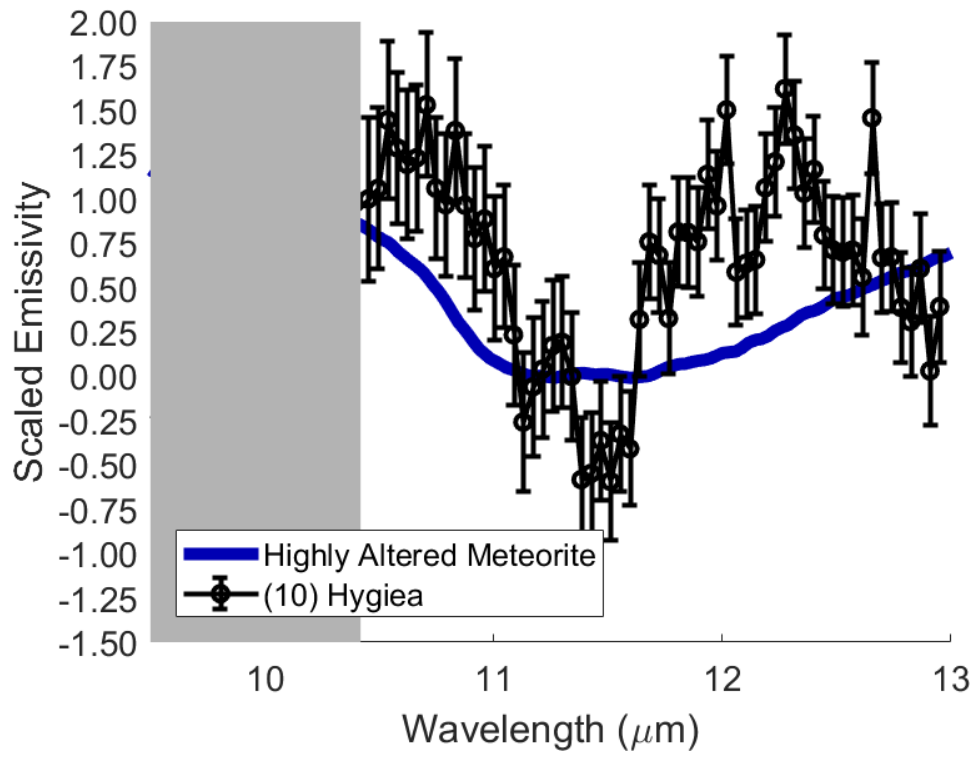


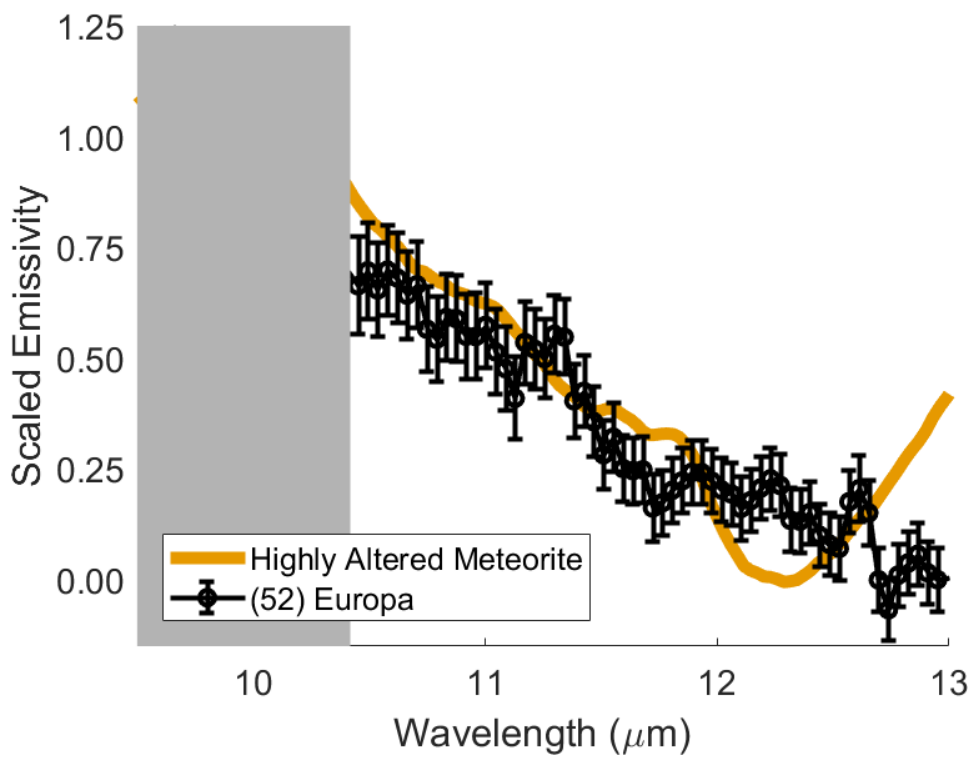
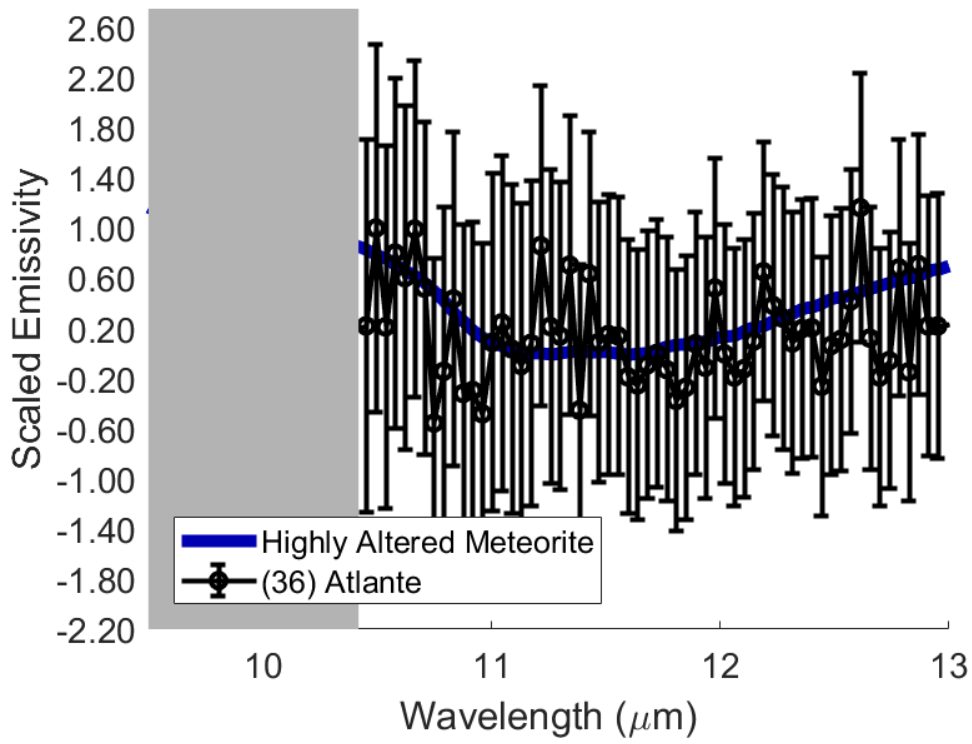


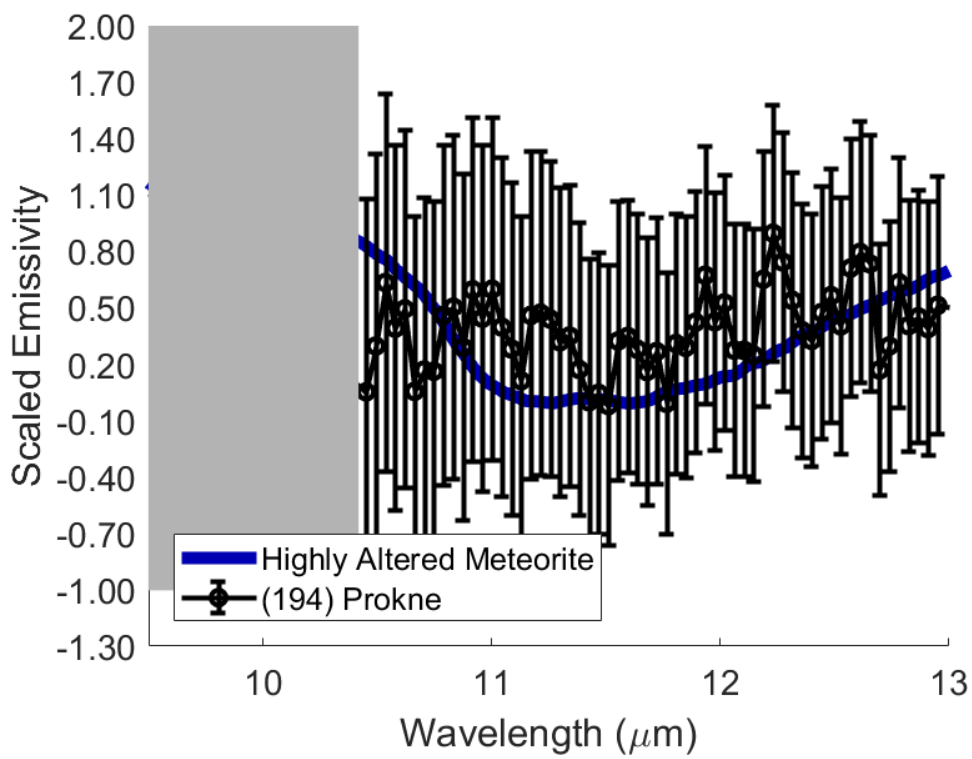
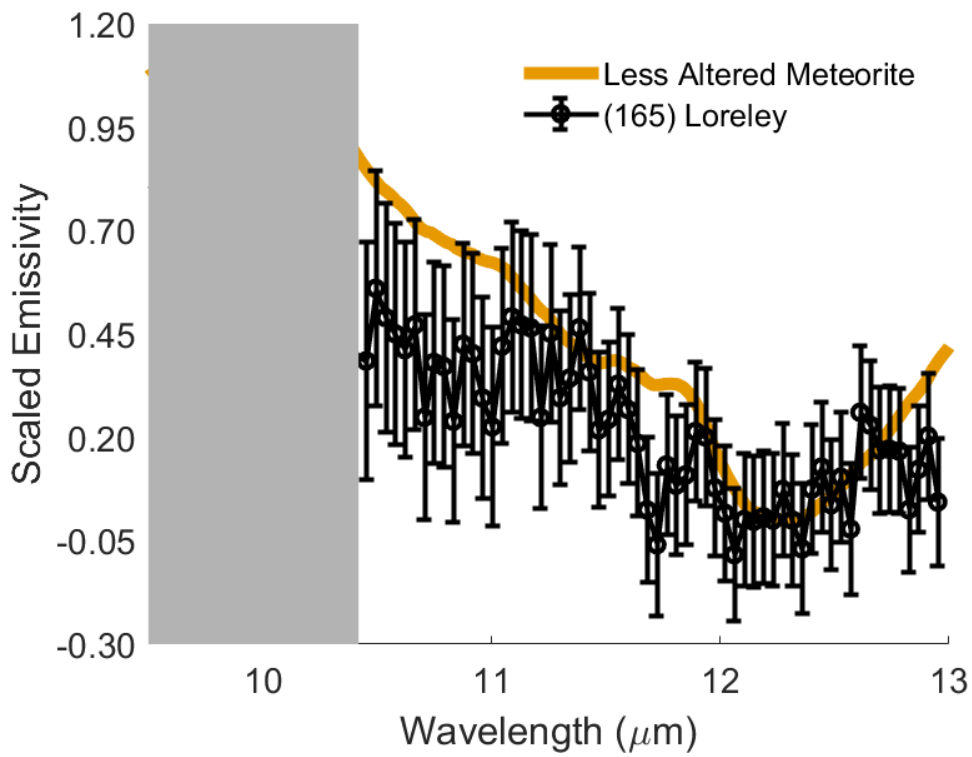


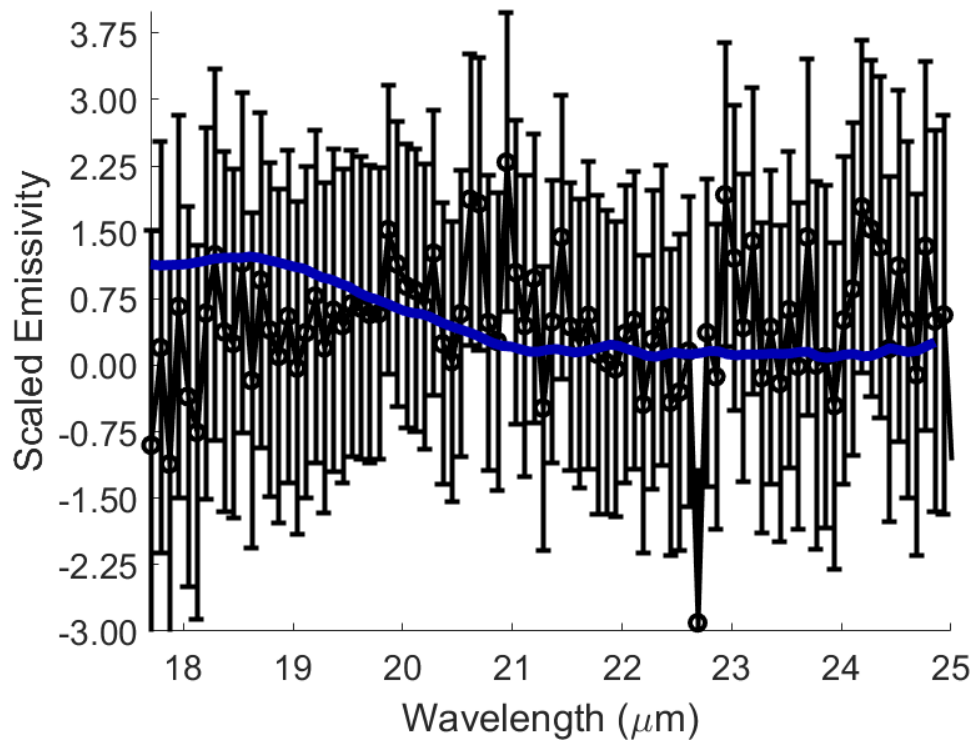
IRTF+BASS











Bibliography

Abreu, N. M., & Brearley, A. J. . (2010). Early solar system processes recorded in the matrices of two highly pristine CR3 carbonaceous chondrites, MET 00426 and QUE 99177. . *Geochimica et Cosmochimica Acta*, 74(3), 1146-1171.

A'Hearn, M. F., & Feldman, P. D. . (1992). Water vaporization on Ceres. *Icarus*, 98(1), 54-60.

Alexander, C. M. O'D, Newsome, S. D., Fogel, M. L., Nittler L. R., Busemann, H., Cody, G. D. (2010). Deuterium enrichments in chondritic macromolecular material— Implications for the origin and evolution of organics, water and asteroids. *Geochimica et Cosmochimica Acta*, 74, 4417-4437.

Alexander, C. M. O'D., Bowden, R., Howard, K. T. (2014). A multi-technique search for the most primitive chondrites. *Lunar and Planetary Science Conference*, abstract 2667.

Alexander, C. M. O'D., Hutchinson, R., Barber, D. J. (1989). Origin of chondrule rims and interchondrule matrices in unequilibrated ordinary chondrites. *Earth and Planetary Science letters*, Vol. 95, 187-207.

Alexander, C. O. D., Barber, D. J., & Hutchison, R. . (1989). The microstructure of Semarkona and Bishunpur. . *Geochimica et Cosmochimica Acta*, 53(11), 3045-3057.

Alexander, C. O. D., Bowden, R., Fogel, M. L., Howard, K. T., Herd, C. D. K., & Nittler, L. R. (2012). The provenances of asteroids, and their contributions to the volatile inventories of the terrestrial planets. *Science*, 337(6095), 721-723.

- Alexander, C. O. D., Fogel, M., Yabuta, H., & Cody, G. D. . (2007). The origin and evolution of chondrites recorded in the elemental and isotopic compositions of their macromolecular organic matter. *Geochimica et Cosmochimica Acta*, *71(17)*, 4380-4403.
- Alexander, C. O. D., Greenwood, R. C., Bowden, R., Gibson, J. M., Howard, K. T., & Franchi, I. A. (in press.). A mutli-technique search for the most primitive CO chondrites. . *Geochimica et Cosmochimica Acta*.
- A'Hearn, M. F., & Feldman, P. D. (1992). Water vaporization on Ceres. *Icarus*, *98(1)*, 54-60.
- Ammannito, E., DeSanctis, M.C., Ciarniello, M., Frigeri, A., Carrozzo, F.G., Combe, J.P., Ehlmann, B.L., Marchi, S., McSween, H.Y., Raponi, A. and Toplis, M.J., . (2016). Distribution of phyllosilicates on the surface of Ceres. *Science*, *353(6303)*, aaf4279.
- Anders, E., & Grevesse, N. . (1989). Abundances of the elements: Meteoritic and solar. . *Geochimica et Cosmochimica acta*, *53(1)*, 197-214.
- Barucci, M. A., Doressoundiram, A., Fulchignoni, M., Florczak, M., Lazzarin, M., Angeli, C., & Lazzaro, D. (1998). Search for aqueously altered materials on asteroids. . *Icarus*, *132(2)*, 388-396.
- Barucci, M. A., Dotto, E., Brucato, J. R., Müller, T. G., Morris, P., Doressoundiram, A., Fulchignoni, M., De Sanctis, M. C., Owen T., Crovisier, J., Le Bras, A., Colangeli, L., Mennella, V. (2002). 10 Hygiea: ISO Infrared Observations. . *Icarus*, *Vol.*, *156*, 202-210.

- Barucci, M.A., Dotto, E., Brucato, J.R., Müller, T.G., Morris, P., Doressoundiram, A., Fulchignoni, M., De Sanctis, M.C., Owen, T., Crovisier, J. and Le Bras, A., (2002). 10 Hygiea: ISO infrared observations. *Icarus*, 156(1), 202-210.
- Beck, P., Garenne, A., Quirico, E., Bonal, L., Montes-Hernandez, G., Moynier, F. (2013). Transmission infrared spectra (2-25 microns) of carbonaceous chondrites (CI, CM, CV-CK, CR, C2 ungrouped): mineralogy, water, asteroidal processes. *Icarus*, Vol. 229, 263-277.
- Beck, P., Garenne, A., Quirico, E., Bonal, L., Montes-Hernandez, G., Moynier, F., & Schmitt, B. (2014). Transmission infrared spectra (2–25 μ m) of carbonaceous chondrites (CI, CM, CV–CK, CR, C2 ungrouped): Mineralogy, water, and asteroidal processes. *Icarus*, 229, 263-277.
- Beck, P., Quirico, E., Montes-Hernandez, G., Bonal, L., Bollard, J., Orthous-Daunay, F.-R., Howard, K. T., Schmitt, B., Brissaud, O., Deschamps, F., Wunder, B., Guillot, S. (2010). Hydrous mineralogy of CM and CI chondrites from infrared spectroscopy and their relationship with low albedo asteroids. *Geochimica. Cosmochimica. Acta*, Vol. 74, 4881-4892. .
- Bell, P. M., Mao, H. K. (1976). Optical spectra and electron paramagnetic resonance of lunar and synthetic glasses: A study of the effects of controlled atmosphere, composition and temperature. *Proceedings of 7th Lunar Science Conference*, 2543-2599.
- Binzel, R. P., Rivkin, A. S., Stuart, J. S., Harris, A. W., Bus, S. J., & Burbine, T. H. (2004). Observed spectral properties of near-Earth objects: results for population distribution, source regions, and space weathering processes. *Icarus*, 170(2), 259-294.

- Bischoff, A. (1998). Aqueous alteration of carbonaceous chondrites: Evidence for preaccretionary alteration—A review. . *Meteoritics & Planetary Science*, 33(5), 1113-1122.
- Bishop, J. L., Dyar, M. D., Sklute, E. C., Drief, A. (2008a). Physical alteration of antigorite: a Mössbauer spectroscopy, reflectance spectroscopy and TEM study with applications to Mars. *Clay Mins.*, Vol. 43, 55-67.
- Bishop, J. L., Lane, M. D., Dyar, M. D., Brown, A. J. (2008b). Reflectance and emission spectroscopy study of four groups of phyllosilicates: smectites, kaolinite-serpentines, chlorites and micas. *Clay Minerals*, Vol. 43, 35-54. .
- Bishop, J. L., Mustard, J. F., Pieters, C. M., Hiroi, T. (1998). Recognition of minor constituents in reflectance spectra of Allan Hills 84001 chips and the importance for remote sensing in Mars. *Meteoritics and Planetary Science*, Vol. 33, 693-698.
- Bishop, J., Muard, E., Dyar, M. D. (2002). The influence of octahedral and tetrahedral cation substitution on the structure of smectites and serpentines as observed through infrared spectroscopy. *Clay Minerals*, Vol. 37, 617-628.
- Bland, P. A., Berry, F. J., Cadogan, J. M., Howard, K. T., Cressey, G. (2012). Fe-bearing mineral abundance in primitive chondrites by Mössbauer Spectroscopy. *Met. Soc. abstract* #5304.
- Bland, P. A., Cressey, G., & Menzies, O. N. . (2004). Modal mineralogy of carbonaceous chondrites by X-ray diffraction and Mössbauer spectroscopy. *Meteoritics & Planetary Science*, 39(1), 3-16.

- Bland, P. A., Cressey, G., Menzies, O. N., (2004). Modal mineralogy of carbonaceous chondrites by X-ray diffraction and Mössbauer spectroscopy. *Met. & Plan. Sci., Vol. 39, Nr. 1, 3-16. Met. & Plan. Sci., Vol. 39, Nr. 1, 3-16.*
- Bland, P. A., & Travis, B. J. (2017). Giant convecting mud balls of the early solar system. *Science Advances, 3(7), e1602514.*
- Bonal, L., Bourot-Denise, M., Quirico, E., Montagnac, G., Lewin, E. (2007). Organic matter and metamorphic history of CO chondrites. *Geochimica et Cosmochimica Acta, Vol. 71, 1605-1623.*
- Bonal, L., Quirico, E., Flandinet, L., Montagnac, G. (2016). Thermal history of type 3 chondrites from Antarctic meteorite collection determined by Raman spectroscopy of their polyaromatic carbonaceous matter. *Geochimica et Cosmochimica Acta, 189, 312-337.*
- Bottke Jr., W. F., Durda, D. D., Nesvorný, D., Jedicke, R., Morbidelli, A., Vokrouhlicky, D., Levison, H. (2005). The fossilized size distribution of the main asteroid belt. *Icarus, 175, 111-140.*
- Bradley, J. P., Ishii, H. A. . (2008). Comment on “The shape and composition of interstellar silicate grains. *Astronomy and Astrophysics, Vol. 486, 781-784.*
- Brearley, A. J. . (1993). Matrix and fine-grained rims in the unequilibrated CO3 chondrite, ALHA77307: Origins and evidence for diverse, primitive nebular dust components. . *Geochimica et Cosmochimica Acta, 57(7), 1521-1550.*
- Brearley, A. J. . (1999). Origin of graphitic carbon and pentlandite in matrix olivines in the Allende meteorite. *Science, 285(5432), 1380-1382.*

- Brearley, A. J. (2006). The action of water. . *Meteorites and the early solar system II*, 943, 587-624.
- Brearley, A. J. (2012). MIL 07687---An Intriguing, Very Low Petrologic Type 3 Carbonaceous Chondrite with a Unique Style of Aqueous Alteration. *LPSC abstract 1233*.
- Brearley, A. J., & Hutcheon, I. D. (2002). Carbonates in the Y791198 CM2 chondrite: zoning and Mn-Cr systematics. *Meteoritics and Planetary Science Supplement*, 37, A23.
- Brearley, A. J., & Jones, R. H. (1998). Chondritic meteorites. *Reviews in Mineralogy and Geochemistry*, 36(1), 3-1.
- Brearley, A. J., Hutcheon, I. D., . (2000). Carbonates in the CM1 Chondrite ALH84034: Mineral chemistry, zoning and Mn-Cr systematics. *LPSC, Abstract #1407*.
- Browning, L. B., McSween, H. Y., & Zolensky, M. E. (1996). Correlated alteration effects in CM carbonaceous chondrites. . *Geochimica et Cosmochimica Acta*, 60(14), 2621-2633.
- Bunch, T. E., & Chang, S. (1980). Carbonaceous chondrites—II. Carbonaceous chondrite phyllosilicates and light element geochemistry as indicators of parent body processes and surface conditions. . *Geochimica et Cosmochimica Acta*, 44(10), 1543-1577.
- Burbine, T. H., Binzel, R. P., Bus, S. J., Clark, B. E. (2001). K asteroids and CO3/CV3 chondrites. *Meteoritics and Planetary Science*, 36, 245-253.
- Burbine, T. H., McCoy, T. J., Hinrichs, J. L., Lucey, P. G. (2006). Spectral properties of angrites. *Meteoritics and Planetary Science*, 41, 1139-1145.
- Burgess R., Wright I. P. and Pillinger C. T. (1991). Determination of sulfur-bearing components in C1 and C2 carbonaceous chondrites by stepped combustion. *Meteoritics*, Vol. 26, 54–64.

- Burns, R. G. (1993). *Mineralogical Applications of Crystal Field Theory*. Cambridge University Press.
- Burns, R. G. (1993). Origin of electronic spectra of minerals in the visible to near-infrared region. In *Remote Geochemical Analysis* (eds. Pieteres, C. M., Englert, P. A.).
- Burns, R. G., & Huggins, F. E. (1972). Cation determinative curves for Mg-Fe-Mn olivines from vibrational spectra.
- Burns, R. G., Huggins, F. E. (1972). Cation determinative curves for Mg-Fe-Mn olivines from vibrational spectra. *Am. Min.*, Vol. 57, 967-985.
- Bus, S. J., & Binzel, R. P. (2002a). Phase II of the small main-belt asteroid spectroscopic survey: A feature-based taxonomy. *Icarus*, 158(1), 146-177.
- Bus, S. J., and R. P. Binzel. (2002b). Phase II of the Small Main-Belt Asteroid Spectroscopic Survey: The observations. *Icarus*, Vol. 158, 106-145, doi:10.1006/icar.2002.6857.
- Calvin W. M., King, T. V. V. (1997). Spectral characteristics of iron-bearing phyllosilicates: Comparison to Orgueil (CI1), Murchison and Murray (CM2). *Met. Planet. Soc. Vol. 32*, 693-701.
- Campins, H., Emery, J. P., Kelley, M., Fernández, Y., Licandro, J., Delbó, M., Barucci, A., Dotto, E. (2009). Spitzer observations of spacecraft target 162173 (1999 JU3). *A&A*, Vol. 503, L17-L20.
- Campins, H., Hargrove, K., Pinilla-Alonso, N., Howell, E.S., Kelley, M.S., Licandro, J., Mothé-Diniz, T., Fernández, Y. and Ziffer, J. (2010). Water ice and organics on the surface of the asteroid 24 Themis. *Nature*, 464(7293), 1320-1321.

- Campins, H., Hargrove, K., Pinilla-Alonso, N., Howell, E.S., Kelley, M.S., Licandro, J., Mothé-Diniz, T., Fernández, Y. and Ziffer, J. (2010). Water ice and organics on the surface of the asteroid 24 Themis. *Nature*, 464(7293), 1320-1321.
- Campins, H., Morbidelli, A., Tsiganis, K., de León, Licandro, J., Lauretta, D. (2010). The origin of Asteroid 101995 (1999 RQ36). *Ap. J. Letters*, Vol. 721, L53-L57.
- Cannon, K. M., Mustard, J. F., Parman, S. W., Sklute, E. C., Dyar, M. D., Cooper, R. F. (2017). Spectral properties of Martian and other planetary glasses and their detection in remotely sensed data. *Journal of Geophysical Research: Planets*, 122, 1-20.
- Castillo-Rogez, J. C., & Schmidt, B. E. (2010). Geophysical evolution of the Themis family parent body. *Geophysical Research Letters*, 37(10).
- Cellino, A., Bus, S. J., Doressoundiram, A., Lazzaro, D. (2002). Spectroscopic Properties of Asteroid Families. *Asteroids III*, Eds. W. Bottke, A. Cellino, P. Paolicchi, R. P. Binzel.
- Chambers, J. E. (2014). Giant planet formation with pebble accretion. *Icarus*, 233, 83-100.
- Chesley SR, Farnocchia D, Nolan MC, Vokrouhlický D, Chodas PW, Milani A, Spoto F, Rozitis B, Benner LA, Bottke WF, Busch MW. (2014). Orbit and bulk density of the OSIRIS-REx target Asteroid (101955) Bennu. *Icarus*, 235, 5-22.
- Chick, K. M., & Cassen, P. (1997). Thermal processing of interstellar dust grains in the primitive solar environment. *The Astrophysical Journal*, 477(1), 398.
- Chizmadia L. J., Brearley, A. J. (2008). Mineralogy, aqueous alteration, and primitive textural characteristics of fine-grained rims in the Y-791198 CM2 carbonaceous chondrite:

TEM observations and comparison to ALHA81002. *Geochimica et Cosmochimica Acta*, 72, 602-625.

Chizmadia, L. J. (2007). Reproduction of phyllosilicate textures in CM2 chondrites during experimental hydration of amorphous silicate smokes. *LPSC abstract 1005*.

Chizmadia, L. J., & Brearley, A. J. (2003). Mineralogy and textural characteristics of fine-grained rims in the Yamato 791198 CM2 carbonaceous chondrite: Constraints on the location of aqueous alteration. *LPSC abstract 1419*.

Chizmadia, L. J., & Nuth III, J. A. (2006). Kinetics of phyllosilicate formation in hydrated magnesiosilicate smokes. *Meteoritics and Planetary Science Supplement*, 41, 5166.

Choe, W. H., Huber, H., Rubin, A. E., Kallemeyn, G. W., Wasson, J. T. (2010). Compositions and taxonomy of 15 unusual carbonaceous chondrites. *Met. & Planet. Sc.*, Vol. 45, No. 4, 531-554.

Ciarniello M, De Sanctis MC, Ammannito E, Raponi A, Longobardo A, Palomba E, Carrozzo FG, Tosi F, Li JY, Schröder SE, Zambon F. (2017). Spectrophotometric properties of dwarf planet Ceres from the VIR spectrometer on board the Dawn mission. *Astronomy & Astrophysics*, 598, A130.

Clark, B. E., Binzel, R. P., Howell, E. S., Cloutis E. A., Ockert-Bell, M., Christensen, P., Barucci, M. A., DeMeo, F., Lauretta, D. S., Connolly Jr., H., Soderberg, A., Hergenrother, C., Lim, L., Emery, J., Mueller, M. (2011). Asteroid (101955) 1999 RQ36: Spectroscopy from 0.4 to 2.4- μm and meteorite analogs. *Icarus*, 216, 462-475.

Clark, B. E., Hapke, B., Pieters, C., & Britt, D. (2002). Asteroid space weathering and regolith evolution. *Asteroids III*, 585.

- Clark, B.E., Ziffer, J., Nesvorný, D., Campins, H., Rivkin, A.S., Hiroi, T., Barucci, M.A., Fulchignoni, M., Binzel, R.P., Fornasier, S. and DeMeo, F., (2010). Spectroscopy of B-type asteroids: Subgroups and meteorite analogs. *Journal of Geophysical Research: Planets*, 115(E6).
- Clark, R. N. (1999). Spectroscopy of rocks and minerals, and principles of spectroscopy. *Manual of remote sensing*, 3, 3-58.
- Clark, R. N. (1999). Spectroscopy of Rocks and Minerals, and Principles of Spectroscopy. *In Remote Sensing for the Earth Sciences Volume 3: Manual of Remote Sensing (eds. Rencz, A. N. Ryerson, R. A.) John Wiley & Sons, Inc. pp. 3-58.*
- Clark, R. N., King, T. V., Klejwa, M., Swayze, G. A., & Vergo, N. (1990). High spectral resolution reflectance spectroscopy of minerals. *Journal of Geophysical Research: Solid Earth*, 95(B8), 12653-12680.
- Cloutis, E. A., Hiroi, T., Gaffey, M. J., Alexander, C. O. D., & Mann, P. (2011a). Spectral reflectance properties of carbonaceous chondrites: 1. CI chondrites. *Icarus*, 212(1), 180-209.
- Cloutis, E. A., Hudon, P., Hiroi, T., & Gaffey, M. J. (2012a). Spectral reflectance properties of carbonaceous chondrites: 3. CR chondrites. *Icarus*, 217(1), 389-407.
- Cloutis, E. A., Hudon, P., Hiroi, T., Gaffey, M. J., & Mann, P. (2011b). Spectral reflectance properties of carbonaceous chondrites: 2. CM chondrites. *Icarus*, 216(1), 309-346.
- Cloutis, E. A., Hudon, P., Hiroi, T., Gaffey, M. J., Mann, P. (2012). Spectral reflectance properties of carbonaceous chondrites – 5: CO chondrites. *Icarus*, Vol. 220, 466-486.

- Cloutis, E. A., Hudon, P., Hiroi, T., Gaffey, M. J., Mann, P., & Bell, J. F. (2012b). Spectral reflectance properties of carbonaceous chondrites: 6. CV chondrites. *Icarus*, 221(1), 328-358.
- Cohen, B. A., Swindle, T. D., & Kring, D. A. (2000). Support for the lunar cataclysm hypothesis from lunar meteorite impact melt ages. *Science*, 290(5497), 1754-1756.
- Cohen, M., Witteborn, F. C., Roush, T., Bregman, J., & Wooden, D. (1998). Spectral irradiance calibration in the infrared. VIII. 5-14 micron spectroscopy of the asteroids Ceres, Vesta, and Pallas. *The Astronomical Journal*, 115(4), 1671.
- Combe JP, Raponi A, De Sanctis MC, Tosi F, Ammannito E, Byrne S, Giacomo Carrozzo F, Hayne PO, Hughson KH, Johnson KE, Landis ME (2016) Exposed H2O-rich areas detected on Ceres with Dawn Visible and Infrared Mapping Spectrometer. In *AAS/Division for Planetary Sciences Meeting Abstracts* (Vol. 48).
- Connolly, H. C., & Jones, R. H. . (2016). Chondrules: The Canonical and Non-canonical View. . *Journal of Geophysical Research: Planets*.
- Cooper, B. L., Salisbury, J. W., Killen, R. M., & Potter, A. E. (2002). Mid-infrared spectral features of rocks and their powders. *Journal of Geophysical Research: Planets*, 107(E4).
- Crisp, J., Kahle, A. B., Abbott, E. A. (1990). Thermal infrared spectral character of Hawaiian basaltic glasses. *Journal of Geophysical Research*, Vol. 95, 21657-216999.
- Cronin, J. R., & Chang, S. (1993). Organic matter in meteorites: Molecular and isotopic analyses of the Murchison meteorite. In *The chemistry of life's origins* (pp. 209-258). Springer Netherlands.

- Cushing, M. C., Vacca, W. D., & Rayner, J. T. (2004). Spextool: a spectral extraction package for SpeX, a 0.8-5.5 micron cross-dispersed spectrograph. *Publications of the Astronomical Society of the Pacific*, 116(818), 362.
- Cyr, K. E., Sears, W. D., & Lunine, J. I. (1998). Distribution and evolution of water ice in the solar nebula: Implications for solar system body formation. *Icarus*, 135(2), 537-548.
- Davidson, J., Nittler, L. R., Alexander, C. M. O'D., Stroud, R. M. (2014). Petrography of very primitive CO₃ chondrites: Dominion Range 08006, Miller Range 07687, and four others. *LPSC abstract 1384*.
- Davidson, J., Nittler, L. R., Stroud, R. M., Takigawa, A., Dregorio, B. T., Alexander, C. M. O'D., Kilcoyne, A. L. D., Cody, G. D. (2015). Organic matter in the unique carbonaceous chondrite Miller Range 07687: A coordinated in situ nano-SIMS, FIB-TEM, and XANES study. *LPSC abstract 1609*.
- Davidsson, B.J.R., Sierks, H., Guettler, C., Marzari, F., Pajola, M., Rickman, H., A'Hearn, M.F., Auger, A.T., El-Maarry, M.R., Fornasier, S. and Gutiérrez, P.J., (2016). The primordial nucleus of comet 67P/Churyumov-Gerasimenko. *Astronomy & Astrophysics*, 592, A63.
- De Angelis, S., Manzari, P., De Sanctis, M. C., Ammannito, E., & Di Iorio, T. (2016). VIS-IR study of brucite–clay–carbonate mixtures: Implications for Ceres surface composition. *Icarus*, 280, 315-327.
- de León, J., Campins, H., Tsiganis, K., Morbidelli, A., & Licandro, J. (2010). Origin of the near-Earth asteroid Phaethon and the Geminids meteor shower. *Astronomy & Astrophysics*, 513, A26.

- de Leuw, S., Rubin, A. E., Wasson, J. T. (2010). Carbonates in CM chondrites: Complex formational histories and comparison to carbonates in CI chondrites. . *Met. & Plan. Sci.*, Vol. 45, Nr. 4, 513-530.
- De Pater, I., & Lissauer, J. J. (2015). *Planetary sciences*. Cambridge University Press.
- De Sanctis, M.C., Ammannito, E., Raponi, A., Marchi, S., McCord, T.B., McSween, H.Y., Capaccioni, F., Capria, M.T., Carrozzo, F.G., Ciarniello, M. and Longobardo, A.,. (2015). Ammoniated phyllosilicates with a likely outer solar system origin on (1) Ceres. *Nature*, 528(7581), 241-244.
- Delbó, M., & Harris, A. W. (2002). Physical properties of near-Earth asteroids from thermal infrared observations and thermal modeling. *Meteoritics & Planetary Science*, 37(12), 1929-1936.
- Delbo, M., Mueller, M., Emery, J. P., Rozitis, B., & Capria, M. T. (2015). Asteroid thermophysical modeling. *Asteroids IV*, 1, 107.
- DeMeo, F. E., Alexander, C. M. O. D., Walsh, K. J., Chapman, C. R., & Binzel, R. P. (2015). The Compositional Structure of the Asteroid Belt. *Asteroids IV*, 1, 13.
- DeMeo, F. E., Binzel, R. P., Slivan, S. M., & Bus, S. J. (2009). An extension of the Bus asteroid taxonomy into the near-infrared. *Icarus*, 202(1), 160-180.
- DeMeo, F. E., Binzel, R. P., Slivan, S. M., & Bus, S. J. (2009). An extension of the Bus asteroid taxonomy into the near-infrared. *Icarus*, 202(1), 160-180.
- Desch, S. J., Connolly, Jr., H. C. (2002). A model of the thermal processing of particles in the solar nebula shocks: Application to cooling rates of chondrules. *Meteoritics and Planetary Science*, Vol. 37, 183-207.

- Dodson-Robinson, S. E., Willacy, K., Bodenheimer, P., Turner, N. J., & Beichman, C. A. (2009). Ice lines, planetesimal composition and solid surface density in the solar nebula. *Icarus*, 200(2), 672-693.
- Dominik, C., Blum, J., Cuzzi, J., & Wurm, G. (2006). Growth of dust as the initial step toward planet formation. *Stars and Protoplanets V*
- Donaldson Hanna KL, Schrader DL, Bowles NE, Clark BE, Cloutis EA, Connolly Jr HC, Hamilton VE, Keller LP, Lauretta DS, Lim LF, McCoy TJ. (2017). Spectral Characterization of Analog Samples in Anticipation of OSIRIS-REx's Arrival at Bennu. ACM, abstract
- Dotto, E., Barucci, M. A., Müller, T. G., Brucato, J. R., Fulchignoni, M., Mennella, V., & Colangeli, L. (2002). ISO observations of low and moderate albedo asteroids-PHT-P and PHT-S results. *Astronomy & Astrophysics*, 393(3), 1065-1072.
- Dotto, E., Barucci, M.A., Crovisier, J., Doressoundiram, A., Encrenaz, T., Fulchignoni, M., Knacke, R., Lellouch, E., Morris, P.W., Müller, T.G. and Owen, T. (1999). ISO observations of asteroids. *In The Universe as Seen by ISO (Vol. 427, p. 165)*.
- Duke, D. A., Stephens, J. D. (1964). Infrared investigation of the olivine group minerals. *Am. Min. Vol. 49, 1388-1406*.
- Dyar, M. D., Delaney, J. S., Sutton, S. R., Schaefer, M. W. (1998). Fe³⁺ distribution in oxidized olivine: a cynchrotron micro-XANES study. *American Mineralogist*, 83, 1361-1365.
- Dyar, M. D., Sklute, E. C., Menzies, O. N., Bland, P. A., Lindsley, D., Glotch, T., Lane, M. D., Schaffer, M. W., Wopenka, B., Klima, R., Bishop, J. L., Hiroi, T., Pieters, C.,

- Sunshine, J. (2009). Spectroscopic characteristics of synthetic olivine: An integrated multi-wavelength and multi-technique approach. *American Mineralogist*, Vol. 94, 883-898.
- Dyar, M.D., Sklute, E.C., Menzies, O.N., Bland, P.A., Lindsley, D., Glotch, T., Lane, M.D., Schaefer, M.W., Wopenka, B., Klima, R. and Bishop, J.L. (2009). Spectroscopic characteristics of synthetic olivine: An integrated multi-wavelength and multi-technique approach. *American Mineralogist*, 94(7), 883-898.
- Ebel, D. S., Brunner, C., Konrad, K., Leftwich, K., Erb, I., Lu, M., Rodriguez, H., Crapster-Pregnot, E. J., Friedrich, J. M., Weisberg, M. K. (2016). Abundance, major element composition and size of component and matrix in CV, CO, and Acfer 094 chondrites. *Geochimica et Cosmochimica Acta*, 172, 322-356.
- Emery, J. P., Cruikshank, D. P., & Van Cleve, J. (2006). Thermal emission spectroscopy (5.2–38 μm) of three Trojan asteroids with the Spitzer Space Telescope: Detection of fine-grained silicates. *Icarus*, 182(2), 496-512.
- Emery, J. P., Fernández, Kelley, M. S. P., Warden (née Crane), K. T., Hergenrother, C., Lauretta, D. S., Drake, M. J., Campins, H. Ziffer, J. (2014). Thermal infrared observations and thermophysical characterization of OSIRIS-REx target asteroid (101955) Bennu. *Icarus*, 234, 17-35.
- Estep-Barnes, P. A. (1977). Infrared Spectroscopy. In *Physical Methods in Determinative Mineralogy, 2nd Edition* (eds., Zussman, J).
- Farmer, V. C., & Palmieri, F. (1977). The characterization of soil minerals by infrared spectroscopy. In *Soil components* (pp. 573-670). Springer Berlin Heidelberg.

- Fegley Jr, B. (2000). Kinetics of gas-grain reactions in the solar nebula. In *From Dust to Terrestrial Planets* (pp. 177-200). Springer Netherlands.
- Feierberg, M. A., Lebofsky, L. A., & Larson, H. P. (1981). Spectroscopic evidence for aqueous alteration products on the surfaces of low-albedo asteroids. *Geochimica et Cosmochimica Acta*, 45(6), 971-981.
- Florczak, M., Lazzaro, D., Mothé-Diniz, T., Angeli, C. A., & Betzler, A. S. (1999). A spectroscopic study of the Themis family. *Astronomy and Astrophysics Supplement Series*, 134(3), 463-471.
- Fornasier, S., Lantz, C., Barucci, M. A., & Lazzarin, M. (2014). Aqueous alteration on main belt primitive asteroids: Results from visible spectroscopy. *Icarus*, 233, 163-178.
- Fornasier, S., Lazzarin, M., Barbieri, C., & Barucci, M. A. (1999). Spectroscopic comparison of aqueous altered asteroids with CM2 carbonaceous chondrite meteorites. *Astronomy and Astrophysics Supplement Series*, 135(1), 65-73.
- Fornasier, S., Lazzarin, M., Barbieri, C., Barucci, M. A.,. (1999). Spectroscopic comparison of aqueously altered asteroids with CM2 carbonaceous chondrite meteorites. *Astron. & Astrophys. Suppl. Ser., Vol. 135*, 65-73. .
- Fowler, J. W., & Chillemi, J. R. (1992). IRAS asteroid data processing. . *The IRAS Minor Planet Survey*, 17, 43.
- Fox, K., Williams, I. P., & Hughes, D. W. (1983). The rate profile of the Geminid meteor shower. *Monthly Notices of the Royal Astronomical Society*, 205(4), 1155-1169.
- Fu, R. R., Elkins-Tanton, L. T., (2014). The fate of magmas in planetesimals and the retention of primitive chondritic crusts. *Earth and Planet. Sci. Let. Vol. 390*, 128-137.

- Fujiya, W., Sugiura, N., Sano, Y., & Hiyagon, H. (2013). Mn–Cr ages of dolomites in CI chondrites and the Tagish Lake ungrouped carbonaceous chondrite. *Earth and Planetary Science Letters*, 362, 130-142.
- Gaffey, M. J. (1976). Spectral reflectance characteristics of the meteorite classes. *Journal of Geophysical Research*, Vol. 81, No. 5, 905-920.
- Gaffey, M. J. (1997). Surface Lithologic heterogeneity of asteroid 4 Vesta. *Icarus*, 127, 130-157.
- Gaffey, S. J., McFadden, L. A., Nash, D., Pieters, C. M., (1993). Ultraviolet, Visible and Near-Infrared Reflectance Spectroscopy: Laboratory Spectra of Geologic Materials. in *Remote Geochemical Analysis: Elemental and Mineralogical Composition*. Eds. Pieters, C. M., Englert, P. A. J., Cambridge University Press. .
- Giuranna, M., Roush, T. L., Duxbury, T., Hogan, R. C., Carli, C., Geminale, A., & Formisano, V. (2011). Compositional interpretation of PFS/MEx and TES/MGS thermal infrared spectra of Phobos. *Planetary and Space Science*, 59(13), 1308-1325.
- Gradie, J., & Tedesco, E. (1982). Compositional structure of the asteroid belt. *Science*, 216(4553), 1405-1407.
- Greenwood, R. C., Franchi, I. A., Alexander, C. M. O'D., Howard, K. T. (2016). Continuing the search for the most primitive CO chondrites: the oxygen isotope perspective. *LPSC abstract 2206*.
- Greshake, A. (1997). The primitive matrix components of the unique carbonaceous chondrite Acfer 094: A TEM study. *Geochimica et Cosmochimica Acta*, Vol. 61, No. 2, 437-452.

- Grimm, R. E., & McSween, H. Y. . (1993). Heliocentric zoning of the asteroid belt by aluminum-26 heating. *LPSC, abstract 577*. .
- Grimm, R. E., & McSween, H. Y. (1989). Water and the thermal evolution of carbonaceous chondrite parent bodies. *Icarus*, 82(2), 244-280.
- Grossman, L., & Larimer, J. W. (1974). Early chemical history of the solar system. *Reviews of Geophysics*, 12(1), 71-101.
- Grossman, J. N., Brearley, J. (2005). The onset of metamorphism in ordinary and carbonaceous chondrites. *Meteoritics and Planetary Science*, 40, Nr. 1, 87-122.
- Grossman, J. N., Rubin, A. E. (2006). Dominion Range 03238: A possible missing link in the metamorphic sequence of CO3 chondrites. *LPSC abstract 1383*.
- Hackwell, J. A., D. W. Warren, M. Chatelain, Y. Dotan, P. Li, D. K. Lynch, D. Mabry, R. W. Russell, and R. Young (1990) "A Low Resolution Array Spectrograph for the 2.9-13.5 mm Spectral Region" Proc. SPIE Conference 1235 on *Instrumentation in Astronomy VII*, 1235, 171-180.
- Hallenbeck, S. L., Nuth III, J. A., Daukantas, P. L. (1998). Mid-infrared spectral evolution of amorphous magnesium silicate smokes annealed in vacuum: Comparison to cometary spectra. . *Icarus*, 131, 198-209.
- Hallenbeck, S. L., Nuth III, J. A., Nelson, R. N. (2000). Evolving optical properties of annealing silicate grains: From amorphous condensate to crystalline mineral. *The Astrophysical Journal*, 535, 247-255.

- Hanowski, N. P., & Brearley, A. J. . (2001). Aqueous alteration of chondrules in the CM carbonaceous chondrite, Allan Hills 81002: Implications for parent body alteration. . *Geochimica et Cosmochimica Acta*, 65(3), 495-518.
- Hargrove, K. D., Emery, J. P., Campins, H., & Kelley, M. S. (2015). Asteroid (90) Antiope: Another icy member of the Themis family? . *Icarus*, 254, 150-156.
- Hargrove, K. D., Kelley, M. S., Campins, H., Licandro, J., & Emery, J. (2012). Asteroids (65) Cybele, (107) Camilla and (121) Hermione: Infrared spectral diversity among the Cybeles. . *Icarus*, 221(1), 453-455.
- Hargrove, K. D., Kelley, M. S., Campins, H., Licandro, J., Emery, J.,. (2012). Asteroids (65) Cybele, (107) Camilla and (121) Hermione: Infrared spectral diversity among the Cybeles. *Icarus*, Vol. 221, 453-455.
- Harris, A. W. (1998). A Thermal Model for Near-Earth Asteroids. *Icarus*, Vol. 131, 291-301.
- Harvey, R. P., & Cassidy, W. A. (1989). A statistical comparison of Antarctic finds and modern falls: Mass frequency distributions and relative abundance by type. *Meteoritics*, 24(1), 9-14.
- Hasegawa, S., Müller, T. G., Kawakami, K., Kasuga, T., Wada, T., Ita, Y., Takato, N., Terada, H., Fujiyoshi, T., Abe, M.,. (2008). Albedo, size, surface characteristics of Hayabusa-2 sample return target 162173 1999 JU3 from Akari and Subaru observations. *Publ. Astron. Soc. Japan*, Vol. 60, S399-S405.
- Hayashi, C., Hoshi, R., & Sugimoto, D. (1981). *Progress Theoret. Phys. Suppl*, 70, 35.

Henderson, B. G., Lucey, P. G., & Jakosky, B. M. (1996). New laboratory measurements of mid-IR emission spectra of simulated planetary surfaces. *Journal of Geophysical Research: Planets*, 101(E6), 14969-14975.

Hiroi, T., Zolensky, M. E., Pieters, C. M., Lipschutz, M. E., (1996). Thermal metamorphism of the C, G, B, and F asteroids seen from the 0.7 μm , 3 μm , and UV absorption strengths in comparison with carbonaceous chondrites. *Met. & Planet. Sci.*, Vol. 31, 321-327.

Horgan, B. H. N., Cloutis, E. A., Mann, P., Bell III, J. F. (2016). Near-infrared spectra of ferrous mineral mixtures and methods for identification in planetary surface spectra. *Icarus*, Vol. 234, 132-154.

Houck, J.R., Roellig, T.L., Van Cleve, J., Forrest, W.J., Herter, T., Lawrence, C.R., Matthews, K., Reitsema, H.J., Soifer, B.T., Watson, D.M. and Weedman, D., (2004). The Infrared Spectrograph*(IRS) on the Spitzer Space Telescope. *The Astrophysical Journal Supplement Series*, 154(1), 18.

Howard, K. T., Alexander, C. M. O'D. (2013b). A new classification scheme for aqueously altered carbonaceous chondrites based on total phyllosilicate abundance. *Lunar & Planet. Sci. abstract #2598*.

Howard, K. T., Alexander, C. M. O'D., Dyl, K. A. (2014). PSD-XRD modal mineralogy of type 3.00 chondrites: initial asteroidal water mass fractions and implications for CM chondrites. *LPSC abstract 1830*.

Howard, K. T., Alexander, C. O. D., Schrader, D. L., & Dyl, K. A. (2015). Classification of hydrous meteorites (CR, CM and C2 ungrouped) by phyllosilicate fraction: PSD-XRD

modal mineralogy and planetesimal environments. *Geochimica et Cosmochimica Acta*, 149, 206-222.

Howard, K. T., Benedix, G. K., Bland, P. A., & Cressey, G. (2009). Modal mineralogy of CM2 chondrites by X-ray diffraction (PSD-XRD). Part 1: Total phyllosilicate abundance and the degree of aqueous alteration. *Geochimica et Cosmochimica Acta*, 73(15), 457.

Howard, K. T., Benedix, G. K., Bland, P. A., & Cressey, G. (2010). Modal mineralogy of CV3 chondrites by X-ray diffraction (PSD-XRD). *Geochimica et Cosmochimica Acta*, 74(17), 5084-5097.

Howard, K. T., Benedix, G. K., Bland, P. A., & Cressey, G. (2011). Modal mineralogy of CM chondrites by X-ray diffraction (PSD-XRD): Part 2. Degree, nature and settings of aqueous alteration. . *Geochimica et Cosmochimica Acta*, 75(10), 2735-2751.

Howard, K. T., Benedix, G. K., Bland, P. A., Gibson, J., Greenwood, R. C., Franchi, I. A., Cressey, G. (2013a). Non-progressive aqueous alterations of CM carbonaceous chondrites: the perspective of modal mineralogy and bulk O-isotopes. *LPSC abstract #2520*.

Howard, K. T., Davidson, J., Alexander, C. M. O'D., Abreu, N. M. (2015a). The glue that holds worlds together: abundance, origin and significance of amorphous Fe, Mg silicate in carbonaceous chondrites. *LPSC abstract 2244*.

Howell, E. S., Rivkin, A. S., Vilas, F., Magri, C., Nolan, M C., Vervack, R., J., Jr., Fernandez, Y. R. (2011). Hydrated silicates on main belt asteroids: Correlation of the 0.7- and 3 micron absorption bands. *EPSC abstract*.

Hsieh, H. H., & Jewitt, D. (2006). A population of comets in the main asteroid belt. *Science*, 312(5773), 561-563.

- Hunt, G. R. (1977). Spectral signatures of particulate minerals in the visible and near infrared. . *Geophysics*, 42(3), 501-513.
- Hunt, G. R., & Logan, L. M. (1972). Variation of single particle mid-infrared emission spectrum with particle size. *Applied Optics*, 11(1), 142-147.
- Hunt, G. R., & Vincent, R. K. (1968). The behavior of spectral features in the infrared emission from particulate surfaces of various grain sizes. *Journal of Geophysical Research*, 73(18), 6039-6046.
- Huss, G. R., Rubin, A. E., & Grossman, J. N. (2006). Thermal metamorphism in chondrites. . *Meteorites and the early solar system II*, 943, 567-586.
- Jewitt, D., & Li, J. (2010). Activity in Geminid Parent (3200) Phaethon. *The Astronomical Journal*, 140(5), 1519.
- Johnson, T. V., Fanale, F. P. (1973). Optical properties of carbonaceous chondrites and their relationship to asteroids. *Journal of Geophysical Research*, Vol. 78, No. 35, 8507-8518.
- Johansen, A., Blum, J., Tanaka, H., Ormel, C., Bizzarro, M., & Rickman, H. (2014). The multifaceted planetesimal formation process. *Protostars and Planets VI*
- Jones, R. H., Lee, T. Y. P. H. O. O. N., Connolly Jr, H. C., Love, S. G., & Shang, H. S. I. E. N. . (2000). Formation of chondrules and CAIs: Theory vs. observation. *Protostars and planets IV*, 1, 927.
- Jones, R. H., Lee, T., Connolly Jr, H. C., Love, S. G., & Shang, H. (2000). Formation of chondrules and CAIs: Theory vs. observation. *Protostars and planets IV*, 1, 927.

- Kallemeyn, G. W., & Wasson, J. T. (1982). The compositional classification of chondrites: III. Ungrouped carbonaceous chondrites. *Geochimica et Cosmochimica Acta*, 46(11), 2217-2228.
- Keil, K., Stoeffler, D., Love, S. G., & Scott, E. R. D. (1997). Constraints on the role of impact heating and melting in asteroids. *Meteoritics & Planetary Science*, 32(3), 349-363.
- Keller, H. U. (1989). Comets: Dirty snowballs or icy dirtballs. In *Physics and Mechanics of Cometary Materials (Vol. 302)*.
- Keller, L. P., Messenger, S. (2011). On the origins of GEMS grains. *Geochimica et Cosmochimica Acta*, 75, 5336-5365.
- Kelley, M. S., Woodward, C. E., Gehrz, R. D., Reach, W. T., & Harker, D. E. (2017). Mid-infrared spectra of comet nuclei. *Icarus*, 284, 344-358.
- Kemper, F., Vriend, W. J., Tielens, A. (2004). The absence of crystalline silicates in the diffused interstellar medium. *The Astrophysical Journal*, 609, 827-837.
- Kemper, F., Vriend, W. J., Tielens, A. G. G. M. (2005). Erratum: "The absence of crystalline silicates in the diffuse interstellar medium. *The Astrophysical Journal*, 633, 534.
- Kimura, M., Grossman, J. N., & Weisberg, M. K. . (2008). Fe-Ni metal in primitive chondrites: Indicators of classification and metamorphic conditions for ordinary and CO chondrites. . *Meteoritics & Planetary Science*, 43(7), 1161-1177.
- King, A. J., Schofield, P. F., Howard, K. T., Russell, S. S. (2014). Modal Mineralogy of CI and CI-like chondrites by position sensitive detector X-ray diffraction. *Lunar and Planet. Sci. abstract #1861*.

- King, P. L., McMillan, P. F., Moore, G. M. (2004). Infrared spectroscopy of silicate glasses with application to natural systems. *In Infrared Spectroscopy in Geochemistry, Exploration Geochemistry and Remote Sensing. (Eds. King, P.L., Ramsey, M.S., & Swayze, G.A.,) Mineral. Assoc. Canada, Short Course Series, vol. 33, 93-133.*
- King, T. V. V., Ridley, W. I. (1987). Relation of the spectroscopic reflectance of olivine to mineral chemistry and some remote sensing implications. *Journal of Geophysical Research, 92, No. B11, 11457-11469.*
- Krot, A. N., Hutcheon, I. D., Brearley, A. J., Pravdivsteva, O. V., Petaev, M. I. (2005) Timescales and settings for alteration of chondritic meteorites. *Meteorites and the early solar system II, 943, 525-554.*
- Krot, A. N., Scott, E. R., & Zolensky, M. E. (1995). Mineralogical and chemical modification of components in CV3 chondrites: Nebular or asteroidal processing? *Meteoritics, 30(6), 748-775.*
- Krot, A. N., Scott, E. R., & Zolensky, M. E. (1997). Origin of fayalitic olivine rims and lath-shaped matrix olivine in the CV3 chondrite Allende and its dark inclusions. *Meteoritics & Planetary Science, 32(1), 31-49.*
- Küppers M, O'rourke L, Bockelée-Morvan D, Zakharov V, Lee S, von Allmen P, Carry B, Teyssier D, Marston A, Müller T, Crovisier J. (2014). Localized sources of water vapour on the dwarf planet (1) Ceres. *Nature, 505(7484), 525.*
- Kurahashi, E., Kita, N. T., Nagahara, H., Morishita, Y. (2008). 26Al-26Mg systematics of chondrules in a primitive CO chondrite. *Geochimica et Cosmochimica Acta, 72, 15, 3865-3882.*

- Landsman, Z. A., Licandro, J., Campins, H., Ziffer, J., de Prá, M., & Cruikshank, D. P. . (2016). The Veritas and Themis asteroid families: 5–14 μm spectra with the Spitzer Space Telescope. *Icarus*, 269, 62-74.
- Lantz, C., Brunetto, R., Barucci, M.A., Dartois, E., Duprat, J., Engrand, C., Godard, M., Ledu, D. and Quirico, E.,. (2015). Ion irradiation of the Murchison meteorite: Visible to mid-infrared spectroscopic results. *Astronomy & Astrophysics*, 577, A41.
- Larson, H. P., Feierberg, M. A., & Lebofsky, L. A. . (1983). The composition of asteroid 2 Pallas and its relation to primitive meteorites. *Icarus*, 56(3), 398-408.
- Lauretta, D. S., Hua, X., & Buseck, P. R. (2000). Mineralogy of fine-grained rims in the ALH 81002 CM chondrite. *Geochimica et Cosmochimica Acta*, 64(19), 3263-3273.
- Lauretta, D. S., the OSIRIS-REx Team. (2012). An overview of the OSIRIS-REx asteroid sample return mission. *LPSC abstract #2491*.
- Lazzaro, D., Barucci, M. A., Perna, D., Jasmim, F. L., Yoshikawa, M., & Carvano, J. M. F. (2013). Rotational spectra of (162173) 1999 JU3, the target of the Hayabusa2 mission. *Astronomy & Astrophysics*, 549, L2.
- Le Guillou, C., Brearley, A. (2014). Relationships between organics, water and early stages of aqueous alteration in the pristine CR3.0 chondrite, MET 00426. *Geochimica et Cosmochimica Acta*, 131, 344-367.
- Lebofsky, L. A. (1980). Infrared reflectance spectra of asteroids-A search for water of hydration. *The Astronomical Journal*, 85, 573-585.

- Leroux H., Cuvillier P., Zanda B. and Hewins R. H. (2015). GEMS-like material in the matrix of the Paris meteorite and the early stages of alteration of CM chondrites. *Geochimica. Cosmochimica. Acta* 170, 247-265.
- Levison, H. F., Kretke, K. A., & Duncan, M. J. (2015). Growing the gas-giant planets by the gradual accumulation of pebbles. *Nature*, 524(7565), 322-324.
- Licandro, J., Campins, H., Kelley, M., Hargrove, K., Pinilla-Alonso, N., Cruikshank, D., Rivkin, A.S. and Emery, J.,. (2011). (65) Cybele: detection of small silicate grains, water-ice, and organics. *Astronomy & Astrophysics*, 525, A34.
- Licandro, J., Campins, H., Mothé-Diniz, T., Pinilla-Alonso, N., & De León, J. (2007). The nature of comet-asteroid transition object (3200) Phaethon. *Astronomy & Astrophysics*, 461(2), 751-757.
- Licandro, J., Hargrove, K., Kelley, M., Campins, H., Ziffer, J., Alí-Lagoa, V., Fernández, Y. and Rivkin, A.,. (2012). 5–14 μm Spitzer spectra of Themis family asteroids. *Astronomy & Astrophysics*, 537, A73.
- Logan, L. M., Hunt, G. R., Salisbury, J. W., & Balsamo, S. R. . (1973). Compositional implications of Christiansen frequency maximums for infrared remote sensing applications. *Journal of Geophysical Research*, 78(23), 4983-5003.
- Lunine, J. I. (2006). Origin of water ice in the solar system. *Meteorites and the early solar system II*, 309-319.
- Lynch, D.K., Russell, R.W., Rudy, R.J., Mazuk, S., Venturini, C.C., Hammel, H.B., Sykes, M.V., Puetter, R.C. and Perry, R.B.,. (2007). Infrared Spectra of Deimos (1-13 μm) and Phobos (3-13 μm). *The Astronomical Journal*, 134(4), 1459.

Marchis, F., Enriquez, J. E., Emery, J. P., Mueller, M., Baek, M., Pollock, J., Assafin, M., Vieira Martins, R., Berthier, J., Vachier, F., Cruikshank, D. P., Lim, L. F., Reichart, D. E., Ivarsen, K. M. (2012). Multiple asteroid systems: Dimensions and thermal properties from Spitzer Space Telescope and ground-based observations. *Icarus*, 221, 1130-1161.

Marchis, F., Vachier, F., Ďurech, J., Enriquez, J. E., Harris, A. W., Dalba, P. A., Berthier, J., Emery, J. P., Bouy, H., Melbourne, J., Stockton, A., Fassnacht, C. D., Dupuy, T. J., Strajnic, J. (2013). Characteristics and large bulk density of the C-type main-belt triple asteroid (93) Minerva. *Icarus*, 224, 178-191.

Marsset, M., Vernazza, P., Birlan, M., DeMeo, F., Binzel, R.P., Dumas, C., Milli, J. and Popescu, M., (2016). Compositional characterisation of the Themis family. *Astronomy & Astrophysics*, 586, A15.

McAdam, M. M., Sunshine, J. M., Howard, K. T., & McCoy, T. M. . (2015). Aqueous alteration on asteroids: Linking the mineralogy and spectroscopy of CM and CI chondrites. *Icarus*, 245, 320-332.

McAdam, M. M., Sunshine, J. M., Howard, K. T., McCoy, T. J., Alexander, C. M. O'D., Davidson, J. (2015). Aqueous alteration in CR meteorites as seen with VIS/NIR and MIR spectroscopy. *LPSC abstract 2540*.

McAdam, M. M., Sunshine, J. M., Kelley, M. S. T., (2013). Composition and degree of alteration of dark asteroids. *DPS abstract*.

McAdam, M. M., Sunshine, J. M., Kelley, M. S. T., (2014). Alteration on asteroids: Insights from CM/CI meteorite mineralogy and midwave infrared spectroscopy. *ACM abstract* .

- McSween Jr., H. Y., Ghosh, A., Grimm, R. E., Wilson, L., Young, E. D. (2002). Thermal evolution models of asteroids. in *Asteroids III* pp. 559-571. Eds. Bottke Jr., W. F., Cellino, A., Paolicchi, P., Binzel, R. P. University of Arizona Press.
- McSween, H. Y. (1977). Carbonaceous chondrites of the Ornans type: A metamorphic sequence. . *Geochimica et Cosmochimica Acta*, 41(4), 477-491.
- McSween, H. Y. (1987). Aqueous alteration in carbonaceous chondrites: Mass balance constraints on matrix mineralogy. *Geochimica et Cosmochimica Acta*, 51(9), 2469-2477.
- McSween, H. Y. (1979). Alteration in CM carbonaceous chondrites inferred from modal and chemical variations in matrix. *Geochimica et Cosmochimica Acta*, 43(11), 1761-1767-1765-1770.
- McSween, H. Y., Castillo-Rogez, J., Emery, J. P., & De Sanctis, M. C. (2016). Rationalizing the Composition and Alteration of Ceres. *LPSC abstract 1258*.
- Messenger, S., Nakamura-Messenger, K., Keller, L. P., Clemett, S. J. (2015). Report: Pristine stratospheric collection of interplanetary dust on an oil-free polyurethane foam substrate. *Meteoritics and Planetary Science*, 50, N. 8, 1468-1485.
- Messenger, S., Sandford, S., & Brownlee, D. (2006). The population of starting materials available for solar system construction. *Meteorites and the early solar system II*, 1, 187-208.
- Metzler, K., Bischoff, A., & Stöffler, D. (1992). Accretionary dust mantles in CM chondrites: Evidence for solar nebula processes. *Geochimica et Cosmochimica Acta*, 56(7), 2873-2897.

- Michalski, J. R., Kraft, M. D., Sharp, T. G., Williams, L. B., Christensen, P. R. (2005). Mineralogical constraints on the high-silica Martian surface component observed by TES. *Icarus*, Vol. 174, 161-177.
- Milliken, R. E., & Rivkin, A. S. (2009). Brucite and carbonate assemblages from altered olivine-rich materials on Ceres. *Nature Geoscience*, 2(4), 258-261.
- Min, M., Dullemond, C. P., Kama, M., & Dominik, C. (2011). The thermal structure and the location of the snow line in the protosolar nebula: Axisymmetric models with full 3-D radiative transfer. *Icarus*, 212(1), 416-426.
- Morbidelli, A., & Nesvorný, D. (1999). Numerous weak resonances drive asteroids toward terrestrial planets orbits. *Icarus*, 139(2), 295-308.
- Morbidelli, A., Brassier, R., Gomes, R., Levison, H. F., & Tsiganis, K. . (2010). Evidence from the asteroid belt for a violent past evolution of Jupiter's orbit. . *The Astronomical Journal*, 140(5), 1391.
- Morlok, A., Stojic, A., Weber, I., Hiesinger, H., Zanetti, M., Helbert, J. (2016). Mid-infrared bi-directional reflectance spectroscopy of impact melt glasses and tektites. *Icarus*, Vol. 278, 162-179.
- Moroz, L. V., Basilevsky, A. T., Hiroi, T., Rout, S. S., Baither, D., van der Bogert, C. H., Yakovlev, O. I., Fisenko, A. V., Semjonova, L. F., Rusakov, V. S., Khramov, D. A., Zinovieva, N. G., Arnold, G., Pieters, C. M. (2009). Spectral properties of simulated impact glasses produced from martian soil analog JSC Mars-1. *Icarus*, Vol. 202, 336-353.

- Morris, R. V., Le, L., Lane, M. D., Golden, D. C., Shelfer, T. D., Lofgren, G. E., Christensen, P. R. (2000). Multidisciplinary study of synthetic Mars global average soil glass. *LPSC abstract 1611*.
- Moyano-Camero, C. E., Trigo-Rodríguez, J. M., Llorca, J., Fornasier, S., Barucci, M. A., & Rimola, A. (2016). A plausible link between the asteroid 21 Lutetia and CH carbonaceous chondrites. *Meteoritics & Planetary Science*, *51*(10), 1795-1812.
- Mustard, J. F. . (2017). From planets to crops and back: Remote sensing makes sense. *Journal of Geophysical Research: Planets*.
- Mustard, J. F., & Hays, J. E. (1997). Effects of hyperfine particles on reflectance spectra from 0.3 to 25 μm . *Icarus*, *125*(1), 145-163.
- Mysen, B., Richet, P. (2005). Silicate Glasses and Melts: Properties and Structure. Elsevier Developments in Geochemistry 10.
- Nakamura, T. (2005). Post-hydration thermal metamorphism of carbonaceous chondrites. *Journal of Mineralogical and Petrological Sciences*, *100*(6), 260-272.
- Nash, D. B., Salisbury, J. W., (1991). Infrared reflectance spectra (2.2-15 μm) of plagioclase feldspars. *Geophys. Res. Lett.* Vol. 18, No. 6, 1151-1154.
- Nesvorný, D., Bottke, W. F., Levison, H. F., & Dones, L. (2003). Recent origin of the Solar System dust bands. *The Astrophysical Journal*, *591*(1), 486.
- Neveu, M., Desch, S. J., & Castillo-Rogez, J. C. (2015). Core cracking and hydrothermal circulation can profoundly affect Ceres' geophysical evolution. *Journal of Geophysical Research: Planets*, *120*(2), 123-154.

- Nicodemus, F. E. (1965). Directional reflectance and emissivity of an opaque surface. *Applied Optics*, Vol. 4, No. 7, 767-773.
- Nittler, L. R., Alexander, C. M. O'D., Stroud, R. M. . (2013). High abundance of presolar materials in CO₃ chondrite Dominion Range 08006. *LPSC abstract 2367*.
- Nuth III, J. A., Brearley, A. J., Scott, E. R. D. (2005). Microcrystals and amorphous material in comets and primitive meteorites: Keys to understanding processes in the early Solar System. *Chondrites and the Protoplanetary Disk ASP Conference Series*, Vol. 341, 675-700.
- Pieters, C. M., & Hiroi, T. (2004, March). RELAB (Reflectance Experiment Laboratory): A NASA multiuser spectroscopy facility. In *Lunar and Planetary Science Conference* (Vol. 35).
- Platz T, Nathues A, Schorghofer N, Preusker F, Mazarico E, Schröder SE, Byrne S, Kneissl T, Schmedemann N, Combe JP, Schäfer M. (2016). Surface water-ice deposits in the northern shadowed regions of Ceres. *Nature Astronomy*, 1, 0007.
- Podolak, M., & Zucker, S. . (2004). A note on the snow line in protostellar accretion disks. *Meteoritics & Planetary Science*, 39(11), 1859-1868.
- Ramsey, M. S., & Christensen, P. R. (1998). Mineral abundance determination: Quantitative deconvolution of thermal emission spectra. *Journal of Geophysical Research: Solid Earth*, 103(B1), 577-596.
- Rayner, J.T., Toomey, D.W., Onaka, P.M., Denault, A.J., Stahlberger, W.E., Vacca, W.D., Cushing, M.C. and Wang, S.,. (2003). SpeX: A medium-resolution 0.8-5.5 micron

- spectrograph and imager for the NASA Infrared Telescope Facility. *Publications of the Astronomical Society of the Pacific*, 115(805), 362.
- Rivkin, A. S., & Emery, J. P. (2010). Detection of ice and organics on an asteroidal surface. *Nature*, 464(7293), 1322-1323.
- Rivkin, A. S., & Emery, J. P. (2010). Detection of ice and organics on an asteroidal surface. *Nature*, 464(7293), 1322-1323.
- Rivkin, A. S., Howell, E. S., Emery, J. P., Volquardsen, E. L. (2013). The Ch asteroids: Connecting a visible taxonomic class to 3- μ m spectral shape. *DPS abstract*.
- Rivkin, A. S., Howell, E. S., Vilas, F., & Lebofsky, L. A. (2002). Hydrated minerals on asteroids: The astronomical record. *Asteroids III*, 1, 235-253.
- Rivkin, A. S., Howell, E. S., Vilas, F., Lebofsky, L. A. (2002). Hydrated minerals on asteroids: astronomical record. In *Asteroids III* (eds. Bottke, W. F., Jr., Cellino, A., Paolicchi, P., Binzel, R. P.) University of Arizona Press. .
- Rivkin, A. S., Thomas, C. A., Howell, E. S., & Emery, J. P. (2015). The Ch-class asteroids: Connecting a visible taxonomic class to a 3 μ m band shape. *The Astronomical Journal*, 150(6), 198.
- Rivkin, A. S., Volquardsen, E. L., & Clark, B. E. (2006). The surface composition of Ceres: Discovery of carbonates and iron-rich clays. *Icarus*, 185(2), 563-567.
- Rubin, A. E. (2010). Physical properties of chondrules in different chondrite groups: Implications for multiple melting events in dusty environments. *Geochimica et Cosmochimica Acta*, 74(16), 4807-4828.

- Rubin, A. E., Trigo-Rodríguez, J. M., Huber, H., & Wasson, J. T. (2007). Progressive aqueous alteration of CM carbonaceous chondrites. *Geochimica et Cosmochimica Acta*, *71*(9), 2361-2382.
- Rubin, A. E., Trigo-Rodríguez, J. M., Huber, H., Wasson, J. T., (2007). Progressive aqueous alteration of CM carbonaceous chondrites. *Geochimica. Cosmochimica. Acta*, *Vol. 71*, 2361-2382.
- Salisbury, J. W. (1993). Mid-infrared Spectroscopy: Laboratory Data. *In Remote Geochemical Analysis (eds. Pieteres, C. M., Englert, P. A.)*.
- Salisbury, J. W., & Eastes, J. W. (1985). The effect of particle size and porosity on spectral contrast in the mid-infrared. *Icarus*, *64*(3), 586-588.
- Salisbury, J. W., D'Aria, D. M., & Jarosewich, E. (1991). Midinfrared (2.5–13.5 μm) reflectance spectra of powdered stony meteorites. *Icarus*, *92*(2), 280-297.
- Salisbury, J. W., Eastes, J. W. (1985). The effect of particle size and porosity on spectral contrast in the mid-infrared. *Icarus*, *Vol. 64*, 586-588.
- Salisbury, J. W., Wald, A. (1992). The role of volume scattering in reducing spectral contrast of reststrahlen bands in spectra of powdered minerals. *Icarus*, *Vol. 96*, 121-128.
- Salisbury, J. W., Wald, A., & D'Aria, D. M. (1994). Thermal-infrared remote sensing and Kirchhoff's law: 1. Laboratory measurements. *Journal of Geophysical Research: Solid Earth*, *99*(B6), 11897-11911.
- Salisbury, J. W., Walter, L. S., Vergo, N. (1992). Mid-infrared (2.1-25 μm) spectra of minerals: First edition. *USGS Open-file Report 87-263*.

- Salisbury, J. W., Walter, L. S., Vergo, N., (1992). Mid-Infrared (2.1-25 μm) Spectra of Minerals: First Edition. *U.S. Geological Survey. Open-File Report 87-263*.
- Sasselov, D. D., & Lecar, M. (2000). On the snow line in dusty protoplanetary disks. . *The Astrophysical Journal*, 528(2), 995.
- Scheeres, D. J., Britt, D., Carry, B., & Holsapple, K. A. (2015). Asteroid interiors and morphology. *Asteroids IV*, 745-766.
- Scott, E. R. D., Jones, R. H., (1990). Disentangling nebular and asteroidal features of CO₃ carbonaceous chondrite meteorites. *Geochimica Cosmochimica Acta*, 54, 2485-2502.
- Sugiura, N., & Fujiya, W. (2014). Correlated accretion ages and $\epsilon^{54}\text{Cr}$ of meteorite parent bodies and the evolution of the solar nebula. *Meteoritics & Planetary Science*, 49(5), 772-787.
- Sunshine, J. M., Pieters, C. M. (1998). Determining the composition of olivine from reflectance spectroscopy. *Journal of Geophysical Research*, 103, No. 36, 13675-13688.
- Swinyard, B. M., Rieke, G. H., Ressler, M., Glasse, A., Wright, G. S., Ferlet, M., Wells, M. (2004). Sensitivity estimates for the mid-infrared instrument (MIRI) on the JWST. *Proceedings of SPIE 5487, Optical, Infrared and Millimeter Space Telescopes*, 785.
- Takir, D., & Emery, J. P. (2012). Outer main belt asteroids: Identification and distribution of four 3- μm spectral groups. *Icarus*, 219(2), 641-654.
- Takir, D., Emery, J. P., Mcsween, H. Y., Hibbitts, C. A., Clark, R. N., Pearson, N., & Wang, A. (2013). Nature and degree of aqueous alteration in CM and CI carbonaceous chondrites. *Meteoritics & Planetary Science*, 48(9), 1618-1637.

- Tarte, P. (1963). Etude infra-rouge des orthosilicates et des orthogermanates. *Spectrochim. Vol. 19, 25-47.*
- Taylor, G. J., Maggiore, P., Scott, E. R. D., Rubin, A. E., Keil, K. (1987). Original structure, and fragmentation and reassembly histories of asteroids: evidence from meteorites. *Icarus, 69, 1-13.*
- Tholen, D. J. (1984). Asteroid taxonomy from cluster analysis of photometry, Ph.D. dissertation, *Univ. of Ariz., Tucson.*
- Tholen, D. J., & Barucci, M. A. . (1989). Asteroid taxonomy. *In Asteroids II (pp. 298-315).*
- Thomas, P. C., & Robinson, M. S. (2005). Seismic resurfacing by a single impact on the asteroid 433 Eros. *Nature, 436(7049), 366-369.*
- Thompson, J. L., Salisbury, J. W. (1993). The mid-infrared reflectance of mineral mixtures (7-14 μm). *Remote Sensing Environment, 45, 1-13.*
- Tomeoka, K., & Buseck, P. R. (1985). Indicators of aqueous alteration in CM carbonaceous chondrites: Microtextures of a layered mineral containing Fe, S, O and Ni. . *Geochimica et Cosmochimica Acta, 49(10), 2149-2163.*
- Tomeoka, K., McSween Jr, H. Y., & Buseck, P. R. (1989). Mineralogical alteration of CM carbonaceous chondrites: A review. *In Proceedings of the NIPR Symposium on Antarctic Meteorites (Vol. 2, pp. 221-234).*
- Tompkins, S., Pieteres, C. M. (2010). Spectral characteristics of lunar impact melts and inferred mineralogy. *Meteoritics and Planetary Science, Vol. 45, 1152-1169.*
- Tonui, E., Zolensky, M., Hiroi, T., Nakamura, T., Lipschutz, M. E., Wang, M. S., & Okudaira, K. (2014). Petrographic, chemical and spectroscopic evidence for thermal

metamorphism in carbonaceous chondrites I: CI and CM chondrites. *Geochimica et Cosmochimica Acta*, 126, 284-306.

Turner, N. J., Fromang, S., Gammie, C., Klahr, H., Lesur, G., Wardle, M., & Bai, X. N. (2014). Transport and accretion in planet-forming disks. *Protostars and Planets VI*, 411-432.

Trigo-Rodriguez, J. M., Rubin, A. E., Wasson, J. T. (2006). Non-nebular origin of dark mantles around chondrules and inclusions in CM chondrites. *Geochimica. Cosmochimica Acta*, Vol. 70, 1271-1290.

Velbel, M. A., Long, D. T., Gooding, J. L. (1991). Terrestrial weathering of Antarctic stone meteorites: Formation of Mg-carbonates on ordinary chondrites. *Geochimica et Cosmochimica Acta*, 55, 67-76.

Velbel, M. A., Palmer, E. E. (2011). Fine grained serpentine in CM2 carbonaceous chondrites and its implications for the extent of aqueous alteration on the parent body: a review. *Clays and Clay Minerals*, Vol. 59, No. 4, 416-432.

Velbel, M. A., Tonui, E. K., & Zolensky, M. E. (2012). Replacement of olivine by serpentine in the carbonaceous chondrite Nogoya (CM2). *Geochimica et Cosmochimica Acta*, 87, 117-135.

Vernazza, P., Carry, B., Emery, J., Hora, J. L., Cruikshank, D., Binzel, R. P., Jackson, J., Helbert, J., Maturilli, A.,. (2010). Mid-infrared spectral variability for compositionally similar asteroids: Implications for asteroid particle size distributions. *Icarus*, Vol. 207, 800-809.

- Vernazza, P., Castillo-Rogez, J., Beck, P., Emery, J., Brunetto, R., Delbo, M., Marsset, M., Marchis, F., Groussin, O., Zanda, B. and Lamy, P. (2017). Different origins or different evolutions? Decoding the spectral diversity among C-type asteroids. *The Astronomical Journal*, 153(2), 72.
- Vernazza, P., Zanda, B., Binzel, R. P., Hiroi, T., DeMeo, F. E., Birlan, M., Hewins, R., Ricci, L., Barge, P., Lockhart, M. (2014). Multiple and Fast: the accretion of ordinary chondrite parent bodies. *The Astrophysical Journal*, 791, 120-142. .
- Vilas, F. (1994). A cheaper, faster, better way to detect water of hydration on solar system bodies. *Icarus*, 111(2), 456-467.
- Vilas, F. (2008). Spectral characteristics of Hayabusa-2 near-Earth asteroid targets 162173 1999 JU3 and 2001 QC34. *The Astronomical Journal*, 135(4), 1101.
- Vilas, F., & Gaffey, M. J. (1989). Phyllosilicate absorption features in main-belt and outer-belt asteroid reflectance spectra. In *Bulletin of the American Astronomical Society* (Vol. 21, p. 966).
- Vilas, F., & Gaffey, M. J. (1989). Phyllosilicate absorption features in main-belt and outer-belt asteroid reflectance spectra. In *Bulletin of the American Astronomical Society* (Vol. 21, p. 966).
- Walsh, K. J., Morbidelli, A., Raymond, S. N., O'Brien, D. P., & Mandell, A. M. (2011). A low mass for Mars from Jupiter/'s early gas-driven migration. *Nature*, 475(7355), 206-209.
- Warren, P. H. (2011). Stable-isotopic anomalies and the accretionary assemblage of the Earth and Mars: A subordinate role for carbonaceous chondrites. *Earth and Planetary Science Letters*, 311(1), 93-100.

- Weisberg, M. K., McCoy, T. J., & Krot, A. N. (2006). Systematics and evaluation of meteorite classification. *Meteorites and the early solar system II*, 19.
- Weisberg, M. K., McCoy, T. J., & Krot, A. N. (2006). Systematics and evaluation of meteorite classification. In D. S. Lauretta, *Meteorites and the early solar system II*, (p. 19).
- Weisberg, M. K., Prinz, M., Clayton, R. N., & Mayeda, T. K. (1997). CV3 chondrites: Three subgroups, not two. *Meteoritics and Planetary Science Supplement*, 32.
- Wells, M., Pel, J.W., Glasse, A., Wright, G.S., Aitink-Kroes, G., Azzollini, R., Beard, S., Brandl, B.R., Gallie, A., Geers, V.C. and Glauser, A.M.,. (2015). The mid-infrared instrument for the James Webb Space telescope, VI: the medium resolution spectrometer. *Publications of the Astronomical Society of the Pacific*, 127(953), 646.
- Werner, M.W., Roellig, T.L., Low, F.J., Rieke, G.H., Rieke, M., Hoffmann, W.F., Young, E., Houck, J.R., Brandl, B., Fazio, G.G. and Hora, J.L. (2004). The Spitzer space telescope mission. *The Astrophysical Journal Supplement Series*, 154(1), 1.
- Wooden, D., Desch, S., Harker, D., Gail, H-P., Keller, L. (2007). Comet Grains and Implications for Heating and Radial Mixing in the Protoplanetary Disk. in *Protostars and Planets* (eds. Reipurth, B., Jewett, D., Keil, K.).
- Xu, S., Binzel, R. P., Burbine, T. H., Bus, S. J. . (1995). Small Main-Belt Asteroid Spectroscopic Survey: Initial Results. *Icarus*, 115, 1-35.
- Xu, S., Binzel, R. P., Burbine, T. H., Bus, S. J. (1995). Small Main-Belt Asteroid Spectroscopic Survey: Initial Results. *Icarus*, 115, 1-35.

- Yang, B., Wahhaj, Z., Beauvalet, L., Marchis, F., Dumas, C., Marsset, M., Nielsen, E. L., Vachier, F. . (2016). Extreme AO observations of two triple asteroid systems with SPHERE. *The Astrophysical Journal Letters*, 820, L35.
- Yoshikawa, M., Yano, H., & Kawaguchi, J. (2008). Japan's future plans for missions to primitive bodies: Hayabusa-2, Hayabusa-MK2, and Marco Polo. *LPSC, Abstract #1747*.
- Young, E. D., Ash, R. D., England, P., & Rumble, D. . (1999). Fluid flow in chondritic parent bodies: Deciphering the compositions of planetesimals. *Science*, 286(5443), 1331-1335.
- Young, E. D., Zhang, K. K., & Schubert, G. (2003). Conditions for pore water convection within carbonaceous chondrite parent bodies—Implications for planetesimal size and heat production. . *Earth and Planetary Science Letters*, 213(3), 249-259.
- Ziffer, J., Campins, H., Licandro, J., Walker, M.E., Fernandez, Y., Clark, B.E., Mothé-Diniz, T., Howell, E. and Deshpande. (2011). Near-infrared spectroscopy of primitive asteroid families. *Icarus*, 213(2), 538-546.
- Zolensky, M., Barrett, R., & Browning, L. (1993). Mineralogy and composition of matrix and chondrule rims in carbonaceous chondrites. *Geochimica et Cosmochimica Acta*, 57(13), 3123-3148.
- Zolensky, M.E., Mittlefehldt, D.W., Lipschutz, M.E., Wang, M.S., Clayton, R.N., Mayeda, T.K., Grady, M.M., Pillinger, C. and David, B.. (1997). CM chondrites exhibit the complete petrologic range from type 2 to 1. *Geochimica. Cosmochimica. Acta*, Vol. 61, No. 23, 5099-5115.

